SHANKOPATHIES: SHANK PROTEIN DEFICIENCY-INDUCED SYNAPTIC DISEASES

EDITED BY: Elodie Ey, Thomas Bourgeron, Tobias Maria Boeckers, Eunjoon Kim and Kihoon Han

PUBLISHED IN: Frontiers in Molecular Neuroscience, Frontiers in Neural Circuits, Frontiers in Cellular Neuroscience and Frontiers in Synaptic Neuroscience

frontiers Research Topics

frontiers

ISSN 1664-8714
ISBN 978-2-88963-567-2
DOI 10.3389/978-2-88963-567-2

About Frontiers

Frontiers is more than just an open-access publisher of scholarly articles: it is a pioneering approach to the world of academia, radically improving the way scholarly research is managed. The grand vision of Frontiers is a world where all people have an equal opportunity to seek, share and generate knowledge. Frontiers provides immediate and permanent online open access to all its publications, but this alone is not enough to realize our grand goals.

Frontiers Journal Series

The Frontiers Journal Series is a multi-tier and interdisciplinary set of open-access, online journals, promising a paradigm shift from the current review, selection and dissemination processes in academic publishing. All Frontiers journals are driven by researchers for researchers; therefore, they constitute a service to the scholarly community. At the same time, the Frontiers Journal Series operates on a revolutionary invention, the tiered publishing system, initially addressing specific communities of scholars, and gradually climbing up to broader public understanding, thus serving the interests of the lay society, too.

Dedication to Quality

Each Frontiers article is a landmark of the highest quality, thanks to genuinely collaborative interactions between authors and review editors, who include some of the world's best academicians. Research must be certified by peers before entering a stream of knowledge that may eventually reach the public - and shape society; therefore, Frontiers only applies the most rigorous and unbiased reviews.
Frontiers revolutionizes research publishing by freely delivering the most outstanding research, evaluated with no bias from both the academic and social point of view. By applying the most advanced information technologies, Frontiers is catapulting scholarly publishing into a new generation.

What are Frontiers Research Topics?

Frontiers Research Topics are very popular trademarks of the Frontiers Journals Series: they are collections of at least ten articles, all centered on a particular subject. With their unique mix of varied contributions from Original Research to Review Articles, Frontiers Research Topics unify the most influential researchers, the latest key findings and historical advances in a hot research area! Find out more on how to host your own Frontiers Research Topic or contribute to one as an author by contacting the Frontiers Editorial Office: researchtopics@frontiersin.org

SHANKOPATHIES: SHANK PROTEIN DEFICIENCY-INDUCED SYNAPTIC DISEASES

Topic Editors:
Elodie Ey, Institut Pasteur, France
Thomas Bourgeron, Institut Pasteur, France
Tobias Maria Boeckers, University of Ulm, Germany
Eunjoon Kim, Institute for Basic Science (IBS), South Korea
Kihoon Han, College of Medicine, Korea University, South Korea

Citation: Ey, E., Bourgeron, T., Boeckers, T. M., Kim, E., Han, K., eds. (2020). Shankopathies: Shank Protein Deficiency-Induced Synaptic Diseases. Lausanne: Frontiers Media SA. doi: 10.3389/978-2-88963-567-2

Table of Contents

frontiers in Molecular Neuroscience

EDITORIAL
published: 07 February 2020
doi: 10.3389/fnmol.2020.00011

Editorial: Shankopathies: Shank Protein Deficiency-Induced Synaptic Diseases

Elodie Ey[1]*, *Thomas Bourgeron*[1]*, *Tobias M. Boeckers*[2]*, *Eunjoon Kim*[3,4]* and *Kihoon Han*[5]*

[1] Human Genetics and Cognitive Functions, Institut Pasteur, UMR 3571 CNRS, Université de Paris, Paris, France, [2] Institute for Anatomy and Cell Biology, Ulm University, Ulm, Germany, [3] Center for Synaptic Brain Dysfunctions, Institute for Basic Science, Daejeon, South Korea, [4] Department of Biological Sciences, Korea Advanced Institute of Science and Technology, Daejeon, South Korea, [5] Department of Neuroscience, and Biomedical Sciences, Korea University College of Medicine, Seoul, South Korea

Keywords: Shank, Shankopathies, neuropsychiatric disorders, modulating factors, brain regions

Editorial on the Research Topic

Shankopathies: Shank Protein Deficiency-Induced Synaptic Diseases

SHANK (also known as ProSAP) proteins are postsynaptic core scaffolds involved in excitatory synapse development, function, and plasticity. The three members of the SHANK family (SHANK1, SHANK2, and SHANK3) differ in their temporal and regional expression patterns in the central nervous system and non-neuronal tissue during development. Mutations in the cognate genes are associated with various neuropsychiatric conditions, such as autism spectrum disorders, Phelan-McDermid syndrome, intellectual disability, schizophrenia, and bipolar disorder. Exactly how defects in SHANK proteins contribute to these conditions is currently under active investigation.

The present Research Topic provides an overview of current knowledge on the involvement of SHANK genes in neuropsychiatric disorders. Shankopathies are explored at different scales: genes, proteins, cells, synapses, neural circuits, behaviors, and environment. For example, Eltokhi et al. observed that the large phenotypic diversity of patients carrying *SHANK2* mutations is reflected in the phenotypic diversity displayed by the various *Shank2* mouse models. Hassani Nia and Kreienkamp reviewed the effects of *Shank3* mutations on the gene, protein, and synaptic signaling. Both reviews provide a comprehensive state-of-the-art overview on *SHANK2* and *SHANK3* different scales. An example of how mouse models can closely mimic human Shankopathies was provided by the comprehensive characterization of the *Shank3*^{Q321R} knock-in model conducted by Yoo et al..

The other contributions address two major questions for Shankopathies: (i) Are there specific modulating factors for Shankopathies and (ii) Which brain regions are specifically affected by Shankopathies?

Concerning the first question, three putative modulating factors were examined; namely, pharmacological intervention (pharmacological modulation of phenotypes), sexual hormones, and zinc. Sungur et al. explored whether *Shank1* mutant mice and control mice were equally sensitive to amphetamine and methylenedioxymethamphetamine. In *Shank2* mutant mice, Ey et al. demonstrated that the abnormal social behavior of *Shank2* knockout mice was associated with a deficit in social motivation, but with an intact social recognition phenotype. They also highlighted that methylphenidate is ineffective in restoring typical activity levels in hyperactive *Shank2* knockout mice. By contrast, Berkel et al. examined the role of an inherent modulating factor; namely, sexual hormones, on *Shank1*, *Shank2*, and *Shank3* gene transcription and protein

OPEN ACCESS

Edited and reviewed by:
Robert J. Harvey, University of the Sunshine Coast, Australia

***Correspondence:**
Elodie Ey
elodie.ey@pasteur.fr
Thomas Bourgeron
thomas.bourgeron@pasteur.fr
Tobias M. Boeckers
Tobias.Boeckers@dzne.de
Eunjoon Kim
kime@kaist.ac.kr
Kihoon Han
neurohan@korea.ac.kr

Received: *06 December 2019*
Accepted: *14 January 2020*
Published: *07 February 2020*

Citation:
Ey E, Bourgeron T, Boeckers TM, Kim E and Han K (2020) Editorial: Shankopathies: Shank Protein Deficiency-Induced Synaptic Diseases. Front. Mol. Neurosci. 13:11. doi: 10.3389/fnmol.2020.00011

levels. The role of sexual hormones as transcriptional fine-tuners, especially shortly before or after birth, might explain sex-related differences in patients and animal models. Finally, zinc was identified as a potentially major modulating factor in Shankopathies, given its role in recruiting Shank2 and Shank3 at synapses, as well as having a key role in the gastro-intestinal tract, as reviewed by Hagmeyer et al.. At the molecular level, the mode of regulation of AMPA receptor (AMPAR) subunit composition by *Shank2*, *Shank3* and zinc was explored by Ha et al.. Zinc regulated the switch during development of AMPARs lacking GluA2 to AMPARs containing GluA2, while Shank2 and Shank3 also regulated this process. At the scale of the organism, Fourie et al. tested the effect of long-term zinc supplementation in alimentation of the *Shank3*$^{\Delta ex13-16}$ mouse model. Importantly, some aspects of synaptic transmission and some behavioral traits, such as self-grooming, were rescued. Taken together, the studies on zinc presented in this Research Topic present evidence that zinc is a promising potential new therapeutic agent for Shankopathies.

Regarding the second question on brain regions specifically affected by Shankopathies, different approaches were used to investigate the effect of *Shank* mutations at the different scales of observation. Yoo et al. highlighted that a conditional *Shank3* knockout (targeting exons 14–16, encoding the PDZ domain) in GABAergic neurons (enriched in the striatum) induces a strong reduction of excitatory synaptic inputs onto dorsal striatal neurons as observed in global *Shank3*$^{\Delta ex14-16}$ mutant mice. However, the conditional knockout leads to milder social deficits and stereotyped behaviors than global *Shank3*$^{\Delta ex14-16}$ mutant mice. Using magnetic resonance imaging (MRI), Schoen et al. examined mouse brain anatomy during development showing that total brain volume, cerebellar volume, and cortical thickness were unaffected in homozygous and heterozygous *Shank3* mutant mice and the prenatal zinc deficiency model compared to wild-type controls. By contrast, the striatal volume and the globus pallidus volume were increased in both models, while the changes in the thalamus were reduced in the *Shank3* mouse model and increased in the prenatal zinc deficiency mouse model. Transcriptomic analyses allowed (Jin et al.) to identify brain region-specific modulation of gene expression in different *Shank3* models, across age classes and between brain regions (prefrontal cortex, striatum, and hippocampus). This analysis highlighted an important modulation of the expression of myelin-related and ribosome-related genes. At the protein level, Heise et al. found that *Shank2* and *Shank3* mutant mice displayed a reduced expression of receptors specific to excitatory synaptic transmission in the striatum and in the thalamus (for *Shank2* also in the cortex and cerebellum). These models were compared to another mouse model of neurodevelopmental disorders, the *Cntn4* mutant that displays increased surface expression of glutamatergic receptors (GluA1 and GluA2) in the striatum or downregulation of GABAergic receptors (GABAA) in several brain regions. Finally, the involvement of the reward system was examined directly and indirectly. In the direct approach, Bariselli et al. knocked down *Shank3* in the ventral tegmental area in mice and observed a dysfunction in social-seeking behavior. The indirect approach concerned the characterization of a *Shank2* model in another species, namely the *Shank2*$^{\Delta ex31}$ mutant rat, characterized by Modi et al.. *Shank2*$^{\Delta ex31}$ mutant rats displayed an atypically high motivation to collect food reward, in parallel with social deficits, impaired learning, increased activity, and repetitive circling, combined with increased striatal activity and decreased hippocampal function.

In summary, this Research Topic provided a multi-scale overview of the current state of knowledge on Shankopathies. The research studies contribute to the understanding of the spectrum of disorders related to *SHANK* mutations, as well as providing prospects for new potential therapeutic strategies, targeting specific brain regions or modulating factors.

AUTHOR CONTRIBUTIONS

All authors listed have made a substantial, direct and intellectual contribution to the work, and approved it for publication.

FUNDING

This work was supported by the Centre National de la Recherche Scientifique, the Université de Paris, the Institut Pasteur, and the Bettencourt-Schueller foundation (to EE and TB), by the Deutsche Forschungsgemeinschaft (DFG, German Research Foundation)-Projektnummer 251293561-SFB 1149 (project A2) (to TMB), by the Institute for Basic Science (IBS-R002-D1 to EK), and by the National Research Foundation of Korea (2018R1C1B6001235 to KH). TMB was further supported by the BIU2 initiative, the Else Kröner Foundation, the Innovative Medicines Initiative (IMI) Joint Undertaking under grant agreement no. 777394 (AIMS 2 Trials), which is composed of financial contributions from the European Union and EFPIA companies' in-kind contribution and the DZNE, Ulm site.

Conflict of Interest: The authors declare that the research was conducted in the absence of any commercial or financial relationships that could be construed as a potential conflict of interest.

frontiers in Synaptic Neuroscience

PERSPECTIVE
published: 23 May 2018
doi: 10.3389/fnsyn.2018.00011

Prospects of Zinc Supplementation in Autism Spectrum Disorders and Shankopathies Such as Phelan McDermid Syndrome

Simone Hagmeyer[1,2†], *Ann Katrin Sauer*[1,2,3†] *and Andreas M. Grabrucker*[3,4,5*]

[1]*Institute for Anatomy and Cell Biology, Ulm University, Ulm, Germany,* [2]*WG Molecular Analysis of Synaptopathies, Department of Neurology, Neurocenter of Ulm University, Ulm, Germany,* [3]*Department of Biological Sciences, University of Limerick, Limerick, Ireland,* [4]*Bernal Institute, University of Limerick, Limerick, Ireland,* [5]*Health Research Institute (HRI), University of Limerick, Limerick, Ireland*

The loss of one copy of SHANK3 (SH3 and multiple ankyrin repeat domains 3) in humans highly contributes to Phelan McDermid syndrome (PMDS). In addition, SHANK3 was identified as a major autism candidate gene. Interestingly, the protein encoded by the SHANK3 gene is regulated by zinc. While zinc deficiency depletes synaptic pools of Shank3, increased zinc levels were shown to promote synaptic scaffold formation. Therefore, the hypothesis arises that patients with PMDS and Autism caused by Shankopathies, having one intact copy of SHANK3 left, may benefit from zinc supplementation, as elevated zinc may drive remaining Shank3 into the post-synaptic density (PSD) and may additional recruit Shank2, a second zinc-dependent member of the SHANK gene family. Further, elevated synaptic zinc levels may modulate E/I ratios affecting other synaptic components such as NMDARs. However, several factors need to be considered in relation to zinc supplementation such as the role of Shank3 in the gastrointestinal (GI) system—the location of zinc absorption in humans. Therefore, here, we briefly discuss the prospect and impediments of zinc supplementation in disorders affecting Shank3 such as PMDS and propose a model for most efficacious supplementation.

Keywords: Zn, autism, ASD, synapse, trace metal, 22q13, 22q13.3

OPEN ACCESS

Edited by:
Eunjoon Kim,
Institute for Basic Science (IBS), South Korea

Reviewed by:
Carlo Sala,
Istituto di Neuroscienze (IN), Italy
Eun-Jae Lee,
Asan Medical Center, South Korea

***Correspondence:**
Andreas M. Grabrucker
andreas.grabrucker@ul.ie

†These authors have contributed equally to this work.

Received: *05 April 2018*
Accepted: *08 May 2018*
Published: *23 May 2018*

Citation:
Hagmeyer S, Sauer AK and Grabrucker AM (2018) Prospects of Zinc Supplementation in Autism Spectrum Disorders and Shankopathies Such as Phelan McDermid Syndrome. Front. Synaptic Neurosci. 10:11. doi: 10.3389/fnsyn.2018.00011

INTRODUCTION

Shank3 and PMDS

Phelan McDermid syndrome (PMDS, also 22q13 deletion syndrome or 22q13.3 deletion syndrome) is classified as a syndromic form of autism due to a majority of patients falling on the autism spectrum, displaying autistic or autism-like behavioral traits, caused by a 22q13.3 deletion that includes the SHANK3 gene. Patients otherwise present with minor facial dysmorphic features, global developmental delay, mental retardation, as well as absent or delayed language acquisition. In addition, ADHD, seizures and gastrointestinal (GI) disorders are common medical comorbid conditions (Wong et al., 1997; Bonaglia et al., 2001; Phelan and McDermid, 2012; Kolevzon et al., 2014; Pfaender et al., 2017).

Heterozygous loss of SHANK3 seems to be a major factor contributing to the pathology of PMDS. In addition, SHANK3 is major autism candidate gene (Leblond et al., 2014). In several

patients with autism, deletions, nonsense, missense and splice site mutations have been found that affect the function of one SHANK3 allele (Durand et al., 2007; Gauthier et al., 2009). Proteins of the SHANK (also known as Proline-rich synapse-associated protein ProSAP) family are major scaffold proteins within the post-synaptic density (PSD) of excitatory synapses (Boeckers et al., 2002). A mouse model for PMDS reflecting autistic traits seen in human patients has been published (Bozdagi et al., 2010) and several homozygous Shank3 mutant animals were reported to display autism-like phenotypes including impaired social behavior and ultrasonic vocalizations, repetitive behavior, anxiety and learning and memory problems (Peça et al., 2011; Wang et al., 2011; Schmeisser et al., 2012).

Interestingly, while pharmacological approaches using IGF-1 and CDPPB, a mGluR5 positive allosteric modulator, were partly successful in restoring function in Shank3 deletion model systems (Bozdagi et al., 2010; Verpelli et al., 2011; Wang et al., 2016; Vicidomini et al., 2017), the regulation of Shank2 and Shank3 by zinc may be another promising approach to rescue Shank3 function.

Zinc and Shank3

The heterozygous loss of the SHANK3 gene results in reduced Shank3 protein levels in PMDS patients. In mutant mice that lack the SHANK3 gene and may function as an animal model for PMDS, a comparable decrease in Shank3 protein levels can be monitored (Peça et al., 2011; Wang et al., 2011; Schmeisser et al., 2012). Intriguingly, a similar reduction in Shank3 protein levels was also observed in animals exposed to a mild zinc deficiency during their embryonic development and in primary hippocampal neurons cultured under zinc deficient conditions (Grabrucker et al., 2011, 2014).

Isoforms of Shank3 and the SHANK family member Shank2 that contain the C-terminal SAM domain directly bind zinc (Baron et al., 2006; Gundelfinger et al., 2006; Grabrucker et al., 2011). Additionally, *in vitro* studies showed that the SAM domain of Shank3 is responsible for its synaptic localization (Boeckers et al., 2005) and oligomerization at the postsynaptic density of glutamatergic synapses (Naisbitt et al., 1999; Baron et al., 2006). The recruitment and multimerization of Shank3 at the PSD is a crucial step in the processes of synapse development and maturation (Grabrucker et al., 2009) and was shown to be highly zinc dependent (Gundelfinger et al., 2006; Grabrucker et al., 2011; Tao-Cheng et al., 2016). Experiments in primary hippocampal neuronal cultures showed that the synaptic localization and protein concentration of Shank3 and Shank2 are highly responsive to alterations in neuronal zinc homeostasis (Grabrucker et al., 2014). In ultrastructural analyses, an increased recruitment of Shank3 to the PSD upon zinc supplementation or stimulation was observed (Tao-Cheng et al., 2016). In addition to that, the presence of zinc was crucial to maintain the augmented Shank3 label intensity at the PSD (Tao-Cheng et al., 2016), and increased the number of synaptic contacts with a "mature" PSD (Grabrucker et al., 2011). On the contrary, an increased number of synapses without a prominent PSD was reported under zinc deficient conditions (Grabrucker et al., 2011), but also Shank deficient conditions. Furthermore, the reduction of neuronal zinc levels by exposure to the highly potent zinc chelators CaEDTA and TPEN resulted in a significant reduction in the number of Shank3 immunoreactive puncta per dendritic length as well as in their fluorescence intensity (Grabrucker et al., 2011, 2014). Additionally, a similar reduction of Shank3 protein levels at synapses was detected by western blot analyses (Grabrucker et al., 2011, 2014). As a consequence of zinc depletion, Shank3 is predominantly diffusely localized in dendritic localizations (Grabrucker et al., 2011) and might enter an inactive state there (Arons et al., 2016) indicating that zinc is crucial for stabilizing Shank3 at the postsynaptic site (Grabrucker et al., 2011; Arons et al., 2016).

Interestingly, the supplementation of primary hippocampal neurons with zinc chloride increased Shank3 immunofluorescence levels and therefore the concentration of Shank3 proteins at synapses (Grabrucker et al., 2011, 2014). In line with the described findings obtained from *in vitro* experiments, prenatal zinc deficiency in mice was found to tremendously affect synaptic Shank3 (Grabrucker et al., 2014). Prenatal zinc deficient pups that were nursed by zinc deficient mothers showed a significant reduction in brain zinc and Shank3 levels. A loss of synaptic Shank3 comparable to that observed in Shank3 knock-out mice was detected in immunohistochemical and biochemical analyses of prenatal zinc deficient animals (Grabrucker et al., 2014). Again, a redistribution of Shank3 from the synaptic site to the cytoplasm was reported (Grabrucker et al., 2014). However, the reduction in zinc levels and the concomitant lack of Shank3 was fully rescued by cross-fostering prenatal zinc deficient pups by mothers fed a zinc adequate control diet indicating that zinc supplementation is sufficient to restore previously diminished Shank3 levels *in vivo* (Grabrucker et al., 2014).

Taken together, reduced Shank3 protein levels comparable to those observed in models of PMDS can be caused by the depletion of zinc emphasizing the strong regulatory effect of zinc on synaptic Shank3. On the other hand, remaining Shank3 protein, and possibly in addition Shank2 proteins, can be recruited to synapses by increasing zinc levels. Therefore, we hypothesize that supplementation with zinc may rescue the loss of Shank3 in PMDS and through this modify the resulting phenotype. It was shown that re-establishing Shank3 levels after birth can ameliorate autism-like symptoms in mice (Mei et al., 2016). However, performing zinc supplementation in Shank3 deficient conditions *in vivo* may face challenges given the reported role of Shank3 in the GI system.

Shank3 and Zinc Transporters

Aside from GI problems, zinc deficiency was shown to be highly prevalent in individuals with PMDS (Grabrucker et al., 2014; Pfaender and Grabrucker, 2014; Pfaender et al., 2017) and ASD (Yasuda et al., 2011; Arora et al., 2017). With the GI system taking center stage in the maintenance of zinc homeostasis, regulation of zinc levels within the body occurs with help of various proteins including members of the Zinc Transporter (ZnT) and Zrt-and Irt-like proteins (ZIP) superfamily of zinc transporters, and metallothioneins (MT; Fukada et al., 2011; Zhao et al., 2014). In humans, dietary zinc uptake primarily occurs within small

intestinal enterocytes (Krebs, 2000; Wang and Zhou, 2010) with ZnT and ZIP transporter moving zinc across cellular membranes and into organelles (Hershfinkel, 2005). Especially, Zip2 and Zip4 proteins act as key players of zinc absorption in enterocytes. Not surprisingly, mutated ZIP4 leads to severe impairments in zinc uptake as seen in the autosomal recessive inherited disorder *Acrodermatitis enteropathica (AE)*. AE patients require lifelong zinc substitution in very large doses as treatment (around 200 mg daily instead of the required daily intake in healthy individuals of 15 mg; Maverakis et al., 2007; Andrews, 2008; Pfaender et al., 2017).

Besides its various other functions in the immune system and during brain development, zinc also plays a vital role in the developing GI system and effects gut morphology (Vela et al., 2015). While current research reports high prevalence of GI disorders and zinc deficiency in neurodevelopmental disorders such as non-syndromic and syndromic ASD, it might also have provided a potential link between these dysfunctions (Vela et al., 2015; Pfaender et al., 2017).

Pfaender et al. (2017) showed that besides its function as postsynaptic scaffolding protein in the brain, Shank3 can additionally be found in human and murine enterocytes in the GI tract. In the same study, analysis of key regulators of trace metal homeostasis revealed significant alterations of ZIP2 and ZIP4 expression on mRNA and protein level in enterocytes generated from PMDS patient derived induced pluripotent stem cells (hiPSC) compared to healthy controls. More so, ZIP2 and ZIP4 expression levels in enterocytes seemed to be dependent on Shank3 protein levels, which was confirmed by overexpression and knockdown experiments in the intestinal Caco-2 cell-line model. Co-immunofluorescence of Shank3 and Zip4 in hiPSC derived enterocytes and co-immunoprecipitation experiments of Shank3 protein using wildtype mouse intestinal epithelial lysate and human enterocyte cell lysates shows that Shank3 proteins seem capable of forming a protein complex with Zip4 and to a lesser extent with Zip2 (Pfaender et al., 2017).

Given that Shank3 levels both *in vitro* and *in vivo* regulate zinc transporter expression, a possible explanation for high incidence rates of zinc deficiency in PMDS can be found. However, the loss of zinc transporters in the GI tract may present a significant challenge for zinc supplementation and similar to AE patients, high levels and daily lifelong supplementation may be needed. Therefore, supplementation with commercially available supplements and dosages reflecting the required daily intake of healthy individuals may not suffice. However, chronic high levels of zinc intake that are not toxic *per se* may have secondary effects for example on copper levels and may be a challenge especially for children with PMDS.

PERSPECTIVES

ZnAAs as Effective Zinc Supplement in PMDS

In the case of a diet low in zinc, Zip4 at the plasma membrane of enterocytes is upregulated to maximize absorption of zinc (Dufner-Beattie et al., 2004). However, this mechanism seems impaired upon Shank3 depletion (Pfaender et al., 2017). Using novel types of zinc supplements, it is possible to utilize alternative routes of zinc uptake. Recently, we have shown that zinc amino acid complexes (ZnAAs) may provide such alternative absorption/transport pathway opportunity (Sauer et al., 2017). Due to the overall amino acid-like structure, ZnAAs based supplements are taken up by amino acid transporters. For example, using hiPSC from AE patients, we could show that while an inorganic zinc supplement such as $ZnCl_2$ performed significantly worse in AE patient cells with non-functional Zip4 compared to control cells, ZnAAs were able to deliver zinc into enterocytes effectively and without significant difference between AE and healthy cells (Sauer et al., 2017). The chemistry of ZnAAs that may be comprised of different amino acids such as glutamate, methionine and lysine, among others, in the form of ZnGlu, ZnMet, ZnLys, allows for release of the zinc (once inside cells or the systemic circulation) whereby zinc will be able to participate in its physiological functions such as the regulation of Shank2 and Shank3 proteins at synapses.

Therefore, we propose that although supplementation of trace minerals in humans or animals can be performed using different types of supplements, the most suited supplement should be selected, considering the special GI physiology under Shank3 depleted conditions such as PMDS. With a significantly higher demand than that of trace minerals, amino acids will have over a thousand-fold more transporters than any trace mineral. Thus, a selection of ZnAAs for supplementation in PMDS might secure the highest efficacy of zinc supplementation (**Figure 1**). ZnAAs are currently available on the market as mineral supplement for animals, where they are safe and effective and should be explored in human studies in future. In contrast, using inorganic zinc supplements might need high dosages and long supplementation times until effects might be measurable in Shank3 mouse models and human patients.

Benefits of Zinc Supplementation in PMDS and ASD—A Hypothesis

Based on the current data, a model can be proposed according to which zinc supplementation in Shankopathies may be a promising approach. This is based on several observations. First, restoring Shank3 levels in adult mice ameliorates their autism phenotype. Second, increased zinc levels are able to increase synaptic Shank3 levels, which may compensate the loss of one functional copy of the gene. Third, in addition, recruitment of the zinc-dependent Shank2 may contribute to the compensating effect (**Figure 2**). Given that Shank proteins are found in a complex of further autism associated proteins such as Neurexin (Nrxn) and Neuroligin (Nlgn), as well as mTOR, strengthening Shank3 scaffolds may also be beneficial in cases of mutation of other proteins of the proposed autism associated pathway at excitatory synapses (Bourgeron, 2009).

While PMDS is a very rare syndrome, the prevalence of mutations in Shank3 and Shank2 is higher in the ASD

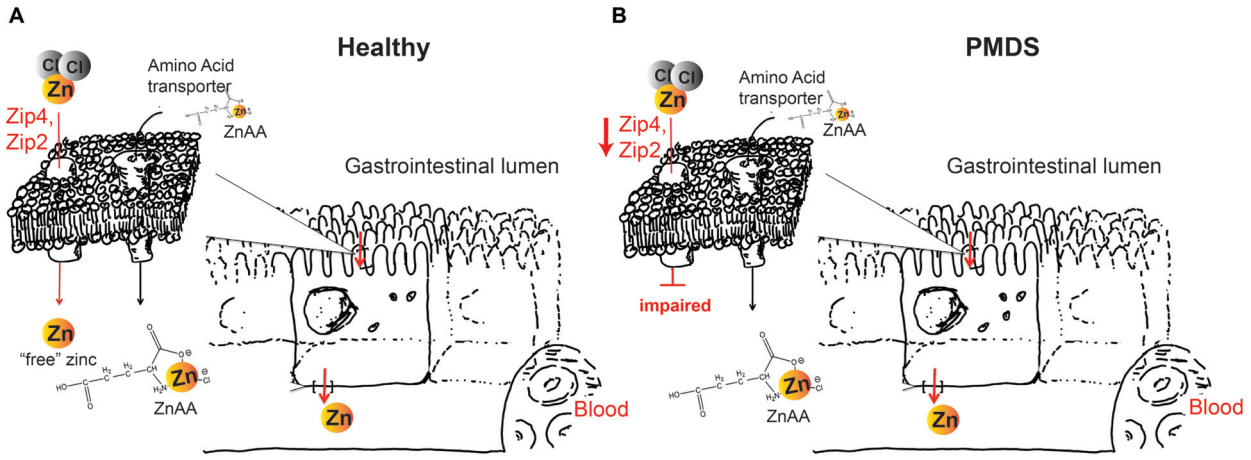

FIGURE 1 | (A) Zinc supplements based on zinc salts such as $ZnCl_2$ or ZnO will dissociate in solution. In healthy individuals, zinc importers Zip4 and Zip2 take up this "free" (aqueous) zinc ions into enterocytes, which subsequently release zinc on the basolateral side into the blood circulation. Zinc amino acid compounds (ZnAA) are relatively stable and are taken up by amino acid transporters. **(B)** In Phelan McDermid syndrome (PMDS) patients, Zip4 and Zip2 may be affected. Thus, uptake of inorganic zinc supplements may be impaired. In contrast, due to the amino acid-like structure, ZnAAs can still be taken up by amino acid transporters possibly providing more efficient supplementation in PMDS patients.

population (∼1.5% and 0.17%, respectively, Leblond et al., 2014). In addition, Shank proteins are physiologically linked to proteins with mutations reported in the ASD population such as NMDAR (Pan et al., 2015), Nrxn/Nlgn complexes (Yoo, 2015; Onay et al., 2017) and mGluR5-mTOR (Fragile X syndrome: 1%–2% of patients with ASD, Tuberous sclerosis: ∼1% of patients with ASD; Abrahams and Geschwind, 2008). Therefore, this group of patients may benefit from modulation of Shank2/3 via zinc as well.

Besides effects on the Shank2/3 scaffold, activation of zinc signaling may have effects on further synaptic proteins and thereby synapse function (Sensi et al., 2009, 2011). For example, zinc acts as allosteric inhibitor of GluN1/GluN2A (NMDA) receptors (Paoletti et al., 1997). However, it was shown that a postsynaptic increase in zinc can also activate NMDA receptors in a Src tyrosine kinase dependent manner, which may be an important contributor to the rescue of ASD behaviors (Lee et al., 2015). Further, zinc may inhibit $GABA_A$ receptors (Smart et al., 1994). Thus, zinc modulates excitatory synaptic transmission as well as inhibitory synaptic transmission and may be an important player in maintaining the balance between excitation (E) and inhibition (I). Changes in E/I ratio have been reported to be important in the pathogenesis ASD (Rubenstein and Merzenich, 2003) and altered zinc homeostasis may positively influence the E/I ratio.

In addition, zinc has inhibitory effects on voltage-gated ion channels (Blakemore and Trombley, 2017), and is linked to BDNF signaling via metalloproteinase activation, which plays an important role in Trk receptor activation (Hwang et al., 2005).

However, with zinc being a non-genetic factor, dosage is important. While genetic models of Shank3 deficiency follow a pattern of full loss (homozygous deletion) or loss of half of Shank3 (heterozygous deletion), zinc will act along a large spectrum of dosages. Finding the correct dosage may be complicated. In addition, it is hard to estimate after which time effects may be observable. While zinc is taken up quickly in the body, it does not cross freely the blood-brain barrier (BBB). A constant elevated serum zinc level may be necessary to generate a sufficient concentration gradient to drive zinc uptake into the brain. Both, dosage and treatment times will be dependent on the type of zinc supplement used. In addition, treatment should be performed as early as possible and therefore, efficacy might critically depend on the ability to diagnose PMDS/ASD early in development. According to previously published data (Grabrucker et al., 2011), forming and immature synapses are characterized by Shank2 and Shank3 family members at the PSD and are more reactive to zinc than mature synapses that also contain the zinc-independent Shank1. Thus, strengthening the Shank2 and Shank3 scaffold to reach a threshold for the synapse to mature will be most critical during the time window of brain development with maximal need for establishment of synaptic contacts to lie down the basic connectivity in and in between brain regions. However, it is possible that some brain regions maintain plasticity throughout later development and will still benefit from increased zinc levels. In line with this, re-expression of Shank3 in adult mice that developed in absence of Shank3 was able to rescue social interaction deficits and repetitive grooming behavior, but not anxiety and motor coordination deficits (Mei et al., 2016). This hints to different time windows in development, where supplementation will be able to rescue different features of ASD to different extent.

Taken together, to move forward in animal studies and finally human studies, various factors need to be considered. The type of supplement needs to ensure effective zinc uptake, but also zinc delivery into the brain. Here, recently developed nanoparticles delivering zinc across the BBB may be promising (Chhabra et al., 2015; Vilella et al., 2017). Additionally, the standard laboratory

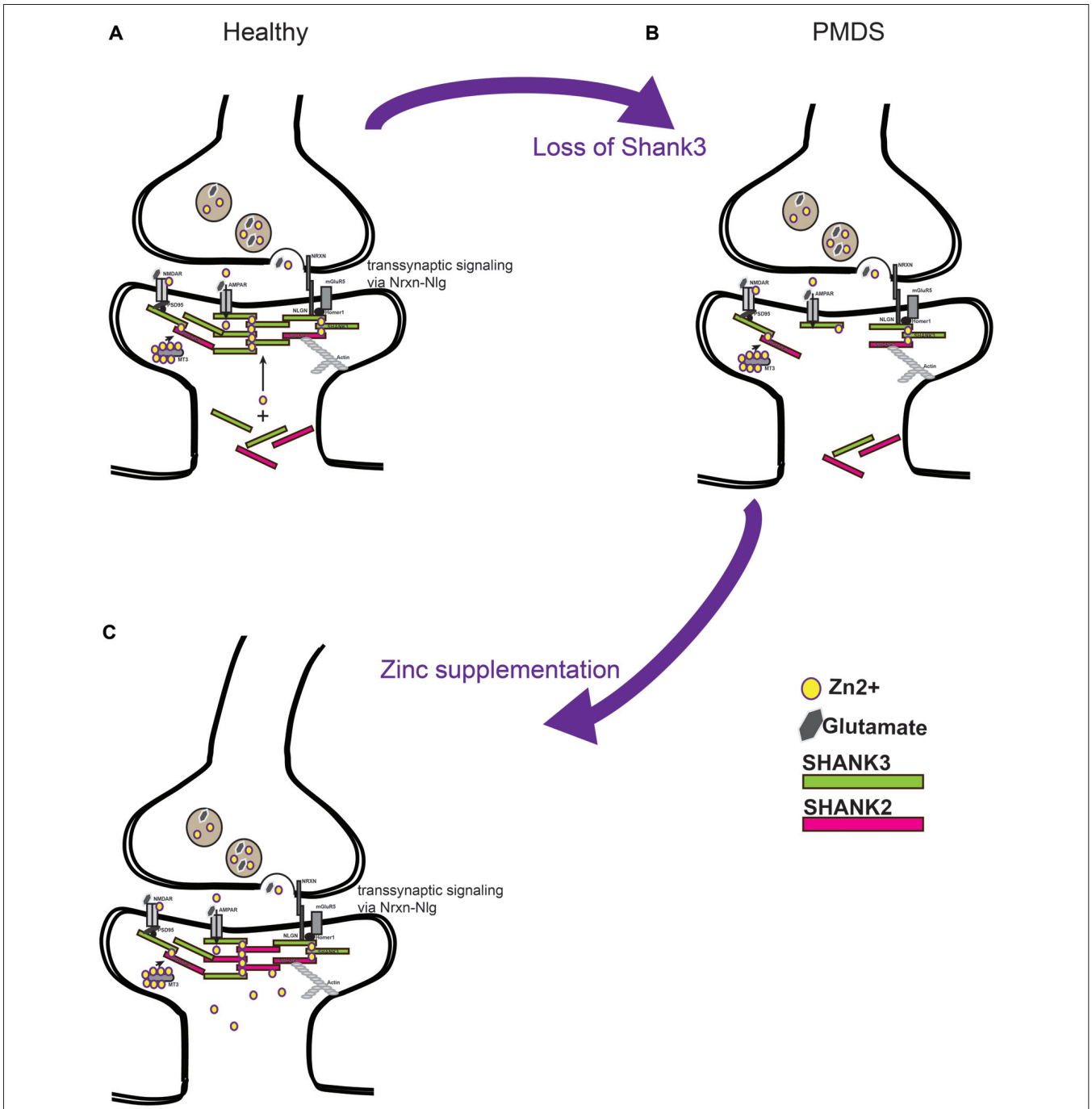

FIGURE 2 | (A) Current models predict a soluble pool of Shank proteins at the post-synapse, as well as a post-synaptic density (PSD) bound pool recruited to the PSD by zinc binding. PSD bound Shank scaffolds proteins link receptors at the membrane to the actin cytoskeleton. Further, by binding with Neuroligin (Nlg) and Neurexin (Nrxn) complexes, the level of Shank3 at the PSD provides a transsynaptic signal to the pre-synapse to coordinate synaptic plasticity of both parts of the synapse. **(B)** Loss of Shank3 proteins at the synapse may destabilize synapses and prevent their maturation or formation. Heterozygous deletion or mutation of Shank3 in humans leaves one copy of the gene intact that produces proteins. **(C)** Increasing zinc levels by zinc supplementation might restore Shank3 levels by recruitment of Shank3 from the soluble synaptic pool to the PSD bound pool and might recruit additional Shank2 proteins. Strengthening the PSD scaffold in this way may compensate some deficits seen in forms of ASD caused by imbalance in the Nrxn-Nlg-Shank pathway.

diet for Shank mouse models has to be carefully controlled for zinc content. Fortified diets used for mice may contain up to five times higher zinc levels as the required daily dosage for mice and it may be possible that heterozygous Shank3 mice on this diet already represent models of low zinc supplementation. While this concentration of zinc may not be enough to cause significant

effects, it might contribute to the relatively mild phenotype of heterozygous mice, despite human patients being heterozygous as well. Finally, the age of mice and duration of treatment, as well as dosage of zinc supplementation need to be carefully selected.

Human studies using zinc supplementation in ASD patients so far reported mixed results. While some studies found benefits (Russo and Devito, 2011), the results were less clear in others. In future, the cohort of participants with ASD needs to be more carefully selected based on their underlying genetic mutation, and treatment performed early in life for a long time using therapeutic dosages of classic zinc supplements or alternative forms of zinc supplementation.

AUTHOR CONTRIBUTIONS

SH, AKS and AG developed the hypothesis of the study and together drafted the manuscript.

FUNDING

SH is a member of the international PhD program in molecular medicine of Ulm University and funded by Evangelisches Studienwerk Villigst e.V. AG is supported by the Juniorprofessuren-Program of the State of Baden-Wuerttemberg.

REFERENCES

Abrahams, B. S., and Geschwind, D. H. (2008). Advances in autism genetics: on the threshold of a new neurobiology. *Nat. Rev. Genet.* 9, 341–355. doi: 10.1038/nrg2346

Andrews, G. K. (2008). Regulation and function of Zip4, the acrodermatitis enteropathica gene. *Biochem. Soc. Trans.* 36, 1242–1246. doi: 10.1042/BST0361242

Arons, M. H., Lee, K., Thynne, C. J., Kim, S. A., Schob, C., Kindler, S., et al. (2016). Shank3 is part of a zinc-sensitive signaling system that regulates excitatory synaptic strength. *J. Neurosci.* 36, 9124–9134. doi: 10.1523/JNEUROSCI.0116-16.2016

Arora, M., Reichenberg, A., Willfors, C., Austin, C., Gennings, C., Berggren, S., et al. (2017). Fetal and postnatal metal dysregulation in autism. *Nat. Commun.* 8:15493. doi: 10.1038/ncomms15493

Baron, M. K., Boeckers, T. M., Vaida, B., Faham, S., Gingery, M., Sawaya, M. R., et al. (2006). An architectural framework that may lie at the core of the postsynaptic density. *Science* 311, 531–535. doi: 10.1126/science.1118995

Blakemore, L. J., and Trombley, P. Q. (2017). Zinc as a neuromodulator in the central nervous system with a focus on the olfactory bulb. *Front. Cell. Neurosci.* 11:297. doi: 10.3389/fncel.2017.00297

Boeckers, T. M., Bockmann, J., Kreutz, M. R., and Gundelfinger, E. D. (2002). ProSAP/Shank proteins—a family of higher order organizing molecules of the postsynaptic density with an emerging role in human neurological disease. *J. Neurochem.* 81, 903–910. doi: 10.1046/j.1471-4159.2002.00931.x

Boeckers, T. M., Liedtke, T., Spilker, C., Dresbach, T., Bockmann, J., Kreutz, M. R., et al. (2005). C-terminal synaptic targeting elements for postsynaptic density proteins ProSAP1/Shank2 and ProSAP2/Shank3. *J. Neurochem.* 92, 519–524. doi: 10.1111/j.1471-4159.2004.02910.x

Bonaglia, M. C., Giorda, R., Borgatti, R., Felisari, G., Gagliardi, C., Selicorni, A., et al. (2001). Disruption of the ProSAP2 gene in a t(12;22)(q24.1;q13.3) is associated with the 22q13.3 deletion syndrome. *Am. J. Hum. Genet.* 69, 261–268. doi: 10.1086/321293

Bourgeron, T. (2009). A synaptic trek to autism. *Curr. Opin. Neurobiol.* 19, 231–234. doi: 10.1016/j.conb.2009.06.003

Bozdagi, O., Sakurai, T., Papapetrou, D., Wang, X., Dickstein, D. L., Takahashi, N., et al. (2010). Haploinsufficiency of the autism-associated Shank3 gene leads to deficits in synaptic function, social interaction, and social communication. *Mol. Autism.* 1:15. doi: 10.1186/2040-2392-1-15

Chhabra, R., Ruozi, B., Vilella, A., Belletti, D., Mangus, K., Pfaender, S., et al. (2015). Application of polymeric nanoparticles for CNS targeted zinc delivery *in vivo*. *CNS Neurol. Disord. Drug Targets* 14, 1041–1053. doi: 10.2174/1871527314666150821111455

Dufner-Beattie, J., Kuo, Y. M., Gitschier, J., and Andrews, G. K. (2004). The adaptive response to dietary zinc in mice involves the differential cellular localization and zinc regulation of the zinc transporters ZIP4 and ZIP5. *J. Biol. Chem.* 279, 49082–49090. doi: 10.1074/jbc.M409962200

Durand, C. M., Betancur, C., Boeckers, T. M., Bockmann, J., Chaste, P., Fauchereau, F., et al. (2007). Mutations in the gene encoding the synaptic scaffolding protein SHANK3 are associated with autism spectrum disorders. *Nat. Genet.* 39, 25–27. doi: 10.1038/ng1933

Fukada, T., Yamasaki, S., Nishida, K., Murakami, M., and Hirano, T. (2011). Zinc homeostasis and signaling in health and diseases: zinc signaling. *J. Biol. Inorg. Chem.* 16, 1123–1134. doi: 10.1007/s00775-011-0797-4

Gauthier, J., Spiegelman, D., Piton, A., Lafrenière, R. G., Laurent, S., St-Onge, J., et al. (2009). Novel de novo SHANK3 mutation in autistic patients. *Am. J. Med. Genet. B Neuropsychiatr. Genet.* 150B, 421–424. doi: 10.1002/ajmg.b.30822

Grabrucker, S., Jannetti, L., Eckert, M., Gaub, S., Chhabra, R., Pfaender, S., et al. (2014). Zinc deficiency dysregulates the synaptic ProSAP/Shank scaffold and might contribute to autism spectrum disorders. *Brain* 137, 137–152. doi: 10.1093/brain/awt303

Grabrucker, A. M., Knight, M. J., Proepper, C., Bockmann, J., Joubert, M., Rowan, M., et al. (2011). Concerted action of zinc and ProSAP/Shank in synaptogenesis and synapse maturation. *EMBO J.* 30, 569–581. doi: 10.1038/emboj.2010.336

Grabrucker, A., Vaida, B., Bockmann, J., and Boeckers, T. M. (2009). Synaptogenesis of hippocampal neurons in primary cell culture. *Cell Tissue Res.* 338, 333–341. doi: 10.1007/s00441-009-0881-z

Gundelfinger, E. D., Boeckers, T. M., Baron, M. K., and Bowie, J. U. (2006). A role for zinc in postsynaptic density asSAMbly and plasticity? *Trends Biochem. Sci.* 31, 366–373. doi: 10.1016/j.tibs.2006.05.007

Hershfinkel, M. (2005). "Zn^{2+}, a dynamic signaling molecule," in *Molecular Biology of Metal Homeostasis and Detoxification: From Microbes to Man*, eds M. J. Tamas and E. Martinoia (Berlin: Springer), 131–154.

Hwang, J. J., Park, M. H., Choi, S. Y., and Koh, J. Y. (2005). Activation of the Trk signaling pathway by extracellular zinc. Role of metalloproteinases. *J. Biol. Chem.* 280, 11995–12001. doi: 10.1074/jbc.M403172200

Kolevzon, A., Angarita, B., Bush, L., Wang, A. T., Frank, Y., Yang, A., et al. (2014). Phelan-McDermid syndrome: a review of the literature and practice parameters for medical assessment and monitoring. *J. Neurodev. Disord.* 6:39. doi: 10.1186/1866-1955-6-39

Krebs, N. F. (2000). Overview of zinc absorption and excretion in the human gastrointestinal tract. *J. Nutr.* 130, 1374–1377. doi: 10.1093/jn/130.5.1374s

Leblond, C. S., Nava, C., Polge, A., Gauthier, J., Huguet, G., Lumbroso, S., et al. (2014). Meta-analysis of SHANK Mutations in Autism Spectrum Disorders: a gradient of severity in cognitive impairments. *PLoS Genet.* 10:e1004580. doi: 10.1371/journal.pgen.1004580

Lee, E. J., Lee, H., Huang, T. N., Chung, C., Shin, W., Kim, K., et al. (2015). Trans-synaptic zinc mobilization improves social interaction in two mouse models of autism through NMDAR activation. *Nat. Commun.* 6:7168. doi: 10.1038/ncomms8168

Maverakis, E., Fung, M. A., Lynch, P. J., Draznin, M., Michael, D. J., Ruben, B., et al. (2007). Acrodermatitis enteropathica and an overview of zinc metabolism. *J. Am. Acad. Dermatol.* 56, 116–124. doi: 10.1016/j.jaad.2006.08.015

Mei, Y., Monteiro, P., Zhou, Y., Kim, J. A., Gao, X., Fu, Z., et al. (2016). Adult restoration of Shank3 expression rescues selective autistic-like phenotypes. *Nature* 530, 481–484. doi: 10.1038/nature16971

Naisbitt, S., Kim, E., Tu, J. C., Xiao, B., Sala, C., Valtschanoff, J., et al. (1999). Shank, a novel family of postsynaptic density proteins that binds to the NMDA receptor/PSD-95/GKAP complex and cortactin. *Neuron* 23, 569–582. doi: 10.1016/s0896-6273(00)80809-0

Onay, H., Kacamak, D., Kavasoglu, A. N., Akgun, B., Yalcinli, M., Kose, S., et al. (2017). Mutation analysis of the *NRXN1* gene in autism spectrum disorders. *Balkan J. Med. Genet.* 19, 17–22. doi: 10.1515/bjmg-2016-0031

Pan, Y., Chen, J., Guo, H., Ou, J., Peng, Y., Liu, Q., et al. (2015). Association of genetic variants of GRIN2B with autism. *Sci Rep.* 5:8296. doi: 10.1038/srep08296

Paoletti, P., Ascher, P., and Neyton, J. (1997). High-affinity zinc inhibition of NMDA NR1-NR2A receptors. *J. Neurosci.* 17, 5711–5725. doi: 10.1523/JNEUROSCI.17-15-05711.1997

Peça, J., Feliciano, C., Ting, J. T., Wang, W., Wells, M. F., Venkatraman, T. N., et al. (2011). Shank3 mutant mice display autistic-like behaviours and striatal dysfunction. *Nature* 472, 437–442. doi: 10.1038/nature09965

Pfaender, S., and Grabrucker, A. M. (2014). Characterization of biometal profiles in neurological disorders. *Metallomics* 6, 960–977. doi: 10.1039/c4mt00008k

Pfaender, S., Sauer, A. K., Hagmeyer, S., Mangus, K., Linta, L., Liebau, S., et al. (2017). Zinc deficiency and low enterocyte zinc transporter expression in human patients with autism related mutations in SHANK3. *Sci. Rep.* 7:45190. doi: 10.1038/srep45190

Phelan, K., and McDermid, H. E. (2012). The 22q13.3 deletion syndrome (Phelan-McDermid Syndrome). *Mol. Syndromol.* 2, 186–201. doi: 10.1159/000334260

Rubenstein, J. L., and Merzenich, M. M. (2003). Model of autism: increased ratio of excitation/inhibition in key neural systems. *Genes Brain Behav.* 2, 255–267. doi: 10.1034/j.1601-183x.2003.00037.x

Russo, A. J., and Devito, R. (2011). Analysis of copper and zinc plasma concentration and the efficacy of zinc therapy in individuals with asperger's syndrome, pervasive developmental disorder not otherwise specified (PDD-NOS) and autism. *Biomark Insights* 6, 127–133. doi: 10.4137/BMI.S7286

Sauer, A. K., Pfaender, S., Hagmeyer, S., Tarana, L., Mattes, A. K., Briel, F., et al. (2017). Characterization of zinc amino acid complexes for zinc delivery *in vitro* using Caco-2 cells and enterocytes from hiPSC. *Biometals* 30, 643–661. doi: 10.1007/s10534-017-0033-y

Schmeisser, M. J., Ey, E., Wegener, S., Bockmann, J., Stempel, A. V., Kuebler, A., et al. (2012). Autistic-like behaviours and hyperactivity in mice lacking ProSAP1/Shank2. *Nature* 486, 256–260. doi: 10.1038/nature11015

Sensi, S. L., Paoletti, P., Bush, A. I., and Sekler, I. (2009). Zinc in the physiology and pathology of the CNS. *Nat. Rev. Neurosci.* 10, 780–791. doi: 10.1038/nrn2734

Sensi, S. L., Paoletti, P., Koh, J. Y., Aizenman, E., Bush, A. I., and Hershfinkel, M. (2011). The neurophysiology and pathology of brain zinc. *J. Neurosci.* 31, 16076–16085. doi: 10.1523/JNEUROSCI.3454-11.2011

Smart, T. G., Xie, X., and Krishek, B. J. (1994). Modulation of inhibitory and excitatory amino acid receptor ion channels by zinc. *Prog. Neurobiol.* 42, 393–441. doi: 10.1016/0301-0082(94)90082-5

Tao-Cheng, J. H., Toy, D., Winters, C. A., Reese, T. S., and Dosemeci, A. (2016). Zinc stabilizes Shank3 at the postsynaptic density of hippocampal synapses. *PLoS One* 11:e0153979. doi: 10.1371/journal.pone.0153979

Vela, G., Stark, P., Socha, M., Sauer, A. K., Hagmeyer, S., and Grabrucker, A. M. (2015). Zinc in gut-brain interaction in autism and neurological disorders. *Neural Plast.* 2015:972791. doi: 10.1155/2015/972791

Verpelli, C., Dvoretskova, E., Vicidomini, C., Rossi, F., Chiappalone, M., Schoen, M., et al. (2011). Importance of Shank3 protein in regulating metabotropic glutamate receptor 5 (mGluR5) expression and signaling at synapses. *J. Biol. Chem.* 286, 34839–34850. doi: 10.1074/jbc.M111.258384

Vicidomini, C., Ponzoni, L., Lim, D., Schmeisser, M. J., Reim, D., Morello, N., et al. (2017). Pharmacological enhancement of mGlu5 receptors rescues behavioral deficits in SHANK3 knock-out mice. *Mol. Psychiatry* 22, 689–702. doi: 10.1038/mp.2016.30

Vilella, A., Belletti, D., Sauer, A. K., Hagmeyer, S., Sarowar, T., Masoni, M., et al. (2017). Reduced plaque size and inflammation in the APP23 mouse model for Alzheimer's disease after chronic application of polymeric nanoparticles for CNS targeted zinc delivery. *J. Trace Elem. Med. Biol.* doi: 10.1016/j.jtemb.2017.12.006 [Epub ahead of print].

Wang, X., Bey, A. L., Katz, B. M., Badea, A., Kim, N., David, L. K., et al. (2016). Altered mGluR5-Homer scaffolds and corticostriatal connectivity in a Shank3 complete knockout model of autism. *Nat. Commun.* 7:11459. doi: 10.1038/ncomms11459

Wang, X., McCoy, P. A., Rodriguiz, R. M., Pan, Y., Je, H. S., Roberts, A. C., et al. (2011). Synaptic dysfunction and abnormal behaviors in mice lacking major isoforms of Shank3. *Hum. Mol. Genet.* 20, 3093–3108. doi: 10.1093/hmg/ddr212

Wang, X., and Zhou, B. (2010). Dietary zinc absorption: a play of Zips and ZnTs in the gut. *IUBMB Life* 62, 176–182. doi: 10.1002/iub.291

Wong, A. C., Ning, Y., Flint, J., Clark, K., Dumanski, J. P., Ledbetter, D. H., et al. (1997). Molecular characterization of a 130-kb terminal microdeletion at 22q in a child with mild mental retardation. *Am. J. Hum. Genet.* 60, 113–120.

Yasuda, H., Yoshida, K., Yasuda, Y., and Tsutsui, T. (2011). Infantile zinc deficiency: association with autism spectrum disorders. *Sci. Rep.* 1:129. doi: 10.1038/srep00129

Yoo, H. (2015). Genetics of autism spectrum disorder: current status and possible clinical applications. *Exp. Neurobiol.* 24, 257–272. doi: 10.5607/en.2015.24.4.257

Zhao, L., Xia, Z., and Wang, F. (2014). Zebrafish in the sea of mineral (iron, zinc, and copper) metabolism. *Front. Pharmacol.* 5:33. doi: 10.3389/fphar.2014.00033

Conflict of Interest Statement: The authors declare that the research was conducted in the absence of any commercial or financial relationships that could be construed as a potential conflict of interest.

frontiers in Molecular Neuroscience

ORIGINAL RESEARCH
published: 19 June 2018
doi: 10.3389/fnmol.2018.00107

Hyperactivity and Hypermotivation Associated With Increased Striatal mGluR1 Signaling in a Shank2 Rat Model of Autism

Meera E. Modi[1†], Julie M. Brooks[1†], Edward R. Guilmette[1†], Mercedes Beyna[1†], Radka Graf[1†], Dominik Reim[2], Michael J. Schmeisser[2,3,4], Tobias M. Boeckers[2], Patricio O'Donnell[1†] and Derek L. Buhl[1*†]*

[1]Pfizer Internal Medicine Research Unit, Pfizer Inc., Cambridge, MA, United States, [2]Institute for Anatomy and Cell Biology, Ulm University, Ulm, Germany, [3]Division of Neuroanatomy, Institute of Anatomy, Otto-von-Guericke University, Magdeburg, Germany, [4]Leibniz Institute for Neurobiology, Magdeburg, Germany

Mutations in the *SHANK* family of genes have been consistently identified in genetic and genomic screens of autism spectrum disorder (ASD). The functional overlap of *SHANK* with several other ASD-associated genes suggests synaptic dysfunction as a convergent mechanism of pathophysiology in ASD. Although many ASD-related mutations result in alterations to synaptic function, the nature of those dysfunctions and the consequential behavioral manifestations are highly variable when expressed in genetic mouse models. To investigate the phylogenetic conservation of phenotypes resultant of *Shank2* loss-of-function in a translationally relevant animal model, we generated and characterized a novel transgenic rat with a targeted mutation of the *Shank2* gene, enabling an evaluation of gene-associated phenotypes, the elucidation of complex behavioral phenotypes, and the characterization of potential translational biomarkers. The *Shank2* loss-of-function mutation resulted in a notable phenotype of hyperactivity encompassing hypermotivation, increased locomotion, and repetitive behaviors. Mutant rats also expressed deficits in social behavior throughout development and in the acquisition of operant tasks. The hyperactive phenotype was associated with an upregulation of mGluR1 expression, increased dendritic branching, and enhanced long-term depression (LTD) in the striatum but opposing morphological and cellular alterations in the hippocampus (HP). Administration of the mGluR1 antagonist JNJ16259685 selectively normalized the expression of striatally mediated repetitive behaviors and physiology but had no effect on social deficits. Finally, *Shank2* mutant animals also exhibited alterations in electroencephalography (EEG) spectral power and event-related potentials, which may serve as translatable EEG biomarkers of synaptopathic alterations. Our results show a novel hypermotivation phenotype that is unique to the rat model of *Shank2* dysfunction, in addition to the traditional hyperactive and repetitive behaviors observed in mouse models. The hypermotivated and hyperactive phenotype is associated with striatal dysfunction, which should be explored further as a targetable mechanism for impairment in ASD.

Keywords: SHANK, Shank2, autism spectrum disorders, rat model, mGluR, motivation

OPEN ACCESS

Edited by:
Kimberly Frances Raab-Graham, Wake Forest School of Medicine, United States

Reviewed by:
Craig M. Powell, University of Texas Southwestern Medical Center, United States
Valerie J. Bolivar, Wadsworth Center, United States

***Correspondence:**
Meera E. Modi
meera.modi@childrens.harvard.edu
Derek L. Buhl
derek.buhl@gmail.com

†Present address:
Meera E. Modi, Harvard Medical School/Boston Children's Hospital Boston, Boston, MA, United States
Julie M. Brooks, Alkermes Inc., Waltham, MA, United States
Edward R. Guilmette and Mercedes Beyna, Biogen Inc., Cambridge, MA, United States,
Radka Graf, Axial Therapeutics, Boston, MA, United States,
Patricio O'Donnell and Derek L. Buhl, Translational Research & Early Clinical Translational Science CNS, Takeda Pharmaceuticals, Cambridge, MA, United States

Received: *08 November 2017*
Accepted: *19 March 2018*
Published: *19 June 2018*

Citation:
Modi ME, Brooks JM, Guilmette ER, Beyna M, Graf R, Reim D, Schmeisser MJ, Boeckers TM, O'Donnell P and Buhl DL (2018) Hyperactivity and Hypermotivation Associated With Increased Striatal mGluR1 Signaling in a Shank2 Rat Model of Autism. Front. Mol. Neurosci. 11:107. doi: 10.3389/fnmol.2018.00107

INTRODUCTION

Mutations within the *SHANK* family of genes (comprising *SHANK1*, *PROSAP1/SHANK2* and *PROSAP2/SHANK3*) are over-represented in the autism spectrum disorder (ASD) population and are the cause of specific disorders such as Phelan-McDermid Syndrome (Jiang and Ehlers, 2013). Inherited and *de novo SHANK2* mutations have been identified in several independent families with ASD (Berkel et al., 2010; Leblond et al., 2012; Monteiro and Feng, 2017), many of which lie in functional binding domains for proteins interacting with SHANK2 within the synapse, making *SHANK2* mutation a representative model of the synaptopathy observed in ASD (Berkel et al., 2012; Jiang and Ehlers, 2013).

Synaptopathic consequences of *Shank* mutations are particularly evident in striatal function. Dysregulation of striatal circuits resulting in abnormal social motivation has been hypothesized as a mechanism for the behavioral characteristics in ASD (Chevallier et al., 2012, 2016). Accumulating evidence has also implicated the striatum in the phenomenology of repetitive behaviors (Kohls et al., 2014). Further, the corticolimbic-ventro-striatal network is dysregulated in patients with ASD and obsessive-compulsive disorder (Ameis and Catani, 2015; Wood and Ahmari, 2015; Bariselli et al., 2016). Given its role in both social motivation and production of motivated and habitual repetitive behaviors, the striatum may consequently serve as a locus for the pathogenic processes that result in the symptomatology of ASD.

Mutation of *Shank3* results in altered dendritic arborization, synaptic transmission, postsynaptic density (PSD) composition and excitatory/inhibitory balance in medium spiny neurons (MSNs) of the striatum (Peca et al., 2011; Filice et al., 2016; Jaramillo et al., 2016; Mei et al., 2016; Wang et al., 2016; Reim et al., 2017; Vicidomini et al., 2017), as well as hypoactivity (Kouser et al., 2013; Speed et al., 2015) and perseverative overgrooming (Kouser et al., 2013; Speed et al., 2015; Jaramillo et al., 2016, 2017), linking repetitive behaviors to altered striatal physiology (Dhamne et al., 2017; Kabitzke et al., 2018). *Shank3* mutation impairs the striatopallidal synapses of striatal MSNs and enhancement of their activity decreases overgrooming (Wang et al., 2017). Mutation of *Shank2* has been similarly implicated in repetitive behaviors in mice; however, *Shank2* mutation primarily manifests as hyperactivity (Schmeisser et al., 2012; Won et al., 2012) as opposed to the hypoactivity observed in multiple *Shank3* mouse models (Kouser et al., 2013; Speed et al., 2015; Jaramillo et al., 2016). *Shank2* mutant mice have substantially increased locomotor activity relative to wild type mice and engage in a repetitive jumping behavior at the expense of species-typical digging behaviors (Schmeisser et al., 2012; Won et al., 2012). Accompanying the hyperactive behavior is an upregulation of ionotropic glutamate receptors, most broadly within the striatum in the *Shank2* mutant mouse (Schmeisser et al., 2012). Together, these findings indicate that in the mouse, mutation of *Shank* genes results in functional changes in the striatum that are likely associated with prominent repetitive and hyperactive phenotypes.

The neural circuits underlying motivation and repetitive behaviors have been historically characterized in rat models due to their ability to rapidly acquire complex, striatally mediated tasks (Hart et al., 2014; Jaramillo and Zador, 2014). To explore the relationship between the striatal cellular and molecular consequences of *Shank2* mutation and the repetitive and motivational phenotypes associated with striatal dysregulation in rats, we generated a novel transgenic *Shank2* mutant rat. This model has enabled the assessment of complex social and motivated behaviors and the identification of a potentially translational electroencephalography (EEG) based biomarker of neural circuit dysfunction that has not been shown in previous mouse models.

Similar to *Shank2* mutant mice, our rat model exhibits social and repetitive impairments and corresponding cellular alterations. *Shank2* mutant rats additionally have a profound phenotype of hyperactivity and hypermotivation that can be ameliorated through the administration of dopamine receptor 1 (D1R) or metabotropic glutamate receptor 1 (mGluR1) antagonists that normalize the observed electrophysiological alterations in the striatum. The characterization of phenotypes that are both consistent across species and amenable to pharmacological manipulation opens the door for the identification of drug treatment strategies for the impairments of ASD with high translational validity.

MATERIALS AND METHODS

Model Generation

Animals

In collaboration with Horizon Discovery, we generated a transgenic Sprague-Dawley rat line expressing a targeted deletion of the *Shank2* gene that causes a frameshift and a premature stop (hereafter homozygous mutants referred to as KO; heterozygous, HET; and wild type, WT) using zinc finger nuclease technology. The deletion was designed to mimic one identified in ASD patients that disrupts the PDZ domain of the protein (Berkel et al., 2012). This study was carried out in accordance with the recommendations of the Guide for the Care and Use of Laboratory Animals. The protocol was approved by the Pfizer Institutional Animal Care and Use Committee.

Generation of Rats Carrying the Shank2 Deletion

A deletion was introduced using zinc finger nuclease technology. The endonucleases targeted the GACCGGG GACTTCTTGA TTGAGGTAGG ACACAGGTG sequence flanking the region of interest (**Supplementary Figure S1A**). Deletion was confirmed at both the genomic as well as mRNA level (**Figure 1B**; **Supplementary Figure S1A**). Two founder lines (Lines 8a and 13) were generated and initially characterized for consistency of phenotype in locomotor activity. Line 13 was maintained and used for all further experiments.

After the model was established, all animals were bred, genotyped, and raised until weaning (P21) at Charles River Laboratories (Wilmington, MA, USA). Experimental animals were produced by F1 HET × HET paired matings to produce

litters containing all genotypes in Mendelian ratios. The F1 parents were generated from crosses between KO males and outbred Sprague-Dawley females. Prior to use, the genotype of all experimental animals was determined by Charles River genotyping service. Animals were shipped to Pfizer (Cambridge, MA, USA) between 21 days and 42 days. Because of intra-animal aggression observed in KO animals, all animals were singly housed after shipment in irradiated Innovive Caging (17'L × 13.4"W × 9.9"H) with Alpha-dry bedding with Bed-r'Nest and Nylabone enrichment. Animals were fed Lab Diet 5053 PicoLab Rodent Diet 20 and water *ad libitum*, except where otherwise noted. Animals were maintained at a temperature of 20–26°C, 30%–70% humidity with a 12:12 light:dark cycle.

Genotyping

Tail snips from rats were used for genomic DNA (gDNA) isolation. Tissue was digested using proteinase K and gDNA was isolated using Qiagen's Blood and Tissue DNeasy kit. A total of 2 μl of gDNA was used for genomic PCR using the following primers: forward: 5′-TGGGTCAACACTGCTCTCTG-3′ and reverse: 5′-AGACTCCTCAAATGATCAAGCATTAC-3′. The expected PCR product sizes for WT and KO (exon 31 deleted) in Line 13 was 1171 and 501, respectively.

RT-PCR

Brain cortical RNA was isolated using Qiazol RNA isolation. Briefly, animals were euthanized humanely under approved animal use and care protocols. After dissection, total brains were flash frozen in liquid nitrogen and stored at −80°C until RNA isolation. Frozen brains were homogenized in Qiazol with a 5 mm bead in Tissuelyzer (Qiagen) for 5 min at 25 Hz and RNA isolation proceeding as per Qiagen protocol. Quantitated RNA was converted to cDNA using VILO Superscript cDNA synthesis reagent (Invitrogen). PCR amplification of WT or exon 31 deleted mRNA was performed with PCR primers E30: 5′-GAGGGCTTTGGATTTGTG-3′; and E32: 5′-GACGACCTTAAGGACGAG-3′ with the expected PCR products for WT and KO mRNA of 248 bp and 123 bp, respectively.

Western Blot

SHANK2 levels were analyzed from WT and KO animals from Line 13. One cortical hemisphere/animal from four male rats per genotype (at 7 weeks of age) were processed into filtered synaptosome fractions for analysis. In each lane, 30 μg of total protein was loaded on a 6% NuPAGE gel. The deletion of SHANK2 was confirmed using the SHANK2 (S23b-6) antibody from Novus Biologicals (#NBP1-44509), generated against the 84–309 amino acids of rat SHANK2 (SH3/PDZ domains) and does not cross-react with either SHANK1 or SHANK3, at a concentration of 1:4000 and normalized to the transferrin receptor (85 kDa) from (Invitrogen #13-6800) at a concentration of 1:2000.

Behavioral Assays

Behavioral assays were performed in several cohorts of adult rats (>8 weeks of age, singly housed, male-unless otherwise noted) bred at Charles River Laboratories and tested at Pfizer. Cohort 1 was used for social investigation assays, including juvenile play (N = 8/genotype at 5–6 weeks), social recognition (n = 10/genotype at 8 weeks), and social approach (N = 13/genotype at 9 weeks). Cohort 2 was used for the open field assay to derive locomotion, rearing, and repetitive circling (N = 11/genotype). Cohort 3 was used for the operant conditioning assay (N = 8/genotype). Cohort 4 was used for the location discrimination touchscreen task (N = 5–8/genotype).

Juvenile Play

Juvenile male animals (5–6 weeks of age) of each genotype (KO, WT) were tested for the exhibition of play behaviors with WT age-matched male conspecifics. Experimental animals were marked and placed in a new test cage and allowed to acclimate for at least 1 h. A novel animal was then introduced to the cage for 5 min during which the animals were allowed to freely interact. The social exposure occurred during the dark phase of the circadian cycle (6–9 pm). The interaction was video recorded under red light conditions with an infrared camera and score by hand using JWatcher[1] for three types of behaviors: nape attacks, pinning and supine. Social play behaviors were categorized based on published descriptions of rat social play (Veenema and Neumann, 2009).

Social Recognition

Adult males of each genotype (WT and KO) were tested for social investigation and recognition of 12 juvenile male rats (5–7 weeks, weighing a minimum of 100 g less than the adults). Experimental subjects were placed in individual test cages and all animals were acclimated to the test room for 1 h prior to testing. The juvenile was then introduced to the test cage and allowed to freely interact with the experimental subject for 4 min. The juveniles were then removed and the animals were separated for 30 min before the juveniles were re-introduced for a second 4-min investigation period. Both investigations were video recorded and hand-scored for time spent in olfactory investigation of either the head or anogenital area of juveniles using JWatcher.

Social Approach

Adult male rats of each genotype (WT and KO) were tested for social approach in a three-chambered test arena. The custom built test chamber was 60 × 30 × 20 cm (W × D × H). The corrals were made from clear PVC pipe (5" diameter) with holes (1") drilled throughout. Each animal was placed in the center arena for 5 min and allowed to explore the entire arena for an additional 10 min in the absence of conspecifics. A corral encaging an adult male conspecific was then introduced to one of the two outer chambers and an empty corral was introduced to the other chamber. The experimental animal was then allowed to explore the entire arena again for 10 min. Finally, a novel animal was added to the previously empty corral and the experimental animal had another 10-min exploration period. All stimulus animals were previously acclimated to the corrals to minimize stress-induced behaviors. Time the experimental

[1] http://www.jwatcher.ucla.edu

animal spent investigating each chamber and the total distance traveled was scored using CleverSys TopScan (CleverSys Inc., Reston, VA, USA).

Open Field Activity and Repetitive Activity

Adult male rats of each genotype (WT and KO) were acclimated to the test room for 1 h and then place individually in a VersaMax AccuScan locomotion chamber for a 1-h test period. The animals were allowed to freely move around an unlit chamber, and their location was tracked by the disruption of IR beams. The total distance traveled, the time spent in the center area, vertical rearing and circling (both clockwise and counterclockwise) was interpolated through the pattern of beams broken based on the manufacturer programmed settings.

Operant Conditioning and Progressive Ratio Response

Eight male rats of each genotype (WT and KO) were food-restricted to 80%–85% of their free feeding body weight and introduced to a MedAssociates (Fairfax, VT, USA) dual lever, pellet reward operant response chamber. Animals were acclimated to the chamber and food reward (sucrose diet pellets) for 1 h on the first day of training. On the second day of training, the response levers were introduced such that one lever was paired with food reward delivery ("active" lever) and one was unpaired ("inactive" lever) at an FR1 schedule modified to elicit response at both levers. Training continued until 80 responses were obtained during a 60-min trial for each group. All animals were then advanced to a progressive ratio reward schedule during which the number of lever presses required to obtain a reward increased non-linearly with each subsequent trial. The number of presses on the active lever and the inactive lever was recorded. The breakpoint was defined as the number of lever presses per single reward at which the animals were unwilling to work. The breakpoint was used as a measure of motivation. The number of lever presses on the active vs. inactive lever was used as a measure of goal directed vs. hyperactive behavior (goal directed behavior should be specific to the active lever only). For one testing session the animals were allowed to consume the reward pellets to satiety for 1 h prior to testing as opposed to the typical conditions in which the animals only had access to a standard rat diet. The breakpoint was compared between the "reward sated" session and the typical "reward hungry" sessions as a measure of the sensitivity of breakpoint to reward value. For three additional testing sessions, each 1 week apart, the animals were treated with the dopamine D1 receptor antagonist SCH-39166 (0, 0.01, 0.1 mg/kg, I.P.) in a randomized fashion and the effect of the pharmacological manipulation on breakpoint was measured.

Location Discrimination Touchscreen Task

Eight WT and five KO male rats were food restricted to 80%–85% of their free feeding body weight. Equal groups were used initially but three of the KO failed to acquire the early testing behaviors and were removed from the study. Rats were then habituated to the touchscreen chamber and the behavior of the animal was shaped such that the animal learned to touch the illuminated stimulus on the screen. This pretraining phase is composed of five stages in which animals progressed through training in a criteria-dependent manner. After this period, the rats advanced to the acquisition of the location discrimination reversal task in which animals were required to make seven correct touches to a response window in eight consecutive trials. Once this criterion was met, the rule changed and the opposite location was then assigned as correct and was rewarded (total of 50 trials or 60 min time point). This acquisition phase was continued until an animal achieved the initial acquisition followed by a reversal in three of four consecutive sessions.

Pharmacological Modulation of Open Field Activity and Repetitive Activity

For behavioral pharmacological experiments, Cohort 4 was used for the dopamine D1 receptor antagonist (SCH-39166 0, 0.01, or 0.1 mg/kg, I.P.) open field experiment using a randomized within-subjects design (N = 10–11/genotype). Cohort 5 was used for the mGluR1 receptor antagonist (JNJ16259685 0 or 0.63 mg/kg, S.C.) open field and social behavior experiment using a randomized within-subjects design (N = 10/genotype). Animals received a subcutaneous injection 30 min prior to testing. Testing was conducted in the pharmacological experiments as described above.

Synaptic Protein Analysis

Proteomic Analysis of Brain Homogenate

Adult animals were anesthetized via CO_2 and rapidly decapitated (N = 4/genotype). The hippocampus (HP) and striatum were rapidly dissected out and frozen in liquid N_2, and brain samples were kept at −80°C until assayed. Subcellular fractionation of the samples was then performed to isolate synpatosomal fractions and western blot interrogation of synaptic proteins expression was done as previously described with minor modifications (Schmeisser et al., 2012; Distler et al., 2014). Briefly, the sections were homogenized in HEPES-buffered sucrose and separated into synaptosomal fractions. Equal amounts of protein 10–20 μg were separated by SDS-polyacrylamide gel electrophoresis and then blotted onto polyvinylidene fluoride membranes. The membranes were incubated with specific primary antibodies and then visualized with HRP-conjugated secondary antibodies on X-ray film. The films were imaged and the gray value was quantified using ImageJ and normalized to the gray value of actin.

Anatomical Analysis

Adult animals (N = 5/genotype) were anesthetized via CO_2 and then rapidly decapitated. Brains were removed, fixed in 10% formalin, and divided into rostral/caudal blocks and stained by the rapid Golgi variant by Neurostructural Research[2] as previously described (Valverde, 1993). Coronal sections (120 μm) were mounted, and striatal MSNs and HP CA1 pyramidal cells were imaged using a Zeiss bright field microscope. Camera lucida drawings were prepared from n = 4–7 randomly selected neurons per brain that met selection criteria (well-stained, arbor not obscured by other anatomy,

[2]http://www.neurostructural.org

soma in the middle third of the tissue section, and the appearance of spines). Neuronal morphology was quantified using Sholl and branch point analyses of the basilar arbor of hippocampal CA1 pyramidal (HPp) cells and the full arbor of MSN. The soma size of all neurons were also analyzed. Results were generated from values averaged across individual neurons per animal (WT: $N = 5$, $n = 32$ neurons; KO: $N = 5$, $n = 31$ neurons).

Electrophysiological Characterizations

In Vitro Slice Preparation

Acute slices (300 μm) were prepared from adult male and female animals of each genotype (WT and KO). The results from both male and female animals were statistically compared, found to be not different and then pooled to increase statistical power. Rats were anesthetized with isoflurane (4%) and transcardially perfused prior to decapitation with oxygenated ice-cold artificial cerebral spinal fluid (aCSF) containing (in mM): NaCl, 125; $NaHCO_3$, 25; glucose, 10; KCl, 3.5; NaH_2PO_4, 1.25; $CaCl_2$, 0.5; $MgCl_2$, 3; pH 7.4, osmolarity 295 mOsm, constantly oxygenated with 95% O_2 and 5% CO_2. Coronal slices containing the dorsal HP or sagittal slices containing the striatum and preserving corticostriatal fiber tracts were sectioned using a Vibratome. Slices were incubated in oxygenated aCSF warmed to ∼34°C for at least 1 h prior to recording. Field excitatory postsynaptic potentials (fEPSPs) or whole-cell patch-clamp recordings were performed. For each experiment, individual slices were placed in a submersion-type recording chamber superfused with oxygenated aCSF (fEPSP flow rate of 2.5 mL/min; whole-cell flow rate of 2 mL/min) and maintained at 33–34°C. Recording aCSF formulations were adjusted to include 2 mM $CaCl_2$ and 1 mM $MgCl_2$.

In Vitro Field Recordings in Hippocampus

Field EPSPs were recorded using a multi-channel recording system (MED64, Alpha MED Scientific). Slices were transferred to one of four MED-P515A recording chambers containing 64 planar micro-electrodes arranged in an 8 × 8 grid embedded in the center of a transparent glass cylinder (10 mm depth). The recording chambers were connected to a 64-channel amplifier which was divided using a 4-way splitter such that four slices were recorded simultaneously. Each slice was in a separate chamber with 16 channels active in an 8 × 2 configuration. Each electrode across all chambers corresponded to a single amplifier channel. This orientation provided each electrode the ability to deliver stimuli as well as record electrophysiological signals. fEPSPs were evoked in the Schaffer collateral fiber pathway in the CA1 region with a biphasic square-wave pulse (0.20 ms; 0.05 Hz) delivered through one electrode. Only those electrodes positioned beneath the stratum radiatum of the CA1 region of the HP were utilized for stimulation or recording. Electrophysiological signals were high-pass filtered at 0.1 Hz and digitized at 20 kHz using MED64 Mobius acquisition software (WitWerx Inc., Santa Cruz, CA, USA).

To characterize the synaptic input-output relationship, fEPSPs were measured at fixed increments between 10–100 μA in slices from WT female $N = 2$ animals, WT male $N = 6$ animals, KO female $N = 3$ animals, KO male $N = 6$ animals. The stimulus intensity for the remainder of the session was set at a level that elicited ∼50% of the maximum fEPSP response (20–50 μA). Changes in synaptic plasticity were examined following a 10 min stable baseline recording. Long-term potentiation (LTP) was induced with a high frequency theta burst stimulation (TBS; 5 trains of 4 pulses at 100 Hz repeated twice) given at the same stimulus intensity used for the 0.05 Hz test stimuli in slices from WT female $N = 5$ animals, WT male $N = 5$ animals, KO female $N = 5$ animals, KO male $N = 4$ animals. Long-term depression (LTD) was induced using a paired-pulse low frequency stimulation (PP-LFS) protocol, which included 900 paired stimuli (50 ms interstimulus interval) delivered at a 1-Hz frequency (Kemp and Bashir, 1999) in slices from WT male $N = 6$ animals, KO male $N = 6$ animals. Peak fEPSP amplitudes were calculated using the MED64 hardware and software packages. The percent change in amplitude was measured by comparing the mean fEPSP amplitude during the 10 min baseline with the mean fEPSP amplitude during the last 10 min of recording.

Whole-Cell Patch Clamp Recordings

Whole-cell voltage clamp recordings were performed from pyramidal cells within the CA1 region of the HP (WT female $N = 11$ cells/5 animals; WT male $N = 9$ cells/7 animals; KO female $N = 10$ cells/5 animals; KO male $N = 8$ cells/6 animals) or MSNs in the ventral striatum (WT male $N = 11$ cells/7 animals; KO male $N = 10$ cells/8 animals. Cells were identified using infrared differential interference contrast (IR-DIC) video microscopy (Olympus BX50-WI) using a 40× water-immersion objective. Visual guidance was obtained with an IR-sensitive CCD camera (DAGE-MTI) connected to a monitor. Patch pipettes (6–10 MΩ) were made from 1.5 mm O.D. boroscilicate glass tubing (World Precision Instruments, Sarasota, FL, USA) and filled with (in mM): $CSCH_3SO_3$, 126; HEPES, 10; $MgCl_2$ 2; CsCL, 20; Spermine, 0.1; QX-314, 1; Mg-ATP, 2; Na_2-ATP, 2; and GTP, 0.3; EGTA, 8; pH 7.3; osmolarity 280 mOsm. In a subset of cells Neurobiotin 488 (0.125%) was added to the internal recording solution for histological identification of recorded cells. Whole-cell recordings were acquired with a computer-controlled Multiclamp 700B amplifier (Axon Instruments, Foster City, CA, USA), digitized (Digidata, Axon Instruments) and sampled with Axoscope 9.0 (Axon Instruments) at a rate of 10 kHz. Electrode potentials were adjusted to zero before recording without correcting the liquid junction potential. Experiments began after reaching a steady resting state (approximately 5 min) and input resistance was monitored continuously with a 5 mV hyperpolarizing pulse (500 ms) given with every afferent stimulus.

Excitatory postsynaptic currents (EPSCs) were evoked using a bipolar electrode made from a twisted pair of Teflon-coated tungsten wires (tips approximately 200 μm apart; FHC, Bowdoin, ME, USA). In all whole cell experiments, afferent stimulation was elicited at a baseline frequency of 0.066 Hz. Neurons were voltage-clamped at a membrane potential of −70 mV except where noted. For hippocampal AMPA/NMDA

ratio experiments, the stimulating electrode was placed in the Schaffer collateral pathway in the most lateral aspect of the CA1 region, no less than 500 μm from the recorded pyramidal cell in the presence of picrotoxin (10 μM). Upon establishing a steady baseline (10 min), the cell was held at −80 mV for 10 sweeps to record fast AMPA-mediated currents evoked by electrical stimulation. The cell was then held at +40 mV and fast AMPA- and slower NMDA-mediated synaptic currents were recorded for 10 min. Subsequently, the AMPA EPSC was isolated at +40 mV via bath application of the NMDA receptor antagonist DL-AP5 (100 μM). The AMPA to NMDA ratio was determined by dividing the peak of the response at −80 mV (AMPA) by the value obtained subtracting the response 40 ms following stimulation at +40 mV before and after DL-AP5 (NMDA; Counotte et al., 2014). For corticostriatal LTD experiments, the stimulating electrode was placed in the white matter at the PFC-striatum border. Following steady baseline, LTD was induced by pairing low frequency presynaptic stimulation (p-LFS; 1 Hz, 480 pulses) with postsynaptic depolarization by holding the membrane potential at −50 mV. Similar to extracellular recordings, the percent change in amplitude was measured by comparing the mean fEPSP amplitude during the 10 min baseline with the mean fEPSP amplitude during the last 10 min of recording. All fEPSP and EPSC amplitudes were averaged per minute with the exception of AMPA/NMDA values, which represent the average of 10 consecutive sweeps.

In Vivo Field Potential Recording

Rats of each genotype (n = 8 KO and n = 7 WT) were surgically implanted with titanium recording screws located over the left medial frontal cortex (AP +0.15 cm, ML +0.15 cm relative to Bregma) and the left parietal cortex (AP −0.37 cm, ML +0.22 cm relative to Bregma) for recording and screws over the left cerebellum and the right cerebellum for reference and grounding, respectively. The screws were implanted stereotaxically under isoflurane (2%) anesthesia and wired to a custom electronic interface board (EIB; ADPT-HS-18-Push Pin; Neuralynx Inc., Bozeman, MT, USA). The EIB connected via an Omnetics connector to the HS-18 headstage preamplifier and data was acquired using a Neuralynx Digital Lynx Data Acquisition System. After a minimum of 1 week of surgical recovery, the animals were acclimated to the recording chambers and the tethering procedure for three sessions. Recording experiments began at least 3 weeks after surgery to allow for recovery of neural tissue and receding of inflammatory response. During each recording session animals were allowed to habituate to the recording cage for 30 min and then signal quality was assessed for an additional 30 min. Baseline signal was recorded for 30 min and then auditory evoked responses were recorded in response to a white noise tone at 70 db, 80 db and 90 db. The tones were presented in a paired pulse paradigm in a train of 200 tones with 500 ms between the paired pulses and 10 s between each trial. The baseline signal was analyzed for spectral power using the fast Fourier transform with a 1.024 s Hanning window resulting in 0.9766 Hz resolution using Spike 2 (CED Cambridge, UK). Event related signals were extracted in a window from 100 ms pre-stimulus to 700 ms post-stimulus relative to the first tone to encompass the response to both tones. Average waveforms were calculated for each subject by averaging the 800 ms window across the 200 trials. Waveform features including P1, N1, P2 and N2 amplitude and latencies were calculated from the averaged waveform for each subject. P1 suppression was calculated as the ratio of P1 after tone 1 to P1 after tone 2 for each subject. Grand averaged waveforms for each genotype were generated by averaging the averaged waveforms for each subject.

RESULTS

The stastical comparisons, results, means, SEM and groups for each result described in the text are enumerated in **Supplementary Table S1**.

Model Generation

Shank2 KO rat lines were generated at Horizon Discovery by targeting exon 31 for deletion by zinc finger nuclease technology. Two lines, 8A and 13 were confirmed by sequencing (data not shown). Line 13 has a 437 bp deletion around and including the entire exon 31, thereby causing a frameshift and premature stop codon in all three known isoforms of the rat Shank2 mRNA (**Figure 1A**). Deletion was confirmed at the genomic (**Supplementary Figure S1A**), mRNA (**Figure 1B**), and protein level (**Figure 1C** and **Supplementary Figure S1B**). Changes in the rat Shank2 mRNA was confirmed by RT-PCR using primers E30: 5′-GAGGGCTTTGGATTTGTG-3′ and E32: 5′-GACGACCTTAAGGACGAG-3′, with the expected PCR products for WT and KO mRNA of 248 bp and 123 bp, respectively (**Figure 1B**; arrows showing expected WT and KO PCR products). SHANK2 deletion was confirmed in synaptosomes and whole brain lysates via western blot using an antibody raised against the targeted SH3/PDZ domain of the protein (**Figure 1C**).

Shank2 KOs Social Deficits Across Development

Consistent with the hypothesis that motivational abnormalities in autism underlie social impairments (Chevallier et al., 2012), KO rats also demonstrate deficits in social interactions across development. Compared to WTs, KO animals fail to both initiate play behaviors (nape attack) and respond appropriately to social solicitation (supine) when interacting with a WT juvenile conspecific (**Figure 2A**; *genotype*: $F_{(1,14)} = 28.32$, $p = 0.0001$). The KO deficit is maintained into adulthood as evidenced by a decrease in olfactory investigation of a juvenile animal, commensurate with a lack of social recognition. As expected, WT animals showed a decrease in olfactory investigation time during re-exposure to a familiar conspecific after a 30-min delay; however, investigation by KO animals does not change (**Figure 2B**; *genotype*: $F_{(1,24)} = 38.5$, $p < 0.0001$). In the three-chambered social investigation paradigm, however, KO animals show a preference for a novel animal over a novel object as

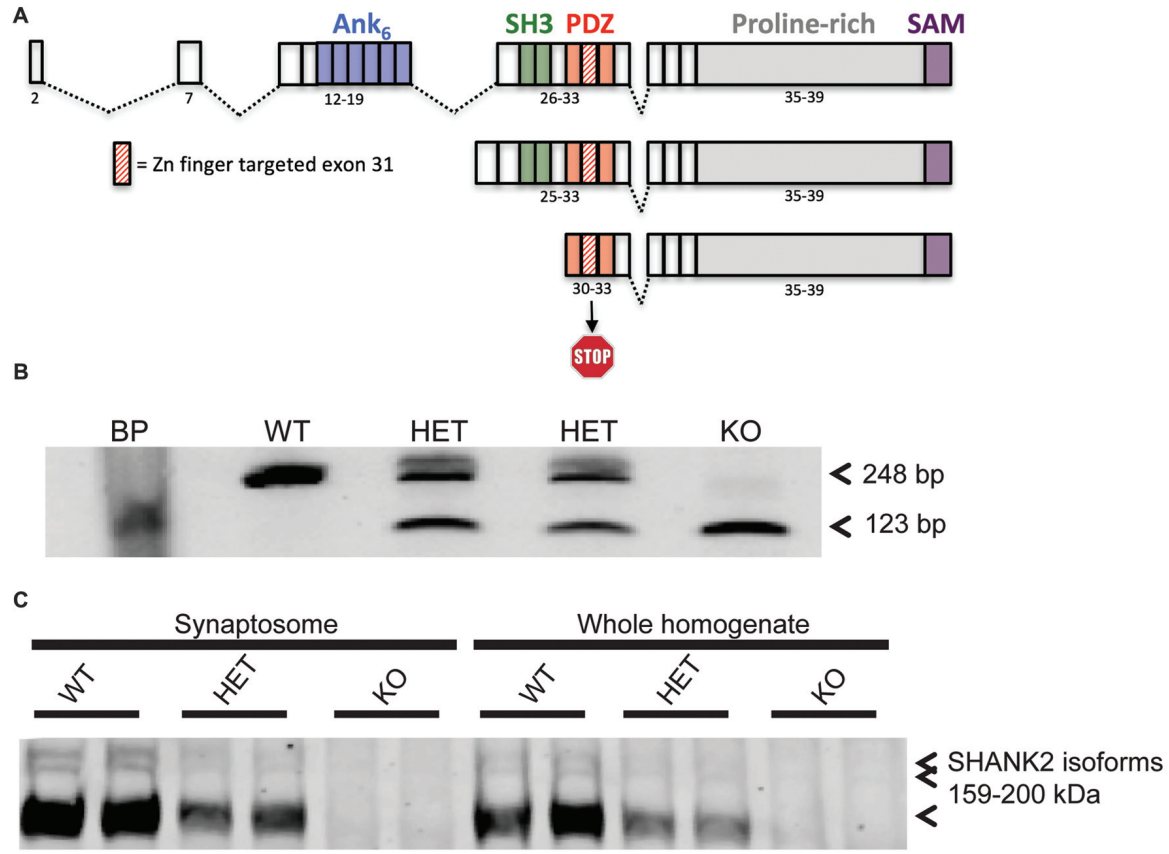

FIGURE 1 | Generation of the *Shank2* mutant rat. **(A)** 437 bp genomic DNA (gDNA) deletion, encompassing exon 31 in the PDZ domain of the rat *Shank2* gene, results in a frameshift mutation and premature stop codon in the resultant mRNA transcript. **(B)** RT-PCR analysis of WT, HET and KO rat Shank2 mRNA around exon 31. Arrows indicate the WT (upper–248 bp) and KO (lower–123 bp) expected PCR products in the resultant Zn-finger KO mRNA. **(C)** No detectable expression of any of the three variants of full length SHANK2 protein product is detected in the KO animals in either whole brain homogenate or enriched synaptosomal fractions (see entire western blot in **Supplementary Figure S1B**).

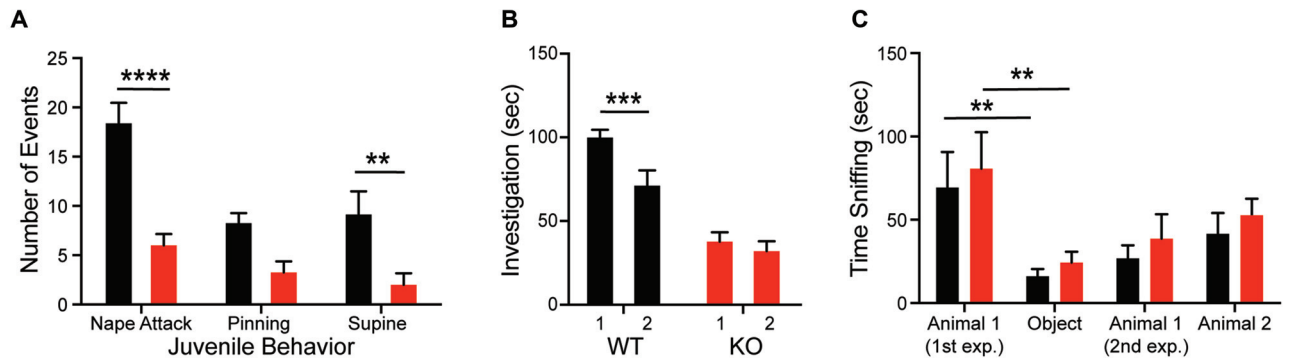

FIGURE 2 | *Shank2* mutation results in impaired social behavior. *Shank2* KOs engage in less social interaction as juveniles **(A)** and as adults **(B)**. The decreased social interaction impairs social recognition **(B)** but not social preference **(C)**. In all panels WT animals are in black and KO animals are in red. Bars indicate SEM. $^{**}p < 0.01$, $^{***}p < 0.001$, $^{****}p < 0.0001$.

measured by time with nose in proximity to the stimulus cup, similar to WT animals (**Figure 2C**; *stimulus*: $F_{(3,54)} = 10.2$, $p < 0.0001$). While both groups also show a preference for the novel animal over a familiar animal, this effect is not significant for either genotype. There are also no significant differences in time spent in each chamber between the genotypes.

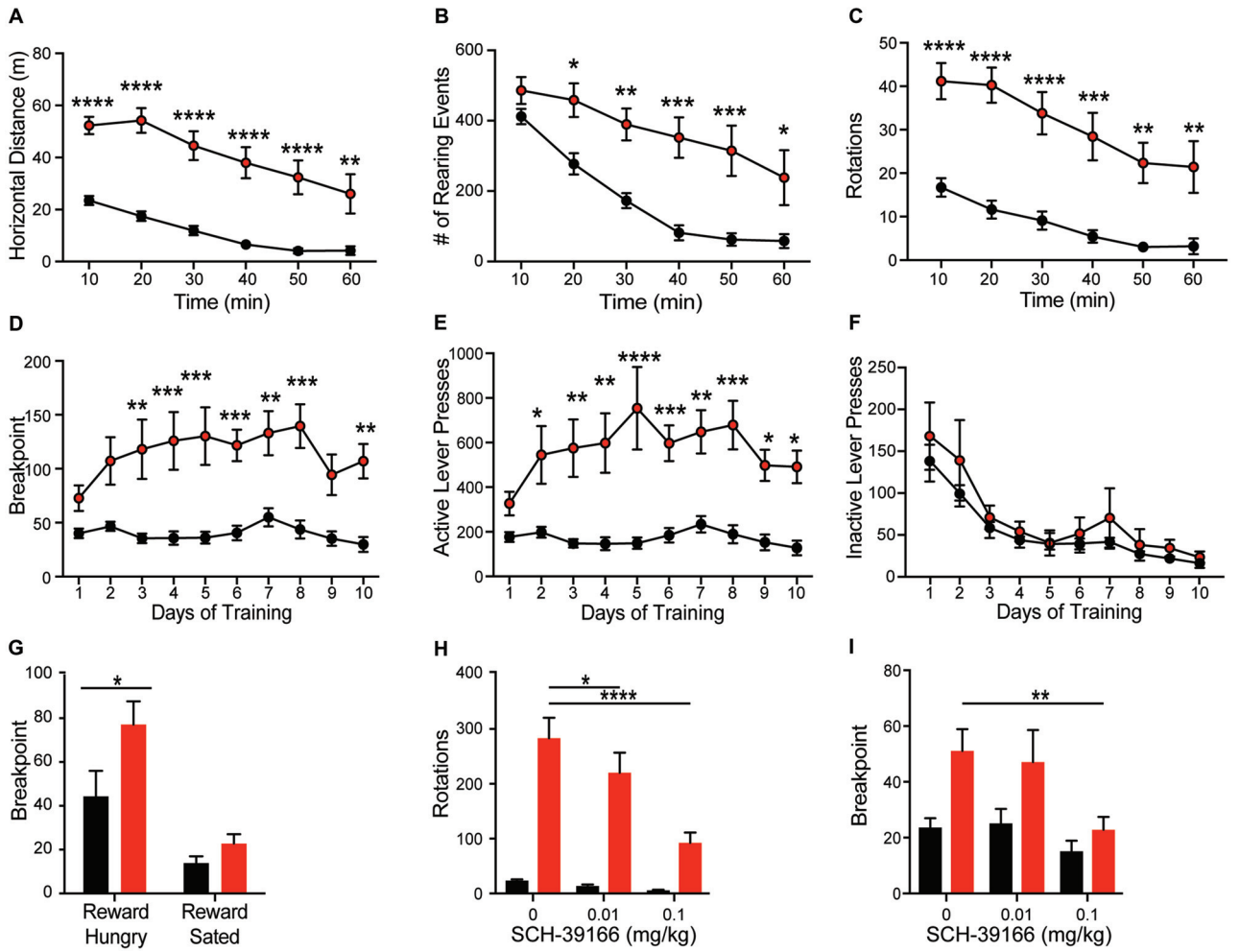

FIGURE 3 | *Shank2* mutation results in increased locomotion, stereotypic and motivated behavior. *Shank2* KOs exhibit increased locomotion **(A)**, vertical rearing **(B)**, and rotations **(C)** in the open field arena relative to WT animals. In the progressive ratio operant task, KOs have an increased breakpoint (number of lever presses at which the animal will cease to work for a fixed reward) **(D)**. The increased response is specific to the active lever **(E)**, not the inactive lever **(F)**, suggesting the increased breakpoint is motivationally driven. Devaluation of the reward through pre-feeding to satiety prior to testing decreases the breakpoint of both WT and KO rats **(G)**. Both the repetitive circling **(H)** and increased breakpoint **(I)** can be reduced by administration of the D1 receptor antagonist SCH-39166. In all panels WT animals are in black and KO animals are in red. Bars indicate SEM. $^{*}p < 0.05$, $^{**}p < 0.01$, $^{***}p < 0.001$, $^{****}p < 0.0001$.

Shank2 KOs Exhibit Hyperactivity and Repetitive Behavior

Consistent with the dominant phenotype seen in *Shank2* mouse models (Schmeisser et al., 2012; Won et al., 2012), we observe hyperactivity in Shank2 KO rats. Open field analysis reveals increased horizontal distance traveled (**Figure 3A**; *genotype* $F_{(1,20)} = 32.46$, $p < 0.0001$) and decreased thigmotaxis (graph not shown; $F_{(1,20)} = 6.743$, $p < 0.0001$) relative to WTs. Decreased thigmotaxis, though, cannot be separated from general increase in locomotion in these analyses. KOs also exhibit increased rearing (**Figure 3B**; *genotype* $F_{(1,20)} = 15.81$, $p < 0.001$) and repetitive circling (**Figure 3C**; *genotype* $F_{(1,20)} = 25.57$, $p < 0.0001$). These latter phenotypes are unique to the rat mutant model and are not seen in mouse models of Shank2 mutation. KOs engage in ∼10-fold more rotations than WT animals, with no orientation bias (not shown). Importantly, KOs also show a similar rate of habituation to the chamber as WT animals, but never return to WT levels in any locomotor behavior.

Deletion of Shank2 Results in a Hypermotivation Phenotype

Hyperactivity and repetitive behaviors are attributed to disruption of striatal motivational circuits (Kim et al., 2016; Szechtman et al., 2017). To explore whether repetitive phenotypes in *Shank2* mutant rats are associated with increased motivated behavior, animals were assessed in a progressive ratio operant response task. KO rats exhibit a significantly higher breakpoint than WTs (**Figure 3D**; *genotype* $F_{(1,14)} = 17.83$, $p = 0.0009$). The increase in response is specific to the reward-associated lever (**Figures 3E,F**; active, *genotype* $F_{(1,14)} = 19.21$,

$p = 0.0006$; inactive, $F_{(1,14)} = 0.756$, $p = 0.3992$), and devaluation of the reward by pre-feeding to satiety decreases response in KO rats similarly to other genotypes (**Figure 3G**; reward hungry vs. reward sated; *genotype* $F_{(1,14)} = 4.664$, $p = 0.0486$). Together, these behaviors suggest an enhancement in motivated response independent of hyperactivity.

D1 Dopamine Receptor Regulation of Both Hypermotivated and Repetitive Phenotypes

Enhancement of striatal D1 receptor (D1R) signaling, particularly within the ventral striatum, contributes to hyperactivity, repetitive behavior, and motivated behavior (Aberman et al., 1998; Shi and McGinty, 2011). To test the sensitivity of *Shank2* mutation-induced behaviors with dopamine receptor modulation, we evaluated the effect of the selective D1/D5R antagonist SCH-39166 on both repetitive circling and the hypermotivated response in progressive ratio. SCH-39166 dose-dependently reduces the production of repetitive circling in KO animals (**Figure 3H**; *dose*: $F_{(2,38)} = 22.86$, $p < 0.0001$; *dose* × *genotype*: $F_{(2,38)} = 16$, $p < 0.0001$). A Sidak's *post hoc* test shows an effect of drug in the KO animals (vehicle vs. 0.01 mg/kg SCH-39166, $p = 0.0168$; vs. 0.1 mg/kg, $p = 0.0001$); however, in WT animals, $p > 0.05$ for both comparisons. Similarly, 0.1 mg/kg of SCH-39166 also decreases the breakpoint in progressive ratio (**Figure 3I**; *dose* $F_{(2,28)} = 5.033$, $p = 0.0136$). A Sidak's *post hoc* test shows an effect of drug in the KO animals (vehicle vs. 0.1 mg/kg SCH-39166, $p = 0.0388$); however, in WT animals, $p > 0.05$ for both comparisons. The inhibitory effect of the D1/D5R antagonist on the production of these behaviors is consistent with striatal dysregulation (Higa et al., 2017).

Shank2 KO Animals Exhibit Paradoxical Task Acquisition Deficits

The differential role of Shank proteins in distinct brain regions may result in discordant behavioral phenotypes after *Shank2* mutation (Reim et al., 2017). Despite the hypermotivated response in progressive ratio, KOs take significantly longer to acquire the association between the lever press and reward during training using a fixed ratio (**Figure 4A**; *interaction* $F_{(9,126)} = 2.832$, $p = 0.0046$). Consistent with this learning deficit, KOs also exhibit a delay in acquisition in a location discrimination touchscreen task; significantly more trials are needed for the KO to learn the reward-action pairing (∼11 days compared to 4 days for WT animals; **Figure 4B**; unpaired Student's *t*-test; $p = 0.033$), with several KO animals never learning the association. The impairments in complex task acquisition suggest hippocampal memory alterations resultant of *Shank2* mutation.

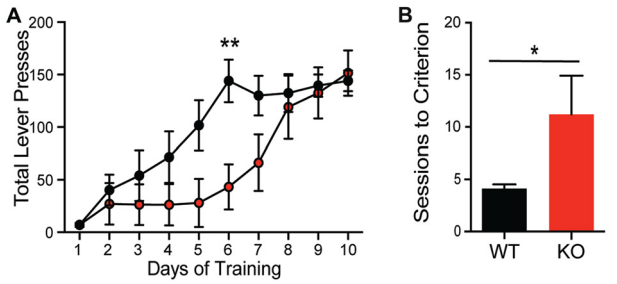

FIGURE 4 | *Shank2* mutation results in impaired acquisition of operant behavior. *Shank2* KOs require more training to acquire both the operant lever press task **(A)** and a location discrimination touchscreen task **(B)**. In all panels WT animals are in black and KO animals are in red. Bars indicate SEM. $^{*}p < 0.05$, $^{**}p < 0.01$.

Opposing Anatomical Alterations in Striatum and Hippocampus

To explore the mechanisms contributing to the observed behavioral phenotypes, expression of postsynaptic proteins and cellular morphology in the HP and striatum were evaluated. In contrast to the dramatic behavioral phenotypic changes, there was no change in synaptic protein expression in the HP resulting from *Shank2* mutation in male rats (**Figure 5A**, **Supplementary Figure S2**). In HPp neurons, KO animals have smaller somas (**Figure 5B**; unpaired *t*-test, $p = 0.0374$) and decreased dendritic branching (**Figure 5C**; Wilcoxin rank-sum test, $p = 0.0002$) per animal (averaged across neurons). Consistent with the enhancement of behaviors mediated by the striatum and the impairment in operant learning, KO animals also exhibit reciprocally aberrant phenotypes in the anatomical alterations. KO rats have a significant upregulation of mGluR1 in the striatum compared to WT animals (**Figure 5D**; unpaired *t*-test, $p = 0.0034$), but no other significant changes in synaptic protein expression (**Supplementary Figure S1**). The MSNs of KO animals have larger neuronal somas (**Figure 5E**; unpaired *t*-test, $p = 0.0477$) and increased branching of the proximal dendritic arbor (**Figure 5F**; Wilcoxin rank-sum test, $p < 0.0001$).

Functional Impairment in Hippocampal and Striatal *in Vitro* Physiology

To determine whether morphological and molecular alterations in hippocampal and striatal neurons are accompanied by changes in synapse physiology, extracellular and whole-cell patch clamp recordings were conducted in both brain regions. In the HPp, input-output curves do not differ between genotypes (data not shown; $F_{(9,135)} = 0.2655$, $p = 0.98$), indicating no change in basal synaptic transmission in the SC-CA1 pathway. However, there is a difference in the ratio of AMPA/NMDA currents within the HPp. Whole-cell voltage clamp recordings of HPp neurons indicate the alterations in hippocampal plasticity result from a reduction in AMPA/NMDA current ratio in KO rats (**Figure 6A**; unpaired *t*-test, $p = 0.015$), driven by an increase in NMDA-mediated current (**Figures 6B,C**; unpaired *t*-test, $p = 0.0134$). A failure is also observed in the maintenance of both synaptic potentiation and depression of evoked fEPSP amplitudes recorded in the HPp of KO animals. LTP induction results in a significant increase in synaptic response in WT (20 ± 2.22%), but not KO rats (8 ± 3.68%), observed 30 min post-stimulation (**Figures 6D,E**, unpaired *t*-test $p = 0.0108$). Similarly, LTD induction leads to an enduring reduction in fEPSP amplitude in WT (27 ± 6.67%), that is not observed

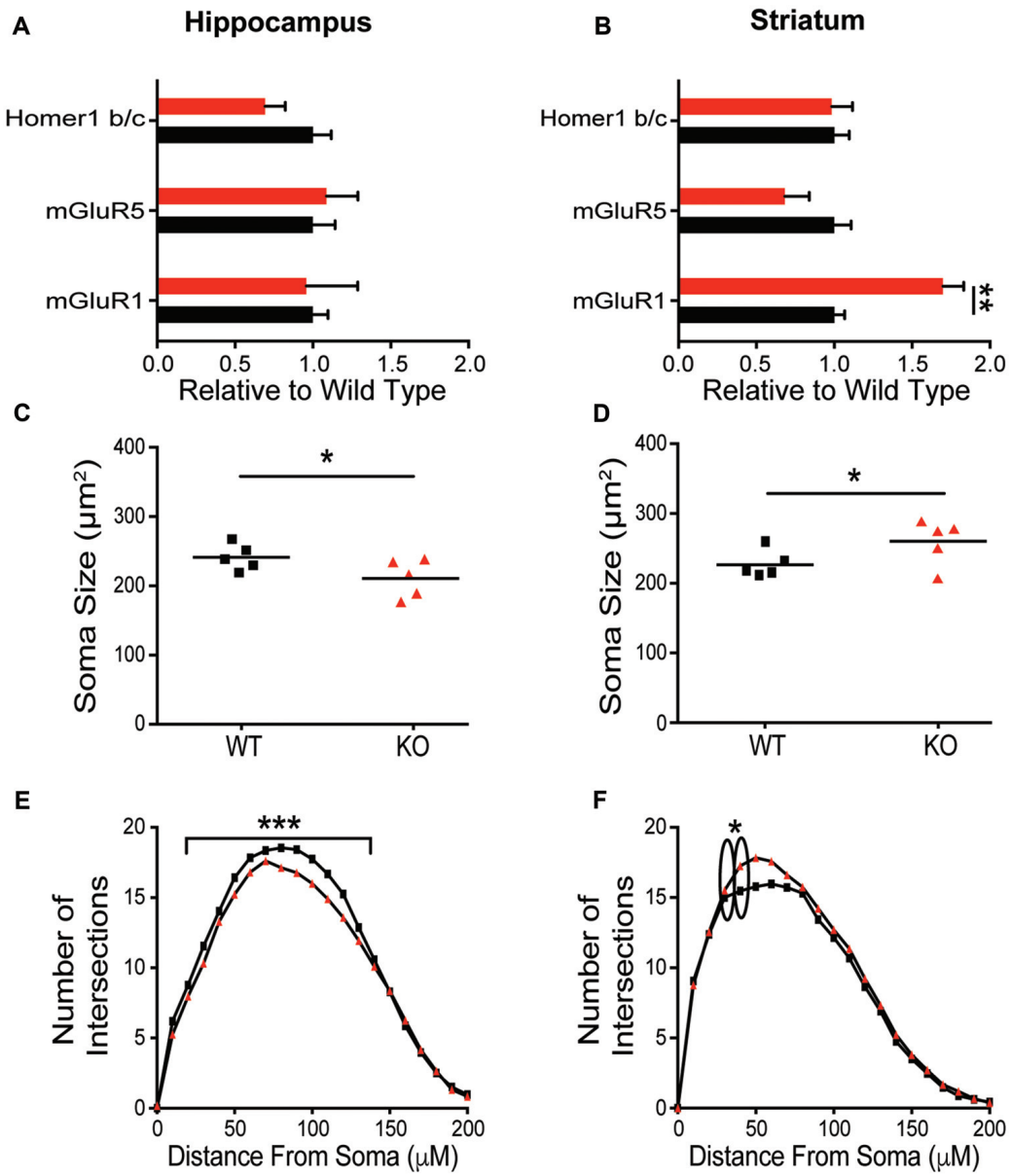

FIGURE 5 | Differential molecular alterations in the hippocampus (HP) and striatum resultant of *Shank2* mutations. *Shank2* mutation does not alter the expression of synaptic proteins (**Supplementary Figure S2**) or metabotropic glutamate receptor related proteins in the HP **(A)**. Values are expressed as fold change relative to the average WT value. The soma size of CA1 hippocampal pyramidal (HPp) neurons is smaller in KO relative to WT rats **(B)** and there is a reduction in basilar dendritic arborization **(C)** as evidenced by Golgi staining and quantification. However, in medium spiny neurons (MSNs) of the striatum, detailed analysis reveals an upregulation of mGluR1 protein expression in male KO rats **(D)** despite a lack of change in synaptic protein level (**Supplementary Figure S2**). Striatal MSNs in contrast to HPps of KO rats have larger soma **(E)** and increased proximal dendritic branching **(F)** relative to WT animals. In all panels WT animals are in black and KO animals are in red. Bars indicate SEM. $*p < 0.05$, $**p < 0.01$, $***p < 0.001$.

in KOs (4 ± 6.00%) 40 min post-stimulation (**Figures 6F,G**; unpaired *t*-test, $p < 0.025$).

Given the observed overexpression of striatal mGluR1 in male KO animals and the suggested role mGluR1 plays in LTD induction at excitatory synapses (Luscher and Huber, 2010), corticostriatal LTD is next examined. Consistent with behavioral and molecular findings, MSN recordings from KO animals show enhanced synaptic response (**Figures 7A,B**). Specifically, corticostriatal LTD induction results in significantly greater reduction of EPSC amplitude in KOs vs. WT (43 ± 4.75% vs. 28 ± 4.98%), measured at 40 min post-stimulation (**Figure 7B**; unpaired *t*-test, $p = 0.0438$). The enhanced LTD observed in mutant animals supports a pathological mechanism of increased activation of mGluR1 in the striatum.

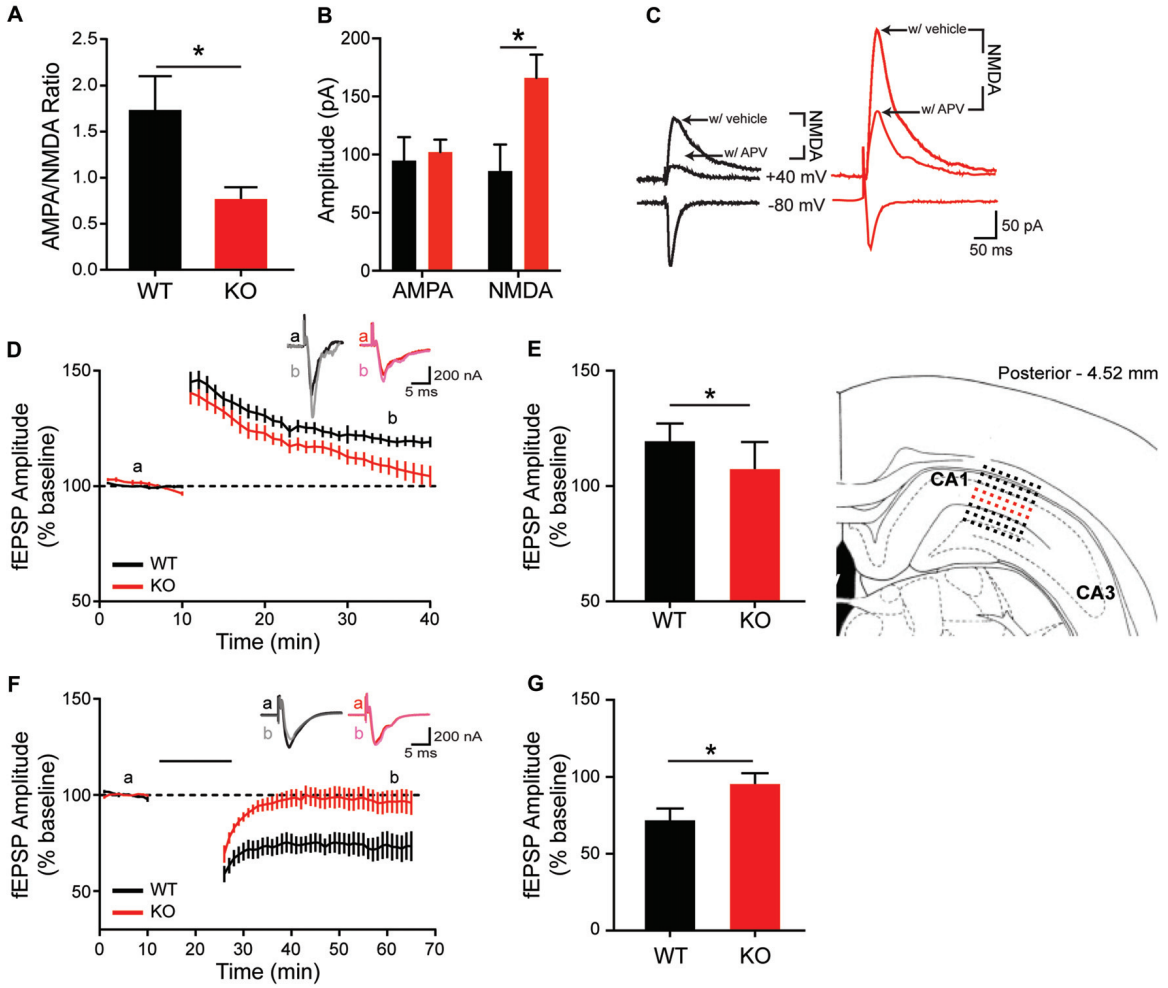

FIGURE 6 | Altered *in vitro* hippocampal physiology of the *Shank2* KO rat. In the CA1 region of the HP, there is a reduction of the ratio of AMPA/NMDA synaptic currents **(A)** that is driven by an increase in the NMDA current **(B,C)**. KO rats also fail to maintain long-term potentiation (LTP) (**D,E**; brain slice depicts location of field recording), with significantly smaller fEPSPs 30 min after theta burst stimulation **(E)**. Inlaid traces are representative fEPSPs from the indicated time periods. KO rats also fail to achieve long-term depression (LTD) **(F)** with significantly larger field potentials 40 min after paired pulse low frequency stimulation (indicated by black bar) **(G)**. Bars indicate SEM. *$p < 0.05$.

Characterization of *in Vivo* Electrophysiological Biomarker of Shank2 Mutation

Given the changes in synaptic plasticity we observed subcortically, we hypothesized a change in cortical processing accessible via *in vivo* neurophysiology would be present, thereby lending to a potential translational biomarker. EEG can be similarly collected in both rodent models and subjects with autism, making EEG-based biomarkers particularly amenable for preclinical to clinical translation (Jeste et al., 2015). During baseline conditions, analysis of EEG spectrum reveals a significant effect of genotype on spectral power (*interaction* $F_{(4,52)} = 5.335$, $p = 0.0011$; *genotype* $F_{(1,13)} = 5.6692$, $p = 0.0329$). This effect was driven by a significant reduction in parietal cortex delta (1–4 Hz) power in KOs compared to WTs (**Figure 8A**; Sidak's test, $p < 0.0001$), however it is unknown if this is a state or a trait based phenomenon. Auditory evoked potentials are also altered in KOs relative to WTs (**Figure 8B**). At 80 db, the p120 amplitude for both S1 and S2 presentations is greater in KOs vs. WTs (**Figure 8C**; $p = 0.044$ and $p = 0.0045$, respectively). In KO animals, the early component latencies (p20 and n40) are significantly delayed for S1 and S2 (**Figure 8C**; S1-p20 $p = 0.0008$; S2-p20 $p = 0.0481$; **Figure 8C**, S1-N40 $p = 0.0083$; S2-N40 $p = 0.0205$). Similar effects are seen at both 70 db and 90 db (data not shown).

Rescue of Striatal LTD and Repetitive Behavior by mGluR1 Antagonism

To explore the association between increased mGluR1 receptor expression and enhanced corticostriatal LTD with aberrant repetitive behavior, the mGluR1 selective antagonist

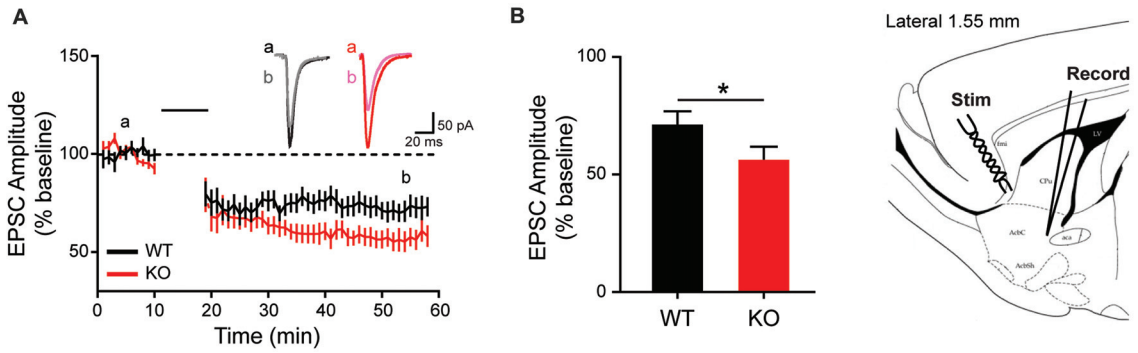

FIGURE 7 | Altered long term depression in the striatum of the *Shank2* KO rat. In the striatum (brain slice depicts location of stimulating and recording electrode), KO rats show enhanced LTD **(A)** with increased depression relative to baseline 40 min after low frequency presynaptic stimulation (indicated by black bar) **(B)**. In all panels WT animals are in black and KO animals are in red. Bars indicate SEM. $^{*}p < 0.05$.

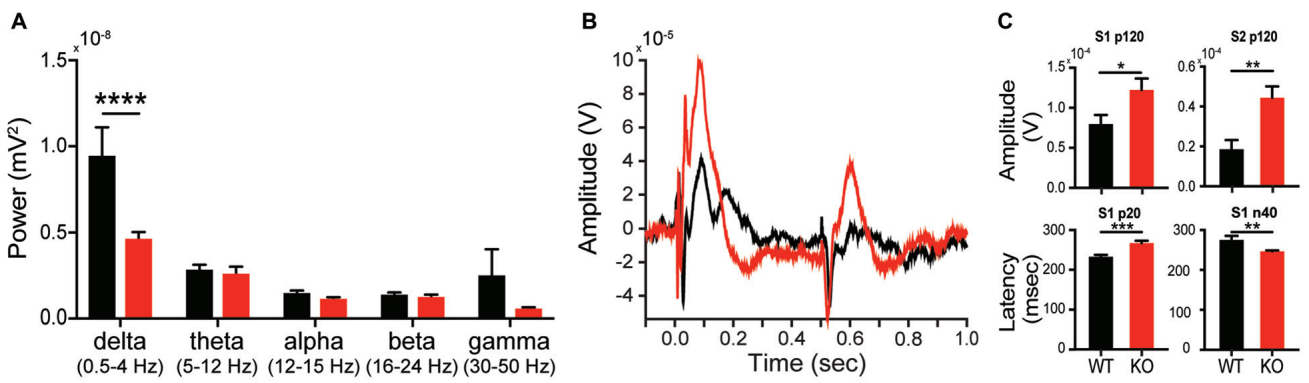

FIGURE 8 | Altered *in vivo* electrophysiology of the *Shank2* KO rat. Alterations in neural responsiveness can be seen *in vivo*. KOs exhibit a reduction in spectral power in the delta frequency compared to WT animals during resting state conditions **(A)**. KOs have an altered evoked response to paired auditory stimuli **(B)**, with an increase in p120 amplitude and an increase in the latency of the p20 and n40 components of the cortical neural response **(C)**. In all panels WT animals are in black and KO animals are in red. Bars indicate SEM. $^{*}p < 0.05$, $^{**}p < 0.01$, $^{***}p < 0.001$, $^{****}p < 0.0001$.

JNJ16259685 was administered *in vitro* and *in vivo*. In comparison to vehicle recordings depicted in **Figures 7A**, **9A** (black and red lines for WT and KO, respectively), JNJ16259685 (100 nM) reduces corticostriatal LTD in both genotypes (**Figures 9A–C**; *treatment* $F_{(1,40)} = 19.65$, $p < 0.0001$ gray and orange lines for WT and KO, respectively). EPSC amplitude is increased by mGluR1 antagonist treatment (**Figure 9C**) in WT ($p = 0.0169$) and KO ($p = 0.0015$). After treatment, there is no significant difference between EPSC amplitude in vehicle treated WT rats and JNJ16259685 treated KO rats ($p = 0.1551$). Similar to D1-selective antagonism, administration of 0.63 mg/kg JNJ16259685 (∼100% receptor occupancy (Lavreysen et al., 2004)) significantly reduces repetitive behaviors in the open field. In KO rats, both vertical rearing (**Figure 9E**; *interaction* $F_{(1,18)} = 4.615$, $p = 0.456$) and repetitive circling (**Figure 9D**; *interaction* $F_{(1,18)} = 23.21$, $p = 0.0001$; *dose* $F_{(1,18)} = 33.8$, $p < 0.0001$; Sidak *post hoc* $p < 0.0001$) are significantly decreased by mGluR1 antagonism, while no effect is seen in WT animals (Sidak *post hoc* $p = 0.7042$. Interestingly, the behavioral effect of JNJ16259685 is specific to repetitive behaviors, as there is no significant effect of drug on overall locomotion, social investigation, or novel object investigation (**Figures 9F,G**).

DISCUSSION

Consistent with analogous mouse models, *Shank2* mutation in rats results in hyperactivity and repetitive behaviors associated with striatal alterations. In addition to locomotor behaviors, our *Shank2* KO rats exhibit a novel hypermotivated response that is likely explained by striatal overexpression of mGluR1, altered neuronal morphology, and changes in MSN activity-dependent plasticity. Consistent with these findings, the mGluR1 antagonist JNJ16259685 normalizes striatal physiology and striatally mediated behaviors. In contrast to enhanced striatal function, *Shank2* mutant rats also demonstrate impairments in learning and decreased hippocampal plasticity and neuronal growth.

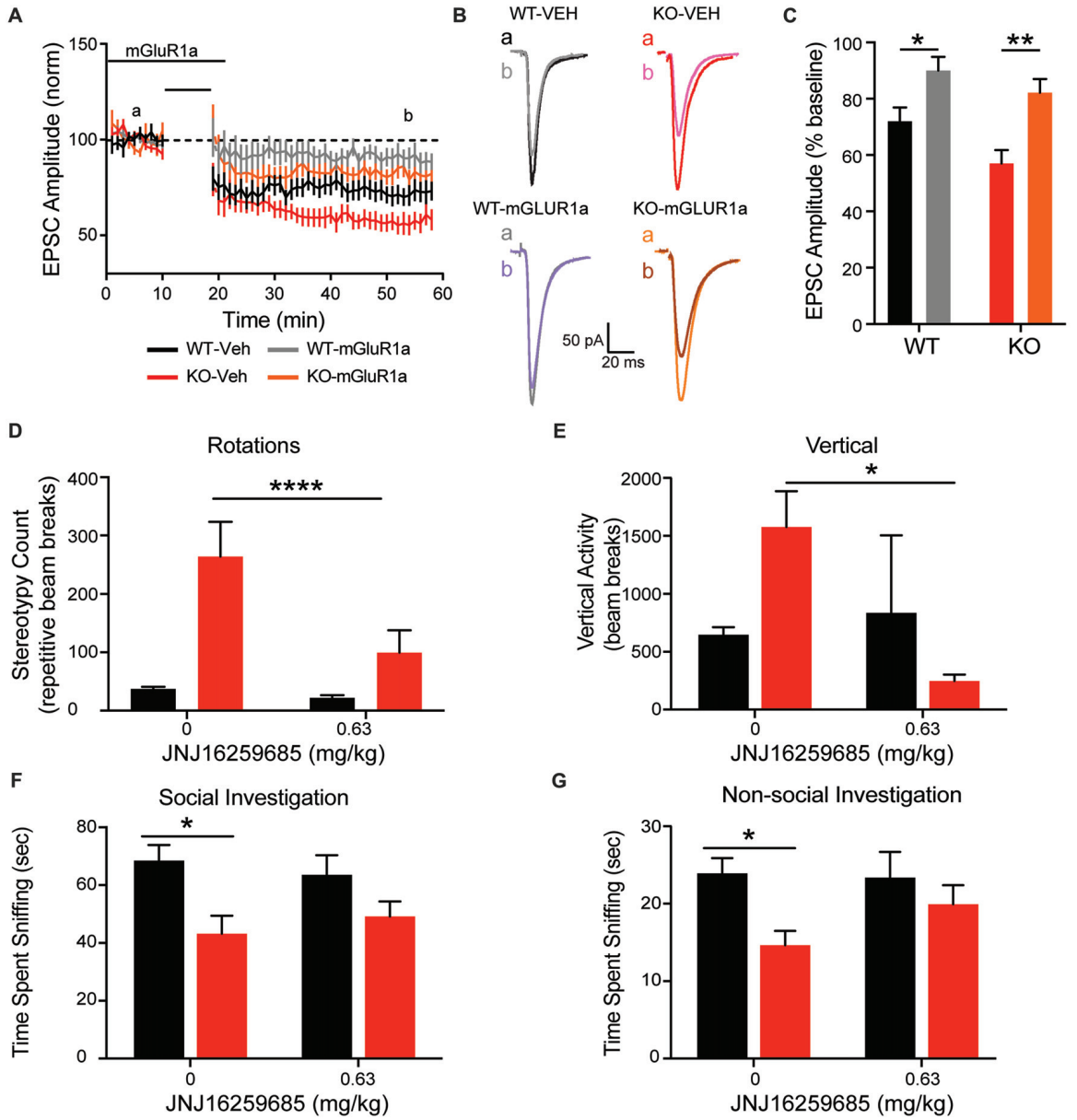

FIGURE 9 | mGluR1 antagonist JNJ16259685 rescues both striatal physiology and behavior. Administration of the selective mGluR1 antagonist JNJ16259685 normalizes the enhanced striatal LTD response of the KO animals **(A)**. Traces are representative EPSPs from the indicated time periods **(B)**. Treatment significantly reduced the depression in both WT and KO rats **(C)**. Blocking mGluR1 receptors *in vivo* selectively rescues the striatally mediated stereotypic behaviors, including rotations **(D)** and rearing **(E)**, but does not have an effect on social **(G)** or non-social **(F)** investigation. In all panels WT animals are in black and KO animals are in red. Note the data in **(A)** for vehicle WT and KO data (black and red lines, respectively) are also depicted in **Figure 7A**. Bars indicate SEM. $^{*}p < 0.05$, $^{**}p < 0.01$, $^{****}p < 0.0001$.

Striatal Dysregulation in the Shank2 Mutant Rat

Hyperactivity and repetitive behaviors have been consistently observed across Shank-associated mouse models (Peca et al., 2011; Schmeisser et al., 2012; Won et al., 2012; Bariselli et al., 2016; Wang et al., 2016). The replicability of these phenotypes across mouse strains, and now species, makes repetitive behavior the most robust behavioral phenotype in Shank models (Jiang and Ehlers, 2013). Interestingly, our model also exhibits a hypermotivation phenotype that is also likely mediated by striatal function. Hyperactivity, repetitive behavior, and motivation have distinct underlying circuitries, however, all three are associated with striatal function, indicating a common node of pathophysiology (Britt et al., 2012). *Shank3* mutation disrupts the development of normal corticostriatal connectivity and ventral striatal maturation,

implicating this family of proteins in the development of striatal circuits (Bariselli et al., 2016; Peixoto et al., 2016). While *Shank3* has been characterized as the "striatal" Shank protein, *Shank2* is also expressed in the rat striatum and may reciprocally regulate the expression of other SHANK proteins in this region (Böckers et al., 2004; Schmeisser et al., 2012; Han et al., 2013). In our model, striatal cellular morphology, physiology, and plasticity are disrupted following *Shank2* mutation. Remediation of striatal mGluR1 upregulation selectively rescues the repetitive but not the social phenotype, indicating the potential contribution of alternate mechanisms to different aspects autism symptomatology.

Opposing Effect of Shank2 Mutation in Striatum and Hippocampus

In contrast to the enhancement of striatal activity, hippocampal function is depressed in Shank2 KO rats structurally, with decreased dendritic branching and soma size; cellularly, demonstrated by reduced synaptic plasticity; and behaviorally, as evidenced by impaired operant conditioning. Recent investigations into SHANK3 suggest regionally distinct functionality of SHANK proteins. Proteomic analysis of the PSD demonstrated *Shank3* mutation primarily disrupted glutamate receptor subunits in the striatum but cytoskeletal components in the HP (Reim et al., 2017). Interactome construction has also revealed a regional specificity of SHANK3 functionality that is not seen in its binding partners (Lee et al., 2017). Given the overlapping functionality within Shank proteins, Shank2 disruption may also result in comparable alterations. Nonetheless, further characterization is needed to determine whether region-specific functionality in Shank2 contributes to the opposing phenotypes described here.

Mechanisms of Shank-Mediated Dysregulation

We show that *Shank2* mutation leads to several structural and functional changes in the striatum, including enhanced mGluR1 protein expression. Similar to our model, positive modulation of mGluR1a activity increases MSN dendritic spine density in ventral striatum (Gross et al., 2016). Consistent with these structural findings, we observe an enhancement of corticostriatal synaptic depression in *Shank2* mutant MSNs, in which mGluR1 is highly expressed in dendrites and spines (Testa et al., 1998). Activation of these postsynaptic receptors increases intracellular calcium (Pisani et al., 2000) through either polyphosphoinositide hydrolysis coupling (Casabona et al., 1997) or via activation of phospholipase C (Fagni et al., 2000). Given that increased postsynaptic calcium concentration is a critical mediator of striatal synaptic plasticity (Calabresi et al., 1992), this is a mechanism by which increased mGluR1 expression may enhance corticostriatal LTD. These data, together with loss of corticostriatal LTD following application of an mGluR1 antagonist (**Figures 5A–C**), support the assertion that striatal mGluR1 overexpression mediates aberrant striatal function and behavior in *Shank2* KO animals.

Alteration of Glutamate Receptor Proteins After Shank2 Mutation

While the *Shank2* rat model shows only subtle, region-specific upregulation of mGluR1 protein, mouse models of *Shank2* mutation exhibit broad disruption of glutamate receptor subunit expression. *Shank2* transgenic mice have a dramatic upregulation of ionotropic receptors in the striatum and, to a lesser extent, the HP (Schmeisser et al., 2012). The differences in glutamate receptor dysregulation between these models are unclear, despite the use of identical protocols. However, the functional alterations in our rat model overlap with specific features of both *Shank2* mutant mouse models (Schmeisser et al., 2012; Won et al., 2012) but do not provide a consensus phenotype. The discordance of molecular but not behavioral phenotypes resultant from *Shank2* mutation in mice and rats suggests that alterations in glutamate receptor expression may not be a pathogenic locus of this mutation. Instead, changes in receptor expression profiles may be pathological manifestations that vary based on species, mutation, and environment resultant of an unidentified common mechanism.

Importance of Circuit-Specific Modulation

Pharmacotherapeutic development for autism has primarily focused on treatments for social impairments, yet repetitive behaviors are a central component of ASD currently lacking FDA-approved treatments. Repetitive behaviors have greater translational face validity, are easier to quantify, and can be measured more objectively than social impairment in rodent models (Kaiser and Feng, 2015). Rescue of repetitive but not social phenotypes with mGluR1 inhibition in this study suggests the striatal circuit should be selectively modulated and may represent a tractable target for these symptoms. However, given the expression profile, mGluR1 inhibition to target striatal dysfunction could potentially lead to "off-circuit" effects. As the molecular alterations in our model are regionally specific, identifying circuit-selective modulators will be important. Regionally specific modulation of metabotropic glutamate receptors by SHANK protein mutation could be a source of the variability seen in the behavioral efficacy of drugs targeting these receptors. The opposing hippocampal and striatal alterations in our model suggest that circuit-selective methods of pharmacological manipulation are likely necessary for the successful treatment of the impairments in autism. This model uniquely enables the screening of novel compounds for both the desired repetitive behavioral effects and counter screening for cognitive effects.

Benefits of Rat Transgenic Models

The characterization of human *Shank2* mutations in both rat and mouse models enables the assessment of species-specific preclinical model strengths. *Shank2* mutation in a rat model empowers more sophisticated characterization of the neural

circuits and provides a better systems-level understanding of the relationship between synaptic dysfunction and behavioral phenotypes. Rats are also amenable to more complex surgical and electrophysiological manipulations due to their larger size. Further, there is greater homology in the metabolic pathways of rats and humans relative to mice and humans, making them the preferred animal model for drug development (Jaramillo and Zador, 2014; Ellenbroek and Youn, 2016; Homberg et al., 2017). Finally, more sophisticated behavioral endpoints can be assessed in rats due to their enhanced cognitive capabilities and diverse social behavioral repertoire, which is particularly relevant to the modeling of ASD-related mutations. Through the use of a rat genetic model, we have identified a unique hypermotivation phenotype and demonstrated social impairments early in development, extending the behavioral phenotypes previously seen in mouse models. These phenotypes have given credence to the hypothesis of autism as a disorder of motivation and striatal function (Chevallier et al., 2012) and inspire further investigation into the ability to selectively pharmacologically manipulate corticostriatal circuits for the treatment of ASD.

AUTHOR CONTRIBUTIONS

MM, JB, MS, TB, PO and DB conceptualized the experiments and edited the manuscript. MM, JB, EG, MB, RG and DR designed and executed the experiments and analyzed the data. MM, JB and DB wrote the manuscript.

ACKNOWLEDGMENTS

The research conducted at Pfizer was funded by the Neuroscience Research Unit of Pfizer Inc. Salary support for DB, EG, RG, JB, PO, MB and MM was also provided by Pfizer Inc. The research conducted at the University of Ulm was funded from the Innovative Medicines Initiative Joint Undertaking under grant agreement n° 115300, resources of which are composed of financial contribution from the European Union's Seventh Framework Programme (FP7/2007-2013) and EFPIA companies' in kind contribution (EU-AIMS to TB). MJS was supported by the Care-for-Rare Foundation and the Eliteprogramm of the Baden-Württemberg Stiftung; DR by a scholarship of the International Graduate School in Molecular Medicine of Ulm University. We would like to thank the animal care staff in the Worldwide Department of Comparative Medicine at Pfizer Inc. for their support in the care and testing of the animals in this study.

SUPPLEMENTARY MATERIAL

The Supplementary Material for this article can be found online at: https://www.frontiersin.org/articles/10.3389/fnmol.2018.00107/full#supplementary-material

FIGURE S1 | Generation and validation of the Shank2 KO rat model. Genomic PCR strategy **(A)** determined gDNA sequence deleted in two rat Shank2 KO lines (8A and 13) including PCR strategy design and primers to detect deletions. DNA gel is example of WT, Het and KO animals' genomic PCR results showing expected gPCR products of 1171 bp (WT) and 501 bp (KO). **(B)** Entire Shank2 western blot of whole brain and synaptosome preparations for WT, Het and KO animals from **Figure 1C**.

FIGURE S2 | Lack of change in synaptic protein expression in *Shank2* KO rat. Neither the HP **(A)** nor the striatum **(B)** show significant changes in synaptic protein expression unlike in the *Shank2* mutnat mouse. Values are expressed as fold change relative to the average WT value. Bars indicate SEM.

TABLE S1 | Comprehensive statistics table.

REFERENCES

Aberman, J. E., Ward, S. J., and Salamone, J. D. (1998). Effects of dopamine antagonists and accumbens dopamine depletions on time-constrained progressive-ratio performance. *Pharmacol. Biochem. Behav.* 61, 341–348. doi: 10.1016/s0091-3057(98)00112-9

Ameis, S. H., and Catani, M. (2015). Altered white matter connectivity as a neural substrate for social impairment in Autism Spectrum Disorder. *Cortex* 62, 158–181. doi: 10.1016/j.cortex.2014.10.014

Bariselli, S., Tzanoulinou, S., Glangetas, C., Prévost-Solié, C., Pucci, L., Viguié, J., et al. (2016). SHANK3 controls maturation of social reward circuits in the VTA. *Nat. Neurosci.* 19, 926–934. doi: 10.1038/nn.4319

Berkel, S., Marshall, C. R., Weiss, B., Howe, J., Roeth, R., Moog, U., et al. (2010). Mutations in the SHANK2 synaptic scaffolding gene in autism spectrum disorder and mental retardation. *Nat. Genet.* 42, 489–491. doi: 10.1038/ng.589

Berkel, S., Tang, W., Treviño, M., Vogt, M., Obenhaus, H. A., Gass, P., et al. (2012). Inherited and *de novo* SHANK2 variants associated with autism spectrum disorder impair neuronal morphogenesis and physiology. *Hum. Mol. Genet.* 21, 344–357. doi: 10.1093/hmg/ddr470

Böckers, T. M., Segger-Junius, M., Iglauer, P., Bockmann, J., Gundelfinger, E. D., Kreutz, M. R., et al. (2004). Differential expression and dendritic transcript localization of Shank family members: identification of a dendritic targeting element in the 3' untranslated region of Shank1 mRNA. *Mol. Cell. Neurosci.* 26, 182–190. doi: 10.1016/j.mcn.2004.01.009

Britt, J. P., Benaliouad, F., McDevitt, R. A., Stuber, G. D., Wise, R. A., and Bonci, A. (2012). Synaptic and behavioral profile of multiple glutamatergic inputs to the nucleus accumbens. *Neuron* 76, 790–803. doi: 10.1016/j.neuron.2012.09.040

Calabresi, P., Maj, R., Pisani, A., Mercuri, N. B., and Bernardi, G. (1992). Long-term synaptic depression in the striatum: physiological and pharmacological characterization. *J. Neurosci.* 12, 4224–4233.

Casabona, G., Knöpfel, T., Kuhn, R., Gasparini, F., Baumann, P., Sortino, M. A., et al. (1997). Expression and coupling to polyphosphoinositide hydrolysis of group I metabotropic glutamate receptors in early postnatal and adult rat brain. *Eur. J. Neurosci.* 9, 12–17. doi: 10.1111/j.1460-9568.1997.tb01348.x

Chevallier, C., Kohls, G., Troiani, V., Brodkin, E. S., and Schultz, R. T. (2012). The social motivation theory of autism. *Trends Cogn. Sci.* 16, 231–239. doi: 10.1016/j.tics.2012.02.007

Chevallier, C., Tonge, N., Safra, L., Kahn, D., Kohls, G., Miller, J., et al. (2016). Measuring social motivation using signal detection and reward responsiveness. *PLoS One* 11:e0167024. doi: 10.1371/journal.pone.0167024

Counotte, D. S., Schiefer, C., Shaham, Y., and O'Donnell, P. (2014). Time-dependent decreases in nucleus accumbens AMPA/NMDA ratio and incubation of sucrose craving in adolescent and adult rats. *Psychopharmacology* 231, 1675–1684. doi: 10.1007/s00213-013-3294-3

Dhamne, S. C., Silverman, J. L., Super, C. E., Lammers, S. H. T., Hameed, M. Q., Modi, M. E., et al. (2017). Replicable *in vivo* physiological and behavioral phenotypes of the Shank3B null mutant mouse model of autism. *Mol. Autism* 8:26. doi: 10.1186/s13229-017-0142-z

Distler, U., Schmeisser, M. J., Pelosi, A., Reim, D., Kuharev, J., Weiczner, R., et al. (2014). In-depth protein profiling of the postsynaptic density from mouse

hippocampus using data-independent acquisition proteomics. *Proteomics* 14, 2607–2613. doi: 10.1002/pmic.201300520

Ellenbroek, B., and Youn, J. (2016). Rodent models in neuroscience research: is it a rat race? *Dis. Model. Mech.* 9, 1079–1087. doi: 10.1242/dmm.026120

Fagni, L., Chavis, P., Ango, F., and Bockaert, J. (2000). Complex interactions between mGluRs, intracellular Ca^{2+} stores and ion channels in neurons. *Trends Neurosci.* 23, 80–88. doi: 10.1016/s0166-2236(99)01492-7

Filice, F., Vörckel, K. J., Sungur, A. O., Wohr, M., and Schwaller, B. (2016). Reduction in parvalbumin expression not loss of the parvalbumin-expressing GABA interneuron subpopulation in genetic parvalbumin and shank mouse models of autism. *Mol. Brain* 9:10. doi: 10.1186/s13041-016-0192-8

Gross, K. S., Brandner, D. D., Martinez, L. A., Olive, M. F., Meisel, R. L., and Mermelstein, P. G. (2016). Opposite effects of mGluR1a and mGluR5 activation on nucleus accumbens medium spiny neuron dendritic spine density. *PLoS One* 11:e0162755. doi: 10.1371/journal.pone.0162755

Han, K., Holder, J. L. Jr., Schaaf, C. P., Lu, H., Chen, H., Kang, H., et al. (2013). SHANK3 overexpression causes manic-like behaviour with unique pharmacogenetic properties. *Nature* 503, 72–77. doi: 10.1038/nature12630

Hart, G., Leung, B. K., and Balleine, B. W. (2014). Dorsal and ventral streams: the distinct role of striatal subregions in the acquisition and performance of goal-directed actions. *Neurobiol. Learn. Mem.* 108, 104–118. doi: 10.1016/j.nlm.2013.11.003

Higa, K. K., Young, J. W., Ji, B., Nichols, D. E., Geyer, M. A., and Zhou, X. (2017). Striatal dopamine D1 receptor suppression impairs reward-associative learning. *Behav. Brain Res.* 323, 100–110. doi: 10.1016/j.bbr.2017.01.041

Homberg, J. R., Wohr, M., and Alenina, N. (2017). Comeback of the rat in biomedical research. *ACS Chem. Neurosci.* 8, 900–903. doi: 10.1021/acschemneuro.6b00415

Jaramillo, T. C., Speed, H. E., Xuan, Z., Reimers, J. M., Escamilla, C. O., Weaver, T. P., et al. (2017). Novel Shank3 mutant exhibits behaviors with face validity for autism and altered striatal and hippocampal function. *Autism Res.* 10, 42–65. doi: 10.1002/aur.1664

Jaramillo, T. C., Speed, H. E., Xuan, Z., Reimers, J. M., Liu, S., and Powell, C. M. (2016). Altered striatal synaptic function and abnormal behaviour in Shank3 exon4–9 deletion mouse model of autism. *Autism Res.* 9, 350–375. doi: 10.1002/aur.1529

Jaramillo, S., and Zador, A. M. (2014). Mice and rats achieve similar levels of performance in an adaptive decision-making task. *Front. Syst. Neurosci.* 8:173. doi: 10.3389/fnsys.2014.00173

Jeste, S. S., Frohlich, J., and Loo, S. K. (2015). Electrophysiological biomarkers of diagnosis and outcome in neurodevelopmental disorders. *Curr. Opin. Neurol.* 28, 110–116. doi: 10.1097/WCO.0000000000000181

Jiang, Y. H., and Ehlers, M. D. (2013). Modeling autism by SHANK gene mutations in mice. *Neuron* 78, 8–27. doi: 10.1016/j.neuron.2013.03.016

Kabitzke, P. A., Brunner, D., He, D., Fazio, P. A., Cox, K., Sutphen, J., et al. (2018). Comprehensive analysis of two Shank3 and the Cacna1c mouse models of autism spectrum disorder. *Genes Brain Behav.* 17, 4–22. doi: 10.1111/gbb.12405

Kaiser, T., and Feng, G. (2015). Modeling psychiatric disorders for developing effective treatments. *Nat. Med.* 21, 979–988. doi: 10.1038/nm.3935

Kemp, N., and Bashir, Z. I. (1999). Induction of LTD in the adult hippocampus by the synaptic activation of AMPA/kainate and metabotropic glutamate receptors. *Neuropharmacology* 38, 495–504. doi: 10.1016/s0028-3908(98)00222-6

Kim, H., Lim, C. S., and Kaang, B. K. (2016). Neuronal mechanisms and circuits underlying repetitive behaviors in mouse models of autism spectrum disorder. *Behav. Brain Funct.* 12:3. doi: 10.1186/s12993-016-0087-y

Kohls, G., Yerys, B. E., and Schultz, R. T. (2014). Striatal development in autism: repetitive behaviors and the reward circuitry. *Biol. Psychiatry* 76, 358–359. doi: 10.1016/j.biopsych.2014.07.010

Kouser, M., Speed, H. E., Dewey, C. M., Reimers, J. M., Widman, A. J., Gupta, N., et al. (2013). Loss of predominant Shank3 isoforms results in hippocampus-dependent impairments in behavior and synaptic transmission. *J. Neurosci.* 33, 18448–18468. doi: 10.1523/JNEUROSCI.3017-13.2013

Lavreysen, H., Wouters, R., Bischoff, F., Nóbrega Pereira, S., Langlois, X., Blokland, S., et al. (2004). JNJ16259685, a highly potent, selective and systemically active mGlu1 receptor antagonist. *Neuropharmacology* 47, 961–972. doi: 10.1016/j.neuropharm.2004.08.007

Leblond, C. S., Heinrich, J., Delorme, R., Proepper, C., Betancur, C., Huguet, G., et al. (2012). Genetic and functional analyses of SHANK2 mutations suggest a multiple hit model of autism spectrum disorders. *PLoS Genet.* 8:e1002521. doi: 10.1371/journal.pgen.1002521

Lee, Y., Kang, H., Lee, B., Zhang, Y., Kim, Y., Kim, S., et al. (2017). Integrative analysis of brain region-specific Shank3 interactomes for understanding the heterogeneity of neuronal pathophysiology related to SHANK3 mutations. *Front. Mol. Neurosci.* 10:110. doi: 10.3389/fnmol.2017.00110

Luscher, C., and Huber, K. M. (2010). Group 1 mGluR-dependent synaptic long-term depression: mechanisms and implications for circuitry and disease. *Neuron* 65, 445–459. doi: 10.1016/j.neuron.2010.01.016

Mei, Y., Monteiro, P., Zhou, Y., Kim, J. A., Gao, X., Fu, Z., et al. (2016). Adult restoration of Shank3 expression rescues selective autistic-like phenotypes. *Nature* 530, 481–484. doi: 10.1038/nature16971

Monteiro, P., and Feng, G. (2017). SHANK proteins: roles at the synapse and in autism spectrum disorder. *Nat. Rev. Neurosci.* 18, 147–157. doi: 10.1038/nrn.2016.183

Peca, J., Feliciano, C., Ting, J. T., Wang, W., Wells, M. F., Venkatraman, T. N., et al. (2011). Shank3 mutant mice display autistic-like behaviours and striatal dysfunction. *Nature* 472, 437–442. doi: 10.1038/nature09965

Peixoto, R. T., Wang, W., Croney, D. M., Kozorovitskiy, Y., and Sabatini, B. L. (2016). Early hyperactivity and precocious maturation of corticostriatal circuits in Shank3B$^{-/-}$ mice. *Nat. Neurosci.* 19, 716–724. doi: 10.1038/nn.4260

Pisani, A., Bernardi, G., Bonsi, P., Centonze, D., Giacomini, P., and Calabresi, P. (2000). Cell-type specificity of mGluR activation in striatal neuronal subtypes. *Amino Acids* 19, 119–129. doi: 10.1007/s007260070040

Reim, D., Distler, U., Halbedl, S., Verpelli, C., Sala, C., Bockmann, J., et al. (2017). Proteomic analysis of post-synaptic density fractions from Shank3 mutant mice reveals brain region specific changes relevant to autism spectrum disorder. *Front. Mol. Neurosci.* 10:26. doi: 10.3389/fnmol.2017.00026

Schmeisser, M. J., Ey, E., Wegener, S., Bockmann, J., Stempel, A. V., Kuebler, A., et al. (2012). Autistic-like behaviours and hyperactivity in mice lacking ProSAP1/Shank2. *Nature* 486, 256–260. doi: 10.1038/nature11015

Shi, X., and McGinty, J. F. (2011). D1 and D2 dopamine receptors differentially mediate the activation of phosphoproteins in the striatum of amphetamine-sensitized rats. *Psychopharmacology* 214, 653–663. doi: 10.1007/s00213-010-2068-4

Speed, H. E., Kouser, M., Xuan, Z., Reimers, J. M., Ochoa, C. F., Gupta, N., et al. (2015). Autism-associated insertion mutation (InsG) of Shank3 exon 21 causes impaired synaptic transmission and behavioral deficits. *J. Neurosci.* 35, 9648–9665. doi: 10.1523/JNEUROSCI.3125-14.2015

Szechtman, H., Ahmari, S. E., Beninger, R. J., Eilam, D., Harvey, B. H., Edemann-Callesen, H., et al. (2017). Obsessive-compulsive disorder: insights from animal models. *Neurosci. Biobehav. Rev.* 76, 254–279. doi: 10.1016/j.neubiorev.2016.04.019

Testa, C. M., Friberg, I. K., Weiss, S. W., and Standaert, D. G. (1998). Immunohistochemical localization of metabotropic glutamate receptors mGluR1a and mGluR2/3 in the rat basal ganglia. *J. Comp. Neurol.* 390, 5–19. doi: 10.1002/(sici)1096-9861(19980105)390:1<5::aid-cne2>3.3.co;2-c

Valverde, F. (1993). The rapid Golgi technique for staining CNS neurons: light microscopy. *Neurosci. Protocols* 1, 1–9.

Veenema, A. H., and Neumann, I. D. (2009). Maternal separation enhances offensive play-fighting, basal corticosterone and hypothalamic vasopressin mRNA expression in juvenile male rats. *Psychoneuroendocrinology* 34, 463–467. doi: 10.1016/j.psyneuen.2008.10.017

Vicidomini, C., Ponzoni, L., Lim, D., Schmeisser, M. J., Reim, D., Morello, N., et al. (2017). Pharmacological enhancement of mGlu5 receptors rescues behavioral deficits in SHANK3 knock-out mice. *Mol. Psychiatry* 22:784. doi: 10.1038/mp.2016.70

Wang, X., Bey, A. L., Katz, B. M., Badea, A., Kim, N., David, L. K., et al. (2016). Altered mGluR5-Homer scaffolds and corticostriatal connectivity in a Shank3 complete knockout model of autism. *Nat. Commun.* 7:11459. doi: 10.1038/ncomms11459

Wang, W., Li, C., Chen, Q., van der Goes, M. S., Hawrot, J., Yao, A. Y., et al. (2017). Striatopallidal dysfunction underlies repetitive behavior in Shank3-

deficient model of autism. *J. Clin. Invest.* 127, 1978–1990. doi: 10.1172/JCI 87997

Won, H., Lee, H. R., Gee, H. Y., Mah, W., Kim, J. I., Lee, J., et al. (2012). Autistic-like social behaviour in Shank2-mutant mice improved by restoring NMDA receptor function. *Nature* 486, 261–265. doi: 10.1038/nature11208

Wood, J., and Ahmari, S. E. (2015). A framework for understanding the emerging role of corticolimbic-ventral striatal networks in OCD-associated repetitive behaviors. *Front. Syst. Neurosci.* 9:171. doi: 10.3389/fnsys.2015. 00171

Conflict of Interest Statement: DB, JB, PO, MB, EG, RG and MM are former employees of Pfizer, Inc. MB and EG are currently employees of Biogen, Inc. PD and DB are currently employees of Takeda Pharmaceuticals. MM is currently at Harvard Medical School/Boston Children's Hospital. JB is currently an employee at Alkermes, and RG is an employee of Axial Therapeutics. All were employed solely by Pfizer during the execution of the described experiments.

The remaining authors declare that the research was conducted in the absence of any commercial or financial relationships that could be construed as a potential conflict of interest.

frontiers in Molecular Neuroscience

ORIGINAL RESEARCH
published: 19 June 2018
doi: 10.3389/fnmol.2018.00212

Heterogeneity of Cell Surface Glutamate and GABA Receptor Expression in Shank and CNTN4 Autism Mouse Models

*Christopher Heise[1,2], Jonathan M. Preuss[1], Jan C. Schroeder[1], Chiara R. Battaglia[1], Jonas Kolibius[1], Rebecca Schmid[1], Michael R. Kreutz[2], Martien J. H. Kas[3,4], J. Peter H. Burbach[4] and Tobias M. Boeckers[1]**

[1]*Institute for Anatomy and Cell Biology, Ulm University, Ulm, Germany,* [2]*RG Neuroplasticity, Leibniz Institute for Neurobiology, Magdeburg, Germany,* [3]*Groningen Institute for Evolutionary Life Sciences, University of Groningen, Groningen, Netherlands,* [4]*Department of Translational Neuroscience, Brain Center Rudolf Magnus, University Medical Center Utrecht, Utrecht, Netherlands*

Autism spectrum disorder (ASD) refers to a large set of neurodevelopmental disorders, which have in common both repetitive behavior and abnormalities in social interactions and communication. Interestingly, most forms of ASD have a strong genetic contribution. However, the molecular underpinnings of this disorder remain elusive. The *SHANK3* gene (and to a lesser degree *SHANK2*) which encode for the postsynaptic density (PSD) proteins SHANK3/SHANK2 and the *CONTACTIN 4* gene which encodes for the neuronal glycoprotein CONTACTIN4 (CNTN4) exhibit mutated variants which are associated with ASD. Like many of the other genes associated with ASD, both *SHANKs* and *CNTN4* affect synapse formation and function and are therefore related to the proper development and signaling capability of excitatory and inhibitory neuronal networks in the adult mammal brain. In this study, we used mutant/knock-out mice of Shank2 (*Shank2*$^{-/-}$), Shank3 (*Shank3*$\alpha\beta^{-/-}$), and Cntn4 (*Cntn4*$^{-/-}$) as ASD-models to explore whether these mice share a molecular signature in glutamatergic and GABAergic synaptic transmission in ASD-related brain regions. Using a biotinylation assay and subsequent western blotting we focused our analysis on cell surface expression of several ionotropic glutamate and GABA receptor subunits: GluA1, GluA2, and GluN1 were analyzed for excitatory synaptic transmission, and the α1 subunit of the $GABA_A$ receptor was analyzed for inhibitory synaptic transmission. We found that both *Shank2*$^{-/-}$ and *Shank3*$\alpha\beta^{-/-}$ mice exhibit reduced levels of several cell surface glutamate receptors in the analyzed brain regions—especially in the striatum and thalamus—when compared to wildtype controls. Interestingly, even though *Cntn4*$^{-/-}$ mice also show reduced levels of some cell surface glutamate receptors in the cortex and hippocampus, increased levels of cell surface glutamate receptors were found in the striatum. Moreover, *Cntn4*$^{-/-}$ mice do not only show brain region-specific alterations

OPEN ACCESS

Edited by:
Sabine Levi,
Institut National de la Santé et de la Recherche Médicale (INSERM), France

Reviewed by:
Enrica Maria Petrini,
Fondazione Istituto Italiano di Technologia, Italy
Hiroko Bannai,
Japan Science and Technology Agency (JST), Japan

***Correspondence:**
Tobias M. Boeckers
tobias.boeckers@uni-ulm.de

Received: *13 February 2018*
Accepted: *30 May 2018*
Published: *19 June 2018*

Citation:
Heise C, Preuss JM, Schroeder JC, Battaglia CR, Kolibius J, Schmid R, Kreutz MR, Kas MJH, Burbach JPH and Boeckers TM (2018) Heterogeneity of Cell Surface Glutamate and GABA Receptor Expression in Shank and CNTN4 Autism Mouse Models. Front. Mol. Neurosci. 11:212. doi: 10.3389/fnmol.2018.00212

Abbreviations: ACSF, artificial cerebrospinal fluid; ASD, autism spectrum disorders; d, distilled; E/I, excitation/inhibition; kDa, kilo Dalton; LTP, long-term potentiation; PBS, phosphate buffered saline; PSD, postsynaptic density; RPM, rotations per minute; SDS, sodium dodecyl sulfate; SDS-PAGE, sodium dodecyl sulfate polyacrylamide gel electrophoresis; Shank, SH3 and multiple ankyrin repeat domains 3, also known as ProSAP.

in cell surface glutamate receptors but also a downregulation of cell surface GABA receptors in several of the analyzed brain regions. The results of this study suggest that even though mutations in defined genes can be associated with ASD this does not necessarily result in a common molecular phenotype in surface expression of glutamatergic and GABAergic receptor subunits in defined brain regions.

Keywords: autism spectrum disorder, autism mouse models, Shank2, Shank3, Cntn4, synapse, cell surface receptors, biotinylation assay

INTRODUCTION

The term autism spectrum disorder (ASD) refers to a spectrum of heterogeneous developmental disorders, which share two striking behavioral phenotypes: patients exhibit repetitive, stereotypic behavior and they also show impaired social communication and behavior. Importantly, ASD has a strong genetic component: if one sibling has ASD, the other has a 25× higher risk of developing ASD as compared to the general population; the concordance rate of monozygotic twins is 70%–90% compared with 0%–10% in dizygotic twins and males have a four times higher risk of developing ASD as compared to females (Moessner et al., 2007; Fassio et al., 2011). ASD also appears to be linked with changes in excitatory and/or inhibitory network activity as up to one-third of the ASD patients also suffer from epilepsy (Rapin, 1997; Tuchman and Rapin, 2002). This may be related to the fact that several of the genes related to ASD are synaptic proteins or proteins, which have synaptic functions (Mullins et al., 2016). It should be noted that the majority of ASD cases are due to genetic variations in a multitude of genes and only a minority of cases can be linked to monogenetic variants of genes, such as variations in the *SHANK3*, *SHANK2* and *CONTACTIN4* (CNTN4) genes (Pinto et al., 2010; Leblond et al., 2014; Mullins et al., 2016). But even in the cases where ASD can be associated with a variant of a single gene, our knowledge of how these genes are linked to this disorder needs to be improved and will likely better our understanding not only of those specific ASD cases but also of mechanisms underlying the entire range of ASD.

The *SHANK* gene family (*SHANK1*, *SHANK2* and *SHANK3)* encodes for postsynaptic density (PSD) associated proteins at the excitatory synapse that act as scaffolds and interconnect neurotransmitter receptors and cell adhesion molecules—both by direct and indirect interactions with a large group of other PSD associated proteins (Boeckers et al., 2002; Grabrucker et al., 2011; Jiang and Ehlers, 2013). Several research groups have demonstrated the importance of Shanks for the proper functioning of the excitatory synapse and excitatory synaptic transmission (Sala et al., 2001; Peca et al., 2011; Schmeisser et al., 2012; Vicidomini et al., 2017) and Shank3 haploinsufficiency has not only been linked to ASD but also to schizophrenia and neuropsychiatric symptoms in the Phelan-McDermid syndrome (Guilmatre et al., 2014). CNTN4/BIG-2, an neuronal glycoprotein, which belongs to a subfamily of the immunoglobulin superfamily of cell adhesion molecules (Oguro-Ando et al., 2017) is known to guide axons during development. This function has been studied in the development of the olfactory and visual neural circuit (Kaneko-Goto et al., 2008; Osterhout et al., 2015). However, the precise role of CNTN4 in establishing neural networks and synaptic contacts remains to be clarified.

Unraveling the molecular and network abnormalities in the brain that cause ASD has proven to be a difficult task and has been carried out in a multidisciplinary fashion (Baudouin et al., 2012; Bourgeron, 2015; Mullins et al., 2016). Part of this research has focused on comparing ASD related genes with respect to function, subcellular localization and the expression pattern in the brain. Other lines of research took advantage of mouse models for monogenetic ASD to unravel novel ASD specific phenotypes at the electrophysiological and biochemical level. We followed the latter approach and utilized mutant/knock-out mice of Shank2 ($Shank2^{-/-}$), Shank3 ($Shank3\alpha\beta^{-/-}$) and Cntn4 ($Cntn4^{-/-}$) to see whether these mice share common cell surface expression patterns of glutamate and GABA receptors in ASD related brain areas: cortex, striatum, hippocampus, thalamus and cerebellum (Ameis et al., 2011; Peca et al., 2011; Becker and Stoodley, 2013; Schuetze et al., 2016). To this end, a cell surface biotinylation protocol was established on acute coronal mouse brain slices containing the aforementioned brain regions, followed by a western blot analysis for several ionotropic glutamate and GABA receptor subunits. Antibodies directed against GluA1, GluA2 and GluN1 were used for the analysis of excitatory synaptic transmission, and antibodies raised against the α1 subunit of the $GABA_A$ receptor were used for the analysis of inhibitory synaptic transmission.

Here, we report that $Shank2^{-/-}$ and $Shank3\alpha\beta^{-/-}$ mice have reduced expression levels of several cell surface glutamate receptors which is most evident in the striatum and thalamus. $Shank2^{-/-}$ also present lower expression levels in the cortex and cerebellum. In contrast, $Cntn4^{-/-}$ mice have lower expression levels of cell surface glutamate receptors in the cortex and hippocampus but increased expression levels of cell surface glutamate receptors in the striatum. In addition, $Cntn4^{-/-}$ mice differ from $Shank2^{-/-}$ and $Shank3\alpha\beta^{-/-}$ mice since they not only show brain region specific changes in cell surface glutamate receptors but also a downregulation of cell surface GABA receptors in several brain regions. Taken together, the results of this study indicate that monogenetic variants in genes associated with ASD may not necessarily have a common molecular phenotype at the level of excitatory and inhibitory signaling components such as ionotropic glutamate and GABA receptors.

This raises the question whether variants in genes related to ASD may have commonalities at other levels of information processing, such as at the level of neuronal networks, which has become a relevant aspect in ASD research (Baudouin et al., 2012; Zikopoulos and Barbas, 2013; Bourgeron, 2015; Mullins et al., 2016).

MATERIALS AND METHODS

Animal Ethics Statement

Shank2$^{-/-}$, *Shank3*αβ$^{-/-}$ and *Cntn4*$^{-/-}$ mice were previously described (Kaneko-Goto et al., 2008; Schmeisser et al., 2012). All mice were kept in specific pathogen-free animal facilities and all animal experiments in this study were performed based on the guidelines for the welfare of experimental animals issued by the Federal Government of Germany and by the local ethics committee (Ulm University), ID Number: 0.103.

Primary Antibodies

Primary antibodies used for western blotting were diluted 1:500 (except for actin which was diluted 1:100,000). The following primary antibodies were purchased from commercial suppliers: Actin (Sigma-Aldrich Cat# A2228 RRID:AB_476697), NR1/GluN1 (Sigma-Aldrich Cat# G8913 RRID:AB_259978), GluA1 (SynapticSystems Cat# 182011 RRID:AB_2113443), GluA2 (SynapticSystems Cat# 182111 RRID:AB_10645888), $GABA_AR\alpha1$ (NeuroMab Cat# N95/35 RRID:AB_2108811), pERK (Cell Signalling Cat# 9101 RRID:AB_2297442), mGluR5 (Millipore Cat# AB5675 RRID:AB_2295173).

Secondary Antibodies

Secondary antibodies used for western blotting were HRP-conjugated (Dako, Glostrup, Denmark, dilution 1:1000).

Slice Preparation

The slice preparation protocol was derived from studies implementing classical electrophysiological recordings of acute brain slices (Mathis et al., 2011; Whitehead et al., 2013; Heise et al., 2017). Briefly, adult male mice aged 3–6 months (one *Shank2*$^{-/-}$, *Shank3*αβ$^{-/-}$, or *Cntn4*$^{-/-}$ and a corresponding wildtype control mouse) were sacrificed and brains were extracted on ice in a petri dish filled with ice cold artificial cerebrospinal fluid (ACSF; NaCl, 120 mM; KCl, 2.5 mM; NaH_2PO_4, 1.25 mM; $NaHCO_3$, 22 mM; Glucose, 10 mM; $MgSO_4$, 2 mM; pH 7.4; oxygenation with 95% O_2/5% CO_2). Then, 300 µm coronal slices were made using a vibratome (Thermo scientific, Vibratom Microm HM 650V; "cutting frequency" = 100, "speed" = 10) beginning rostrally at Bregma 3.20 mm. Slices containing striatum and anterior cortex portions were gathered between Bregma 1.50 mm and Bregma 0.00 mm. Slices containing hippocampus, thalamus and posterior cortex portions were gathered between Bregma −1.00 mm and Bregma −3.00 mm. Lastly, slices containing cerebellum were gathered between Bregma −5.80 mm and Bregma −7.80 mm. After slicing, sections were immediately transferred to a 2 l glass beaker filled with ice cold ACSF (oxygenation with 95% O_2/5% CO_2) until all slices were gathered and cell surface biotinylation (see below) was carried out. View Supplementary Figure S2,1 for a visual impression of the aforementioned slices.

Cell Surface Biotinylation

Cell surface biotinylation and NeutrAvidin pull-down was carried out with slight modifications of previously published work (Whitehead et al., 2013). Briefly, slices were transferred from the 2 l beaker (see "Slice Preparation" section above) to 6-well plates where they were incubated with ice cold Sulfo-NHS-SS-Biotin (Thermo #21331; 1 mg/ml solubilized in ACSF) on a horizontal shaker (Heidolph, Unimax 1010; around 90 rotations per minute (RPM)) for 45 min at 4°C. Then, several washing steps followed to stop the biotinylation reaction, each lasting 5 min on the horizontal shaker at 4°C: two washes with ice cold 10 mM glycine (solubilized in ACSF) and a final wash with ice cold TBS (150 mM NaCl, 50 mM Tris HCl, pH 7.4).

Extraction of Brain Regions

Brain regions of interest (cortex, striatum, hippocampus, thalamus and cerebellum) were dissected from the various coronal brain slices using small forceps (Fine Science Tools, Heidelberg, Germany) under an Olympus SZ40 stereoscope. Anterior and posterior cortex sections (see above) were pooled.

Lysis, NeutrAvidin Pull-Down, Input (Total) and Biotinylated Fraction (Surface)

Extracted, biotinylated brain regions (see above) were collected in 1.5 ml Eppendorf tubes containing 600 µl of lysis buffer (25 mM Tris (pH 7.6), 150 mM NaCl, 1% TritonTM X-100, 0.5% sodium deoxycholate, 0.1% sodium dodecyl sulfate (SDS), 2 mM NaF, 1 mM EDTA and a cocktail of protease inhibitors (Roche), diluted in dH_2O). Tissue was then lysed on ice using a potter and centrifuged at 12000 *g* (Eppendorf; 5430R) for 15 min at 4°C to remove nuclei and cellular debris. Supernatant was transferred to fresh, precooled 1.5 ml Eppendorf tubes. Samples were then analyzed by Bradford assay to assess protein concentration. Samples were adjusted to 1 µg/µl using lysis buffer and 2× 25 µl were taken from each sample as input controls (5%) and stored at 4°C until later use (see below). Five-hundred microliter of 1 µg/µl sample were transferred to a new precooled 1.5 ml Eppendorf tube and 100 µl of 50% Neutravidin agarose resin (Thermo: #29200) slurry were added and incubated overnight on a test-tube-rotator (Shijders, 34528) at 4°C. The next day, several washing steps followed: 3× washes with ice cold lysis buffer and 2× washes with ice cold TBS (cocktail of protease inhibitors). Between each wash samples were put on the test-tube-rotator at 4°C for 30 min, followed by a centrifugation step at 1000 *g* to separate the Neutravidin agarose matrix and the attached biotinylated proteins from the supernatant. After the last washing step, proteins were eluted from the matrix with 60 µl of 4× loading dye (200 mM Tris-HCL, pH 6.8, 200 mM DTT, 4%SDS, 4 mM EDTA, 40% glycerol, 0.02% bromophenolblue), yielding the biotinylated fraction with biotinylated cell-surface-bound proteins, henceforth referred to as the surface fraction. At this point, input samples from the previous day were also diluted with 4× loading dye, yielding the input controls which contain

both biotinylated and non-biotinylated proteins, henceforth referred to as the total protein fraction. Finally, samples were boiled for 5 min at 95°C, put directly on ice, centrifuged at 12,000 *g*, and saved for subsequent Western Blot analysis at −20°C.

Western Blot Analysis

For western blotting, one input control (5%) and half of the biotin fraction of the wildtype mouse and the corresponding *Shank2*$^{-/-}$, *Shank3*αβ$^{-/-}$, or *Cntn4*$^{-/-}$ mouse were loaded on one gel to compare the signal intensities of the fractions as faithfully as possible. Per experimental round, a second gel with the same loading was carried out to increase the amount of different antibodies that could be used per round. Western blot analysis was carried out according to standard protocols (Laemmli, 1970). HRP-conjugated secondary antibodies were used together with the SuperSignal detection system (Thermo Scientific) to visualize protein bands.

Quantification of Protein Band Signal Intensity and Data Analysis

Digital files from the SuperSignal detection system were analyzed with the open source program ImageJ (US National Institutes of Health). Average band intensities of the signal of interest were calculated, adjusting for background noise. Then, the average band intensity of each surface fraction was divided by the corresponding average band intensity in the total fraction, yielding the "surface/total ratio." After this, data was normalized to the average "surface/total ratio" of the wildtype control and the mutant mouse model of the experimental round, yielding the "normalized surface/total ratio." In order to easily interpret changes between wildtype and mutant mice, the wildtype average was then set to 1 by dividing data by the mean of the wildtype control across experimental rounds. Statistical analysis was carried out using a student's *t*-test. For total protein analysis, average band intensities of the signal of interest in the total fraction were normalized by actin and the wildtype average was then set to 1 as described above.

Neuronal Stimulation Protocol

For the experiment pertaining to neuronal stimulation using "high potassium," coronal slices containing the hippocampus were initially gathered in two 2 l glass beakers (one for the control and one for the experimental group) containing ice cold ACSF as described above. After 15 min, the ACSF in the glass beakers was exchanged quickly for an ice cold ACSF without $MgSO_4$ but with 2 mM $CaCl_2$ instead (all other buffer components were equal and again oxygenation took place with 95% O_2/5% CO_2; incubation for 30 min). Then, the temperature was raised 1°C/min to a final temperature of nearly 37°C. As soon as the final temperature was reached, a 4 M KCl stock (diluted in dH_2O) was added to the ACSF of the experimental group to yield a final concentration of 50 mM KCl ("high potassium"). For the control group, no KCl but instead the corresponding volume of dH_2O was added. After 5 min, slices were transferred to new 2 l glass beakers containing ice cold ACSF without $MgSO_4$ but with 2 mM $CaCl_2$ (again oxygenation took place with 95% O_2/5% CO_2). Then, cell surface biotinylation, extraction of the hippocampus, tissue lysis, NeutrAvidin pull-down and western blot analysis took place as described above (however, every buffer in downstream applications—e.g., the lysis buffer—contained 2 mM $CaCl_2$).

RESULTS

The Implemented Experimental Design Yields Clean Cell Surface Fractions and Acute Slices With Intact Intracellular Signaling Properties

The first aim of this study was to test whether the employed cell surface biotinylation protocol for acute coronal brain slices yields relatively pure cell surface fractions and whether the cell surface biotinylation is really a prerequisite for receptor accumulation in the cell surface fraction, as would be expected. For this analysis, we utilized hippocampal tissue extracted from slices between Bregma −1.00 mm and Bregma −3.00 mm (see "Materials and Methods" section and Supplementary Figure S1) which expresses high levels of ionotropic glutamate receptors (Schwenk et al., 2014). To test for the purity of the cell surface fraction we carried out a western blot analysis with actin as an abundant intracellular protein and found that actin is present in the total protein fraction which contains non-biotinylated and biotinylated proteins but is almost absent in cell surface fractions (**Figure 1A**). To test whether the cell surface biotinylation protocol is necessary to accumulate glutamate and GABA receptors in the cell surface fraction, we carried out our experimental procedure either with (+) or without (−) the use of NHS-SS-Biotin and found that, as expected, NHS-SS-Biotin is needed for the accumulation of $GABA_AR\alpha1$, GluN1, GluA2, GluA1 and mGluR5 in the surface fraction (**Figure 1A**).

Lastly, we wanted to test whether our slice preparation and subsequent experimental procedures yield acute coronal brain slices with intact physiological properties. As an indication for the ability of the slices to react in a physiologically relevant manner we chose to stimulate our slices with "high potassium" (extracellular KCl concentration of 50 mM for 5 min at 37°C), which is a classical protocol to stimulate neurons *in vitro* and *ex vivo* and is related to an increase in ERK phosphorylation and various associated neuronal processes such as long-term potentiation (LTP). For this analysis, we again utilized hippocampal tissue extracted from slices between Bregma −1.00 mm and Bregma −3.00 mm since many studies utilizing this high potassium protocol to induce neuronal stimulation and ERK phosphorylation took advantage of hippocampal neurons (Sala et al., 2000; Lundquist and Dudek, 2006). We found that stimulating our slices before cell surface biotinylation, indeed, leads to an increase of ERK phosphorylation relative to non-stimulated controls, yielding increased levels of phospho-ERK running at 42 and 44 kDa in the sodium dodecyl sulfate polyacrylamide gel electrophoresis (SDS-PAGE; **Figure 1B**).

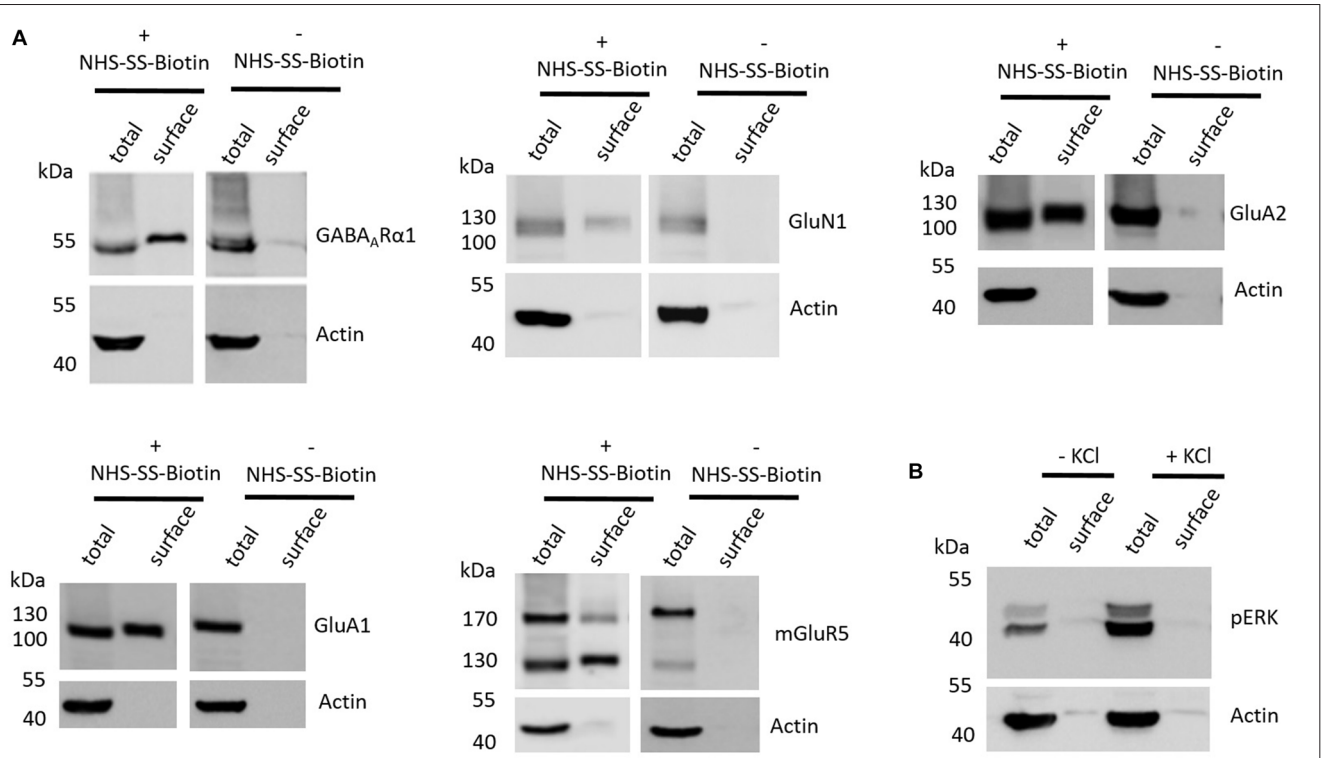

FIGURE 1 | Various controls of the cell surface biotinylation procedure confirm a properly functioning experimental design yielding acute coronal slices with physiological signaling properties. **(A)** Representative western blots (WBs) showing band intensities of hippocampal total protein and cell surface sample with or without prior cell surface biotinylation reveal that cell surface samples are almost devoid of typical intracellular proteins and that biotinylation is necessary for enrichment of proteins in the cell surface sample. The cell surface biotinylation protocol either was (+NHS-SS-Biotin) or was not (−NHS-SS-Biotin) carried out on acute coronal wildtype slices containing the hippocampus prior to dissection and lysis of hippocampal tissue from the slice. Total protein samples (total) and samples containing biotinylated cell surface proteins (surface) were analyzed by WB for GABA$_A$Rα1, GluN1, GluA2, GluA1, mGluR5 and actin. **(B)** Representative WBs showing band intensities of hippocampal total protein and cell surface sample with or without "high potassium" stimulation prior to cell surface biotinylation reveal that total protein samples exhibit an increased phospho ERK signal intensity after "high potassium" stimulation relative to control samples. Neuronal stimulation of acute coronal wildtype slices by 50 mM KCl for 5 min at 37°C either was (+KCl) or was not (−KCl) performed before cell surface biotinylation and subsequent dissection and lysis of hippocampal tissue from the slice. Total protein samples (total) and samples containing biotinylated cell surface proteins (surface) were analyzed by WB for pERK and actin.

Shank2$^{-/-}$ and *Shank3*αβ$^{-/-}$ Mice Exhibit Reduced Cell Surface Glutamate Receptor Levels in the Striatum and Other ASD Related Brain Regions

We started our investigation of cell surface glutamate and GABA receptor expression levels in ASD mouse models by applying the cell surface biotinylation protocol to acute slices from *Shank2*$^{-/-}$ and *Shank3*αβ$^{-/-}$ mice and comparing them to wildtype controls. After biotinylation, the following ASD related brain regions were dissected from the slices, lysed and analyzed by western blot: cortex, striatum, hippocampus, thalamus and cerebellum (Supplementary Figure S1). Immunodetection was carried out with antibodies directed against GABA$_A$Rα1, GluA2, GluN1, GluA1 and mGluR5 and revealed that signal intensities in the cell surface fractions were high enough for quantification in most brain regions, whereas quantification of mGluR5 was limited to the hippocampus (Supplementary Figure S2,1).

Interestingly, we found that both *Shank2*$^{-/-}$ and *Shank3*αβ$^{-/-}$ mice exhibit a reduction of several cell surface glutamate receptors in the analyzed brain regions—especially in the striatum and thalamus (**Figures 2**, **3**, **5**). More precisely, *Shank3*αβ$^{-/-}$ mice exhibit significantly reduced cell surface expression levels of GluN1 and GluA2 in the striatum and thalamus and *Shank2*$^{-/-}$ mice have significantly reduced cell surface expression levels of GluN1 in the striatum and cortex. Furthermore, we found that *Shank3*αβ$^{-/-}$ and *Shank2*$^{-/-}$ mice exhibit significantly reduced cell surface expression levels of GluA1 in the hippocampus and GluA2 in the cerebellum, respectively. Additionally, several other cell surface glutamate receptors showed trends ($p \leq 0.10$) for a downregulation in the analyzed brain regions (**Figures 2**, **3**, **5**). In the cortex, *Shank2*$^{-/-}$ and *Shank3*αβ$^{-/-}$ mice both showed no altered cell surface expression of GABA$_A$Rα1, GluA2, GluA1 and *Shank3*αβ$^{-/-}$ mice also showed no alteration of GluN1 levels. In the striatum, *Shank2*$^{-/-}$ and *Shank3*αβ$^{-/-}$ mice both showed no altered cell surface expression of GABA$_A$Rα1 and GluA1 and *Shank2*$^{-/-}$ mice also showed no alteration of GluA2 levels. As for the hippocampus, *Shank2*$^{-/-}$ and *Shank3*αβ$^{-/-}$ mice both showed no altered cell surface expression of GABA$_A$Rα1, GluA2, NR 1

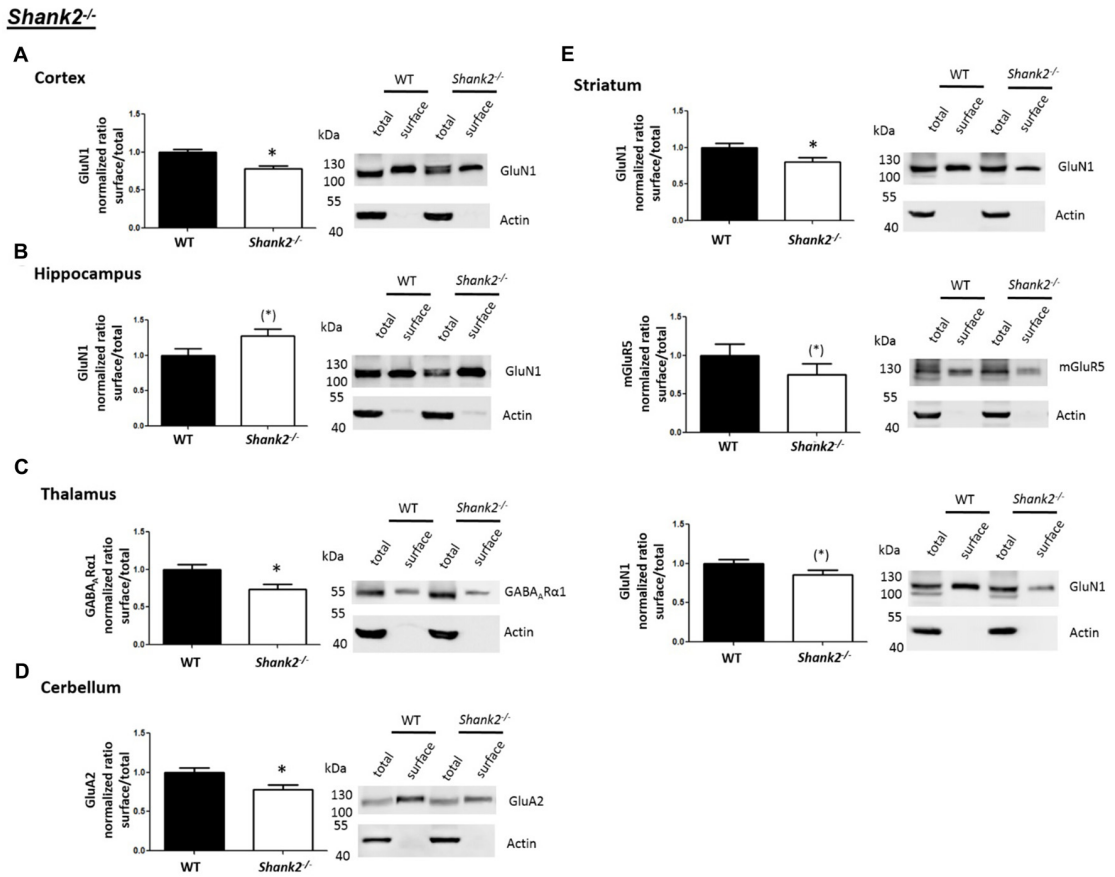

FIGURE 2 | Analysis of cell surface glutamate and GABA receptor subunits in autism spectrum disorder (ASD) related brain regions of *Shank2*$^{-/-}$ mice. **(A–E)** Representative WBs showing band intensities of total protein and cell surface sample in cortex **(A)**, striatum **(B)**, hippocampus **(C)**, thalamus **(D)** and cerebellum **(E)** of wildtype and *Shank2*$^{-/-}$ mice reveal a downregulation of cell surface glutamate receptor subunits in *Shank2*$^{-/-}$ mice. Immunodetections were carried out with antibodies directed against $GABA_AR\alpha1$, GluA2, GluN1, GluA1, mGluR5 and actin. For $GABA_AR\alpha1$, GluA2, and actin all brain regions were analyzed. For GluN1 all brain regions except the cerebellum were analyzed. For GluA1 all brain regions except the thalamus and cerebellum were analyzed. For mGluR5 only the hippocampus was analyzed. Only statistically significant data ($p < 0.05$; see below) or data with strong trends ($p < 0.10$; see below) is shown. To the left of each representative WB, the respective quantification of the surface/total ratio is shown. Vertical axis shows the mean fold change vs. the wildtype control (control set to a value of 1). Error bars are SEMs. $n \geq 5$ per group. $^*p < 0.05$, $^{(*)}p < 0.10$.

or mGluR5 and *Shank3*αβ$^{-/-}$ mice also showed no alteration of GluA1 levels. For the thalamus we observed no altered cell surface expression of $GABA_AR\alpha1$ in *Shank3*αβ$^{-/-}$ mice and *Shank2*$^{-/-}$ mice showed no alteration of GluA2 or GluN1 levels. Lastly, in the cerebellum *Shank2*$^{-/-}$ and *Shank3*αβ$^{-/-}$ mice both showed no altered cell surface expression of $GABA_AR\alpha1$ and *Shank3*αβ$^{-/-}$ mice showed no alteration in GluA2 levels (**Figures 2**, **3**, **5**). Of note, no differences in total expression levels of the analyzed receptors were found between *Shank2*$^{-/-}$ or *Shank3*αβ$^{-/-}$ mice and wildtype controls (Supplementary Figure S2,2).

Cntn4$^{-/-}$ Mice Exhibit Altered Cell Surface Glutamate and GABA Receptor Levels in ASD Related Brain Regions

We then expanded our investigation of cell surface glutamate and GABA receptors in ASD mouse models by applying the cell surface biotinylation protocol to acute slices from *Cntn4*$^{-/-}$ mice and comparing them to wildtype controls. Again, western blotting was carried out to analyze samples from the cortex, striatum, hippocampus, thalamus and cerebellum (Supplementary Figure S1).

In contrast to the findings of *Shank2*$^{-/-}$ and *Shank3*αβ$^{-/-}$ mice, we found that *Cntn4*$^{-/-}$ mice exhibit reduced cell surface glutamate receptor levels in the cortex and hippocampus but increased cell surface glutamate receptor levels in the striatum when compared to wildtype controls (**Figures 4**, **5**). More precisely, *Cntn4*$^{-/-}$ mice exhibit significantly reduced cell surface expression levels of GluA2 and GluN1 in the cortex, reduced cell surface expression levels of GluA2 and mGluR5 in the hippocampus, and increased cell surface expression levels of GluA2 and GluA1 in the striatum. In addition to these dysregulations of cell surface glutamate receptor levels we also found changes in cell surface GABA receptor levels in several brain regions (**Figures 4**, **5**). More precisely, we found

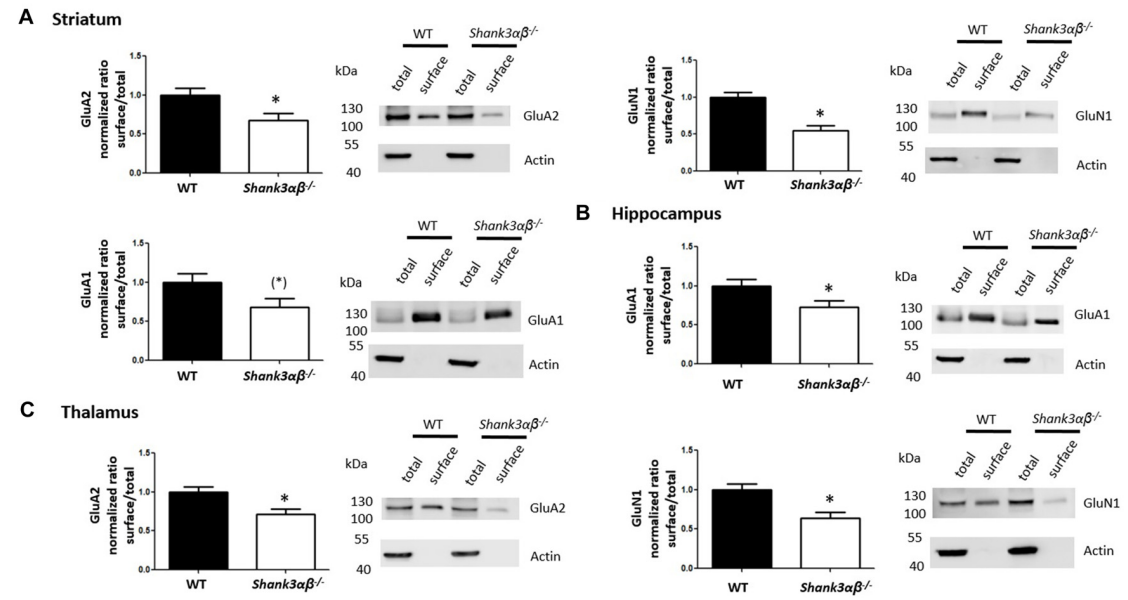

FIGURE 3 | Analysis of cell surface glutamate and GABA receptor subunits in ASD related brain regions of *Shank3*αβ$^{-/-}$ mice. **(A–C)** Representative WBs showing band intensities of total protein and cell surface sample in striatum **(A)**, hippocampus **(B)** and thalamus **(C)** of wildtype and *Shank3*αβ$^{-/-}$ mice reveal a downregulation of cell surface glutamate receptor subunits in *Shank3*αβ$^{-/-}$ mice. Immunodetections were carried out with antibodies directed against $GABA_AR\alpha1$, GluA2, GluN1, GluA1, mGluR5, and actin. For $GABA_AR\alpha1$, GluA2 and actin all brain regions were analyzed. For GluN1 all brain regions except the cerebellum were analyzed. For GluA1 all brain regions except the thalamus and cerebellum were analyzed. For mGluR5 only the hippocampus was analyzed. Only statistically significant data ($p < 0.05$; see below) or data with strong trends ($p < 0.10$; see below) is shown. To the left of each representative WB, the respective quantification of the surface/total ratio is shown. Vertical axis shows the mean fold change vs. the wildtype control (control set to a value of 1). Error bars are SEMs. $n \geq 5$ per group. $^{*}p < 0.05$, $^{(*)}p < 0.10$.

reduced cell surface $GABA_AR\alpha1$ levels in the hippocampus and thalamus and a trend for reduced cell surface $GABA_AR\alpha1$ levels in the cortex. In contrast, except for reduced thalamic cell surface $GABA_AR\alpha1$ levels in *Shank2*$^{-/-}$ mice (**Figures 2**, **5**), no further differences between *Shank2*$^{-/-}$ or *Shank3*αβ$^{-/-}$ and wildtype mice could be identified with regard to cell surface $GABA_AR\alpha1$ levels. In the cortex, *Cntn4*$^{-/-}$ mice displayed no significantly altered cell surface expression of $GABA_AR\alpha1$ and GluA1 and in the striatum $GABA_AR\alpha1$ and GluN1 levels were not altered. As for the hippocampus, *Cntn4*$^{-/-}$ mice displayed no significantly altered cell surface expression of GluN1 and GluA1 and in the thalamus *Cntn4*$^{-/-}$ mice displayed no changes in GluA2 and GluN1 levels. Lastly, in the cerebellum *Cntn4*$^{-/-}$ mice displayed no significantly altered cell surface expression of $GABA_AR\alpha1$ and GluA2 (**Figures 4**, **5**). Of note, no differences in total expression levels of the analyzed receptors were found between *Cntn4*$^{-/-}$ mice and wildtype controls (Supplementary Figure S2,2).

DISCUSSION

Epidemiological studies suggest that up to 1% of the world's population may be diagnosed with ASD (Elsabbagh et al., 2012; Christensen et al., 2016) and, therefore, understanding the genetic/molecular underpinnings of this class of psychiatric disorders is of great importance. Years of research have generated data which clearly suggests a strong genetic component involved in the etiology of ASDs—e.g., variations in the *SHANK2*, *SHANK3* and *CNTN4* genes have been associated with an increased risk for developing ASD and many knockout mice of these genes display abnormalities in behavior and social interactions reminiscent of ASD patients (Leblond et al., 2012; Provenzano et al., 2012; Schmeisser et al., 2012; Jiang and Ehlers, 2013). Nonetheless, the scientific community lacks a unifying theory backed up by experimental data to explain how a plethora of genetic variations leads to a condition with similar core symptoms, albeit with a great heterogeneity and variability (Mullins et al., 2016).

In this study, we compared cell surface expression levels of several glutamate and GABA receptors in ASD related brain region of three different ASD mouse models (*Shank2*$^{-/-}$, *Shank3*αβ$^{-/-}$ and *Cntn4*$^{-/-}$) aiming on unraveling molecular abnormalities in excitatory and/or inhibitory signaling components which are common to all three mouse models. It is important to note that the mouse models used in this study differ with respect to their ASD-related behavior: *Shank2*$^{-/-}$ and *Shank3*αβ$^{-/-}$ mice clearly show repetitive, stereotyped behavior and deficits in social interactions, though in varying degrees (Schmeisser et al., 2012; Vicidomini et al., 2017; Monteiro and Feng, 2017), whereas ASD-related behavior

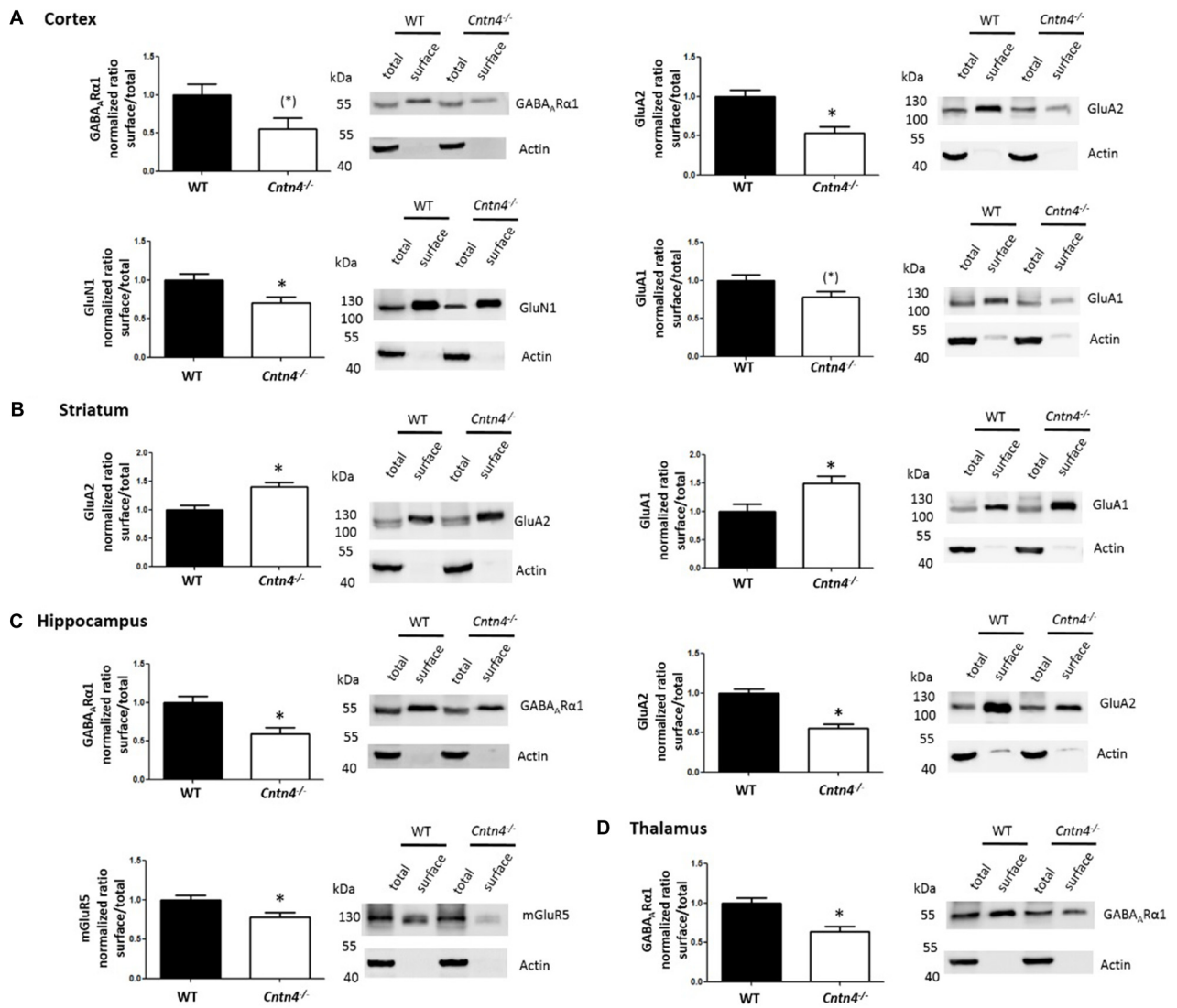

FIGURE 4 | Analysis of cell surface glutamate and GABA receptor subunits in ASD related brain regions of *Cntn4*$^{-/-}$ mice. **(A–D)** Representative WBs showing band intensities of total protein and cell surface sample in cortex **(A)**, striatum **(B)**, hippocampus **(C)** and thalamus **(D)** of wildtype and *Cntn4*$^{-/-}$ mice reveal a dysregulation of cell surface glutamate and GABA receptor subunits in *Cntn4*$^{-/-}$ mice. Immunodetections were carried out with antibodies directed against $GABA_AR\alpha1$, GluA2, GluN1, GluA1, mGluR5, and actin. For $GABA_AR\alpha1$, GluA2, and actin all brain regions were analyzed. For GluN1 all brain regions except the cerebellum were analyzed. For GluA1 all brain regions except the thalamus and cerebellum were analyzed. For mGluR5 only the hippocampus was analyzed. Only statistically significant data ($p < 0.05$; see below) or data with strong trends ($p < 0.10$; see below) is shown. To the left of each representative WB, the respective quantification of the surface/total ratio is shown. Vertical axis shows the mean fold change vs. the wildtype control (control set to a value of 1). Error bars are SEMs. $n \geq 5$ per group. $^{*}p < 0.05$, $^{(*)}p < 0.10$.

in *Cntn4*$^{-/-}$ has been less well characterized but appears to be much less pronounced (Molenhuis et al., 2016). Our data suggest that—as might have been expected—genetic deficiency of *Shank2* and *Shank3* yields relatively similar changes in cell surface glutamate and GABA receptor expression levels: on the whole, a downregulation of cell surface ionotropic glutamate receptor subunits (GluN1, GluA2 and GluA1) could be observed in several ASD-related brain regions (especially in the striatum and thalamus) whereas almost no changes in the expression of cell surface ionotropic GABA receptors was seen. Since ionotropic receptors at the cell surface are well-positioned to take part in neuronal signaling at the synapse, our data suggests a reduction in the excitation/inhibition (E/I) ratio in several brain regions of *Shank2*$^{-/-}$ and *Shank3*$\alpha\beta^{-/-}$ mice. In line with this hypothesis, *Shank3* deficient mice have been reported to have a reduced striatal/cortico-striatal glutamatergic synaptic

		Shank2$^{-/-}$ mice	*Shank3αβ*$^{-/-}$ mice	*Cntn4*$^{-/-}$ mice
Cortex	$GABA_AR\alpha1$	N/S (p = 0.54) 0.07 ± 0.11	N/S (p = 0.14) -0.19 ± 0.13	(↓)
	GluA2	N/S (p = 0.83) -0.03 ± 0.13	N/S (p = 0.19) -0.14 ± 0.10	↓
	GluN1	↓	N/S (p = 0.82) 0.02 ± 0.11	↓
	GluA1	N/S (p =0.21) -0.28 ± 0.20	N/S (p = 0.92) 0.02 ± 0.20	(↓)
Striatum	$GABA_AR\alpha1$	N/S (p = 0.17) 0.18 ± 0.12	N/S (p = 0.13) 0.18 ± 0.11	N/S (p = 0.11) 0.22 ± 0.12
	GluA2	N/S (p = 0.83) -0.04 ± 0.17	↓	↑
	GluN1	↓	↓	N/S (p = 0.38) -0.09 ± 0.10
	GluA1	N/S (p = 0.16) 0.29 ± 0.18	(↓)	↑
Hippocampus	$GABA_AR\alpha1$	N/S (p = 0.48) -0.14 ± 0.20	N/S (p = 0.42) 0.06 ± 0.08	↓
	GluA2	N/S (p = 0.65) -0.12 ± 0.26	N/S (p = 0.64) -0.07 ± 0.14	↓
	GluN1	(↑)	N/S (p = 0.21) -0.22 ± 0.17	N/S (p = 0.32) 0.12 ± 0.12
	GluA1	N/S (p = 0.39) -0.35 ± 0.38	↓	N/S (p = 0.35) 0.19 ± 0.19
	mGluR5	(↓)	N/S (p = 0.30) 0.09 ± 0.08	↓
Thalamus	$GABA_AR\alpha1$	↓	N/S (p = 0.33) 0.13 ± 0.13	↓
	GluA2	N/S (p = 0.59) 0.01 ± 0.18	↓	N/S (p = 0.88) 0.02 ± 0.10
	GluN1	(↓)	↓	N/S (p = 0.66) 0.07 ± 0.15
Cerbellum	$GABA_AR\alpha1$	N/S (p = 0.18) 0.21 ± 0.15	N/S (p = 0.40) -0.20 ± 0.24	N/S (p = 0.56) 0.10 ± 0.17
	GluA2	↓	N/S (p = 0.76) 0.08 ± 0.25	N/S (p = 0.23) 0.03 ± 0.02

FIGURE 5 | Summary of cell surface glutamate and GABA receptor subunit analysis in ASD related brain regions of *Shank2*$^{-/-}$, *Shank3αβ*$^{-/-}$ and *Cntn4*$^{-/-}$ mice. Summarized cell surface glutamate and GABA receptor subunit analysis reveals a commonality of *Shank2*$^{-/-}$ and *Shank3αβ*$^{-/-}$ mice with respect to dysregulations of cell surface receptors relative to wildtype controls whereas *Cntn4*$^{-/-}$ mice appear to differ from the *Shank* deficient mice in this respect. On the whole, *Shank2*$^{-/-}$ and *Shank3αβ*$^{-/-}$ mice display reduced levels of cell surface glutamate receptor subunits in most of the analyzed brain regions, whereas dysregulation of cell surface $GABA_AR\alpha1$ levels is minimal. In contrast, *Cntn4*$^{-/-}$ mice display dysregulations of both cell surface glutamate and GABA receptor subunits. Summary is based on quantifications of surface/total ratio (**Figures 2**–**4**). ↓, ↑ $p < 0.05$; (↓), (↑) $p < 0.10$. In the case of non-significant data (N/S) which does not show trends ($p > 0.10$) the difference of means (wildtype—autism mouse model) ± SEM and the corresponding *p*-value is shown. Numbers are rounded to two decimal places. Upregulated (↑); downregulated (↓).

transmission and a reduced spine density in the striatum (Peca et al., 2011). Additionally, several *Shank2* and *Shank3* deficiency mouse models display a reduced glutamatergic synaptic transmission and a reduced spine density/PSD ultrastructure in the hippocampus (Schmeisser et al., 2012; Won et al., 2012; Jiang and Ehlers, 2013). Unfortunately, to our knowledge there is no published electrophysiological or electron microscopy data of the thalamus available for *Shank* deficient mice but it would be intriguing to find out whether thalamic abnormalities in glutamatergic signaling could be identified. In the case of *Cntn4*$^{-/-}$ mice we also found abnormalities in cell surface receptors. However, we observed that these mice exhibit both brain region specific down- and upregulations of cell surface glutamate receptors and brain region specific downregulations of GABAergic cell surface receptors. Essential differences between Cntn4 and Shanks may underlie these differential changes observed in our mouse models. In particular, the expression of Cntn4 in the brain is far lower and more restricted than that of

the Shanks. Overall, Cntn4 expression is low in the brain with a few hotspots such as several thalamic nuclei, hippocampal CA regions and several cortical cell-types, including pyramidal as well as GABAergic neurons (Habib et al., 2016; Tasic et al., 2016; Oguro-Ando et al., 2017). This expression pattern may be related to the changes in cell-surface receptor expression levels observed in the *Cntn4*$^{-/-}$ mice.

The findings of this study point towards the possibility that there may not be a common molecular phenotype that all ASD mouse models share. On the one hand, it suggests that other levels of molecular and cellular processes may be a common point of convergence. On the other hand, it indicates that gene-specific effects may diversify phenotypes as is also observed in individuals with ASD who display great heterogeneity in symptoms, severity, and comorbidities. Therefore, future treatment of ASD patients might have to be highly individualized.

Of note, our study differs from virtually all previous biochemical studies of synaptic proteins in ASD mouse models since we implemented a biotinylation assay to analyze cell surface bound receptors as opposed to the commonly used analysis of synaptosomal/PSD fractions. Obviously, the advantage of analyzing cell surface receptors is that the data has more implications for synaptic signal transmission, since synaptosomal/PSD fractions will contain many receptors, which cannot participate in synaptic signaling, as they are not localized at the cell surface (e.g., localization in the spine before exocytosis or after endocytosis). This is of particular relevance for the research in the field of ASD since it is likely that the common

		Shank2 deficient mutants		*Shank3* deficient mutants	
		cell surface	synaptosome/ PSD preperation	cell surface	synaptosome/ PSD preperation
Cortex	$GABA_AR\alpha1$	↓	N/I[1-8]	N/S	N/I[1-8]
	GluA2	N/S	N/S[1] N/I[2-8]	N/S	N/S[1,6,8] N/I[2-5,7]
	GluN1	N/S	N/S[1] N/I[2-8]	N/S	↓[8] N/S[1,6,8] N/I[2-5,7]
	GluA1	N/S	N/S[1] N/I[2-8]	N/S	N/S[1,6,8] N/I[2-5,7]
	mGluR5	N/I	N/I[1-8]	N/I	N/I[1-8]
Striatum	$GABA_AR\alpha1$	N/S	N/I[1-8]	N/S	N/S[2] N/I[1,3-8]
	GluA2	N/S	↑[1] N/I[2-8]	↓	↓[2,3,5,6,8] N/S[1,8] N/I[4,7]
	GluN1	↓	↑[1] N/I[2-8]	↓	↓[3,8] N/S[1,2,5,6] N/I[4,7]
	GluA1	N/S	N/S[1] N/I[2-8]	(↓)	↓[3] N/S[1,2,5,6,8] N/I[4,7]
	mGluR5	N/I	N/I[1-8]	N/I	N/S[2] N/I[1,3-8]
Hippocampus	$GABA_AR\alpha1$	N/S	N/I[1-8]	N/S	N/S[2] N/I[1,3-8]
	GluA2	N/S	N/S[1] N/I[2-8]	N/S	N/S[1,7] N/I[2-6,8]
	GluN1	(↑)	↑[1] N/I[2-8]	N/S	N/S[1,7] N/I[2-6,8]
	GluA1	N/S	N/S[1] N/I[2-8]	↓	N/S[1,2,7] N/I[3-6,8]
	mGluR5	(↓)	N/I[1-8]	N/S	N/S[2] N/I[1,3-8]
Thalamus	$GABA_AR\alpha1$	↓	N/I[1-8]	N/S	N/I[1-8]
	GluA2	N/S	N/I[1-8]	↓	N/I[1-8]
	GluN1	(↓)	N/I[1-8]	↓	N/I[1-8]
	GluA1	N/I	N/I[1-8]	N/I	N/I[1-8]
	mGluR5	N/I	N/I[1-8]	N/I	N/I[1-8]
Cerebellum	$GABA_AR\alpha1$	N/S	N/I[1-8]	N/S	N/I[1-8]
	GluA2	↓	↓[1] N/I[2-8]	N/S	N/S[6] N/I[1-5,7,8]
	GluN1	N/I	N/I[1-8]	N/I	N/S[6] N/I[1-5,7,8]
	GluA1	N/I	↓[1] N/I[2-8]	N/I	↓[6] N/I[1-5,7,8]
	mGluR5	N/I	N/I[1-8]	N/I	N/I[1-8]

FIGURE 6 | Comparison of cell surface glutamate receptor subunit analysis with synaptosome/postsynaptic density (PSD) preparation analysis of glutamate receptors in ASD related brain regions in *Shank2* and *Shank3* deficient mice. Cell surface glutamate receptor subunit analysis and synaptosome/PSD preparation analysis reveals that the results of both methods do not necessarily show similar trends but both approaches usually generate converging data. [1]Refers to data from Schmeisser et al. (2012). [2]Refers to data from Peca et al. (2011). [3]Refers to data from Reim et al. (2017). [4]Refers to data from Peter et al. (2016). [5]Refers to data from Jaramillo et al. (2016). [6]Refers to data from Mei et al. (2016). [7]Refers to data from Kouser et al. (2013). [8]Refers to data from Zhou et al. (2016); note that in this study two different and *Shank3* deficient mice were analyzed. Cell surface refers to data from the current work: ↓ $p < 0.05$; (↓), (↑) $p < 0.10$. N/I stands for not investigated and N/S stands for non-significant results. Figure only shows data from brain regions/antibody detections which were addressed in this study. Upregulated ↑; downregulated ↓.

abnormality that all forms of ASD share might be alterations at the level of neuronal signaling/neuronal networks (Bourgeron, 2015; Mullins et al., 2016). The reader should, however, keep in mind that the biochemical experimental approach of our study does not allow a discrimination of neuronal subtypes, extrasynaptic and synaptic receptors or neurons and glia cells. And since e.g., astrocytes have been shown to express glutamate receptors (Spreafico et al., 1994; Seifert et al., 1997; Gallo and Ghiani, 2000; Verkhratsky and Kirchhoff, 2007) they, too, should be kept in mind when interpreting our data in terms of neuronal/network signaling and changes in the E/I balance (Hansson and Rönnbäck, 2003; Araque and Navarrete, 2010). In line with this, *Shank2* deficiency in defined neuronal cell types appears to change E/I (Kim et al., 2018), suggesting that neuron-type-specific effects of Shank deletions must be addressed in future work. Nonetheless, one should also bear in mind in this context that the striatum is somewhat of an exception since around 95% of striatal neurons are GABAergic medium sized spiny neurons (Yager et al., 2015). So in the case of the striatum our data may, indeed, represent receptor levels of a rather restricted number of neural cells and probably reflects receptor levels of medium sized spiny neurons to a large degree. Lastly, future work on ASD mouse models would greatly benefit from an experimental design which can distinguish between extrasynaptic and synaptic receptors since, e.g., extrasynaptic $GABA_A$ receptors have been shown to modulate epileptic seizures in mouse models by affecting tonic inhibition (Glykys and Mody, 2006; Heise et al., 2017) and it is known that ASD patients have an increased risk for developing epileptic seizures (Besag, 2018).

If one compares the data of this study with the available data of brain region specific synaptosome/PSD fraction analysis we find that in many cases the trends are similar, in others they are not (**Figure 6**). Thus, this study is also a cautionary note that one should be careful when inferring properties of synaptic signaling from synaptosomal/PSD fraction data. The best approach would be to combine synaptosome/PSD fraction analysis with biotinylation assays to get a more complete overview of the proteome at the synapse.

AUTHOR CONTRIBUTIONS

CH and JP carried out the majority of experiments and data analysis. Also, JS, CB, JK and RS helped in carrying out some of the experiments of this work. CH established the experimental design in the laboratory, carried out the literature research, wrote the manuscript and created the figures. MKas and JPB provided mice for the Cntn4 experiments and provided input to the manuscript. MK and TB designed the experiments, revised the text and provided expertise for the project.

FUNDING

TB is supported by grants from the Deutsche Forschungsgemeinschaft (DFG: SFB1149, TPA02), and BIU2 at Ulm University and by the Virtual Institute within the Helmholtz Gesellschaft ("RNA Dysmetabolism in ALS and FTD," VH-VI-510). MK is supported by grants from the DFG (Kr1879/5-1/6-1/SFB 779 TPB8), Bundesministerium für Bildung und Forschung (BMBF) "Energi" FKZ: 01GQ1421B, The EU Joint Programme—Neurodegenerative Disease Research (JPND) project STAD and the Leibniz Foundation (WGL—Pakt für Forschung). The research leading to these results has received funding from the People Programme (Marie Curie Actions) of the European Union's Seventh Framework Programme FP7/2007-2013/under REA grant agreement n° 289581 and received support from the Innovative Medicines Initiative Joint Undertaking under grant agreement n° 115300, resources of which are composed of financial contribution from the European Union's Seventh Framework Programme (FP7/2007-2013) and EFPIA companies' in kind contribution (EU-AIMS, n 115300).

ACKNOWLEDGMENTS

We thank Maria Manz for the outstanding technical support and we would like to thank Dr. Jürgen Bockmann for help with regards to mouse breeding. We would also like to thank Michael B. Lever for recommending the cell surface biotinylation protocol and Débora Garrido for providing information on Shank model comparison. We thank Dr. Yoshihiro Yoshihara for providing the *Cntn4*$^{-/-}$ mice.

SUPPLEMENTARY MATERIAL

The Supplementary Material for this article can be found online at: https://www.frontiersin.org/articles/10.3389/fnmol.2018.00212/full#supplementary-material

REFERENCES

Ameis, S. H., Fan, J., Rockel, C., Voineskos, A. N., Lobaugh, N. J., Soorya, L., et al. (2011). Impaired structural connectivity of socio-emotional circuits in autism spectrum disorders: a diffusion tensor imaging study. *PLoS One* 6:e28044. doi: 10.1371/journal.pone.0028044

Araque, A., and Navarrete, M. (2010). Glial cells in neuronal network function. *Philos. Trans. R. Soc. Lond. B Biol. Sci.* 365, 2375–2381. doi: 10.1098/rstb.2009.0313

Baudouin, S. J., Gaudias, J., Gerharz, S., Hatstatt, L., Zhou, K., Punnakkal, P., et al. (2012). Shared synaptic pathophysiology in syndromic and nonsyndromic rodent models of autism. *Science* 338, 128–132. doi: 10.1126/science.1224159

Becker, E. B., and Stoodley, C. J. (2013). Autism spectrum disorder and the cerebellum. *Int. Rev. Neurobiol.* 113, 1–34. doi: 10.1016/B978-0-12-418700-9.00001-0

Besag, F. M. (2018). Epilepsy in patients with autism: links, risks and treatment challenges. *Neuropsychiatr. Dis. Treat.* 14, 1–10. doi: 10.2147/NDT.s120509

Boeckers, T. M., Bockmann, J., Kreutz, M. R., and Gundelfinger, E. D. (2002). ProSAP/Shank proteins—a family of higher order organizing molecules of the postsynaptic density with an emerging role in human

neurological disease. *J. Neurochem.* 81, 903–910. doi: 10.1046/j.1471-4159.2002.00931.x

Bourgeron, T. (2015). From the genetic architecture to synaptic plasticity in autism spectrum disorder. *Nat. Rev. Neurosci.* 16, 551–563. doi: 10.1038/nrn3992

Christensen, D. L., Baio, J., Van Naarden Braun, K., Bilder, D., Charles, J., Constantino, J. N., et al. (2016). Prevalence and characteristics of autism spectrum disorder among children aged 8 years—autism and developmental disabilities monitoring network, 11 sites, united states, 2012. *MMWR Surveill. Summ.* 65, 1–23. doi: 10.15585/mmwr.ss6503a1

Elsabbagh, M., Divan, G., Koh, Y. J., Kim, Y. S., Kauchali, S., Marcin, C., et al. (2012). Global prevalence of autism and other pervasive developmental disorders. *Autism Res.* 5, 160–179. doi: 10.1002/aur.239

Fassio, A., Patry, L., Congia, S., Onofri, F., Piton, A., Gauthier, J., et al. (2011). SYN1 loss-of-function mutations in autism and partial epilepsy cause impaired synaptic function. *Hum. Mol. Genet.* 20, 2297–2307. doi: 10.1093/hmg/ddr122

Gallo, V., and Ghiani, C. A. (2000). Glutamate receptors in glia: new cells, new inputs and new functions. *Trends Pharmacol. Sci.* 21, 252–258. doi: 10.1016/s0165-6147(00)01494-2

Glykys, J., and Mody, I. (2006). Hippocampal network hyperactivity after selective reduction of tonic inhibition in $GABA_A$ receptor α5 subunit-deficient mice. *J. Neurophysiol.* 95, 2796–2807. doi: 10.1152/jn.01122.2005

Grabrucker, A. M., Schmeisser, M. J., Schoen, M., and Boeckers, T. M. (2011). Postsynaptic ProSAP/Shank scaffolds in the cross-hair of synaptopathies. *Trends Cell Biol.* 21, 594–603. doi: 10.1016/j.tcb.2011.07.003

Guilmatre, A., Huguet, G., Delorme, R., and Bourgeron, T. (2014). The emerging role of SHANK genes in neuropsychiatric disorders. *Dev. Neurobiol.* 74, 113–122. doi: 10.1002/dneu.22128

Habib, N., Li, Y., Heidenreich, M., Swiech, L., Avraham-Davidi, I., Trombetta, J. J., et al. (2016). Div-Seq: single-nucleus RNA-Seq reveals dynamics of rare adult newborn neurons. *Science* 353, 925–928. doi: 10.1126/science.aad7038

Hansson, E., and Rönnbäck, L. (2003). Glial neuronal signaling in the central nervous system. *FASEB J.* 17, 341–348. doi: 10.1096/fj.02-0429rev

Heise, C., Taha, E., Murru, L., Ponzoni, L., Cattaneo, A., Guarnieri, F. C., et al. (2017). eEF2K/eEF2 pathway controls the excitation/inhibition balance and susceptibility to epileptic seizures. *Cereb. Cortex* 27, 2226–2248. doi: 10.1093/cercor/bhw075

Jaramillo, T. C., Speed, H. E., Xuan, Z., Reimers, J. M., Liu, S., and Powell, C. M. (2016). Altered striatal synaptic function and abnormal behaviour in Shank3 Exon4–9 deletion mouse model of autism. *Autism Res.* 9, 350–375. doi: 10.1002/aur.1529

Jiang, Y. H., and Ehlers, M. D. (2013). Modeling autism by SHANK gene mutations in mice. *Neuron* 78, 8–27. doi: 10.1016/j.neuron.2013.03.016

Kaneko-Goto, T., Yoshihara, S., Miyazaki, H., and Yoshihara, Y. (2008). BIG-2 mediates olfactory axon convergence to target glomeruli. *Neuron* 57, 834–846. doi: 10.1016/j.neuron.2008.01.023

Kim, R., Kim, J., Chung, C., Ha, S., Lee, S., Lee, E., et al. (2018). Cell-type-specific Shank2 deletion in mice leads to differential synaptic and behavioral phenotypes. *J. Neurosci.* 38, 4076–4092. doi: 10.1523/JNEUROSCI.2684-17.2018

Kouser, M., Speed, H. E., Dewey, C. M., Reimers, J. M., Widman, A. J., Gupta, N., et al. (2013). Loss of predominant Shank3 isoforms results in hippocampus-dependent impairments in behavior and synaptic transmission. *J. Neurosci.* 33, 18448–18468. doi: 10.1523/JNEUROSCI.3017-13.2013

Laemmli, U. K. (1970). Cleavage of structural proteins during the assembly of the head of bacteriophage T4. *Nature* 227, 680–685. doi: 10.1038/227680a0

Leblond, C. S., Heinrich, J., Delorme, R., Proepper, C., Betancur, C., Huguet, G., et al. (2012). Genetic and functional analyses of SHANK2 mutations suggest a multiple hit model of autism spectrum disorders. *PLoS Genet.* 8:e1002521. doi: 10.1371/journal.pgen.1002521

Leblond, C. S., Nava, C., Polge, A., Gauthier, J., Huguet, G., Lumbroso, S., et al. (2014). Meta-analysis of SHANK mutations in autism spectrum disorders: a gradient of severity in cognitive impairments. *PLoS Genet.* 10:e1004580. doi: 10.1371/journal.pgen.1004580

Lundquist, J. J., and Dudek, S. M. (2006). Differential activation of extracellular signal-regulated kinase 1 and a related complex in neuronal nuclei. *Brain Cell Biol.* 35, 267–281. doi: 10.1007/s11068-008-9018-7

Mathis, D. M., Furman, J. L., and Norris, C. M. (2011). Preparation of acute hippocampal slices from rats and transgenic mice for the study of synaptic alterations during aging and amyloid pathology. *J. Vis. Exp.* 49:2330. doi: 10.3791/2330

Mei, Y., Monteiro, P., Zhou, Y., Kim, J. A., Gao, X., Fu, Z., et al. (2016). Adult restoration of Shank3 expression rescues selective autistic-like phenotypes. *Nature* 530, 481–484. doi: 10.1038/nature16971

Moessner, R., Marshall, C. R., Sutcliffe, J. S., Skaug, J., Pinto, D., Vincent, J., et al. (2007). Contribution of SHANK3 mutations to autism spectrum disorder. *Am. J. Hum. Genet.* 81, 1289–1297. doi: 10.1086/522590

Molenhuis, R. T., Bruining, H., Remmelink, E., de Visser, L., Loos, M., Burbach, J. P., et al. (2016). Limited impact of Cntn4 mutation on autism-related traits in developing and adult C57BL/6J mice. *J. Neurodev. Disord.* 8:6. doi: 10.1186/s11689-016-9140-2

Monteiro, P., and Feng, G. (2017). SHANK proteins: roles at the synapse and in autism spectrum disorder. *Nat. Rev. Neurosci.* 18, 147–157. doi: 10.1038/nrn.2016.183

Mullins, C., Fishell, G., and Tsien, R. W. (2016). Unifying views of autism spectrum disorders: a consideration of autoregulatory feedback loops. *Neuron* 89, 1131–1156. doi: 10.1016/j.neuron.2016.02.017

Oguro-Ando, A., Zuko, A., Kleijer, K. T. E., and Burbach, J. P. H. (2017). A current view on contactin-4, -5, and -6: implications in neurodevelopmental disorders. *Mol. Cell. Neurosci.* 81, 72–83. doi: 10.1016/j.mcn.2016.12.004

Osterhout, J. A., Stafford, B. K., Nguyen, P. L., Yoshihara, Y., and Huberman, A. D. (2015). Contactin-4 mediates axon-target specificity and functional development of the accessory optic system. *Neuron* 86, 985–999. doi: 10.1016/j.neuron.2015.04.005

Peca, J., Feliciano, C., Ting, J. T., Wang, W., Wells, M. F., Venkatraman, T. N., et al. (2011). Shank3 mutant mice display autistic-like behaviours and striatal dysfunction. *Nature* 472, 437–442. doi: 10.1038/nature09965

Peter, S., Ten Brinke, M. M., Stedehouder, J., Reinelt, C. M., Wu, B., Zhou, H., et al. (2016). Dysfunctional cerebellar Purkinje cells contribute to autism-like behaviour in Shank2-deficient mice. *Nat. Commun.* 7:12627. doi: 10.1038/ncomms12627

Pinto, D., Pagnamenta, A. T., Klei, L., Anney, R., Merico, D., Regan, R., et al. (2010). Functional impact of global rare copy number variation in autism spectrum disorders. *Nature* 466, 368–372. doi: 10.1038/nature09146

Provenzano, G., Zunino, G., Genovesi, S., Sgadó, P., and Bozzi, Y. (2012). Mutant mouse models of autism spectrum disorders. *Dis. Markers* 33, 225–239. doi: 10.3233/DMA-2012-0917

Rapin, I. (1997). Autism. *N. Engl. J. Med.* 337, 97–104. doi: 10.1056/NEJM199707103370206

Reim, D., Distler, U., Halbedl, S., Verpelli, C., Sala, C., Bockmann, J., et al. (2017). Proteomic analysis of post-synaptic density fractions from Shank3 mutant mice reveals brain region specific changes relevant to autism spectrum disorder. *Front. Mol. Neurosci.* 10:26. doi: 10.3389/fnmol.2017.00026

Sala, C., Piëch, V., Wilson, N. R., Passafaro, M., Liu, G., and Sheng, M. (2001). Regulation of dendritic spine morphology and synaptic function by Shank and Homer. *Neuron* 31, 115–130. doi: 10.1016/s0896-6273(01)00339-7

Sala, C., Rudolph-Correia, S., and Sheng, M. (2000). Developmentally regulated NMDA receptor-dependent dephosphorylation of cAMP response element-binding protein (CREB) in hippocampal neurons. *J. Neurosci.* 20, 3529–3536. doi: 10.1523/JNEUROSCI.20-10-03529.2000

Schmeisser, M. J., Ey, E., Wegener, S., Bockmann, J., Stempel, A. V., Kuebler, A., et al. (2012). Autistic-like behaviours and hyperactivity in mice lacking ProSAP1/Shank2. *Nature* 486, 256–260. doi: 10.1038/nature11015

Schuetze, M., Park, M. T., Cho, I. Y., MacMaster, F. P., Chakravarty, M. M., and Bray, S. L. (2016). Morphological alterations in the thalamus, striatum, and pallidum in autism spectrum disorder. *Neuropsychopharmacology* 41, 2627–2637. doi: 10.1038/npp.2016.64

Schwenk, J., Baehrens, D., Haupt, A., Bildl, W., Boudkkazi, S., Roeper, J., et al. (2014). Regional diversity and developmental dynamics of the AMPA-receptor proteome in the mammalian brain. *Neuron* 84, 41–54. doi: 10.1016/j.neuron.2014.08.044

Seifert, G., Rehn, L., Weber, M., and Steinhauser, C. (1997). AMPA receptor subunits expressed by single astrocytes in the juvenile mouse hippocampus. *Mol. Brain Res.* 47, 286–294. doi: 10.1016/s0169-328x(97)00059-4

Spreafico, R., Frassoni, C., Arcelli, P., Battaglia, G., Wenthold, R. J., and De Biasi, S. (1994). Distribution of AMPA selective glutamate receptors in the thalamus of adult rats and during postnatal development. A light and ultrastructural immunocytochemical study. *Dev. Brain Res.* 82, 231–244. doi: 10.1016/0165-3806(94)90166-x

Tasic, B., Menon, V., Nguyen, T. N., Kim, T. K., Jarsky, T., Yao, Z., et al. (2016). Adult mouse cortical cell taxonomy revealed by single cell transcriptomics. *Nat. Neurosci.* 19, 335–346. doi: 10.1038/nn.4216

Tuchman, R., and Rapin, I. (2002). Epilepsy in autism. *Lancet Neurol.* 1, 352–358. doi: 10.1016/S1474-4422(02)00160-6

Verkhratsky, A., and Kirchhoff, F. (2007). NMDA receptors in glia. *Neuroscientist* 13, 28–37. doi: 10.1177/1073858406294270

Vicidomini, C., Ponzoni, L., Lim, D., Schmeisser, M. J., Reim, D., Morello, N., et al. (2017). Pharmacological enhancement of mGlu5 receptors rescues behavioral deficits in SHANK3 knock-out mice. *Mol. Psychiatry* 22:784. doi: 10.1038/mp.2016.70

Whitehead, G., Jo, J., Hogg, E. L., Piers, T., Kim, D. H., Seaton, G., et al. (2013). Acute stress causes rapid synaptic insertion of Ca^{2+} -permeable AMPA receptors to facilitate long-term potentiation in the hippocampus. *Brain* 136, 3753–3765. doi: 10.1093/brain/awt293

Won, H., Lee, H. R., Gee, H. Y., Mah, W., Kim, J. I., Lee, J., et al. (2012). Autistic-like social behaviour in Shank2-mutant mice improved by restoring NMDA receptor function. *Nature* 486, 261–265. doi: 10.1038/nature11208

Yager, L. M., Garcia, A. F., Wunsch, A. M., and Ferguson, S. M. (2015). The ins and outs of the striatum: role in drug addiction. *Neuroscience* 301, 529–541. doi: 10.1016/j.neuroscience.2015.06.033

Zhou, Y., Kaiser, T., Monteiro, P., Zhang, X., Van der Goes, M. S., Wang, D., et al. (2016). Mice with Shank3 mutations associated with ASD and schizophrenia display both shared and distinct defects. *Neuron* 89, 147–162. doi: 10.1016/j.neuron.2015.11.023

Zikopoulos, B., and Barbas, H. (2013). Altered neural connectivity in excitatory and inhibitory cortical circuits in autism. *Front. Hum. Neurosci.* 7:609. doi: 10.3389/fnhum.2013.00609

Conflict of Interest Statement: The authors declare that the research was conducted in the absence of any commercial or financial relationships that could be construed as a potential conflict of interest.

frontiers in Molecular Neuroscience

REVIEW
published: 19 July 2018
doi: 10.3389/fnmol.2018.00240

Distinct Phenotypes of *Shank2* Mouse Models Reflect Neuropsychiatric Spectrum Disorders of Human Patients With *SHANK2* Variants

Ahmed Eltokhi[1,2,3], *Gudrun Rappold*[2] *and Rolf Sprengel*[1,3]*

[1]*Max Planck Research Group "Molecular Neurobiology", Max Planck Institute for Medical Research, Heidelberg, Germany,*
[2]*Department of Human Molecular Genetics, Institute of Human Genetics, Heidelberg University, Heidelberg, Germany,*
[3]*Institute for Anatomy and Cell Biology, Heidelberg University, Heidelberg, Germany*

The SHANK scaffolding proteins are important organizers for signaling proteins in the postsynapse of excitatory neurons. The functional significance of SHANK proteins becomes apparent by the wide spectrum of neurodevelopmental and neuropsychiatric disorders associated with *SHANK* variants in human patients. A similar diversity of neuropsychiatric-like phenotypes is described for numerous *Shank2* and *Shank3* knockout (KO) mouse lines. In this review, we will focus on and discuss the experimental results obtained from different, but genetically related and therefore comparable, *Shank2* mouse models. First, we will describe the distinct *SHANK2* variant-mediated neurodevelopmental and neuropsychiatric disorders in human patients. Then we will discuss the current knowledge of the expressed SHANK2 isoforms in the mouse, and we will describe the genetic strategies used for generating three conventional and seven conditional *Shank2* mouse lines. The distinct impairments i.e., autistic-like and mania-like behavior and the alterations on the molecular, electrophysiological and behavioral levels will be compared between the different *Shank2* mouse models. We will present our view as to why in these mouse models a spectrum of phenotypes can arise from similar *Shank2* gene manipulations and how *Shank2* mutant mice can be used and should be analyzed on the behavioral level in future research.

Keywords: SHANK2 domains, SHANK2 isoforms, *SHANK2* gene variants, autism spectrum disorder, intellectual disability, schizophrenia, *Shank2* knockout mice, behavioral tests

OPEN ACCESS

Edited by:
Eunjoon Kim,
Institute for Basic Science (IBS), South Korea

Reviewed by:
Andreas Martin Grabrucker, University of Limerick, Ireland
Chiara Verpelli, Istituto di Neuroscienze (IN), Italy

***Correspondence:**
Rolf Sprengel
rolf.sprengel@mpimf-heidelberg.mpg.de

Received: *31 March 2018*
Accepted: *21 June 2018*
Published: *19 July 2018*

Citation:
Eltokhi A, Rappold G and Sprengel R (2018) Distinct Phenotypes of Shank2 Mouse Models Reflect Neuropsychiatric Spectrum Disorders of Human Patients With SHANK2 Variants. Front. Mol. Neurosci. 11:240. doi: 10.3389/fnmol.2018.00240

INTRODUCTION

Gene variants of the multi-domain postsynaptic scaffolding proteins included in the SHANK family (also known as ProSAP) are significantly associated with autism spectrum disorders (ASD). After the first publication of a *SHANK3* variant in human patients with ASD (Durand et al., 2007), numerous studies confirmed the close link between *SHANK* variants and ASD and intellectual disability (ID; see https://gene.sfari.org). In humans, three different genes, *SHANK 1*, *2* and *3* produce several SHANK isoforms via internal promoters and alternative splice products

(Lim et al., 1999; for review see Sala et al., 2015). SHANK proteins are master scaffolding proteins in the postsynapse of excitatory neurons. There, they are critically involved in the morphogenesis of spines (Sala et al., 2001). Within the spine, SHANK proteins form a net-like matrix structure (Baron et al., 2006; Hayashi et al., 2009) that serves as a scaffold for the organization of other postsynaptic proteins including N-methyl-D-aspartate receptors (NMDAR), L-α-amino-3-hydroxy-5-methyl-4-isoxazolepropionic acid receptors (AMPAR) and the metabotropic glutamate receptors (mGluRs; Sheng and Kim, 2011; Jacob and Weinberg, 2015; for review see Verpelli et al., 2012). The longest isoforms of SHANK1–3 contain several protein-protein interaction sites: the N-terminal ankyrin repeat-containing (ANK) domain, the Src homology 3 (SH3) domain, the PSD-95/Discs large/zona occludens (PDZ) domain, the proline-rich region (PRR) and the sterile alpha motif (SAM) in the C-terminal domain. The N-terminal ANK domain interacts with the cytoskeletal protein alpha-fodrin (Böckers et al., 2001) and the SH3 domain binds to glutamate receptor-interacting protein (GRIP), which is important for AMPAR trafficking (Lu and Ziff, 2005). The PDZ site in SHANKs can bind to the adaptor protein guanylate kinase-associated protein (GKAP; Naisbitt et al., 1999). GKAP itself can bind to the postsynaptic density molecule 95 (PSD95; Naisbitt et al., 1997) that is in contact with the glutamate gated ion channels, NMDAR (Kornau et al., 1995) and AMPAR (Kim et al., 2001; Uemura et al., 2004; for review see Boeckers et al., 2002). Most clearly the interaction of SHANK and Homer proteins via the PRR was noted (Naisbitt et al., 1999; Tu et al., 1999). This interaction allows the coupling of mGluRs to Ca^{2+} release from endoplasmic reticulum (ER) in the postsynaptic density. Cortactin, a molecule involved in actin polymerization, was also shown to bind to PRR (Ammer and Weed, 2008). The C-terminal SAM domain serves as a Zn^{2+} dependent dimerization domain for SHANKs (Baron et al., 2006; Gundelfinger et al., 2006).

This complex multidomain structure of the SHANK proteins and the diversity of SHANK1–3 isoforms might be one reason for the broad spectrum of *SHANK* variant-associated neurodevelopmental and neuropsychiatric disorders. Distinct *SHANK* mutations can yield different protein products, with a specific combination of protein domains, different from that of the WT protein. This, in turn, can affect the potential protein-protein interactions, thus altering the role of the protein in neurons. In ASD patients, chromosomal deletions, translocations, gene duplications, gene fragment deletions and coding mutations in all three *SHANK* genes were identified (see https://gene.sfari.org) but the simple haploinsufficiency caused by the mutation is unlikely to explain the broad spectrum of phenotypes. In order to dissect the causal link between *SHANK* variants and the underlying molecular mechanisms of neurodevelopmental and neuropsychiatric disorders, numerous mouse models for *"shankopathies"* were generated (**Table 1**, **Figure 1**). For SHANK3, 14 mouse lines, generated with different gene-targeted strategies, are published (**Figure 1**). Interestingly, the behavioral analysis of the *Shank3* knockout (KO) mouse lines revealed differences in social and repetitive behavior as well as in cognitive functions, similar to the distinct neuropsychiatric phenotypes of different patients. These behavioral inconsistencies were explained partially by the residual SHANK3 isoforms that could be expressed from the targeted *Shank3* gene in mice (Bozdagi et al., 2010; Peca et al., 2011; Yang et al., 2012) as discussed in detail in a recent review (Monteiro and Feng, 2017). However, in all 10 different *Shank2* KO mouse lines, the gene KO strategies were very similar leading to protein products truncated within the PDZ domain or the PRR, both present in all SHANK2 isoforms of the WT mice (**Figure 1**). Nevertheless, the phenotype of the three conventional and seven conditional *Shank2* KO mouse lines diverged between the different lines. This phenotypic variability is reminiscent of the fact that in human patients, *SHANK2* variants are not only significantly associated with ASD or ID, but also with schizophrenia (SCZ), a correlation that cannot be stated as strong for *SHANK3* variants (Peykov et al., 2015; Homann et al., 2016; de Sena Cortabitarte et al., 2017).

TABLE 1 | Genetically modified mouse lines encoding gene-targeted mutations of endogenous *Shank* genes and one transgenic mouse line expressing a SHANK3-GFP that are made available to public in the mouse genome informatics database (http://www.informatics.jax.org).

SHANK1	SHANK3	
Shank1$^{Gt(E055G03)Wrst}$	*Shank3*$^{tm1a(KOMP)Mbp}$	*Shank3*^{tm1Yhj}
Shank1$^{Gt(E127E12)Wrst}$	*Shank3*$^{tm1c(KOMP)Mbp}$	*Shank3*$^{tm1.1Yhj}$
Shank1$^{Gt(IST12658A7)Tigm}$	*Shank3*$^{tm1d(KOMP)Mbp}$	*Shank3*$^{tm1.2Yhj}$
Shank1^{tm1Shng}	*Shank3*$^{tm1e(KOMP)Mbp}$	*Shank3*^{tm1Geno}
	Shank3$^{tm1a(KOMP)Wtsi}$	*Shank3*$^{tm1.1Geno}$
SHANK2	*Shank3*$^{tm1e(KOMP)Wtsi}$	*Shank3*^{tm1Gfng}
Shank2$^{Gt(OST148685)Lex}$	*Shank3*$^{tm1.1Bux}$	*Shank3*^{tm2Gfng}
Shank2$^{tm1.1Bcgen}$	*Shank3*$^{tm1.2Bux}$	*Shank3*$^{tm3.1Gfng}$
Shank2^{tm1Tmb}	*Shank3*$^{tm1.1Pfw}$	*Shank3*$^{tm4.1Gfng}$
Shank2$^{tm1.1Tmb}$	*Shank3*^{tm1Cmpl}	*Shank3*$^{tm5.1Gfng}$
Shank2^{tm1Mgle}	*Tg*$^{(Shank3-EGFP)1Hzo}$	

Mouse lines in blue are not published but commercially available.

SHANK2 GENE VARIANTS IN NEURODEVELOPMENTAL AND NEUROPSYCHIATRIC DISORDERS

After the first identification of *SHANK2* gene mutations in patients with ASD and ID (Berkel et al., 2010), several other publications described further variations in the *SHANK2* gene locus in patients with neuropsychiatric disorders. They identified *SHANK2* variations including truncations, missense mutations, gene deletions and mutations in the *SHANK2* promoter regions; all of these findings solidified the causal link of *SHANK2* variants to ASD and ID (Pinto et al., 2010; Wischmeijer et al., 2011; Leblond et al., 2012, 2014; Prasad et al., 2012; Chilian et al., 2013; Schluth-Bolard et al., 2013; Bowling et al., 2017; Yuen et al., 2017). Interestingly, an association between *SHANK2* gene mutations and SCZ was described in Peykov et al. (2015). By sequencing the *SHANK2* gene in 481 SCZ patients and 659 unaffected individuals, Peykov et al. (2015) identified several non-synonymous variants exclusively in SCZ patients (Supplementary Table S1). This association was confirmed by

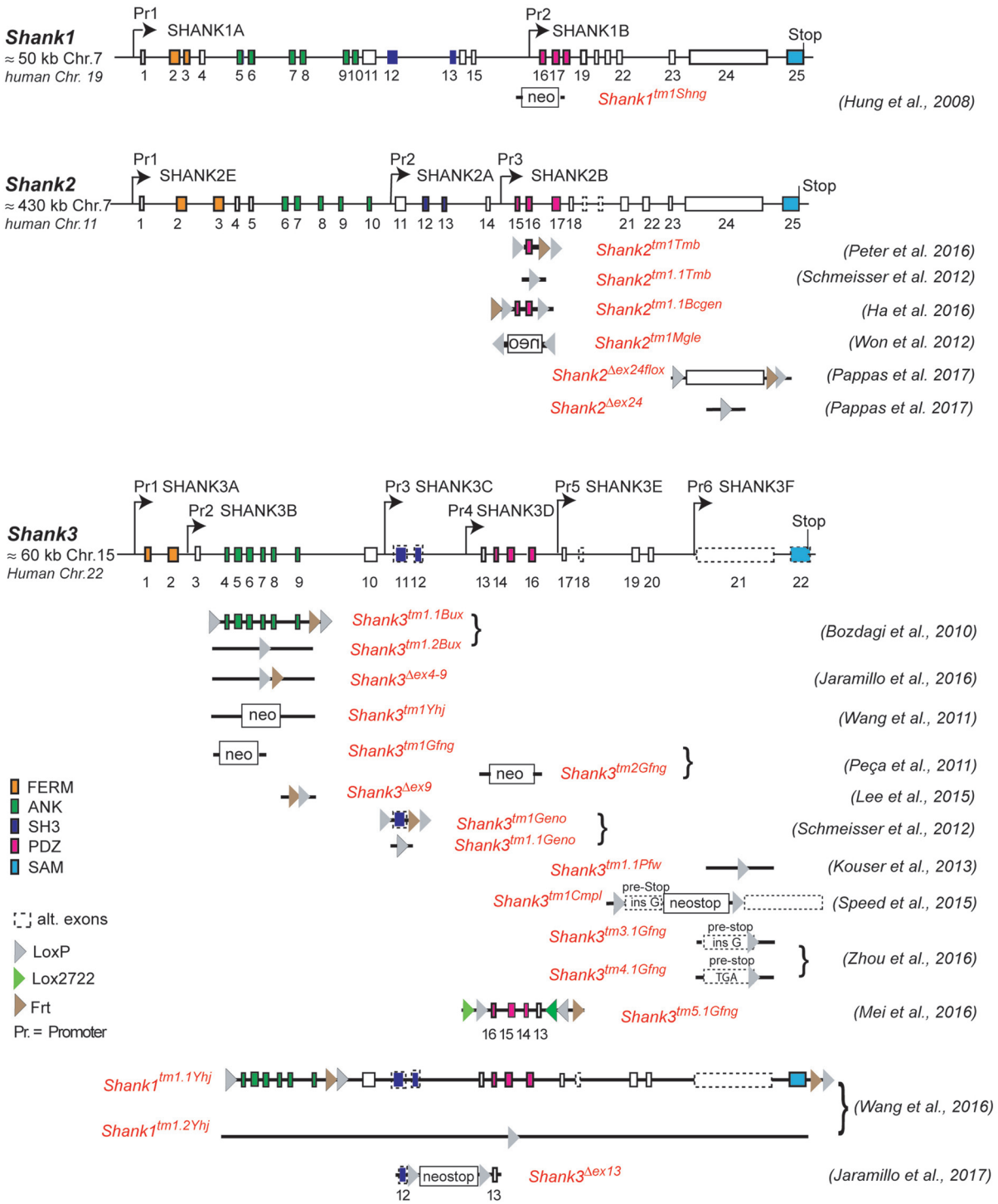

FIGURE 1 | Gene structure and gene segment deletions in gene-targeted *Shank* mouse models. Structures of the mouse *Shank1*, *Shank2* and *Shank3* genes are depicted. Exons are given in rectangles; alternative spliced exons are in dashed lines. Positions of promoters (Pr) for the expression of the different isoforms of the *Shank1–3* gene loci are indicated. Positions of the neomycin (neo) selection marker, loxP, lox2722 and Frt sites in the targeted alleles are indicated. Targeted gene segments flanked by two loxP or two lox2722 elements can be removed or inverted by tissue-specific expression of Cre to generate a conditional *Shank* knockout (KO) or *Shank* knockin mouse models. neo = selection marker, sense orientation; oen = neo selection marker, reverse orientation. References for the first publication of the mouse lines are given. FERM (F for 4.1 protein, E for ezrin, R for radixin and M for moesin), ANK (ankyrin repeat domain), SH3 (Src homology 3), PDZ (PSD-95/Discs large/zona occludens), SAM (sterile alpha motife). (Hung et al., 2008; Bozdagi et al., 2010; Peca et al., 2011; Wang et al., 2011, 2016; Schmeisser et al., 2012; Won et al., 2012; Kouser et al., 2013; Lee J. et al., 2015; Speed et al., 2015; Ha et al., 2016; Jaramillo et al., 2016, 2017; Mei et al., 2016; Peter et al., 2016; Zhou et al., 2016; Pappas et al., 2017).

a study reporting seven siblings in a family with SCZ spectrum disorders carrying a missense variant in the *SHANK2* gene (Homann et al., 2016).

How Divergent Phenotypes Can Arise From Different *SHANK2* Variants

Mutations in Different Protein Interaction Domains

As outlined above, the comprehensive analysis of patients harboring *SHANK2* alterations with neurodevelopmental and neuropsychiatric disorders revealed a wide range of phenotypic expression, with various symptoms of ASD, ID, and SCZ. Moreover, the severity of *SHANK2*-associated disorders and cognitive deficiency is highly variable among patients. Imprecise clinical diagnoses and the clinical data from different clinics might explain this inconsistency. However, the *SHANK2* variants as such also need to be considered as one reason for such variability. Different mutations in the *SHANK2* gene can lead to increased or decreased expression of the SHANK2 protein, dysfunctional SHANK2 protein domains or truncated protein products lacking protein interaction domains. This can, in turn, alter protein-protein interactions and the organization of the postsynaptic protein network. Therefore, different *SHANK2* mutations can lead to different alterations in molecular and cellular processes in the neurons, resulting in a wide range of behavioral phenotypes.

This perspective finds support in the rescue experiment of SHANK2 knockdown by overexpression of human SHANK2 variants in rat primary cultures (Berkel et al., 2012). The SHANK2A(R462X) variant accumulated in the soma and the dendrites, whereas overexpressed SHANK2A-WT selectively located in dendritic spines (Berkel et al., 2012). The SHANK2A(T1127M) and SHANK2A(L1008_P1009dup) variants were confined into synapses with lower SHANK2A immunosignal compared to SHANK2A-WT (Berkel et al., 2012), indicating that various mutations can lead to a decrease in the total final amount of SHANK2A present at the synapse, which could be an important factor in the pathophysiology of the neuropsychiatric disorder. Furthermore, the dendritic spine volume was only significantly increased by the overexpression of SHANK2A-WT, whereas all three SHANK2A variants (R462X, T1127M, L1008_P1009dup) did not have the potential to increase the spine volume. Similarly, the SHANK2 knockdown, which provoked a reduced spine volume, an increased number of immature spines and a dendritic complexity near the cell body, was rescued to different degrees when SHANK2A variants were co-expressed with the SHANK2 knockdown shRNA in rat primary neurons thus suggesting a dosage effect in the case of SHANK2. The SHANK2A-WT and SHANK2A(L1008_P1009dup) were able to rescue the dendritic spine and the dendritic arbor development but SHANK2A(R462X) and SHANK2A(T1127M) could not rescue the reduced spine volume. Consistently, SHANK2A(R462X) failed to rescue the enhanced growth of dendrites to a normal level, whereas the SHANK2A(T1127M) and SHANK2A(L1008_P1009dup) were able to rescue the phenotype similar to the SHANK2A-WT. From these cell culture studies, it can be concluded that the *SHANK2* gene is involved in at least two separate functions: the control of dendrite morphology and the regulation of spine size.

Genetic and Epigenetic Modulations

In addition to the nature of *SHANK2* variants, other genetic, epigenetic and environmental factors have a strong influence on the expression of the *SHANK2* variant-mediated neuropsychiatric disorders. For example, the same *SHANK2* variants were found in patients with different clinical features (**Table 2**). SHANK2(K535R) and SHANK2(P587S) variants were each identified in one ASD patient and in one patient with ID (Berkel et al., 2010). Similarly, SHANK2(A577V), previously misnamed as A578V, was associated with different characteristics of SCZ spectrum disorders in seven brothers (Homann et al., 2016). SHANK2(S610Y) was found in two patients: one with ID and the other with catatonic SCZ (Berkel et al., 2010; Peykov et al., 2015). The SHANK2(A1731S) variant was present in four patients with different subtypes of SCZ spectrum disorders (Peykov et al., 2015). In addition, some synonymous variants appear in patients with ASD, ID and SCZ, but not in healthy controls (Berkel et al., 2010; Rauch et al., 2012;

TABLE 2 | Five single point mutations in the coding region (c.) of the *SHANK2* gene leading to five amino acid residue exchanges (p.) that are associated with different neuropsychiatric disorders.

Point mutation	Amino acid residue exchange	Number of patients	Diagnosis	Transmission source	References
c.1604A >G	p.K535R	2	1 ASD	n.a	Berkel et al. (2010)
			1 ID	n.a	
c.1730C >T	p.A577V	7	5 SCZ	Mother	Homann et al. (2016)
			1 Schizotypal personality	Mother	
			1 Schizoaffective	Mother	
c.1759C >T	p.P587S	2	1 Autism	Mother	Berkel et al. (2010)
			1 ID	n.a	
c.1829C >A	p.S610Y	2	1 Catatonic SCZ	n.a	Berkel et al. (2010)
			1 ID with Autistic features	Father	Peykov et al. (2015)
c.5191G >T	p.A1731S	4	3 Paranoid SCZ	Mother	Peykov et al. (2015)
			1 Disorganized SCZ	Mother	

ASD, Autism spectrum disorder; ID, Intellectual disability; SCZ, Schizophrenia; n.a., not available. (NCBI reference sequence: NM_012309.4; for the full list of identified SHANK2 variants in patients, see supplementary information).

Peykov et al., 2015; Supplementary Table S1). The influence of other genes on the phenotypic expression of the *SHANK2* variants became most obvious in patients with an inherited *SHANK2* variant-associated ASD or SCZ, which had not been diagnosed in their parents. The aforementioned SHANK2(A577V) variant found in seven schizophrenic male brothers, for example, was inherited from a healthy mother (Homann et al., 2016). This was also the case for five different SHANK2 variants: T438M, P1144L, V1608I, L1646M and A1731S (Peykov et al., 2015) and for several other variants identified in ASD patients (Supplementary Table S1) suggesting that sexually dimorphic pathways have an effect on the penetrance of these variants. Together, all these findings strongly support the proposed multiple hit model of neurodevelopmental and neuropsychiatric disorders (Leblond et al., 2012). Additionally, epigenetic factors most likely affect the penetrance of *SHANK2* variants. A DNA hypermethylation value of 5 CpG positions within the *SHANK2* gene was found in a male patient with ID and developmental delay (Kolarova et al., 2015), suggesting that *SHANK2* expression is sensitive to the DNA methylation pattern. Other epigenetic mechanisms such as histone acetylation are expected to regulate the expression of the *SHANK2* gene in an isoform-specific manner. Furthermore, one long non-coding variant associated to *SHANK2* has been found to be up-regulated in blood samples of ASD patients (Wang et al., 2015).

SHANK2 ISOFORMS IN MICE

For the design and the possible impact of *Shank2* gene manipulation in mice, the detailed knowledge of the different SHANK2 isoforms and their expression pattern in the mouse brain is a prerequisite. As *Shank1–3* can express many different SHANK isoforms using several promoters and alternative splicing (**Figure 1**), the different SHANK isoforms are proposed to have different functions during developmental stages (Jiang and Ehlers, 2013). According to the NCBI database, 21 putative isoforms are predicted to be expressed by the *Shank2* gene locus on chromosome 7 in mice. Cloned rat cDNAs for the SHANK2 isoforms, SHANK2E, SHANK2A and SHANK2B, provide experimental evidence that these three isoforms are differentially expressed in the rat brain (**Figure 2**; Boeckers et al., 1999a,b; Han et al., 2006). Three different promoters are recruited for the expression of SHANK2E, SHANK2A and SHANK2B. The 5' located promoter is used to generate the largest isoform, SHANK2E. The SHANK2E encoding transcript contains a 5'-untranslated exon, which is designated as exon 1. The promoters for the initiation of *Shank2a* and *Shank2b* transcripts are located in introns 10 and 14, respectively. For the translation of *Shank2a* and *Shank2b* transcripts, intron-located translational start codons open the translational reading frames (**Figure 2**).

The mouse *Shank2* gene contains 25 exons. The alternative splicing of exon 19, 20 and 23 and the internal alternative splice donor site in exon 22 can lead to additional isoforms of SHANK2E, SHANK2A and SHANK2B. Using rat brain and human brain-derived cDNAs, the presence and absence of the alternatively spliced *Shank2a* exons were experimentally verified in rats and humans. The transcripts with exons 19, 20 and 23 seem to be underrepresented in peripheral tissues, whereas they seem to be dominantly expressed in the brain (Böckers et al., 2004; Leblond et al., 2012). It is important to mention that the short SHANK2C isoform, which is obtained by an alternative splicing event of exon 22 in humans (Leblond et al., 2012), cannot be detected in the transcriptom of mice and rats. The description of the presence or absence of exon 19 and 20 in the NCBI database-predicted 21 SHANK2 isoforms in mice is inconsistent and needs to be verified. This might explain why different numbers of exons in the *Shank2* gene loci are given in different genome browsers (e.g., in Ensemble: ENSMUSG00000037541, the mouse *Shank2* gene is composed of 23 exons).

As shown in **Figure 2**, SHANK2E is the full-length SHANK2 isoform containing an ANK domain, SH3 domain, PDZ domain, PRR and SAM domain, which is located on the SHANK2 C-terminal synaptic targeting elements (Böckers et al., 2004; Boeckers et al., 2005). In the brain, SHANK2E is expressed at different levels in different regions with the highest expression in the cerebellum (Leblond et al., 2012). The shortest SHANK2 isoform, SHANK2B (named as SHANK2C in Monteiro and Feng, 2017), contains just the PDZ, PRR and SAM domains (**Figure 2**). As determined by mRNA analysis in humans and rats, *SHANK2* expression is strongest in the brain, but *SHANK2* mRNA can also be PCR-amplified in most peripheral tissues with the exception of skeletal muscles and heart (Leblond et al., 2012). The *SHANK2B* RT-PCR products confirmed the differential *SHANK2B* expression in all human brain regions (Leblond et al., 2012), a finding that had already been well documented in rats by classical *in situ* RNA hybridization studies showing brain region-specific as well as developmentally controlled expression of SHANK1–3 (Böckers et al., 2004). According to this study, SHANK2 is co-expressed with SHANK1 during the early days of development, whereas SHANK3 reaches its maximum expression at postnatal day P16. By using the laminar organization of the cerebellum and the hippocampus, the authors showed convincingly that: (i) *Shank1* and *Shank2* mRNA co-exist in Purkinje cells (PCs) and their dendrites, whereas *Shank3* mRNA was found only in the cerebellar granular cells; and (ii) *Shank2* mRNA expression in the hippocampus is restricted to the cell layer of principal neurons, while the signals for the *Shank1* and *Shank3* mRNA can be detected in the molecular layers as well (Böckers et al., 2004).

In biochemical studies using rats, SHANK2 and SHANK3 seemed to be essential elements for the proper organization of the PSD. They localize to the PSD via their SAM domain and interactions with Zn^{2+} ions, which can be enhanced by the activity and synaptic release of Zn^{2+}. In contrast, SHANK1 is recruited to the PSD by a pre-formed scaffold via its PDZ domain (Baron et al., 2006; Gundelfinger et al., 2006; Grabrucker et al., 2011). Thus, all SHANKs can respond to activity and synaptic events that might underlie learning and memory. However, SHANK1 is lacking the capability to localize to immature/inactive synapses, which

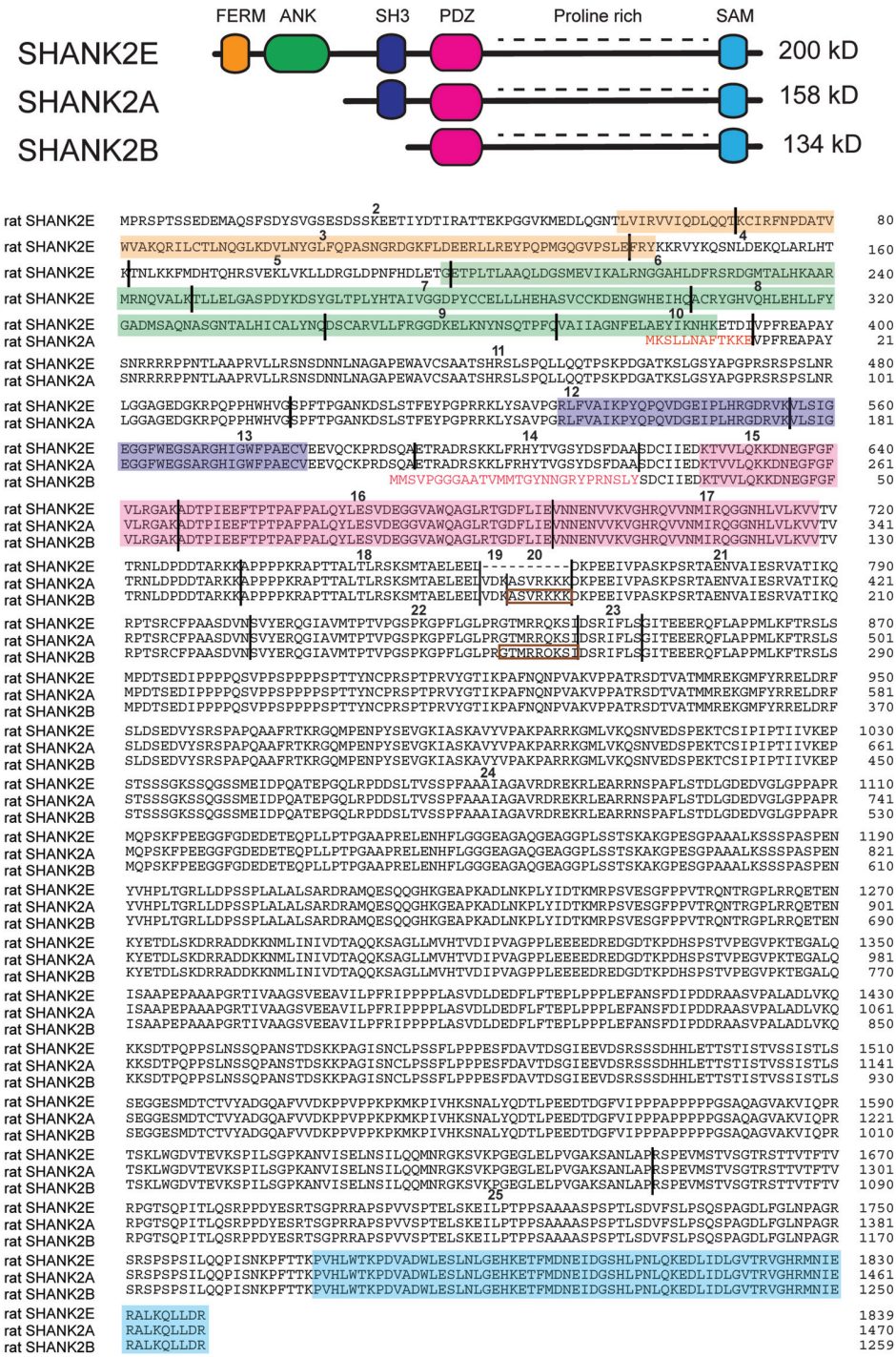

FIGURE 2 | SHANK2 isoforms in the rat evaluated by direct cDNA cloning. (Top) Schematic view of different conserved protein domains in SHANK2 isoforms. (Bottom) Amino acid residue sequence alignment of the SHANK2E (AY298755; Han et al., 2006), SHANK2A (AJ249562; Boeckers et al., 1999a) and SHANK2B (AF060116 or AJ131899; Du et al., 1998; Boeckers et al., 1999b) isoforms. (Bottom) Amino acid residue sequence alignment of the SHANK2E (AY298755; Han et al., 2006), SHANK2A (AJ249562; Boeckers et al., 1999a) and SHANK2B (AF060116 or AJ131899; Du et al., 1998; Boeckers et al., 1999b) isoforms. The SHANK2 protein domains are color-coded. The positions of the introns in the coding regions are indicated by vertical black lines. Exons are numbered starting with exon 2 as the first translated exon. N-terminal amino acid residues of isoform A and B are given in red. The sequences inside the brown rectangles are absent in some other *Shank2* transcripts. The N-terminal sequence of isoform A is encoded by the three terminal end of intron 10. The N-terminal sequence of isoform B is encoded in intron 14. Isoform C which is found in humans cannot be detected in mouse or rat mRNAs.

seems to be SAM domain/Zn^{2+}-dependent (Schmeisser and Verpelli, 2016). During neuronal development, the subcellular distribution of SHANK2 proteins changes and immunoelectron microscopy studies revealed that SHANK2 accumulation shifts in the developing, cortical nuerons. At postnatal day P5, SHANK is accumulated in the lamellipodium, then shifts into the cytoplasm of the cell bodies and in the growing neurites at P8, and finally to the PSD at P10, which supports the idea that it may play a role in multiple cell biological frameworks of neurons (Boeckers et al., 1999a). Interestingly, on the electrophysiological level, SHANK1 and SHANK2, but not SHANK3 virus-mediated knockdown reduced the number of spines and the AMPAR responses at CA3-to-CA1 synapses in acute hippocampal slice cultures (Shi et al., 2017). Due to this functional divergence of SHANK proteins, it is not surprising that in ASD patients, *SHANK2* and *SHANK3* mutations are over-represented (Leblond et al., 2014).

MODELING *SHANK2* MUTATIONS IN MICE

The multiple genetic, epigenetic and environmental factors affecting the phenotypic expression of ASD and SCZ disorders are a major issue when we try to understand the molecular, anatomical, physiological and behavioral phenotypes of *SHANK2* variants. Analyzing genetically comparable inbred mice should at least minimize the environmental and epigenetic components when mice are raised and housed under comparable conditions. Observations of male and female single-housed or cohort-housed mice with identical or mixed genotypes, and either with conditional gene deletions or gene overexpression, offer multiple options to investigate different aspects of the neurodevelopmental and neuropsychiatric disorders in an animal model. Already in 2007, Crawley and Tordjman proposed several behavioral tasks that are suitable for the analysis of autistic behavior in mice (Crawley, 2007; Tordjman et al., 2007).

Distinct Phenotypes of the Different *Shank2* Knockout Mice

The proposal of Crawley and Tordjman likely promoted the generation of several gene-targeted mutations in mice modeling human *SHANK1, 2* and *3* mutations-associated ASD (**Figure 1**). In 2012, the first two *Shank2* KO mouse models ($Shank2^{-/-}$) were generated. Both mouse models resembled two PDZ domain-microdeletions found in two human patients (Berkel et al., 2010). Mice of both lines showed comparable cognitive and social impairments. In $Shank2^{\Delta ex16}$ mice (named $Shank2^{\Delta ex7}$), exon 16 was deleted (Schmeisser et al., 2012). In $Shank2^{\Delta ex15-16}$ mice (named $Shank2^{\Delta ex6-7}$), the exons 15-16 encoding gene segment was replaced by a loxP site flanked inverse-oriented neomycin resistance (neo) selection marker (Won et al., 2012). Although no residual SHANK2 expression was detected in homozygous $Shank2^{\Delta ex16}$ or $Shank2^{\Delta ex15-16}$ mice as determined by immunoblots and immunohistology, and although the genetic background of the two mouse lines was similar (C57Bl/6N and C57Bl/6J), significant differences on the molecular, electrophysiological, synaptic composition and anatomical levels of $Shank2^{\Delta ex16}$ or $Shank2^{\Delta ex15-16}$ were evident (**Table 3**, Supplementary Table S2). The impairment of synaptic plasticity at hippocampal CA1 synapses showed opposite results in the two mouse lines and the NMDAR response was increased in $Shank2^{\Delta ex16}$ but decreased in $Shank2^{\Delta ex15-16}$ mice. In addition, the spine number and spine density were reduced in CA1 pyramidal cells of $Shank2^{\Delta ex16}$, whereas $Shank2^{\Delta ex15-16}$ mice showed normal spine numbers and density (**Table 3**, Supplementary Table S2).

ss

In 2017, Lim et al. (2017) substantiated the distinct phenotypes of $Shank2^{\Delta ex16}$ and $Shank2^{\Delta ex15-16}$ mice by a direct comparison of the two mouse lines in a mixed C57Bl/6N × C57Bl/6J background. The differences in gene expression (Supplementary Table S2) and synaptic properties such as the AMPA/NMDA ratio and long-term potentiation

TABLE 3 | Distinct endophenotypes in genetically very similar gene-manipulated, conventional *Shank2* knockout mice.

	$Shank2^{\Delta ex15-16}$	$Shank2^{\Delta ex16}$	$Shank2^{\Delta ex24}$
Body weight	Normal	Reduced	Normal
Spines morphology (hippocampus)	Spines density, number or length	Spines density and number	PSDs
Synaptic transmission	Basal synaptic transmission and mEPSC NMDA/AMPA ratio	Synaptic transmission, mEPSC amplitude and mEPSC frequency	n.a.
	NMDA/AMPA ratio	NMDA/AMPA ratio	NMDA/AMPA ratio
Synaptic plasticity (CA1)	LTP	LTP	n.a.
	LTD	LTD	n.a.
Hyperactivity	Yes	Yes	Yes
Anxiety	Yes	Yes	n.a.
Repetitive behavior	Jumping and upright scrabbling	Stereotypic behavior (self-grooming)	Self-grooming
Spatial learning	Spatial learning and memory in the Morris water maze	Spatial memory in the Morris water maze	Spatial learning in the Morris water maze
Social interact	Social interaction	Social interaction	Social interaction
L838,417 treatment	Spatial memory deficit	Spatial memory deficit	n.a.
References	Won et al. (2012) Lim et al. (2017)	Schmeisser et al. (2012) Lim et al. (2017)	Pappas et al. (2017)

n.a., not available; Green = no alteration; blue = decrease; red = increase.

(LTP; Neves et al., 2008) as well as differences in the inhibitory signaling were directly correlated to the *Shank2* Δex*16* and Δex*15-16* gene-targeted mutations. The *Shank2*$^{\Delta ex15-16}$ mice exhibited a decreased $GABA_AR$-mediated inhibition, most likely caused by the reduced expression of the GABAR gene, *Gabra2*. Interestingly, a similar discrepancy between the phenotypic expression of *Shank2* Δex*16* and Δex*15-16* gene deletions was found when the two gene deletions were restricted to cerebellar PCs (Ha et al., 2016; Peter et al., 2016; Supplementary Table S2). These mouse lines were generated by combining the floxed *Shank2 ex16* or the floxed *Shank2 ex15-16* gene, with transgenic Cre-expressing mouse lines that used the PC specific Pcp2 promoter, also called L7 promoter, for PC specific inactivation of the *Shank2* gene (**Figure 1**). *Shank2*$^{\Delta ex15-16-Pcp2-Cre}$ mice showed impaired motor coordination and learning in the Erasmus ladder test, but normal motor performance in the rotarod test. However, they exhibited neither repetitive behavior nor social interaction deficits, but only a mild anxiety-like behavior. In contrast, *Shank2*$^{\Delta ex16-L7-Cre}$ mice showed normal motor performance in the Erasmus ladder with no anxiety-like behavior, but deficits in social interaction as well as social novelty recognition. Thus, similar inactivation of the *Shank2* gene in cerebellar PCs produced distinct phenotypes at the molecular and up to the behavioral level. Similarly in two recent mouse models restricting the Δex*15-16* deletion in two specific cell types; one in excitatory neurons (*Shank2*$^{\Delta ex15-16-CaMK2a-Cre}$) and the other in GABAergic inhibitory neurons (*Shank2*$^{\Delta ex15-16-Viaat-Cre}$, Kim et al., 2018), *Shank2*$^{\Delta ex15-16-CaMK2a-Cr}$ and *Shank2*$^{\Delta ex15-16-Viaat-Cre}$ mice showed differences on the electrophysiological level by reduced mEPSC frequency in hippocampal CA1 neurons in *Shank2*$^{\Delta ex15-16-CaMK2a-Cre}$ but not in *Shank2*$^{\Delta ex15-16-Viaat-Cre}$ mice. *Shank2*$^{\Delta ex15-16-CaMK2a-Cre}$ mice showed increased anxiety-like but normal repetitive behaviors in comparison to *Shank2*$^{\Delta ex15-16-Viaat-Cre}$ mice, which showed no anxiety-like but increased repetitive behaviors (Supplementary Table S2). Thus, in *Shank2* KO mice, a residual expression of truncated proteins or mRNAs, which differs between the *Shank2* mouse lines (**Figure 3**), might disturb the structure or the flexibility of the SHANK scaffold at different levels and thus the flexibility of the postsynaptic protein organization. This impaired synaptic function might vary in different neurons or even be different in various synapses of the same neuron. These finding in cell type specific *Shank2* KO mice underlines observations that very similar *SHANK2* mutations can lead to a different phenotype, as noticed by the wide behavioral spectrum of ASD described for patients with mutations in the *SHANK2* genes (Supplementary Table S1).

In 2017, a third conventional *Shank2* KO mouse was generated by the out-of-frame deletion of *Shank2* exon 24, which deleted the PRR region (Pappas et al., 2017). These *Shank2*$^{\Delta ex24}$ KO mice exhibited a pronounced behavioral difference compared to the published ASD-like behavior of *Shank2*$^{\Delta ex16}$ and *Shank2*$^{\Delta ex15-16}$ (**Table 3**, Supplementary Table S2). *Shank2*$^{\Delta ex24}$ mice showed a bipolar-associated mania-like behavior. *Shank2*$^{\Delta ex24}$ mice were hyperactive in the home cage and open field test, showed a decrease in repetitive behaviors such as self-grooming, had no social preference in the social affiliation test nor did they show a SCZ-like behavior. Instead, *Shank2*$^{\Delta ex24}$ mice showed anhedonia-like behavior and disturbed circadian rhythms. Some of these unique behavioral impairments persisted even in conditional *Shank2*$^{\Delta ex24}$ mice (Supplementary Table S2; Pappas et al., 2017). When exon 24 of *Shank2* was removed in cerebellar PCs, *Shank2*$^{\Delta ex24-Pcp2-Cre}$ mice showed an impaired motor performance in the rotarod (Pappas et al., 2017). The Cre-mediated removal of exon 24 in the neocortex in *Shank2*$^{\Delta ex24-Emx1-Cre}$ was correlated with

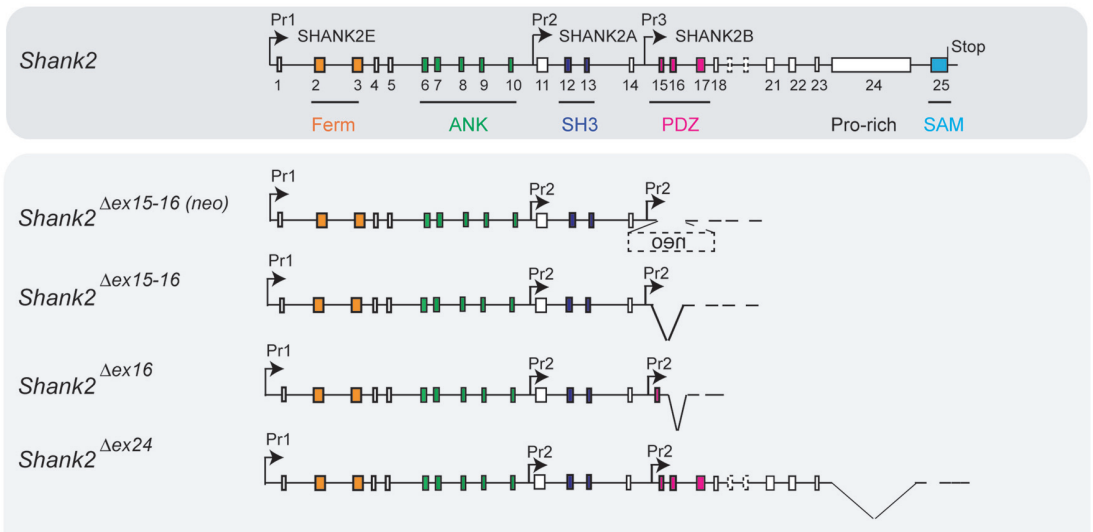

FIGURE 3 | Putative pre-mRNA transcripts in homozygous *Shank2* KO mice. Schematic view of the *Shank2* gene and the putative pre-mRNA that can be expressed by the four different gene-targeted alleles of the *Shank2* mouse models with very distinct phenotypes. Symbols are as in **Figure 2**.

mania-like behavior, hyperactivity, impaired spatial memory and a surprisingly significant social preference in female mice (Pappas et al., 2017). The developmental contribution of the *Shank2*$^{\Delta ex24}$ was unraveled by the conditional deletion of exon 24 in forebrain postnatally, using the developmentally-controlled promoter for the alpha subunit of Ca^{2+}-calmodulin dependent protein kinase II (CaMKII) for Cre expression. Thus, when exon 24 was deleted efficiently in 3 weeks old *Shank2*$^{\Delta ex24-CaMKI2a-Cre}$ mice, they didn't show any hyperactivity, which was used as signature for the mania-like behavior of the global *Shank2*$^{\Delta ex24}$ mice (Pappas et al., 2017).

How Can the Distinct Phenotypes of the Different *Shank2* Knockout Mice Be Explained?

The heterogeneity in the phenotypic expression of all three conventional and seven conditional *Shank2*-"deficient" mouse models indicated that there is no clearly defined SHANK2 deficiency-mediated phenotype. Similar to human patients, each *Shank2* KO mouse line showed a distinct neuropsychiatric-like phenotype, which was dependent on the specific type of *Shank2* mutation. In contrast to humans, where genetic and environmental factors cannot be excluded as cofactors for the penetrance of abnormal social behavior, the common social experience of experimental mouse cohorts can largely exclude environmental factors. Therefore, it is more likely that similar genetic modulations still express different truncated SHANK2 proteins at different levels (**Figure 3**), which might disturb the balanced co-expression of both SHANK1 and SHANK3 isoforms and exert more different dominant-negative effects on other protein interacting partners, that can be recognized by different behavioral outcomes. Experimental evidence for disturbed or unbalanced expression of SHANK proteins was provided by the virus-mediated overexpression in mice of the truncated SHANK2A(R462X) variant (Berkel et al., 2012), initially identified in one ASD patient (Berkel et al., 2010; Supplementary Table S2). Neurons in hippocampal cultures showed impaired spine development, characterized by their filopodia-like structure. In CA1 cells from acute hippocampal slices, reduced mEPSC amplitudes could be recorded which were correlated to impaired cognitive function, demonstrating that the truncated SHANK2 proteins can disturb the physiological function of the coordinated SHANK expression in the CNS.

Thus, as already described for similar *Shank3* KO mouse models, the *Shank2* KO lines are characterized by functionally distinct molecular, electrophysiological and neurophysiological phenotypes. In particular, the opposing effect of the disturbed excitatory and inhibitory responses of CA1 pyramidal cells in *Shank2*$^{\Delta ex15-16}$ and *Shank2*$^{\Delta ex16}$ was unexpected and still is not well understood. Already small differences in the genetic background could be responsible for this drastic difference. Moreover, it might be interesting to find out whether female and male mice or littermates with the very same *Shank2* KO mutation show different neuropsychiatric-like behavior, as described in human patients for four and seven siblings, who inherited the *SHANK2* mutation from their healthy mothers (**Table 2**). The careful comparative analysis of individual *Shank2* KO littermates of the same KO mouse line might identify epigenetic and environmental ASD or SCZ-facilitating factors; although this is a major and long-lasting endeavor.

INSIGHT INTO ASD PATHOGENESIS AND TREATMENT FROM *SHANK2* KNOCKOUT MOUSE MODELS

The finding of distinct phenotypes of genetically very similar *Shank2* KO mice finds further strong support by the pharmacological treatment strategies of the different *Shank2* KO mice. In the *Shank2*$^{\Delta ex15-16}$ mice, the hippocampal NMDAR function in brain slices was decreased (Won et al., 2012). The treatment of *Shank2*$^{\Delta ex15-16}$ with D-cycloserine, a partial agonist at the glycine-binding site of NMDARs, increased the NMDAR responses and rescued the social impairments of *Shank2*$^{\Delta ex15-16}$ mice. Similarly, the administration of a positive allosteric modulator of mGluR5, 3-cyano-N-(1,3-diphenyl-1H-pyrazol-5-yl benzamide (CDPPB), which enhances the NMDAR function via mGluR5 activation, rescued the NMDAR signaling impairments, as measured in hippocampal CA1 cells. The CDPPB-mediated recovery of NMDAR function in *Shank2*$^{\Delta ex15-16}$ mice was correlated with normalized social interaction of CDPPB treated *Shank2*$^{\Delta ex15-16}$ mice. However, hyperactivity and anxiety-like behaviors were not recovered (Won et al., 2012).

A different approach to activate the NMDAR function in *Shank2*$^{\Delta ex15-16}$ mice was carried out by inducing postsynaptic Zn^{2+} elevation using a Zn^{2+} chelator, clioquinol (Lee E. J. et al., 2015). Zn^{2+} is mainly derived from presynaptic pools and activates NMDAR through postsynaptic activation of the tyrosine kinase Src (Manzerra et al., 2001). Treating *Shank2*$^{\Delta ex15-16}$ mice with clioquinol enhanced social interaction, but did not had any effect on social novelty recognition, anxiety-like behavior, hyperactivity and repetitive behavior. The functional NMDAR rescue was demonstrated by restoring NMDAR signaling at hippocampal (SC-CA1) synapses (Lee E. J. et al., 2015). Although the pharmacological treatment of *Shank2*$^{\Delta ex15-16}$ mice was carried out 30–120 min before the behavioral tests, and even though the recovery of the NMDAR function was shown at hippocampal synapses, other brain regions, e.g., the oxytocin neurons in the hypothalamus, might also be involved in producing social incompetence and could be good candidate targets for pharmacological therapy.

In addition to the stimulation of the glutamatergic system, the enhancement of the inhibitory synaptic activity can reverse genetically-based ASD-associated deficits. In *Shank2*$^{\Delta ex15-16}$ mice, *Gabra2* expression on RNA level as well as $GABA_A$ receptor-mediated inhibitory neurotransmission in CA1 hippocampal slices were reduced in *Shank2*$^{\Delta ex15-16}$, but not in *Shank2*$^{\Delta ex16}$ mice. Treatment with an allosteric modulator of $GABA_A$ receptor, L838,417, reversed the spatial memory deficits of the *Shank2*$^{\Delta ex15-16}$ mice, but not those of *Shank2*$^{\Delta ex16}$ mice (Lim et al., 2017). However, L838,417

had no significant effects on anxiety-like behavior or social impairment in *Shank2*$^{\Delta ex15-16}$ mice. Whether or not long or short-term treatment in young and adult mice will have a persistent rescue effect remains to be investigated. The pharmacological rescues showed that the identification of the underlying electrophysiological mechanism for the type of ASD is mandatory for a successful treatment. Since a detailed electrophysiological differential diagnosis of ASD patients is not feasible, the *Shank* mutant mice are the best accessible tools to dissect different ASD endophenotypes of *SHANK* mutations at the molecular, anatomical, electrophysiological and behavioral levels.

BEHAVIORAL TEST BATTERY FOR *SHANK2* MOUSE MODELS

The widely varying phenotypes of *Shank2* mouse models for ASD and other neuropsychiatric disorders can be grouped into several categories: molecular, anatomical, hormonal, immunological, neurophysiological and behavioral. The detailed description within all six categories is crucial for the putative therapeutic treatment which, if successful, will likely to alleviate only some of ASD, SCZ or cognitive phenotypes. Standardized molecular, anatomical and neuronal activity analyses are straightforward and comparable between different studies, at least when the analyzed mutant and control mice are derived from the same colony, are age-matched, of the same gender, and when the genetic background of the mice used in different studies is similar. A major issue is comparing behavioral phenotypes determined in different laboratories (Schellinck et al., 2010), which can be a reason for the difference in behavior between the *Shank2* mouse models.

For the comparable description of ASD and other neuropsychiatric disorder phenotypes in *Shank2* mouse models, it is obligatory to exclude gross physical abnormalities (Crawley, 2007). General health, body weight and neurological reflexes including eye blink, ear reflex and whisker twitch should be investigated. The three-stage SHIRPA procedure (Immelmann and Beer, 1989) can be performed to assess mice phenotypes for obvious physical, behavioral and morphological impairments before testing social behavior and cognition. In the best case, a complete ethogram of the *Shank2* mutant mouse line, before and after genetic or pharmacological rescue, should be determined to cover the expected wide spectrum of phenotypes. If only a partial ethogram is provided, at least the full range of social and cognitive performance tests should be presented. As suggested (Crawley, 2007; Tordjman et al., 2007), a consistent "multi-trait" analysis of cognitive and social behavior is necessary for the dissection of the clinically heterogeneous ASD spectrum in the different mouse models.

First Simple Behavioral Tests

For *Shank2* mouse models, the first behavioral observations can already be started when the mouse is still used to live in its home cage. The burrowing or marble burying tests are indicators for anxiety and obsessive-compulsive disorders (Broekkamp et al., 1986; Borsini et al., 2002; Deacon, 2006; Thomas et al., 2009; Angoa-Pérez et al., 2013). The nest building test (Deacon, 2012) is considered a potential endophenotype relevant to the negative symptoms of SCZ (Amann et al., 2010) and depression. The unbiased physical performance and activity, as well as circadian rhythm of mice, can be recorded in the home cage (LABORAS system from Metris) and the running wheel; motor coordination in rotarod and Erasmus ladder test (Dunham and Miya, 1957; Van Der Giessen et al., 2008; Vandeputte et al., 2010; Luong et al., 2011). For anxiety testing, which is considered one of the most important co-morbidities of neuropsychiatric disorders, the zero-maze, elevated zero-maze and elevated plus-maze (Handley and Mithani, 1984; Pellow et al., 1985; Lister, 1987; Shepherd et al., 1994; Heisler et al., 1998; Cook et al., 2001) and the dark-light compartment (Crawley and Goodwin, 1980) can be used.

The Four Most Important Diagnostic Symptoms Need to Be Investigated

The behavioral test battery of *Shank2* mouse models should focus primarily on diagnostic symptoms of ASD: abnormal social interactions, deficits in communication, high levels of repetitive behaviors and cognitive dysfunction. However, to express cognitive and social competence in a behavioral test, anxiety and other stress factors have to be minimized. Pre-handling of the mice for at least 1 week is obligatory before testing the social behavior and memory (Fridgeirsdottir et al., 2014). In addition, increased stress by different housing conditions might affect the results (Kamakura et al., 2016). During the handling phase, repetitive behaviors (self-grooming, jumping and climbing) can be recorded in the LABORAS, and repetitive digging behavior in the marble burying assay. Social ability is usually assessed in the three-chambered box (Moy et al., 2004), the partition test apparatus (Kudryavtseva, 2003) and reciprocal social interaction in a novel arena (Silverman et al., 2010). When communicating information, olfactory stimulations as well as vocalizations in the ultrasonic ranges are used to enhance social bonding between mice, which can be evaluated by the olfactory habituation/dishabituation test (Wesson et al., 2008) and by measuring ultrasonic vocalizations (USV). As a measure of cognitive function, the spatial working reference memory can be tested in the T-maze and spatial reference memory in the Morris water maze, Y- or Radial-maze. The simple puzzle box is testing the goal-oriented performance of mice, which can give early hints of cognitive functions (Ben Abdallah et al., 2011). Social transmission of food preference has been used as a method for studying memory by several laboratories (Wrenn, 2004).

Additional Behavioral Assays Analogous to Other Symptoms of Neuropsychiatric Disorders

Patients with neuropsychiatric disorders suffer from a wide range of symptoms which can be measured in *Shank2* mice to some extent. Depression in mice can be noticed in the forced swim test, the tail-suspension tests (Porsolt et al., 1977; Steru

TABLE 4 | Summary of behavioral tests that can be used in the test battery for *Shank2* mouse models and other mice with potential neuropsychiatric-like phenotype.

Targeted domain	Behavioral tests	Targeted domain	Behavioral tests
General	- SHIRPA	**Mania**	- Circadian rhythm in running wheel - Videotaped observations of home cage sleep and activity patterns
Hyper/hypo activity	- Locomotor activity in the home cage - Locomotor activity in the open field	**Seizure**	- Sensitivity to audiogenic seizures - Sensitivity to drug-induced seizures
Anxiety	- Elevated plus-maze - Elevated zero-maze - Dark-light compartment - Open field - Marble burying - Shock-probe burying - Vogel conflict test - Hyponeophagia	**Depression**	- Forced swim test - Tail-suspension test - Visible Burrow System - Learned helplessness test - Sucrose preference task - Circadian rhythm - Social interaction - Sexual behavior
Motor learning, balance, coordination and impulsivity	- Rotarod - Running wheel - Open field - Horizontal bar - Static rods - Parallel bars - Mouse cylinder test - Elevated bridge - Swim test - Staircase test - Hanging wire test - Hind-paw footprint test - Balance beam test - Erasmus ladder test - Eye-blink conditioning test - Cliff avoidance test - 5-Choice serial reaction time task - Stop-signal reaction time task	**Cognitive, attention and memory function**	- Novel object recognition task - Morris water maze - Fear conditioning - Pre-pulse inhibition - Mazes (Barnes, Radial, Y and T) - Hole-board - Odorant-based tasks - Operant conditioning - 5-Choice serial reaction time task - Set-shifting task - Latent inhibition test - Social transmission of food preference task - Eye-blink conditioning
		Response to sensory stimuli	- Acoustic startle - Tactile startle - Hot plate - Von Frey hairs - Attentional neglect tape test
Repetitive behavior, resistance to change in routine	- Hole-board - Marble burying - Reversal learning in the Morris water maze or Y-maze - Self-grooming - Motor stereotypies (rearing and jumping)	**Aggression**	- Resident-intruder test - Isolation-induced fighting - Tube test
Social interaction, communication and social dominance	- 3-chamber social test - Direct social interaction - Social conditioned place preference task - Operant conditioning - Partition test - Visible Burrow System - Juvenile play - Whisker trimming - Nest building - USV during social interaction - USV by separated pups - Retrieval of separated pups - Olfactory habituation/dishabituation measures - Tube test		

et al., 1985) and by anhedonia in the sucrose preference test (Papp et al., 1991; Tye et al., 2013). Deficits in sensory processing can be considered a symptom of SCZ, which can be evaluated by the Pre-Pulse Inhibition (PPI) of Acoustic Startle Response (ASR; Braff and Geyer, 1990; Swerdlow et al., 1994). Other symptoms of SCZ, such as delusions and auditory hallucinations, still cannot be fully assessed in mice (Chadman et al., 2009). If necessary, learning and memorizing fear can be examined as the last step in the test battery. However, the analysis of contextual and cued fear learning (Maren, 2001) or the passive avoidance test (Gray and McNaughton, 2000) are usually not performed with *Shank2* mouse models (for the summary of tests see **Table 4**).

CONCLUSION

The different alterations in synaptic responses, synaptic plasticity, social interaction and exploration behavior, as well as therapeutic responses in *Shank2* KO mice emphasize that a balanced, physiologically-controlled expression of SHANKs is necessary for the appropriate organization of postsynaptic proteins and receptors at excitatory synapses. In addition, the comparison between *Shank2* KO mouse lines strongly suggests that truncated SHANK2 isoforms or their mRNAs disrupt the homeostasis of SHANK proteins and their function as major scaffolding organizers in the postsynaptic matrix. Different *Shank2* mutations might yield different protein products with potentially contrasting effects at the synapse (e.g., increasing or decreasing its strength), thus leading to a diversity of phenotypes. However, epigenetic factors as well as inconsistent analysis of the various *Shank2* mouse lines cannot yet be completely ruled out.

PERSPECTIVE

Understanding the detailed function of the multitude of SHANK isoforms is one of the biggest challenges in cognitive neuroscience. The disturbed balance of different SHANK proteins within individual postsynapses significantly affects the plasticity of synapses, possibly by changing the composition of the postsynaptic scaffold, which translates to a rearrangement of the glutamate receptors and measurable alterations in the glutamatergic signaling. For *in vivo* analysis of certain SHANK2 isoforms in mice, certain exons or *SHANK* internal promoters could be eliminated or certain SHANK isoforms could be overexpressed by viruses or transgenes. New genetic engineering techniques can generate relatively quickly novel *Shank2* mouse lines. However, in future studies with novel constitutive and conditional *Shank2* mouse lines, the expression of the residual truncated isoforms should be analyzed in more details, and the full battery of behavioral analysis covering ASD, SCZ, mania and Attention Deficit Hyperactivity Disorder (ADHD) has to be applied, since the existing *Shank2* mouse models showed very distinct, unpredictable phenotype despite very similar genetic manipulations. In addition, males and females and real littermates need to be compared in detail to unravel epigenetic, environmental and gender effects on the expression of the phenotypes. More importantly, the current *Shank2* mouse models provided first insights into molecular and physiological changes underlying ASD-related symptoms. The *Shank2* mutant mice showed that ASD-related symptoms can be diminished by pharmacological treatment of the mutant mice, which can guide future therapeutic strategies for ASD patients. Now the application of spatio-temporal removal of SHANK2 using cell-type specific Cre or CreERT2 mice can identify those neuronal connections and circuits that have the strongest impact on the expression of the ASD-like phenotype. Moreover, conditional *Shank2* KO mice can help to dissect the neurodevelopmental vs. the transient deficiencies mediated by the SHANK depletion. Once the most crucial neuronal circuits and cell types are identified, those neuronal populations can be targeted and analyzed in great detail in behaving mice by novel physiological technologies, e.g., multicellular recordings and optogenetics, which allow the recording, visualization and manipulation of neuronal activity ensembles during social interaction, repetitive behavior, vocalization and cognition, or even during different phases of sleep. Due to the very distinct phenotypes of different *Shank2* mouse lines, it will be exciting to see how their altered neuronal network activity is correlated with the impaired social behavior.

AUTHOR CONTRIBUTIONS

All authors significantly contributed to the manuscript. AE and RS wrote the first draft and provided the figures, tables and supplementary information. GR critically revised the manuscript.

FUNDING

This work was supported by a grant from the Ingeborg Ständer Foundation to RS. AE received a PhD fellowship from Heidelberg Bioscience International Graduate School (HBIGS).

ACKNOWLEDGMENTS

We would like to thank Trey Chiu and Flavia-Bianca Cristian for proofreading. We would also like to sincerely thank Shaimaa Madbouly for her constant support.

SUPPLEMENTARY MATERIAL

The Supplementary Material for this article can be found online at: https://www.frontiersin.org/articles/10.3389/fnmol.2018.00240/full#supplementary-material

REFERENCES

Amann, L. C., Gandal, M. J., Halene, T. B., Ehrlichman, R. S., White, S. L., McCarren, H. S., et al. (2010). Mouse behavioral endophenotypes for schizophrenia. *Brain Res. Bull.* 83, 147–161. doi: 10.1016/j.brainresbull.2010.04.008

Ammer, A. G., and Weed, S. A. (2008). Cortactin branches out: roles in regulating protrusive actin dynamics. *Cell Motil. Cytoskeleton* 65, 687–707. doi: 10.1002/cm.20296

Angoa-Pérez, M., Kane, M. J., Briggs, D. I., Francescutti, D. M., and Kuhn, D. M. (2013). Marble burying and nestlet shredding as tests of repetitive, compulsive-like behaviors in mice. *J. Vis. Exp.* 82:50978. doi: 10.3791/50978

Baron, M. K., Boeckers, T. M., Vaida, B., Faham, S., Gingery, M., Sawaya, M. R., et al. (2006). An architectural framework that may lie at the core of the postsynaptic density. *Science* 311, 531–535. doi: 10.1126/science.1118995

Ben Abdallah, N. M., Fuss, J., Trusel, M., Galsworthy, M. J., Bobsin, K., Colacicco, G., et al. (2011). The puzzle box as a simple and efficient behavioral test for exploring impairments of general cognition and executive functions in mouse models of schizophrenia. *Exp. Neurol.* 227, 42–52. doi: 10.1016/j.expneurol.2010.09.008

Berkel, S., Marshall, C. R., Weiss, B., Howe, J., Roeth, R., Moog, U., et al. (2010). Mutations in the SHANK2 synaptic scaffolding gene in autism spectrum disorder and mental retardation. *Nat. Genet.* 42, 489–491. doi: 10.1038/ng.589

Berkel, S., Tang, W., Trevino, M., Vogt, M., Obenhaus, H. A., Gass, P., et al. (2012). Inherited and *de novo* SHANK2 variants associated with autism spectrum disorder impair neuronal morphogenesis and physiology. *Hum. Mol. Genet.* 21, 344–357. doi: 10.1093/hmg/ddr470

Boeckers, T. M., Bockmann, J., Kreutz, M. R., and Gundelfinger, E. D. (2002). ProSAP/Shank proteins—a family of higher order organizing molecules of the postsynaptic density with an emerging role in human neurological disease. *J. Neurochem.* 81, 903–910. doi: 10.1046/j.1471-4159.2002.00931.x

Boeckers, T. M., Kreutz, M. R., Winter, C., Zuschratter, W., Smalla, K. H., Sanmarti-Vila, L., et al. (1999a). Proline-rich synapse-associated protein-1/cortactin binding protein 1 (ProSAP1/CortBP1) is a PDZ-domain protein highly enriched in the postsynaptic density. *J. Neurosci.* 19, 6506–6518. doi: 10.1523/jneurosci.19-15-06506.1999

Boeckers, T. M., Winter, C., Smalla, K. H., Kreutz, M. R., Bockmann, J., Seidenbecher, C., et al. (1999b). Proline-rich synapse-associated proteins ProSAP1 and ProSAP2 interact with synaptic proteins of the SAPAP/GKAP family. *Biochem. Biophys. Res. Commun.* 264, 247–252. doi: 10.1006/bbrc.1999.1489

Boeckers, T. M., Liedtke, T., Spilker, C., Dresbach, T., Bockmann, J., Kreutz, M. R., et al. (2005). C-terminal synaptic targeting elements for postsynaptic density proteins ProSAP1/Shank2 and ProSAP2/Shank3. *J. Neurochem.* 92, 519–524. doi: 10.1111/j.1471-4159.2004.02910.x

Böckers, T. M., Mameza, M. G., Kreutz, M. R., Bockmann, J., Weise, C., Buck, F., et al. (2001). Synaptic scaffolding proteins in rat brain. Ankyrin repeats of the multidomain Shank protein family interact with the cytoskeletal protein α-fodrin. *J. Biol. Chem.* 276, 40104–40112. doi: 10.1074/jbc.m102454200

Böckers, T. M., Segger-Junius, M., Iglauer, P., Bockmann, J., Gundelfinger, E. D., Kreutz, M. R., et al. (2004). Differential expression and dendritic transcript localization of Shank family members: identification of a dendritic targeting element in the 3′ untranslated region of Shank1 mRNA. *Mol. Cell. Neurosci.* 26, 182–190. doi: 10.1016/j.mcn.2004.01.009

Borsini, F., Podhorna, J., and Marazziti, D. (2002). Do animal models of anxiety predict anxiolytic-like effects of antidepressants? *Psychopharmacology* 163, 121–141. doi: 10.1007/s00213-002-1155-6

Bowling, K. M., Thompson, M. L., Amaral, M. D., Finnila, C. R., Hiatt, S. M., Engel, K. L., et al. (2017). Genomic diagnosis for children with intellectual disability and/or developmental delay. *Genome Med.* 9:43. doi: 10.1186/s13073-017-0433-1

Bozdagi, O., Sakurai, T., Papapetrou, D., Wang, X., Dickstein, D. L., Takahashi, N., et al. (2010). Haploinsufficiency of the autism-associated Shank3 gene leads to deficits in synaptic function, social interaction and social communication. *Mol. Autism* 1:15. doi: 10.1186/2040-2392-1-15

Braff, D. L., and Geyer, M. A. (1990). Sensorimotor gating and schizophrenia. Human and animal model studies. *Arch. Gen. Psychiatry* 47, 181–188. doi: 10.1001/archpsyc.1990.01810140081011

Broekkamp, C. L., Rijk, H. W., Joly-Gelouin, D., and Lloyd, K. L. (1986). Major tranquillizers can be distinguished from minor tranquillizers on the basis of effects on marble burying and swim-induced grooming in mice. *Eur. J. Pharmacol.* 126, 223–229. doi: 10.1016/0014-2999(86)90051-8

Chadman, K. K., Yang, M., and Crawley, J. N. (2009). Criteria for validating mouse models of psychiatric diseases. *Am. J. Med. Genet. B Neuropsychiatr. Genet.* 150B, 1–11. doi: 10.1002/ajmg.b.30777

Chilian, B., Abdollahpour, H., Bierhals, T., Haltrich, I., Fekete, G., Nagel, I., et al. (2013). Dysfunction of SHANK2 and CHRNA7 in a patient with intellectual disability and language impairment supports genetic epistasis of the two loci. *Clin. Genet.* 84, 560–565. doi: 10.1111/cge.12105

Cook, M. N., Williams, R. W., and Flaherty, L. (2001). Anxiety-related behaviors in the elevated zero-maze are affected by genetic factors and retinal degeneration. *Behav. Neurosci.* 115, 468–476. doi: 10.1037//0735-7044.115.2.468

Crawley, J., and Goodwin, F. K. (1980). Preliminary report of a simple animal behavior model for the anxiolytic effects of benzodiazepines. *Pharmacol. Biochem. Behav.* 13, 167–170. doi: 10.1016/0091-3057(80)90067-2

Crawley, J. N. (2007). Mouse behavioral assays relevant to the symptoms of autism. *Brain Pathol.* 17, 448–459. doi: 10.1111/j.1750-3639.2007.00096.x

Deacon, R. M. (2012). Assessing burrowing, nest construction, and hoarding in mice. *J. Vis. Exp.* 59:e2607. doi: 10.3791/2607

Deacon, R. M. (2006). Digging and marble burying in mice: simple methods for *in vivo* identification of biological impacts. *Nat. Protoc.* 1, 122–124. doi: 10.1038/nprot.2006.20

de Sena Cortabitarte, A., Degenhardt, F., Strohmaier, J., Lang, M., Weiss, B., Roeth, R., et al. (2017). Investigation of SHANK3 in schizophrenia. *Am. J. Med. Genet. B Neuropsychiatr. Genet.* 174, 390–398. doi: 10.1002/ajmg.b.32528

Du, Y., Weed, S. A., Xiong, W. C., Marshall, T. D., and Parsons, J. T. (1998). Identification of a novel cortactin SH3 domain-binding protein and its localization to growth cones of cultured neurons. *Mol. Cell. Biol.* 18, 5838–5851. doi: 10.1128/mcb.18.10.5838

Dunham, N. W., and Miya, T. S. (1957). A note on a simple apparatus for detecting neurological deficit in rats and mice. *J. Am. Pharm. Assoc. Am. Pharm. Assoc.* 46, 208–209. doi: 10.1002/jps.3030460322

Durand, C. M., Betancur, C., Boeckers, T. M., Bockmann, J., Chaste, P., Fauchereau, F., et al. (2007). Mutations in the gene encoding the synaptic scaffolding protein SHANK3 are associated with autism spectrum disorders. *Nat. Genet.* 39, 25–27. doi: 10.1038/ng1933

Fridgeirsdottir, G. A., Hillered, L., and Clausen, F. (2014). Escalated handling of young C57BL/6 mice results in altered Morris water maze performance. *Ups. J. Med. Sci.* 119, 1–9. doi: 10.3109/03009734.2013.847511

Grabrucker, A. M., Knight, M. J., Proepper, C., Bockmann, J., Joubert, M., Rowan, M., et al. (2011). Concerted action of zinc and ProSAP/Shank in synaptogenesis and synapse maturation. *EMBO J.* 30, 569–581. doi: 10.1038/emboj.2010.336

Gray, J. A., and McNaughton, N. (2000). *The Neuropsychology of Anxiety: An Enquiry into the Functions of the Septo-Hippocampal System.* 2nd Edn. New York, NY: Oxford University Press.

Gundelfinger, E. D., Boeckers, T. M., Baron, M. K., and Bowie, J. U. (2006). A role for zinc in postsynaptic density asSAMbly and plasticity? *Trends Biochem. Sci.* 31, 366–373. doi: 10.1016/j.tibs.2006.05.007

Ha, S., Lee, D., Cho, Y. S., Chung, C., Yoo, Y. E., Kim, J., et al. (2016). Cerebellar Shank2 regulates excitatory synapse density, motor coordination and specific repetitive and anxiety-like behaviors. *J. Neurosci.* 36, 12129–12143. doi: 10.1523/jneurosci.1849-16.2016

Han, W., Kim, K. H., Jo, M. J., Lee, J. H., Yang, J., Doctor, R. B., et al. (2006). Shank2 associates with and regulates Na^+/H^+ exchanger 3. *J. Biol. Chem.* 281, 1461–1469. doi: 10.1074/jbc.M509786200

Handley, S. L., and Mithani, S. (1984). Effects of α-adrenoceptor agonists and antagonists in a maze-exploration model of 'fear'-motivated behaviour. *Naunyn Schmiedebergs Arch. Pharmacol.* 327, 1–5. doi: 10.1007/bf00504983

Hayashi, M. K., Tang, C., Verpelli, C., Narayanan, R., Stearns, M. H., Xu, R. M., et al. (2009). The postsynaptic density proteins Homer and Shank form a polymeric network structure. *Cell* 137, 159–171. doi: 10.1016/j.cell.2009.01.050

Heisler, L. K., Chu, H. M., Brennan, T. J., Danao, J. A., Bajwa, P., Parsons, L. H., et al. (1998). Elevated anxiety and antidepressant-like responses in serotonin 5-HT1A receptor mutant mice. *Proc. Natl. Acad. Sci. U S A* 95, 15049–15054. doi: 10.1073/pnas.95.25.15049

Homann, O. R., Misura, K., Lamas, E., Sandrock, R. W., Nelson, P., McDonough, S. I., et al. (2016). Whole-genome sequencing in multiplex families with psychoses reveals mutations in the SHANK2 and SMARCA1 genes segregating with illness. *Mol. Psychiatry* 21, 1690–1695. doi: 10.1038/mp.2016.24

Hung, A. Y., Futai, K., Sala, C., Valtschanoff, J. G., Ryu, J., Woodworth, M. A., et al. (2008). Smaller dendritic spines, weaker synaptic transmission, but enhanced spatial learning in mice lacking Shank1. *J. Neurosci.* 28, 1697–1708. doi: 10.1523/jneurosci.3032-07.2008

Immelmann, K., and Beer, C. (1989). *A Dictionary of Ethology.* Cambridge, MA: Harvard University Press.

Jacob, A. L., and Weinberg, R. J. (2015). The organization of AMPA receptor subunits at the postsynaptic membrane. *Hippocampus* 25, 798–812. doi: 10.1002/hipo.22404

Jaramillo, T. C., Speed, H. E., Xuan, Z., Reimers, J. M., Escamilla, C. O., Weaver, T. P., et al. (2017). Novel Shank3 mutant exhibits behaviors with face validity for autism and altered striatal and hippocampal function. *Autism Res.* 10, 42–65. doi: 10.1002/aur.1664

Jaramillo, T. C., Speed, H. E., Xuan, Z., Reimers, J. M., Liu, S., and Powell, C. M. (2016). Altered striatal synaptic function and abnormal behaviour

in Shank3 Exon4–9 deletion mouse model of autism. *Autism Res.* 9, 350–375. doi: 10.1002/aur.1529

Jiang, Y. H., and Ehlers, M. D. (2013). Modeling autism by SHANK gene mutations in mice. *Neuron* 78, 8–27. doi: 10.1016/j.neuron.2013.03.016

Kamakura, R., Kovalainen, M., Leppaluoto, J., Herzig, K. H., and Makela, K. A. (2016). The effects of group and single housing and automated animal monitoring on urinary corticosterone levels in male C57BL/6 mice. *Physiol. Rep.* 4:e12703. doi: 10.14814/phy2.12703

Kim, C. H., Chung, H. J., Lee, H. K., and Huganir, R. L. (2001). Interaction of the AMPA receptor subunit GluR2/3 with PDZ domains regulates hippocampal long-term depression. *Proc. Natl. Acad. Sci. U S A* 98, 11725–11730. doi: 10.1073/pnas.211132798

Kim, R., Kim, J., Chung, C., Ha, S., Lee, S., Lee, E., et al. (2018). Cell-type-specific shank2 deletion in mice leads to differential synaptic and behavioral phenotypes. *J. Neurosci.* 38, 4076–4092. doi: 10.1523/jneurosci.2684-17.2018

Kolarova, J., Tangen, I., Bens, S., Gillessen-Kaesbach, G., Gutwein, J., Kautza, M., et al. (2015). Array-based DNA methylation analysis in individuals with developmental delay/intellectual disability and normal molecular karyotype. *Eur. J. Med. Genet.* 58, 419–425. doi: 10.1016/j.ejmg.2015.05.001

Kornau, H. C., Schenker, L. T., Kennedy, M. B., and Seeburg, P. H. (1995). Domain interaction between NMDA receptor subunits and the postsynaptic density protein PSD-95. *Science* 269, 1737–1740. doi: 10.1126/science.7569905

Kouser, M., Speed, H. E., Dewey, C. M., Reimers, J. M., Widman, A. J., Gupta, N., et al. (2013). Loss of predominant Shank3 isoforms results in hippocampus-dependent impairments in behavior and synaptic transmission. *J. Neurosci.* 33, 18448–18468. doi: 10.1523/jneurosci.3017-13.2013

Kudryavtseva, N. N. (2003). Use of the "partition" test in behavioral and pharmacological experiments. *Neurosci. Behav. Physiol.* 33, 461–471. doi: 10.1023/A:1023411217051

Leblond, C. S., Heinrich, J., Delorme, R., Proepper, C., Betancur, C., Huguet, G., et al. (2012). Genetic and functional analyses of SHANK2 mutations suggest a multiple hit model of autism spectrum disorders. *PLoS Genet.* 8:e1002521. doi: 10.1371/journal.pgen.1002521

Leblond, C. S., Nava, C., Polge, A., Gauthier, J., Huguet, G., Lumbroso, S., et al. (2014). Meta-analysis of SHANK Mutations in Autism Spectrum Disorders: a gradient of severity in cognitive impairments. *PLoS Genet.* 10:e1004580. doi: 10.1371/journal.pgen.1004580

Lee, J., Chung, C., Ha, S., Lee, D., Kim, D. Y., Kim, H., et al. (2015). Shank3-mutant mice lacking exon 9 show altered excitation/inhibition balance, enhanced rearing, and spatial memory deficit. *Front. Cell. Neurosci.* 9:94. doi: 10.3389/fncel.2015.00094

Lee, E. J., Lee, H., Huang, T. N., Chung, C., Shin, W., Kim, K., et al. (2015). Trans-synaptic zinc mobilization improves social interaction in two mouse models of autism through NMDAR activation. *Nat. Commun.* 6:7168. doi: 10.1038/ncomms8168

Lim, S., Naisbitt, S., Yoon, J., Hwang, J. I., Suh, P. G., Sheng, M., et al. (1999). Characterization of the Shank family of synaptic proteins. Multiple genes, alternative splicing, and differential expression in brain and development. *J. Biol. Chem.* 274, 29510–29518. doi: 10.1074/jbc.274.41.29510

Lim, C. S., Kim, H., Yu, N. K., Kang, S. J., Kim, T., Ko, H. G., et al. (2017). Enhancing inhibitory synaptic function reverses spatial memory deficits in Shank2 mutant mice. *Neuropharmacology* 112, 104–112. doi: 10.1016/j.neuropharm.2016.08.016

Lister, R. G. (1987). The use of a plus-maze to measure anxiety in the mouse. *Psychopharmacology* 92, 180–185. doi: 10.1007/bf00177912

Lu, W., and Ziff, E. B. (2005). PICK1 interacts with ABP/GRIP to regulate AMPA receptor trafficking. *Neuron* 47, 407–421. doi: 10.1016/j.neuron.2005.07.006

Luong, T. N., Carlisle, H. J., Southwell, A., and Patterson, P. H. (2011). Assessment of motor balance and coordination in mice using the balance beam. *J. Vis. Exp.* 49:2376. doi: 10.3791/2376

Manzerra, P., Behrens, M. M., Canzoniero, L. M., Wang, X. Q., Heidinger, V., Ichinose, T., et al. (2001). Zinc induces a Src family kinase-mediated up-regulation of NMDA receptor activity and excitotoxicity. *Proc. Natl. Acad. Sci. U S A* 98, 11055–11061. doi: 10.1073/pnas.191353598

Maren, S. (2001). Neurobiology of Pavlovian fear conditioning. *Annu. Rev. Neurosci.* 24, 897–931. doi: 10.1146/annurev.neuro.24.1.897

Mei, Y., Monteiro, P., Zhou, Y., Kim, J. A., Gao, X., Fu, Z., et al. (2016). Adult restoration of Shank3 expression rescues selective autistic-like phenotypes. *Nature* 530, 481–484. doi: 10.1038/nature16971

Monteiro, P., and Feng, G. (2017). SHANK proteins: roles at the synapse and in autism spectrum disorder. *Nat. Rev. Neurosci.* 18, 147–157. doi: 10.1038/nrn.2016.183

Moy, S. S., Nadler, J. J., Perez, A., Barbaro, R. P., Johns, J. M., Magnuson, T. R., et al. (2004). Sociability and preference for social novelty in five inbred strains: an approach to assess autistic-like behavior in mice. *Genes Brain Behav.* 3, 287–302. doi: 10.1111/j.1601-1848.2004.00076.x

Naisbitt, S., Kim, E., Tu, J. C., Xiao, B., Sala, C., Valtschanoff, J., et al. (1999). Shank, a novel family of postsynaptic density proteins that binds to the NMDA receptor/PSD-95/GKAP complex and cortactin. *Neuron* 23, 569–582. doi: 10.1016/s0896-6273(00)80809-0

Naisbitt, S., Kim, E., Weinberg, R. J., Rao, A., Yang, F. C., Craig, A. M., et al. (1997). Characterization of guanylate kinase-associated protein, a postsynaptic density protein at excitatory synapses that interacts directly with postsynaptic density-95/synapse-associated protein 90. *J. Neurosci.* 17, 5687–5696. doi: 10.1523/JNEUROSCI.17-15-05687.1997

Neves, G., Cooke, S. F., and Bliss, T. V. (2008). Synaptic plasticity, memory and the hippocampus: a neural network approach to causality. *Nat. Rev. Neurosci.* 9, 65–75. doi: 10.1038/nrn2303

Papp, M., Willner, P., and Muscat, R. (1991). An animal model of anhedonia: attenuation of sucrose consumption and place preference conditioning by chronic unpredictable mild stress. *Psychopharmacology* 104, 255–259. doi: 10.1007/bf02244188

Pappas, A. L., Bey, A. L., Wang, X., Rossi, M., Kim, Y. H., Yan, H., et al. (2017). Deficiency of Shank2 causes mania-like behavior that responds to mood stabilizers. *JCI Insight* 2:e92052. doi: 10.1172/jci.insight.92052

Peca, J., Feliciano, C., Ting, J. T., Wang, W., Wells, M. F., Venkatraman, T. N., et al. (2011). Shank3 mutant mice display autistic-like behaviours and striatal dysfunction. *Nature* 472, 437–442. doi: 10.1038/nature09965

Pellow, S., Chopin, P., File, S. E., and Briley, M. (1985). Validation of open:closed arm entries in an elevated plus-maze as a measure of anxiety in the rat. *J. Neurosci. Methods* 14, 149–167. doi: 10.1016/0165-0270(85)90031-7

Peter, S., Ten Brinke, M. M., Stedehouder, J., Reinelt, C. M., Wu, B., Zhou, H., et al. (2016). Dysfunctional cerebellar Purkinje cells contribute to autism-like behaviour in Shank2-deficient mice. *Nat. Commun.* 7:12627. doi: 10.1038/ncomms12627

Peykov, S., Berkel, S., Schoen, M., Weiss, K., Degenhardt, F., Strohmaier, J., et al. (2015). Identification and functional characterization of rare SHANK2 variants in schizophrenia. *Mol. Psychiatry* 20, 1489–1498. doi: 10.1038/mp.2014.172

Pinto, D., Pagnamenta, A. T., Klei, L., Anney, R., Merico, D., Regan, R., et al. (2010). Functional impact of global rare copy number variation in autism spectrum disorders. *Nature* 466, 368–372. doi: 10.1038/nature09146

Porsolt, R. D., Bertin, A., and Jalfre, M. (1977). Behavioral despair in mice: a primary screening test for antidepressants. *Arch. Int. Pharmacodyn. Ther.* 229, 327–336.

Prasad, A., Merico, D., Thiruvahindrapuram, B., Wei, J., Lionel, A. C., Sato, D., et al. (2012). A discovery resource of rare copy number variations in individuals with autism spectrum disorder. *G3* 2, 1665–1685. doi: 10.1534/g3.112.004689

Rauch, A., Wieczorek, D., Graf, E., Wieland, T., Endele, S., Schwarzmayr, T., et al. (2012). Range of genetic mutations associated with severe non-syndromic sporadic intellectual disability: an exome sequencing study. *Lancet* 380, 1674–1682. doi: 10.1016/S0140-6736(12)61480-9

Sala, C., Piëch, V., Wilson, N. R., Passafaro, M., Liu, G., and Sheng, M. (2001). Regulation of dendritic spine morphology and synaptic function by Shank and Homer. *Neuron* 31, 115–130. doi: 10.1016/s0896-6273(01)00339-7

Sala, C., Vicidomini, C., Bigi, I., Mossa, A., and Verpelli, C. (2015). Shank synaptic scaffold proteins: keys to understanding the pathogenesis of autism and other synaptic disorders. *J. Neurochem.* 135, 849–858. doi: 10.1111/jnc.13232

Schellinck, H. M., Cyr, D. P., and Brown, R. E. (2010). "Chapter 7—how many ways can mouse behavioral experiments go wrong? Confounding variables in mouse models of neurodegenerative diseases and how to control them," in *Advances in the Study of Behavior*, eds H. J. Brockmann, T. J. Roper, M. Naguib, K. E. Wynne-Edwards, J. C. Mitani and L. W. Simmons (Burlington, MA: Academic Press), 255–366.

Schluth-Bolard, C., Labalme, A., Cordier, M. P., Till, M., Nadeau, G., Tevissen, H., et al. (2013). Breakpoint mapping by next generation sequencing reveals causative gene disruption in patients carrying apparently balanced chromosome rearrangements with intellectual deficiency and/or congenital malformations. *J. Med. Genet.* 50, 144–150. doi: 10.1136/jmedgenet-2012-101351

Schmeisser, M. J., Ey, E., Wegener, S., Bockmann, J., Stempel, A. V., Kuebler, A., et al. (2012). Autistic-like behaviours and hyperactivity in mice lacking ProSAP1/Shank2. *Nature* 486, 256–260. doi: 10.1038/nature11015

Schmeisser, M. J., and Verpelli, C. (2016). "Chapter 10—SHANK mutations in intellectual disability and autism spectrum disorder," in *Neuronal and Synaptic Dysfunction in Autism Spectrum Disorder and Intellectual Disability*, eds C. Sala and C. Verpelli (San Diego, CA: Academic Press), 151–160.

Sheng, M., and Kim, E. (2011). The postsynaptic organization of synapses. *Cold Spring Harb. Perspect. Biol.* 3:a005678. doi: 10.1101/cshperspect.a005678

Shepherd, J. K., Grewal, S. S., Fletcher, A., Bill, D. J., and Dourish, C. T. (1994). Behavioural and pharmacological characterisation of the elevated "zero-maze" as an animal model of anxiety. *Psychopharmacology* 116, 56–64. doi: 10.1007/bf02244871

Shi, R., Redman, P., Ghose, D., Liu, Y., Ren, X., Ding, L. J., et al. (2017). Shank proteins differentially regulate synaptic transmission. *eNeuro* 4:ENEURO.0163-15.2017. doi: 10.1523/ENEURO.0163-15.2017

Silverman, J. L., Yang, M., Lord, C., and Crawley, J. N. (2010). Behavioural phenotyping assays for mouse models of autism. *Nat. Rev. Neurosci.* 11, 490–502. doi: 10.1038/nrn2851

Speed, H. E., Kouser, M., Xuan, Z., Reimers, J. M., Ochoa, C. F., Gupta, N., et al. (2015). Autism-associated insertion mutation (InsG) of Shank3 exon 21 causes impaired synaptic transmission and behavioral deficits. *J. Neurosci.* 35, 9648–9665. doi: 10.1523/JNEUROSCI.3125-14.2015

Steru, L., Chermat, R., Thierry, B., and Simon, P. (1985). The tail suspension test: a new method for screening antidepressants in mice. *Psychopharmacology* 85, 367–370. doi: 10.1007/bf00428203

Swerdlow, N. R., Braff, D. L., Taaid, N., and Geyer, M. A. (1994). Assessing the validity of an animal model of deficient sensorimotor gating in schizophrenic patients. *Arch. Gen. Psychiatry* 51, 139–154. doi: 10.1001/archpsyc.1994.03950020063007

Thomas, A., Burant, A., Bui, N., Graham, D., Yuva-Paylor, L. A., and Paylor, R. (2009). Marble burying reflects a repetitive and perseverative behavior more than novelty-induced anxiety. *Psychopharmacology* 204, 361–373. doi: 10.1007/s00213-009-1466-y

Tordjman, S., Drapier, D., Bonnot, O., Graignic, R., Fortes, S., Cohen, D., et al. (2007). Animal models relevant to schizophrenia and autism: validity and limitations. *Behav. Genet.* 37, 61–78. doi: 10.1007/s10519-006-9120-5

Tu, J. C., Xiao, B., Naisbitt, S., Yuan, J. P., Petralia, R. S., Brakeman, P., et al. (1999). Coupling of mGluR/Homer and PSD-95 complexes by the Shank family of postsynaptic density proteins. *Neuron* 23, 583–592. doi: 10.1016/s0896-6273(00)80810-7

Tye, K. M., Mirzabekov, J. J., Warden, M. R., Ferenczi, E. A., Tsai, H. C., Finkelstein, J., et al. (2013). Dopamine neurons modulate neural encoding and expression of depression-related behaviour. *Nature* 493, 537–541. doi: 10.1038/nature11740

Uemura, T., Mori, H., and Mishina, M. (2004). Direct interaction of GluRdelta2 with Shank scaffold proteins in cerebellar Purkinje cells. *Mol. Cell. Neurosci.* 26, 330–341. doi: 10.1016/j.mcn.2004.02.007

Van Der Giessen, R. S., Koekkoek, S. K., van Dorp, S., De Gruijl, J. R., Cupido, A., Khosrovani, S., et al. (2008). Role of olivary electrical coupling in cerebellar motor learning. *Neuron* 58, 599–612. doi: 10.1016/j.neuron.2008.03.016

Vandeputte, C., Taymans, J. M., Casteels, C., Coun, F., Ni, Y., Van Laere, K., et al. (2010). Automated quantitative gait analysis in animal models of movement disorders. *BMC Neurosci.* 11:92. doi: 10.1186/1471-2202-11-92

Verpelli, C., Schmeisser, M. J., Sala, C., and Boeckers, T. M. (2012). Scaffold proteins at the postsynaptic density. *Adv. Exp. Med. Biol.* 970, 29–61. doi: 10.1007/978-3-7091-0932-8_2

Wang, X., Bey, A. L., Katz, B. M., Badea, A., Kim, N., David, L. K., et al. (2016). Altered mGluR5-Homer scaffolds and corticostriatal connectivity in a Shank3 complete knockout model of autism. *Nat. Commun.* 7:11459. doi: 10.1038/ncomms11459

Wang, X., McCoy, P. A., Rodriguiz, R. M., Pan, Y., Je, H. S., Roberts, A. C., et al. (2011). Synaptic dysfunction and abnormal behaviors in mice lacking major isoforms of Shank3. *Hum. Mol. Genet.* 20, 3093–3108. doi: 10.1093/hmg/ddr212

Wang, Y., Zhao, X., Ju, W., Flory, M., Zhong, J., Jiang, S., et al. (2015). Genome-wide differential expression of synaptic long noncoding RNAs in autism spectrum disorder. *Transl. Psychiatry* 5:e660. doi: 10.1038/tp.2015.144

Wesson, D. W., Donahou, T. N., Johnson, M. O., and Wachowiak, M. (2008). Sniffing behavior of mice during performance in odor-guided tasks. *Chem. Senses* 33, 581–596. doi: 10.1093/chemse/bjn029

Wischmeijer, A., Magini, P., Giorda, R., Gnoli, M., Ciccone, R., Cecconi, L., et al. (2011). Olfactory receptor-related duplicons mediate a microdeletion at 11q13.2q13.4 associated with a syndromic phenotype. *Mol. Syndromol.* 1, 176–184. doi: 10.1159/000322054

Won, H., Lee, H. R., Gee, H. Y., Mah, W., Kim, J. I., Lee, J., et al. (2012). Autistic-like social behaviour in Shank2-mutant mice improved by restoring NMDA receptor function. *Nature* 486, 261–265. doi: 10.1038/nature11208

Wrenn, C. C. (2004). Social transmission of food preference in mice. *Curr. Protoc. Neurosci.* 8:8.5G. doi: 10.1002/0471142301.ns0805gs28

Yang, M., Bozdagi, O., Scattoni, M. L., Wöhr, M., Roullet, F. I., Katz, A. M., et al. (2012). Reduced excitatory neurotransmission and mild autism-relevant phenotypes in adolescent Shank3 null mutant mice. *J. Neurosci.* 32, 6525–6541. doi: 10.1523/JNEUROSCI.6107-11.2012

Yuen, R. K. C., Merico, D., Bookman, M., L Howe, J., Thiruvahindrapuram, B., Patel, R. V., et al. (2017). Whole genome sequencing resource identifies 18 new candidate genes for autism spectrum disorder. *Nat. Neurosci.* 20, 602–611. doi: 10.1038/nn.4524

Zhou, Y., Kaiser, T., Monteiro, P., Zhang, X., Van der Goes, M. S., Wang, D., et al. (2016). Mice with Shank3 mutations associated with ASD and schizophrenia display both shared and distinct defects. *Neuron* 89, 147–162. doi: 10.1016/j.neuron.2015.11.023

Conflict of Interest Statement: The authors declare that the research was conducted in the absence of any commercial or financial relationships that could be construed as a potential conflict of interest.

frontiers in Molecular Neuroscience

PERSPECTIVE
published: 07 August 2018
doi: 10.3389/fnmol.2018.00268

Functional Relevance of Missense Mutations Affecting the N-Terminal Part of Shank3 Found in Autistic Patients

*Fatemeh Hassani Nia and Hans-Jürgen Kreienkamp**

Institute for Human Genetics, University Medical Center Hamburg-Eppendorf, Hamburg, Germany

Genetic defects in *SHANK* genes are associated with autism. Deletions and truncating mutations suggest haploinsufficiency for Shank3 as a major cause of disease which may be analyzed in appropriate Shank deficient mouse models. Here we will focus on the functional analysis of missense mutations found in *SHANK* genes. The relevance of most of these mutations for Shank function, and their role in autism pathogenesis is unclear. This is partly due to the fact that mutations spare the most well studied functional domains of Shank3, such as the PDZ and SAM domains, or the short proline-rich motifs which are required for interactions with postsynaptic partners Homer, Cortactin, dynamin, IRSp53 and Abi-1. One set of mutations affects the N-terminal part, including the highly conserved SPN domain and ankyrin repeats. Functional analysis from several groups has indicated that these mutations (e.g., R12C; L68P; R300C, and Q321R) interfere with the critical role of Shank3 for synapse formation. More recently the structural analysis of the SPN-ARR module has begun to shed light on the molecular consequences of mutations in the SPN of Shank3. The SPN was identified as a Ras association domain, with high affinities for GTP-bound, active forms of Ras and Rap. The two autism related mutations in this part of the protein, R12C and L68P, both abolish Ras binding. Further work is directed at identifying the consequences of Ras binding to Shank proteins at postsynaptic sites.

Keywords: ankyrin repeat, intramolecular interaction, dendritic spine, f-actin, fodrin, mGluR5, ras proteins

OPEN ACCESS

Edited by:
Eunjoon Kim,
Institute for Basic Science (IBS), South Korea

Reviewed by:
Chiara Verpelli,
Istituto di Neuroscienze (IN), Italy
Mingjie Zhang,
Hong Kong University of Science and Technology, Hong Kong

****Correspondence:***
Hans-Jürgen Kreienkamp
kreienkamp@uke.de

Received: *31 May 2018*
Accepted: *16 July 2018*
Published: *07 August 2018*

Citation:
Hassani Nia F and Kreienkamp H-J (2018) Functional Relevance of Missense Mutations Affecting the N-Terminal Part of Shank3 Found in Autistic Patients. Front. Mol. Neurosci. 11:268. doi: 10.3389/fnmol.2018.00268

AUTISM SPECTRUM DISORDERS (ASD)

Autism spectrum disorders (ASD) are neurodevelopmental disorders characterized by delayed acquisition of speech, deficits in social interactions and stereotypic behaviors. In recent years several molecular genetic studies in large cohorts of patients have shown that the pathogenesis of ASDs involves a strong genetic component (Leblond et al., 2014). In several cases, potentially pathogenic mutations were identified in genes coding for synaptic proteins (Kelleher et al., 2012). These include cell adhesion proteins of the Neuroligin and Neurexin families (Jamain et al., 2003); proteins involved in signaling (e.g., regulators of small G-protein signaling such as Epac or SynGAP Woolfrey et al., 2009; Clement et al., 2012); and scaffold proteins of excitatory, glutamatergic synapses, including all three members of the Shank family (Durand et al., 2007; Moessner et al., 2007; Gauthier et al., 2009; Berkel et al., 2010). Based on these findings autism has been considered as a synaptic disease or synaptopathy, with individual mutations suspected to affect synapse formation and/or synaptic signal transduction and plasticity.

Since the introduction of exome sequencing into human genetic diagnostics, many more sequence variants continue to be discovered in ASD patients. The diagnostic challenge is then for a given patient to navigate through all these variants and make a more or less educated guess whether the variation at hand is benign or likely to be pathogenic and causative to disease. This is particularly true for missense mutations where it is difficult to assess pathogenicity in the absence of further knowledge of the functional characteristics of the encoded protein.

SHANK/PROSAP PROTEINS

Shank/ProSAP proteins (Shank1–3) are major scaffold proteins of the postsynaptic density (PSD); via multiple interactions they connect different types of glutamate receptor complexes with signaling molecules and the actin cytoskeleton of the dendritic spine. The ability of Shank3 to multimerize via its C-terminal SAM domain has led to the suggestion that formation of Shank clusters is a key event in PSD assembly (Baron et al., 2006). Shank proteins appear to function entirely through the establishment of molecular interactions with other PSD proteins; for this they employ a number of protein interaction motifs which are depicted in **Table 1**.

Loss of one copy of the region on chromosome 22 which includes the *SHANK3* gene leads to 22q13 deletion/Phelan-McDermid syndrome, which is associated with severe intellectual disability (Bonaglia et al., 2006). More generally, *SHANK* gene dosage appears to be important as duplication of the *SHANK3* gene also leads to a neurological phenotype (Han et al., 2013). In autism and also schizophrenia cases, insertions, deletions, nonsense and splice site mutations have been observed on one *SHANK3* allele which lead to loss or truncation of the protein. By introducing some of these changes into the genome of mice, Zhou et al. (2016) observed that different mutations may affect brain function in very different ways, depending on cell type and developmental stage. In addition to these presumably loss of function variants, a number of missense mutations have been found in individual autism patients (Durand et al., 2007; Moessner et al., 2007; Gauthier et al., 2009). Interestingly, the relevance of most of these mutations for Shank3 function, and their role in autism pathogenesis is unclear. This is partly due to the genetics of the patients; thus some variations found in *SHANK3* in autism patients are inherited from healthy parents (e.g., R12C and R300C), ruling out a dominant effect on disease. Whereas, all other mutations are extremely rare, R300C is found 15 times in a database of exomes of 64.000, mostly healthy individuals (Exac database), suggesting that it could be a polymorphism rather than a pathogenic mutation. In contrast, P141A and Q312R variants occur *de novo* in the affected children (Moessner et al., 2007; Boccuto et al., 2013). The L68P mutant described by Gauthier et al. (2009) was inherited, but from an epileptic father, suggesting that it may affect neurological functions in different ways, dependent on environmental and other genetic factors.

A second problem lies in the fact that mutations spare the most well studied functional domains of Shank3. Thus, so far no mutations have been identified in patients which affect the PDZ and SAM domains, or those short sequence motifs which are required for interactions with postsynaptic partners Homer, Cortactin, dynamin, IRSp53, and Abi-1. Instead, missense mutations are found in the N-terminal region including the ankyrin repeats (see below), and in the long proline rich segment between PDZ and SAM domains which has been characterized as an "intrinsically disordered region." As a consequence, it has been difficult to design functional assays where one could actually show that these mutations interfere with specific functions of the Shank3 protein. Intriguingly, mice lacking only the Ank repeat containing forms of Shank3 (Shank3A$^{-/-}$ mice) show a much milder behavioral phenotype than mice lacking most variants of the protein [Shank3B$^{-/-}$ mice (Peça et al., 2011)]. Thus, the N-terminal part of Shank3 is highly affected by mutations in human patients, but its relevance in mutant mice is unclear. This leaves us with the more general open question whether rare missense mutations found in patients are indeed pathogenic, or simply represent extremely rare polymorphisms.

STRUCTURE OF THE N-TERMINAL REGION OF SHANK3

Long variants of Shank proteins contains in their N-terminal part a set of seven Ankyrin repeats, followed by the SH3 domain (the "Sh" and "ank" in Shank). In addition, the Ank domains are preceded by a conserved domain which was initially overlooked when Shank domains were assigned. We termed this the Shank/ProSAP N-terminal (SPN) domain. This about 90 amino acid domain is most similar to the so-called F_0 motif in the FERM domain of talin, which itself is a major scaffold of focal adhesions (Goult et al., 2010). Using X-ray crystallography, Lilja et al. (2017) solved the three dimensional structure of an N-terminal fragment of rat Shank3, consisting of the SPN and Ank domains. Here the SPN domain was confirmed to fold in a ubiquitin like (ubl) fold, like the talin F_0 domain. A set of seven ankyrin repeats was observed in this structure, which was linked to the SPN motif by a 19 amino acid long linker region. This linker and the SPN domain fold back against the Ank repeats, leading to an extended interface between both domains which confirms a previously detected intramolecular interaction between SPN and Ank (Mameza et al., 2013). The structure also provides a molecular framework for further analysis of missense mutations, as the positions of mutated residues can be viewed in a 3D model (**Figure 1**).

MOLECULAR INTERACTIONS

Using both unbiased approaches such as yeast two hybrid screening, as well as educated guesses based on functional data, several interaction partners for the Ank domain have been identified: (a) Sharpin, a cytosolic signaling protein (Lim et al., 2001); (b) α-fodrin, a cytoskeletal protein which provides a link to the actin cytoskeleton (Bockers et al., 2001); (c) ion channels of the HCN family (Yi et al., 2016). Whereas, it is unclear whether Sharpin is present at postsynaptic

TABLE 1 | Functional effects of mutations affecting the N-terminus of Shank3, the upper graphic shows the domain structure of Shank3, and lists the missense mutations found in autistic patients which affect the N-terminal part of the protein.

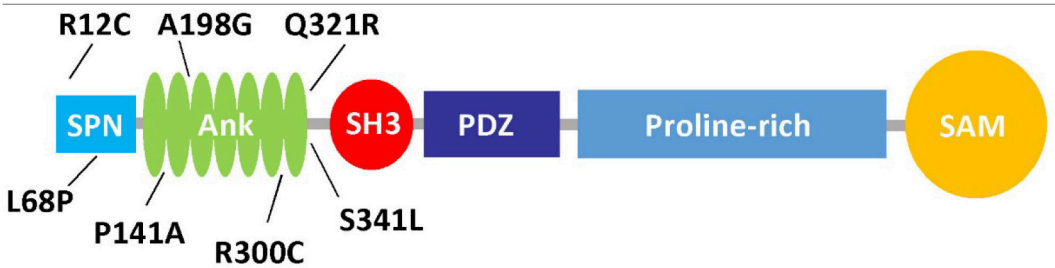

Alteration	References	Inheritance	Domain	Effect on mol. interactions	Effect on dendritic spines	Effect on synaptic signaling
R12C	Durand et al., 2007	Mother (social phobia)	SPN	Ras: reduced Intramolecular: none	Density: moderate reduction Morphology: no effect F-actin: moderate reduction	Trans-synaptic: disrupted Support of mGluR5 pathway: disrupted Inhibition of integrin: lost
L68P	Gauthier et al., 2009	Father (epilepsy)	SPN	Ras: lost Fodrin: up (ns) Sharpin: up Intramolecular: lost	Density: no effect	Inhibition of integrin: lost
P141A	Boccuto et al., 2013	*de novo*	Ank	n.d.	n.d.	n.d.
A198G	Durand et al., 2007	Mother (healthy)	Ank	n.d.	n.d.	n.d.
R300C	Durand et al., 2007	Mother (healthy)	Ank	Fodrin: none Sharpin: up	Density: moderate reduction Morphology: no effect F-actin: moderate reduction	Trans-synaptic: disrupted
Q321R	Moessner et al., 2007	*de novo*	Ank	Fodrin: none Sharpin: up	Density: moderate reduction Morphology: shorter spines with larger heads F-actin: no effect	Trans-synaptic: disrupted
S341L	Moessner et al., 2007	Father (healthy)	Ank	n.d.	n.d.	n.d.

N.d, not determined; ns, the observed effect was not statistically different from WT.

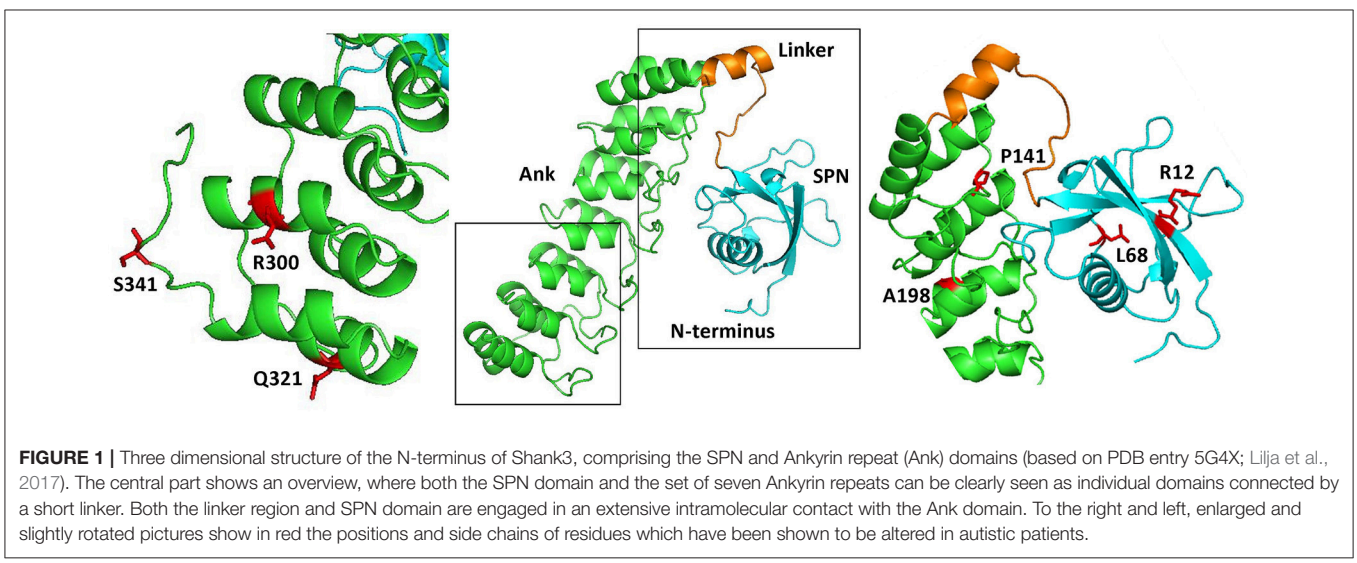

FIGURE 1 | Three dimensional structure of the N-terminus of Shank3, comprising the SPN and Ankyrin repeat (Ank) domains (based on PDB entry 5G4X; Lilja et al., 2017). The central part shows an overview, where both the SPN domain and the set of seven Ankyrin repeats can be clearly seen as individual domains connected by a short linker. Both the linker region and SPN domain are engaged in an extensive intramolecular contact with the Ank domain. To the right and left, enlarged and slightly rotated pictures show in red the positions and side chains of residues which have been shown to be altered in autistic patients.

sites in neurons together with Shank, both α-fodrin and HCN channels can be envisioned to play a role in the assumed function of Shank proteins, namely organizing the postsynaptic density and linking membrane proteins with the submembranous cytoskeleton. Intriguingly, the three interactors do not share any sequence homology or common sequence motifs which might predict a common way of binding to the Ank domain.

Initially we observed that the SPN domain is locked in an intramolecular interaction with the Ank domain, blocking access of Ank domain ligands α-fodrin and Sharpin (Mameza et al., 2013). The ubl fold of the SPN (and F_0 of talin) is similar to that observed in Ras association domains. Indeed we observed that the SPN binds to active (GTP bound) Ras family members (HRas, KRas; as well as Rap1 variants) with high affinity, whereas GDP-bound Ras proteins do not bind.

MOLECULAR EFFECTS OF MISSENSE MUTATIONS

The effects of several missense mutations found in autism patients on these interactions has been studied in some detail, mostly in biochemical assays using pulldown and co-immunoprecipitation experiments (see **Table 1**). Mutations in the Ank domain appeared to have a rather moderate effect on binding of this domain to either Sharpin or α-fodrin. In contrast, both mutations in the SPN domain (R12C and L68P) interfered with binding to Ras family small G-proteins. In the case of R12C, this could be rationalized by molecular modeling of the Shank3/Ras complex. Here, Arg12 is facing Ras and is involved in forming an ion pair with Glu37 of Ras. Mutation to Cysteine obviously eliminates this interaction and leads to loss of affinity for GTP-bound forms of HRas and Rap1. The L68P mutation interferes not only with Ras binding, but also with the intramolecular interaction with the Ank domain. Leu68 is located in the inner hydrophobic core of the SPN domain, and it is likely that a proline residue at this position will lead to an unfolding of the domain, thereby eliminating both interactions (with Ras and with the Ank domain). As a consequence, access to the Ank domain is no longer blocked by the SPN motif, leading to improved binding of Sharpin, α-fodrin and exogenously applied SPN domain (Mameza et al., 2013). These data suggest that the L68P mutation most likely induces a permanently open conformation of the N-terminal portion of Shank3, where the function of the Ank domain is unregulated and interaction with small G-proteins of Ras family eliminated (Mameza et al., 2013; Lilja et al., 2017).

FUNCTIONAL EFFECTS OF MISSENSE MUTATIONS IN THE FORMATION OF DENDRITIC SPINES

Expression of missense mutant variants of Shank3 in primary hippocampal neurons showed that the normal synaptic targeting of Shank3 was not affected by these mutations (Arons et al., 2012; Durand et al., 2012). Overexpression of Shank3 WT significantly increased dendritic spine density and decreased the number of filopodia; Shank3 constructs carrying the N-terminal mutations showed a more moderate effect on spine formation (Arons et al., 2012; Durand et al., 2012). Shank3 WT affects spine maturation by forming spines with larger heads compared to control neurons transfected with GFP. However, Shank3 carrying the *de novo* mutation Q321R caused only a slight increase in the head width but also a decrease in the length of spines. Overexpression of Shank3 variants containing the two inherited mutations R12C and R300C had no significant effect on spine size; thus these mutations disrupt the role of Shank3 on spine maturation (Durand et al., 2012).

The reduction of mEPSC frequency in Shank3 knockdown neurons (expressing a shShank3 construct) was fully restored to control levels by transfection with a shShank3-resistant form of WT Shank3 and the L68P mutant, suggesting that the L68P mutant supports normal excitatory synaptic transmission and does in this respect not result in a loss of function (Mameza et al., 2013). In another study, overexpression of Shank3 WT in hippocampal neurons significantly increased mEPSC frequency compared to the control neurons transfected with GFP, while missense mutations (R12C, R300C, Q321R) increased mEPSC frequency but not as much as WT (Durand et al., 2012).

The ASD-associated mutations in the Ank domain affect F-actin content in dendritic spines. Overexpression of Shank3 WT increased the F-actin recruitment to the dendritic spines compare to control GFP transfected neurons. Here, R12C and R300C mutant constructs had an intermediate effect on the level of F-actin in the dendritic spines and the Q321R variant had no effect. Thus, these mutations disrupt the regulatory effect of Shank3 on actin dynamics and remodeling in spines and at the postsynaptic density. This effect of Shank3 is independent of the known Shank3 interaction partner Cortactin, as WT and control neurons did not show a significant difference in the postsynaptic levels of this important regulator of actin in dendritic spines (Durand et al., 2012).

FUNCTIONAL EFFECTS OF MISSENSE MUTATIONS IN TRANSSYNAPTIC SIGNALING

Shank3 has been reported to affect not only the postsynaptic but also presynaptic function of excitatory synapses, by regulating the activity of Neuroligin/Neurexin complexes. Though SAPAP is likely to be the most specific, high affinity interactor of Shank3 in the PSD (Zeng et al., 2016), the PDZ domain of Shank3 may also directly interact with the cytoplasmic tails of postsynaptic Neuroligins (Meyer et al., 2004). Using quantitative immunofluorescent microscopy, Arons et al. (2012) showed that ASD-associated mutations in Shank3 (R12C, R300C, Q321R) interfere with the role of Shank3 in transsynaptic signaling. Unlike the overexpressed Shank3 WT, these three mutants failed to increase the level of postsynaptic Homer1 and presynaptic VGLUT1. In addition, the size of the total recycling pool of synaptic vesicles at presynaptic sites contacting dendritic profiles of neurons expressing these mutant variants of Shank3 significantly decreased compared to neurons expressing Shank3 WT. Paired whole-cell recordings showed that with all mutations, the amplitude of both AMPAR and NMDAR EPSCs decreased, and the synaptic failure rate increased compared to cells overexpressing Shank3 WT (Arons et al., 2012).

In a follow-up study, Arons et al. (2016) addressed the role of one of the mutations found in ASD patients (R12C) in the regulation of Shank3 function by Zinc. Using FRAP (fluorescence

recovery after photobleaching) assays they showed that increases in the zinc level induces stabilization of Shank3 (R12C similar to WT) and that depletion of zinc with the zinc-specific reagent TPEN increase the fraction of the both WT and R12C mutant in the immobile pool. These data suggest that zinc sensitive dynamics of Shank3 (which likely depends on an intact SAM domain; Baron et al., 2006) was not altered by this mutation. Nevertheless, the inability of the R12C variant of Shank3 to mimic the effect of Shank3 WT in enhancing presynaptic levels of VGLUT1 after zinc treatment confirmed that it is incapable of *trans*-synaptic signaling (Arons et al., 2016).

FUNCTIONAL EFFECTS OF MISSENSE MUTATIONS IN SYNAPTIC SIGNALING

A study in 2011 showed that the R12C mutation impairs the role of Shank3 in supporting the mGluR5 pathway. Using DHPG as an agonist of group I mGluRs, it was observed that in neurons transfected with a Shank3 knockdown construct (shShank3), the mGluRI signaling pathway leading to phosphorylation of ERK1/2 and CREB was impaired. Overexpression of shShank3-resistant Shank3 WT and also full-length mGluR5 were able to rescue DHPG-induced ERK1/2 activation, while the Shank3 R12C mutant was not able to do so (Verpelli et al., 2011).

The ability of the SPN domain to bind active, GTP-bound Ras proteins might affect signal transduction at synapses in different ways. Thus, Shank3 (and Shank1) could be downstream effectors of Ras signaling, in a so far unidentified signaling pathway. Alternatively, Shank3 could function to sequester active G-proteins, thus limiting their availability for other pathways. Indeed, such a scenario has been observed as both Shank1 and Shank3 were reported to negatively regulate integrin activation. This occurs due to sequestration of active Rap1 proteins via the Shank SPN domain. Both SPN domain mutations (L68P and R12C) that disrupt the binding of Shank to G-proteins also impair the inhibitory effect of Shank3 on integrin activation. Overexpression of Shank3 constructs in the rat hippocampal neurons showed that WT Shank3, but not the L68P mutant suppress formation of filopodia by inhibiting integrin activity. Also, overexpression of Shank3 WT in Shank3 KO cortical neurons plated on laminin inhibited β1-integrin activity in neuronal growth cones, while overexpressed L68P mutant failed to do so (Lilja et al., 2017).

FUTURE PERSPECTIVES AND OPEN QUESTIONS

Particularly the N-terminal portion of Shank3 is affected by missense mutations found in autism patients. Therefore, we and others have attempted to analyze the functional relevance of these mutations on a structural, molecular and cell biological level. For several mutations it is now clear that they do affect molecular interactions of the Shank3 protein; in particular, the R12C mutation rather selectively affects the binding of small G-proteins. In contrast, the L68P appears to destroy the folding of the SPN domain, thereby disrupting all of its interactions and also its regulatory effect on the Ank repeats. While the role of Arg12 and Leu68 maybe explained by the structural analysis of the Shank3 N-terminus, this is much less clear for the other five mutations which alter residues in the Ank domain. This is due to the fact that, so far, we do not know how Ank interaction partners (Sharpin, α-fodrin, HCN1) actually bind to the Ank repeats. There is no single motif in either interaction partner which has been mapped with some precision, and there is also no consensus between these three possible partners. Further analysis, accompanied by structural analysis of a possible Ank/ligand complex might help to elucidate the relevance of ASD-associated variants here.

A second open question is: how do the deficits in molecular interactions which have been identified for several variants, actually correlate with the cellular phenotype observed in neuronal cells? This is currently most unclear for the R12C mutant, which alters F-actin content as well as the form of dendritic spines, which interferes with mGluR5 signaling and which disrupts the transsynaptic strengthening of synaptic connections (see **Table 1**). The SPN domain and Arg12 are far removed in linear sequence from the PDZ domain (which binds to Neuroligin) and from the homer binding motif which links Shank3 to the Homer/mGluR5 complex. The same holds true for Arg300 and Gln321 in the Ank motif; nevertheless, mutations in both residues also interfere with spine formation induced by Shank3, and with transsynaptic signaling. These observations suggest that a possible link between the Shank3 N-terminus and the actin-based cytoskeleton needs to be studied further. This link could be provided by the actin-associated α-fodrin (which binds to the Ank repeats). However, binding to α-fodrin is only slightly affected by the missense mutations discussed here. An alternative view, which has been suggested by Arons et al. (2016) is a possible switch of Shank3 between open and closed conformations. In this way, the N-terminal (SPN and Ank) domains would interact with the C-terminal, proline rich motifs which harbor binding sites for actin regulators (cortactin; Abi-1; IRSp53) and the homer/mGluR5 complex. Through this (so far undefined) interaction, it might be explained how the N-terminus of Shank3 leads to dysregulation of the well-studied C-terminal interactions of this protein. Again, both biochemical and structural analyses will be extremely helpful to elucidate these conformational changes.

AUTHOR CONTRIBUTIONS

All authors listed have made a substantial, direct and intellectual contribution to the work, and approved it for publication.

ACKNOWLEDGMENTS

Work in the authors' laboratory is supported by Deutscher Akademischer Austauschdienst (DAAD; to FHN) and Deutsche Forschungsgemeinschaft (DFG; to H-JK).

REFERENCES

Arons, M. H., Lee, K., Thynne, C. J., Kim, S. A., Schob, C., Kindler, S., et al. (2016). Shank3 is part of a zinc-sensitive signaling system that regulates excitatory synaptic strength. *J. Neurosci.* 36, 9124–9134. doi: 10.1523/JNEUROSCI.0116-16.2016

Arons, M. H., Thynne, C. J., Grabrucker, A. M., Li, D., Schoen, M., Cheyne, J. E., et al. (2012). Autism-associated mutations in ProSAP2/Shank3 impair synaptic transmission and neurexin-neuroligin-mediated transsynaptic signaling. *J. Neurosci.* 32, 14966–14978. doi: 10.1523/JNEUROSCI.2215-12.2012

Baron, M. K., Boeckers, T. M., Vaida, B., Faham, S., Gingery, M., Sawaya, M. R., et al. (2006). An architectural framework that may lie at the core of the postsynaptic density. *Science* 311, 531–535. doi: 10.1126/science.1118995

Berkel, S., Marshall, C. R., Weiss, B., Howe, J., Roeth, R., Moog, U., et al. (2010). Mutations in the SHANK2 synaptic scaffolding gene in autism spectrum disorder and mental retardation. *Nat. Genet.* 42, 489–491. doi: 10.1038/ng.589

Boccuto, L., Lauri, M., Sarasua, S. M., Skinner, C. D., Buccella, D., Dwivedi, A., et al. (2013). Prevalence of SHANK3 variants in patients with different subtypes of autism spectrum disorders. *Eur. J. Hum. Genet.* 21, 310–316. doi: 10.1038/ejhg.2012.175

Bockers, T. M., Mameza, M. G., Kreutz, M. R., Bockmann, J., Weise, C., Buck, F., et al. (2001). Synaptic scaffolding proteins in rat brain. ankyrin repeats of the multidomain Shank protein family interact with the cytoskeletal protein alpha-fodrin. *J. Biol. Chem.* 276, 40104–40112. doi: 10.1074/jbc.M102454200

Bonaglia, M. C., Giorda, R., Mani, E., Aceti, G., Anderlid, B. M., Baroncini, A., et al. (2006). Identification of a recurrent breakpoint within the SHANK3 gene in the 22q13.3 deletion syndrome. *J. Med. Genet.* 43, 822–828. doi: 10.1136/jmg.2005.038604

Clement, J. P., Aceti, M., Creson, T. K., Ozkan, E. D., Shi, Y., Reish, N. J., et al. (2012). Pathogenic SYNGAP1 mutations impair cognitive development by disrupting maturation of dendritic spine synapses. *Cell* 151, 709–723. doi: 10.1016/j.cell.2012.08.045

Durand, C. M., Betancur, C., Boeckers, T. M., Bockmann, J., Chaste, P., Fauchereau, F., et al. (2007). Mutations in the gene encoding the synaptic scaffolding protein SHANK3 are associated with autism spectrum disorders. *Nat. Genet.* 39, 25–27. doi: 10.1038/ng1933

Durand, C. M., Perroy, J., Loll, F., Perrais, D., Fagni, L., Bourgeron, T., et al. (2012). SHANK3 mutations identified in autism lead to modification of dendritic spine morphology via an actin-dependent mechanism. *Mol. Psychiatry* 17, 71–84. doi: 10.1038/mp.2011.57

Gauthier, J., Spiegelman, D., Piton, A., Lafrenière, R. G., Laurent, S., St-Onge, J., et al. (2009). Novel *de novo* SHANK3 mutation in autistic patients. *Am. J. Med. Genet. B Neuropsychiatr. Genet.* 150B, 421–424. doi: 10.1002/ajmg.b.30822

Goult, B. T., Bouaouina, M., Elliott, P. R., Bate, N., Patel, B., Gingras, A. R., et al. (2010). Structure of a double ubiquitin-like domain in the talin head: a role in integrin activation. *EMBO J.* 29, 1069–1080. doi: 10.1038/emboj.2010.4

Han, K., Holder, J. L. Jr., Schaaf, C. P., Lu, H., Chen, H., Kang, H., et al. (2013). SHANK3 overexpression causes manic-like behaviour with unique pharmacogenetic properties. *Nature* 503, 72–77. doi: 10.1038/nature12630

Jamain, S., Quach, H., Betancur, C., Rastam, M., Colineaux, C., Gillberg, I. C., et al. (2003). Mutations of the X-linked genes encoding neuroligins NLGN3 and NLGN4 are associated with autism. *Nat. Genet.* 34, 27–29. doi: 10.1038/ng1136

Kelleher, R. J. 3rd, Geigenmüller, U., Hovhannisyan, H., Trautman, E., Pinard, R., Rathmell, B., et al. (2012). High-throughput sequencing of mGluR signaling pathway genes reveals enrichment of rare variants in autism. *PLoS ONE* 7:e35003. doi: 10.1371/journal.pone.0035003

Leblond, C. S., Nava, C., Polge, A., Gauthier, J., Huguet, G., Lumbroso, S., et al. (2014). Meta-analysis of SHANK mutations in autism spectrum disorders: a gradient of severity in cognitive impairments. *PLoS Genet.* 10:e1004580. doi: 10.1371/journal.pgen.1004580

Lilja, J., Zacharchenko, T., Georgiadou, M., Jacquemet, G., De Franceschi, N., Peuhu, E., et al. (2017). SHANK proteins limit integrin activation by directly interacting with Rap1 and R-Ras. *Nat. Cell Biol.* 19, 292–305. doi: 10.1038/ncb3487

Lim, S., Sala, C., Yoon, J., Park, S., Kuroda, S., Sheng, M., et al. (2001). Sharpin, a novel postsynaptic density protein that directly interacts with the shank family of proteins. *Mol. Cell Neurosci.* 17, 385–397. doi: 10.1006/mcne.2000.0940

Mameza, M. G., Dvoretskova, E., Bamann, M., Hönck, H. H., Güler, T., Boeckers, T. M., et al. (2013). SHANK3 gene mutations associated with autism facilitate ligand binding to the Shank3 ankyrin repeat region. *J. Biol. Chem.* 288, 26697–26708. doi: 10.1074/jbc.M112.424747

Meyer, G., Varoqueaux, F., Neeb, A., Oschlies, M., and Brose, N. (2004). The complexity of PDZ domain-mediated interactions at glutamatergic synapses: a case study on neuroligin. *Neuropharmacology* 47, 724–733. doi: 10.1016/j.neuropharm.2004.06.023

Moessner, R., Marshall, C. R., Sutcliffe, J. S., Skaug, J., Pinto, D., Vincent, J., et al. (2007). Contribution of SHANK3 mutations to autism spectrum disorder. *Am. J. Hum. Genet.* 81, 1289–1297. doi: 10.1086/522590

Peça, J., Feliciano, C., Ting, J. T., Wang, W., Wells, M. F., Venkatraman, T. N., et al. (2011). Shank3 mutant mice display autistic-like behaviours and striatal dysfunction. *Nature* 472, 437–442. doi: 10.1038/nature09965

Verpelli, C., Dvoretskova, E., Vicidomini, C., Rossi, F., Chiappalone, M., Schoen, M., et al. (2011). Importance of Shank3 protein in regulating metabotropic glutamate receptor 5 (mGluR5) expression and signaling at synapses. *J. Biol. Chem.* 286, 34839–34850. doi: 10.1074/jbc.M111.258384

Woolfrey, K. M., Srivastava, D. P., Photowala, H., Yamashita, M., Barbolina, M. V., Cahill, M. E., et al. (2009). Epac2 induces synapse remodeling and depression and its disease-associated forms alter spines. *Nat. Neurosci.* 12, 1275–1284. doi: 10.1038/nn.2386

Yi, F., Danko, T., Botelho, S. C., Patzke, C., Pak, C., Wernig, M., et al. (2016). Autism-associated SHANK3 haploinsufficiency causes Ih channelopathy in human neurons. *Science* 352:aaf2669. doi: 10.1126/science.aaf2669

Zeng, M., Shang, Y., Guo, T., He, Q., Yung, W. H., Liu, K., et al. (2016). A binding site outside the canonical PDZ domain determines the specific interaction between Shank and SAPAP and their function. *Proc. Natl. Acad. Sci. U.S.A.* 113, E3081–E3090. doi: 10.1073/pnas.1523265113

Zhou, Y., Kaiser, T., Monteiro, P., Zhang, X., Van der Goes, M. S., Wang, D., et al. (2016). Mice with Shank3 mutations associated with ASD and schizophrenia display both shared and distinct defects. *Neuron* 89, 147–162. doi: 10.1016/j.neuron.2015.11.023

Conflict of Interest Statement: The authors declare that the research was conducted in the absence of any commercial or financial relationships that could be construed as a potential conflict of interest.

frontiers in Molecular Neuroscience

ORIGINAL RESEARCH
published: 31 August 2018
doi: 10.3389/fnmol.2018.00250

Integrative Brain Transcriptome Analysis Reveals Region-Specific and Broad Molecular Changes in *Shank3*-Overexpressing Mice

Chunmei Jin[1,2†], Hyojin Kang[3†], Jae Ryun Ryu[2,4], Shinhyun Kim[1,2], Yinhua Zhang[1,2], Yeunkum Lee[1,2], Yoonhee Kim[1,2] and Kihoon Han[1,2]*

[1] Department of Neuroscience, College of Medicine, Korea University, Seoul, South Korea, [2] Department of Biomedical Sciences, College of Medicine, Korea University, Seoul, South Korea, [3] Supercomputing Center, Korea Institute of Science and Technology Information, Daejeon, South Korea, [4] Department of Anatomy, College of Medicine, Korea University, Seoul, South Korea

Variants of the SH3 and multiple ankyrin repeat domain 3 (*SHANK3*) gene, encoding excitatory postsynaptic core scaffolding proteins, are causally associated with numerous neurodevelopmental and neuropsychiatric disorders, including autism spectrum disorder (ASD), bipolar disorder, intellectual disability, and schizophrenia (SCZ). Although detailed synaptic changes of various *Shank3* mutant mice have been well characterized, broader downstream molecular changes, including direct and indirect changes, remain largely unknown. To address this issue, we performed a transcriptome analysis of the medial prefrontal cortex (mPFC) of adult *Shank3*-overexpressing transgenic (TG) mice, using an RNA-sequencing approach. We also re-analyzed previously reported RNA-sequencing results of the striatum of adult *Shank3* TG mice and of the prefrontal cortex of juvenile $Shank3^{+/\Delta C}$ mice with a 50–70% reduction of Shank3 proteins. We found that several myelin-related genes were significantly downregulated specifically in the mPFC, but not in the striatum or hippocampus, of adult *Shank3* TG mice by comparing the differentially expressed genes (DEGs) of the analyses side by side. Moreover, we also found nine common DEGs between the mPFC and striatum of *Shank3* TG mice, among which we further characterized ASD- and SCZ-associated G protein-coupled receptor 85 (*Gpr85*), encoding an orphan *Gpr* interacting with PSD-95. Unlike the mPFC-specific decrease of myelin-related genes, we found that the mRNA levels of *Gpr85* increased in multiple brain regions of adult *Shank3* TG mice, whereas the mRNA levels of its family members, *Gpr27* and *Gpr173*, decreased in the cortex and striatum. Intriguingly, in cultured neurons, the mRNA levels of *Gpr27*, *Gpr85*, and *Gpr173* were modulated by the neuronal activity. Furthermore, exogenously expressed GPR85 was co-localized with PSD-95 and Shank3 in cultured neurons and negatively regulated the number of excitatory synapses, suggesting its potential role in homeostatic regulation of excitatory synapses in *Shank3* TG neurons. Finally, we performed a gene set enrichment analysis of the

OPEN ACCESS

Edited by:
Deepak Prakash Srivastava, King's College London, United Kingdom

Reviewed by:
Carlo Sala, Istituto di Neuroscienze (IN), Italy
Michael Schön, Universität Ulm, Germany

***Correspondence:**
Kihoon Han
neurohan@korea.ac.kr

† These authors have contributed equally to this work

Received: *26 April 2018*
Accepted: *02 July 2018*
Published: *31 August 2018*

Citation:
Jin C, Kang H, Ryu JR, Kim S, Zhang Y, Lee Y, Kim Y and Han K (2018) Integrative Brain Transcriptome Analysis Reveals Region-Specific and Broad Molecular Changes in Shank3-Overexpressing Mice. Front. Mol. Neurosci. 11:250. doi: 10.3389/fnmol.2018.00250

RNA-sequencing results, which suggested that *Shank3* could affect the directional expression pattern of numerous ribosome-related genes in a dosage-dependent manner. To sum up, these results reveal previously unidentified brain region-specific and broad molecular changes in *Shank3*-overexpressing mice, further elucidating the complexity of the molecular pathophysiology of *SHANK3*-associated brain disorders.

Keywords: Shank3, mPFC, striatum, transcriptome, myelin, GPR85, ribosome

INTRODUCTION

SH3 and multiple ankyrin repeat domain 3 (*SHANK3*), also known as proline-rich synapse-associated protein 2 (*ProSAP2*), is a gene that encodes excitatory synaptic core scaffolding proteins that organize the macromolecular protein complex of the postsynaptic density (PSD) (Naisbitt et al., 1999; Sheng and Kim, 2000). Clinically, deletions of the chromosomal region containing *SHANK3* cause Phelan–McDermid syndrome (Wilson et al., 2003; Costales and Kolevzon, 2015; Harony-Nicolas et al., 2015), and a variety of point mutations and small deletions of *SHANK3* have been causally associated with numerous neurodevelopmental and neuropsychiatric disorders, including autism spectrum disorder (ASD), intellectual disability, and schizophrenia (SCZ) (Grabrucker et al., 2011; Duffney et al., 2015), which have been modeled by several lines of knock-out and knock-in mouse models (Jiang and Ehlers, 2013; Yoo et al., 2014; Schmeisser, 2015; Monteiro and Feng, 2017). Moreover, duplications of *SHANK3* have also been found in patients with Asperger's syndrome, attention-deficit hyperactivity disorder (ADHD) (Moessner et al., 2007), bipolar disorder (Han et al., 2013), and SCZ (Failla et al., 2007), and the transgenic mice that mildly overexpress Shank3 proteins (∼50%) display manic-like hyperkinetic behaviors and spontaneous seizures (Han et al., 2013; Choi and Han, 2015; Lee et al., 2018). These results indicate that proper expression and function of Shank3 are critical for normal synaptic development and function. Indeed, Shank3-dependent molecular, structural, and functional changes of excitatory synapses have been deeply characterized from *in vitro* and *in vivo* studies to elucidate some of the key underlying pathophysiological mechanisms (Han et al., 2013; Wang et al., 2016) and to provide potential therapeutic approaches for *SHANK3*-associated brain disorders, mainly ASDs (Bozdagi et al., 2013; Shcheglovitov et al., 2013; Duffney et al., 2015; Bidinosti et al., 2016; Vicidomini et al., 2016; Wang et al., 2016).

In contrast, it still remains largely unknown how different variants of a single gene, *SHANK3*, can lead to diverse phenotypic outcomes or clinical symptoms. Possible explanations could be that *SHANK3* expresses numerous Shank3 protein isoforms due to alternative splicing and multiple internal promoters, and that different brain regions express different combinations and levels of these Shank3 isoforms (Wang et al., 2014). Furthermore, we recently demonstrated that Shank3 protein interactomes of different brain regions consist of both brain region-specific (major portion) and common interactors (minor portion), which, together with the isoform diversity, suggest that alterations of Shank3 expression or function could have some distinct effects in different brain regions (Lee et al., 2017b). Supporting this hypothesis, it was reported that the functional changes of different brain regions could vary even in a single *Shank3* mutant mouse line (Peca et al., 2011; Lee et al., 2015; Zhou et al., 2016). Nevertheless, these results are so far limited to the characterizations of synaptic changes in *Shank3* knock-out mice. Broader downstream molecular changes, including direct and indirect changes, of Shank3 that might be possible even in non-neuronal cell types remain scarcely investigated.

To address this issue, in this study, we performed a transcriptome analysis of the medial prefrontal cortex (mPFC) of *Shank3*-overexpressing transgenic (TG) mice (Han et al., 2013) and compared the result with previously reported transcriptome analyses of the striatum of *Shank3* TG mice (Lee et al., 2017d) and the prefrontal cortex (PFC) of *Shank3* heterozygous (*Shank3*$^{+/\Delta C}$, heterozygous mice for C-terminal exon 21 deletion of *Shank3*) mice (Duffney et al., 2015; Qin et al., 2018). We focused on the mPFC and striatum for several reasons. The mPFC has well-established roles in top-down regulatory control over various subcortical nuclei involved in regulating emotional, social, and cognitive behaviors (Russo and Nestler, 2013; Riga et al., 2014), which are impaired in brain disorders associated with *SHANK3* mutations. The striatum is a key component of the brain motor and reward systems (Balleine et al., 2007; Russo and Nestler, 2013), abnormalities of which may contribute to behavioral symptoms observed in ASD, bipolar disorder, or SCZ. Furthermore, Shank3 is highly expressed in the mPFC and striatum (Monteiro and Feng, 2017), and indeed, molecular, cellular, and electrophysiological defects in the mPFC and striatal neurons are observed in numerous rodent models having *Shank3* mutations (Peca et al., 2011; Lee et al., 2015; Harony-Nicolas et al., 2017; Bey et al., 2018).

From integrative analyses and experimental validations, we found that the expression levels of myelin-related genes were downregulated specifically in the mPFC, but not in the striatum or hippocampus, of *Shank3* TG mice. Meanwhile, the expression of *Gpr85*, encoding an orphan G protein-coupled receptor, was increased in multiple brain regions of *Shank3* TG mice. We then further characterized the functional effects of this gene on excitatory synapses. Finally, we found that Shank3 affected the directional expression pattern of numerous ribosome-related genes in a dosage-dependent manner. To sum up, these results provide new insights into the complexity and heterogeneity of the molecular pathophysiology of *SHANK3*-associated brain disorders.

MATERIALS AND METHODS

Mice

The enhanced green fluorescent protein (EGFP)-*Shank3* transgenic (TG) mice used in this study have been described previously (Han et al., 2013; Lee et al., 2017a,b,d). The male wild-type (WT) and TG mice were bred and maintained in a C57BL/6J background according to the Korea University College of Medicine Research Requirements, and all the experimental procedures were approved by the Committees on Animal Research at the Korea University College of Medicine (KOREA-2016-0096). The mice were fed and had access to water *ad libitum* and were housed under a 12-h light–dark cycle. For all experiments, "control WT mice" means WT littermates of the TG mice used for experiments.

RNA Sequencing and Analysis

The mice (10- to 12-week-old male WT and *Shank3* TG) were deeply anesthetized with isoflurane and decapitated. The mPFC was dissected from each brain using a brain matrix (Alto, SA-2175, coronal 1 mm). Specifically, we put brains in contact with the front side (olfactory bulb side) of the matrix and cut off the first 2 mm of brains including the olfactory bulb. Then, we dissected out the next 2 mm of the remaining brain tissue. From the resulting coronal sections, we further dissected the mPFC area as shown in Figure 1A of Lee et al. (2017b). After dissection, the mPFC was immediately placed in a RNAlater solution (Ambion) and stored at 4°C overnight. The mPFC from two mice of same genotype was pooled to make one RNA sample, and a total three pairs of RNA samples (three WT and three *Shank3* TG; thus total six mice per each genotype) were processed for RNA sequencing. RNA extraction, library preparation, cluster generation, and sequencing were performed by Macrogen Inc. (Seoul, Korea). RNA samples for sequencing were prepared using a TruSeq Stranded mRNA LT Sample Prep Kit (Illumina) according to the manufacturer's instructions. An Illumina's HiSeq 2000 was used for sequencing to generate 101-bp paired-end reads (**Supplementary Table S1**). Raw data were submitted to the GEO (Gene Expression Omnibus) repository under the accession number GSE113368.

Transcript abundance was estimated with Salmon (v0.9.1) (Patro et al., 2017) in quasi-mapping-based mode onto the *Mus musculus* genome (GRCm38) with GC bias correction (–gcBias). Quantified gene-level abundance data were imported to R (v.3.6.0) with the tximport (Soneson et al., 2015) package, and differential gene expression analysis was carried out using R/Bioconductor DEseq2 (v1.19.11) (Love et al., 2014). Normalized read counts were computed by dividing the raw read counts by size factors and fitted to a negative binomial distribution. The *P*-values were first corrected by applying an empirical estimation of the null distribution using the R fdrtool (v.1.2.15) package and then adjusted for multiple testing with the Benjamini–Hochberg correction. Genes with an adjusted *P*-value of <0.05 were considered as differentially expressed. Volcano plots were generated using the R ggplot2 (v.2.2.1) package.

The gene ontology (GO) and Kyoto Encyclopedia of Genes and Genomes (KEGG) pathway analyses were performed using DAVID software (version 6.8) (Huang da et al., 2009). Mouse gene names were converted to human homologs using the Mouse Genome Informatics (MGI) database[1].

To define "myelin-related genes," a total of 333 human and mouse genes were extracted from five query terms ("central nervous system myelination," "myelination," "structural constituent of myelin sheath," "myelin sheath," and "myelin sheath adaxonal region") from AmiGO[2].

Gene set enrichment analysis (GSEA)[3] (Subramanian et al., 2005) was used to determine whether *a priori*-defined gene sets would show statistically significant differences in expression between *Shank3* TG and WT mice. Enrichment analysis was performed using GSEAPreranked (gsea-3.0.jar) module on gene set collections H (Hallmark gene sets; 50 gene sets) and CP (KEGG; 186 gene sets) downloaded from Molecular Signature Database (MSigDB) v6.1[4]. GSEAPreranked was applied using the list of all genes expressed, ranked by the fold change, and multiplied by the inverse of the *P*-value with recommended default settings (1,000 permutations and a classic scoring scheme). The false discovery rate (FDR) was estimated to control the false-positive finding of a given normalized enrichment score (NES) by comparing the tails of the observed and null distributions derived from 1,000 gene set permutations. The gene sets with an FDR of <0.05 were considered as significantly enriched.

RNA Purification and qRT-PCR

Real-time quantitative reverse transcription PCR (qRT-PCR) was performed as described previously (Kim et al., 2016; Lee et al., 2017a). In brief, total RNA was extracted from the brain regions of WT and *Shank3* TG mice or cultured rat neurons using an miRNeasy Mini Kit (Qiagen) according to the manufacturer's instructions. Two micrograms of total RNA were used for the cDNA synthesis using iScript^{TM} cDNA Synthesis Kit (Bio-Rad). Target mRNAs were detected and quantified by a real-time PCR instrument (CFX96 Touch, Bio-Rad) using SYBR Green master mix (Bio-Rad). The results were analyzed using the comparative *C*t method normalized against the housekeeping gene *Gapdh*. The primer sequences for real-time PCR are as follows:

Mouse *Plp1* forward 5′ CCCACCCCTATCCGCTAGTT 3′,
reverse 5′ CAGGAAAAAAAGCACCATTGTG 3′
Mouse *Myrf* forward 5′ TGGCAACTTCACCTACCACA 3′,
reverse 5′ GTGGAACCTCTGCAAAAAGC 3′
Mouse *Mobp* forward 5′ AACTCCAAGCGTGAGATCGT 3′,
reverse 5′ CTCGGTCACTTCTTCCTTGG 3′
Mouse *Mbp* forward 5′ ACACACGAGAACTACCCATT ATGG 3′,
reverse 5′ AGAAATGGACTACTGGGTTTTCATCT 3′
Mouse *Tspan2* forward 5′ TGCGGTGCATCAAGTATCTG 3′,

[1]http://www.informatics.jax.org/homology.shtml
[2]http://amigo.geneontology.org/amigo
[3]http://software.broadinstitute.org/gsea
[4]http://software.broadinstitute.org/gsea/msigdb

reverse 5′ ATAACGGCTGATCCGGCTA 3′
Mouse *Cldn11* forward 5′ GTGGTGGGTTTCGTCAC GAG 3′,
reverse 5′ CGTCCATTTTTCGGCAGGTG 3′
Mouse *Mog* forward 5′ CTGTTTGTTATTGTGCCTGTT CTTG 3′,
reverse 5′ AGTCTTCGGTGCAGCCAGTT 3′
Mouse *Mag* forward 5′ GGTGTTGAGGGAGGCAGTTG 3′,
reverse 5′ CGTTCTCTGCTAGGCAAGCA 3′
Mouse *Shank3* forward 5′ TGGTTGGCAAGAGATCCAT 3′,
reverse 5′ TTGGCCCCATAGAACAAAAG 3′
Mouse *Gpr27* forward 5′ GAAGAGGCTGTGCAAGA TGTT 3′,
reverse 5′ AGCTCCCGGTTGAAGAGGA 3′
Mouse *Gpr85* forward 5′ ATGCAGCCGACAACATTT TGC 3′,
reverse 5′ CAGGTGGAGCCATTTTTGACA 3′
Mouse *Gpr173* forward 5′ CTGCACAAGGCTCCTTA CTAC 3′,
reverse 5′ CAGCCATAAAGGCCACAATCTTA 3′
Mouse *Gapdh* forward 5′ GGCATTGCTCTCAATGACAA 3′,
reverse 5′ CCCTGTTGCTGTAGCCGTAT 3′
Rat *Gpr27* forward 5′ GAAGAGGCTGTGCAAGATGTT 3′,
reverse 5′ AGCTCCCGGTTGAAGAGGA 3′
Rat *Gpr85* forward 5′ TCAGCGTCACCAGATACTTAGC 3′,
reverse 5′ CCAAACACGTCCAAAAGGTCA 3′
Rat *Gpr173* forward 5′ CTGCACAAGGCTCCTTACTAC 3′,
reverse 5′ CAGCCATAAAGGCCACAATCTTA 3′
Rat *Gapdh* forward 5′ GGATACTGAGAGCAAGAGAGA 3′,
reverse 5′ TTATGGGGTCTGGGATGGAA 3′

cDNA Constructs

The full-length mouse *Gpr85* cDNA was PCR amplified from mouse brain cDNA library and subcloned into pRK5-Myc plasmid (WT and Δ*C* constructs). Mutagenesis reaction was performed using QuikChange II XL site-directed mutagenesis kit (Agilent Technologies) according to the manufacturer's instructions to generate pRK5-Myc-GPR85 M152T construct (forward 5′ GGGGAATGCCGTGGCCACGGACAGAG 3′ and reverse 5′ CTCTGTCCGTGGCCACGGCATTCCCC 3′ primers). The pRK5-HA-Shank3 construct was described previously (Choi et al., 2015b). The construct contains a HA-tag followed by the full-length rat *Shank3* mRNA (NM_021676.1) with entire coding region and 3′UTR.

Neuron Culture, Drug Treatment, Transfection, and Immunocytochemistry

Cultured cortical and hippocampal neurons were prepared from embryonic day 18 rat brains as described previously (Lee et al., 2017c). Dissociated neurons on poly-L-lysine-coated six-well plates or coverslips were placed in a neurobasal medium supplemented with B27 (Invitrogen), 0.5 mM L-glutamine, and penicillin/streptomycin (Thermo Fisher Scientific). For the drug treatment, cultured cortical neurons at days *in vitro* (DIV) 21 were treated with either picrotoxin (50 μM, Sigma-Aldrich) or tetrodotoxin (1 μM, Alomone Labs) for an indicated period and processed for RNA extraction. For immunocytochemistry, cultured hippocampal neurons at DIV 7 were transfected with Myc-GPR85 (alone or together with HA-Shank3 construct) constructs using calcium phosphate. The neurons were fixed with 4% PFA/sucrose, permeabilized with 0.2% Triton X-100, and incubated with HA (Santa Cruz, sc-7392), Myc (Santa Cruz, sc-40; Abcam, AB9106), and PSD-95 (NeuroMab, 75-028) primary and dye-conjugated secondary antibodies (Jackson ImmunoResearch). For surface staining, the neurons were incubated with Myc antibody before the permeabilization process. Images were acquired by confocal microscopy (Zeiss, LSM780) and quantified using ImageJ software in a blinded manner. Specifically, dendritic segments (length of at least 50 μm, measured by ImageJ) of the primary or secondary branches of neurons were randomly selected by an analyzer blinded to the transfected construct, and puncta along the dendritic segments were manually counted. The results were collected from three independent experiments (i.e., three independent rounds of neuron culture to image analysis; total n = 16, 16, 24 neurons for WT, Δ*C*, and M152T constructs were measured, respectively).

Quantification and Statistical Analysis

Values from at least three independent experiments were used for quantification and statistical analysis. This means that we performed at least three independent technical experiments, and we used different biological samples for each technical experiment. *P*-values were calculated by two-tailed unpaired Student's *t*-test unless otherwise specified, using GraphPad Prism 6 software. All data are presented as the mean ± SEM. $^{*}P < 0.05$; $^{**}P < 0.01$; and $^{***}P < 0.001$.

RESULTS

Identification and Comparison of DEGs From the Transcriptome Analysis of *Shank3* TG mPFC

To investigate molecular changes in the mPFC of *Shank3* TG mice, we performed a transcriptome analysis (RNA sequencing [RNA-seq]) of mPFC tissue from adult (10- to 12-week-old) WT and *Shank3* TG mice (**Supplementary Tables S1, S2**). We reasoned that this unbiased approach might highlight the major molecular changes or signaling pathways affected by mild Shank3 overexpression in the mPFC, as was done to reveal the altered mTORC1 signaling in the striatum of *Shank3* TG mice (Lee et al., 2017d). After applying adjusted *P* values (<0.05, Benjamini–Hochberg correction) to the transcriptome analysis, we identified 195 differentially expressed genes (DEGs) (82 upregulated and 113 downregulated) in the *Shank3* TG mPFC compared with the WT mPFC (**Figure 1A** and **Supplementary Table S3**). Based on the fold change values, odorant-binding protein 2B (*Obp2b*), C-type lectin domain family 1 member B (*Clec1b*), and secretagogin, EF-hand calcium-binding protein (*Scgn*) were the top three upregulated genes, whereas transmembrane protein 212 (*Tmem212*), calpain 11 (*Capn11*), and solute carrier family 5 member 11 (*Slc5a11*) were the top three downregulated

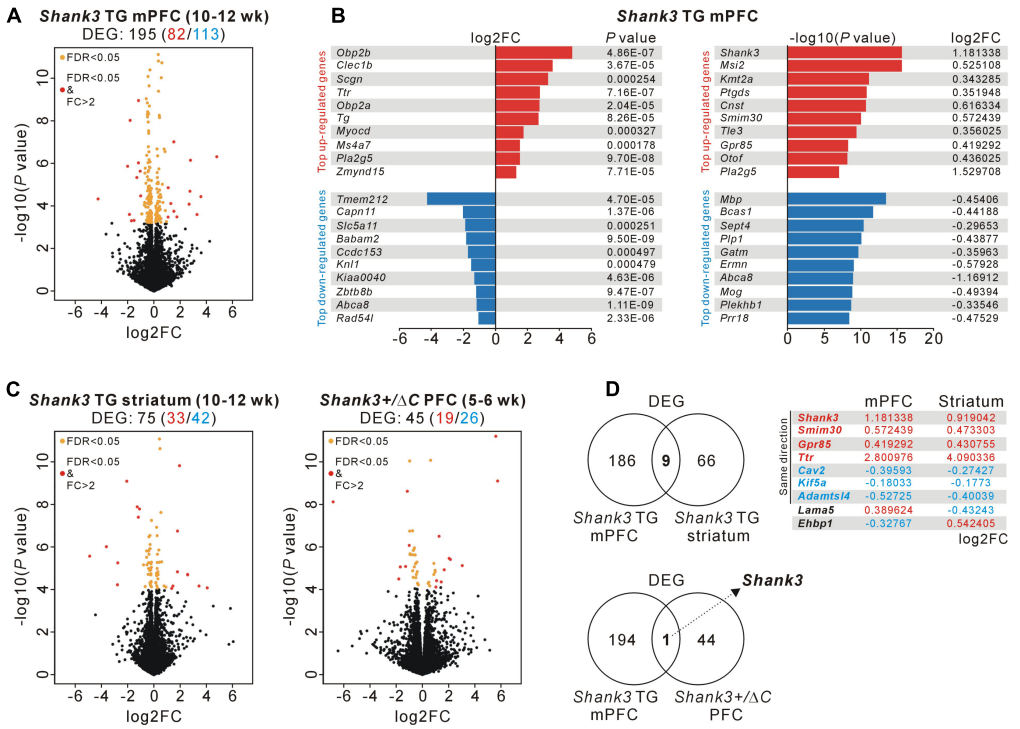

FIGURE 1 | RNA-seq and DEG analyses in the *Shank3* TG mPFC and striatum and in the *Shank3*$^{+/\Delta C}$ PFC. **(A)** Volcano plot for the mPFC RNA-seq analysis of 10- to 12-week-old *Shank3* TG mice. Differentially expressed genes (DEGs), defined by FDR < 0.05, are shown as orange (FC ≤ 2) and red (FC > 2) circles. FC, fold change. The complete lists of the RNA-seq analysis and DEGs are provided in **Supplementary Tables S2, S3**. **(B)** List of top 10 upregulated and downregulated DEGs [based on the fold changes (left) and based on the *P*-values (right)] from the mPFC RNA-seq analysis of *Shank3* TG mice. **(C)** Volcano plots for the striatum RNA-seq analysis of 10- to 12-week-old *Shank3* TG mice (left) and for the PFC RNA-seq analysis of 5- to 6-week-old *Shank3*$^{+/\Delta C}$ mice (right). The complete lists of DEGs are provided in **Supplementary Tables S4, S5**, respectively. **(D)** The Venn diagrams show the numbers of common DEGs between the mPFC and striatum of *Shank3* TG mice (nine genes, upper) and between the mPFC of *Shank3* TG mice and the PFC of *Shank3*$^{+/\Delta C}$ mice (only *Shank3*, lower). For the nine common DEGs between the mPFC and striatum of *Shank3* TG mice, the $\log_2$FC values for each brain region are shown.

genes (**Figure 1B**, left). In contrast, based on the *P* values, *Shank3*, Musashi RNA-binding protein 2 (*Msi2*), and lysine methyltransferase 2A (*Kmt2a*) were the top three upregulated genes, whereas myelin basic protein (*Mbp*), breast carcinoma-amplified sequence 1 (*Bcas1*), and septin 4 (*Sept4*) were the top three downregulated genes (**Figure 1B**, right).

Next, we tried to understand how specific the *Shank3* TG mPFC DEGs were by comparing them with DEGs from two recently published *Shank3*-related RNA-seq studies. One was from the striatum of adult (10- to 12-week-old) *Shank3* TG mice (Lee et al., 2017d), with which we aimed to identify both brain region-specific (i.e., mPFC- or striatum-specific) and, if any, broad (i.e., common to multiple brain regions) molecular changes in adult *Shank3* TG mice. The other was from the PFC of juvenile (5- to 6-week-old) *Shank3*$^{+/\Delta C}$ mice (Qin et al., 2018), which are heterozygous mice for C-terminal exon 21 deletion of *Shank3*. The *Shank3*$^{+/\Delta C}$ mice show a 50–70% reduction of Shank3 proteins in the PFC and display several autism-like behaviors, including social preference deficits and repetitive behaviors, together with molecular and functional changes of excitatory synapses in the PFC (Duffney et al., 2015). Despite the age difference (adult versus juvenile) between the mice used for the analyses, we hypothesized that we might be able to identify *Shank3* dosage-dependent molecular changes in the PFC region by comparing the RNA-seq results of *Shank3* TG mPFC and *Shank3*$^{+/\Delta C}$ PFC.

We downloaded the raw data sets of the *Shank3* TG striatum and *Shank3*$^{+/\Delta C}$ PFC RNA-seq analyses and re-processed them using the same protocol as for the *Shank3* TG mPFC RNA-seq analysis to compare the DEGs in greater detail. This approach identified 75 DEGs (33 upregulated and 42 downregulated) in the *Shank3* TG striatum (**Figure 1C**, left and **Supplementary Table S4**) and 45 DEGs (19 upregulated and 26 downregulated) in the *Shank3*$^{+/\Delta C}$ PFC (**Figure 1C**, right and **Supplementary Table S5**), compared with corresponding WT controls. When we compared the DEG lists of the *Shank3* TG mPFC and striatum, nine genes were common to both, including *Shank3* (**Figure 1D**, upper). *Shank3*, small integral membrane protein 30 (*Smim30*), G protein-coupled receptor 85 (*Gpr85*), and transthyretin (*Ttr*) were upregulated, whereas caveolin 2 (*Cav2*), kinesin family member 5A (*Kif5a*), and ADAMTS like 4 (*Adamtsl4*) were downregulated, in both brain regions of *Shank3* TG mice compared with WT mice. Intriguingly, in the case of two genes, laminin subunit alpha 5 (*Lama5*) and EH domain-binding protein 1 (*Ehbp1*), the directions of changes in expression were the opposite in the mPFC and striatum of

Shank3 TG mice. *Lama5* was upregulated and downregulated in the mPFC and striatum of *Shank3* TG mice compared with WT mice, respectively. Meanwhile, *Ehbp1* was downregulated and upregulated in the *Shank3* TG mPFC and striatum, respectively. In contrast to the nine common DEGs between *Shank3* TG mPFC and striatum, there was only one common DEG, *Shank3*, between the *Shank3* TG mPFC and *Shank3*$^{+/\Delta C}$ PFC (**Figure 1D**, lower). Overall, these results indicate that the majority of the DEGs of the adult *Shank3* TG mPFC and striatum were specific to each brain region, and that there was no common DEG, except for *Shank3* itself, between the adult *Shank3* TG mPFC and the juvenile *Shank3*$^{+/\Delta C}$ PFC.

Decrease of Myelin-Related mRNA Levels Specifically in the mPFC of *Shank3* TG Mice

The fact that there were not many overlaps between the DEGs of three RNA-seq analyses prompted us to investigate whether the biological pathways represented by them could be different. Even though the gene identities of DEGs were different, it is still possible that they could be involved in the same or similar biological pathways. To test this, we performed GO and KEGG pathway analyses for the DEGs of the *Shank3* TG mPFC, striatum, and *Shank3*$^{+/\Delta C}$ PFC.

For the 195 DEGs of the adult *Shank3* TG mPFC, "central nervous system myelination" in the biological process category, "structural constituent of myelin sheath" and "heparin binding" in the molecular function category, and "extracellular matrix," "myelin sheath," "proteinaceous extracellular matrix," and "extracellular exosome" in the cellular component category were observed to be significant (**Figure 2A** and **Supplementary Table S6**). For the 75 DEGs of the adult *Shank3* TG striatum, "integrin-mediated signaling pathway" and "platelet activation" in the biological process category were significant, but there was no significant term in the molecular function, cellular component, or KEGG category (**Figure 2B** and **Supplementary Table S7**). For the 45 DEGs of the juvenile *Shank3*$^{+/\Delta C}$ PFC, we did not find any significant term in the categories, possibly because the number of genes was too small (**Supplementary Table S8**). The results suggest that not only the identities of genes but also the representative biological pathways of the DEGs of the *Shank3* TG mPFC, striatum, and *Shank3*$^{+/\Delta C}$ PFC were largely different.

Gene ontology analysis revealed that the myelin-related genes were enriched specifically in the DEGs of the *Shank3* TG mPFC. Indeed, when analyzing the list of *Shank3* TG mPFC DEGs, we identified 27 myelin-related genes (see methods for the definition of myelin-related genes), most of which (25 of 27) were downregulated in the mPFC of *Shank3* TG mice compared with WT mice (**Supplementary Table S9**). We validated eight of the decreased myelin-related DEGs (*Mobp*, *Mbp*, *Tspan2*, *Cldn11*, *Myrf*, *Mog*, *Mag*, and *Plp1*) by qRT-PCR analyses of the *Shank3* TG mPFC (**Figure 2C**). We also confirmed that the mRNA levels of eight validated myelin-related genes were not altered in the striatum and hippocampus of *Shank3* TG mice compared with WT mice (**Figure 2D**). These results indicate that the mRNA levels of myelin-related genes were altered specifically in the mPFC, but not in the striatum or the hippocampus, of adult *Shank3* TG mice. None of the 27 myelin-related DEGs of the *Shank3* TG mPFC were found in the *Shank3*$^{+/\Delta C}$ PFC DEGs, suggesting the normal expression of the genes in *Shank3*$^{+/\Delta C}$ mice (**Supplementary Table S5**). However, direct qRT-PCR validations are necessary to confirm this.

Increase of *Gpr85* mRNA Levels in the Multiple Brain Regions of *Shank3* TG Mice

Next, we attempted to identify whether there were any commonly altered DEGs among the multiple brain regions of *Shank3* TG mice, which might provide additional insights into the molecular pathophysiology of *Shank3* overexpression. Therefore, we re-evaluated the nine, including *Shank3*, shared DEGs between the *Shank3* TG mPFC and striatum (**Figure 1D**, upper). Among them, *Gpr85* (also called *Sreb2* for superconserved receptor expressed in brain 2), an upregulated DEG in both mPFC and striatum of *Shank3* TG mice, was significant, because of its known associations with SCZ and ASDs (Matsumoto et al., 2008; Fujita-Jimbo et al., 2015).

There are three members in the *Sreb* gene family, *Sreb1* (*Gpr27*), *Sreb2* (*Gpr85*), and *Sreb3* (*Gpr173*), which have previously been shown to be expressed in the central nervous system (Matsumoto et al., 2000, 2005). Thus, we performed qRT-PCR for *Gpr27*, *Gpr85*, and *Gpr173* in the cortex, hippocampus, striatum, and cerebellum of adult (10-week-old) WT and *Shank3* TG mice (**Figure 3A**). We found that the mRNA levels of *Gpr85* were significantly upregulated in the four brain regions of *Shank3* TG mice compared with WT mice. Intriguingly, however, *Gpr27* and *Gpr173* mRNAs showed trends of downregulation in the four brain regions of *Shank3* TG mice. Specifically, *Gpr27* mRNA was significantly downregulated in the cortex, and *Gpr173* mRNA was significantly downregulated in the cortex and striatum of *Shank3* TG mice (**Figure 3A**). When we performed qRT-PCR analysis of the juvenile (5-week-old) WT and *Shank3* TG cortex and hippocampus, *Gpr85* mRNA was found to be significantly upregulated in the hippocampus, but not in the cortex, of *Shank3* TG mice, whereas *Gpr27* and *Gpr173* showed normal expression in both brain regions, suggesting age-dependent expression changes in *Gpr27*, *Gpr85*, and *Gpr173* in *Shank3* TG brains (**Figure 3B**). *Gpr27*, *Gpr85*, and *Gpr173* mRNA levels were slightly higher in the adult stage compared with the juvenile stage of the WT cortex (**Figure 3C**).

Next, we investigated what the potential mechanisms underlying the altered expression of *Gpr27*, *Gpr85*, and *Gpr173* in *Shank3* TG brains could be. It has been previously reported that Shank3 proteins undergo synapse-to-nucleus shuttling in an activity-dependent manner, and that Shank3 proteins may regulate the expression of several genes in the nucleus (Grabrucker et al., 2014). However, *Gpr27*, *Gpr85*, and *Gpr173* were not in the list of potential "Shank3 target genes" reported in the study. Therefore, we tested whether the neuronal activity could regulate *Gpr27*, *Gpr85*, and *Gpr173* expression. We previously showed increased excitatory, but decreased inhibitory,

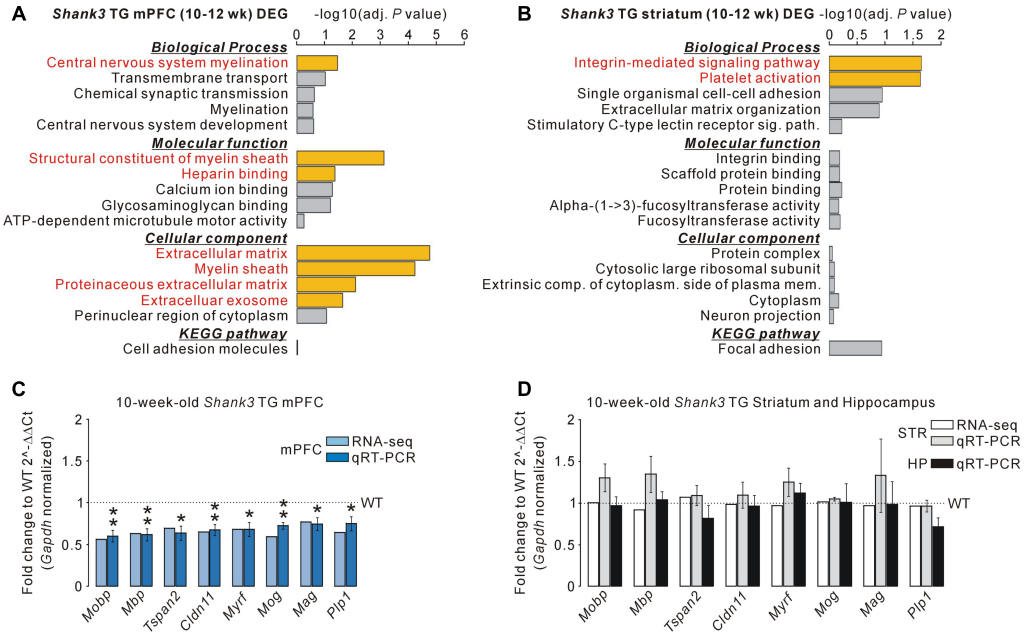

FIGURE 2 | Decreased mRNA levels of myelin-related genes specifically in the mPFC, but not striatum and hippocampus, of *Shank3* TG mice. **(A)** Gene ontology (GO) and Kyoto Encyclopedia of Genes and Genomes (KEGG) pathway analyses of the DEGs of the *Shank3* TG mPFC. Significant terms (Benjamini adjusted *P*-value < 0.05) are highlighted in red. The complete list of analyses is provided in **Supplementary Table S6**. **(B)** GO and KEGG pathway analyses of the DEGs of the *Shank3* TG striatum. The complete list of analyses is provided in **Supplementary Table S7**. **(C)** qRT-PCR validation of the eight myelin-related DEGs decreased in the *Shank3* TG mPFC (dark blue bar) compared with WT mice (n = 5 animals per genotype; unpaired two-tailed Student's t-test). The fold change value for each gene from the mPFC RNA-seq analysis is also shown (light blue bar). **(D)** qRT-PCR analysis of the eight myelin-related DEGs of the *Shank3* TG mPFC in the *Shank3* TG striatum (STR, gray bar) and hippocampus (HP, black bar) compared with WT mice (n = 4 animals per genotype; unpaired two-tailed Student's t-test). The fold change value for each gene from the striatum RNA-seq analysis is also shown (white bar). Data are presented as mean ± SEM. $^*P < 0.05$ and $^{**}P < 0.01$.

synaptic function, and spontaneous seizures in *Shank3* TG mice (Han et al., 2013), which suggests increased neuronal activity. We treated cultured cortical neurons of DIV 21 with either picrotoxin (a blocker for inhibitory $GABA_A$ receptor) or tetrodotoxin (TTX, a sodium channel blocker inhibiting action potential firing) for three different time periods (30 min, 1 h, and 5 h) to increase and decrease neuronal activity, respectively, and measured the mRNA levels of *Gpr27*, *Gpr85*, and *Gpr173*. For the picrotoxin treatment, we found that *Gpr27* and *Gpr173* mRNAs were decreased when neurons were treated for 30 min, whereas *Gpr85* mRNA was increased when neurons were treated for 5 h (**Figure 3D**). For TTX treatment, *Gpr85* and *Gpr173* mRNAs were decreased when neurons were treated for 30 min, but there was no change in the mRNA levels in the rest of conditions (**Figure 3E**). Taken together, these results suggest that the mRNA levels of *Gpr85* and its family members, *Gpr27* and *Gpr173*, were altered in the multiple brain regions of adult *Shank3* TG mice, possibly due to increased neuronal activity.

Negative Regulation of Excitatory Synapse Number by GPR85 in Cultured Hippocampal Neurons

GPR85 is an orphan G protein-coupled receptor (GPCR), and its molecular functions in neurons remain largely unknown. Nevertheless, a recent study showed that GPR85 could interact and co-localize with a core excitatory synaptic protein, PSD-95, in neurons (Fujita-Jimbo et al., 2015). As PSD-95 forms a protein complex with Shank3 through another protein, guanylate kinase-associated protein/synapse-associated protein-associated protein (GKAP/SAPAP) (Naisbitt et al., 1999; Kim and Sheng, 2004; Sheng and Hoogenraad, 2007; Sheng and Kim, 2011), it is possible that GPR85 can also indirectly interact with Shank3 at neuronal excitatory synapses.

To test this, we generated an N-terminal Myc-tagged GPR85 construct with which surface GPR85 proteins expressed in cultured hippocampal neurons could be detected (**Figure 4A**). As previously reported (Fujita-Jimbo et al., 2015), surface GPR85 proteins were co-localized with endogenous PSD-95 proteins in cultured neurons (**Figure 4B**, upper). Moreover, when co-transfected with Shank3, the surface GPR85 and Shank3 proteins were found to be highly co-localized along neuronal dendrites, suggesting that they could form protein complexes in neurons (**Figure 4B**, lower).

Next, we investigated the functional effects of GPR85 overexpression, which might mimic its increased expression in *Shank3* TG neurons, on excitatory synapses by measuring the PSD-95 puncta density. We used three different GPR85 constructs, WT, Δ*C* without last four amino acid residues critical for PSD-95 interaction (Fujita-Jimbo et al., 2015), and

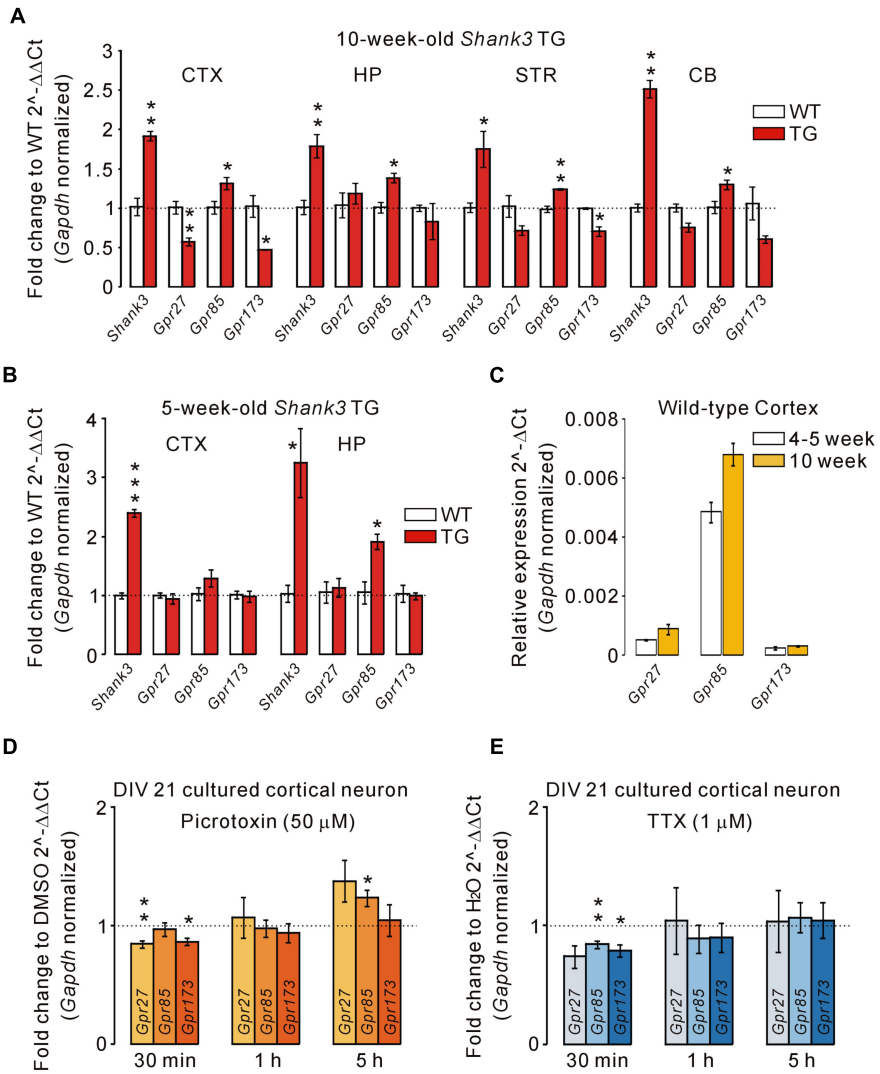

FIGURE 3 | Altered mRNA levels of *Gpr27*, *Gpr85*, and *Gpr173* in multiple brain regions of *Shank3* TG mice. **(A)** qRT-PCR analysis of *Gpr27*, *Gpr85*, and *Gpr173* in the adult *Shank3* TG cortex (CTX), hippocampus (HP), striatum (STR), and cerebellum (CB) compared with WT mice (n = 4 animals per genotype; unpaired two-tailed Student's t-test). *Shank3* was used as a positive control. **(B)** qRT-PCR analysis of *Gpr27*, *Gpr85*, and *Gpr173* in the juvenile *Shank3* TG cortex and hippocampus compared with WT mice (n = 4 animals per genotype; unpaired two-tailed Student's t-test). **(C)** qRT-PCR analysis of the relative expression of *Gpr27*, *Gpr85*, and *Gpr173* between the cortical tissues of juvenile and adult WT mice (n = 3 animals). **(D)** qRT-PCR analysis of *Gpr27*, *Gpr85*, and *Gpr173* in the cultured cortical neurons of days *in vitro* (DIV) 21 treated with picrotoxin for the indicated periods of time (n = 5 biological replicates; unpaired two-tailed Student's t-test). Dimethyl sulfoxide (DMSO) was a vehicle control. h, hour. **(E)** qRT-PCR analysis of *Gpr27*, *Gpr85*, and *Gpr173* in the neurons treated with tetrodotoxin (TTX) for the indicated periods (n = 4 biological replicates; unpaired two-tailed Student's t-test). H_2O was a vehicle control. Data are presented as mean ± SEM. $^*P < 0.05$, $^{**}P < 0.01$, and $^{***}P < 0.001$.

M152T mutant identified in an ASD patient (Fujita-Jimbo et al., 2015). We transfected each of the GPR85 constructs to culture hippocampal neurons of DIV 7 and fixed the neurons and immunostained for PSD-95 at DIV 21. We found that the neurons transfected with GPR85 WT had significantly less PSD-95 puncta along the dendrites compared with nearby untransfected neurons (**Figure 4C**, upper). Moreover, GPR85 Δ*C* and M152T constructs also showed decreased PSD-95 puncta density, similar to the WT construct (**Figure 4C**, middle and lower). To sum up, these results suggest that GPR85 could form a protein complex with PSD-95 and Shank3 at neuronal excitatory synapses where it likely exerts a negative effect on the synaptic development and/or maintenance (**Figure 4D**).

GSEA of the Transcriptome Analyses of the *Shank3* TG mPFC and Striatum and of the *Shank3*$^{+/\Delta C}$ PFC

The above-mentioned results were based on the DEGs of RNA-seq analyses, which focused on significantly altered, but a small subset of, genes. We performed GSEA of the *Shank3* TG mPFC and striatum and of the *Shank3*$^{+/\Delta C}$ PFC RNA-seq analyses

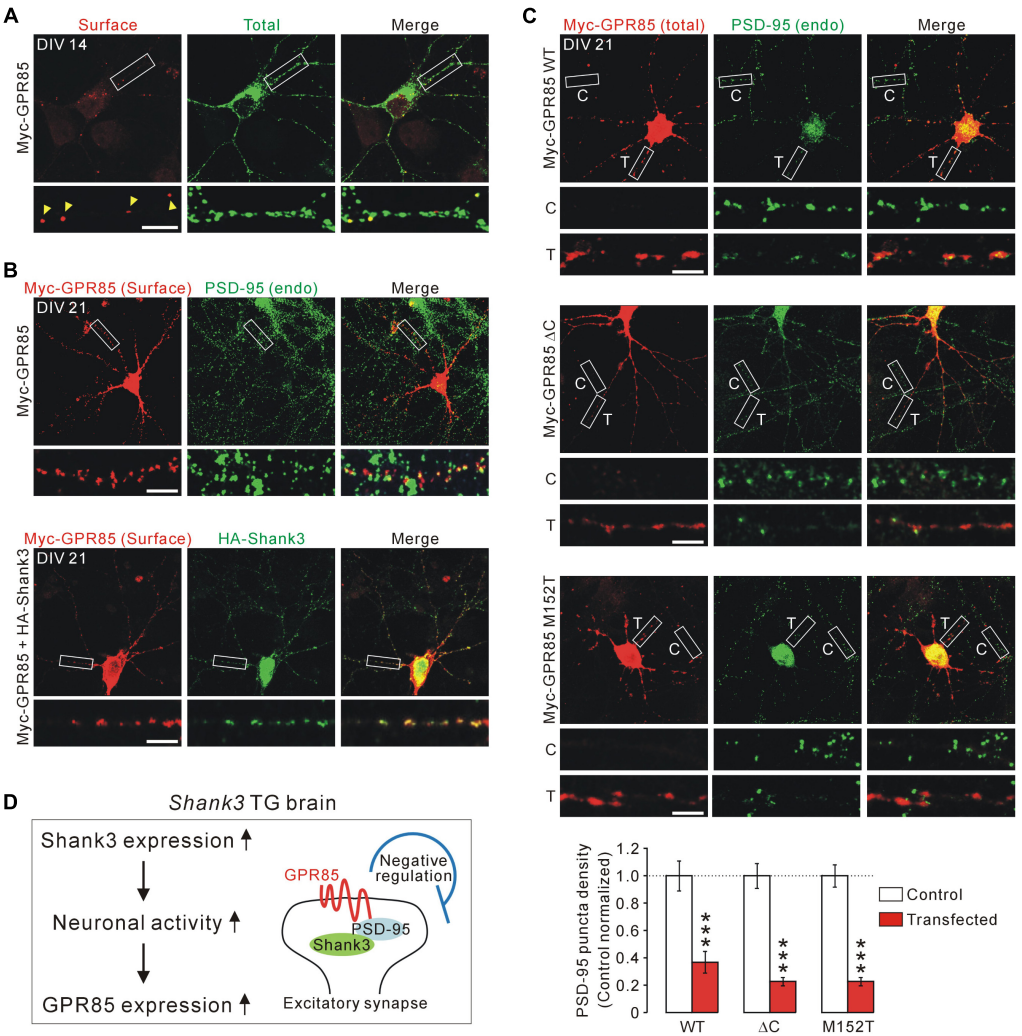

FIGURE 4 | Localization and function of GPR85 in excitatory synapses of cultured hippocampal neurons. **(A)** Representative immunostaining image shows the surface and total protein expression of Myc-GPR85 in cultured hippocampal neurons of DIV 14. Scale bar, 10 μm. **(B)** Representative immunostaining images show co-localizations of surface Myc-GPR85 puncta with endogenous (endo) PSD-95 (upper) and with exogenous HA-Shank3 (lower) proteins in cultured hippocampal neurons of DIV 21. **(C)** Representative immunostaining images and quantification show the decreased density of PSD-95 in cultured hippocampal neurons of DIV 21 transfected with Myc-GPR85 constructs (WT, Δ*C*, or M152T), compared with nearby untransfected neurons (n = 16, 16, 24 neurons for WT, Δ*C*, and M152T constructs, respectively; unpaired two-tailed Student's t-test). C, control; T, transfected. **(D)** The proposed hypothesis suggests that GPR85 expression is increased in *Shank3* TG neurons due to increased neuronal activity and that GPR85 forms a complex with Shank3 via PSD-95 to negatively regulate the number of excitatory synapses. Data are presented as mean ± SEM. ***$P < 0.001$.

to identify meaningful "molecular signatures" based on the broader or overall expression changes in the transcriptome. We applied two different groups of gene sets (hallmark and KEGG gene sets) to the three RNA-seq analyses, which revealed significantly enriched terms from each transcriptome (**Figure 5** and **Supplementary Tables S10–S12**).

In particular, we found that several enriched terms were common among the analyses of the *Shank3* TG mPFC and striatum and the *Shank3*$^{+/\Delta C}$ PFC. First, for the hallmark gene sets, "Myc target V1" was represented by the downregulated genes of *Shank3* TG mPFC and the upregulated genes of *Shank3* TG striatum (**Figure 5A**). Second, for the KEGG gene sets, "ribosome" was represented by the downregulated genes of both *Shank3* TG mPFC and striatum (**Figure 5B**). Third, for the hallmark gene sets, "epithelial mesenchymal transition" was enriched by the upregulated genes of both *Shank3* TG mPFC and *Shank3*$^{+/\Delta C}$ PFC, whereas "Myc target V1" was represented by the downregulated genes of *Shank3* TG mPFC and the upregulated genes of *Shank3*$^{+/\Delta C}$ PFC (**Figure 5C**). Finally, for the KEGG gene sets, "ribosome" was enriched by the downregulated genes of *Shank3* TG mPFC and the upregulated genes of *Shank3*$^{+/\Delta C}$ PFC (**Figure 5D**).

Among the GSEA results, we further investigated the ribosome-related gene expression changes, because those genes were downregulated in the *Shank3* TG mPFC and striatum but upregulated in the *Shank3*$^{+/\Delta C}$ PFC (**Figure 6A**), thus

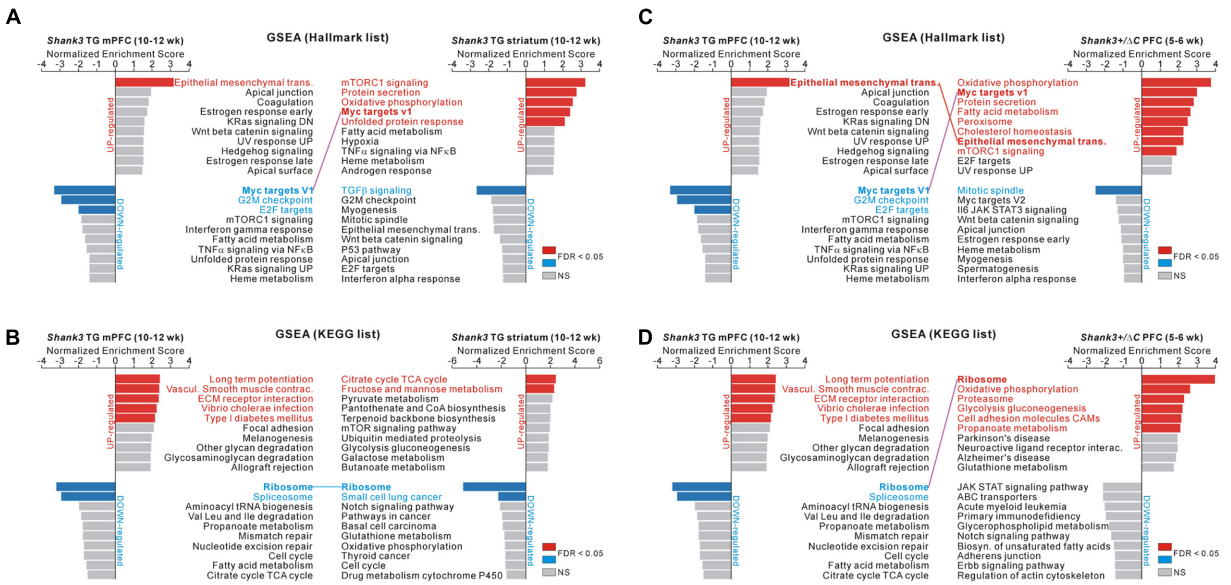

FIGURE 5 | GSEA of the *Shank3* TG mPFC and striatum and *Shank3*$^{+/\Delta C}$ PFC RNA-seq results. **(A)** The bar graphs show normalized enrichment scores (NESs) of the gene set enrichment analysis (GSEA) on the hallmark gene sets for the *Shank3* TG mPFC (left) and striatum (right) RNA-seq analyses. Significant gene sets (FDR < 0.05) are highlighted in red and blue for upregulated and downregulated genes, respectively. The common term, "Myc targets V1," between the *Shank3* TG mPFC and striatum, is connected with a purple line. **(B)** The bar graphs show NES of GSEA on the KEGG gene sets for the *Shank3* TG mPFC (left) and striatum (right) RNA-seq analyses. The common term, "ribosome," is connected with a blue line. **(C)** The bar graphs show NES of GSEA on the hallmark gene sets for the *Shank3* TG mPFC (left) and the *Shank3*$^{+/\Delta C}$ PFC (right). The common terms, "epithelial mesenchymal transition" and "Myc targets V1," are connected with red and purple lines, respectively. **(D)** The bar graphs show the NES of GSEA on the KEGG gene sets for the *Shank3* TG mPFC (left) and the *Shank3*$^{+/\Delta C}$ PFC (right). The common term, "ribosome," is connected with a purple line. The complete list that contains the results of the GSEA is provided in **Supplementary Tables S10–S12**.

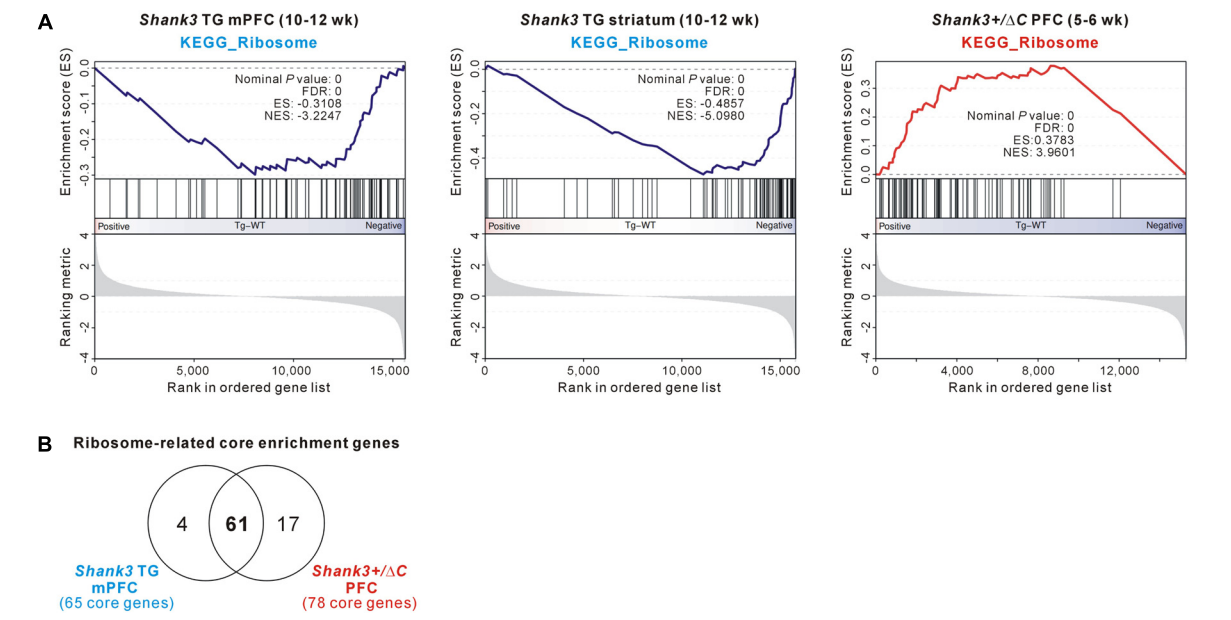

FIGURE 6 | The ribosome-related molecular signature commonly detected in the *Shank3* TG mPFC and striatum and *Shank3*$^{+/\Delta C}$ PFC RNA-seq results. **(A)** The enrichment plots of RNA-seq analyses of *Shank3* TG mPFC (left) and striatum (middle) and *Shank3*$^{+/\Delta C}$ PFC (right) of the KEGG ribosome gene set. **(B)** The Venn diagram shows the number of common ribosome-related core enrichment genes between the *Shank3* TG mPFC (65 downregulated core genes) and the *Shank3*$^{+/\Delta C}$ PFC (78 upregulated core genes). The lists of core genes are provided in **Supplementary Table S13**.

possibly modulated in a *Shank3* dosage-dependent manner. Moreover, it was previously reported that neuronal mTORC1 signaling, which regulates ribosome biogenesis and function (Jastrzebski et al., 2007; Iadevaia et al., 2014), can be altered by *Shank3* overexpression or knock-down (Bidinosti et al., 2016; Lee et al., 2017d). Therefore, we compared the ribosome-related GSEA core enrichment genes of the *Shank3* TG mPFC and the *Shank3*$^{+/\Delta C}$ PFC. There were 65 downregulated and 78 upregulated ribosome-related core genes in the *Shank3* TG mPFC and the *Shank3*$^{+/\Delta C}$ PFC RNA-seq analyses, respectively (**Supplementary Table S13**), and surprisingly, 61 genes (74.4% of total) were found to be shared between them (**Figure 6B**). Overall, these results suggest that there could be some shared molecular signatures between the different brain regions of *Shank3* TG mice and between the PFC regions of *Shank3* TG and *Shank3*$^{+/\Delta C}$ mice, and that ribosome-related changes could be a potential candidate.

DISCUSSION

In this study, we performed RNA-seq analysis of the mPFC of *Shank3* TG mice and compared the result, side by side, with the previously reported RNA-seq analyses of the striatum of *Shank3* TG mice and the PFC of *Shank3*$^{+/\Delta C}$ mice. We found that the expression of myelin-related genes specifically decreased in the mPFC and the expression of *Gpr85* increased in multiple brain regions of *Shank3* TG mice by comparing the DEGs of different RNA-seq analyses. Moreover, the GSEA results suggested that the expression of a group of ribosome-related genes could be altered in a *Shank3* dosage-dependent manner, at least in the PFC regions of mice. One obvious limitation of our analysis is that we compared DEGs from the mPFC of "adult" *Shank3* TG mice and from the PFC of "juvenile" *Shank3*$^{+/\Delta C}$ mice. Indeed, when we compared the transcriptomes of "adult" WT mPFC and "juvenile" WT PFC (**Supplementary Table S14**), or "adult" TG mPFC and "juvenile" WT PFC (**Supplementary Table S15**), there were about 5,300 DEGs in both cases, suggesting that developmental stages largely affect gene expression profiles (note that we therefore compared *Shank3*-dependent DEGs normalized to the age-matched WT controls). Furthermore, considering differential *Shank3* expression in brain across developmental stages (Wang et al., 2014), it is possible that DEGs of the PFC of juvenile *Shank3*$^{+/\Delta C}$ mice can be different from those of adult *Shank3*$^{+/\Delta C}$ mice. Therefore, further validation will be necessary to confirm that a group of ribosome-related genes of PFC are altered in a *Shank3* dosage-dependent manner. In contrast, it is also possible that additional common DEGs, other than ribosome-related genes, may be identified if we compare *Shank3* TG mice and *Shank3*$^{+/\Delta C}$ mice of similar developmental stages.

The brain region-specific Shank3 isoform expression (Wang et al., 2014) and Shank3 interactome (Lee et al., 2017b) have been suggested to contribute to the phenotypic complexity and heterogeneity of *SHANK3*-associated brain disorders. It is also possible that such protein-level diversity of Shank3 might contribute to the brain region-specific changes of transcriptome in *Shank3* mutant mice. For example, Shank3 proteins can undergo synapse-to-nucleus shuttling in an activity-dependent manner to regulate the expression of several genes in the nucleus (Grabrucker et al., 2014). Certain Shank3 isoforms may be more preferentially targeted to the nucleus or some Shank3 interactors may be involved in the synapse-to-nucleus shuttling of Shank3. If so, each brain region could have different levels of Shank3 proteins in the nucleus. Further investigations about Shank3-dependent gene expression and its regulation will be necessary to test this intriguing hypothesis.

It was unexpected that the mRNA levels of myelin-related genes would be altered in the mPFC of adult *Shank3* TG mice. As the majority of Shank3 proteins in the brain function at the neuronal excitatory synapses, it is likely that the altered expression of myelin-related genes could be an indirect effect of Shank3 overexpression in the neurons. Indeed, it has been reported that the neuronal activity can promote oligodendrogenesis and myelination (Gibson et al., 2014; Mitew et al., 2018). However, this might not be the case for *Shank3* TG mice where the neuronal activity is expected to increase (Han et al., 2013), but the expression of myelin-related genes decreases. As an alternative possibility, various types of behavioral stress, including neonatal maternal separation, chronic social isolation, and chronic social defeat, can impair myelination in rodents, mainly in the PFC regions (Liu et al., 2012; Lehmann et al., 2017; Yang et al., 2017). Moreover, increased serum levels of stress hormone corticosterone and altered hypothalamic-pituitary-adrenal (HPA) axis have been observed in human patients and animal models of mania (Daban et al., 2005; Leussis et al., 2013). Therefore, as an animal model of mania (Han et al., 2013; Lee et al., 2018), *Shank3* TG mice might also have increased levels of stress hormones, which could secondarily affect the expression of myelin-related genes in the mPFC. Further validation of myelin-related phenotypes of the mPFC, together with measurements of stress hormone levels, in *Shank3* TG mice could be an interesting topic of the future study.

Among the common DEGs between the mPFC and striatum of adult *Shank3* TG mice, we further characterized *Gpr85* and its family members *Gpr27* and *Gpr173*. In the cortex, hippocampus, striatum, and cerebellum of adult *Shank3* TG mice, the mRNA levels of *Gpr85* increased, whereas those of *Gpr27* and *Gpr173* decreased, compared with WT mice, suggesting some compensatory changes in expression among the family members. In particular, when we treated cultured cortical neurons with picrotoxin to increase the neuronal activity and thereby possibly mimick the neurons of *Shank3* TG mice, we observed an increase in *Gpr85*, but a decrease in *Gpr27* and *Gpr173*, mRNA levels. Therefore, elevated neuronal activity could, at least in part, contribute to the altered expression of *Gpr85*, *Gpr27*, and *Gpr173* in *Shank3* TG brains. It was unexpected that, in the case of *Gpr173*, mRNA levels were also reduced under decreased neuronal activity by TTX treatment. Detailed transcriptional (or post-transcriptional) mechanisms underlying activity-dependent expression changes of *Gpr85*, *Gpr27*, and *Gpr173* need to be further investigated.

Beyond their relationship at the level of transcriptional regulation, we further investigated the functional interaction between Shank3 and GPR85 at neuronal excitatory synapses, based on the recently reported protein–protein interactions between PSD-95 and GPR85 (Fujita-Jimbo et al., 2015). Indeed, GPR85 proteins were found to be co-localized with PSD-95 and Shank3 along the neuronal dendrites, suggesting that increased GPR85 in *Shank3* TG neurons could be targeted to the excitatory synapses. To replicate this condition, we overexpressed GPR85 in cultured hippocampal neurons and found that GPR85 significantly decreased the number of excitatory synapses. Even GPR85 proteins without the C-terminal four residues or those harboring an ASD-associated variant (M152T) were nonetheless found to decrease excitatory synapses in cultured neurons, suggesting that these mutant proteins may still exert their negative effect at excitatory synapses. It is not uncommon that PSD-95-interacting proteins negatively regulate excitatory synaptic development and function. For example, Neph2/Kirrel3, an adhesion molecule interacting with PSD-95, negatively regulates excitatory synaptic transmission in the dentate granule neurons of the hippocampus (Choi et al., 2015a; Roh et al., 2017). Although the detailed underlying mechanisms need to be further investigated, we speculate that an activity-dependent increase of *Gpr85* expression, together with its negative regulation of excitatory synapses, could represent a homeostatic response in *Shank3* TG neurons. In the original paper describing the *Shank3* TG mice (Han et al., 2013), we found increased excitatory synapse number in TG neurons compared with WT neurons. We speculate that Shank3 overexpression in TG neurons increases excitatory synapse number, which in turn elevates neuronal activity to induce *Gpr85* mRNA expression. GPR85 proteins in *Shank3* TG neurons may have negative effects on excitatory synapse number, but its expression level may not be enough to fully normalize synapse number to the WT level. Meanwhile, in our GPR85 overexpression experiment, we could observe decreased synapse number because we overexpressed GPR85 very high level for a long period (2 weeks). Considering the associations of *GPR85*/*SREB2* with ASDs and SCZ (Matsumoto et al., 2008; Chen et al., 2012; Radulescu et al., 2013; Fujita-Jimbo et al., 2015), more investigations about the functional relationship between Shank3 and GPR85 would provide information on the detailed mechanisms of activity-dependent synaptic regulation and their potential implications in multiple brain disorders.

To identify meaningful molecular signatures based on broader expression changes, instead of the DEGs, we performed a GSEA of the RNA-seq results, which revealed some commonly enriched terms among the *Shank3* TG mPFC and striatum and the *Shank3*$^{+/\Delta C}$ PFC. Notably, ribosome-related genes were downregulated in the *Shank3* TG mPFC and striatum but upregulated in the *Shank3*$^{+/\Delta C}$ PFC, suggesting that those genes could be altered in a *Shank3* dosage-dependent manner. Indeed, when we compared the ribosome-related core enrichment genes of the *Shank3* TG mPFC and the *Shank3*$^{+/\Delta C}$ PFC, most were shared and showed the opposite directional changes in expression in the two mice. Although it is not currently easy to explain how the level of Shank3 proteins affects the expression of a group of ribosome-related genes, changes in mTORC1 signaling, which regulates ribosome biogenesis and function (Jastrzebski et al., 2007; Iadevaia et al., 2014), might be involved. It was found that the reduced Shank3 expression decreased mTORC1 activity by increasing steady-state levels of Cdc2-like kinase 2 (CLK2) (Bidinosti et al., 2016). The CLK2 phosphorylates and activates the regulatory subunit of protein phosphatase 2A (PP2A), which in turn inhibits AKT, a positive upstream regulator of mTORC1. Moreover, we recently showed that the mTORC1 activity is decreased in the striatum of *Shank3* TG mice, possibly due to the aberrant protein interactions between Shank3 and some upstream regulators of mTORC1 (Lee et al., 2017d). A comprehensive analysis of mTORC1 activity in various brain regions of *Shank3* mutant mice, together with the direct measurement of ribosomal quantity (both mRNA and protein) and activity, could provide important clues regarding the detailed mechanisms behind this. In this regard, it is worth noting that in a recent quantitative proteomic analysis of the striatal PSD of *Shank3* mutant mice (*Shank3*$\Delta 11^{-/-}$), the levels of several ribosomal proteins were increased compared with WT mice (Reim et al., 2017). Shank3 proteins are coupled with metabotropic glutamate receptors (mGluRs) via Homer (Tu et al., 1999) and regulate their synaptic expression and signaling (Verpelli et al., 2011; Vicidomini et al., 2016; Wang et al., 2016). mGluR signaling is a key regulator of synaptic local translation (Waung and Huber, 2009; Luscher and Huber, 2010). Therefore, abnormal mGluR signaling and altered levels of ribosomal proteins may together lead to changes in synaptic mRNA translation in *Shank3* mutant mice, which can be an important topic of future study.

CONCLUSION

In conclusion, using unbiased transcriptome analyses, our study reveals both brain region-specific and broad, previously unidentified molecular changes in *Shank3*-overexpressing mice. These results further elucidate the complexity and heterogeneity of the molecular pathophysiology of *SHANK3*-associated brain disorders and also highlight the need for subsequent studies on relevant molecular pathways, which could be applied, in the long term, for the development of the better therapeutic approaches.

AUTHOR CONTRIBUTIONS

CJ, JR, SK, YZ, YL, YK, and KH designed and performed the experiments. HK and KH analyzed and interpreted the data, and wrote the paper. All authors read and approved the manuscript.

FUNDING

This work was supported by the National Research Foundation of Korea (NRF) grants funded by the Korea Government Ministry of Science and ICT (NRF-2015M3C7A1028790 and NRF-2018R1C1B6001235), by the grant of the Korea Health Technology R&D Project through the Korea Health

Industry Development Institute (KHIDI) funded by the Korea Government Ministry of Health and Welfare (HI16C0090), by the Korea Institute of Science and Technology Information (K-18-L12-C08-S01), and by the Korea University grant (K1800771).

SUPPLEMENTARY MATERIAL

The Supplementary Material for this article can be found online at: https://www.frontiersin.org/articles/10.3389/fnmol.2018.00250/full#supplementary-material

REFERENCES

Balleine, B. W., Delgado, M. R., and Hikosaka, O. (2007). The role of the dorsal striatum in reward and decision-making. *J. Neurosci.* 27, 8161–8165.

Bey, A. L., Wang, X., Yan, H., Kim, N., Passman, R. L., Yang, Y., et al. (2018). Brain region-specific disruption of Shank3 in mice reveals a dissociation for cortical and striatal circuits in autism-related behaviors. *Transl. Psychiatry* 8:94. doi: 10.1038/s41398-018-0142-6

Bidinosti, M., Botta, P., Kruttner, S., Proenca, C. C., Stoehr, N., Bernhard, M., et al. (2016). CLK2 inhibition ameliorates autistic features associated with SHANK3 deficiency. *Science* 351, 1199–1203. doi: 10.1126/science.aad5487

Bozdagi, O., Tavassoli, T., and Buxbaum, J. D. (2013). Insulin-like growth factor-1 rescues synaptic and motor deficits in a mouse model of autism and developmental delay. *Mol. Autism* 4:9. doi: 10.1186/2040-2392-4-9

Chen, Q., Kogan, J. H., Gross, A. K., Zhou, Y., Walton, N. M., Shin, R., et al. (2012). SREB2/GPR85, a schizophrenia risk factor, negatively regulates hippocampal adult neurogenesis and neurogenesis-dependent learning and memory. *Eur. J. Neurosci.* 36, 2597–2608. doi: 10.1111/j.1460-9568.2012.08180.x

Choi, S.-Y., and Han, K. (2015). Emerging role of synaptic actin-regulatory pathway in the pathophysiology of mood disorders. *Anim. Cells Syst.* 19, 283–288.

Choi, S. Y., Han, K., Cutforth, T., Chung, W., Park, H., Lee, D., et al. (2015a). Mice lacking the synaptic adhesion molecule Neph2/Kirrel3 display moderate hyperactivity and defective novel object preference. *Front. Cell. Neurosci.* 9:283. doi: 10.3389/fncel.2015.00283

Choi, S. Y., Pang, K., Kim, J. Y., Ryu, J. R., Kang, H., Liu, Z., et al. (2015b). Post-transcriptional regulation of SHANK3 expression by microRNAs related to multiple neuropsychiatric disorders. *Mol. Brain* 8:74. doi: 10.1186/s13041-015-0165-3

Costales, J. L., and Kolevzon, A. (2015). Phelan-McDermid Syndrome and SHANK3: implications for Treatment. *Neurotherapeutics* 12, 620–630.

Daban, C., Vieta, E., Mackin, P., and Young, A. H. (2005). Hypothalamic-pituitary-adrenal axis and bipolar disorder. *Psychiatr. Clin. North Am.* 28, 469–480.

Duffney, L. J., Zhong, P., Wei, J., Matas, E., Cheng, J., Qin, L., et al. (2015). Autism-like deficits in shank3-deficient mice are rescued by targeting actin regulators. *Cell Rep.* 11, 1400–1413. doi: 10.1016/j.celrep.2015.04.064

Failla, P., Romano, C., Alberti, A., Vasta, A., Buono, S., Castiglia, L., et al. (2007). Schizophrenia in a patient with subtelomeric duplication of chromosome 22q. *Clin. Genet.* 71, 599–601.

Fujita-Jimbo, E., Tanabe, Y., Yu, Z., Kojima, K., Mori, M., Li, H., et al. (2015). The association of GPR85 with PSD-95-neuroligin complex and autism spectrum disorder: a molecular analysis. *Mol. Autism* 6:17. doi: 10.1186/s13229-015-0012-5

Gibson, E. M., Purger, D., Mount, C. W., Goldstein, A. K., Lin, G. L., Wood, L. S., et al. (2014). Neuronal activity promotes oligodendrogenesis and adaptive myelination in the mammalian brain. *Science* 344:1252304. doi: 10.1126/science.1252304

Grabrucker, A. M., Schmeisser, M. J., Schoen, M., and Boeckers, T. M. (2011). Postsynaptic ProSAP/Shank scaffolds in the cross-hair of synaptopathies. *Trends Cell Biol.* 21, 594–603. doi: 10.1016/j.tcb.2011.07.003

Grabrucker, S., Proepper, C., Mangus, K., Eckert, M., Chhabra, R., Schmeisser, M. J., et al. (2014). The PSD protein ProSAP2/Shank3 displays synapto-nuclear shuttling which is deregulated in a schizophrenia-associated mutation. *Exp. Neurol.* 253, 126–137. doi: 10.1016/j.expneurol.2013.12.015

Han, K., Holder, J. L. Jr., Schaaf, C. P., Lu, H., Chen, H., Kang, H., et al. (2013). SHANK3 overexpression causes manic-like behaviour with unique pharmacogenetic properties. *Nature* 503, 72–77. doi: 10.1038/nature12630

Harony-Nicolas, H., De Rubeis, S., Kolevzon, A., and Buxbaum, J. D. (2015). Phelan mcdermid syndrome: from genetic discoveries to animal models and treatment. *J. Child Neurol.* 30, 1861–1870. doi: 10.1177/0883073815600872

Harony-Nicolas, H., Kay, M., Hoffmann, J. D., Klein, M. E., Bozdagi-Gunal, O., Riad, M., et al. (2017). Oxytocin improves behavioral and electrophysiological deficits in a novel Shank3-deficient rat. *eLife* 6:e18904. doi: 10.7554/eLife.18904

Huang da, W., Sherman, B. T., and Lempicki, R. A. (2009). Systematic and integrative analysis of large gene lists using DAVID bioinformatics resources. *Nature Protoc.* 4, 44–57. doi: 10.1038/nprot.2008.211

Iadevaia, V., Liu, R., and Proud, C. G. (2014). mTORC1 signaling controls multiple steps in ribosome biogenesis. *Semin. Cell Dev. Biol.* 36, 113–120. doi: 10.1016/j.semcdb.2014.08.004

Jastrzebski, K., Hannan, K. M., Tchoubrieva, E. B., Hannan, R. D., and Pearson, R. B. (2007). Coordinate regulation of ribosome biogenesis and function by the ribosomal protein S6 kinase, a key mediator of mTOR function. *Growth Fact.* 25, 209–226.

Jiang, Y. H., and Ehlers, M. D. (2013). Modeling autism by SHANK gene mutations in mice. *Neuron* 78, 8–27. doi: 10.1016/j.neuron.2013.03.016

Kim, E., and Sheng, M. (2004). PDZ domain proteins of synapses. *Nat. Rev. Neurosci.* 5, 771–781.

Kim, Y., Zhang, Y., Pang, K., Kang, H., Park, H., Lee, Y., et al. (2016). Bipolar disorder associated microRNA, miR-1908-5p, regulates the expression of genes functioning in neuronal glutamatergic synapses. *Exp. Neurobiol.* 25, 296–306. doi: 10.5607/en.2016.25.6.296

Lee, B., Zhang, Y., Kim, Y., Kim, S., Lee, Y., and Han, K. (2017a). Age-dependent decrease of GAD65/67 mRNAs but normal densities of GABAergic interneurons in the brain regions of Shank3-overexpressing manic mouse model. *Neurosci. Lett.* 649, 48–54. doi: 10.1016/j.neulet.2017.04.016

Lee, Y., Kang, H., Lee, B., Zhang, Y., Kim, Y., Kim, S., et al. (2017b). Integrative analysis of brain region-specific Shank3 interactomes for understanding the heterogeneity of neuronal pathophysiology related to SHANK3 mutations. *Front. Mol. Neurosci.* 10:110. doi: 10.3389/fnmol.2017.00110

Lee, Y., Kim, D., Ryu, J. R., Zhang, Y., Kim, S., Kim, Y., et al. (2017c). Phosphorylation of CYFIP2, a component of the WAVE-regulatory complex, regulates dendritic spine density and neurite outgrowth in cultured hippocampal neurons potentially by affecting the complex assembly. *Neuroreport* 28, 749–754. doi: 10.1097/WNR.0000000000000838

Lee, Y., Kim, S. G., Lee, B., Zhang, Y., Kim, Y., Kim, S., et al. (2017d). Striatal transcriptome and interactome analysis of Shank3-overexpressing mice reveals the connectivity between Shank3 and mTORC1 signaling. *Front. Mol. Neurosci.* 10:201. doi: 10.3389/fnmol.2017.00201

Lee, J., Chung, C., Ha, S., Lee, D., Kim, D. Y., Kim, H., et al. (2015). Shank3-mutant mice lacking exon 9 show altered excitation/inhibition balance, enhanced rearing, and spatial memory deficit. *Front. Cell. Neurosci.* 9:94. doi: 10.3389/fncel.2015.00094

Lee, Y., Zhang, Y., Kim, S., and Han, K. (2018). Excitatory and inhibitory synaptic dysfunction in mania: an emerging hypothesis from animal model studies. *Exp. Mol. Med.* 50:12. doi: 10.1038/s12276-018-0028-y

Lehmann, M. L., Weigel, T. K., Elkahloun, A. G., and Herkenham, M. (2017). Chronic social defeat reduces myelination in the mouse medial prefrontal cortex. *Sci. Rep.* 7:46548. doi: 10.1038/srep46548

Leussis, M. P., Berry-Scott, E. M., Saito, M., Jhuang, H., De Haan, G., Alkan, O., et al. (2013). The ANK3 bipolar disorder gene regulates psychiatric-related behaviors that are modulated by lithium and stress. *Biol. Psychiatry* 73, 683–690. doi: 10.1016/j.biopsych.2012.10.016

Liu, J., Dietz, K., Deloyht, J. M., Pedre, X., Kelkar, D., Kaur, J., et al. (2012). Impaired adult myelination in the prefrontal cortex of socially isolated mice. *Nat. Neurosci.* 15, 1621–1623. doi: 10.1038/nn.3263

Love, M. I., Huber, W., and Anders, S. (2014). Moderated estimation of fold change and dispersion for RNA-seq data with DESeq2. *Genome Biol.* 15:550.

Luscher, C., and Huber, K. M. (2010). Group 1 mGluR-dependent synaptic long-term depression: mechanisms and implications for circuitry and disease. *Neuron* 65, 445–459. doi: 10.1016/j.neuron.2010.01.016

Matsumoto, M., Beltaifa, S., Weickert, C. S., Herman, M. M., Hyde, T. M., Saunders, R. C., et al. (2005). A conserved mRNA expression profile of SREB2 (GPR85) in adult human, monkey, and rat forebrain. *Brain Res. Mol. Brain Res.* 138, 58–69.

Matsumoto, M., Saito, T., Takasaki, J., Kamohara, M., Sugimoto, T., Kobayashi, M., et al. (2000). An evolutionarily conserved G-protein coupled receptor family, SREB, expressed in the central nervous system. *Biochem. Biophys. Res. Commun.* 272, 576–582.

Matsumoto, M., Straub, R. E., Marenco, S., Nicodemus, K. K., Matsumoto, S., Fujikawa, A., et al. (2008). The evolutionarily conserved G protein-coupled receptor SREB2/GPR85 influences brain size, behavior, and vulnerability to schizophrenia. *Proc. Natl. Acad. Sci. U.S.A.* 105, 6133–6138. doi: 10.1073/pnas.0710717105

Mitew, S., Gobius, I., Fenlon, L. R., Mcdougall, S. J., Hawkes, D., Xing, Y. L., et al. (2018). Pharmacogenetic stimulation of neuronal activity increases myelination in an axon-specific manner. *Nat. Commun.* 9:306. doi: 10.1038/s41467-017-02719-2

Moessner, R., Marshall, C. R., Sutcliffe, J. S., Skaug, J., Pinto, D., Vincent, J., et al. (2007). Contribution of SHANK3 mutations to autism spectrum disorder. *Am. J. Hum. Genet.* 81, 1289–1297.

Monteiro, P., and Feng, G. (2017). SHANK proteins: roles at the synapse and in autism spectrum disorder. *Nat. Rev. Neurosci.* 18, 147–157. doi: 10.1038/nrn.2016.183

Naisbitt, S., Kim, E., Tu, J. C., Xiao, B., Sala, C., Valtschanoff, J., et al. (1999). Shank, a novel family of postsynaptic density proteins that binds to the NMDA receptor/PSD-95/GKAP complex and cortactin. *Neuron* 23, 569–582.

Patro, R., Duggal, G., Love, M. I., Irizarry, R. A., and Kingsford, C. (2017). Salmon provides fast and bias-aware quantification of transcript expression. *Nat. Methods* 14, 417–419. doi: 10.1038/nmeth.4197

Peca, J., Feliciano, C., Ting, J. T., Wang, W., Wells, M. F., Venkatraman, T. N., et al. (2011). Shank3 mutant mice display autistic-like behaviours and striatal dysfunction. *Nature* 472, 437–442. doi: 10.1038/nature09965

Qin, L., Ma, K., Wang, Z. J., Hu, Z., Matas, E., Wei, J., et al. (2018). Social deficits in Shank3-deficient mouse models of autism are rescued by histone deacetylase (HDAC) inhibition. *Nat. Neurosci.* 21, 564–575. doi: 10.1038/s41593-018-0110-8

Radulescu, E., Sambataro, F., Mattay, V. S., Callicott, J. H., Straub, R. E., Matsumoto, M., et al. (2013). Effect of schizophrenia risk-associated alleles in SREB2 (GPR85) on functional MRI phenotypes in healthy volunteers. *Neuropsychopharmacology* 38, 341–349. doi: 10.1038/npp.2012.184

Reim, D., Distler, U., Halbedl, S., Verpelli, C., Sala, C., Bockmann, J., et al. (2017). Proteomic analysis of post-synaptic density fractions from Shank3 mutant mice reveals brain region specific changes relevant to autism spectrum disorder. *Front. Mol. Neurosci.* 10:26. doi: 10.3389/fnmol.2017.00026

Riga, D., Matos, M. R., Glas, A., Smit, A. B., Spijker, S., and Van Den Oever, M. C. (2014). Optogenetic dissection of medial prefrontal cortex circuitry. *Front. Syst. Neurosci.* 8:230. doi: 10.3389/fnsys.2014.00230

Roh, J. D., Choi, S. Y., Cho, Y. S., Choi, T. Y., Park, J. S., Cutforth, T., et al. (2017). Increased excitatory synaptic transmission of dentate granule neurons in mice lacking PSD-95-interacting adhesion molecule Neph2/Kirrel3 during the early postnatal period. *Front. Mol. Neurosci.* 10:81. doi: 10.3389/fnmol.2017.00081

Russo, S. J., and Nestler, E. J. (2013). The brain reward circuitry in mood disorders. *Nat. Rev. Neurosci.* 14, 609–625. doi: 10.1038/nrn3381

Schmeisser, M. J. (2015). Translational neurobiology in Shank mutant mice–model systems for neuropsychiatric disorders. *Ann. Anat.* 200, 115–117. doi: 10.1016/j.aanat.2015.03.006

Shcheglovitov, A., Shcheglovitova, O., Yazawa, M., Portmann, T., Shu, R., Sebastiano, V., et al. (2013). SHANK3 and IGF1 restore synaptic deficits in neurons from 22q13 deletion syndrome patients. *Nature* 503, 267–271. doi: 10.1038/nature12618

Sheng, M., and Hoogenraad, C. C. (2007). The postsynaptic architecture of excitatory synapses: a more quantitative view. *Annu. Rev. Biochem.* 76, 823–847.

Sheng, M., and Kim, E. (2000). The Shank family of scaffold proteins. *J. Cell Sci.* 113(Pt 11), 1851–1856.

Sheng, M., and Kim, E. (2011). The postsynaptic organization of synapses. *Cold Spring Harb. Perspect. Biol.* 3:a005678. doi: 10.1101/cshperspect.a005678

Soneson, C., Love, M. I., and Robinson, M. D. (2015). Differential analyses for RNA-seq: transcript-level estimates improve gene-level inferences. *F1000Res.* 4:1521. doi: 10.12688/f1000research.7563.2

Subramanian, A., Tamayo, P., Mootha, V. K., Mukherjee, S., Ebert, B. L., Gillette, M. A., et al. (2005). Gene set enrichment analysis: a knowledge-based approach for interpreting genome-wide expression profiles. *Proc. Natl. Acad. Sci. U.S.A.* 102, 15545–15550.

Tu, J. C., Xiao, B., Naisbitt, S., Yuan, J. P., Petralia, R. S., Brakeman, P., et al. (1999). Coupling of mGluR/Homer and PSD-95 complexes by the Shank family of postsynaptic density proteins. *Neuron* 23, 583–592.

Verpelli, C., Dvoretskova, E., Vicidomini, C., Rossi, F., Chiappalone, M., Schoen, M., et al. (2011). Importance of Shank3 protein in regulating metabotropic glutamate receptor 5 (mGluR5) expression and signaling at synapses. *J. Biol. Chem.* 286, 34839–34850. doi: 10.1074/jbc.M111.258384

Vicidomini, C., Ponzoni, L., Lim, D., Schmeisser, M. J., Reim, D., Morello, N., et al. (2016). Pharmacological enhancement of mGlu5 receptors rescues behavioral deficits in SHANK3 knock-out mice. *Mol. Psychiatry* 22, 689–702. doi: 10.1038/mp.2016.30

Wang, X., Bey, A. L., Katz, B. M., Badea, A., Kim, N., David, L. K., et al. (2016). Altered mGluR5-Homer scaffolds and corticostriatal connectivity in a Shank3 complete knockout model of autism. *Nat. Commun.* 7:11459. doi: 10.1038/ncomms11459

Wang, X., Xu, Q., Bey, A. L., Lee, Y., and Jiang, Y. H. (2014). Transcriptional and functional complexity of Shank3 provides a molecular framework to understand the phenotypic heterogeneity of SHANK3 causing autism and Shank3 mutant mice. *Mol. Autism* 5:30. doi: 10.1186/2040-2392-5-30

Waung, M. W., and Huber, K. M. (2009). Protein translation in synaptic plasticity: mGluR-LTD, Fragile X. *Curr. Opin. Neurobiol.* 19, 319–326. doi: 10.1016/j.conb.2009.03.011

Wilson, H. L., Wong, A. C., Shaw, S. R., Tse, W. Y., Stapleton, G. A., Phelan, M. C., et al. (2003). Molecular characterisation of the 22q13 deletion syndrome supports the role of haploinsufficiency of SHANK3/PROSAP2 in the major neurological symptoms. *J. Med. Genet.* 40, 575–584.

Yang, Y., Cheng, Z., Tang, H., Jiao, H., Sun, X., Cui, Q., et al. (2017). Neonatal maternal separation impairs prefrontal cortical myelination and cognitive functions in rats through activation of Wnt signaling. *Cereb. Cortex* 27, 2871–2884. doi: 10.1093/cercor/bhw121

Yoo, J., Bakes, J., Bradley, C., Collingridge, G. L., and Kaang, B. K. (2014). Shank mutant mice as an animal model of autism. *Philos. Trans. R. Soc. Lond. B Biol. Sci.* 369:20130143. doi: 10.1098/rstb.2013.0143

Zhou, Y., Kaiser, T., Monteiro, P., Zhang, X., Van Der Goes, M. S., Wang, D., et al. (2016). Mice with Shank3 mutations associated with ASD and schizophrenia display both shared and distinct defects. *Neuron* 89, 147–162. doi: 10.1016/j.neuron.2015.11.023

Conflict of Interest Statement: The authors declare that the research was conducted in the absence of any commercial or financial relationships that could be construed as a potential conflict of interest.

frontiers in Molecular Neuroscience

ORIGINAL RESEARCH
published: 25 September 2018
doi: 10.3389/fnmol.2018.00337

Sex Hormones Regulate *SHANK* Expression

*Simone Berkel[1†], Ahmed Eltokhi[1,2†], Henning Fröhlich[1], Diana Porras-Gonzalez[1], Rafiullah Rafiullah[1], Rolf Sprengel[2] and Gudrun A. Rappold[1]**

[1]*Department of Human Molecular Genetics, Institute of Human Genetics, Ruprecht-Karls-University, Heidelberg, Germany,*
[2]*Research Group of the Max Planck Institute for Medical Research at the Institute of Anatomy and Cell Biology, Ruprecht-Karls-University, Heidelberg, Germany*

Autism spectrum disorders (ASD) have a higher prevalence in male individuals compared to females, with a ratio of affected boys compared to girls of 4:1 for ASD and 11:1 for Asperger syndrome. Mutations in the *SHANK* genes (comprising *SHANK1*, *SHANK2* and *SHANK3*) coding for postsynaptic scaffolding proteins have been tightly associated with ASD. As early brain development is strongly influenced by sex hormones, we investigated the effect of dihydrotestosterone (DHT) and 17β-estradiol on *SHANK* expression in a human neuroblastoma cell model. Both sex hormones had a significant impact on the expression of all three *SHANK* genes, which could be effectively blocked by androgen and estrogen receptor antagonists. In neuron-specific androgen receptor knock-out mice (Ar^{NesCre}), we found a nominal significant reduction of all *Shank* genes at postnatal day 7.5 in the cortex. In the developing cortex of wild-type (WT) CD1 mice, a sex-differential protein expression was identified for all Shanks at embryonic day 17.5 and postnatal day 7.5 with significantly higher protein levels in male compared to female mice. Together, we could show that *SHANK* expression is influenced by sex hormones leading to a sex-differential expression, thus providing novel insights into the sex bias in ASD.

Keywords: autism spectrum disorders (ASD), sex differences, *SHANK*, SH-SY5Y cells, dihydrotestosterone, 17β-estradiol, androgen receptor knock-out mouse

OPEN ACCESS

Edited by:
Eunjoon Kim, Institute for Basic Science (IBS), South Korea

Reviewed by:
Yong-Seok Lee, Seoul National University College of Medicine, South Korea
Andreas Martin Grabrucker, University of Limerick, Ireland

****Correspondence:***
Gudrun A. Rappold
gudrun.rappold@med.uni-heidelberg.de

[†]These authors have contributed equally to this work

Received: *30 April 2018*
Accepted: *28 August 2018*
Published: *25 September 2018*

Citation:
Berkel S, Eltokhi A, Fröhlich H, Porras-Gonzalez D, Rafiullah R, Sprengel R and Rappold GA (2018) Sex Hormones Regulate SHANK Expression. Front. Mol. Neurosci. 11:337. doi: 10.3389/fnmol.2018.00337

INTRODUCTION

Autism Spectrum disorders (ASD) are neurodevelopmental disorders characterized by restricted and repetitive behaviors, lack of imaginative play and impaired social interaction coupled with verbal and non-verbal communication deficits. Heritability is estimated between 70%–90%, and one out of 68 children in the United States is affected (Bailey et al., 1995; Developmental Disabilities Monitoring Network Surveillance Year 2010 Principal Investigators, Centers for Disease Control and Prevention (CDC), 2014). ASD symptoms persist throughout life and prenatal impairments develop into a postnatal manifestation (Rabaneda et al., 2014).

ASD occur more frequently in males compared to females with a ratio of 4:1 for ASD and 11:1 for Asperger syndrome (Gillberg et al., 2006; Fombonne, 2009; Werling, 2016); however, the mechanism behind this sex-differential risk is not well understood. A diagnostic bias may explain part of these differences as ASD are more visible and easier to be diagnosed in males (Bargiela et al., 2016). One hypothesis to explain the sex-differential risk postulates that ASD risk genes show sex-dimorphic expression as they may reside on the sex chromosomes and are influenced by skewed X chromosome inactivation or sex-specific imprinting defects on autosomes. Another hypothesis

claims that ASD risk genes interact with sexually dimorphic pathways (Baron-Cohen et al., 2011; Werling et al., 2016). Prenatal and neonatal brain development is known to be influenced by sex hormones, suggesting that they may indeed play a role in the sex-differential expression of ASD symptoms (Werling, 2016). Estrogen enhances synaptogenesis and modulates synaptic plasticity and presumably has a neuroprotective effect (Beyer, 1999). Furthermore, a subset of adolescent ASD individuals presented elevated androgen levels (Tordjman et al., 1997) and individual differences in the development of typical autistic traits were shown to be influenced by fetal testosterone levels (Auyeung et al., 2009). To this end, a high testosterone level during development has been postulated as a risk factor for ASD (Baron-Cohen et al., 2011). Differences in synaptic composition and regional cerebral plasticity between the sexes were also proposed to account for the sex bias in ASD (Mottron et al., 2015).

SHANK proteins (SHANK1, SHANK2 and SHANK3) are scaffolding proteins at the postsynaptic site of excitatory synapses in the central nervous system (Kreienkamp, 2008), crucial for the formation, organization and signaling of excitatory synapses. *SHANK* gene variants have been associated with ASD, intellectual disability and schizophrenia (Leblond et al., 2014; Eltokhi et al., 2018).

To identify a putative regulatory role of sex hormones on *SHANK* expression, we first treated a human neuroblastoma cell line, SH-SY5Y, with dihydrotestosterone (DHT) or 17β-estradiol and quantified *SHANK* gene expression. In addition, *Shank* gene expression was evaluated pre- and postnatally in the cortex of mice lacking the androgen receptor (Ar) in neurons (Ar^{NesCre} mice). Moreover, we examined *Shank* gene and protein expression in the cortex of male and female wild-type (WT) CD1 mice at two different early developmental stages.

MATERIALS AND METHODS

Animals

Mice were housed in the Interfacultary Biomedical Facility at the Heidelberg University (IBF), under a 12 h light-dark cycle and given *ad libitum* access to water and food. All procedures were conducted in strict compliance with the National Institutes of Health Guidelines for the Care and Use of Laboratory Animals and approved by the German Animal Welfare Act and performed according to the regulations of animal experimentation within Heidelberg University and the European Union (European Communities Council Directive 2010/63/EU (local license number: T-03/16, T-24/14)). CD1 (ICR) mice (Charles River) were used for sex-specific expression analyses at different developmental stages ($n = 16$ animals of each sex). The embryonic stage was calculated by vaginal plug check and by controlling the morphological parameters which accord to the respective Theiler stage. The day of birth was considered as postnatal day (P) 0.5. Sex genotyping was performed by PCR detection of the male-specific *Sry* gene on tail biopsies. Neuron-specific Ar knock-out mice (Ar^{NesCre}) were generated by crossing female homozygous floxed Ar (*Arflox*) mice (*B6N.129-*$Ar^{tm1Verh}$/Cnrm; De Gendt et al., 2004) with male Nestin-Cre deleter mice ($Tg^{(Nes-cre)1Kln}$; MGI:2176173; Tronche et al., 1999) hemizygous for the floxed *Ar* allele. *Arflox* mice were obtained from the European Mouse Mutant Archive (EMMA, #02579) which had been backcrossed into the C57Bl/6N background for over 12 generations prior to the arrival at the IBF animal facility, as published previously (Fröhlich et al., 2017). Adult mice were sacrificed using CO_2 and early postnatal animals were decapitated, then the frontal part of the cortex was dissected for further analysis.

Cre induced site-specific recombination was checked on cortical cDNA from E17.5 and P7.5 WT and Ar^{NesCre} brains by qPCR using a specific reverse primer residing in the floxed exon 2 to determine exon 2 deletion. Primer sequences are given in **Supplementary Table Sl**.

Cell Culture

Human neuroblastoma cells (SH-SY5Y) were grown on 75 cm flasks in Dulbecco's modified Eagle medium (DMEM, Thermo Fisher Scientific), supplemented with 15% fetal calf serum, 1% non-essential amino acids and 1% Penicillin-streptomycin at 37°C in a humidified environment with 5% CO_2. Cells were split at 80%–90% confluency and 8×10^5 cells were plated per well on a 6-well cell culture plate in phenol red-free DMEM (Thermo Fisher Scientific) containing 1% charcoal dextran-treated calf serum for 24 h. Cells were treated either with 100 nM DHT (dissolved in methanol; Sigma-D-073-1ML), mock (100% methanol with the same dilution factor as DHT), 100 nM DHT combined with 1 μM flutamide (Sigma-F9397) or mock together with flutamide. To investigate the effect of 17β-estradiol, cells were treated either with 100 nM 17β-estradiol dissolved in 100% ethanol (Sigma-E8875), mock (100% ethanol with the same dilution factor as 17β-estradiol), 100 nM 17β-estradiol combined with 100 nM MPP (1,3-*Bis*(4-hydroxyphenyl)-4-methyl-5-[4-(2-piperidinylethoxy)phenol]-1*H*-pyrazole-dihydrochloride; Sigma-M7068), mock together with MPP, 100 nM 17β-estradiol plus 100 nM PHTPP (4-[2-Phenyl-5, 7-*bis*(trifluoromethyl)pyrazolo[1,5-*a*]pyrimidin-3-yl]phenol; Tocris-2662), mock plus PHTPP, 100 nM 17β-estradiol plus both MPP and PHTPP or mock plus both MPP and PHTPP. Cells were harvested after 4 h of treatment for mRNA and after 48 h for protein analyses.

Quantitative Real Time PCR (qPCR)

Total RNA from SH-SY5Y cells (five experiments with six biological replicates for each condition), CD1 and Ar^{NesCre} mouse cortices at E17.5 and P7.5 was extracted with TRIzol (Invitrogen) according to the manufacturer's instructions. Reverse transcription was performed using the SuperScript™ VILO™ cDNA Synthesis Kit (Invitrogen). Quantitative PCR was conducted using the SYBR Green Lo-Rox Fast Mix (Bioline) and the ABI 7,500 Fast Real-Time PCR system (Applied Biosystems). Each sample was analyzed in triplicates. Relative mRNA levels were assessed using the relative standard curve method by normalization to the following reference RNAs: ribosomal *18S RNA*, glyceraldehyde 3-phosphate dehydrogenase (*GAPDH*) mRNA, heat shock protein family D (HSP60) member1 (*HSPD1*)

mRNA, succinate dehydrogenase complex subunit A mRNA (*SDHA*) and hypoxanthine phosphoribosyltransferase 1 mRNA (*HPRT1*). For the SH-SY5Y cell treatment with 17β-estradiol, only *18S*, *HSPD1* and *SDHA* were used as reference mRNAs, as *Gapdh* and *Hprt1* mRNA levels were influenced by estradiol (Schroder et al., 2009). Our analysis confirmed their differential expression in SH-SY5Y cells after 17β-estradiol treatment when normalized to *18S* (**Supplementary Table S2A**). The relative expression values for mock treatment were set to 1. Calculated values are presented as normalized relative expression ratios. The sequences for the oligonucleotides used are given in **Supplementary Table S1**.

Protein Analysis

Immunefluorescence microscopy was carried out on fixed SH-SY5Y cells using the primary antibodies anti-Ar (Abcam, ab74272, 1:100 dilution) and anti-estrogen receptor α (Abcam, ab661002, 1:100 dilution), and as secondary antibodies Alexa fluor 488 goat anti-rabbit or Alexa fluor 488 goat anti-mouse (Thermo Fisher Scientific, 1:1,000 dilution).

Protein extraction from SH-SY5Y cells and from mouse frontal cortex (using the Polytron PT1200E, Kinematica AG) was performed at 4°C using RIPA buffer supplemented with SIGMAFAST protease inhibitor (S8820; Sigma). Protein concentrations were determined with the BCA protein assay kit (Pierce). Western blot analysis was executed using the Odyssey Infrared Imaging System (LI-COR Biosciences). Twenty microgram of proteins were separated on Novex WedgeWell 4%–12% Tris Glycine Gels (Thermo Fisher Scientific) and transferred to PVDF membrane (Millipore). PVDF membranes were probed with mouse anti-pan-SHANK (1:500; Neuromab), mouse monoclonal β3-tubulin (1:20,000; Promega-G7121), anti-SHANK1 (Synaptic Systems, polyclonal rabbit purified antibody, 1:500 dilution), anti-SHANK2 (Synaptic Systems, polyclonal guinea pig antiserum, 1:500 dilution), anti-SHANK3 (ab140030, Abcam, 1:1,000 dilution). IRDye 800CW donkey anti-mouse, IRDye 680LT donkey anti-guinea pig or IRDye 680RD donkey anti-rabbit (1:15,000 dilution; LI-COR Biosciences) immuno-positive signals were quantified using the Image Studio Lite 3.1 software (LI-COR Biosciences). The Page Ruler Prestained Protein ladder (10–180 kDa) and the Spectra Multicolor High Range Protein ladder (40–300 kDa; Thermo Fisher Scientific) were used as protein size marker. Shank expression was normalized to the amount of β3-tubulin and the values obtained for the male cortices were set to 1.

nCounter Analysis

Total RNA from conditional Ar^{NesCre} mouse brain cortex was extracted with TRIzol (Invitrogen) and the gene expression profile was investigated by nCounter expression analysis at the nCounter Core Facility Heidelberg, using the nCounter Dx analysis system GEN1 (NanoString Technologies). A customized Elements codeset with seven target genes and four reference genes was applied. (For probe design see **Supplementary Table S3**). The detailed workflow is described at https://www.nanostring.com/support/product-support/support-workflow. Background correction and normalization of data were performed using the nSolver Analysis Software 3.0 (NanoString Technologies). A positive control and reference gene normalization was performed according to the Gene expression analysis guideline from NanoString Technologies[1]. The most stable expressed genes *Gapdh*, *Hspd1*, *Sdha* and *Hprt1* were selected for normalization based on the geNorm method (Vandesompele et al., 2002). The unit of measurement is given in "codeset counts" and the codeset counts of the WT animals were set to 100%. The absolute numbers are provided in **Supplementary Table S4**.

Statistical Analysis

IBM SPSS STATISTICS 21, Prism 6 software (GraphPad Software) and Microsoft Office Excel software were used for data analysis. Two-way ANOVA was performed for comparing RNA expression levels between hormone-treated and mock-treated SH-SY5Y cells with treatment and experiment as the two factors. To compare gene expression levels between male and female cortices, two-way ANOVA was used with litter and sex as influencing factors. According to Bonferroni correction for multiple testing, a P-value threshold of ≤ 0.01 was considered significant ($n = 5$ different tests). For the expression analysis in the conditional Ar^{NesCre} mouse to compare differences between the WT and the knock-out mice and for the quantification of the Shank protein in male and female cortices in the western blot experiments, an unpaired two-tailed Student's t-test was used, with a P-value of ≤ 0.05 considered as nominal significant. All data are presented as mean values ± standard error of the mean (SEM).

RESULTS

SHANK Expression in Human Cells Treated With Dihydrotestosterone and 17β-Estradiol

To receive a first indication whether androgen has an effect on *SHANK* gene expression, we employed a human neuroblastoma cell model (SH-SY5Y). SH-SY5Y cells express all three SHANKs, as well as the androgen, estrogen α and β receptors (AR, ERα and ERβ; Chamniansawat and Chongthammakun, 2009, 2010; Sarachana et al., 2011; Grassi et al., 2013; Sarachana and Hu, 2013). The expression of AR and ERα in the SH-SY5Y cells is shown in **Supplementary Figure S1A**. After stimulation with DHT for 2 h, the overall expression of AR increased in the cells. Stimulation with 17 β-estradiol did not increase the expression level of ERα, but more protein was found in the nucleus (**Supplementary Figure S1A**).

To determine a regulatory influence on *SHANK* gene expression, we treated SH-SY5Y cells with the androgen DHT at different concentrations (1 nM, 10 nM and 100 nM; **Supplementary Figure S1B**). Based on the literature, DHT concentrations between 1 nM and 100 nM are considered

[1]https://www.nanostring.com/application/files/7715/1251/5220/Gene_Expression_Data_Analysis_Guidelines.pdf; accessed June 2018

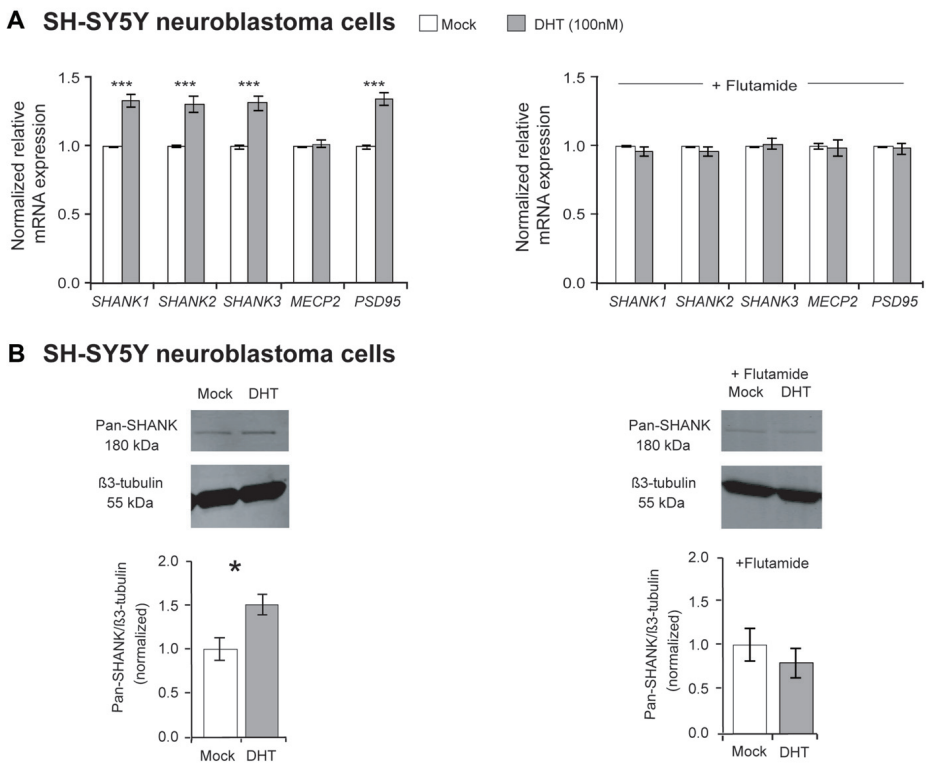

FIGURE 1 | Effect of dihydrotestosterone (DHT) on *SHANK* gene expression in SH-SY5Y cells. **(A)** Quantification of *SHANK*, *MECP2* and *PSD95* gene expression by qPCR after 4 h of treatment with either 100 nM DHT or a combination of 100 nM DHT and 1 μM flutamide (n = 5 experiments with six biological replicates for each condition). Gene expression was normalized against five reference genes (*18S*, *GAPDH*, *HPRT1*, *HSPD1* and *SDHA*; two-way ANOVA, $^{***}P \leq 0.001$, vs. mock). Bonferroni threshold: n = 5 tests, $P \leq 0.01$. **(B)** An increase of SHANK protein levels by 50% was identified after 48 h of 100 nM DHT treatment by western blot analysis, whereas no difference was determined after 48 h of treatment with DHT combined with flutamide (n = 5 experiments, unpaired two-tailed Student's t-tests, $^{*}P \leq 0.05$). Error bars indicate standard error of the mean (SEM).

to be within the physiological range and have been used in similar studies (Sarachana et al., 2011; Grassi et al., 2013). The strongest effects on *SHANK* expression were obtained by treatment with 100 nM for 4 h. *SHANK* gene expression was measured by qPCR and normalized to five androgen-independent reference RNAs: the ribosomal *18S* RNA, the mRNAs for glyceraldehyde 3-phosphate dehydrogenase (*GAPDH*), the heat shock protein family D (HSP60) member1 (*HSPD1*), the succinate dehydrogenase complex subunit A mRNA (*SDHA*) and hypoxanthine phosphoribosyltransferase 1 mRNA (*HPRT1*). The androgen independance of the reference genes was shown by the unchanged levels of *GAPDH*, *HPRT1*, *HSPD1* and *SDHA* normalized to *18S* in DHT and mock-treated SH-SY5Y cells (**Supplementary Table S2A**). *PSD95*, a gene known to be regulated by sex hormones (Akama and McEwen, 2003; Liu et al., 2008), and the X-chromosomal gene *MECP2*, which shows a transient sex-specific expression difference in the developing rat brain (Kurian et al., 2007), were included as additional markers in the expression analysis.

Our mRNA expression analysis showed that the DHT treatment significantly elevated the expression of all three *SHANK* genes by about 35% (P-values ≤ 0.001), compared to mock-treated SH-SY5Y cells (**Figure 1A**). Expression levels of *MECP2* were not influenced, whereas *PSD95* expression was significantly increased after DHT treatment (**Figure 1A**). The regulatory effect of DHT on *SHANK* gene expression could also be detected by an increased SHANK immuno-signal in western blots using an anti-pan-SHANK antibody and an anti-SHANK3 antibody (**Figure 1B**, **Supplementary Figures S1C,D**). When the SH-SY5Y cells were treated with DHT combined with the anti-androgen flutamide, the regulatory effect of DHT on *SHANK* and *PSD95* mRNA levels was completely abolished and as shown with a pan-Shank antibody also on the protein level, demonstrating that the increased *SHANK* and *PSD95* levels after DHT treatment are mediated by the stimulation of the AR (**Figures 1A,B**).

To elucidate if estrogens also regulate *SHANK* gene expression, 100 nM 17β-estradiol was used to stimulate the estrogen receptors in SH-SY5Y cells. After 17β-estradiol treatment for 4 h, a minor enhancement of *SHANK, MECP2* and *PSD95* expression could be observed. Now we restricted the normalization against reference gene expression of *18S*, *HSPD1* and *SDHA*, since *GAPDH* and *HPRT1* expression was affected by 17β-estradiol (**Supplementary Table S2A**). Our quantification revealed an increase of 15% mRNA expression for *SHANK*, *PSD95* and *MECP2*, when compared to mock-treated SH-SY5Y

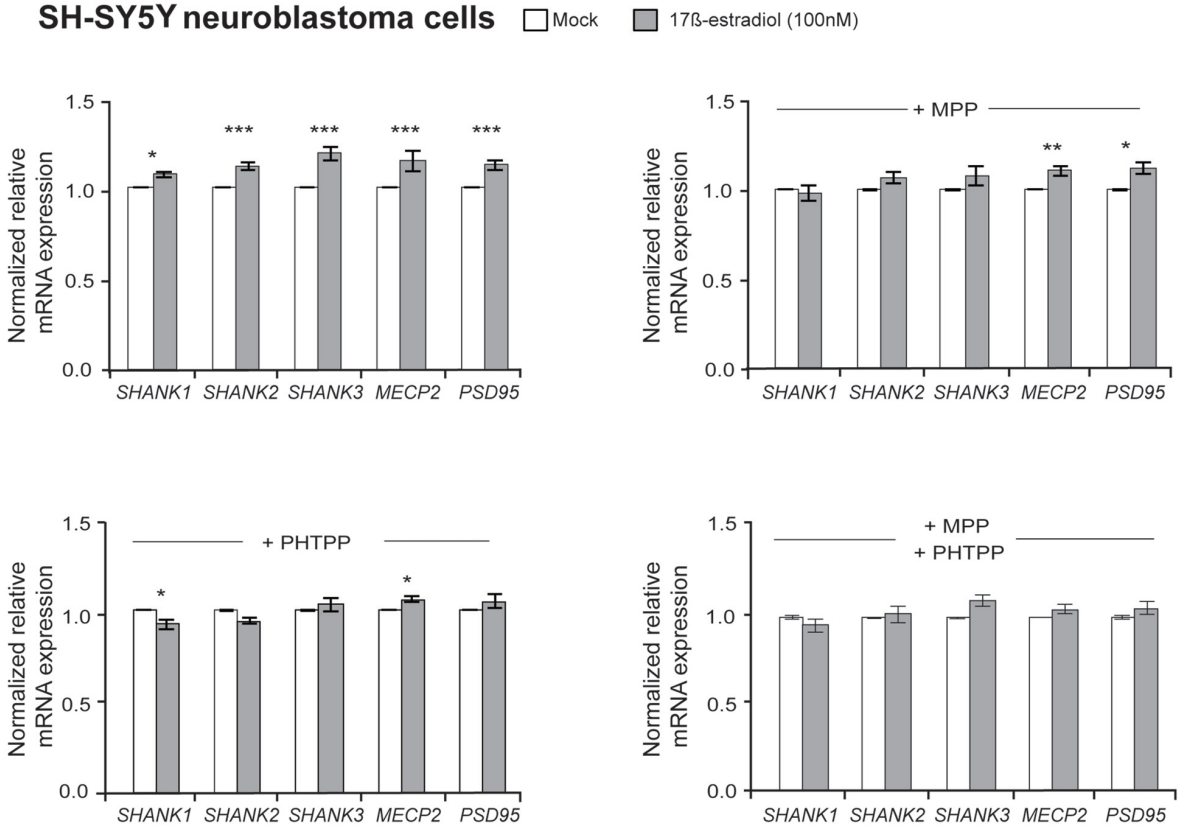

FIGURE 2 | Effect of 17β-estradiol on *SHANK* gene expression in SH-SY5Y cells. Gene expression analysis of *SHANK, MECP2* and *PSD95* after 4 h of treatment with 100 nM 17β-estradiol. The expression was also analyzed after stimulation with 100 nM 17β-estradiol in combination with a selective blocking of estrogen receptor α (100 nM MPP), estrogen receptor β (100 nM PHTPP) or a combination of both (n = 5 experiments with six biological replicates for each condition). Gene expression was normalized against three reference genes (*18S*, *HSPD1* and *SDHA*). Error bars indicate SEM (two-way ANOVA, $^{*}P \leq 0.05$, $^{**}P \leq 0.01$, $^{***}P \leq 0.001$, vs. mock-treatment control). Bonferroni correction: n = 5 tests, $P \leq 0.01$.

cells (P-value for *SHANK1* = 0.02; P-values for *SHANK2*, *SHANK3*, *MECP2* and *PSD95* $\leq$ 0.001; **Figure 2**). However, a regulatory influence on SHANK protein expression could not be detected in immunoblots (**Supplementary Figure S1E**). By blocking the ERα or ERβ receptor subtypes with the selective ERα antagonist MPP or ERβ antagonist PHTPP, the effect of 17β-estradiol on *SHANK* expression by MPP was gone, whereas the blocking of ERβ with the antagonist PHTPP abrogated the effect on *SHANK* and *PSD95* expression (**Figure 2**). The combined blocking of both ERs antagonized the 17β-estradiol-stimulated expression of *SHANK*, *PSD95* and *MECP2* (**Figure 2**). Thus, besides AR, also ERα and ERβ signaling contributes to the expression of *SHANK* genes in the human SH-SY5Y cell line.

Expression Analysis of *Shank* Genes in Neuron-Specific Conditional Androgen Receptor Knock-out Mice (Ar^{NesCre})

To provide *in vivo* evidence for the Ar regulatory influence on *Shank* gene expression during neurodevelopment, we used a neuron-specific Ar knock-out mouse (Ar^{NesCre}; Fröhlich et al., 2017). We analyzed *Shank* mRNA expression in the cortex of Ar^{NesCre} mice at two developmental stages, E17.5 and P7.5 (**Figure 3**, **Supplementary Figure S2A**). In this critical period of brain development, sex differences in the spatiotemporal expression of *Ar*, *Erα* and *Erβ* in mouse brain as well as differences in testosterone levels were previously reported (Mogi et al., 2015). Furthermore, it is known that in the human cortex, size and sex hormone levels differ between males and females (Lombardo et al., 2012; Lai et al., 2013). By nCounter analysis, we identified a reduced mRNA expression of all three *Shanks* and *Mecp2* in the Ar^{NesCre} mice compared to WT at P7.5 with nominal significance (**Figure 3**), supporting the contribution of Ar signaling in the specific regulation of the *Shank* gene expression during development.

Expression Analysis of the *Shank* Genes and Proteins in the Male and Female Mouse Cortex

Further support for a sex-specific regulation of *Shank* expression could be provided by comparing the expression levels in

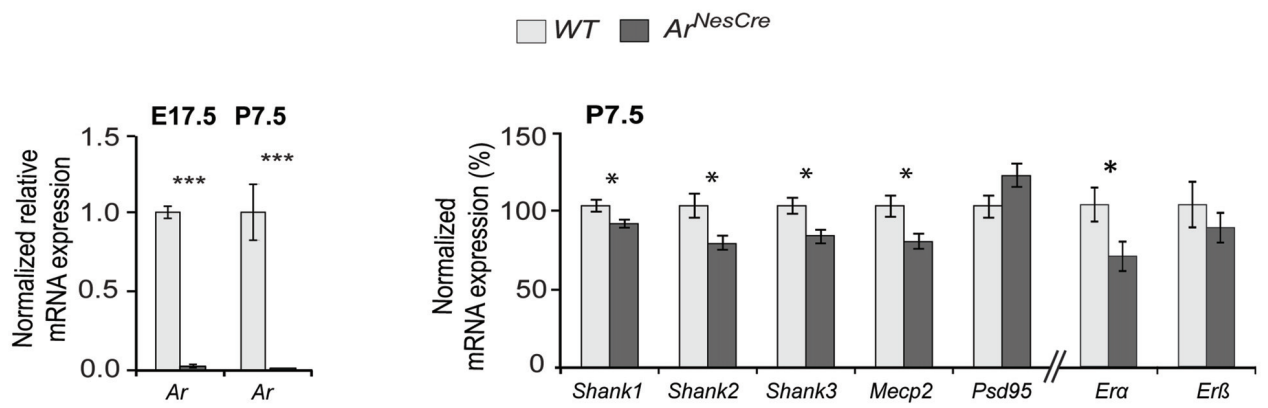

FIGURE 3 | Comparative *Shank* gene expression analysis by nCounter in the cortex of wild-type (WT) and Ar^{NesCre} mice. (Left) Loss of androgen receptor (*Ar*) expression in cortical neurons was confirmed by qPCR. The deletion of *Ar*-exon2 was shown on mRNA level in cortical tissue. (Right) Gene expression analysis in cortex of WT and Ar^{NesCre} mice at P7.5. The loss of Ar resulted in a decreased expression of the *Shank* and *Mecp2* genes (n = 7 WT and seven KO mice, two male and five female animals in each group). The analysis could not be stratified by sex due to low numbers. Gene expression was normalized against four reference genes (*Gapdh*, *Hprt1*, *Hspd1* and *Sdha*). Error bars indicate SEM (unpaired two-tailed Student's *t*-tests, $^{*}P \leq 0.05$; $^{***}P \leq 0.001$).

the frontal cortices of male and female CD1 WT mice at two different developmental stages, E17.5 and P7.5. The sex-independent expression of the reference genes was confirmed by showing equal levels of *Gapdh*, *Sdha*, *Hprt1* and *Hspd1* expression, normalized to *18s*, in male and female mice cortices (**Supplementary Table S2B**). In the comparative qPCR analysis, significantly elevated *Shank1*, *Shank3* and *Mecp2* expression levels could be detected in the cortices of female compared to the male mice at E17.5 (**Supplementary Figure S2B**). At P7.5, our analysis revealed elevated *Shank1* mRNA expression in the female cortex with nominal significance, as well as significantly elevated *Psd95* expression (**Supplementary Figure S2B**). Then we analyzed Shank protein expression in whole protein lysate from the frontal cortex of male and female mice at E17.5 and P7.5 by western blot. In contrast to the mRNA expression analysis, we found significantly higher expression levels for all three Shank proteins in the male compared to female cortices at both developmental stages. Shank expression is decreased in females by 50%–77% at E17.5 (**Figure 4A**) and by 43%–47% at P7.5 (**Figure 4B**), indicating that Shank expression differences are more pronounced at the earlier stage of E17.5.

DISCUSSION

Males show higher prenatal and postnatal testosterone levels than females (Baron-Cohen, 2002; Werling, 2016). Elevated prenatal exposure to testosterone and /or irregular steroidogenic activity have been postulated to be associated with elevated ASD risk (Auyeung et al., 2009). Testosterone is metabolized in the brain into DHT or converted into estradiol by the enzyme aromatase (CYP19A1). Therefore, we have investigated the influence of both hormones on the expression of the *SHANK* genes, which are strongly linked to ASD pathology (Leblond et al., 2014). We could show in the SH-SY5Y neuroblastoma cell line, a widely used neuronal cell model to investigate hormonal influences of androgens and estrogens (Sarachana et al., 2011; Grassi et al., 2013; Nakaso et al., 2014; Sun et al., 2017), that the effect of DHT and 17β-estradiol on the expression of all three Shanks could be effectively blocked by androgen and estrogen receptor antagonists. *SHANK* gene expression was shown to be regulated by DHT, directly modulated by AR signaling. DHT increased *SHANK* mRNA levels by 35% and 17β-estradiol increased *SHANK* mRNA levels by 15%, suggesting a role as transcriptional fine-tuners. Protein levels were found to be increased by DHT treatment by 50%, indicating that the major effect is seen at the level of translation.

More direct evidence for the contribution of AR signaling on the regulation of *SHANK* gene expression could be demonstrated by the analysis of mice with *Ar* gene deletion in neurons (ArNesCre). Ar^{NesCre} mice show reduced sexual, territorial and aggressive behavior (Raskin et al., 2009; Studer et al., 2015). Male Ar^{NesCre} mice lack social memory when presented to male conspecifics but do not show ASD-like impairments in social interactions with other mice (Karlsson et al., 2016). We found that in absence of the Ar in neurons, the expression of all three *Shanks* was reduced and reached nominal significance, supporting the role of Ar activity in the regulation of *Shank* expression during brain development. Previous data has shown that *Ar* and *Shank* genes have overlapping expression patterns in the cortex, striatum and hippocampus (Lein et al., 2007; Fröhlich et al., 2017; Monteiro and Feng, 2017). Androgen- and estrogen-dependent gene regulation has also been described for genes involved in the function of glutamatergic synapses in the medial preoptic area and the ventromedial hypothalamus of rats,

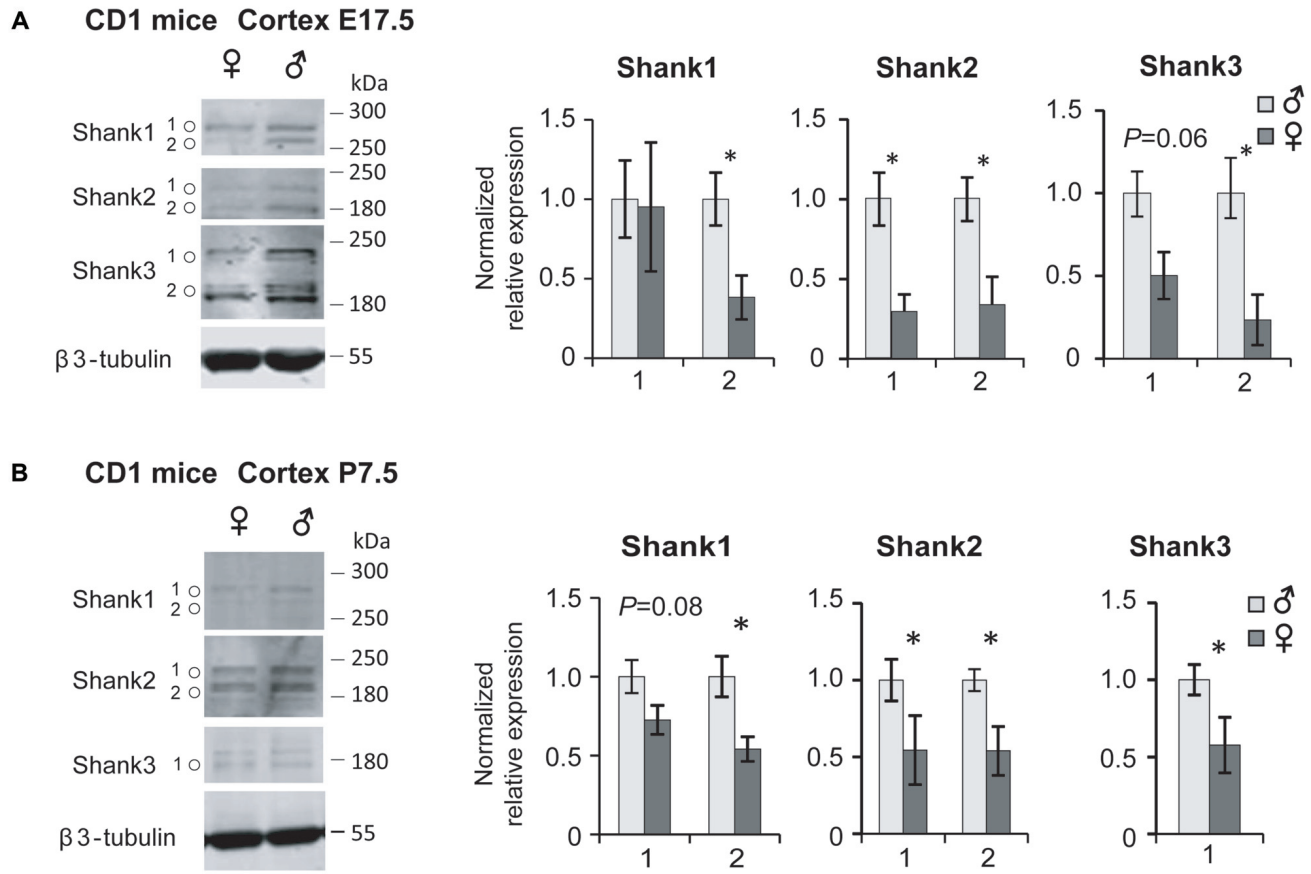

FIGURE 4 | Shank protein analysis in the male and female mouse cortex. Levels of Shank1, Shank2 and Shank3 protein in the frontal cortex of male and female at E17.5 **(A)** and P7.5 **(B)**; (n = 4 of each sex), $^*P < 0.05$, unpaired two-tailed Student's t-tests. Isoform expression differences were observed between the two developmental stages for Shank3.

after exposure to anti-androgenic and/or estrogenic treatment or a combination of both *in utero* (Lichtensteiger et al., 2015). In that study, *Shank1* and *Shank2* expression was altered in young male rats and *Shank2* and *Shank3* in female animals at P6, hereby providing additional *in vivo* evidence of a sex hormone regulation of *Shank* gene expression in specific brain regions.

Palindromic and dihexameric motifs of androgen responsive elements were described in the promoters or enhancers of all three *SHANK* genes: half and full sites in *SHANK2* and half sites in *SHANK1* and *SHANK3* (Wilson et al., 2016). An AR-binding site was also recently identified in an intron and in the distant promoter region of *SHANK2* by ChIP-Seq (Quartier et al., 2018). These results point to a direct regulatory influence of DHT on *SHANK2*. In a different study, direct and indirect interaction partners of SHANKs, such as PSD-95 and the AMPA receptor subunits GluA1 and GluA2, were reported to be androgen-responsive (Trabzuni et al., 2013), suggesting that synergistic effects at the synapse between multiple proteins strengthen the individual effects.

Despite the fact that *Shank1* mRNA expression levels are lower in male mice at P7.5, we could show that protein levels of all Shanks are higher in males during late prenatal and early postnatal cortical development in WT mice (E17.5 and P7.5). The RNA level does not always correlate with protein levels, especially for proteins with a long half-life or in cases of negative feed-back when the increase in protein level decreases the expression of RNA. In a previous study on genome-wide scale, it was also found that the cellular abundance of protein is predominantly controlled at the level of translation (Schwanhausser et al., 2011). Between E17.5 and P7.5, *Ar* expression and testosterone level differ between male and female mice (Mogi et al., 2015). Male mice have about three times higher blood testosterone levels than female embryos at E17 (Vom Saal, 1983) and show significantly higher testosterone levels in the brain (ICR/CD1 strain) at E19 (Mogi et al., 2015). The finding that DHT increases *SHANK* mRNA and protein expression in SH-SY5Y cells, suggests that high levels of testosterone in the male brain may result in elevated SHANK protein expression. The discrepancy between high protein and low mRNA levels in CD1 mice might

be caused by negative feedback mechanisms, suggesting that high Shank protein levels lead to lower Shank mRNA levels. However, SH-SY5Y cells may not entirely reflect the regulatory potential of testosterone signaling in cortical neurons, which are a heterogeneous population of cells that may respond individually differently to DHT. Therefore, the data obtained from established cell lines need to be verified in the living mouse.

In mice, the perinatal developmental period between E17 and P7.5 might be a vulnerable time window for *Shank* expression when sex differences in the cortex might intersect with ASD etiological pathways. Physiologically higher SHANK protein expression levels in males compared to females implicate that genetic variants may have a higher penetrance in males, leading to a larger proportion of males with a diagnosis of ASD. Clinical studies reported elevated androgen levels in ASD-affected individuals (Baron-Cohen, 2002; Werling, 2016). Our results imply that Shank expression may be increased in these individuals, at least during the developmental vulnerable stages. In contrast, most ASD individuals have been identified with *SHANK* deletions and various point mutations, indicating that SHANK levels are very likely reduced in these ASD individuals. Nevertheless, it cannot be excluded that a general dysregulation of SHANK gene expression contributes to ASD pathology, as *SHANK3* gene duplications have also been identified in individuals with Asperger syndrome (Durand et al., 2007).

SHANK genes reside on autosomes, and *SHANK* variants are randomly distributed across male and female subjects. So far, only copy number variant (CNV) deletions encompassing the *SHANK1* gene segregated in male carriers with high-functioning autism and showed a clearly reduced penetrance in female individuals (Sato et al., 2012) and some *SHANK* variants have been found in male autistic patients that were inherited from healthy mothers (for a recent review see (Eltokhi et al., 2018)).

Sex differences in gene expression were previously studied in prenatal and adult neocortical tissue of human post-mortem brain (Trabzuni et al., 2013; Werling et al., 2016). Only a small proportion of the analyzed genes, however, were found to be expressed in a sex-specific manner (96 prenatal, 58 adult; Werling et al., 2016). No evidence was obtained for sex-differential expression of the *SHANKs* or other ASD-associated genes like *RORA* and *FOXP1* (Sarachana et al., 2011; Takayama et al., 2014; Fröhlich et al., 2017). However, in those studies, the analyzed cortical samples were from prenatal (16–22 weeks) or adult samples and did not match with the investigated developmental stages used in our study, suggesting that the days shortly before or after birth are sensitive for sex hormone-regulated SHANK/Shank expression.

Together, we found that the expression of the ASD-associated *SHANK* gene family is upregulated by DHT in SH-SY5Y cells and that in mice all three Shanks showed elevated protein expression levels in males during late prenatal and early postnatal cortical development, that most likely are facilitated by high testosterone levels of males during these developmental time windows. Our results provide novel insights in the understanding of the sex bias in ASD.

AUTHOR CONTRIBUTIONS

GR and SB designed the study. SB performed the mouse experiments and protein analysis. AE performed the cell culture experiments and mRNA expression analysis. HF and RR generated the Ar^{NesCre} mouse line and provided tissue. DP-G contributed to the cell culture and mouse experiments. SB and AE performed the data analysis. SB, AE, GR, HF and RS contributed to the data interpretation. SB, AE and GR wrote the manuscript. All authors contributed to and reviewed the final manuscript.

FUNDING

This study was supported by the Medical Faculty of the Ruprecht-Karls-University Heidelberg. SB was supported by a Frontier grant (ZUK49/Ü5.2.183) and by the Medical Faculty of the Ruprecht-Karls-University Heidelberg. AE received support from an HBIGS PhD fellowship, RR from a DAAD scholarship and RS from the Ingeborg Ständer Foundation.

ACKNOWLEDGMENTS

We thank the nCounter Core Facility Heidelberg at the Institute of Human Genetics for providing nCounter-related services and Christine Fischer for statistical advice.

SUPPLEMENTARY MATERIAL

The Supplementary Material for this article can be found online at: https://www.frontiersin.org/articles/10.3389/fnmol.2018.00337/full#supplementary-material

REFERENCES

Akama, K. T., and McEwen, B. S. (2003). Estrogen stimulates postsynaptic density-95 rapid protein synthesis via the Akt/protein kinase B pathway. *J. Neurosci.* 23, 2333–2339. doi: 10.1523/JNEUROSCI.23-06-02333.2003

Auyeung, B., Baron-Cohen, S., Ashwin, E., Knickmeyer, R., Taylor, K., and Hackett, G. (2009). Fetal testosterone and autistic traits. *Br. J. Psychol.* 100, 1–22. doi: 10.1348/000712608X311731

Bailey, A., Le Couteur, A., Gottesman, I., Bolton, P., Simonoff, E., Yuzda, E., et al. (1995). Autism as a strongly genetic disorder: evidence from a British twin study. *Psychol. Med.* 25, 63–77. doi: 10.1017/s0033291700028099

Bargiela, S., Steward, R., and Mandy, W. (2016). The experiences of late-diagnosed women with autism spectrum conditions: an investigation of the female autism phenotype. *J. Autism Dev. Disord.* 46, 3281–3294. doi: 10.1007/s10803-016-2872-8

Baron-Cohen, S. (2002). The extreme male brain theory of autism. *Trends Cogn. Sci.* 6, 248–254. doi: 10.1016/s1364-6613(02)01904-6

Baron-Cohen, S., Lombardo, M. V., Auyeung, B., Ashwin, E., Chakrabarti, B., and Knickmeyer, R. (2011). Why are autism spectrum conditions more prevalent in males? *PLoS Biol.* 9:e1001081. doi: 10.1371/journal.pbio.1001081

Beyer, C. (1999). Estrogen and the developing mammalian brain. *Anat. Embryol.* 199, 379–390. doi: 10.1007/s004290050236

Chamniansawat, S., and Chongthammakun, S. (2009). Estrogen stimulates activity-regulated cytoskeleton associated protein (Arc) expression via the MAPK- and PI-3K-dependent pathways in SH-SY5Y cells. *Neurosci. Lett.* 452, 130–135. doi: 10.1016/j.neulet.2009.01.010

Chamniansawat, S., and Chongthammakun, S. (2010). Genomic and non-genomic actions of estrogen on synaptic plasticity in SH-SY5Y cells. *Neurosci. Lett.* 470, 49–54. doi: 10.1016/j.neulet.2009.12.053

De Gendt, K., Swinnen, J. V., Saunders, P. T., Schoonjans, L., Dewerchin, M., Devos, A., et al. (2004). A sertoli cell-selective knock-out of the androgen receptor causes spermatogenic arrest in meiosis. *Proc. Natl. Acad. Sci. U S A* 101, 1327–1332. doi: 10.1073/pnas.0308114100

Developmental Disabilities Monitoring Network Surveillance Year 2010 Principal Investigators, Centers for Disease Control and Prevention (CDC). (2014). Prevalence of autism spectrum disorder among children aged 8 years—autism and developmental disabilities monitoring network, 11 sites, United States, 2010. *MMWR Surveill. Summ.* 63, 1–21.

Durand, C. M., Betancur, C., Boeckers, T. M., Bockmann, J., Chaste, P., Fauchereau, F., et al. (2007). Mutations in the gene encoding the synaptic scaffolding protein SHANK3 are associated with autism spectrum disorders. *Nat. Genet.* 39, 25–27. doi: 10.1038/ng1933

Eltokhi, A., Rappold, G., and Sprengel, R. (2018). Distinct phenotypes of Shank2 mouse models reflect neuropsychiatric spectrum disorders of human patients with SHANK2 variants. *Front. Mol. Neurosci.* 11:240. doi: 10.3389/fnmol.2018.00240

Fombonne, E. (2009). Epidemiology of pervasive developmental disorders. *Pediatr. Res.* 65, 591–598. doi: 10.1203/PDR.0b013e31819e7203

Fröhlich, H., Rafiullah, R., Schmitt, N., Abele, S., and Rappold, G. A. (2017). Foxp1 expression is essential for sex-specific murine neonatal ultrasonic vocalization. *Hum. Mol. Genet.* 26, 1511–1521. doi: 10.1093/hmg/ddx055

Gillberg, C., Cederlund, M., Lamberg, K., and Zeijlon, L. (2006). Brief report: "the autism epidemic". The registered prevalence of autism in a Swedish urban area. *J. Autism Dev. Disord.* 36, 429–435. doi: 10.1007/s10803-006-0081-6

Grassi, D., Bellini, M. J., Acaz-Fonseca, E., Panzica, G., and Garcia-Segura, L. M. (2013). Estradiol and testosterone regulate arginine-vasopressin expression in SH-SY5Y human female neuroblastoma cells through estrogen receptors-α and -β. *Endocrinology* 154, 2092–2100. doi: 10.1210/en.2012-2137

Karlsson, S. A., Studer, E., Kettunen, P., and Westberg, L. (2016). Neural androgen receptors modulate gene expression and social recognition but not social investigation. *Front. Behav. Neurosci.* 10:41. doi: 10.3389/fnbeh.2016.00041

Kreienkamp, H. J. (2008). Scaffolding proteins at the postsynaptic density: shank as the architectural framework. *Handb. Exp. Pharmacol.* 186, 365–380. doi: 10.1007/978-3-540-72843-6_15

Kurian, J. R., Forbes-Lorman, R. M., and Auger, A. P. (2007). Sex difference in mecp2 expression during a critical period of rat brain development. *Epigenetics* 2, 173–178. doi: 10.4161/epi.2.3.4841

Lai, M. C., Lombardo, M. V., Suckling, J., Ruigrok, A. N., Chakrabarti, B., Ecker, C., et al. (2013). Biological sex affects the neurobiology of autism. *Brain* 136, 2799–2815. doi: 10.1093/brain/awt216

Leblond, C. S., Nava, C., Polge, A., Gauthier, J., Huguet, G., Lumbroso, S., et al. (2014). Meta-analysis of *SHANK* Mutations in Autism Spectrum Disorders: a gradient of severity in cognitive impairments. *PLoS Genet.* 10:e1004580. doi: 10.1371/journal.pgen.1004580

Lein, E. S., Hawrylycz, M. J., Ao, N., Ayres, M., Bensinger, A., Bernard, A., et al. (2007). Genome-wide atlas of gene expression in the adult mouse brain. *Nature* 445, 168–176. doi: 10.1038/nature05453

Lichtensteiger, W., Bassetti-Gaille, C., Faass, O., Axelstad, M., Boberg, J., Christiansen, S., et al. (2015). Differential gene expression patterns in developing sexually dimorphic rat brain regions exposed to antiandrogenic, estrogenic, or complex endocrine disruptor mixtures: glutamatergic synapses as target. *Endocrinology* 156, 1477–1493. doi: 10.1210/en.2014-1504

Liu, F., Day, M., Muñiz, L. C., Bitran, D., Arias, R., Revilla-Sanchez, R., et al. (2008). Activation of estrogen receptor-β regulates hippocampal synaptic plasticity and improves memory. *Nat. Neurosci.* 11, 334–343. doi: 10.1038/nn2057

Lombardo, M. V., Ashwin, E., Auyeung, B., Chakrabarti, B., Taylor, K., Hackett, G., et al. (2012). Fetal testosterone influences sexually dimorphic gray matter in the human brain. *J. Neurosci.* 32, 674–680. doi: 10.1523/JNEUROSCI.4389-11.2012

Mogi, K., Takanashi, H., Nagasawa, M., and Kikusui, T. (2015). Sex differences in spatiotemporal expression of AR, ERα and ERβ mRNA in the perinatal mouse brain. *Neurosci. Lett.* 584, 88–92. doi: 10.1016/j.neulet.2014.10.028

Monteiro, P., and Feng, G. (2017). SHANK proteins: roles at the synapse and in autism spectrum disorder. *Nat. Rev. Neurosci.* 18, 147–157. doi: 10.1038/nrn.2016.183

Mottron, L., Duret, P., Mueller, S., Moore, R. D., Forgeot, R. D., Jacquemont, S., et al. (2015). Sex differences in brain plasticity: a new hypothesis for sex ratio bias in autism. *Mol. Autism* 6:33. doi: 10.1186/s13229-015-0024-1

Nakaso, K., Tajima, N., Horikoshi, Y., Nakasone, M., Hanaki, T., Kamizaki, K., et al. (2014). The estrogen receptor β-PI3K/Akt pathway mediates the cytoprotective effects of tocotrienol in a cellular Parkinson's disease model. *Biochim. Biophys. Acta* 1842, 1303–1312. doi: 10.1016/j.bbadis.2014.04.008

Quartier, A., Chatrousse, L., Redin, C., Keime, C., Haumesser, N., Maglott-Roth, A., et al. (2018). Genes and pathways regulated by androgens in human neural cells, potential candidates for the male excess in autism spectrum disorder. *Biol. Psychiatry* 84, 239–252. doi: 10.1016/j.biopsych.2018.01.002

Rabaneda, L. G., Robles-Lanuza, E., Nieto-González, J. L., and Scholl, F. G. (2014). Neurexin dysfunction in adult neurons results in autistic-like behavior in mice. *Cell Rep.* 8, 338–346. doi: 10.1016/j.celrep.2014.06.022

Raskin, K., de Gendt, K., Duittoz, A., Liere, P., Verhoeven, G., Tronche, F., et al. (2009). Conditional inactivation of androgen receptor gene in the nervous system: effects on male behavioral and neuroendocrine responses. *J. Neurosci.* 29, 4461–4470. doi: 10.1523/JNEUROSCI.0296-09.2009

Sarachana, T., and Hu, V. W. (2013). Differential recruitment of coregulators to the RORA promoter adds another layer of complexity to gene (dys) regulation by sex hormones in autism. *Mol. Autism* 4:39. doi: 10.1186/2040-2392-4-39

Sarachana, T., Xu, M., Wu, R. C., and Hu, V. W. (2011). Sex hormones in autism: androgens and estrogens differentially and reciprocally regulate RORA, a novel candidate gene for autism. *PLoS One* 6:e17116. doi: 10.1371/journal.pone.0017116

Sato, D., Lionel, A. C., Leblond, C. S., Prasad, A., Pinto, D., Walker, S., et al. (2012). SHANK1 deletions in males with autism spectrum disorder. *Am. J. Hum. Genet.* 90, 879–887. doi: 10.1016/j.ajhg.2012.03.017

Schroder, A. L., Pelch, K. E., and Nagel, S. C. (2009). Estrogen modulates expression of putative housekeeping genes in the mouse uterus. *Endocrine* 35, 211–219. doi: 10.1007/s12020-009-9154-6

Schwanhausser, B., Busse, D., Li, N., Dittmar, G., Schuchhardt, J., Wolf, J., et al. (2011). Global quantification of mammalian gene expression control. *Nature* 473, 337–342. doi: 10.1038/nature10098

Studer, E., Naslund, J., Andersson, E., Nilsson, S., Westberg, L., and Eriksson, E. (2015). Serotonin depletion-induced maladaptive aggression requires the presence of androgens. *PLoS One* 10:e0126462. doi: 10.1371/journal.pone.0126462

Sun, J., Wang, D., Guo, L., Fang, S., Wang, Y., and Xing, R. (2017). Androgen receptor regulates the growth of neuroblastoma cells *in vitro* and *in vivo*. *Front. Neurosci.* 11:116. doi: 10.3389/fnins.2017.00116

Takayama, K., Suzuki, T., Tsutsumi, S., Fujimura, T., Takahashi, S., Homma, Y., et al. (2014). Integrative analysis of FOXP1 function reveals a tumor-suppressive effect in prostate cancer. *Mol. Endocrinol.* 28, 2012–2024. doi: 10.1210/me.2014-1171

Tordjman, S., Ferrari, P., Sulmont, V., Duyme, M., and Roubertoux, P. (1997). Androgenic activity in autism. *Am. J. Psychiatry* 154, 1626–1627. doi: 10.1176/ajp.154.11.1626-a

Trabzuni, D., Ramasamy, A., Imran, S., Walker, R., Smith, C., Weale, M. E., et al. (2013). Widespread sex differences in gene expression and splicing in the adult human brain. *Nat. Commun.* 4:2771. doi: 10.1038/ncomms3771

Tronche, F., Kellendonk, C., Kretz, O., Gass, P., Anlag, K., Orban, P. C., et al. (1999). Disruption of the glucocorticoid receptor gene in the nervous system results in reduced anxiety. *Nat. Genet.* 23, 99–103. doi: 10.1038/12703

Vandesompele, J., De Preter, K., Pattyn, F., Poppe, B., Van Roy, N., De Paepe, A., et al. (2002). Accurate normalization of real-time quantitative RT-PCR data by geometric averaging of multiple internal control genes. *Genome Biol.* 3:RESEARCH0034. doi: 10.1186/gb-2002-3-7-research0034

Vom Saal, F. S. (1983). "The interaction of circulating oestrogens androgens in regulating mammalian sexual differentiation," in *Hormones and Behaviour in Higher Vertebrates*, eds J. Balthazart, E. Pröve and R. Gilles (Berlin Heidelberg: Springer), 159–177.

Werling, D. M. (2016). The role of sex-differential biology in risk for autism spectrum disorder. *Biol. Sex Differ.* 7:58. doi: 10.1186/s13293-016-0112-8

Werling, D. M., Parikshak, N. N., and Geschwind, D. H. (2016). Gene expression in human brain implicates sexually dimorphic pathways in autism spectrum disorders. *Nat. Commun.* 7:10717. doi: 10.1038/ncomms10717

Wilson, S., Qi, J., and Filipp, F. V. (2016). Refinement of the androgen response element based on ChIP-Seq in androgen-insensitive androgen-responsive prostate cancer cell lines. *Sci. Rep.* 6:32611. doi: 10.1038/srep32611

Conflict of Interest Statement: The authors declare that the research was conducted in the absence of any commercial or financial relationships that could be construed as a potential conflict of interest.

frontiers in Molecular Neuroscience

ORIGINAL RESEARCH
published: 04 October 2018
doi: 10.3389/fnmol.2018.00365

Shank2 Mutant Mice Display Hyperactivity Insensitive to Methylphenidate and Reduced Flexibility in Social Motivation, but Normal Social Recognition

Elodie Ey[1], Nicolas Torquet[2], Fabrice de Chaumont[3], Julie Lévi-Strauss[1], Allain-Thibeault Ferhat[1], Anne-Marie Le Sourd[1], Tobias M. Boeckers[4] and Thomas Bourgeron[1,5]*

[1] CNRS UMR 3571, Human Genetics and Cognitive Functions, Institut Pasteur, Paris, France, [2] Sorbonne Université, UPMC Univ Paris 06, INSERM, CNRS, Neuroscience Paris Seine – Institut de Biologie Paris Seine (NPS – IBPS), Paris, France, [3] CNRS UMR 3691, BioImage Analysis, Institut Pasteur, Paris, France, [4] Institute for Anatomy and Cell Biology, Ulm University, Ulm, Germany, [5] Université Paris Diderot, Sorbonne Paris Cité, Human Genetics and Cognitive Functions, Paris, France

Mouse models of autism can be used to study evolutionarily conserved mechanisms underlying behavioral abnormalities in social communication and repetitive behaviors. *SHANK* genes code for synaptic scaffolding proteins at excitatory synapses and mutations in all *SHANK* genes have been associated with autism. Here, we present three behavioral aspects of the mutant mice deleted for exon 16 in *Shank2*. First, we treated *Shank2* mutant mice with methylphenidate to rescue the hyperactivity. Our failure to do so suggests that the hyperactivity displayed by *Shank2* mutant mice is not related to the one displayed by the typical mouse models of hyperactivity, and might be more closely related to manic-like behaviors. Second, by testing the effect of group housing and social isolation on social interest, we highlighted that *Shank2* mutant mice lack the typical flexibility to modulate social interest, in comparison with wild-type littermates. Finally, we established a new protocol to test for social recognition in a social context. We used this protocol to show that *Shank2* mutant mice were able to discriminate familiar and unknown conspecifics in free interactions. Altogether, these studies shed some light on specific aspects of the behavioral defects displayed by the *Shank2* mouse model. Such information could be used to orient therapeutic strategies and to design more specific tests to characterize the complex behavior of mouse models of autism.

Keywords: mouse models, autism, *Shank2*, hyperactivity, methylphenidate, social motivation, ultrasonic vocalization, social recognition

OPEN ACCESS

Edited by:
Markus Wöhr, Philipps-Universität Marburg, Germany

Reviewed by:
Rolf Sprengel, Max-Planck-Institut für Medizinische Forschung, Germany
Maria Passafaro, Università degli Studi di Milano, Italy

****Correspondence:***
Elodie Ey
elodie.ey@pasteur.fr;
eey@pasteur.fr

Received: *12 July 2018*
Accepted: *13 September 2018*
Published: *04 October 2018*

Citation:
Ey E, Torquet N, de Chaumont F, Lévi-Strauss J, Ferhat A-T, Le Sourd A-M, Boeckers TM and Bourgeron T (2018) Shank2 Mutant Mice Display Hyperactivity Insensitive to Methylphenidate and Reduced Flexibility in Social Motivation, but Normal Social Recognition. Front. Mol. Neurosci. 11:365. doi: 10.3389/fnmol.2018.00365

INTRODUCTION

Autism spectrum conditions (ASCs; henceforth autism) are characterized by atypical social communication, including social interactions and verbal and non-verbal communication, as well as stereotyped and repeated behaviors and restricted interests (American Psychiatric Association, 2013). More than 80 genes have been robustly associated with autism (Abrahams et al., 2013).

Among these genes, the *SHANK* family is of interest since mutations in each of the three members of this family (*SHANK1*, *PROSAP1/SHANK2*, and *PROSAP2/SHANK3*) have been identified in patients with autism, but with a gradient of severity (Leblond et al., 2014). Patients carrying a mutation in *SHANK1* display a mild phenotype in social communication and stereotypes, while patients carrying *SHANK2* mutations are more affected in their social interactions and repetitive behaviors. Patients with *SHANK3* mutations are even more severely affected and are also in the great majority of cases diagnosed with intellectual disability.

In the present study, we focused our experiments on mice lacking the Shank2 protein. To date, three different genetic constructions of the model exist (reviewed in Eltokhi et al., 2018): deletion of exon 16 [knock out (Schmeisser et al., 2012; Ey et al., 2013; Lim et al., 2016), conditional knock out in Purkinje cells (Peter et al., 2016)], deletion of exons 15 and 16 [knock out (Won et al., 2012; Lee et al., 2015; Lim et al., 2016), conditional knock out in Purkinje cells (Ha et al., 2016), conditional knock out in excitatory neurons (Kim et al., 2018), conditional knock out in inhibitory neurons (Kim et al., 2018), conditional knock out in parvalbumin-positive neurons (Lee et al., 2018)], deletion of exon 24 [knock out (Pappas et al., 2017), conditional knock out in Purkinje cells (Pappas et al., 2017), conditional knock out in excitatory neurons of neocortex and hippocampus (Pappas et al., 2017)]. All these models display hyperactivity, except the mice mutated conditionally only in Purkinje cells (Ha et al., 2016; Peter et al., 2016; Pappas et al., 2017). As proxies for the core symptoms of autism, a number of studies identified subtle abnormalities in the social domain [reduced interest for social interactions (Schmeisser et al., 2012; Won et al., 2012; Lee et al., 2015; Peter et al., 2016; Kim et al., 2018)] [but not in Ha et al. (2016); Lim et al. (2016); Pappas et al. (2017); and Lee et al. (2018)], reduced interest for social novelty (Schmeisser et al., 2012; Lee et al., 2015; Peter et al., 2016) [but not in Won et al. (2012) and Kim et al. (2018)], atypical ultrasonic communication (Schmeisser et al., 2012; Won et al., 2012; Ey et al., 2013; Ha et al., 2016; Kim et al., 2018), and increased stereotyped behaviors (Ha et al., 2016; Peter et al., 2016; Kim et al., 2018; Lee et al., 2018) [but not in Lee et al. (2015); Pappas et al. (2017); and Kim et al. (2018)].

In this study, we aimed at modulating the behavioral phenotype of the *Shank2*$^{\Delta ex16-/-}$ [hereafter *Shank2* (MGI: 5435698; Schmeisser et al., 2012)] mice using pharmacological treatment or social isolation. For the pharmacological treatment, we used methylphenidate (commercially available for medical use under the name Ritalin®), a treatment for individuals diagnosed with attention-deficit/hyperactivity disorder (ADHD) (Stepanova et al., 2017). To test for social interest, we modulated the motivation to interact with another mouse by including a period of social isolation prior to the social interaction test. Finally, a review of the existing protocols for social recognition in mice (see **Supplementary Material** – Review of social recognition protocols) highlighted that the habituation-dishabituation protocol was ethologically relevant. We adapted this protocol by testing simultaneously the mutant mouse and the wild-type mouse to control rigorously the investigation of social recognition in *Shank2* mutant mice.

MATERIALS AND METHODS

Modulation Through Pharmacological Treatment

We tested males (placebo: 10 *Shank2*$^{+/+}$, 10 *Shank2*$^{+/-}$, 10 *Shank2*$^{-/-}$; treatment: 10 *Shank2*$^{+/+}$, 10 *Shank2*$^{+/-}$, and 10 *Shank2*$^{-/-}$) and females (placebo: 9 *Shank2*$^{+/+}$, 10 *Shank2*$^{+/-}$, 10 *Shank2*$^{-/-}$; treatment: 9 *Shank2*$^{+/+}$, 10 *Shank2*$^{+/-}$, 10 *Shank2*$^{-/-}$) aged of 4–6 months. Female mice were housed in groups of 2–4 per cage, while males were single-housed because of high aggressiveness. *Shank2* mutant mice were initially described in Schmeisser et al. (2012), backcrossed for more than 10 generations on C57Bl/6J. We injected the animals with methylphenidate (MPH; 30 mg/kg; intra-peritoneal injection) or saline solution, 1 h before the test. Whether mice received saline or MPH was randomly chosen before starting the experiment. We tested the animals in the openfield. One hour after the injection, the animals were left to freely explore a round openfield (1 m of diameter) for 30 min (100 lux). We measured the distance traveled and compared it between wild-type, *Shank2*$^{+/-}$ and *Shank2*$^{-/-}$ mice treated with either saline solution or methylphenidate using non-parametric Wilcoxon-Mann-Whitney U-tests given the small sample size and the non-normal distribution of the data.

Modulation Through Social Isolation

We tested 16 *Shank2*$^{+/+}$ and 13 *Shank2*$^{-/-}$ adult females of 4–6 months of age (Schmeisser et al., 2012). We did not use *Shank2*$^{+/-}$ mice in the remaining parts of the paper, given the subtlety of social defects in this genotype (Schmeisser et al., 2012). *Shank2*$^{+/+}$ and *Shank2*$^{-/-}$ mice were tested twice in the occupant-new comer test (Ferhat et al., 2016). On the first time, they were group-housed (2–4 mice per cage) from weaning on. On the second time 3 weeks later, they were isolated for 3 days before the test; this last data had been presented in the original study (Schmeisser et al., 2012). In the occupant-new comer test, a female mouse (occupant) was placed in a test cage (Plexiglas, 50 cm × 25 cm × 30 cm, 100 lux, with fresh bedding) in a soundproof chamber for 30 min habituation. After this time, an unfamiliar group-housed C57Bl/6J adult female (new comer) was introduced. Social interactions were recorded continuously (high-resolution Sony XCD-SX90CR video camera). Ultrasonic vocalizations were recorded simultaneously with a condenser ultrasound microphone Polaroid/CMPA, the interface UltraSoundGate 416-200 and the software Avisoft-SASLab Pro Recorded from Avisoft Bioacoustics (sampling frequency: 300 kHz; FFT-length: 1024 points; 16-bit format). Ultrasonic vocalizations were recorded for the pair of mice tested (one C57Bl/6J new comer and one from the *Shank2* strain, either a wild-type one or a mutant one) since we cannot distinguish the identity of the caller in such a setting. Nevertheless, previous studies suggested that the contribution of the new comer is minor in comparison with that of the

occupant (Hammerschmidt et al., 2012). We recorded manually the time spent in contact and the latency for the first contact. We also measured manually the latency for the first ultrasonic vocalizations and the total number of ultrasonic vocalizations emitted. We manually established the distribution of ultrasonic vocalizations among the following call types (see Ey et al., 2013):

- "short": call duration was less than 5 ms;
- "simple": call duration was longer than 5 ms and the frequency range was smaller than 6.25 kHz (flat) or call duration was longer than 5 ms and the frequency range was larger than 6.25 kHz and there was only one direction of frequency modulation (upward or downward);
- "complex": frequency modulations in more than one direction and frequency range larger than 6.25 kHz (modulated), or inclusion of one or more additional frequency components (harmonic or non-linear phenomena, but no saturation) but no constraint on frequency range (complex);
- "unstructured": no pure tone component, "noisy" calls;
- "frequency jumps" (fq jumps): presence of one or more jump(s) in frequency, without time gap between the consecutive elements; it can include noisy parts within the pure tone call or not.

We used unpaired non-parametric Wilcoxon tests to compare the latency for the first contact, the total time spent in contact, the latency for the first call and the call rate between genotypes within the social condition (either grouped or isolated). We used paired non-parametric Wilcoxon tests to compare the latency for the first contact, the total time spent in contact, the latency for the first call and the call rate between social conditions (grouped or isolated) within genotypes. We used Chi-squared (with a Bonferroni correction for multiple testing) tests to compare the proportions of calls within and between social conditions or genotypes.

New Protocol for Social Recognition

We set up a new habituation-dishabituation test. After carefully reviewing the different protocols available to test social recognition, we found three protocols using free social interactions: two-trial social recognition, social discrimination, habituation-dishabituation (see **Supplementary Material** – Review of social recognition protocols). We adapted the habituation-dishabituation protocol by testing a pair of female mice (one *Shank2*$^{+/+}$ mouse and one *Shank2*$^{-/-}$ mouse) with a juvenile C57Bl/6J female mouse as the stimulus mouse. By testing paired mice, we collected data from the mutant and its control mouse in exactly the same conditions. We tested 12 pairs of one *Shank2*$^{+/+}$ adult female and one *Shank2*$^{-/-}$ adult female (6 months of age), paired together at least 1 week before testing. Juvenile females were housed in groups of four upon arrival at the animal facility (3 weeks of age) and until the end of the experiment. Mice were identified through RFID chips implanted under isoflurane anesthesia and after local sub-cutaneous injection of lidocaine (at 4 weeks of age for the juveniles and at weaning for the tested mice). On the day of testing, mice were habituated to the testing room 20 min before the test. We then introduced the pair of *Shank2* mice in a test cage (50 cm × 50 cm × 30 cm, fresh bedding). The pair of mice was left to explore freely the test cage for 20 min. After this habituation time, we introduced an unknown C57Bl/6J juvenile female mouse (5 weeks of age) and let the mice freely interact for 2 min. After this first encounter, we took out of the cage the juvenile mouse and left it alone in a housing cage for 5 min. We then re-introduced it in the cage for 2 min. We repeated these steps for four encounters with the same juvenile. On the fifth encounter, we introduced another unknown C57Bl/6J juvenile female mouse (5 weeks of age) from another housing cage. During each encounter, a tracking system, Live Mouse Tracker, allowed to individually follow each of the three mice and to automatically extract the time spent in contact with the juvenile for each tested mouse (de Chaumont et al., 2018). We used unpaired non-parametric Wilcoxon tests to compare the total time spent in contact.

We used paired non-parametric Wilcoxon tests to compare the total time spent in contact between *Shank2*$^{+/+}$ and *Shank2*$^{-/-}$ mice (within each pair) for each juvenile encounter. We used paired non-parametric Wilcoxon tests to compare the total time spent in contact within each genotype between the fourth encounter and the fifth one.

Ethic Approval Statement

All experiments involving animals complied with the European ethical regulation, and were validated by the ethical committee CETEA n°89, Institut Pasteur, Paris. These procedures were realized within the project APAFIS#7706-20 161 12317252460 v2.

RESULTS

The Effects of Methylphenidate on Hyperactivity in *Shank2* Mutant Mice

Shank2$^{-/-}$ mice are highly hyperactive in comparison with their wild-type littermates (Schmeisser et al., 2012). Here, we injected adult males and females with methylphenidate (MPH) or saline solution, 1 h before the openfield test. The saline-injected *Shank2*$^{-/-}$ mice traveled significantly longer distances in comparison with saline-injected *Shank2*$^{+/+}$ mice (males: $W = 0$, $p < 0.001$; females: $W = 10.5$, $p = 0.005$) and *Shank2*$^{+/-}$ mice (males: $W = 7$, $p < 0.001$; females: $W = 0$, $p < 0.001$; **Figure 1**). In addition, *Shank2*$^{+/-}$ mice also displayed hyperactivity but to a lower extend in comparison with their wild-type littermates (males: $W = 21.5$, $p = 0.034$; females: $W = 0$, $p < 0.001$). These results confirmed the initially described gene dosage-related hyperactivity in this model (Schmeisser et al., 2012). MPH treatment increased significantly the distance traveled by *Shank2*$^{+/+}$ mice (males: $W = 10$, $p = 0.003$; females: $W = 4.5$, $p = 0.002$) and by *Shank2*$^{+/-}$ mice (males: $W = 10$, $p = 0.002$; females: $W = 5$, $p < 0.001$) in comparison with saline-injected mice of the same genotypes in both sexes. The MPH treatment also increased significantly the distance traveled by *Shank2*$^{-/-}$ female mice in comparison with saline-injected *Shank2*$^{-/-}$ female mice

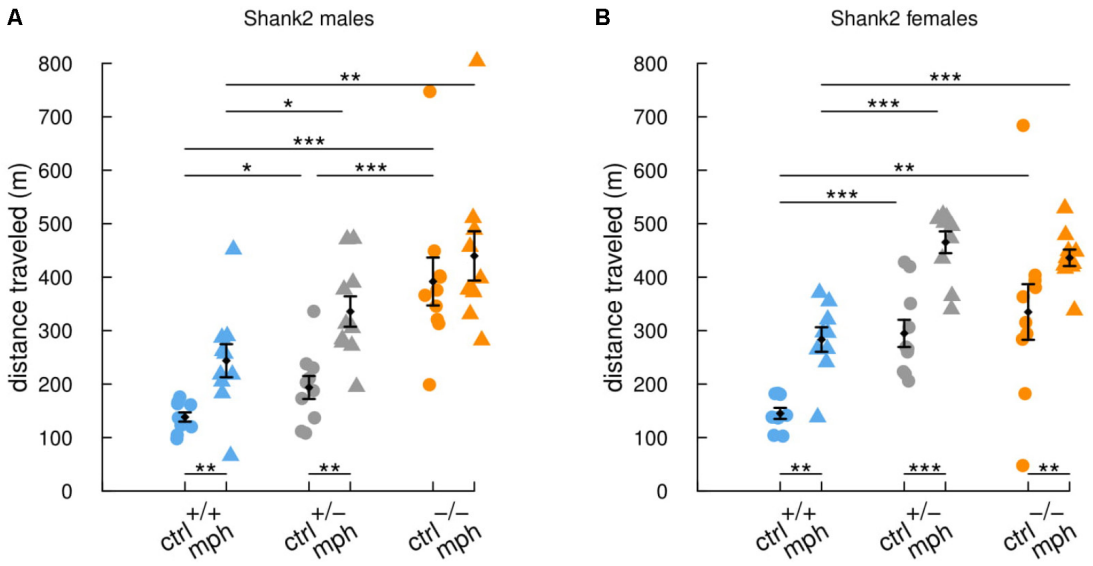

FIGURE 1 | Similar enhancement of activity by methylphenidate treatment in *Shank2* wild-type and mutant mice. Distance traveled in 30-min free exploration of an openfield in **(A)** male and in **(B)** female *Shank2*$^{+/+}$ (blue), *Shank2*$^{+/-}$ (gray) and *Shank2*$^{-/-}$ (orange) mice after methylphenidate treatment (MPH, 30 mg/kg) or after saline injection 1 h before the test. Data are presented as mean ± SEM, with individual points. Uncorrected non-parametric Wilcoxon tests were used (*$p < 0.05$, **$p < 0.01$, ***$p < 0.001$).

($W = 14$, $p = 0.005$; **Figure 1B**). The difference in *Shank2*$^{-/-}$ male mice in comparison with saline-injected *Shank2*$^{-/-}$ males was not significant ($W = 36$, $p = 0.307$; **Figure 1A**), but the hyperactivity was already very high and we might have a saturation effect. In both sexes, MPH-injected *Shank2*$^{-/-}$ mice still traveled significantly longer distances in comparison with MPH-injected *Shank2*$^{+/+}$ mice (males: $W = 8$, $p = 0.002$; females: $W = 2$, $p < 0.001$).

Overall, *Shank2*$^{-/-}$, *Shank2*$^{+/-}$, and *Shank2*$^{+/+}$ mice reacted similarly to the injection of MPH, with an increase in their locomotor activity. MPH was therefore not efficient to rescue hyperactivity in this model.

The Effects of Social Isolation on Social Behavior in *Shank2* Mutant Mice

Many mouse models of autism display only subtle abnormalities in classical behavioral tests for social interest (reviewed in Ferhat et al., 2017). One hypothesis is that the main social problem might reside in the social reward system, which can impair behavioral flexibility [see for instance the lack of social modulation of ultrasonic vocalizations in *Shank1* mutant mice (Wöhr et al., 2011)].

In this study, we therefore compared social interactions and ultrasonic vocalizations in the occupant-new comer test between group-housed and isolated adult female mice from the *Shank2* mutant strain. When females were group-housed, there were no significant differences between *Shank2*$^{+/+}$ mice and *Shank2*$^{-/-}$ mice in the latency for the first contact ($W = 120.5$, $p = 0.482$; **Figure 2A**), in the time spent in contact ($W = 98.5$, $p = 0.826$; **Figure 2B**), in the latency for the first call ($W = 95$, $p = 0.714$; **Figure 2C**), and in the vocal repertoire used (**Figures 3A,B**). The only difference was found in the number of vocalizations emitted, with less vocalizations emitted by *Shank2*$^{-/-}$ mice in comparison with wild-type mice ($W = 150$, $p = 0.046$; **Figure 2D**).

When females were isolated for 3 days, *Shank2*$^{-/-}$ mice spent significantly shorter time in contact with the new comer ($W = 165$, $p = 0.008$; **Figure 2B**) and emitted less ultrasonic vocalizations in comparison with *Shank2*$^{+/+}$ mice ($W = 171$, $p = 0.003$; **Figure 2D**). Interestingly, when considering the ultrasonic vocalization repertoire used, *Shank2*$^{-/-}$ mice emitted significantly more calls from the short and unstructured categories than *Shank2*$^{+/+}$ mice in the isolated condition (**Figures 3A,B**). In contrast, the duration of the calls for each call type did not differ significantly between social conditions or between genotypes (**Figures 3C,D**).

Overall, significant differences in social interaction and communication emerged between *Shank2*$^{-/-}$ and *Shank2*$^{+/+}$ mice only after social isolation, and not when animals were group-housed. These results suggested that *Shank2*$^{-/-}$ mice were impaired in their modulation of social motivation.

Social Recognition in a Social Context in *Shank2* Mutant Mice

In their initial characterization, *Shank2*$^{-/-}$ female mice displayed impairments in social recognition in the three-chambered test, with no significant preference for an unknown conspecific in comparison with a familiar conspecific (Schmeisser et al., 2012; Peter et al., 2016). However, in other studies using the *Shank2*$^{\Delta ex15-16}$ mice, social recognition in the three-chambered test did not differ significantly between homozygous mutant and wild-type (Won et al., 2012; Lee et al., 2015; Kim et al., 2018). In

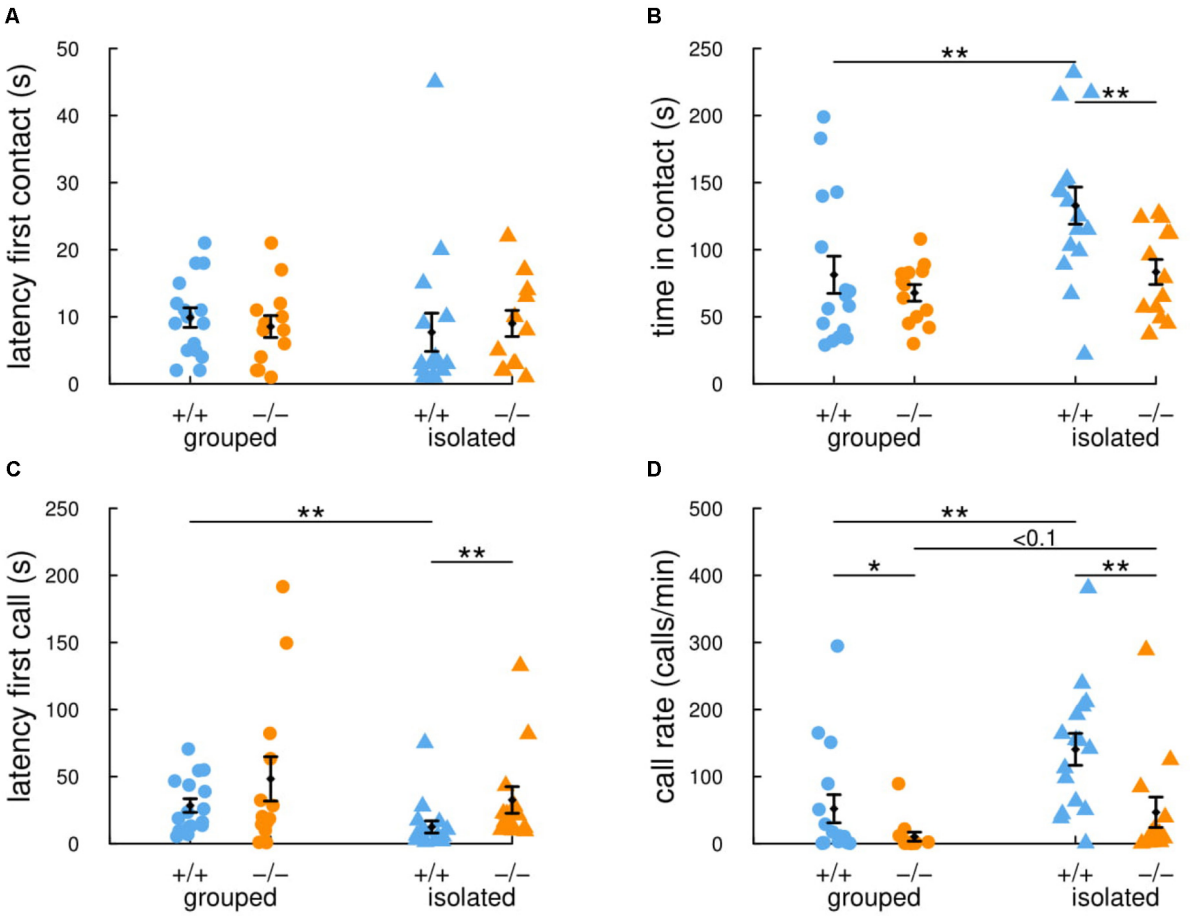

FIGURE 2 | Previous social isolation modulates social communication in wild-type female mice but not in *Shank2* mutant female mice. In the 4-min (i.e., 240 s) occupant-new comer test, the latency to establish the first contact **(A)**, the total time spent in contact **(B)**, the latency to emit the first ultrasonic vocalization **(C)** and the number of calls per minute **(D)** were measured in group-housed mice and in mice isolated for 3 days before testing. Data are presented as mean ± SEM, with individual points. Uncorrected non-parametric Wilcoxon tests were used (*$p < 0.05$, **$p < 0.01$, ***$p < 0.001$).

the present study, we aimed at testing whether social recognition was impaired when mice were freely interacting. We established a habituation-dishabituation test with a pair of adult female mice (one *Shank2*$^{+/+}$ mouse and one *Shank2*$^{-/-}$ mouse, familiar to each other for at least 1 week before the test) interacting repeatedly with a C57Bl/6J juvenile female. After four encounters with the same juvenile, the pair of mice encountered an unknown juvenile on the fifth encounter.

The social recognition protocol appeared to be valid. Indeed, the time that *Shank2*$^{+/+}$ mice spent in contact with the juvenile decreased over the four successive expositions to the same juvenile (**Figure 4**, blue line and dots). Then, they spent a significantly increased time in contact with the second juvenile presented for the fifth encounter ($W = 1$, $p = 0.002$), suggesting that they were able to discriminate their juvenile conspecifics. *Shank2*$^{-/-}$ mice followed a parallel profile despite the fact that they tended to spend shorter time in contact with the juveniles in comparison with their wild-type littermates (encounter 2: $W = 65$, $p = 0.042$; encounter 3: $W = 66$, $p = 0.034$; encounter 5: $W = 65$, $p = 0.042$; **Figure 4**, orange line and dots). As in *Shank2*$^{+/+}$ mice, the time that *Shank2*$^{-/-}$ mice spent in contact with the juvenile between the fourth and the fifth encounters also increased significantly ($W = 0$, $p < 0.001$).

Overall, the *Shank2*$^{-/-}$ mice spent shorter time in contact with the juvenile in comparison with wild-type mice but remained able to differentiate two individuals.

DISCUSSION

Methylphenidate Does Not Rescue the Hyperactivity of the Adult *Shank2*$^{-/-}$ Mice

The psychostimulant methylphenidate inhibits the reuptake of dopamine and norepinephrine (increase of dopamine and norepinephrine extracellular levels) (de la Peña et al., 2018). It is known to be an effective treatment for a subset of patients diagnosed with hyperactivity in humans (reviewed in Stepanova et al., 2017). It appeared to improve inattention, distractibility,

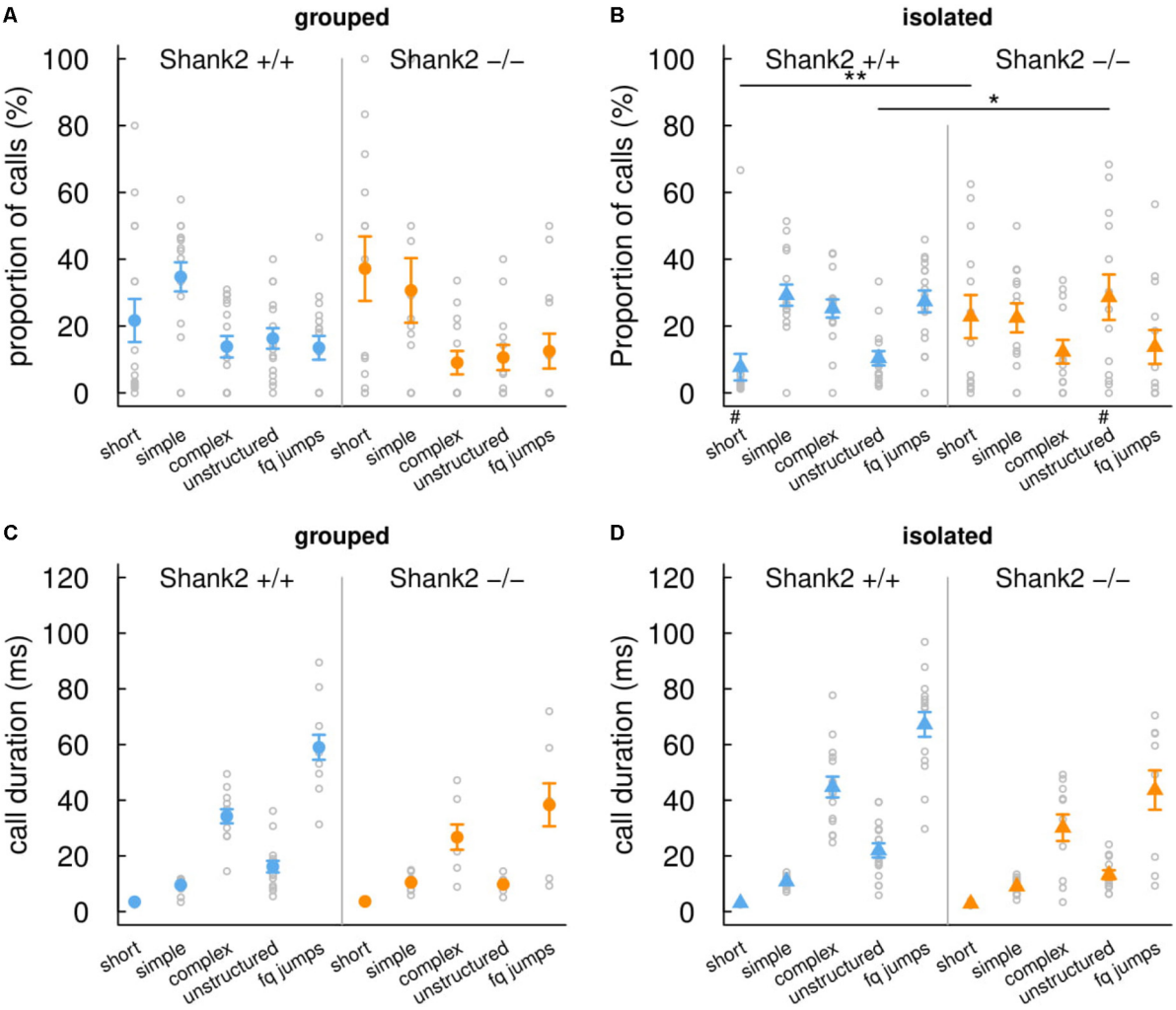

FIGURE 3 | Effects of social isolation on the repertoire and duration of ultrasonic vocalizations emitted by *Shank2* females. Distribution of ultrasonic vocalizations among the five call types recorded during same-sex social interactions (4 min, i.e., 240 s) in group-housed females **(A)** and in females isolated for 3 days **(B)**. Mean duration of the five call types recorded during same-sex social interactions in group-housed females **(C)** and in females isolated for 3 days **(D)**. Data are presented as mean ± SEM, with individual points. Uncorrected Chi-squared tests were used to compare the proportion of each call type between pairs involving one wild-type and pairs involving one *Shank2* mutant mice within a social condition (*$p < 0.05$, **$p < 0.01$) or between social condition (either grouped or isolated) within one genotype ($^{\#}p < 0.05$).

hyperactivity and impulsivity more efficiently than placebo in patients with autism or neurodevelopmental disorders (Quintana et al., 1995; Handen et al., 2000; Research Units on Pediatric Psychopharmacology Autism Network, 2005; Kim et al., 2017). For instance, in a large study conducted by the Research Units on Pediatric Psychopharmacology Autism Network, about half of the patients with autism or neurodevelopmental disorders and hyperactivity responded to methylphenidate treatment (Research Units on Pediatric Psychopharmacology Autism Network, 2005). Nevertheless, methylphenidate appeared to be less efficient and to present more adverse effects (e.g., social withdrawal) in patients with autism than in children developing typical ADHD (Research Units on Pediatric Psychopharmacology Autism Network, 2005; Stepanova et al., 2017). Methylphenidate also tended to increase social withdrawal in patients with ADHD (Research Units on Pediatric Psychopharmacology Autism Network, 2005).

In mice, methylphenidate is used to test the predictive validity of mouse models for ADHD, since it can rescue the hyperactivity of several of these mouse models (de la Peña et al., 2018). In mouse models of autism, methylphenidate did not rescue hyperactivity in *Fmr1*$^{-/-}$ mice (Wrenn et al., 2015). In the first part of the present study, we highlighted that an injection of methylphenidate increased the activity of *Shank2*$^{+/+}$ mice, as expected in wild-type mice, but also increased the activity of *Shank2*$^{+/-}$ and *Shank2*$^{-/-}$ mice. These results show that the hyperactivity of *Shank2*$^{-/-}$ adult mice is not attenuated by methylphenidate, and therefore might not be related to "ADHD-like hyperactivity." Our results are consistent with those from Pappas et al. (2017) who also observed an

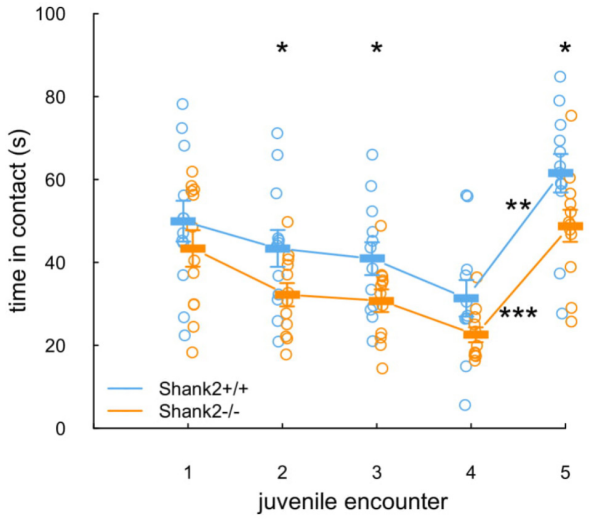

FIGURE 4 | Unaffected social recognition in *Shank2* female mice. In the five repeated exposures (2 min, i.e., 120 s; inter-trial interval: 1 min, i.e., 60 s) of a pair of one *Shank2*$^{+/+}$ mouse and one *Shank2*$^{-/-}$ mouse to an unknown juvenile, the time spent in contact with the juvenile was measured for each tested mouse. The juvenile introduced was the same in encounters one to four; on encounter five, a new juvenile was introduced. Data are presented as mean ± SEM, with individual points. Uncorrected non-parametric paired Wilcoxon tests were used (*$p < 0.05$, **$p < 0.01$, ***$p < 0.001$).

increased hyperactivity in *Shank2*$^{\Delta ex24}$ mutant mice treated with amphetamine (2 mg/kg), while this hyperactivity was rescued by the mood stabilizers valproic acid or lithium (Pappas et al., 2017). These results suggest that the hyperactive phenotype in *Shank2* mutant mice could therefore be reminiscent of the manic-like phenotype of a mouse model for bipolar disorder. To further investigate this parallel with manic-like behavior, future studies on *Shank2* mouse models should include analyses on sleep-wake cycles, impulsivity and preference for reward stimuli (Beyer and Freund, 2017). Investigating the dopaminergic pathway in this model might also provide information on the relatedness of the phenotype of *Shank2* mice with a manic-like phenotype. With preliminary data in an eight-arm radial maze for spatial learning, we already noticed an increased arousal of *Shank2*$^{-/-}$ mice when seeking for the sweet reward in comparison with their wild-type littermates (unpublished data), suggesting an atypical reward seeking behavior. In parallel, clioquinol, a zinc chelator and a ionophore mobilizing trans-synaptic zinc has been shown to rescue the reduced social interest in the three-chambered test in mouse models of autism, but could not rescue the hyperactivity observed in the *Shank2*$^{\Delta ex15-16}$ model (Lee et al., 2015).

Prior Isolation Increases Social Motivation for Conspecific, but Not in the *Shank2*$^{-/-}$ Mice

A reduction of social interactions might originate from abnormalities in the neuronal circuits involved in social reward. The strength of social interactions might then be modulated by the motivation of the individual to interact with peers. We aimed at testing whether mice lacking *Shank2* have the ability to modulate their interest in social interactions. We therefore manipulated their motivation to interact by housing them in groups or isolated.

While wild-type *Shank2*$^{+/+}$ mice housed in isolation increased their social motivation with more time spent in contact and higher call rate compared to the group-housed condition, *Shank2*$^{-/-}$ mutant mice behaved similarly, no matter whether in the isolated or group-housed conditions. Their level of behavioral flexibility in the social domain appeared to be lower in comparison with wild-type mice. Unfortunately, this mouse model has never been tested in a reversal learning task, to assess its cognitive flexibility. Other *Shank2* mouse models were tested for learning and memory but not in a reversal learning task, except the conditional, parvalbumin cell-type specific *Shank2*$^{\Delta ex15-16}$ knock-out mice that displayed typical learning and reversal learning in the Morris water maze task (Lee et al., 2018). Therefore, the cognitive flexibility of *Shank2* mutant mice remains to be further documented to understand whether the present lack of social flexibility is related to a reduced cognitive flexibility.

We could also hypothesize that *Shank2*$^{-/-}$ mice might consider social interactions as more aversive and therefore less rewarding than wild-type *Shank2*$^{+/+}$ mice do. Indeed, our previous work showed that *Shank2*$^{-/-}$ mice emit ultrasonic vocalizations with lower peak frequency in comparison with wild-type littermates (Ey et al., 2013). Interestingly, ultrasonic vocalizations emitted by adult males usually displayed a lower peak frequency in an aversive context (contention stress) than in affiliative social interactions (Chabout et al., 2012). Further experiments will focus on the modulation of the spontaneous home cage behavior between *Shank2*$^{-/-}$ and *Shank2*$^{+/+}$ mice to gather robust data on a more complete behavioral repertoire. Long-term group studies are now possible using a newly developed tracking system, Live Mouse Tracker (de Chaumont et al., 2018). The first experiments with mixed-genotype groups suggest that *Shank2*$^{-/-}$ female mice and their wild-type littermates differ in their involvement in complex social configurations (de Chaumont et al., 2018).

This reduced social reward could be in line with the hypothesis reviewed by Chevallier et al. (2012), in which social deficits in autism might come from social motivation deficits and therefore trigger social cognition deficits, and not the reverse. However, such an approach is still under discussion since evidences are mixed (reviewed in Bottini, 2018).

Shank2$^{-/-}$ Mice Are Able to Integrate Social Cues for Recognition of Conspecific

The three-chamber test provides a binary way to measure the preference for social novelty versus social familiarity: it is a yes/no test (Crawley, 2004). It does not permit to disentangle whether the animal has a reduced motivation for (i.e., is not interested in) social novelty or whether it cannot distinguish the two different mice presented. The paradigm presented here tried to distinguish these two possibilities.

We showed that *Shank2*$^{-/-}$ mice might be less motivated to interact with an unknown conspecific since they tend to spend shorter time in contact with the juvenile in comparison with their wild-type littermates. Nevertheless, they did not display social recognition impairments in this protocol: they still manage to gather information about the identity of the conspecific. *Shank2*$^{-/-}$ mice therefore are able to differentiate individuals from one another, i.e., to perceive and analyze social cues.

This is reminiscent of a series of experiments conducted in patients with autism. During social scene observation, toddlers with autism are less focused on eyes in comparison with neurotypical toddlers (Constantino et al., 2017), but they can be faster at identifying facial information compared with typically developed individuals (Gharib et al., 2015).

Whether the behavior of the *Shank2*$^{-/-}$ mouse is influenced by the behavior of its paired wild-type conspecific is unknown. If there were an influence of the behavior of the *Shank2*$^{+/+}$ mouse on the *Shank2*$^{-/-}$ mouse, this would mean that *Shank2*$^{-/-}$ mice have the ability to socially imitate its paired conspecific, which depicts some interesting social competencies. If *Shank2*$^{-/-}$ mice behave totally independently from the paired *Shank2*$^{+/+}$ mice, this would mean that *Shank2*$^{-/-}$ mice own social recognition ability. To disentangle these two possibilities, it would be interesting to try this protocol of social recognition with different types of pairings (*Shank2*$^{-/-}$ vs. *Shank2*$^{-/-}$, *Shank2*$^{-/-}$ vs. *Shank2*$^{+/+}$, and *Shank2*$^{+/+}$ vs. *Shank2*$^{+/+}$) and also with isolated mice.

CONCLUSION

To summarize, the present study gathers new pieces of information on specific aspects of the behavior of the *Shank2*$^{-/-}$ mice. It shows that the hyperactivity displayed by this model cannot be reduced by methylphenidate. It also highlights that the social deficits displayed by this model might stem from a lack of flexibility in the social motivation. Finally, it provides more details on the social recognition deficits, which were not visible during direct social interactions with a conspecific, i.e., when the tested mice had access to all identity cues of the conspecifics. Interestingly, the reduced social interaction displayed by *Shank2*$^{-/-}$ mice might therefore be misinterpreted as a problem in social cognition. We propose an alternative hypothesis that *Shank2*$^{-/-}$ mice have high capacity to integrate social cues, but once these social cues are integrated, the mice display less social motivation to interact. Such information could be used to orient therapeutic strategies and to design more specific behavioral tests to characterize mouse models of autism.

DATA AVAILABILITY STATEMENT

The raw data supporting the conclusion of the manuscript will be made available by the authors, without undue reservation, to any qualified researcher.

AUTHOR CONTRIBUTIONS

EE, NT, A-TF, and JL-S performed and analyzed the experiments. A-MLS performed the genotyping of the mice. FdC created the tracking system for the social recognition experiments. TMB generated the mouse model. EE and TB conceived the project and wrote the manuscript.

FUNDING

This work was partially funded by the Institut Pasteur, the Bettencourt-Schueller Foundation, the Fondation de France, the Orange Foundation, the Centre National de la Recherche Scientifique, the University Paris Diderot, and the BioPsy LabEX. The research leading to these results has also received support from the Innovative Medicines Initiative Joint Undertaking under grant agreement no. 115300, resources of which are composed of financial contribution from the European Union's Seventh Framework Program (FP7/2007-2013) and EFPIA companies' in kind contribution. The funders had no role in study design, data collection and analysis, decision to publish, or preparation of the manuscript.

ACKNOWLEDGMENTS

We thank the reviewers for helpful comments that improved the manuscript.

SUPPLEMENTARY MATERIAL

The Supplementary Material for this article can be found online at: https://www.frontiersin.org/articles/10.3389/fnmol.2018.00365/full#supplementary-material

REFERENCES

Abrahams, B. S., Arking, D. E., Campbell, D. B., Mefford, H. C., Morrow, E. M., Weiss, L. A., et al. (2013). SFARI Gene 2.0: a community-driven knowledgebase for the autism spectrum disorders (ASDs). *Mol. Autism* 4:36. doi: 10.1186/2040-2392-4-36

American Psychiatric Association (2013). *Diagnostic and Statistical Manual of Mental Disorders, Fifth Edition (DSM-V)*. Washington, DC: American Psychiatric Association. doi: 10.1176/appi.books.9780890425596

Beyer, D. K. E., and Freund, N. (2017). Animal models for bipolar disorder: from bedside to the cage. *Int. J. Bipolar Disord.* 5:35. doi: 10.1186/s40345-017-0104-6

Bottini, S. (2018). Social reward processing in individuals with autism spectrum disorder: a systematic review of the social motivation hypothesis. *Res. Autism Spectr. Disord.* 45, 9–26. doi: 10.1016/j.rasd.2017.10.001

Chabout, J., Serreau, P., Ey, E., Bellier, L., Aubin, T., Bourgeron, T., et al. (2012). Adult male mice emit context-specific ultrasonic vocalizations that are modulated by prior isolation or group rearing environment. *PLoS One* 7:e29401. doi: 10.1371/journal.pone.0029401

Chevallier, C., Kohls, G., Troiani, V., Brodkin, E. S., and Schultz, R. T. (2012). The social motivation theory of autism. *Trends Cogn. Sci.* 16, 231–239. doi: 10.1016/j.tics.2012.02.007

Constantino, J. N., Kennon-McGill, S., Weichselbaum, C., Marrus, N., Haider, A., Glowinski, A. L., et al. (2017). Infant viewing of social scenes is under genetic control and is atypical in autism. *Nature* 547, 340–344. doi: 10.1038/nature22999

Crawley, J. N. (2004). Designing mouse behavioral tasks relevant to autistic-like behaviors. *Ment. Retard. Dev. Disabil. Res. Rev.* 10, 248–258. doi: 10.1002/mrdd.20039

de Chaumont, F., Ey, E., Torquet, N., Lagache, T., Dallongeville, S., Imbert, A., et al. (2018). Live mouse tracker: real-time behavioral analysis of groups of mice. *bioRxiv* [Pre print]. doi: 10.1101/345132

de la Peña, J. B., dela Peña, I. J., Custodio, R. J., Botanas, C. J., Kim, H. J., and Cheong, J. H. (2018). Exploring the validity of proposed transgenic animal models of attention-deficit hyperactivity disorder (ADHD). *Mol. Neurobiol.* 55, 3739–3754. doi: 10.1007/s12035-017-0608-1

Eltokhi, A., Rappold, G., and Sprengel, R. (2018). Distinct phenotypes of *shank2* mouse models reflect neuropsychiatric spectrum disorders of human patients with *shank2* variants. *Front. Mol. Neurosci.* 11:240. doi: 10.3389/fnmol.2018.00240

Ey, E., Torquet, N., Le Sourd, A.-M., Leblond, C. S., Boeckers, T. M., Faure, P., et al. (2013). The Autism *ProSAP1/Shank2* mouse model displays quantitative and structural abnormalities in ultrasonic vocalisations. *Behav. Brain Res.* 256, 677–689. doi: 10.1016/j.bbr.2013.08.031

Ferhat, A.-T., Halbedl, S., Schmeisser, M. J., Kas, M. J., Bourgeron, T., and Ey, E. (2017). Behavioural phenotypes and neural circuit dysfunctions in mouse models of autism spectrum disorder. *Adv. Anat. Embryol. Cell Biol.* 224, 85–101. doi: 10.1007/978-3-319-52498-6-5

Ferhat, A.-T., Torquet, N., Le Sourd, A.-M., de Chaumont, F., Olivo-Marin, J.-C., Faure, P., et al. (2016). Recording mouse ultrasonic vocalizations to evaluate social communication. *J. Vis. Exp.* 112:53871. doi: 10.3791/53871

Gharib, A., Mier, D., Adolphs, R., and Shimojo, S. (2015). Eyetracking of social preference choices reveals normal but faster processing in autism. *Neuropsychologia* 72, 70–79. doi: 10.1016/j.neuropsychologia.2015.04.027

Ha, S., Lee, D., Cho, Y. S., Chung, C., Yoo, Y.-E., Kim, J., et al. (2016). Cerebellar *shank2* regulates excitatory synapse density, motor coordination, and specific repetitive and anxiety-like behaviors. *J. Neurosci.* 36, 12129–12143. doi: 10.1523/JNEUROSCI.1849-16.2016

Hammerschmidt, K., Radyushkin, K., Ehrenreich, H., and Fischer, J. (2012). The Structure and usage of female and male mouse ultrasonic vocalizations reveal only minor differences. *PLoS One* 7:e41133. doi: 10.1371/journal.pone.0041133

Handen, B. L., Johnson, C. R., and Lubetsky, M. (2000). Efficacy of methylphenidate among children with autism and symptoms of attention-deficit hyperactivity disorder. *J. Autism Dev. Disord.* 30, 245–255. doi: 10.1023/A:1005548619694

Kim, R., Kim, J., Chung, C., Ha, S., Lee, S., Lee, E., et al. (2018). Cell-type-specific *shank2* deletion in mice leads to differential synaptic and behavioral phenotypes. *J. Neurosci.* 38, 4076–4092. doi: 10.1523/JNEUROSCI.2684-17.2018

Kim, S.-J., Shonka, S., French, W. P., Strickland, J., Miller, L., and Stein, M. A. (2017). Dose-response effects of long-acting liquid methylphenidate in children with Attention Deficit/Hyperactivity Disorder (ADHD) and Autism Spectrum Disorder (ASD): a pilot study. *J. Autism Dev. Disord.* 47, 2307–2313. doi: 10.1007/s10803-017-3125-1

Leblond, C. S., Nava, C., Polge, A., Gauthier, J., Huguet, G., Lumbroso, S., et al. (2014). Meta-analysis of shank mutations in autism spectrum disorders: a gradient of severity in cognitive impairments. *PLoS Genet.* 10:e1004580. doi: 10.1371/journal.pgen.1004580

Lee, E.-J., Lee, H., Huang, T.-N., Chung, C., Shin, W., Kim, K., et al. (2015). Trans-synaptic zinc mobilization improves social interaction in two mouse models of autism through NMDAR activation. *Nat. Commun.* 6:7168. doi: 10.1038/ncomms8168

Lee, S., Lee, E., Kim, R., Kim, J., Lee, S., Park, H., et al. (2018). *Shank2* deletion in parvalbumin neurons leads to moderate hyperactivity, enhanced self-grooming and suppressed seizure susceptibility in mice. *Front. Mol. Neurosci.* 11:209. doi: 10.3389/fnmol.2018.00209

Lim, C.-S., Kim, H., Yu, N.-K., Kang, S. J., Kim, T., Ko, H.-G., et al. (2016). Enhancing inhibitory synaptic function reverses spatial memory deficits in *shank2* mutant mice. *Neuropharmacology* 112(Pt A), 104–112. doi: 10.1016/j.neuropharm.2016.08.016

Pappas, A. L., Bey, A. L., Wang, X., Rossi, M., Kim, Y. H., Yan, H., et al. (2017). Deficiency of *Shank2* causes mania-like behavior that responds to mood stabilizers. *JCI Insight* 2:92052. doi: 10.1172/jci.insight.92052

Peter, S., ten Brinke, M. M., Stedehouder, J., Reinelt, C. M., Wu, B., Zhou, H., et al. (2016). Dysfunctional cerebellar Purkinje cells contribute to autism-like behaviour in *Shank2*-deficient mice. *Nat. Commun.* 7:12627. doi: 10.1038/ncomms12627

Quintana, H., Birmaher, B., Stedge, D., Lennon, S., Freed, J., Bridge, J., et al. (1995). Use of methylphenidate in the treatment of children with autistic disorder. *J. Autism Dev. Disord.* 25, 283–294. doi: 10.1007/BF02179289

Research Units on Pediatric Psychopharmacology Autism Network. (2005). Randomized, controlled, crossover trial of methylphenidate in pervasive developmental disorders with hyperactivity. *Arch. Gen. Psychiatry* 62, 1266–1274. doi: 10.1001/archpsyc.62.11.1266

Schmeisser, M. J., Ey, E., Wegener, S., Bockmann, J., Stempel, A. V., Kuebler, A., et al. (2012). Autistic-like behaviours and hyperactivity in mice lacking ProSAP1/Shank2. *Nature* 486, 256–260. doi: 10.1038/nature11015

Stepanova, E., Dowling, S., Phelps, M., and Findling, R. L. (2017). Pharmacotherapy of emotional and behavioral symptoms associated with autism spectrum disorder in children and adolescents. *Dialogues Clin. Neurosci.* 19, 395–402.

Wöhr, M., Roullet, F. I., Hung, A. Y., Sheng, M., and Crawley, J. N. (2011). Communication impairments in mice lacking shank1: reduced levels of ultrasonic vocalizations and scent marking behavior. *PLoS One* 6:e20631. doi: 10.1371/journal.pone.0020631

Won, H., Lee, H.-R., Gee, H. Y., Mah, W., Kim, J.-I., Lee, J., et al. (2012). Autistic-like social behaviour in *Shank2*-mutant mice improved by restoring NMDA receptor function. *Nature* 486, 261–265. doi: 10.1038/nature11208

Wrenn, C. C., Heitzer, A. M., Roth, A. K., Nawrocki, L., and Valdovinos, M. G. (2015). Effects of clonidine and methylphenidate on motor activity in Fmr1 knockout mice. *Neurosci. Lett.* 585, 109–113. doi: 10.1016/j.neulet.2014.11.035

Conflict of Interest Statement: The authors declare that the research was conducted in the absence of any commercial or financial relationships that could be construed as a potential conflict of interest.

frontiers in Cellular Neuroscience

ORIGINAL RESEARCH
published: 09 October 2018
doi: 10.3389/fncel.2018.00341

GABA Neuronal Deletion of *Shank3* Exons 14–16 in Mice Suppresses Striatal Excitatory Synaptic Input and Induces Social and Locomotor Abnormalities

*Taesun Yoo[1†], Heejin Cho[1†], Jiseok Lee[2†], Haram Park[1], Ye-Eun Yoo[1], Esther Yang[3], Jin Yong Kim[3], Hyun Kim[3] and Eunjoon Kim[1,2]**

[1]Department of Biological Sciences, Korea Advanced Institute for Science and Technology (KAIST), Daejeon, South Korea, [2]Center for Synaptic Brain Dysfunctions, Institute for Basic Science (IBS), Daejeon, South Korea, [3]Department of Anatomy and Division of Brain Korea 21, Biomedical Science, College of Medicie, Korea University, Seoul, South Korea

Shank3 is an excitatory postsynaptic scaffolding protein implicated in multiple brain disorders, including autism spectrum disorders (ASD) and Phelan-McDermid syndrome (PMS). Although previous neurobiological studies on Shank3 and *Shank3*-mutant mice have revealed diverse roles of Shank3 in the regulation of synaptic, neuronal and brain functions, whether Shank3 expression in specific cell types distinctly contributes to mouse phenotypes remains largely unclear. In the present study, we generated two *Shank3*-mutant mouse lines (exons 14–16) carrying global and GABA neuron-specific deletions and characterized their electrophysiological and behavioral phenotypes. These mouse lines show similar decreases in excitatory synaptic input onto dorsolateral striatal neurons. In addition, the abnormal social and locomotor behaviors observed in global *Shank3*-mutant mice are strongly mimicked by GABA neuron-specific *Shank3*-mutant mice, whereas the repetitive and anxiety-like behaviors are only partially mimicked. These results suggest that GABAergic *Shank3* (exons 14–16) deletion has strong influences on striatal excitatory synaptic transmission and social and locomotor behaviors in mice.

Keywords: autism, Phelan-McDermid syndrome, Shank3, striatum, social interaction, repetitive behavior

OPEN ACCESS

Edited by:
Alessandro Tozzi,
University of Perugia, Italy

Reviewed by:
Maria Passafaro,
Università degli Studi di Milano, Italy
Richard J. Weinberg,
University of North Carolina at Chapel Hill, United States

****Correspondence:***
Eunjoon Kim
kime@kaist.ac.kr

[†]These authors have contributed equally to this work

Received: *01 August 2018*
Accepted: *14 September 2018*
Published: *09 October 2018*

Citation:
Yoo T, Cho H, Lee J, Park H, Yoo Y-E, Yang E, Kim JY, Kim H and Kim E (2018) GABA Neuronal Deletion of Shank3 Exons 14–16 in Mice Suppresses Striatal Excitatory Synaptic Input and Induces Social and Locomotor Abnormalities. Front. Cell. Neurosci. 12:341. doi: 10.3389/fncel.2018.00341

INTRODUCTION

Shank represents a family of postsynaptic scaffolding proteins with three known members: Shank1/ProSAP3, Shank2/ProSAP1 and Shank3/ProSAP2 (Sheng and Kim, 2000; Sheng and Sala, 2001; Boeckers et al., 2002; Sheng and Hoogenraad, 2007; Grabrucker et al., 2011; Sheng and Kim, 2011; Jiang and Ehlers, 2013; Sala et al., 2015; Monteiro and Feng, 2017; Mossa et al., 2017). Shank proteins interact with many other synaptic proteins and are known to regulate excitatory synapse assembly as well as excitatory synaptic transmission and plasticity.

Mutations of *SHANK3* (Boeckers et al., 1999; Lim et al., 1999; Naisbitt et al., 1999; Tu et al., 1999) have been implicated in diverse brain disorders, including autism spectrum disorders (ASD), neurological and psychiatric symptoms of Phelan-McDermid syndrome (PMS), schizophrenia, intellectual disability and mania (Phelan et al., 1993; Bonaglia et al., 2001; Wilson et al., 2003; Durand et al., 2007; Moessner et al., 2007; Gauthier et al., 2010; Bonaglia et al., 2011; Hamdan et al., 2011; Leblond et al., 2012; Boccuto et al., 2013;

Han et al., 2013; Guilmatre et al., 2014; Leblond et al., 2014; Cochoy et al., 2015; De Rubeis et al., 2018).

A number of *Shank3*-mutant mouse lines have been generated and characterized in an effort to understand the *in vivo* functions of Shank3 and identify important mechanisms underlying *Shank3-related* brain disorders (Bozdagi et al., 2010; Peca et al., 2011; Wang et al., 2011; Schmeisser et al., 2012; Yang et al., 2012; Han et al., 2013; Kouser et al., 2013; Lee et al., 2015; Speed et al., 2015; Jaramillo et al., 2016; Mei et al., 2016; Wang et al., 2016; Zhou et al., 2016; Jaramillo et al., 2017; Vicidomini et al., 2017; Bey et al., 2018; Qin et al., 2018).

Given that Shank3 is an important component of excitatory synapses (Boeckers et al., 1999; Lim et al., 1999; Naisbitt et al., 1999; Tu et al., 1999), and that the imbalance of excitation and inhibition (E/I) at synaptic and neuronal levels has been implicated in ASD (Yizhar et al., 2011; Nelson and Valakh, 2015; Lee E. et al., 2017), Shank3 dysfunctions may have significant influences on E/I imbalances associated with ASD. Importantly, however, because *Shank3* is expressed in both excitatory and inhibitory neurons (Han et al., 2013), the consequences of *Shank3* mutations in mixed neuronal populations are not easy to predict and should be assessed by direct cell type-specific *Shank3* deletion *in vivo* for better understanding of related brain regions, cell types, and neural circuits. In further support of the importance of *Shank3* expression in GABAergic neurons, *Shank3* is highly expressed in the striatum (Peca et al., 2011), a brain region enriched with GABAergic neurons and known to be associated with various brain functions as well as neurological and psychiatric disorders (Balleine et al., 2007; Kreitzer and Malenka, 2008; Grueter et al., 2012; Báez-Mendoza and Schultz, 2013). In addition, GABAergic neurons in the striatum have dendritic spines where Shank3 may play important roles in the regulation of spinogenesis and axospinous synapse functions (Harris and Weinberg, 2012; O'Rourke et al., 2012).

To this end, we attempted a GABA neuron-specific deletion of *Shank3* exons 14–16, which encodes the PDZ domain known to interact with many synaptic proteins, including GKAP/SAPAP (Kim and Sheng, 2004; Sheng and Kim, 2011), using the Viaat-Cre mouse line that drives Cre recombinase expression in widespread GABAergic neurons (Chao et al., 2010). The electrophysiological and behavioral phenotypes of these mice were compared with those from mice carrying a global *Shank3* deletion (exons 14–16). We found that GABA neuron-specific *Shank3* deletion induces a strong reduction in excitatory synaptic input onto dorsolateral striatal neurons and abnormal social and locomotor behaviors, while having moderate effects on repetitive and anxiety-like behaviors.

MATERIALS AND METHODS

Animals

Mice carrying a deletion of exons 14–16 of the *Shank3* gene flanked by LoxP sites were designed and generated by Biocytogen. The EGFP+ Neo cassette was eliminated by crossing these mice with *protamine*-Flp mic. EGFP+ Neo cassette-deleted $Shank3^{flox/+}$ mice were crossed with *protamine-Cre* mice, and the resulting mice were then crossed with wild-type (WT) mice to introduce the $Shank3^{\Delta 14-16}$ allele. Experimental $Shank3^{\Delta 14-16}$ global knockout mice were obtained by heterozygous mating ($Shank3^{\Delta 14-16/+} \times Shank3^{\Delta 14-16/+}$). To generate $Shank3^{\Delta 14-16}$ cell type-specific conditional knockout (cKO) mice in which *Shank3* is knocked out in Viaat (vesicular inhibitory amino acid transporter)-expressing GABAergic neurons (*Viaat-Cre;*$Shank3^{fl/fl}$ mice), homozygous $Shank3^{flox/flox}$ female mice were crossed with double-heterozygous *Viaat-Cre;*$Shank3^{flox/+}$ male mice. The control group for the cKO mouse was Cre-negative $Shank3^{flox/flox}$ littermates. *Viaat-Cre*, *protamine-Flp* and *protamine-Cre* mouse lines used in this study were maintained in a C57BL/6J genetic background for more than five generations, a breeding strategy that allowed us to compare all global and *Viaat-Cre* mouse line in the same pure C57BL/6J background. All mice were bred and maintained at the mouse facility of Korea Advanced Institute of Science and Technology (KAIST) according to Animal Research Requirements of KAIST, and all experimental procedures were approved by the Committee of Animal Research at KAIST (KA2016-30). All animals were fed *ad libitum* and housed under the 12 h light/dark cycle (light phase during 1:00 am to 1:00 pm). Polymerase chain reaction (PCR) genotyping of conventional knockout mice was performed using the following primers: for WT allele (276 bp): 5'-GGG TTC CTA TGA CAG CCT CA-3' and 5'-TTC TGC AGG ATA GCC ACC TT-3'; for deletion (del) allele (1,159 bp): 5'-GGG TTC CTA TGA CAG CCT CA-3' and 5'-AGC TCA GCC GTC ATG GAC-3'. Genotypes of *Viaat-Cre;*$Shank3^{fl/fl}$ mice were determined by PCR using the following primers: for floxed (478 bp) or WT allele (276 bp): 5'-GGG TTC CTA TGA CAG CCT CA-3' and 5'-TTC TGC AGG ATA GCC ACC TT-3'; for Viaat-Cre allele (272 bp): 5'-GTG TTG CCG CGC CAT CTG C-3' and 5'-CAC CAT TGC CCC TGT TTC ACT ATC-3'. Only male mice were used for behavioral and electrophysiological experiments. Both male and female were used for biochemical experiments.

Fluorescent *in situ* Hybridization (FISH)

In brief, frozen sections (14 μm thick) were cut coronally through the cortex and striatum formation. Sections were thaw-mounted onto Superfrost Plus Microscope Slides (Fisher Scientific #12-550-15). The sections were fixed in 4% formaldehyde for 10 min, dehydrated in increasing concentrations of ethanol for 5 min, and finally air-dried. Tissues were then pretreated for protease digestion for 10 min at room temperature. Probe hybridization and amplification were performed at 40°C using HybEZ hybridization oven (Advanced Cell Diagnostics, Hayward, CA, USA). The probes used in this study were three synthetic oligonucleotides complementary to the nucleotide (nt) sequence 1488–2346 of Mm-Shank3, nt 62–3113 of Mm-Gad1-C3, nt 552–1506 of Mm-Gad2-C2, nt 464–1415 of Mm-Slc17a7/Vglut1-C2, and nt 1986–2998 of Mm-Slc17a6/Vglut2-C3 (Advanced Cell Diagnostics, Hayward, CA, USA). The labeled probes were conjugated to Alexa Fluor 488, Atto 550, and Atto 647. The sections were hybridized with the labeled probe mixture at 40°C for 2 h per slide. Unbound hybridization probes were removed by washing the sections three times with 1× wash

buffer at room temperature for 2 min. Following steps for signal amplification included incubations at 40°C with Amplifier 1-FL for 30 min, with Amplifier 2-FL for 15 min, with Amplifier 3-FL for 30 min and with Amplifier 4 Alt B-FL for 15 min. Each amplifier solution was removed by washing with 1× wash buffer at room temperature for 2 min. The slides were viewed, analyzed and photographed using TCS SP8 Dichroic/CS (Leica), and the ImageJ program (NIH) was used to analyze the images.

Brain Lysates

Brains from *Shank3*$^{\Delta 14-16}$ mice and their WT littermates (13 weeks; male), and those from *Viaat-Cre;Shank3*$^{fl/fl}$ mice and their WT littermates (12 weeks; female), were extracted and dissected on ice into cortex, thalamus, striatum and hippocampus, followed by homogenization with ice-cold homogenization buffer (0.32 M sucrose, 10 mM HEPES, pH 7.4, 2 mM EDTA, pH 8.0, 2 mM EGTA, pH8.0, protease inhibitors, phosphatase inhibitors). Total lysates were prepared by boiling with β-mercaptoethanol directly after homogenization.

Western Blot

Total brain lysates separated in electrophoresis and transferred to a nitrocellulose membrane were incubated with primary antibodies to Shank3 (#2036 guinea pig polyclonal antibodies raised against aa 1289–1318 of the mouse Shank3 protein, 1:500; Lee et al., 2015) and α-tubulin (Sigma T5168; 1:1,000) at 4°C overnight. Fluorescent secondary antibody signals were detected using *Odyssey® Fc Dual Mode Imaging System*.

Rat Neuron Culture, Immunocytochemistry and Imaging

Primary hippocampal neuronal cultures were prepared from Sprague-Dawley rats at E18 as described previously (Goslin and Banker, 1991). Dissociated neurons were plated in coverslips coated with poly-L-lysine and laminin, and grown in neurobasal media supplemented with B27 (Invitrogen), 0.5 mM glutamax (Invitrogen) and 12.5 μM glutamate (plating media) in a 10% CO_2 incubator. After, this plating media and maintained media were replaced with feeding media (same as plating media only except for glutamate) every week. For immunocytochemistry, cultured neurons (at days *in vitro* or DIV 15) were fixed with 1% paraformaldehyde/1% sucrose (5 min) and methanol (5 min), permeabilized with 0.1% gelatin, 0.3% Triton X-100, 450 mM NaCl in phosphate buffered saline (PBS), and immunostained with primary antibodies against Shank3 (Santa Cruz H-160, 1:200) and GAD67 (Abcam ab26116, 1:200), and FITC-, and Alexa594-conjugated secondary antibodies (Jackson ImmunoResearch). The images were acquired using a confocal microscope (LSM780, Carl Zeiss) with a ×63 objective lens. The Z-stacked images were converted to maximal projection.

Electrophysiology

Mice at P28–35 (for dorsolateral striatum mEPSC and mIPSC) were anesthetized with diethyl ether. Mouse brain sections (300 μm) were sectioned in ice-cold dissection buffer containing (in mM) 212 sucrose, 25 $NaHCO_3$, 10 D-glucose, 2 Na-pyruvate, 1.25 ascorbic acid, 1.25 NaH_2PO_4, 5 KCl, 3.5 $MgSO_4$ and 0.5 $CaCl_2$ bubbled with 95% O_2 and 5% CO_2 gases using Leica VT 1,200 vibratome. The slices were recovered for 30 min and maintained in artificial cerebrospinal fluid (ACSF) at 32°C (in mM: 124 NaCl, 25 $NaHCO_3$, 10 Glucose, 2.5 KCl, 1 NaH_2PO_4, 2.5 $CaCl_2$, 1.3 $MgSO_4$ oxygenated with 95% O_2 and 5% CO_2 gases). All recordings were performed after recovery for additional 30 min at room temperature. During all recordings, brain slices were maintained in a submerge-type recording chamber perfused with 26.5–28°C ACSF (2 ml min^{-1}). Recording and stimulus glass pipettes from borosilicate glass capillaries (Harvard Apparatus) were pulled using an electrode puller (Narishige). All electric responses were amplified and filtered at 2 kHz (Multiclamp 700B, Molecular Devices) and then digitized at 10 kHz (Digidata 1550, Molecular Devices). For whole-cell patch recordings in the dorsolateral striatum, a recording pipette (2.5–3.5 MΩ) was filled with the internal solution (in mM: 100 $CsMeSO_4$, 10 TEA-Cl, 8 NaCl, 10 HEPES, 5 QX-314-Cl, 2 Mg-ATP, 0.3 Na-GTP and 10 EGTA for mEPSCs; 115 CsCl, 10 EGTA, 8 NaCl, 10 TEACl, 10 HEPES, 4 Mg-ATP, 0.3 Na-GTP, 5 QX-314 for mIPSCs) adjusted to pH 7.35 and 285 mOsm. To measure mEPSCs and mIPSCs, dorsolateral striatal MSN neurons were voltage-clamped at −70 mV. For mEPSCs and mIPSCs, picrotoxin (60 μM) and NBQX (10 μM) + APV (50 μM) were added to ACSF with TTX (1 μM), respectively. Responses were recorded for 2 min after maintaining stable baseline for 5 min. MSNs in the dorsal striatum were identified by the soma size (8–12 μm) and basic membrane properties (cell capacitance >100 pF and input resistance >160 MOhm, as reported previously (Cepeda et al., 1998, 2008; Gertler et al., 2008).

Behavioral Assays

Before behavioral experiments, all mice were handled for 10 min per day for 3 days. All behavioral assays were proceeded after 30 min habituation in a dark booth. All tested mice were 2–7 months male mice. The order of behavioral tests was designed in a way to minimize stress in animals. The behavioral tests for global *Shank3*$^{\Delta 14-16}$ and *Viaat-Cre;Shank3*$^{\Delta 14-16}$ mice were performed in the orders described in **Supplementary Table S1**.

Three-Chamber Test

Social approach was measured using the three-chambered test (Moy et al., 2004; Nadler et al., 2004; Silverman et al., 2010). The apparatus is a white acrylic box (60 × 40 × 20 cm) divided into three chambers. The illumination condition was ∼10 lux for global *Shank3*$^{\Delta 14-16}$ mice and 70–80 lux for *Viaat-Cre;Shank3*$^{\Delta 14-16}$ mice. We used a dim light condition (∼10 lux) for global *Shank3*$^{\Delta 14-16}$ mice because a brighter light condition (∼70–80 lux) did not yield optimal results in WT mice. Both left and right side chambers contained a cage in the upper or lower corner for an object or a stranger mouse. Experimental mice were isolated in a single cage for 3 days prior to the test, whereas unfamiliar stranger mice (129S1/SvlmJ

strain) were group-housed (5–7 mice/cage). All stranger mice were age-matched males and were habituated to a corner cage during the previous day (30 min). The test consisted of three phases: empty-empty (habituation), stranger1-object (S1-O) and stranger1-stranger2 (S1-S2). In the first (habituation) phase, a test mouse was placed in the center area of the three-chambered apparatus, and allowed to freely explore the whole apparatus for 10 min. The mouse was then gently guided to the center chamber while an inanimate blue cylindrical object (O) and a WT stranger mouse, termed stranger 1 (S1), were placed in the two corner cages. The positions of object (O) and S1 were alternated between tests to prevent side preference. In the S1-O phase, the test mouse was allowed to explore the stranger mouse or the object freely for 10 min. Before the third S1-S2 phase, the subject mouse was again gently guided to the center chamber while the object was replaced with a new WT stranger mouse, termed stranger 2 (S2). The subject mouse again was allowed to freely explore all three chambers and interact with both stranger mice for 10 min. The duration of sniffing, defined as positioning of the nose of the test mouse within 2.5 cm from a cage, was measured using Ethovision XT10 (Noldus) software.

Direct Social Interaction Test

Each individual mouse spent 10 min in a gray box (30 × 30 × 30 cm; ∼25–30 lux) for two consecutive days for habituation. On day 3, pairs of mice of the same genotype (originally housed separately) were placed in the test box for 10 min. All mice were isolated for 3 days prior to the experimental day. Time spent in nose-to-nose interaction, following, and total interaction were measured manually in a blinded manner. Nose-to-nose interaction was defined as sniffing the head part of the other mouse. Following included the behavior of a mouse following the other mouse as well as nose-to-tail sniffing. Total interaction included nose-to-nose interaction, following, body contact, allo-grooming and mounting.

Courtship Ultrasonic Vocalization

Adult subject male mice were isolated in their home cage for 3 days before the test, whereas age-matched intruder female mice were group-housed (6–7 mice/cage). We did not measure female estrous cycles, assuming that group housing may synchronize the cycles. Basal ultrasonic vocalizations (USVs) of an isolated male mouse in its home cage under a light condition of ∼60 lux in a soundproof chamber were recorded for 5 min in the absence of a female intruder. Next, a randomly chosen stranger C57BL/6J female mouse was introduced into the cage, and female-induced courtship USVs were recorded for 5 min during free interaction between males and females. Avisoft SASLab Pro software was used to automatically analyze the number of USV calls, latency to first call, and total duration of calls from recorded USV files. Signals were filtered from 1 Hz to 100 kHz and digitized with a sampling frequency of 250 kHz, 16 bits per sample (Avisoft UltraSoundGate 116H). To generate spectrograms, the following parameters were used (FFT length: 256, frame size: 100, window: FlatTop, overlap: 75%), resulting in a frequency resolution of 977 Hz and a temporal resolution of 0.256 msec. Frequencies lower than 25 kHz were filtered out to reduce background white noises.

Repetitive Behavior and Self-Grooming Test

Each mouse was placed in a fresh home cage (∼60–70 lux) with bedding and recorded for 20 min. The last 10 min was analyzed manually to measure times spent in self-grooming and digging behavior. Self-grooming behavior was defined as stroking or scratching of its body or face, or licking its body parts. Digging was defined as the behavior of scattering bedding using its head and forelimbs. To further analyze self-grooming behavior, mice were placed in an empty home cage without bedding and were recorded for 20 min. Time spent in self-grooming behavior was counted manually during the last 10 min in a blind manner.

Laboras Test (Long-Term Monitoring)

Each mouse was placed in a single cage and recorded for 96 consecutive hours from the start of the night cycle. Illumination condition during light-on periods was ∼60 lux. Basal activities (locomotion, climbing, rearing, grooming, eating and drinking) were recorded and automatically analyzed by the Laboratory Animal Behavior Observation Registration and Analysis System (LABORAS, Metris). Laboras results were not validated by own manual analyses, given the availability of previous validation results (Van de Weerd et al., 2001; Quinn et al., 2003, 2006; Dere et al., 2015). Mouse movements during the whole 4-day period were used for quantification, except for other behaviors, for which movements during light-off periods were used for more clear results.

Open-Field Test

Mice were put in the center of a white acrylic box (40 × 40 × 40 cm), and their locomotion was recorded with a video camera for 1 h. The illumination of the open field was 90–100 lux. The recorded video was analyzed using Ethovision XT10 software (Noldus). The center zone was defined as an area with 4 × 4 squares when the whole-field was 6 × 6 squares.

Elevated Plus-Maze Test

The maze was elevated to a height of 75 cm from the floor, with two open arms (30 × 6 cm, ∼180 lux) and two closed arms (30 × 6 cm, ∼20 lux). Mice were introduced onto the center of the apparatus with their head toward the open arms and allowed to freely explore the environment for 8 min. Amounts of time spent in open or closed arms and number of transitions were measured by Ethovision XT10 software (Noldus).

Light-Dark Test

The light-dark apparatus was divided into light and dark chambers (21 × 29 × 20 cm, 700 lux, light chamber; 21 × 13 × 20 cm, ∼5 lux, dark chamber) separated by an entrance in the middle wall (5 × 8 cm). Mice were introduced in the light

chamber with their head toward the opposite side of the dark chamber and allowed to freely explore the apparatus for 10 min. Amounts of time spent in light and dark chambers and number of transitions were analyzed by Ethovision XT10 software (Noldus).

Statistical Analysis

Statistical analyses were performed using GraphPad Prism 5 software. Details of statistical analyses and results are presented in **Supplementary Table S2**. The normality of the data distribution was determined using the D'Agostino and Pearson omnibus normality test, followed by Student's *t*-test (in the case of normal distribution) and Mann-Whitney U test (in the case of non-normal distribution). If, sample is dependent each other, paired *t*-test (in the case of normal distribution), and Wilcoxon signed rank test (in the case of non-normal distribution). Repeated-measures of two-way ANOVA and subsequent Bonferroni *post hoc* multiple comparison tests, performed only when there are significant interactions, were used for the time-varying analysis of open-field test and Laboras test. If a single value makes the data distribution as non-normal and is detected as significant outlier ($^{*}P < 0.05$) under the Grubb's test, we removed the data as outliers. One sample *t*-test was used for the analysis of western blot data. The statistical significance of values are indicated in the figure panels as follows: $^{*}P < 0.05$, $^{**}P < 0.01$, $^{***}P < 0.001$, nd, not detectable and ns, not significant.

RESULTS

Expression of *Shank3* in Both Glutamatergic and GABAergic Neurons

To explore the contributions of *Shank3* expression in excitatory and inhibitory neurons to synaptic functions and behaviors in mice, we first tested whether *Shank3* is expressed in glutamatergic and GABAergic neurons using fluorescence *in situ* hybridization (FISH). *Shank3 in situ* signals were present in Vglut1- and Vglut2-positive glutamatergic neurons in brain regions including the medial prefrontal cortex (mPFC; **Figures 1A,B**), indicative of *Shank3* expression in glutamatergic excitatory neurons. *Shank3* signals were also present in Gad1- and Gad2-positive GABAergic neurons in brain regions including the mPFC and the dorsolateral region of the striatum (**Figures 1C,D**). These results suggest that *Shank3* mRNA is expressed in both glutamatergic and GABAergic neurons. *Shank3* mRNA signals outside of DAPI-labeled nuclei or neighboring cell body regions may represent dendritic (rather than somatic) *Shank3* mRNA, as previously reported (Epstein et al., 2014).

To further characterize Shank3 expression in GABAergic neurons, we immunostained for Shank3 protein in GABAergic neurons in cultured rat hippocampal neurons. Shank3 signals were detected in dendrites of both GAD67 (encoded by Gad1)-positive GABAergic neurons and GAD67-negative cells (**Figure 1E**). In addition, punctate Shank3 signals were observed at shaft excitatory synapses on dendrites of GAD67-positive GABAergic neurons (**Figure 1F**). These results, together with the previously reported positive expression of EGFP-tagged Shank3 in GAD-6–positive GABAergic neurons (Han et al., 2013), suggest that Shank3 is expressed in both glutamatergic and GABAergic neurons.

Generation and Characterization of Global *Shank3*$^{\Delta 14-16}$ and *Viaat-Cre;Shank3*$^{\Delta 14-16}$ Mice

To analyze the effects of cell type-specific *Shank3* deletion, we first generated a new mouse line harboring a cassette containing exons 14–16 of the *Shank3* gene flanked by flox sequences, and then crossed these mice with *protamine-Flp and protamine-Cre* mice to produce mice in which *Shank3* exons 14–16 were globally and homozygously deleted (*Shank3*$^{\Delta 14-16}$ mice; **Figure 2A**). PCR confirmed the genotype of these mice (**Figure 2B**), and immunoblot analyses revealed that the two main splice variants of the Shank3 protein (Shank3a and Shank3c/d) were absent in several brain regions (**Figure 2C**), a result expected based on previous studies on the alternative splicing of *Shank3* (Lim et al., 1999; Maunakea et al., 2010; Waga et al., 2014; Wang et al., 2014).

We next generated mice carrying *Shank3*$^{\Delta 14-16}$ deletion restricted to GABAergic neurons by crossing *Shank3*$^{fl/fl}$ mice with *Viaat-Cre* mouse lines, which drives gene expression globally in GABAergic neurons by the solute carrier family 32 (GABA vesicular transporter) member 1 (Slc32a1 or Viaat/vesicular inhibitory amino acid transporter) promoter (Chao et al., 2010; Kim et al., 2018). *Viaat-Cre;Shank3*$^{\Delta 14-16}$ mice, genotyped by PCR (**Figure 2B**), showed a strong reduction in Shank3a in the striatum (**Figure 2D**), a brain region enriched with GABAergic neurons. Notably, the hippocampus displayed a strong tendency for an increase in *Shank3* expression, likely reflecting compensatory changes in the mutant pyramidal neurons caused by the *Shank3* deletion in GABAergic neurons in the hippocampus or other brain regions.

Suppressed Excitatory Synaptic Transmission in the Dorsolateral Striatum in Global *Shank3*$^{\Delta 14-16}$ and *Viaat-Cre;Shank3*$^{\Delta 14-16}$ Mice

We first measured excitatory and inhibitory synaptic transmission in the dorsal striatum, a region with enriched with GABAergic neurons and implicated in the development of abnormal behaviors in *Shank3*-mutant mice (Peca et al., 2011; Peixoto et al., 2016). Both the frequency and amplitude of mEPSCs were substantially decreased in dorsolateral striatal neurons in global *Shank3*$^{\Delta 14-16}$ mice, with frequency exhibiting a larger decrease; in contrast, mIPSCs were normal (**Figures 3A,B**).

Similar changes were observed in dorsolateral striatal neurons in *Viaat-Cre;Shank3*$^{\Delta 14-16}$ mice: mEPSC frequency and amplitude were decreased, whereas mIPSCs were normal (**Figures 3C,D**). Collectively, these results suggest that global and GABAergic *Shank3* deletions similarly suppress excitatory synaptic transmission in dorsolateral striatal neurons without affecting inhibitory synaptic transmission.

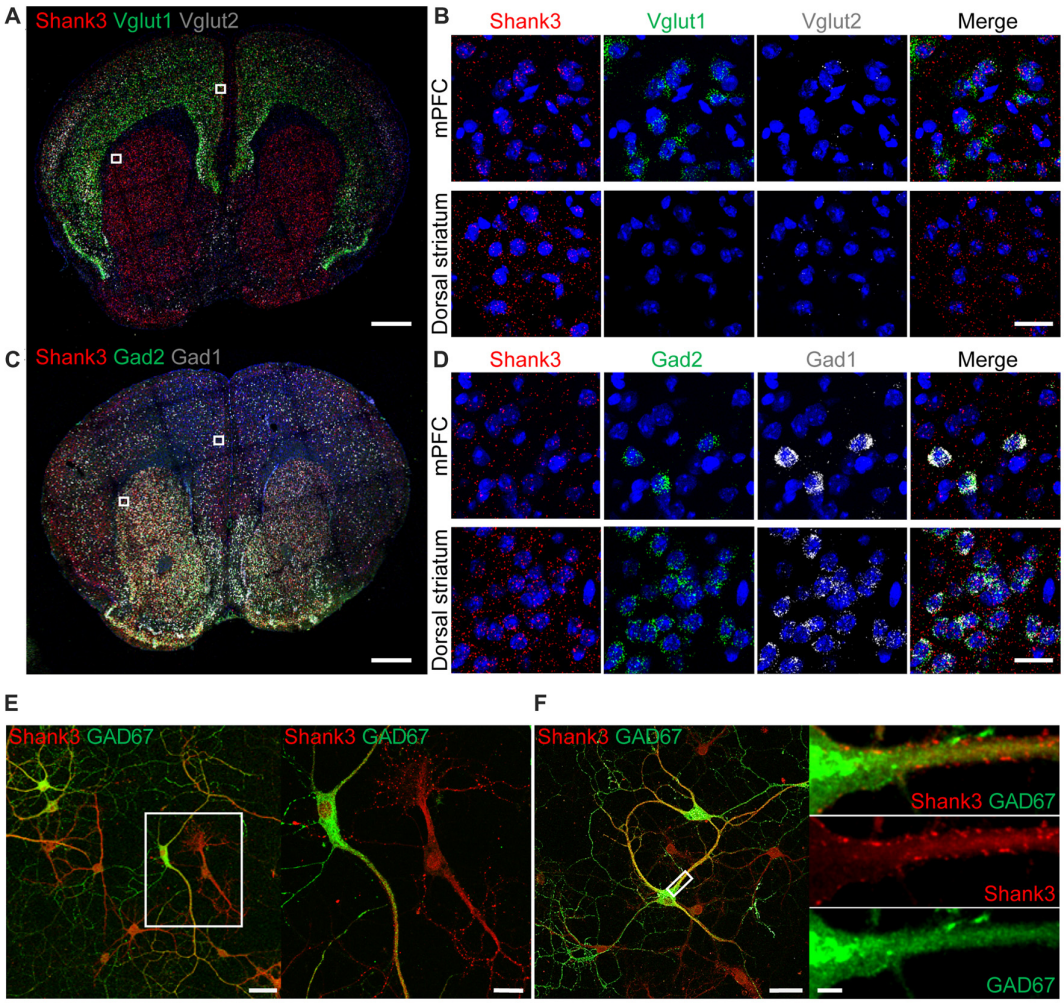

FIGURE 1 | Expression of *Shank3* in both glutamatergic and GABAergic neurons. **(A,B)** Detection of *Shank3* mRNA in *Vglut1/2* mRNA-positive glutamatergic neurons in the prelimbic region of the medial prefrontal cortex (mPFC) in mice (P56) by double-immunofluorescence *in situ* hybridization. Note that *Vglut2* mRNA signals in the mPFC were weaker than those of *Vglut1*, and that, in the dorsolateral striatum, *Vglut1/2* mRNA signals are very weak or absent. Scale bar, 0.5 mm, 20 μm. **(C,D)** Detection of *Shank3* mRNA in Gad1/2-positive GABAergic neurons in the prelimbic region of the mPFC and the dorsolateral region of the striatum of mice (P56) by double-immunofluorescence *in situ* hybridization. Scale bar, 0.5 mm, 20 μm. **(E,F)** Detection of Shank3 proteins in GAD67-positive GABAergic neurons in cultured rat hippocampal neurons at 15 days *in vitro* (DIV 15), as shown by double immunofluorescence staining for Shank3 and GAD67 (encoded by *Gad1*). Scale bar, 50 μm, 20 μm, 50 μm, 5 μm.

Enhanced Direct Social Interaction and Suppressed Social Communication in Global *Shank3*$^{\Delta 14-16}$ and *Viaat-Cre;Shank3*$^{\Delta 14-16}$ Mice

To test the impact of global and GABA neuron-specific deletions of *Shank3* exons 14–16 on behaviors in mice, we subjected *Shank3*$^{\Delta 14-16}$ and *Viaat-Cre;Shank3*$^{\Delta 14-16}$ mice to a battery of behavioral tests. *Shank3*$^{\Delta 14-16}$ mice displayed normal social approach behavior in the three-chamber test, but increased social interaction in the direct social interaction test (**Figures 4A,B**). These mice also showed suppressed USVs upon encounter with a novel female stranger (courtship USVs; **Figure 4C**).

Viaat-Cre;Shank3$^{\Delta 14-16}$ mice showed normal social approach behavior in the three-chamber test but enhanced direct social interaction and suppressed courtship USVs (**Figures 4D–F**), similar to the behaviors observed in global *Shank3*$^{\Delta 14-16}$ mice. These results suggest that social interaction phenotypes induced by global *Shank3*$^{\Delta 14-16}$ deletion is largely recapitulated in mice with *Shank3* exons 14–16 deletion restricted to GABAergic neurons.

Strongly Altered Repetitive Behaviors in Global *Shank3*$^{\Delta 14-16}$ Are Partially Mimicked by *Viaat-Cre;Shank3*$^{\Delta 14-16}$ Mice

In tests for repetitive behaviors, global *Shank3*$^{\Delta 14-16}$ mice displayed enhanced self-grooming in a test cage without bedding (**Figure 5A**), and exhibited enhanced self-grooming but reduced digging in home cages with bedding (**Figure 5B**). In Laboras

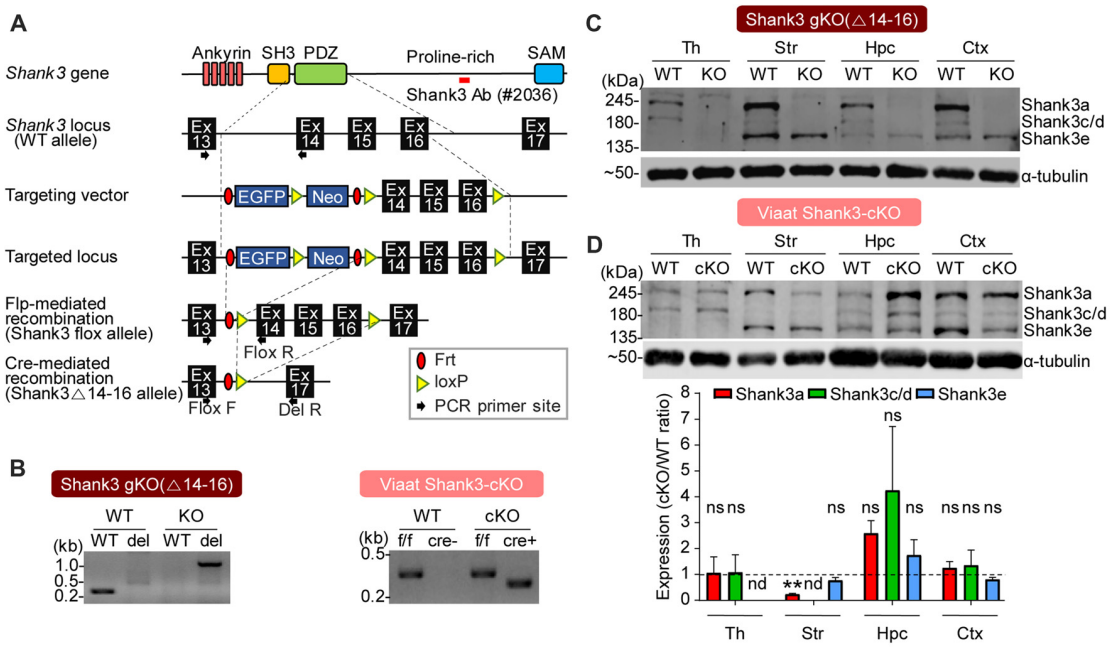

FIGURE 2 | Generation and characterization of global *Shank3*$^{\Delta 14-16}$ and *Viaat-Cre;Shank3*$^{\Delta 14-16}$ mice. **(A)** conditional knockout (cKO) strategy for exons 14–16 of the *Shank3* gene in mice. Ankyrin, ankyrin repeats; SH3, src homology 3 domain; PDZ, PSD-95, Dlg, ZO-1 domain; Pro-rich, proline-rich region; SAM, sterile alpha motif; Ex, exon; Frt, flippase recombinase target; loxP, locus of X-over P1. **(B)** Polymerase chain reaction (PCR) genotyping of global *Shank3*$^{\Delta 14-16}$ and *Viaat-Cre;Shank3*$^{\Delta 14-16}$ mice. Note that the primer set targeting exons 13 and 14 generates a PCR band (276 bp) in the wild-type (WT) allele, but not in the *Shank3*$^{\Delta 14-16}$ (*del*) allele, whereas the primer set targeting exons 13 and 17 generates a PCR band (1159 bp) in the *Shank3*$^{\Delta 14-16}$ (*del*) allele, but not in the WT allele. **(C)** Immunoblot analyses of Shank3 protein splice variants in WT and *Shank3*$^{\Delta 14-16}$ mice (13 weeks; male) using a Shank3-specific antibody (#2036); the target region is indicated in panel **A** as a red bar. Th, thalamus; Str, striatum; Hpc, hippocampus; Ctx, cortex. **(D)** Reduced levels of Shank3 protein variants in different brain regions of *Viaat-Cre;Shank3*$^{\Delta 14-16}$ mice (12 weeks; female). Total brain lysates were analyzed by immunoblotting using a Shank3-specific antibody (#2036). cKO band signals normalized to α-tubulin were normalized to those from WT mice. Data are shown as mean ± SEM. $n = 3$ pairs (WT, cKO), $^{**}P < 0.01$, nd, not detectable, ns, not significant and one sample *t*-test.

cages, where mouse movements are continuously monitored for 4 days, global *Shank3*$^{\Delta 14-16}$ mice showed enhanced self-grooming, although climbing behavior was suppressed (**Figures 5C,D**).

Viaat-Cre;Shank3$^{\Delta 14-16}$ mice showed enhanced self-grooming and suppressed digging in home cages with bedding and enhanced rearing in Laboras cages (long-term monitoring), but normal self-grooming in a novel cage without bedding as well as in Laboras cages (**Figures 5E–H**); these results differed in some respects from those of the global *Shank3*$^{\Delta 14-16}$ mice.

Home-cage digging and Laboras-cage climbing were similarly reduced in global *Shank3*$^{\Delta 14-16}$ and *Viaat-Cre;Shank3*$^{\Delta 14-16}$ mice. These results suggest that the strong self-grooming induced by global *Shank3* deletion is not fully recapitulated by the GABAergic *Shank3* deletion, while the digging and climbing are similarly suppressed by both deletions.

Similar Novelty-Induced Hypoactivity in Global *Shank3*$^{\Delta 14-16}$ and *Viaat-Cre;Shank3*$^{\Delta 14-16}$ Mice

In tests for locomotion, global *Shank3*$^{\Delta 14-16}$ mice displayed reduced locomotor activity in the open-field test, a novel environment (**Figure 6A**). In Laboras cages (long-term monitoring), global *Shank3*$^{\Delta 14-16}$ mice showed strong hypoactivity during the first 2 h and modest hypoactivity measured over the first 6 h; during the last 72 h, a period after full habitation to the environment, *Shank3*$^{\Delta 14-16}$ mice exhibited normal locomotor activity (**Figure 6B**). These results suggest that *Shank3*$^{\Delta 14-16}$ mice show hypoactivity in a novel, but not a familiar, environment.

Viaat-Cre;Shank3$^{\Delta 14-16}$ mice showed decreased locomotor activity in the open-field test and during the first 6 h in Laboras cages (long-term monitoring; **Figures 6C,D**), similar to the novelty-induced hypoactivity in global *Shank3*$^{\Delta 14-16}$ mice. These results suggest that global and GABAergic *Shank3* deletion lead to similar novelty-induced hypoactivity in mice.

Partially Similar Anxiety-Like Behaviors in Global *Shank3*$^{\Delta 14-16}$ and *Viaat-Cre;Shank3*$^{\Delta 14-16}$ Mice

In tests for anxiety-related behaviors, global *Shank3*$^{\Delta 14-16}$ mice did not show anxiety-like behavior in the open-field test, as shown by the normal amount of time spent in the center region of the open-field arena (**Figure 7A**). However, these mice were less anxious in the elevated plus-maze test, spending more time

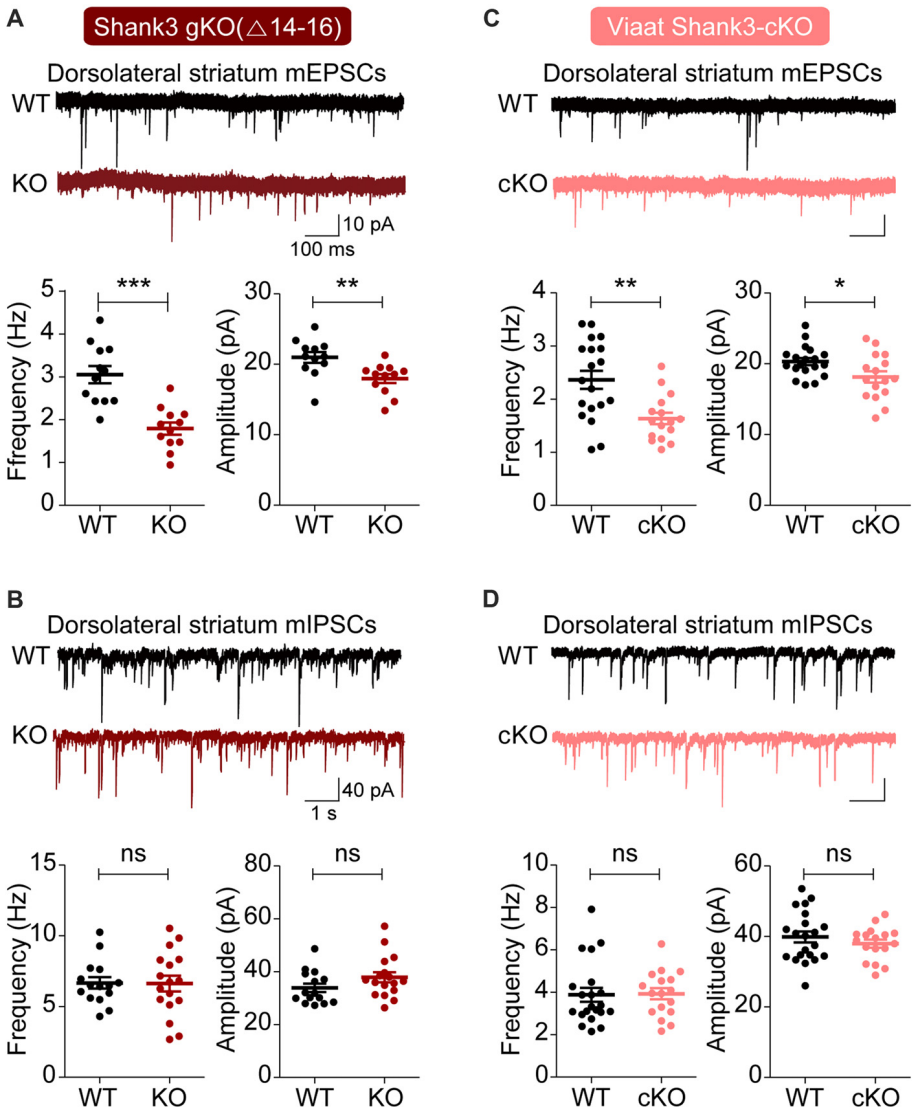

FIGURE 3 | Suppressed excitatory but not inhibitory synaptic transmission in the dorsolateral striatum in global *Shank3*$^{\Delta 14-16}$ and *Viaat-Cre;Shank3*$^{\Delta 14-16}$mice. **(A,B)** Global *Shank3*$^{\Delta 14-16}$ mice (P28–35) show decreased frequency and amplitude of mEPSCs, and normal mIPSCs in dorsolateral striatal neurons. Data are shown as mean ± SEM. n = 12 neurons from four mice (WT), 12, 3 (KO) for mEPSCs, 15, 4 (WT), 17, 4 (KO) for mIPSCs, $^{**}P < 0.01$, $^{***}P < 0.001$, ns, not significant, Student's t-test. **(C,D)** *Viaat-Cre;Shank3*$^{\Delta 14-16}$ mice (P28–35) show decreased frequency and amplitude of mEPSCs, and normal mIPSCs in dorsolateral striatal neurons. n = 19, 5 (WT), 16, 4 (cKO) for mEPSCs, 21, 5 (WT), 17, 5 (cKO) for mIPSCs, $^{*}P < 0.05$, $^{**}P < 0.01$, ns, not significant, Student's t-test (frequency and amplitude of mEPSCs, and amplitude of mIPSC), and Mann-Whitney U test (frequency of mIPSC).

in the open arm (**Figure 7B**), and, conversely, more anxious in the light-dark apparatus, spending less time in the light chamber (**Figure 7C**). *Shank3*$^{\Delta 14-16}$ mice also showed a reduced number of transitions between light and dark chambers in the light-dark apparatus, in line with the hypoactivity of the mice. These results suggest that global *Shank3*$^{\Delta 14-16}$ mice show differential anxiety-like behaviors.

Viaat-Cre;Shank3$^{\Delta 14-16}$ mice were more anxious in open-field and light-dark tests, spending less amount of time in the center region of the open-field arena (**Figure 7D**) and in the light chamber of the light-dark apparatus (**Figure 7F**). However, these mice did not show anxiety-like behavior in the elevated plus-maze test, spending normal amount of time in the open arm (**Figure 7E**).

These results suggest that global and GABAergic *Shank3* deletions similarly induce anxiety-like behaviors in the light-dark test, whereas they have differential influences on other types of anxiety-like behaviors. Therefore, GABAergic *Shank3* deletion seems to strongly contribute to the anxiety-like behavior of global *Shank3*$^{\Delta 14-16}$ mice in the light-dark test. These results also suggest that GABAergic *Shank3* deletion does induce anxiety-like behavior in the open-field test, but this is masked by

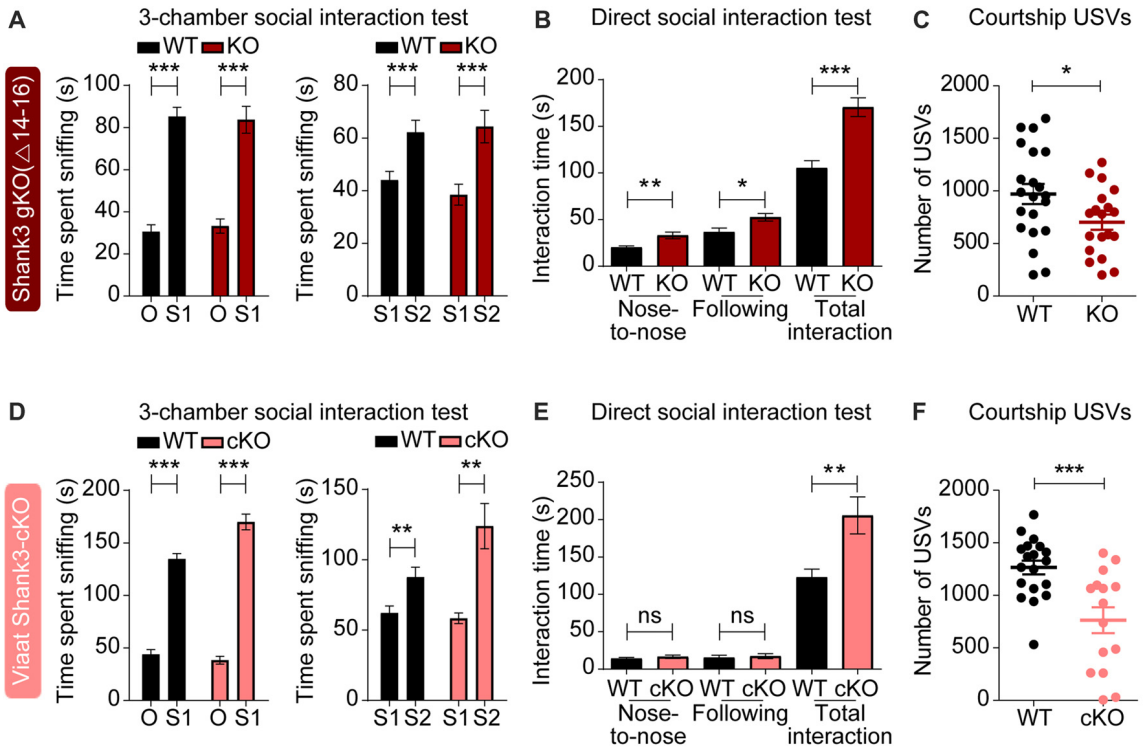

FIGURE 4 | Enhanced direct social interaction and suppressed social communication in global *Shank3*$^{\Delta 14-16}$ and *Viaat-Cre;Shank3*$^{\Delta 14-16}$ mice. **(A)** Normal social approach and social novelty recognition in *Shank3*$^{\Delta 14-16}$ mice (14–21 weeks) in the three-chamber test, as shown by time spent sniffing. S1, stranger; O, object; S2, novel stranger. Data are shown as mean ± SEM. n = 28 (WT) and 22 (KO), $^{***}P < 0.001$, paired t-test. Details on the order of behavioral tests performed on *Shank3*$^{\Delta 14-16}$ mice and conditional *Shank3*$^{\Delta 14-16}$ mouse lines (see below) are described in **Supplementary Table S1**. **(B)** Enhanced social interaction in *Shank3*$^{\Delta 14-16}$ mice (14–20 weeks) in the direct social interaction test, as shown by nose-to-nose interaction, following and total interaction, the latter of which additionally includes allo-grooming and body contacts. Mean ± SEM. n = 20 (WT) and 16 (KO), $^{*}P < 0.05$, $^{**}P < 0.01$, $^{***}P < 0.001$, Student's t-test. **(C)** Suppressed ultrasonic vocalizations (USVs) in *Shank3*$^{\Delta 14-16}$ mice (18–24 weeks), upon encounter with a novel female stranger. n = 21 (WT) and 19 (KO), $^{*}P < 0.05$, Student's t-test. **(D–F)** *Viaat-Cre;Shank3*$^{\Delta 14-16}$ mice (10–13 weeks for **D**, 15–28 weeks for **E**, and 11–21 weeks for **F**) show normal social approach in the three-chamber test **(D)** enhanced direct social interaction **(E)** and suppressed courtship USVs **(F)**. n = 19 mice (WT), 13 (cKO) for three-chamber, 11 (WT), 8 (cKO) for direct social interaction, and 19 (WT), 15 (cKO) for USV, $^{**}P < 0.01$, $^{***}P < 0.001$, ns, not significant, paired t-test (three-chamber test), Mann-Whitney U test (nose to nose time and following time of direct social interaction test), and Student's t-test (total interaction time of direct social interaction test and adult USV test).

global *Shank3* deletion. In contrast, GABAergic *Shank3* deletion seems to have minimal impacts on the anxiety-like behavior in the elevated plus-maze test, suggesting that non-GABAergic *Shank3* deletions are more important for the anxiolytic-like behaivor of global *Shank3*$^{\Delta 14-16}$ mice in the elevated plus-maze.

DISCUSSION

In this study, we investigated the impacts of global and GABA neuron-specific deletion of *Shank3* exons 14–16 on synaptic transmission and behaviors in mice. Global *Shank3*$^{\Delta 14-16}$ mice display decreased excitatory input onto dorsolateral striatal neurons and strong abnormalities in social, repetitive, locomotor and anxiety-like behaviors. The electrophysiological and behavioral (social and locomotor) phenotypes observed in global *Shank3*$^{\Delta 14-16}$ mice are strongly mimicked by *Viaat-Cre;Shank3*$^{\Delta 14-16}$ mice, although the repetitive and anxiety-like behavioral deficits in global *Shank3*$^{\Delta 14-16}$ mice are partially mimicked by *Viaat-Cre;Shank3*$^{\Delta 14-16}$ mice (summarized in **Table 1**).

The result that both the frequency and amplitude of mEPSCs are reduced in global *Shank3*$^{\Delta 14-16}$ mice (**Figure 3**) further strengthens the notion that Shank3 is important for the development and function of excitatory synapses in the dorsal striatum. Similar decreases in the frequency and amplitude of mEPSCs in the dorsal striatum have been observed in the *Shank3* mouse line lacking exons 13–16 (*Shank3B*$^{-/-}$ mice; Peca et al., 2011; Mei et al., 2016; Wang et al., 2017).

A more important finding from our study is that both mouse lines (global and *Viaat-Cre*) show similar decreases in the frequency and amplitude of mEPSCs in dorsolateral striatal neurons (**Figure 3**). This suggests that the suppressed excitatory input onto dorsolateral striatal neurons in these mouse lines are likely to be induced by the deletion of *Shank3* in striatal GABAergic neurons in a cell autonomous manner.

In support of this possibility, our FISH data indicate that *Shank3* mRNAs are expressed in Gad1/2-positive neurons in the

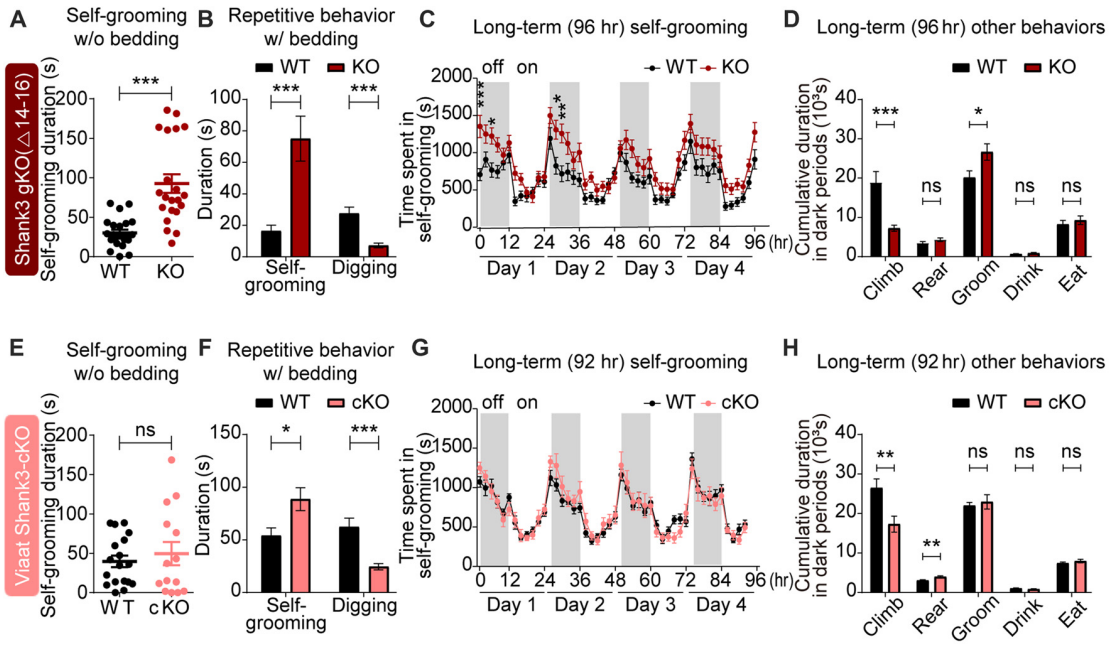

FIGURE 5 | Strongly altered repetitive behaviors in global *Shank3*$^{\Delta 14-16}$ mice are partially mimicked by *Viaat-Cre;Shank3*$^{\Delta 14-16}$ mice. **(A)** Enhanced self-grooming in *Shank3*$^{\Delta 14-16}$ mice (11–14 weeks) in a novel cage without bedding. n = 22 (WT) and 21 (KO), ***$P < 0.001$, Student's t-test. **(B)** Enhanced self-grooming and suppressed digging in *Shank3*$^{\Delta 14-16}$ mice (12–14 weeks) in home cages with bedding. n = 21 (WT) and 20 (KO), ***$P < 0.001$, Mann-Whitney U test. **(C)** Enhanced self-grooming in *Shank3*$^{\Delta 14-16}$ mice (9–14 weeks) in Laboras cages, in which mouse movements are monitored for 4 days. n = 20 (WT) and 21 (KO), *$P < 0.05$, **$P < 0.01$, ***$P < 0.001$, repeated measures two-way ANOVA (genotype p value = 0.0149 and genotype × time p value < 0.0001). **(D)** Enhanced self-grooming and suppressed climbing in *Shank3*$^{\Delta 14-16}$ mice (9–14 weeks) in Laboras cages (long-term monitoring). These graphs are a summary of all types of movements in Laboras cages for 4 days, including self-grooming. n = 20 (WT) and 21 (KO), *$P < 0.05$, ***$P < 0.001$, ns, not significant, Student's t-test. **(E–H)** *Viaat-Cre;Shank3*$^{\Delta 14-16}$ mice (11–15 weeks for **E**, 10–26 weeks (cohort 3: 10–20 weeks, cohort 4: 23–26 weeks) for **F**, 12–14 weeks for **G,H**) show enhanced self-grooming and suppressed digging in home cages with bedding **(F)** but normal self-grooming in a novel cage without bedding **(E)** and normal self-grooming but enhanced rearing and suppressed climbing in Laboras cages (long-term monitoring; **G,H**). n = 18 mice (WT), 14 (cKO) for w/o bedding, 14 (WT), 18 (cKO) for w/bedding, and 15 (WT), 13 (cKO) for Laboras, *$P < 0.05$, **$P < 0.01$, ***$P < 0.001$, repeated measures two-way ANOVA (for Laboras; genotype p value = 0.79), Student's t-test (for self-grooming test, repetitive behavior test, and Laboras (climbing, rearing, grooming and drinking)), and Mann-Whitney U test (for Laboras (eating)).

dorsal striatum in addition to mPFC (**Figure 1**). In addition, the immunostaining result indicates that Shank3-positive punctate structures are observed on the dendrites of GAD67-positive GABAergic neurons in cultured hippocampal neurons. Given that Shank3 is an important component of the postsynaptic density at excitatory synapses (Sheng and Kim, 2000; Sheng and Sala, 2001; Boeckers et al., 2002; Sheng and Hoogenraad, 2007; Grabrucker et al., 2011; Sheng and Kim, 2011; Jiang and Ehlers, 2013; Sala et al., 2015; Monteiro and Feng, 2017; Mossa et al., 2017), the lack of Shank3 in dorsolateral striatal neurons may suppress normal development and maturation of the postsynaptic density, dendritic spines, and excitatory synapses. In addition, previous studies have reported a strong decrease in dendritic spine density in dorsal striatal neurons in *Shank3B*$^{-/-}$ mice (Peca et al., 2011), further suggesting that the decreased mEPSC frequency may be a consequence of postsynaptic changes.

More recently, however, additional analyses of excitatory synaptic inputs onto D1 and D2 medium spiny neurons (MSNs) in the dorsal striatum of *Shank3B*$^{-/-}$ mice have revealed that D2 MSNs show reductions in both presynaptic release and spine density (Wang et al., 2017), suggesting that both pre- and postsynaptic factors may be involved. In addition, a previous study on *Shank3B*$^{-/-}$ mice showed that early abnormal excitability in pyramidal neurons in the somatosensory cortex driven by the limited inhibitory input from neighboring GABAergic neurons induces precocious development of excitatory synapses on dorsomedial striatal neurons that leads to a decrease in the mEPSC frequency at later stages (Peixoto et al., 2016). It is therefore possible that the decreased mEPSC frequency in dorsolateral striatal neurons in global *Shank3*$^{\Delta 14-16}$ and *Viaat-Cre;Shank3*$^{\Delta 14-16}$ mice may represent the consequences of the primary changes occurring in cortical GABAergic neurons.

Behaviorally, global *Shank3*$^{\Delta 14-16}$ mice display altered social and repetitive behaviors, including suppressed courtship USVs and enhanced self-grooming (**Figures 4**, **5**). These mice also show hypoactivity and altered anxiety-like behaviors (**Figures 6**, **7**). Given that *Shank3*$^{\Delta 14-16}$ mice lack the PDZ domain-containing Shank3 variants, Shank3a and Shank3c/d, but retain Shank3e, our mouse line is likely to display behavioral phenotypes similar to those observed in the *Shank3B*$^{-/-}$ mouse line, which globally

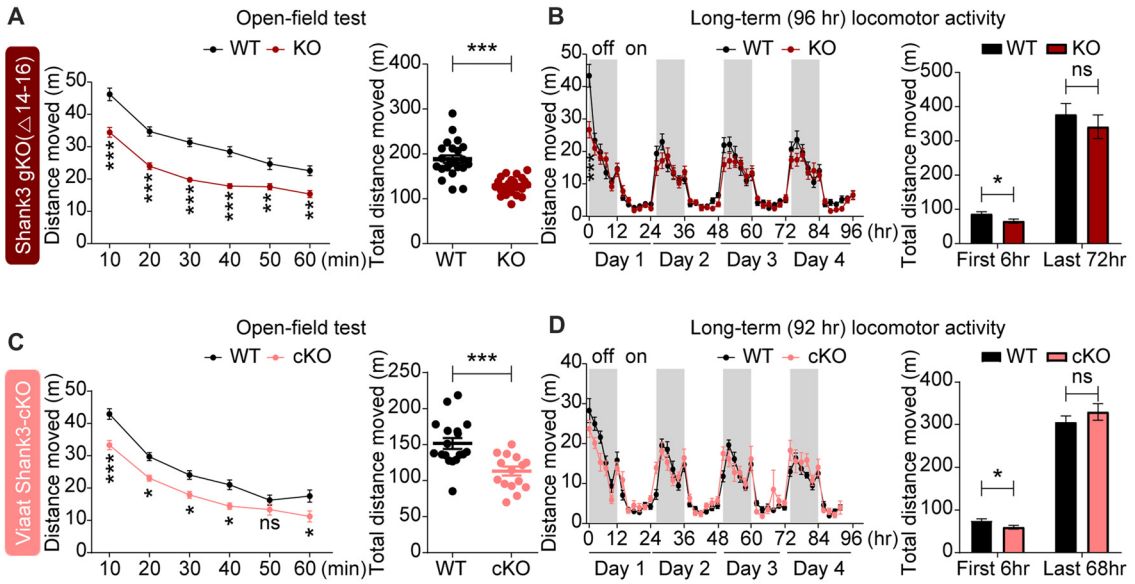

FIGURE 6 | Novelty-induced hypoactivity in global *Shank3*$^{\Delta 14-16}$ and *Viaat-Cre;Shank3*$^{\Delta 14-16}$ mice. **(A)** Suppressed locomotor activity, as measured by distance moved in *Shank3*$^{\Delta 14-16}$ mice (11–13 weeks) in the open-field test. Data are shown as mean ± SEM. n = 23 (WT) and 22 (KO), $^{**}P < 0.01$, $^{***}P < 0.001$, repeated measures two-way ANOVA (genotype p value < 0.0001; genotype × time interaction p value = 0.0109) and Student's t-test. **(B)** *Shank3*$^{\Delta 14-16}$ mice (9–14 weeks) show suppressed locomotor activity during an early period (first 2 and 6 h), but not in the later habituated period (last 72 h), in Laboras cages (long-term monitoring). n = 20 (WT) and 21 (KO), $^{*}P < 0.05$, $^{***}P < 0.001$, repeated measures two-way ANOVA (genotype p value = 0.3711; genotype × time interaction p value < 0.0001) and Student's t-test. **(C,D)** *Viaat-Cre;Shank3*$^{\Delta 14-16}$ mice (8–9 weeks for **C** and 12–14 weeks for **D**) show hypoactivity in the open-field test **(C)** and during the first 6 h but not the last 68 h in Laboras cages (long-term monitoring; **D**). n = 18 (WT), 15 (cKO) for open-field, 15 (WT), 13 (cKO) for Laboras, $^{*}P < 0.05$, $^{***}P < 0.001$, ns, not significant, repeated measures two-way ANOVA (for the left panels in open-field and Laboras results; genotype p values = 0.0006 and 0.7414, time × genotype p values = 0.0454 and 0.0002, respectively), Student's t-test.

lacks exons 13–16 encoding the PDZ domain (Peca et al., 2011). Indeed, *Shank3*$^{\Delta 14-16}$ and *Shank3B*$^{-/-}$ mice show largely similar behaviors, including suppressed courtship USVs, hypoactivity, and anxiety-like behavior (elevated zero maze and light-dark test), although *Shank3B*$^{-/-}$ mice additionally show suppressed social approach (Peca et al., 2011; Dhamne et al., 2017). Another *Shank3*-mutant mice similar to ours is the one lacking exon 13, encoding the PDZ domain (*Shank3*^{E13} mice; Jaramillo et al., 2017). These mice show enhanced self-grooming and social interaction deficits, but normal locomotion and anxiety-related behavior; the partial similarity to our behavioral phenotypes is likely attributable to the different exon targeting strategy (insertion of a stop codon in front of exon 13) in *Shank3*^{E13} mice.

Although the behavioral phenotypes of global *Shank3*$^{\Delta 14-16}$ mice are strong in multiple domains (social, repetitive, locomotor, and anxiety-like), the following points need to be further discussed. First, global *Shank3*$^{\Delta 14-16}$ mice show enhanced direct social interaction, which was unexpected and is at variance with the normal three-chamber social approach observed in these mice. Notably, a previous study on *Shank3*$^{\Delta 4-22}$ mice has reported a similar increase in direct social interaction where *Shank3*$^{\Delta 4-22}$ mice display frequently attempted but unsuccessful social interactions with a stranger C3H mouse, a different strain, that does not reciprocate and terminate the social interaction attempted by the subject mouse (Wang et al., 2016), suggesting that *Shank3*$^{\Delta 4-22}$ mice have normal social interest but struggle with persisting social failures. We could not test whether this is the case for our mice because we used genotype-matched (WT-WT or KO-KO) mouse pairs where monitoring of non-reciprocated social interaction is difficult because of the same coat color and the confusion over retraction vs. rejection. However, our results suggest that social interest is normal in global *Shank3*$^{\Delta 14-16}$ mice, which is different from the significant social interaction deficits observed in many other *Shank3*-mutant mouse lines (Jiang and Ehlers, 2013; Monteiro and Feng, 2017). We propose that the difference in the specific *Shank3* exons deleted in each mouse lines might explain the discrepancy. For instance, the exons deleted in our *Shank3* mice (exons 14–16) are distinct from those deleted in *Shank3B*$^{-/-}$ mice (exon 13–16; Peca et al., 2011). In support of this possibility, a very small difference in the exons deleted in *Shank2*-mutant mice (i.e., exons 6 and 7 vs. exon 7) has been shown to cause strong differences in molecular, synaptic and behavioral phenotypes (Schmeisser et al., 2012; Won et al., 2012; Lim et al., 2017; Wegener et al., 2018).

Another notable result is that global *Shank3*$^{\Delta 14-16}$ mice display anxiolytic-like behavior in the elevated plus-maze whereas they show anxiety-like behavior in the light-dark apparatus and normal anxiety-like behavior in the center region of open-field arena. This could be due to the different anxiogenic components in these tests (Belzung and Griebel, 2001; Carola et al., 2002; Carobrez and Bertoglio, 2005), as exemplified by

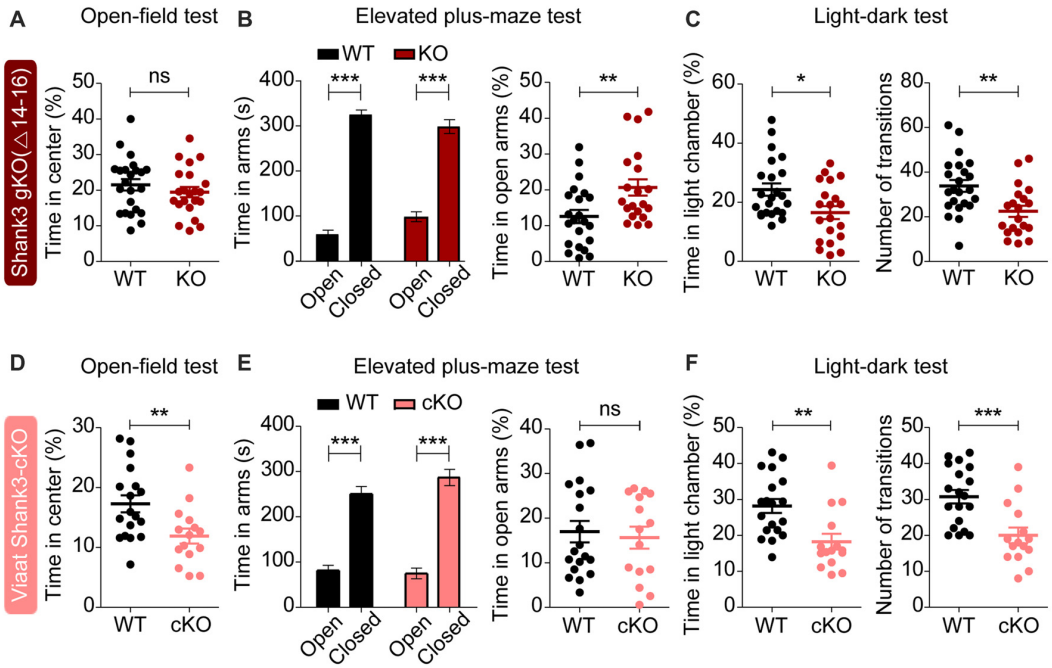

FIGURE 7 | Partially similar anxiety-like behaviors in global *Shank3*$^{\Delta 14-16}$ and *Viaat-Cre;Shank3*$^{\Delta 14-16}$ mice. **(A)** Normal anxiety-like behavior in *Shank3*$^{\Delta 14-16}$ mice (11–13 weeks), as measured by the time spent in the center region of the open field arena in the open-field test. Note that locomotor activity results from the open-field test are described in **Figure 6A**. Data are shown as mean ± SEM. n = 23 (WT) and 22 (KO), ns, not significant, Student's t-test. **(B)** Anxiolytic-like behavior in *Shank3*$^{\Delta 14-16}$ mice (13–21 weeks) in the elevated plus-maze test. n = 22 (WT) and 20 (KO), $^{**}P < 0.01$, $^{***}P < 0.001$, paired t-test (for the left panels), and Student's t-test (for the right panel). **(C)** Anxiety-like behavior in *Shank3*$^{\Delta 14-16}$ mice (14–21 weeks) in the light-dark test. Note that these mice are also hypoactive in this test, as shown by the number of transitions. n = 23 (WT) and 20 (KO), $^{*}P < 0.05$, $^{**}P < 0.01$, Student's t-test. **(D–F)** *Viaat-Cre;Shank3*$^{\Delta 14-16}$ mice (8–9 weeks for **D**, 8–10 weeks for **E**, and 11–20 weeks for **F**) spend a reduced amount of time in the center region of the open-field area (**D**; locomotor activity results are described in **Figure 6C**), a normal amount of time in the open arm of the elevated plus-maze **(E)** and a decreased amount of time in the light chamber of the light-dark apparatus (**F**, left) and show decreased number of transitions (**F**, right). n = 18 (WT), 15 (cKO) for open-field, 19 (WT), 15 (cKO) for elevated plus-maze, and 19 (WT), 15 (cKO) for light-dark, $^{**}P < 0.01$, $^{***}P < 0.001$, Student's t-test (for open-field test, right panel of elevated-plus maze test, and number of transition of light-dark test), paired t-test (for the left panel of elevated plus-maze test), and Mann-Whitney U test (for time in light chamber of light-dark test).

the differential responses of nine different mouse strains to the elevated plus-maze and light-dark tests (Griebel et al., 2000). Notably, *Shank3B*$^{-/-}$ mice (exons 13–16) also display differential anxiety-like behaviors in these assays, being partly similar to our results; normal anxiety-like behavior in elevated plus-maze, anxiety-like behavior in zero maze, light-dark apparatus and open-field center (Peca et al., 2011; Dhamne et al., 2017).

Our results indicate that GABAergic neurons contribute to some of the abnormal behaviors observed in global *Shank3*$^{\Delta 14-16}$ mice. Specifically, the enhanced direct social interaction, suppressed courtship USVs, and novelty-induced hypoactivity observed in global *Shank3*$^{\Delta 14-16}$ mice were also observed in *Viaat-Cre;Shank3*$^{\Delta 14-16}$ mice. In contrast, the strong self-grooming behavior observed in global *Shank3*$^{\Delta 14-16}$ mice were only partially mimicked by *Viaat-Cre;Shank3*$^{\Delta 14-16}$ mice. In anxiety-like behaviors, only the light-dark test results were similar in global *Shank3*$^{\Delta 14-16}$ and *Viaat-Cre;Shank3*$^{\Delta 14-16}$ mice. Therefore, GABA neuronal *Shank3* deletion seems to be more important for social and locomotor behaviors than repetitive and anxiety-like behaviors.

A recent study reported the effects of a deletion of *Shank3* exons 4–22 restricted to Nex-positive glutamatergic neurons in the cortex, hippocampus and amygdala (*Nex-Shank3* cKO mice) and Dlx5/6-positive GABAergic neurons in the striatum (*Dlx5/6-Shank3* cKO mice; Bey et al., 2018). Neither *Nex-Shank3* nor *Dlx5/6-Shank3* cKO mice exhibit social approach deficits, results similar to the normal social approach behavior reported by the same group using mice with a global *Shank3*$^{\Delta 4-22}$ mice (Wang et al., 2016). This phenotype is also similar to the normal social approach behavior observed in our global *Shank3*$^{\Delta 14-16}$ and *Viaat-Cre;Shank3*$^{\Delta 14-16}$ mice.

The suppressed courtship USV and hypoactivity phenotypes observed in global *Shank3*$^{\Delta 4-22}$ mice (Wang et al., 2016) were not recapitulated in either *Nex-Shank3* or *Dlx5/6-Shank3* cKO mice (Bey et al., 2018). These results are different from our findings that both global *Shank3*$^{\Delta 14-16}$ and *Viaat-Cre;Shank3*$^{\Delta 14-16}$ mice show suppressed courtship USV and hypoactivity. Furthermore, the enhanced self-grooming observed in global *Shank3*$^{\Delta 4-22}$ mice (Wang et al., 2016) was observed in *Nex-Shank3* cKO mice, but not in *Dlx5/6-Shank3* cKO mice (Bey et al., 2018). These results are slightly different from our finding that the enhanced self-grooming in global *Shank3*$^{\Delta 14-16}$ mice was partially recapitulated in *Viaat-Cre;Shank3*$^{\Delta 14-16}$mice.

TABLE 1 | Summary of electrophysiological and behavioral phenotypes of global *Shank3*$^{\Delta 14-16}$ and *Viaat-Cre;Shank3*$^{\Delta 14-16}$ mice.

			***Shank3* exons 14-16 global KO**		***Shank3* exons 14-16 Viaat cKO**	
Electrophysiology	**Brain region**	**Measurement**	Frequency	Amplitude	Frequency	Amplitude
	Dorsolateral striatum	mEPSC	↓	↓	↓	↓
		mIPSC	-	-	-	-
Behavior	**Behavioral domain**	**Behavioral test**	***Shank3* exons 14-16 global KO**		***Shank3* exons 14-16 Viaat cKO**	
	Social interaction	3-chamber	-		-	
		Direct interaction	Total interaction ↑ Nose-to-nose ↑ Following ↑		Total interaction ↑ Nose-to-nose, - Following, -	
	Social communication	Adult USV (courtship)	↓		↓	
	Repetitive behavior	Laboras	Self-grooming ↑ Climbing ↓		Rearing ↑ Climbing ↓	
		Self-grooming (w/o bedding)	↑		-	
		Repetitive behavior (with bedding)	Self-grooming ↑ Digging ↓		Self-grooming ↑ Digging ↓	
	Locomotor activity	Laboras (first 6 h)	↓		↓	
		Open-field	↓		↓	
	Anxiety-like behavior	Open field (center time)	-		↓	
		Elevated plus-maze (time in open arms)	↑		-	
		Light/dark box (time in light chamber)	↓		↓	

This table summarizes only the increases or decreases of various electrophysiological and behavioral phenotypes in a given mouse line relative to wild-type (WT)/control mice, but is not intended to compare the phenotypic severities across different mouse lines. -, no significant change; up and down arrows, increases and decreases.

These results indicate that two different global *Shank3* deletions (exons 14–16 and 4–22) in mice lead to remarkably similar behavioral phenotypes in mice in social, repetitive, locomotor and anxiety-like behavioral domains, but that these similarities are minimized by two different cKOs restricted to GABAergic neurons (Dlx5/6 and Viaat). These discrepancies could be attributable to differences in the specific exons of *Shank3* deleted and/or specific characteristics of *Dlx5/6-Cre* vs. *Viaat-Cre* mice (Oh et al., 2005; Goebbels et al., 2006; Chao et al., 2010). For instance, *Dlx5/6-Cre* primarily targets GABAergic neurons in the striatum (Monory et al., 2006), whereas *Viaat-Cre* targets the majority of GABAergic neurons in the brain (Chao et al., 2010). In addition, it could be subtle differences in mouse housing conditions or experimental details.

It remains unclear how GABA neuronal deletion of *Shank3* (exons 14–16) leads to the above mentioned diverse behavioral abnormalities. However, functional defects in the striatum have been strongly implicated in abnormal phenotypes in various *Shank3*-mutant mouse lines (Peca et al., 2011; Schmeisser et al., 2012; Filice et al., 2016; Jaramillo et al., 2016; Mei et al., 2016; Peixoto et al., 2016; Sarowar et al., 2016; Zhou et al., 2016; Jaramillo et al., 2017; Lee Y. et al., 2017; Reim et al., 2017; Vicidomini et al., 2017; Wang et al., 2017; Bey et al., 2018). In addition, a recent study has shown that chemogenetic stimulation of D2, but not D1, MSN activity by DREADD-hM3Dq for the activation of the striatopallidal pathway can rescue self-grooming in *Shank3B*$^{-/-}$ mice (Wang et al., 2017). Therefore, the suppressed excitatory synaptic transmission in dorsolateral striatal neurons in global *Shank3*$^{\Delta 14-16}$ and *Viaat-Cre;Shank3*$^{\Delta 14-16}$ mice might have contributed to the behavioral abnormalities observed in our mouse lines, including enhanced self-grooming. However, the substantial difference between the strong self-grooming in global *Shank3*$^{\Delta 14-16}$ mice and the weak self-grooming in *Viaat-Cre;Shank3*$^{\Delta 14-16}$ mice suggests that GABAergic *Shank3* deletion only partially contribute to the self-grooming phenotype. However, care should be taken in the interpretation because Viaat-mediated GABAergic *Shank3* deletion can affect multiple types of GABAergic neurons.

In conclusion, our results suggest that the deletion of *Shank3* exons 14–16 restricted to GABAergic neurons in mice induces phenotypes that are similar to those induced by global *Shank3* deletion. These include strongly suppressed excitatory synaptic onto dorsolateral striatal neurons and strongly altered social and locomotor behaviors but modestly altered repetitive and anxiety-like behaviors.

AUTHOR CONTRIBUTIONS

TY, JL and HC performed behavioral experiments. TY and JL performed immunoblot experiments. TY, HP and Y-EY performed electrophysiological experiments. EY and JK performed *in situ* hybridization experiments. TY performed hippocampal neuron culture and immunocytochemical experiments. HK and EK designed research and wrote the manuscript.

FUNDING

This study was supported by the Institute for Basic Science (IBS-R002-D1 to EK).

SUPPLEMENTARY MATERIAL

The Supplementary Material for this article can be found online at: https://www.frontiersin.org/articles/10.3389/fncel.2018.00341/full#supplementary-material

REFERENCES

Báez-Mendoza, R., and Schultz, W. (2013). The role of the striatum in social behavior. *Front. Neurosci.* 7:233. doi: 10.3389/fnins.2013.00233

Balleine, B. W., Delgado, M. R., and Hikosaka, O. (2007). The role of the dorsal striatum in reward and decision-making. *J. Neurosci.* 27, 8161–8165. doi: 10.1523/JNEUROSCI.1554-07.2007

Belzung, C., and Griebel, G. (2001). Measuring normal and pathological anxiety-like behaviour in mice: a review. *Behav. Brain Res.* 125, 141–149. doi: 10.1016/s0166-4328(01)00291-1

Bey, A. L., Wang, X., Yan, H., Kim, N., Passman, R. L., Yang, Y., et al. (2018). Brain region-specific disruption of *Shank3* in mice reveals a dissociation for cortical and striatal circuits in autism-related behaviors. *Transl. Psychiatry* 8:94. doi: 10.1038/s41398-018-0142-6

Boccuto, L., Lauri, M., Sarasua, S. M., Skinner, C. D., Buccella, D., Dwivedi, A., et al. (2013). Prevalence of *SHANK3* variants in patients with different subtypes of autism spectrum disorders. *Eur. J. Hum. Genet.* 21, 310–316. doi: 10.1038/ejhg.2012.175

Boeckers, T. M., Bockmann, J., Kreutz, M. R., and Gundelfinger, E. D. (2002). ProSAP/Shank proteins—a family of higher order organizing molecules of the postsynaptic density with an emerging role in human neurological disease. *J. Neurochem.* 81, 903–910. doi: 10.1046/j.1471-4159.2002.00931.x

Boeckers, T. M., Winter, C., Smalla, K. H., Kreutz, M. R., Bockmann, J., Seidenbecher, C., et al. (1999). Proline-rich synapse-associated proteins ProSAP1 and ProSAP2 interact with synaptic proteins of the SAPAP/GKAP family. *Biochem. Biophys. Res. Commun.* 264, 247–252. doi: 10.1006/bbrc.1999.1489

Bonaglia, M. C., Giorda, R., Beri, S., De Agostini, C., Novara, F., Fichera, M., et al. (2011). Molecular mechanisms generating and stabilizing terminal 22Q13 deletions in 44 subjects with Phelan/McDermid syndrome. *PLoS Genet.* 7:e1002173. doi: 10.1371/journal.pgen.1002173

Bonaglia, M. C., Giorda, R., Borgatti, R., Felisari, G., Gagliardi, C., Selicorni, A., et al. (2001). Disruption of the ProSAP2 gene in a t(12;22)(q24.1;Q13.3) is associated with the 22Q13.3 deletion syndrome. *Am. J. Hum. Genet.* 69, 261–268. doi: 10.1086/321293

Bozdagi, O., Sakurai, T., Papapetrou, D., Wang, X., Dickstein, D. L., Takahashi, N., et al. (2010). Haploinsufficiency of the autism-associated *Shank3* gene leads to deficits in synaptic function, social interaction, and social communication. *Mol. Autism* 1:15. doi: 10.1186/2040-2392-1-15

Carobrez, A. P., and Bertoglio, L. J. (2005). Ethological and temporal analyses of anxiety-like behavior: the elevated plus-maze model 20 years on. *Neurosci. Biobehav. Rev.* 29, 1193–1205. doi: 10.1016/j.neubiorev.2005.04.017

Carola, V., D'Olimpio, F., Brunamonti, E., Mangia, F., and Renzi, P. (2002). Evaluation of the elevated plus-maze and open-field tests for the assessment of anxiety-related behaviour in inbred mice. *Behav. Brain Res.* 134, 49–57. doi: 10.1016/s0166-4328(01)00452-1

Cepeda, C., André, V. M., Yamazaki, I., Wu, N., Kleiman-Weiner, M., and Levine, M. S. (2008). Differential electrophysiological properties of dopamine D1 and D2 receptor-containing striatal medium-sized spiny neurons. *Eur. J. Neurosci.* 27, 671–682. doi: 10.1111/j.1460-9568.2008.06038.x

Cepeda, C., Colwell, C. S., Itri, J. N., Chandler, S. H., and Levine, M. S. (1998). Dopaminergic modulation of NMDA-induced whole cell currents in neostriatal neurons in slices: contribution of calcium conductances. *J. Neurophysiol.* 79, 82–94. doi: 10.1152/jn.1998.79.1.82

Chao, H. T., Chen, H., Samaco, R. C., Xue, M., Chahrour, M., Yoo, J., et al. (2010). Dysfunction in GABA signalling mediates autism-like stereotypies and Rett syndrome phenotypes. *Nature* 468, 263–269. doi: 10.1038/nature09582

Cochoy, D. M., Kolevzon, A., Kajiwara, Y., Schoen, M., Pascual-Lucas, M., Lurie, S., et al. (2015). Phenotypic and functional analysis of *SHANK3* stop mutations identified in individuals with ASD and/or ID. *Mol. Autism* 6:23. doi: 10.1186/s13229-015-0020-5

De Rubeis, S., Siper, P. M., Durkin, A., Weissman, J., Muratet, F., Halpern, D., et al. (2018). Delineation of the genetic and clinical spectrum of Phelan-McDermid syndrome caused by *SHANK3* point mutations. *Mol. Autism* 9:31. doi: 10.1186/s13229-018-0205-9

Dere, E., Winkler, D., Ritter, C., Ronnenberg, A., Poggi, G., Patzig, J., et al. (2015). *Gpm6b* deficiency impairs sensorimotor gating and modulates the behavioral response to a 5-HT2A/C receptor agonist. *Behav. Brain Res.* 277, 254–263. doi: 10.1016/j.bbr.2014.04.021

Dhamne, S. C., Silverman, J. L., Super, C. E., Lammers, S. H. T., Hameed, M. Q., Modi, M. E., et al. (2017). Replicable *in vivo* physiological and behavioral phenotypes of the *Shank3B* null mutant mouse model of autism. *Mol. Autism* 8:26. doi: 10.1186/s13229-017-0142-z

Durand, C. M., Betancur, C., Boeckers, T. M., Bockmann, J., Chaste, P., Fauchereau, F., et al. (2007). Mutations in the gene encoding the synaptic scaffolding protein *SHANK3* are associated with autism spectrum disorders. *Nat. Genet.* 39, 25–27. doi: 10.1038/ng1933

Epstein, I., Tushev, G., Will, T. J., Vlatkovic, I., Cajigas, I. J., and Schuman, E. M. (2014). Alternative polyadenylation and differential expression of Shank mRNAs in the synaptic neuropil. *Philos. Trans. R. Soc. Lond. B Biol. Sci.* 369:20130137. doi: 10.1098/rstb.2013.0137

Filice, F., Vörckel, K. J., Sungur, A. O., Wöhr, M., and Schwaller, B. (2016). Reduction in parvalbumin expression not loss of the parvalbumin-expressing GABA interneuron subpopulation in genetic parvalbumin and shank mouse models of autism. *Mol. Brain* 9:10. doi: 10.1186/s13041-016-0192-8

Gauthier, J., Champagne, N., Lafrenière, R. G., Xiong, L., Spiegelman, D., Brustein, E., et al. (2010). *De novo* mutations in the gene encoding the synaptic scaffolding protein *SHANK3* in patients ascertained for schizophrenia. *Proc. Natl. Acad. Sci. U S A* 107, 7863–7868. doi: 10.1073/pnas.0906232107

Gertler, T. S., Chan, C. S., and Surmeier, D. J. (2008). Dichotomous anatomical properties of adult striatal medium spiny neurons. *J. Neurosci.* 28, 10814–10824. doi: 10.1523/JNEUROSCI.2660-08.2008

Goebbels, S., Bormuth, I., Bode, U., Hermanson, O., Schwab, M. H., and Nave, K. A. (2006). Genetic targeting of principal neurons in neocortex and hippocampus of NEX-Cre mice. *Genesis* 44, 611–621. doi: 10.1002/dvg.20256

Goslin, K., and Banker, G. (1991). "Rat hippocampal neurons in low-density culture," in *Culturing Nerve Cells*, eds G. Banker and K. Goslin (Cambridge, MA: The MIT Press), 337–370.

Grabrucker, A. M., Schmeisser, M. J., Schoen, M., and Boeckers, T. M. (2011). Postsynaptic ProSAP/Shank scaffolds in the cross-hair of synaptopathies. *Trends Cell Biol.* 21, 594–603. doi: 10.1016/j.tcb.2011.07.003

Griebel, G., Belzung, C., Perrault, G., and Sanger, D. J. (2000). Differences in anxiety-related behaviours and in sensitivity to diazepam in inbred and outbred strains of mice. *Psychopharmacology* 148, 164–170. doi: 10.1007/s002130050038

Grueter, B. A., Rothwell, P. E., and Malenka, R. C. (2012). Integrating synaptic plasticity and striatal circuit function in addiction. *Curr. Opin. Neurobiol.* 22, 545–551. doi: 10.1016/j.conb.2011.09.009

Guilmatre, A., Huguet, G., Delorme, R., and Bourgeron, T. (2014). The emerging role of SHANK genes in neuropsychiatric disorders. *Dev. Neurobiol.* 74, 113–122. doi: 10.1002/dneu.22128

Hamdan, F. F., Gauthier, J., Araki, Y., Lin, D. T., Yoshizawa, Y., Higashi, K., et al. (2011). Excess of *de novo* deleterious mutations in genes associated with glutamatergic systems in nonsyndromic intellectual disability. *Am. J. Hum. Genet.* 88, 306–316. doi: 10.1016/j.ajhg.2011.02.001

Han, K., Holder, J. L. Jr., Schaaf, C. P., Lu, H., Chen, H., Kang, H., et al. (2013). *SHANK3* overexpression causes manic-like behaviour with unique pharmacogenetic properties. *Nature* 503, 72–77. doi: 10.1038/nature12630

Harris, K. M., and Weinberg, R. J. (2012). Ultrastructure of synapses in the mammalian brain. *Cold Spring Harb. Perspect. Biol.* 4:a005587. doi: 10.1101/cshperspect.a005587

Jaramillo, T. C., Speed, H. E., Xuan, Z., Reimers, J. M., Escamilla, C. O., Weaver, T. P., et al. (2017). Novel *Shank3* mutant exhibits behaviors with face validity for autism and altered striatal and hippocampal function. *Autism Res.* 10, 42–65. doi: 10.1002/aur.1664

Jaramillo, T. C., Speed, H. E., Xuan, Z., Reimers, J. M., Liu, S., and Powell, C. M. (2016). Altered striatal synaptic function and abnormal behaviour in *Shank3* Exon4–9 deletion mouse model of autism. *Autism Res.* 9, 350–375. doi: 10.1002/aur.1529

Jiang, Y. H., and Ehlers, M. D. (2013). Modeling autism by SHANK gene mutations in mice. *Neuron* 78, 8–27. doi: 10.1016/j.neuron.2013.03.016

Kim, R., Kim, J., Chung, C., Ha, S., Lee, S., Lee, E., et al. (2018). Cell-type-specific *shank2* deletion in mice leads to differential synaptic and behavioral phenotypes. *J. Neurosci.* 38, 4076–4092. doi: 10.1523/JNEUROSCI.2684-17.2018

Kim, E., and Sheng, M. (2004). PDZ domain proteins of synapses. *Nat. Rev. Neurosci.* 5, 771–781. doi: 10.1038/nrn1517

Kouser, M., Speed, H. E., Dewey, C. M., Reimers, J. M., Widman, A. J., Gupta, N., et al. (2013). Loss of predominant *Shank3* isoforms results in hippocampus-dependent impairments in behavior and synaptic transmission. *J. Neurosci.* 33, 18448–18468. doi: 10.1523/JNEUROSCI.3017-13.2013

Kreitzer, A. C., and Malenka, R. C. (2008). Striatal plasticity and basal ganglia circuit function. *Neuron* 60, 543–554. doi: 10.1016/j.neuron.2008.11.005

Leblond, C. S., Heinrich, J., Delorme, R., Proepper, C., Betancur, C., Huguet, G., et al. (2012). Genetic and functional analyses of SHANK2 mutations suggest a multiple hit model of autism spectrum disorders. *PLoS Genet.* 8:e1002521. doi: 10.1371/journal.pgen.1002521

Leblond, C. S., Nava, C., Polge, A., Gauthier, J., Huguet, G., Lumbroso, S., et al. (2014). Meta-analysis of SHANK mutations in autism spectrum disorders: a gradient of severity in cognitive impairments. *PLoS Genet.* 10:e1004580. doi: 10.1371/journal.pgen.1004580

Lee, J., Chung, C., Ha, S., Lee, D., Kim, D. Y., Kim, H., et al. (2015). *Shank3*-mutant mice lacking exon 9 show altered excitation/inhibition balance, enhanced rearing and spatial memory deficit. *Front. Cell. Neurosci.* 9:94. doi: 10.3389/fncel.2015.00094

Lee, Y., Kim, S. G., Lee, B., Zhang, Y., Kim, Y., Kim, S., et al. (2017). Striatal transcriptome and interactome analysis of *Shank3*-overexpressing mice reveals the connectivity between *Shank3* and mTORC1 signaling. *Front. Mol. Neurosci.* 10:201. doi: 10.3389/fnmol.2017.00201

Lee, E., Lee, J., and Kim, E. (2017). Excitation/inhibition imbalance in animal models of autism spectrum disorders. *Biol. Psychiatry* 81, 838–847. doi: 10.1016/j.biopsych.2016.05.011

Lim, C. S., Kim, H., Yu, N. K., Kang, S. J., Kim, T., Ko, H. G., et al. (2017). Enhancing inhibitory synaptic function reverses spatial memory deficits in Shank2 mutant mice. *Neuropharmacology* 112, 104–112. doi: 10.1016/j.neuropharm.2016.08.016

Lim, S., Naisbitt, S., Yoon, J., Hwang, J. I., Suh, P. G., Sheng, M., et al. (1999). Characterization of the Shank family of synaptic proteins. Multiple genes, alternative splicing and differential expression in brain and development. *J. Biol. Chem.* 274, 29510–29518. doi: 10.1074/jbc.274.41.29510

Maunakea, A. K., Nagarajan, R. P., Bilenky, M., Ballinger, T. J., D'Souza, C., Fouse, S. D., et al. (2010). Conserved role of intragenic DNA methylation in regulating alternative promoters. *Nature* 466, 253–257. doi: 10.1038/nature09165

Mei, Y., Monteiro, P., Zhou, Y., Kim, J. A., Gao, X., Fu, Z., et al. (2016). Adult restoration of *Shank3* expression rescues selective autistic-like phenotypes. *Nature* 530, 481–484. doi: 10.1038/nature16971

Moessner, R., Marshall, C. R., Sutcliffe, J. S., Skaug, J., Pinto, D., Vincent, J., et al. (2007). Contribution of *SHANK3* mutations to autism spectrum disorder. *Am. J. Hum. Genet.* 81, 1289–1297. doi: 10.1086/522590

Monory, K., Massa, F., Egertová, M., Eder, M., Blaudzun, H., Westenbroek, R., et al. (2006). The endocannabinoid system controls key epileptogenic circuits in the hippocampus. *Neuron* 51, 455–466. doi: 10.1016/j.neuron.2006.07.006

Monteiro, P., and Feng, G. (2017). SHANK proteins: roles at the synapse and in autism spectrum disorder. *Nat. Rev. Neurosci.* 18, 147–157. doi: 10.1038/nrn.2016.183

Mossa, A., Giona, F., Pagano, J., Sala, C., and Verpelli, C. (2017). SHANK genes in autism: defining therapeutic targets. *Prog. Neuropsychopharmacol. Biol. Psychiatry* 84, 416–423. doi: 10.1016/j.pnpbp.2017.11.019

Moy, S. S., Nadler, J. J., Perez, A., Barbaro, R. P., Johns, J. M., Magnuson, T. R., et al. (2004). Sociability and preference for social novelty in five inbred strains: an approach to assess autistic-like behavior in mice. *Genes Brain Behav.* 3, 287–302. doi: 10.1111/j.1601-1848.2004.00076.x

Nadler, J. J., Moy, S. S., Dold, G., Trang, D., Simmons, N., Perez, A., et al. (2004). Automated apparatus for quantitation of social approach behaviors in mice. *Genes Brain Behav.* 3, 303–314. doi: 10.1111/j.1601-183x.2004.00071.x

Naisbitt, S., Kim, E., Tu, J. C., Xiao, B., Sala, C., Valtschanoff, J., et al. (1999). Shank, a novel family of postsynaptic density proteins that binds to the NMDA receptor/PSD-95/GKAP complex and cortactin. *Neuron* 23, 569–582. doi: 10.1016/s0896-6273(00)80809-0

Nelson, S. B., and Valakh, V. (2015). Excitatory/inhibitory balance and circuit homeostasis in autism spectrum disorders. *Neuron* 87, 684–698. doi: 10.1016/j.neuron.2015.07.033

Oh, W.-J., Noggle, S. A., Maddox, D. M., and Condie, B. G. (2005). The mouse vesicular inhibitory amino acid transporter gene: expression during embryogenesis, analysis of its core promoter in neural stem cells and a reconsideration of its alternate splicing. *Gene* 351, 39–49. doi: 10.1016/j.gene.2005.01.009

O'Rourke, N. A., Weiler, N. C., Micheva, K. D., and Smith, S. J. (2012). Deep molecular diversity of mammalian synapses: why it matters and how to measure it. *Nat. Rev. Neurosci.* 13, 365–379. doi: 10.1038/nrn3170

Peca, J., Feliciano, C., Ting, J. T., Wang, W., Wells, M. F., Venkatraman, T. N., et al. (2011). *Shank3* mutant mice display autistic-like behaviours and striatal dysfunction. *Nature* 472, 437–442. doi: 10.1038/nature09965

Peixoto, R. T., Wang, W., Croney, D. M., Kozorovitskiy, Y., and Sabatini, B. L. (2016). Early hyperactivity and precocious maturation of corticostriatal circuits in *Shank3B*$^{-/-}$ mice. *Nat. Neurosci.* 19, 716–724. doi: 10.1038/nn.4260

Phelan, K., Rogers, R. C., and Boccuto, L. (1993). "Phelan-McDermid syndrome," in *GeneReviews((R))*, eds M. P. Adam, H. H. Ardinger, R. A. Pagon, S. E. Wallace, L. J. H. Bean, K. Stephens and A. Amemiya (Seattle, WA: University of Washington), 1993–2018.

Qin, L., Ma, K., Wang, Z.-J., Hu, Z., Matas, E., Wei, J., et al. (2018). Social deficits in *Shank3*-deficient mouse models of autism are rescued by histone deacetylase (HDAC) inhibition. *Nat. Neurosci.* 21, 564–575. doi: 10.1038/s41593-018-0110-8

Quinn, L. P., Stean, T. O., Chapman, H., Brown, M., Vidgeon-Hart, M., Upton, N., et al. (2006). Further validation of LABORAS using various dopaminergic manipulations in mice including MPTP-induced nigro-striatal degeneration. *J. Neurosci. Methods* 156, 218–227. doi: 10.1016/j.jneumeth.2006.03.013

Quinn, L. P., Stean, T. O., Trail, B., Duxon, M. S., Stratton, S. C., Billinton, A., et al. (2003). LABORAS^{TM}: initial pharmacological validation of a system allowing continuous monitoring of laboratory rodent behaviour. *J. Neurosci. Methods* 130, 83–92. doi: 10.1016/s0165-0270(03)00227-9

Reim, D., Distler, U., Halbedl, S., Verpelli, C., Sala, C., Bockmann, J., et al. (2017). Proteomic analysis of post-synaptic density fractions from *Shank3* mutant mice reveals brain region specific changes relevant to autism spectrum disorder. *Front. Mol. Neurosci.* 10:26. doi: 10.3389/fnmol.2017.00026

Sala, C., Vicidomini, C., Bigi, I., Mossa, A., and Verpelli, C. (2015). Shank synaptic scaffold proteins: keys to understanding the pathogenesis of autism and other synaptic disorders. *J. Neurochem.* 135, 849–858. doi: 10.1111/jnc.13232

Sarowar, T., Chhabra, R., Vilella, A., Boeckers, T. M., Zoli, M., and Grabrucker, A. M. (2016). Activity and circadian rhythm influence synaptic *Shank3* protein levels in mice. *J. Neurochem.* 138, 887–895. doi: 10.1111/jnc.13709

Schmeisser, M. J., Ey, E., Wegener, S., Bockmann, J., Stempel, A. V., Kuebler, A., et al. (2012). Autistic-like behaviours and hyperactivity in mice lacking ProSAP1/Shank2. *Nature* 486, 256–260. doi: 10.1038/nature11015

Sheng, M., and Hoogenraad, C. C. (2007). The postsynaptic architecture of excitatory synapses: a more quantitative view. *Annu. Rev. Biochem.* 76, 823–847. doi: 10.1146/annurev.biochem.76.060805.160029

Sheng, M., and Kim, E. (2000). The Shank family of scaffold proteins. *J. Cell Sci.* 113, 1851–1856.

Sheng, M., and Kim, E. (2011). The postsynaptic organization of synapses. *Cold Spring Harb. Perspect. Biol.* 3:a005678. doi: 10.1101/cshperspect.a005678

Sheng, M., and Sala, C. (2001). PDZ domains and the organization of supramolecular complexes. *Annu. Rev. Neurosci.* 24, 1–29. doi: 10.1146/annurev.neuro.24.1.1

Silverman, J. L., Yang, M., Lord, C., and Crawley, J. N. (2010). Behavioural phenotyping assays for mouse models of autism. *Nat. Rev. Neurosci.* 11, 490–502. doi: 10.1038/nrn2851

Speed, H. E., Kouser, M., Xuan, Z., Reimers, J. M., Ochoa, C. F., Gupta, N., et al. (2015). Autism-associated insertion mutation (InsG) of *Shank3* exon 21 causes impaired synaptic transmission and behavioral deficits. *J. Neurosci.* 35, 9648–9665. doi: 10.1523/JNEUROSCI.3125-14.2015

Tu, J. C., Xiao, B., Naisbitt, S., Yuan, J. P., Petralia, R. S., Brakeman, P., et al. (1999). Coupling of mGluR/Homer and PSD-95 complexes by the Shank family of postsynaptic density proteins. *Neuron* 23, 583–592. doi: 10.1016/s0896-6273(00)80810-7

Van de Weerd, H. A., Bulthuis, R. J., Bergman, A. F., Schlingmann, F., Tolboom, J., Van Loo, P. L., et al. (2001). Validation of a new system for the automatic

registration of behaviour in mice and rats. *Behav. Processes* 53, 11–20. doi: 10.1016/s0376-6357(00)00135-2

Vicidomini, C., Ponzoni, L., Lim, D., Schmeisser, M. J., Reim, D., Morello, N., et al. (2017). Pharmacological enhancement of mGlu5 receptors rescues behavioral deficits in *SHANK3* knock-out mice. *Mol. Psychiatry* 22, 689–702. doi: 10.1038/mp.2016.30

Waga, C., Asano, H., Sanagi, T., Suzuki, E., Nakamura, Y., Tsuchiya, A., et al. (2014). Identification of two novel *Shank3* transcripts in the developing mouse neocortex. *J. Neurochem.* 128, 280–293. doi: 10.1111/jnc.12505

Wang, X., Bey, A. L., Katz, B. M., Badea, A., Kim, N., David, L. K., et al. (2016). Altered mGluR5-Homer scaffolds and corticostriatal connectivity in a *Shank3* complete knockout model of autism. *Nat. Commun.* 7:11459. doi: 10.1038/ncomms11459

Wang, W., Li, C., Chen, Q., Van der Goes, M. S., Hawrot, J., Yao, A. Y., et al. (2017). Striatopallidal dysfunction underlies repetitive behavior in *Shank3*-deficient model of autism. *J. Clin. Invest.* 127, 1978–1990. doi: 10.1172/jci87997

Wang, X., McCoy, P. A., Rodriguiz, R. M., Pan, Y., Je, H. S., Roberts, A. C., et al. (2011). Synaptic dysfunction and abnormal behaviors in mice lacking major isoforms of *Shank3*. *Hum. Mol. Genet.* 20, 3093–3108. doi: 10.1093/hmg/ddr212

Wang, X., Xu, Q., Bey, A. L., Lee, Y., and Jiang, Y. H. (2014). Transcriptional and functional complexity of *Shank3* provides a molecular framework to understand the phenotypic heterogeneity of *SHANK3* causing autism and *Shank3* mutant mice. *Mol. Autism* 5:30. doi: 10.1186/2040-2392-5-30

Wegener, S., Buschler, A., Stempel, A. V., Kang, S. J., Lim, C. S., Kaang, B. K., et al. (2018). Defective synapse maturation and enhanced synaptic plasticity in *Shank2* δex7$^{-/-}$ mice. *eNeuro* 5:ENEURO.0398-17.2018. doi: 10.1523/ENEURO.0398-17.2018

Wilson, H. L., Wong, A. C., Shaw, S. R., Tse, W.-Y., Stapleton, G. A., Phelan, M. C., et al. (2003). Molecular characterisation of the 22Q13 deletion syndrome supports the role of haploinsufficiency of *SHANK3/PROSAP2* in the major neurological symptoms. *J. Med. Genet.* 40, 575–584. doi: 10.1136/jmg.40.8.575

Won, H., Lee, H. R., Gee, H. Y., Mah, W., Kim, J. I., Lee, J., et al. (2012). Autistic-like social behaviour in *Shank2*-mutant mice improved by restoring NMDA receptor function. *Nature* 486, 261–265. doi: 10.1038/nature11208

Yang, M., Bozdagi, O., Scattoni, M. L., Wöhr, M., Roullet, F. I., Katz, A. M., et al. (2012). Reduced excitatory neurotransmission and mild autism-relevant phenotypes in adolescent *Shank3* null mutant mice. *J. Neurosci.* 32, 6525–6541. doi: 10.1523/JNEUROSCI.6107-11.2012

Yizhar, O., Fenno, L. E., Prigge, M., Schneider, F., Davidson, T. J., O'Shea, D. J., et al. (2011). Neocortical excitation/inhibition balance in information processing and social dysfunction. *Nature* 477, 171–178. doi: 10.1038/nature10360

Zhou, Y., Kaiser, T., Monteiro, P., Zhang, X., Van der Goes, M. S., Wang, D., et al. (2016). Mice with *Shank3* mutations associated with ASD and schizophrenia display both shared and distinct defects. *Neuron* 89, 147–162. doi: 10.1016/j.neuron.2015.11.023

Conflict of Interest Statement: The authors declare that the research was conducted in the absence of any commercial or financial relationships that could be construed as a potential conflict of interest.

The reviewer RW declared a past co-authorship with one of the authors EK to the handling Editor.

frontiers in Molecular Neuroscience

ORIGINAL RESEARCH
published: 11 October 2018
doi: 10.3389/fnmol.2018.00360

SHANK3 Downregulation in the Ventral Tegmental Area Accelerates the Extinction of Contextual Associations Induced by Juvenile Non-familiar Conspecific Interaction

Sebastiano Bariselli[†], *Alessandro Contestabile*[†], *Stamatina Tzanoulinou*, *Stefano Musardo* and *Camilla Bellone* *

Department of Fundamental Neuroscience, University of Geneva, Centre Médical Universitaire (CMU), Geneva, Switzerland

Haploinsufficiency of the *SHANK3* gene, encoding for a scaffolding protein located in the postsynaptic density of glutamatergic synapse, has been linked to forms of autism spectrum disorders (ASDs). It has been shown that SHANK3 controls the maturation of social reward circuits in the ventral tegmental area (VTA). Whether the impairments in associative learning observed in ASD relate to SHANK3 insufficiency restricted to the reward system is still an open question. Here, we first characterize a social-conditioned place preference (CPP) paradigm based on the direct and free interaction with a juvenile and non-familiar conspecific. In both group- and single-housed C57Bl6/j late adolescence male mice, this CPP protocol promotes the formation of social-induced contextual associations that undergo extinction. Interestingly, the downregulation of *Shank3* expression in the VTA altered the habituation to a non-familiar conspecific during conditioning and accelerated the extinction of social-induced conditioned responses. Thus, inspired by the literature on drugs of abuse-induced contextual learning, we propose that acquisition and extinction of CPP might be used as behavioral assays to assess social-induced contextual association and "social-seeking" dysfunctions in animal models of psychiatric disorders.

Keywords: conditioned place preference, social novelty, VTA, Shank3, isolation

OPEN ACCESS

Edited by:
Eunjoon Kim,
Institute for Basic Science (IBS), South Korea

Reviewed by:
Andreas Martin Grabrucker, University of Limerick, Ireland
Markus Wöhr, Philipps-Universität Marburg, Germany

***Correspondence:**
Camilla Bellone
camilla.bellone@unige.ch

[†]*These authors have contributed equally to this work*

Received: *30 May 2018*
Accepted: *12 September 2018*
Published: *11 October 2018*

Citation:
Bariselli S, Contestabile A, Tzanoulinou S, Musardo S and Bellone C (2018) SHANK3 Downregulation in the Ventral Tegmental Area Accelerates the Extinction of Contextual Associations Induced by Juvenile Non-familiar Conspecific Interaction. Front. Mol. Neurosci. 11:360. doi: 10.3389/fnmol.2018.00360

INTRODUCTION

Haploinsufficiency of the *SHANK3* gene, which encodes for a scaffolding protein located in the postsynaptic density of glutamatergic synapses, has been causally linked to Phelan McDermid syndrome. This syndrome is characterized by intellectual disability, developmental delay, poor motor function and autism spectrum disorder (ASD). To find possible therapeutic interventions, it is fundamental to identify the causative mechanisms and the main neuronal circuits involved in the disease. In humans, emerging evidence suggests an existing association between reward system alterations and ASD (Chevallier et al., 2012). Furthermore, it has been observed that infants with ASD have a diminished response to social reward stimuli that might relate to impairments in social learning (Scott-Van Zeeland et al., 2010). Although *Shank3* knock-out (KO) mice displayed deficits in reinforcement learning (Wang et al., 2016), the contribution of reward system dysfunctions to aberrant behavioral traits observed in ASD animal models remains largely unknown.

SHANK3 is a postsynaptic protein expressed at excitatory inputs where it controls transmission and plasticity (Naisbitt et al., 1999). In mice, the *Shank3* gene is composed of 21 exons with several internal promoters (Jiang and Ehlers, 2013), which encodes for a variety of protein isoforms. Considering the association between ASD and *SHANK3* mutations in humans, several *Shank3* mutant mouse lines have been generated to study both the contribution of the gene to the emergence of ASD-related symptoms and the neuronal circuit dysfunctions underlying aberrant behavioral traits. Sociability, social preference and social novelty recognition abnormalities have been observed with variable severity in mutant mice lacking the different SHANK3 isoforms (Ferhat et al., 2017). Besides its role in controlling sociability and stereotypes in mice, the expression of certain SHANK3 variants is necessary for appropriate learning. In fact, both exon 4–9 and exon 21 deletion lead to impairment in spatial learning (Kouser et al., 2013) and, depending on the genetic background, exon 4–9 KO showed alterations in fear conditioning (Wang et al., 2011; Yang et al., 2012; Drapeau et al., 2014). Recently, it has been demonstrated that a full KO mouse line for all SHANK3 isoforms displays deficits in reinforcement learning (Wang et al., 2016). However, whether the impairments in associative learning are attributable to a SHANK3 insufficiency restricted to the reward system is still an open question.

Rodents can learn to associate environmental cues (conditioned stimuli, CS) with the availability of positive experiences, such as social interaction (unconditioned stimuli, US) resulting in conditioned place preference (CPP) responses. CPP tasks, classically used to study the reinforcing properties of drugs of abuse (Tzschentke, 2007), have been adopted to test the ability of conspecific interaction to promote contextual associative learning (Calcagnetti and Schechter, 1992; Crowder and Hutto, 1992; Van den Berg et al., 1999; Panksepp and Lahvis, 2007; Thiel et al., 2008; Trezza et al., 2009; Kummer et al., 2011; Dölen et al., 2013; Lahvis et al., 2015; Hung et al., 2017). Contextual associations are subject to extinction, a behavioral phenomenon caused by the repeated presentations of contextual cues in the absence of the reinforcer and characterized by a timely reduction of the conditioned responses (for a comprehensive view on extinction theories see Bouton, 2004; Quirk and Mueller, 2008; Dunsmoor et al., 2015). However, although it has been shown that social-induced CPP undergoes extinction in adolescent rats (Trezza et al., 2009), the involvement of SHANK3 in this phenomenon remains elusive.

The reward system originates from the highly heterogeneous dopamine (DA) neurons of the ventral tegmental area (VTA) and controls reinforcement learning. Despite their diversity, at least a subclass of midbrain DA neurons increase their activity in response to unexpected rewards and, after associative learning, to cues predicting reward availability (Schultz et al., 1997; Cohen et al., 2012). Importantly, while optogenetic studies demonstrated the sufficiency of VTA DA neuron stimulation to promote learning (Tsai et al., 2009; Adamantidis et al., 2011), blockade of DA receptors confirmed the necessity of intact DA signaling for reward-induced place preference acquisition (Hoffman and Beninger, 1989; Cunningham et al., 2000; Rezayof et al., 2002; Le Foll et al., 2005; Vidal-Infer et al., 2012). Appropriate synaptic transmission and plasticity at synaptic inputs onto VTA DA neurons are fundamental, not only for the acquisition (Stuber et al., 2008; Huang et al., 2016) but also for the extinction of reinforcement learning (Engblom et al., 2008). Emerging evidence suggests the involvement of the DA system in social-induced learning of new contextual associations. In fact, social-induced CPP activates several regions within the reward system (El Rawas et al., 2012), it is controlled by oxytocin within the VTA and NAc (Dölen et al., 2013; Hung et al., 2017) and is impaired by the DA re-uptake inhibitor, methylphenidate (Trezza et al., 2009). Recently, we demonstrated that an intact excitability and expression of the ASD-associated protein Neuroligin 3 at VTA DA neurons (Bariselli et al., 2018) are necessary for the acquisition of social-induced CPP. However, the role of SHANK3 at VTA neurons in learning and extinction of social-induced contextual associations remained unexplored.

To investigate the involvement of SHANK3 at VTA neurons in controlling social-induced associative learning, we first characterized a social CPP paradigm (Bariselli et al., 2018) based on the direct and free interaction with a juvenile and non-familiar conspecific. The acquisition of CPP does not rely on single-housing and undergoes extinction. Moreover, we found that while the downregulation of *Shank3* expression in the VTA did not prevent the acquisition of a preference for the non-familiar conspecific-associated compartment, it altered the habituation to non-familiar conspecific and accelerated the extinction of social-induced conditioned responses.

MATERIALS AND METHODS

Animals

The experimental procedures described here were conducted in accordance with the Swiss laws and previously approved by the Geneva Cantonal Veterinary Authority. Male C57Bl/6j mice were purchased from Charles River Laboratories and housed in the institutional animal facility under standard 12 h/12 h light/dark cycles with food and water *ad libitum*. Experimental animals were group-housed (2–3 per cage), or single-housed only for the single-housing experimental condition, and tested during late adolescence, at the 8th or 9th week of life. Younger non-familiar male mice (3–4 weeks; sex-matched) were single-housed and used as stimuli animals during the conditioning sessions of the CPP protocol. Behavioral experiments were conducted in a room with fixed illumination (20 Lux) at a temperature between 22°C and 24°C. The experiments were performed in a time window that started approximately 2 h after the end of the dark circle and ended 2 h before the start of the next dark circle.

Real-Time Quantitative Reverse Transcriptase PCR

Total RNA was extracted using the RNeasy PLUS Mini Kit (Qiagen), from the VTA of mice infected either with

shSHANK3 or scrSHANK3. After quantification with Nanodrop Spectrophotometer, 1 μg of RNA was retrotranscribed in cDNA with QuantiTect Reverse Transcription Kit (Qiagen), followed by a PCR amplification of the subsequent transcripts: *SHANK3* forward primer 5′ acgaagtgcctgcgtctggac 3′, reverse primer 5′ ctcttgccaaccattctcatcagtg 3′, *Tyrosine hydroxylase (TH)* forward primer 5′ ccccacctggagtattttgtg 3′, reverse primer 5′ atcacgggcg gacagtagacc 3′, *Actin* forward primer 5′ agagggaaatcgtgcgtgac 3′, reverse primer 5′ caatagtgatgacctggccgt 3′. Reactions were carried out using iTaq™ Universal SYBR® Green Supermix (Biorad) on Applied Biosystems 7,500 Real-Time PCR System (Applied Biosystems, Foster City, CA, USA) by 50°C for 2 min, 95°C for 10 min followed by 40 cycles at 95°C for 15 s and 60°C for 1 min. Melting curve analyses were performed to verify the amplification specificity. Relative quantification of gene expression was performed according to the ΔΔ-Ct method (Livak and Schmittgen, 2001).

Conditioned Place Preference Induced by Non-familiar Conspecific Interaction

The apparatus (Bioseb, Model BIOSEB, *in vivo* Research Instruments, spatial place preference box for mice LE895) used for the CPP protocol consists of two square-shaped chambers (20 × 20 cm) with either gray stripes on white background or black dots on white background. The floor in each of the two chambers has different distinct textures, namely one with a smooth and one with a rough surface. The two chambers are interconnected by a small corridor, with transparent walls

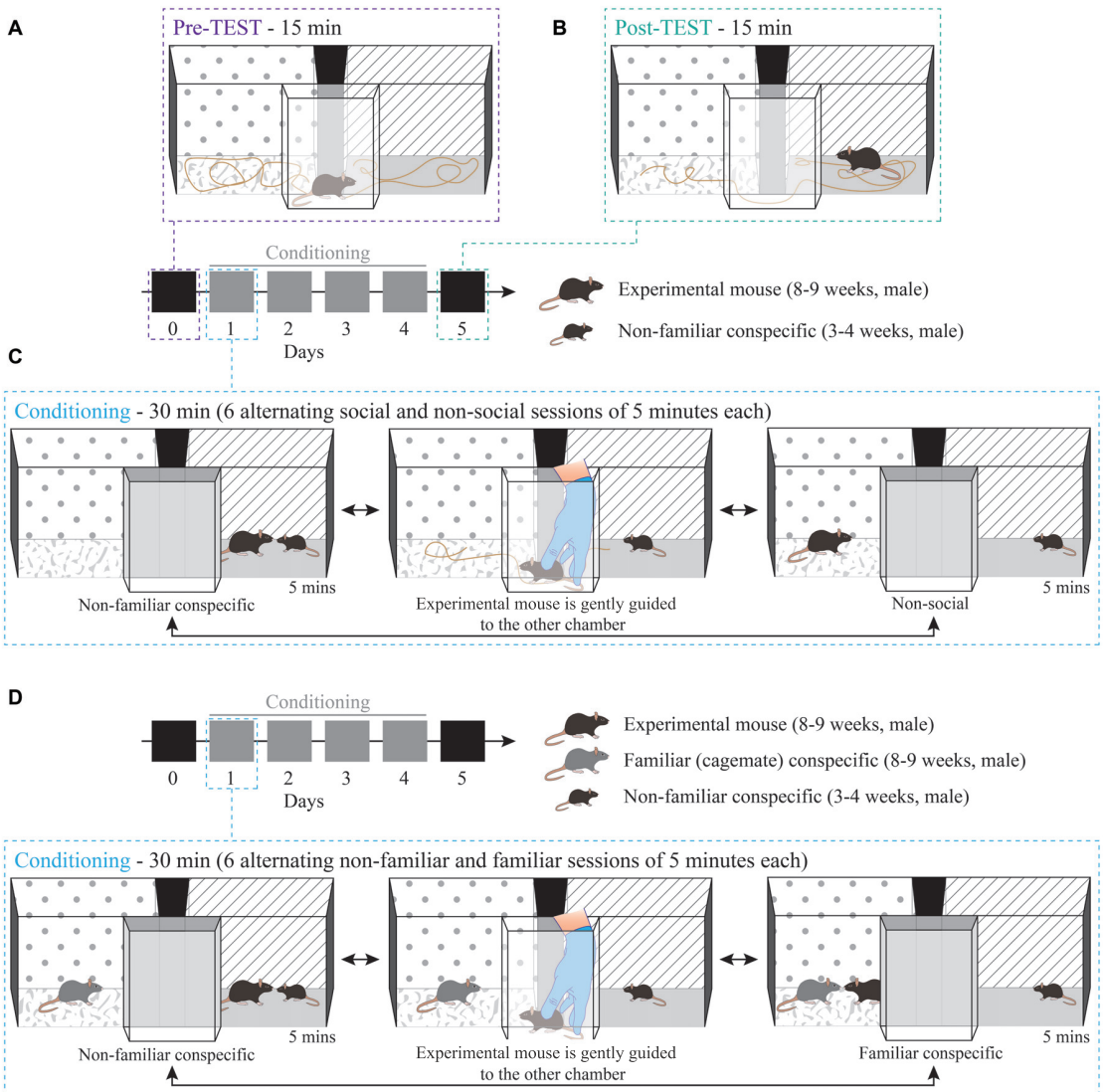

FIGURE 1 | Non-familiar conspecific-induced conditioned place preference (CPP): a variation of social-induced CPP to assess the reinforcing properties of social interaction. Schematic 3D representation of the CPP procedure and apparatus. The protocol consisted of: **(A)** 15 min pre-TEST, **(B)** 15 min post-TEST and **(C)** conditioning phase (30 min per day for four consecutive days). **(D)** Schematic 3D representation of conditioning phase for non-familiar vs. familiar social stimuli protocol, during which the experimental mouse interacted with a non-familiar social stimulus in one chamber and with a familiar (cage-mate) stimulus in the other one.

and floor, and removable doors allow the corridor to be closed (**Figure 1**).

After each pre-TEST, conditioning session, post-TEST and extinction protocol the arena was cleaned thoroughly with 1% acetic acid and allowed to dry before continuing with the next animal.

Day 0—Pre-TEST: experimental mice freely explored the CPP apparatus for 15 min to establish a baseline preference for both chambers (**Figure 1A**). On the same day, stimuli mice were habituated either to one or the other chamber for 15 min. The chamber that they were habituated in was the chamber that they were in during the conditioning sessions.

Days 1–4—Conditioning, paired protocol (non-familiar vs. non-social session): for each experimental mouse, one chamber was randomly assigned as the paired session chamber, with the presence of a non-familiar mouse (US+) and the other as the non-social session chamber (US). This protocol remained stable for each mouse throughout the conditioning sessions of Days 1–4. Experimental mice were subjected to six alternating conditioning sessions of 5 min each, resulting in 30 min of total conditioning time per day (e.g., non-familiar mouse session 1, non-social session 1, non-familiar mouse session 2, non-social session 2, non-familiar mouse session 3, non-social session 3; **Figure 1C**). During each conditioning session, the experimental subjects were allowed to freely interact with social stimuli. To counteract bias formation, each day the starting session was counterbalanced across mice and alternated for each mouse, such that, if for example on day 1 the experimental subject was exposed to the paired session first, on day 2 the conditioning started with the non-social session. After the end of each 5-min trial, the animals were gently guided by the experimenter through the corridor and towards the other chamber (**Figure 1C**), therefore the animals were exposed to the spatial orientation of both chambers and apparatus.

Days 1–4—Conditioning, contingency break protocol: this experimental protocol did not maintain the stable contingencies between chamber and stimulus. Specifically, the assignment of one context to the non-familiar stimulus (US+) and another context to the non-social (US) was inverted each day (e.g., day 1: non-familiar mouse in chamber A vs. non-social in chamber B; day 2: non-familiar mouse in chamber B vs. non-social in chamber A; day 3: non-familiar mouse in chamber A vs. non-social in chamber B; and day 4: non-familiar mouse in chamber B vs. non-social in chamber A).

Days 1–4—Conditioning, paired protocol (familiar session vs. non-familiar session): for each experimental mouse one chamber was assigned as the paired session chamber, with the presence of the non-familiar mouse (US+), and the other chamber was associated with the presence of a cage-mate, the familiar stimulus (US). This protocol remained stable for each mouse throughout the conditioning sessions of Days 1–4. Experimental mice were subjected to six alternating conditioning sessions of 5 min each, resulting in 30 min of total conditioning time per day (e.g., non-familiar mouse session 1, familiar mouse session 1, non-familiar mouse session 2, familiar mouse session 2, non-familiar mouse session 3, familiar mouse session 3; **Figure 1D**). Each day the starting session was counterbalanced across mice and alternated for each mouse. After the end of each 5-min trial, the animals were gently guided by the experimenter through the corridor and towards the other chamber (**Figure 1D**).

We should note that, in this paradigm, the experimental mouse was free to interact with a social stimulus that remained unchanged throughout all the conditioning sessions. Typically, one stimulus mouse was assigned to one experimental animal. Thus, although the stimulus mouse represented a stranger stimulus at the first conditioning session, the non-familiarity aspect was maintained since both experimental and stimuli animals returned to their respective home-cages and kept separated after each conditioning day. Thus, in this case, the US exposure represented a valued condition. In contrast, when the experimental subject had access to the familiar stimulus both in the home-cage and in the conditioned side of the apparatus, the familiar stimulus mouse exposure represented a devalued condition.

Day 5—Post-TEST: 24 h after the last conditioning session, experimental mice were placed in the corridor of the CPP apparatus and, after lifting the removable doors, the animals could freely explore the arena once again for 15 min and establish a preference (**Figure 1B**) in the absence of the US.

Extinction: starting 48 h after the post-TEST session, experimental mice were exposed for several days (5–6 days) to the empty apparatus. In particular, mice were placed in the corridor of the CPP apparatus and, after lifting the removable doors, explored the arena for 15-min-long sessions in the absence of the US. After each extinction session, the arena was cleaned thoroughly with 1% acetic acid and allowed to dry before continuing with the next animal.

The behavior of the animals was tracked automatically with the Ethovision XT software (Noldus, Wageningen, Netherlands) or AnyMAZE and the time spent in the two chambers was recorded for the pre- and post-TEST sessions. Subsequently, the preference index was calculated as: time spent in the non-familiar conspecific-paired chamber divided by the time spent in the non-social chamber for *non-familiar vs. non-social session*, and time spent in the non-familiar conspecific-paired chamber divided by the time spent in the familiar-paired chamber for *familiar session vs. non-familiar session*. Moreover, we calculated the learning index by dividing the preference index calculated at post-TEST by the preference index calculated at pre-TEST. For all behavioral cohorts, the parameters of body and nose-to-nose contact, number of transitions and length of mean visit were analyzed using Ethovision XT.

Stereotaxic Injections

Purified scrShank3 and shShank3 (AAV1-GFP-U6-scrmb-shRNA; titer: 5.9×10^{13} GC/mL and AAV5-ZacF-U6-luc-zsGreen-shShank3; titer: 7.4×10^{13} GC/mL, VectorBioLab) injections were delivered in mice younger than P6 as previously described (Bariselli et al., 2016). After anesthesia induction with a mixture of isoflurane/O_2, C57Bl/6j wildtype pups were placed on a stereotaxic frame (Angle One; Leica, Germany) and a single craniotomy was made over the VTA. To obtain bilateral VTA infection, 200 nl of viral solution was injected

at the following coordinates: ML: 0.15 mm, AP: 0.1 mm, DV: −4.0 and −3.9 mm from lambda through a graduated glass pipette (Drummond Scientific Company, Broomall, PA, USA). After behavioral experiments, *post hoc* analysis was performed to validate the localization of the infection (**Figure 6B**).

Statistical Analysis

Analysis of preference index, learning index and time in each chamber was conducted by performing Shapiro-Wilk analysis to assess the normality of sample distributions. *T*-test with Welch's correction and paired *t*-test were used for comparisons between two sample groups when appropriate. When the normality was violated non-parametric Mann-Whitney and Wilcoxon rank-tests were applied. For multifactorial analysis, repeated-measures two-way ANOVA was performed, and *P* values of main effects and interaction were reported in the figure legends for each experiment. After significant main effects and interactions were revealed, Bonferroni *post hoc* tests were used for between/within group comparisons and reported in the figure legends or graphs. Significance level was set at $P < 0.05$. Statistical outliers were excluded when the time spent in either chamber during apparatus exploration (at pre-TEST, post-TEST or extinction sessions) was deviating for more than two standard deviations from the group mean. Within this manuscript, the non-familiar conspecific-induced CPP protocol was replicated four times in four different and independent animal batches.

RESULTS

Non-familiar Conspecific-Induced CPP Assesses the Reinforcing Properties of Social Interaction

To study the role of SHANK3 in the VTA in mediating the reinforcing properties of social interaction, we modified previously published social-induced CPP protocols to obtain CPP mediated by interaction with a non-familiar conspecific in male mice. The paradigm started with a pre-TEST phase, during which mice explored for 15 min an empty apparatus consisting of two chambers characterized by different contextual cues (**Figure 1A**; see "Materials and Methods" section for further details). We then performed 4 days of conditioning, during which mie learnt to associate one compartment of the apparatus with the presence of a non-familiar (novel) social stimulus while the other compartment was left empty (non-social). During each conditioning day, we rapidly alternated for three times the exposure to the two chambers (**Figure 1C**). Twenty-four hours after the last conditioning session, we measured the acquisition of a place preference for one of the two chambers by quantifying the time spent exploring each compartment of the empty apparatus (**Figure 1B**). In addition, to compare the reinforcing properties of non-familiar vs. familiar conspecific, during the conditioning phase, experimental animals encountered in one chamber a non-familiar mouse, while in the other they were exposed to their familiar cage-mate (**Figure 1D**).

The Acquisition of Non-familiar Conspecific-Induced CPP Does Not Require Single-Housing

Social CPP paradigms are often performed isolating the experimental mice before and/or during the conditioning. Single-housing, possibly through adaptations occurring within the dopaminergic system (Whitaker et al., 2013), enhances sociability (Panksepp and Beatty, 1980; Vanderschuren et al., 1995), increases the incentive value of social stimuli (Van den Berg et al., 1999; Trezza et al., 2009) and seems necessary to obtain social-induced CPP (Trezza et al., 2009). However, under these circumstances, it is difficult to determine whether the animals develop a CPP response because of the aversive properties of social isolation or because of the reinforcing properties of social interaction. Therefore, we tested whether housing conditions affected non-familiar conspecific-induced CPP acquisition in wildtype late adolescent mice (**Figure 2A**). By measuring the time spent in the non-familiar conspecific-paired chamber and the non-social chamber, we calculated a preference index (time spent in non-familiar conspecific-associated chamber/time spent in the non-social chamber) at the pre- and the post-TEST. We found that single-housed mice (during the conditioning) increased their preference index at the post-TEST compared to the pre-TEST (**Figures 2B–D**), indicating that they developed a preference for the non-familiar conspecific-associated chamber during conditioning. Additionally, at the post-TEST, single-housed mice spent a significantly longer time in the non-familiar conspecific-paired chamber compared to the non-social one (**Figure 2E**). This indicates that experimental animals were discriminating between contextual cues and expressing a preference for the ones associated with the interaction with a novel conspecific.

Subsequently, we subjected group-housed mice to the same conditioning paradigm used for single-housed animals. Surprisingly, we found that group-housed mice increased their preference for non-familiar conspecific-associated chamber (**Figures 2F–H**) and discriminated between non-familiar conspecific-associated vs. non-social chamber at the post-TEST (**Figure 2I**). Thus, the non-familiar conspecific-induced CPP paradigm, which relies on the direct and free exploration of a younger and non-familiar conspecific stimulus, allows us to study the reinforcing properties of social interaction without the need to single-house the experimental animals.

To prove the necessity of a contingency between contextual cues and social exposure for the acquisition of non-familiar conspecific-induced CPP, group-housed mice were exposed to the same number of social stimuli presentations, but in alternating chambers (contingency break) during the conditioning phase. In this case, we assigned the non-familiar conspecific-paired chamber as the first chamber in which they were exposed to the non-familiar social stimulus. Under these circumstances, the experimental animals did not increase their preference index (**Figures 2J–L**) and did not show any preference for one of the two chambers at the post-TEST (**Figure 2M**). Finally, to quantify the increase in place preference between pre- and post-TEST and to allow between-group comparisons, we calculated a learning index (preference

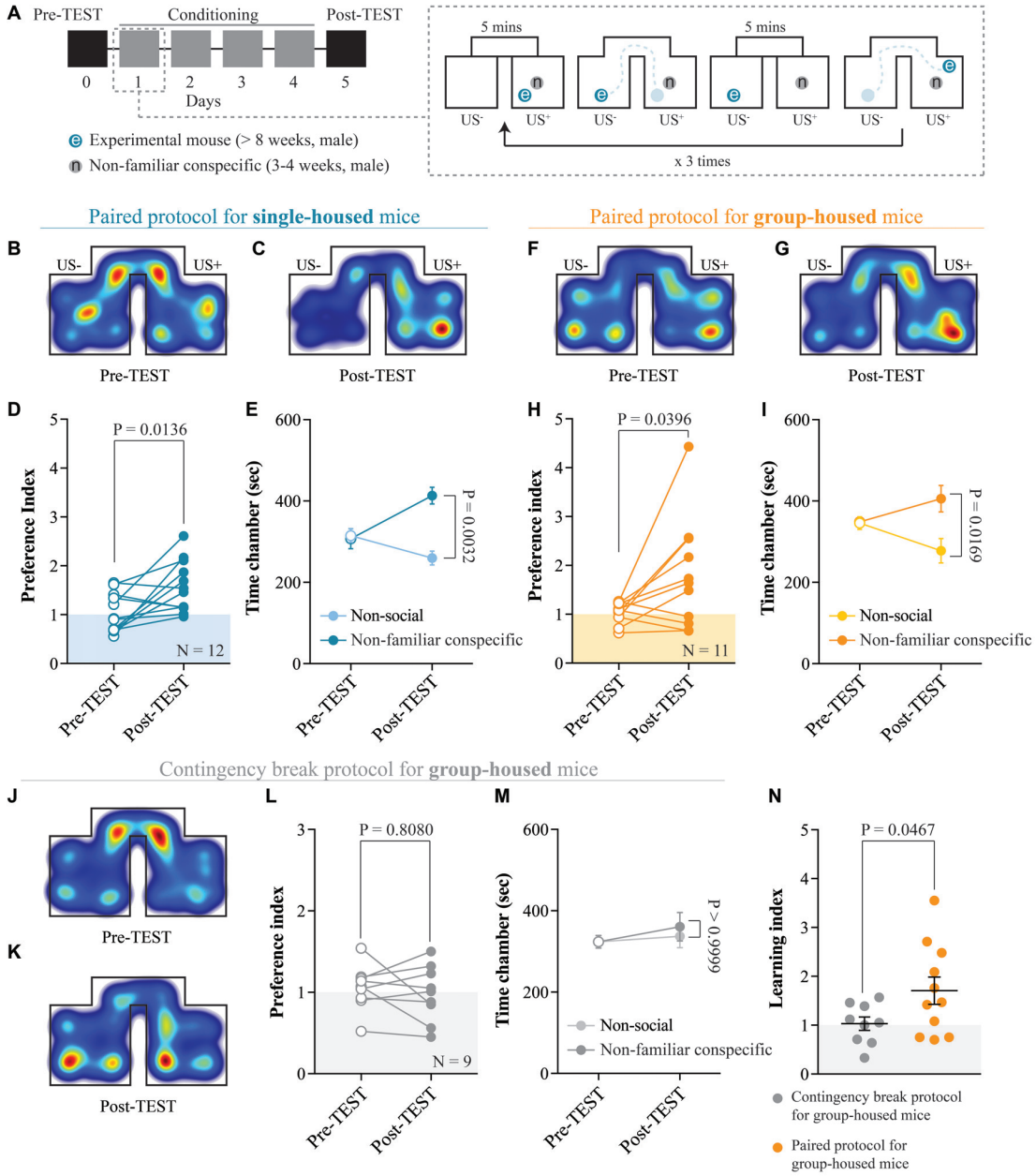

FIGURE 2 | Acquisition of non-familiar conspecific-induced CPP does not require single-housing. **(A)** Left: schematic representation of CPP time-course. Right: schematic representation of a single CPP conditioning alternation. **(B)** Representative apparatus occupancy heat-maps for single-housed mice during pre-TEST and **(C)** post-TEST. **(D)** Preference index calculated at pre- and post-TEST for single-housed mice ($N = 12$; paired t-test: $t_{(11)} = 2.934$; $P = 0.0136$). **(E)** Time spent in non-social and non-familiar conspecific-paired chambers for single-housed mice during pre- and post-TEST ($N = 12$; two-way RM ANOVA: time × chamber interaction: $F_{(1,11)} = 4.021$, $P = 0.0702$; main effect chamber: $F_{(1,11)} = 9.85$, $P = 0.0094$; main effect time: $F_{(1,11)} = 6.363$, $P = 0.0284$; followed by Bonferroni's multiple comparisons test). **(F)** Representative apparatus occupancy heat-maps for group-housed animals at pre-TEST and **(G)** post-TEST. **(H)** Preference index calculated at pre- and post-TEST for group-housed mice ($N = 11$; paired t-test: $t_{(10)} = 2.366$; $P = 0.0396$). **(I)** Time spent in the non-social and non-familiar conspecific-associated chambers for group-housed mice during pre- and post-TEST ($N = 11$; two-way RM ANOVA: time × chamber interaction: $F_{(1,10)} = 5.115$, $P = 0.0472$; main effect chamber: $F_{(1,10)} = 3.019$, $P = 0.1129$; main effect time: $F_{(1,10)} = 0.2936$, $P = 0.5998$; followed by Bonferroni's multiple comparisons test). **(J)** Representative apparatus occupancy heat-maps of group-housed mice subject to CPP contingency break at pre-TEST and **(K)** post-TEST. **(L)** Preference index of group-housed mice subjected to CPP contingency break calculated at pre- and post-TEST ($N = 9$; paired t-test: $t_{(8)} = 0.6537$; $P = 0.8080$). **(M)** Time spent in the two chambers of the apparatus for group-housed mice subjected to CPP contingency break during pre- and post-TEST (the chambers were assigned a non-social and non-familiar property for analyses purposes; $N = 9$; two-way RM ANOVA: time × chamber interaction: $F_{(1,8)} = 0.1864$, $P = 0.6773$; main effect chamber: $F_{(1,8)} = 0.1024$, $P = 0.7572$; main effect time: $F_{(1,8)} = 2.401$, $P = 0.1599$; followed by Bonferroni's multiple comparisons test). **(N)** Learning index calculated for group-housed mice subjected to either a contingency break ($N = 9$) or a paired protocol CPP ($N = 11$; unpaired t-test with Welch's correction: $t_{(14.4)} = 2.175$; $P = 0.0467$). N indicates number of mice. Abbreviations: US, unconditioned stimulus.

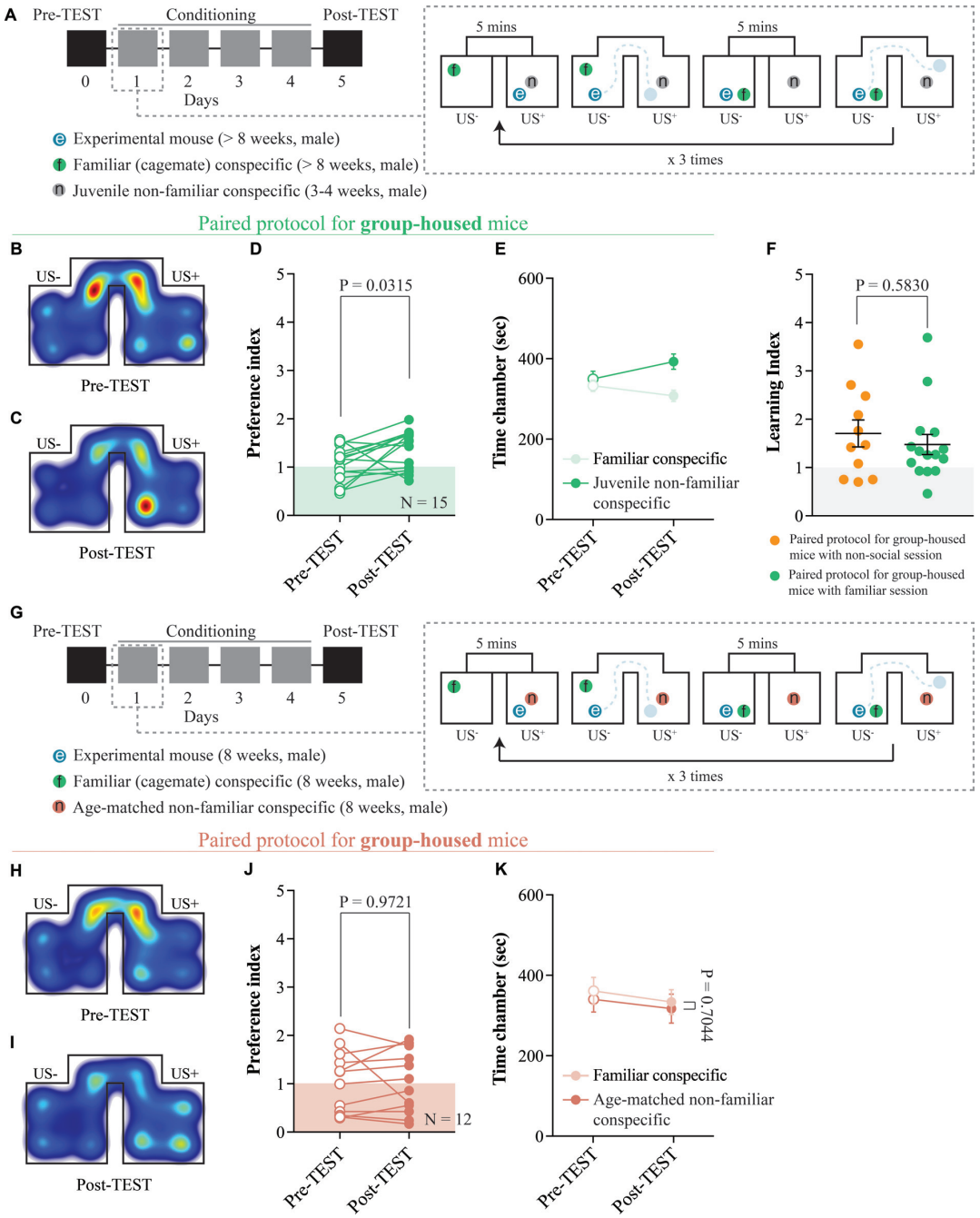

FIGURE 3 | The interaction with a juvenile non-familiar conspecific is reinforcing. **(A)** Left: schematic representation of CPP time-course. Right: schematic representation of a single CPP conditioning alternation between a familiar session and a non-familiar conspecific session. **(B)** Representative apparatus occupancy heat-maps during pre-TEST and **(C)** post-TEST for group-housed mice subjected to this protocol. **(D)** Preference index calculated at pre- and post-TEST for group-housed mice subjected to this protocol ($N = 15$; paired t-test: $t_{(14)} = 2.389$; $P = 0.0315$). **(E)** Time spent in familiar and non-familiar conspecific-paired chambers for group-housed mice subjected to this protocol during pre- and post-TEST ($N = 15$; two-way RM ANOVA: time × chamber interaction: $F_{(1,14)} = 4.525$, $P = 0.0517$; main effect chamber: $F_{(1,14)} = 3.416$, $P = 0.0858$; main effect time: $F_{(1,14)} = 1.657$, $P = 0.2189$). **(F)** Learning index calculated for group-housed mice subjected to either the protocol reported in **Figure 2A** ($N = 11$) or the protocol reported here in **(A)** ($N = 15$; Mann-Whitney test; $P = 0.5830$). **(G)** Left: schematic representation of CPP time-course. Right: schematic representation of a single CPP conditioning alternation between a familiar session and a non-familiar conspecific session. **(H)** Representative apparatus occupancy heat-maps during pre-TEST and **(I)** post-TEST for group-housed mice subjected to this protocol. **(J)** Preference index calculated at pre- and post-TEST for group-housed mice subjected to this protocol ($N = 12$; paired t-test: $t_{(11)} = 0.0358$; $P = 0.9721$). **(K)** Time spent in familiar and non-familiar conspecific-paired chambers for group-housed mice subjected to this protocol during pre- and post-TEST ($N = 12$; two-way RM ANOVA: time × chamber interaction: $F_{(1,11)} = 0.0157$, $P = 0.9026$; main effect chamber: $F_{(1,11)} = 0.0927$, $P = 0.7665$; main effect time: $F_{(1,11)} = 11.1$, $P = 0.0067$). N indicates number of mice. Abbreviations: US, unconditioned stimulus.

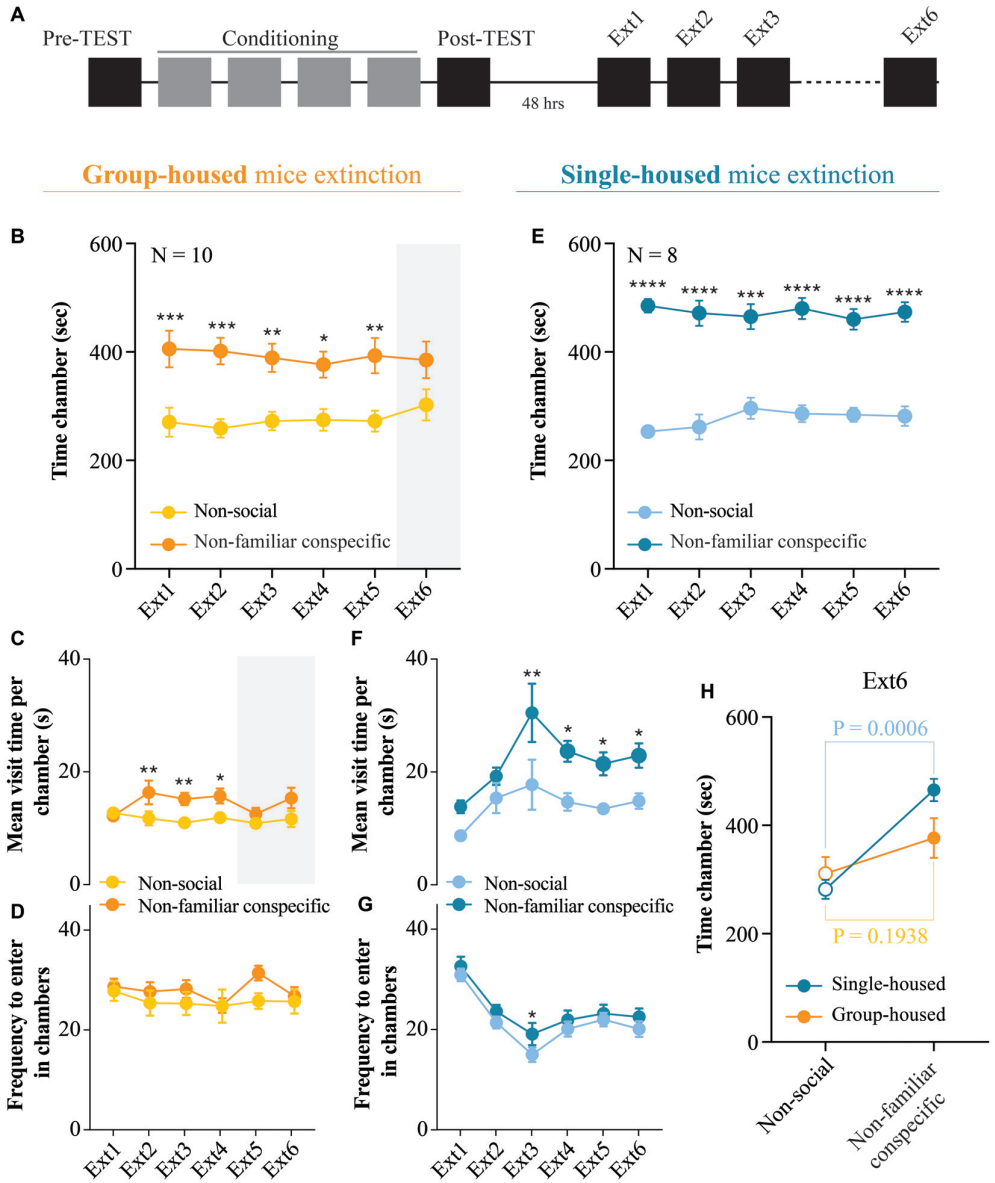

FIGURE 4 | Extinction of non-familiar conspecific-induced CPP is affected by housing condition. **(A)** Schematic representation of CPP acquisition and extinction. **(B)** Time spent in non-social and non-familiar conspecific-paired chambers across extinction sessions for group-housed mice subjected to CPP (N = 10; two-way RM ANOVA: time × chamber interaction: $F_{(5,45)}$ = 0.4486, P = 0.8120; main effect chamber: $F_{(1,9)}$ = 8.484, P = 0.0172; main effect time: $F_{(5,45)}$ = 1.25, P = 0.3021; followed by Bonferroni's multiple comparisons test). **(C)** Mean visit time spent in non-social and non-familiar conspecific-paired chambers across extinction sessions for group-housed mice subjected to CPP (N = 10; two-way RM ANOVA: time × chamber interaction: $F_{(5,45)}$ = 2.642, P = 0.0354; main effect chamber: $F_{(1,9)}$ = 9.002, P = 0.0149; main effect time: $F_{(5,45)}$ = 1.589, P = 0.1827; followed by Bonferroni's multiple comparisons test). **(D)** Frequency to enter in non-social and non-familiar conspecific-paired chambers across extinction sessions for group-housed mice subjected to CPP (N = 10; two-way RM ANOVA: time × chamber interaction: $F_{(5,45)}$ = 1.215, P = 0.3175; main effect chamber: $F_{(1,9)}$ = 2.086, P = 0.1826; main effect time: $F_{(5,45)}$ = 1.361, P = 0.2568). **(E)** Time spent in non-social and non-familiar conspecific-paired chambers across extinction sessions for single-housed mice (N = 8) subjected to a paired protocol (two-way RM ANOVA: time × chamber interaction: $F_{(5,35)}$ = 1.037, P = 0.4113; main effect chamber: $F_{(1,7)}$ = 78.38, P < 0.0001; main effect time: $F_{(5,35)}$ = 0.997, P = 0.4339; followed by Bonferroni's multiple comparisons test). **(F)** Mean visit time spent in non-social and non-familiar conspecific-paired chambers across extinction sessions for single-housed mice (N = 8) subjected to a paired protocol (two-way RM ANOVA: time × chamber interaction: $F_{(5,35)}$ = 0.6993, P = 0.6268; main effect chamber: $F_{(1,7)}$ = 11.16, P = 0.0086; main effect time: $F_{(5,35)}$ = 9.897, P < 0.0001; followed by Bonferroni's multiple comparisons test). **(G)** Frequency to enter in non-social and non-familiar conspecific-paired chambers across extinction sessions for single-housed mice (N = 8) subjected to a paired protocol (two-way RM ANOVA: time × chamber interaction: $F_{(5,35)}$ = 0.6539, P = 0.6600; main effect chamber: $F_{(1,7)}$ = 5.746, P = 0.0401; main effect time: $F_{(5,35)}$ = 18.08, P < 0.0001; followed by Bonferroni's multiple comparisons test). **(H)** Time spent in non-social or non-familiar conspecific-paired chamber at extinction session 6 for single-housed (N = 8) and group-housed (N = 10) mice (two-way ANOVA: time × group: $F_{(1,32)}$ = 3.316, P = 0.0780; main effect group: $F_{(1,32)}$ = 1.149, P = 0.2917; main effect time: $F_{(1,32)}$ = 23.09, P < 0.0001; followed by Bonferroni's multiple comparisons test). N indicates number of mice. Significance: *p < 0.05, **p < 0.01, ***p < 0.001, ****p < 0.0001.

index at the post-TEST/preference index at the pre-TEST). Confirming the validity of the non-familiar conspecific-induced CPP protocol, group-housed mice conditioned with the pairing protocol displayed a significantly higher learning index compared to animals subjected to the contingency break protocol (**Figure 2N**).

The Interaction With a Juvenile, But Not Age-Matched, Non-familiar Conspecific Is Reinforcing

To understand whether the novelty component associated with non-familiar social stimuli is necessary to promote contextual learning, we assessed whether group-housed mice would develop any preference for either an age-matched familiar or a non-familiar juvenile mouse-paired context. By subjecting the animals to conditioning sessions in which they interacted with a non-familiar and a familiar stimulus in different chambers (**Figures 1D**, **3A**), we observed an increase in the preference for the non-familiar conspecific-associated one (**Figures 3B–D**). Additionally, at the post-TEST, mice spent more time in the non-familiar conspecific-paired compartment compared to the one paired with a familiar mouse (**Figure 3E**). Finally, by comparing the learning index obtained from pairing protocols with either non-social session or familiar session, we found no differences in place preference acquisition (**Figure 3F**). Interestingly, when we subjected the animals to conditioning sessions in which they interacted with an age-matched non-familiar and a familiar stimulus in different chambers, we did not observe any preference (**Figures 3G–K**). Altogether, these results indicate that the social interaction with a non-familiar conspecific juvenile is reinforcing and that while the age of the stimulus plays an important role, the CPP is neither driven by social familiarity nor non-social pairing.

Extinction of Non-familiar Conspecific-Induced CPP Is Affected by Housing the Condition

Considering that after the post-TEST, in adolescent rats, social-induced CPP responses are lost within three single exposures to the empty CPP apparatus (Trezza et al., 2009), we investigated whether the non-familiar conspecific-induced conditioned responses can also be extinguished. Thus, we exposed our experimental animals to six extinction sessions, as previously reported (Trezza et al., 2009). Starting 48 h after the post-TEST, both single-housed and group-housed mice freely explored the empty apparatus for 15 min once per day over 6 days (**Figure 4A**). During early extinction sessions, group-housed mice displayed longer exploration of the non-familiar conspecific-associated chamber as compared to the chamber where no social stimulus was present (**Figure 4B**). Moreover, group-housed mice showed an increased duration of the visit of non-familiar conspecific- compared to non-social compartment (**Figure 4C**), while no changes in the number of transitions in each chamber were observed (**Figure 4D**). At extinction session 6, group-housed mice lost their preference for the non-familiar-associated chamber (**Figure 4B**). However, single-housed mice spent a longer time in the non-familiar conspecific-associated compared to non-social compartment throughout all the extinction session performed (**Figure 4E**) and engaged in longer visits of non-familiar conspecific-associated chamber (**Figures 4F,G**). Thus, it is evident that at the sixth extinction session, while group-housed mice extinguished their preference for non-familiar conspecific-associated compartment, single-housed mice retained it (**Figure 4H**). Altogether, these results indicate that while housing conditions do not induce major changes in the acquisition of the non-familiar conspecific-induced CPP, single-housing affects the extinction of contextual associations induced by free interaction with a novel conspecific.

VTA SHANK3 Downregulation Alters the Exploration of Non-familiar Conspecific Without Affecting CPP

Post-natal downregulation of the ASD-related protein SHANK3 in the VTA induces deficits in synaptic transmission, plasticity and social preference dynamics (Bariselli et al., 2016). Since both the excitatory transmission and plasticity at those inputs are essential for associative learning and extinction of reward-induced conditioned responses, we investigated the effects of VTA *Shank3* downregulation on the acquisition and extinction of non-familiar conspecific-induced CPP. More precisely, we downregulated *Shank3* in the VTA of neonatal mice (as previously described in Bariselli et al., 2016; **Figure 5A**), and we group-housed them after weaning for about 5 weeks. At 8 weeks of age (late adolescence), VTA-scrShank3 and VTA-shShank3 mice underwent non-familiar conspecific CPP acquisition and were subsequently sacrificed for histological validation (**Figure 5B**). By performing qPCR experiments on dissected midbrain regions, we found a pronounced downregulation of the longest SHANK3a transcript in AAV-shShank3 compared to AAV-scrShank3 infected animals (**Figure 5C**). This reduction was confirmed by normalizing the levels of the *Shank3a* mRNA to the mRNA encoding for the TH enzyme (**Figure 5D**), a marker of dopaminergic neurons (Stamatakis et al., 2013).

The downregulation of the ASD-associated protein Neuroligin 3 from VTA DA neurons induces an aberrant habituation to non-familiar conspecifics (Bariselli et al., 2018). To assess whether SHANK3 insufficiency at VTA neurons could induce a similar phenotype, we monitored both the distance moved and the reciprocal interaction of VTA-shShank3 and VTA-scrShank3 mice with their social stimuli. We observed that, while VTA-scrShank3 mice showed a progressive reduction in the interaction with the same social stimulus across conditioning days, VTA-shShank3 mice did not habituate to the social stimuli (**Figure 5E**). Importantly, these behavioral deficits were not associated with changes in the distance moved (**Figure 5F**).

When comparing pre- and post-TEST, VTA-scrShank3 mice increased their preference for the non-familiar conspecific-paired chamber (**Figures 5G–I**) and, at the Post-TEST, they displayed a longer exploration of the non-familiar conspecific-associated chamber (**Figure 5J**). When VTA-shShank3 mice were conditioned, they showed a trend towards a higher

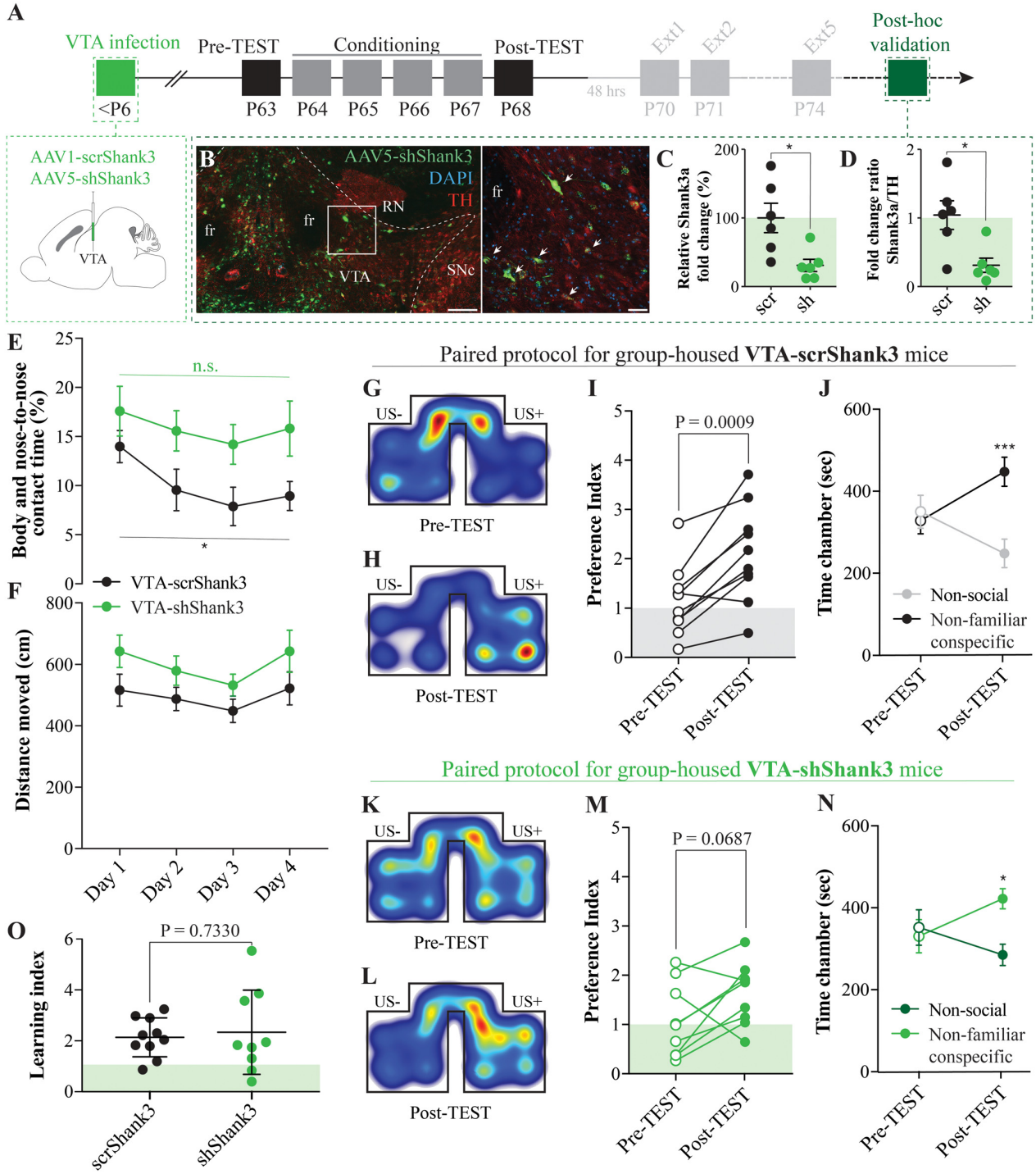

FIGURE 5 | Ventral tegmental area (VTA) SHANK3 downregulation alters the exploration of non-familiar conspecific without affecting CPP. **(A)** Experimental time course of AAV-scrShank3/AAV-shShank3 VTA infection, CPP acquisition, extinction and *post hoc* histological verification of viral infection and effect. **(B)** Histological validation of VTA infection (scale bar: left panel: 150 μm, right panel: 50 μm; white arrows indicate tyrosine hydroxylase (TH)-shShank3 colocalization). **(C)** Relative expression of Shank3a after infection of AAV-scrShank3/AAV-shShank3 in the VTA (unpaired *t*-test: $t_{(10)} = 2.972$; $P = 0.0140$). **(D)** Ratio between Shank3a and TH expression after AAV-scrShank3/AAV-shShank3 infection in the VTA (Mann-Whitney test: $P = 0.0152$). **(E)** Body and nose-to-nose contact time during conditioning days for group-housed VTA-scrShank3 mice ($N = 10$) and VTA-shShank3 ($N = 9$) mice (two-way ANOVA: time × group interaction: $F_{(3,51)} = 0.4552$, $P = 0.7148$; group main effect: $F_{(1,17)} = 4.894$, $P = 0.0409$; main effect time: $F_{(3,51)} = 4.363$, $P = 0.0082$; followed by Bonferroni's multiple comparisons test). **(F)** Distance moved in the arena during conditioning days for group-housed VTA-scrShank3 mice ($N = 10$) and VTA-shShank3 ($N = 9$) mice (two-way ANOVA: time × group interaction:

(*Continued*)

FIGURE 5 | Continued
$F_{(3,51)} = 0.2209$, $P = 0.8814$; group main effect: $F_{(1,17)} = 3.388$, $P = 0.0832$; main effect time: $F_{(3,51)} = 3.707$, $P = 0.0173$). **(G)** Representative occupancy heat-maps for group-housed VTA-scrShank3 mice at pre-TEST and **(H)** post-TEST. **(I)** Preference index calculated at pre- and post-TEST for group-housed VTA-scrShank3 mice ($N = 10$; paired t-test: $t_{(9)} = 4.827$; $P = 0.0009$). **(J)** Time spent in non-social and non-familiar conspecific-paired chamber for group-housed VTA-scrShank3 mice during pre- and post-TEST ($N = 10$; two-way RM ANOVA: time × chamber interaction: $F_{(1,9)} = 25.35$, $P = 0.0007$; main effect chamber: $F_{(1,9)} = 1.918$, $P = 0.1994$; main effect time: $F_{(1,9)} = 0.4628$, $P = 0.5134$; followed by Bonferroni's multiple comparisons test). **(K)** Representative occupancy heat-maps for group-housed VTA-shShank3 mice at pre-TEST and **(L)** post-TEST. **(M)** Preference index calculated at pre- and post-TEST for group-housed VTA-shShank3 mice ($N = 9$; paired t-test: $t_{(8)} = 2.103$; $P = 0.0687$). **(N)** Time spent in non-social and non-familiar conspecific-paired chamber for group-housed VTA-shShank3 mice during pre- and post-TEST ($N = 9$; two-way RM ANOVA: time × chamber interaction: $F_{(1,8)} = 4.943$, $P = 0.0329$; main effect chamber: $F_{(1,8)} = 2.651$, $P = 0.1027$; main effect time: $F_{(1,8)} = 0.119$, $P = 0.7322$; followed by Bonferroni's multiple comparisons test). **(O)** Learning index calculated for VTA-scrShank3 ($N = 10$) and VTA-shShank3 ($N = 9$; unpaired t-test: $t_{(17)} = 0.3468$; $P = 0.7330$). N indicates number of mice. Abbreviations: US, unconditioned stimulus; fr, fasciculus retroflexus; SNc, substantia nigra pars compacta; RN, red nucleus. $^{*}p < 0.05$, $^{***}p < 0.001$.

preference index between pre- and post-TEST (**Figures 5K–M**), and a significant preference for the non-familiar conspecific-associated chamber vs. the non-social chamber at the post-TEST (**Figure 5N**). Since the learning index of VTA-shShank3 mice was comparable to the one measured from VTA-scrShank3, we concluded that *Shank3* downregulation in the VTA was not inducing major abnormalities in the acquisition of non-familiar conspecific-induced CPP (**Figure 5O**).

VTA SHANK3 Downregulation Alters the Extinction of Non-familiar Conspecific-Induced CPP

After 48 h, VTA-scrShank3 mice underwent an extinction protocol (**Figure 6A**) and, by the extinction session 5, they no longer displayed a preference for the non-familiar conspecific-paired chamber (**Figure 6B**). The extinction of the CPP at extinction 5 in VTA-scrShank3 mice was associated with a similar mean duration of the visits of non-familiar conspecific vs. non-social associated chamber (**Figure 6C**), with no differences in the number of transitions within the two compartments (**Figure 6D**). When VTA-shShank3 mice underwent extinction, we noticed that their preference for the non-familiar conspecific-paired chamber was not stable over time and already not significant by the fourth extinction session (**Figure 6E**). This effect was accompanied by a similar duration of the mean visit time of the two compartments at several extinction sessions (**Figures 6F,G**). To directly compare the extinction of non-familiar conspecific-induced place preference between VTA-scrShank3 and VTA-shShank3 mice, we compared the preference index across pre-TEST, post-TEST and extinction sessions. We found that VTA-shShank3, compared to VTA-scrShank3, had a significantly lower preference index, particularly during early extinction sessions indicating an accelerated extinction (**Figure 6H**). Importantly, VTA-shShank3 mice showed an increased distance moved during the experiment as compared to VTA-scrShank3 (**Figure 6I**).

DISCUSSION

Here, we tested whether the downregulation of the ASD-associated gene *Shank3* in the VTA is sufficient to alter the reinforcing properties of social interaction in mice and the extinction of the social-induced contextual associations. Reinforcing properties of social interactions have been previously tested by using protocols that require single-housing before and/or during conditioning. Here, by characterizing a modified version of previously published CPP paradigms, we show that while housing conditions (single-housing vs. group-housing) do not affect the acquisition of a preference for the compartment associated with a non-familiar conspecific, it influences the extinction of non-familiar conspecific-induced contextual associations. By using the newly characterized CPP protocol, we show that the downregulation of *Shank3* impairs habituation to non-familiar conspecifics and accelerates the extinction of social-induced contextual associations.

Direct and Free Interaction With a Juvenile Non-familiar Conspecific Promotes Contextual Learning in Group-Housed C57Bl/6j Mice

Social novelty recognition induces territorial urinary marking (Arakawa et al., 2008), increases exploratory behavior (Ferguson et al., 2000), and produces exploratory preference, which is only expressed during the first 5 min of the three-chamber task (Nadler et al., 2004). For these reasons, we developed a CPP paradigm that requires short (5 min) and repeated episodes of free and direct interaction with a juvenile non-familiar sex-matched social stimulus (Bariselli et al., 2018). Contrary to what has been previously reported (Calcagnetti and Schechter, 1992; Thiel et al., 2008; Fritz et al., 2011; Kummer et al., 2011; Molas et al., 2017), we demonstrate that single-housing is not a necessary condition for the acquisition of a social-induced CPP. However, in the present study, we found that the direct interaction with a non-familiar juvenile mouse is necessary for social-induced contextual learning, which is not observed when experimental and stimuli subjects are age-matched. This difference could be the consequence of offensive behaviors. Considering that offensive behavior is a trait expressed by C57Bl/6 male mice (Crawley et al., 1997) and that aggression promotes place preference in CD1 male mice (Golden et al., 2016), further investigation is needed to address the role of antagonistic and offensive behavior in the acquisition of non-familiar conspecific-induced CPP. Additionally, considering the impact of sexual hormones on the acquisition of reward-induced place preference (Calipari et al., 2017), future studies will need to assess the acquisition of non-familiar conspecific-induced place preference in female mice at various stages of their estrous cycle.

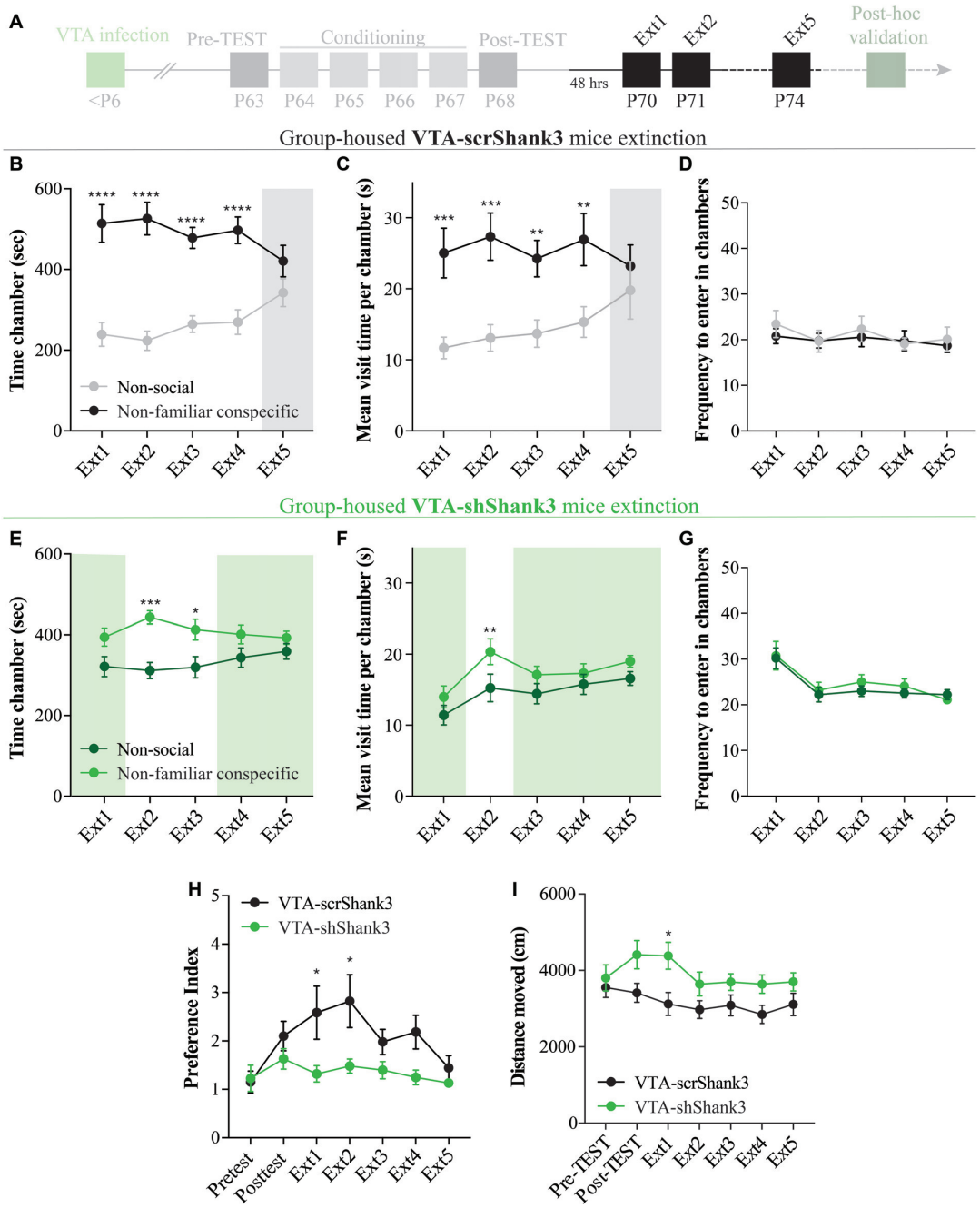

FIGURE 6 | VTA SHANK3 downregulation alters the extinction of non-familiar conspecific-induced CPP. **(A)** Experimental time course of AAV-scrShank3/AAV-shShank3 VTA infection, CPP acquisition and extinction. **(B)** Time spent in non-social and non-familiar conspecific-paired chamber for group-housed VTA-scrShank3 mice across extinction sessions ($N = 10$; two-way RM ANOVA: time × chamber interaction: $F_{(4,36)} = 4.624$, $P = 0.0041$; main effect chamber: $F_{(1,9)} = 18.32$, $P = 0.0020$; main effect time: $F_{(4,36)} = 1.126$, $P = 0.3595$; followed by Bonferroni's multiple comparisons test). **(C)** Mean visit time spent in non-social and non-familiar conspecific-paired chambers across extinction sessions for group-housed VTA-scrShank3 mice subjected to CPP ($N = 10$; two-way RM ANOVA: time × chamber interaction: $F_{(4,36)} = 2.097$, $P = 0.1043$; main effect chamber: $F_{(1,9)} = 23.93$, $P = 0.0012$; main effect time: $F_{(4,36)} = 0.889$, $P = 0.4817$; followed by Bonferroni's multiple comparisons test). **(D)** Frequency to enter in non-social and non-familiar conspecific-paired chambers across extinction sessions for group-housed VTA-scrShank3 mice subjected to CPP ($N = 10$; two-way RM ANOVA: time × chamber interaction: $F_{(4,36)} = 1.443$, $P = 0.2399$; main effect chamber: $F_{(1,9)} = 0.3101$, $P = 0.5912$; main effect time: $F_{(4,36)} = 0.5925$, $P = 0.6703$). **(E)** Time spent in non-social and non-familiar conspecific-paired chambers for group-housed VTA-shShank3 mice during extinction ($N = 9$; two-way ANOVA: time × chamber interaction: $F_{(4,32)} = 1.453$, $P = 0.2394$; main effect chamber: $F_{(1,8)} = 6.002$, $P = 0.0399$; main effect time: $F_{(4,32)} = 4.226$, $P = 0.0074$; followed by Bonferroni's multiple comparisons test). **(F)** Mean visit time spent in non-social and non-familiar conspecific-paired chambers across extinction sessions for group-housed VTA-shShank3 mice subjected to CPP

(*Continued*)

FIGURE 6 | Continued
(N = 9; two-way RM ANOVA: time × chamber interaction: $F_{(4,32)}$ = 1.168, P = 0.3433; main effect chamber: $F_{(1,8)}$ = 4.496, P = 0.0671; main effect time: $F_{(4,32)}$ = 8.131, P = 0.0001; followed by Bonferroni's multiple comparisons test). **(G)** Frequency to enter in non-social and non-familiar conspecific-paired chambers across extinction sessions for group-housed VTA-shShank3 mice subjected to CPP (N = 9; two-way RM ANOVA: time × chamber interaction: $F_{(4,32)}$ = 1.708, P = 0.1725; main effect chamber: $F_{(1,8)}$ = 0.6025, P = 0.4600; main effect time: $F_{(4,32)}$ = 9.554, $P < 0.0001$). **(H)** Preference index calculated during pre-TEST, post-TEST and extinction sessions for group-housed VTA-scrShank3 mice (N = 10) and VTA-shShank3 (N = 9) mice (two-way ANOVA: time × group interaction: $F_{(6,102)}$ = 2.118, P = 0.0575; group main effect: $F_{(1,17)}$ = 5.436, P = 0.0323; main effect time: $F_{(6,102)}$ = 4.953, P = 0.0002; followed by Bonferroni's multiple comparisons test). **(I)** Distance moved in the arena during pre-TEST, post-TEST and extinction sessions for group-housed VTA-scrShank3 mice (N = 10) and VTA-shShank3 (N = 9) mice (two-way ANOVA: time × group interaction: $F_{(6,102)}$ = 3.056, P = 0.0086; group main effect: $F_{(1,17)}$ = 4.211, P = 0.0550; main effect time: $F_{(6,102)}$ = 7.497, $P < 0.0001$; followed by Bonferroni's multiple comparisons test). N indicates number of mice. Significance: $^{*}p < 0.05$, $^{**}p < 0.01$, $^{***}p < 0.001$, $^{****}p < 0.0001$.

Single-Housing Affects the Extinction of Contextual Associations Induced by Non-familiar Interaction

Social-induced CPP undergoes extinction in adolescent rats (Trezza et al., 2009), and we demonstrated that social-induced conditioned responses could be induced and also lost in late adolescent mice. However, we found that housing conditions affect the extinction of the preference for the non-familiar conspecific-paired chamber. In single-housed compared to group-housed animals, the decreased rate of extinction of these conditioned responses might be due to the increased strength of the association between contextual cues (CS) and the presence of a non-familiar conspecific, which would strongly counteract the new association (CS-absence of social stimuli). The increased strength of the associations in single-housed mice could stem from the increased subjective value of social stimuli during the acquisition of the non-familiar conspecific-induced CPP as a consequence of the absence of social contacts in their home-cage. In fact, the saliency of social events is modulated by social context, as, compared to non-lonely individuals, lonely individuals convey higher attention and accuracy in decoding social cues (Pickett et al., 2004) and have a greater ability to recall socially-related information. Alternatively, the absence of social contacts in the home-cage during extinction might favor, in the presence of the contextual cues previously associated with social interaction availability, a behavioral strategy that maximizes the probability of engaging in social interactions (e.g., spending more time in the chamber paired with the exposure to a non-familiar conspecific). Also, in this case, the influence of the primary association on the behavioral outcome would be increased at the expense of the new CS-absence of social interaction association, thus resulting in a reduced extinction of the conditioned response. Considering the effects of single-housing on the extinction of non-familiar conspecific-induced CPP, investigating the behavioral and neuronal mal-adaptations induced by social isolation on the acquisition and extinction of social-induced conditioned responses might be beneficial for individuals affected by "loneliness" (*Cacioppo JT and Cacioppo S, The Lancet, "The growing problem of loneliness"*).

Shank3 Downregulation in the VTA Accelerates the Extinction of Non-familiar Conspecific-Induced CPP

In recent years, several genetic mouse models have been developed to study the involvement of each SHANK3 variant in synaptic and social behavior impairments (Bariselli and Bellone, 2016). The elimination of the major Shank3 isoforms induces aberrant social novelty recognition and social preference (Peça et al., 2011), the latter rescued by Shank3 re-expression at adulthood (Mei et al., 2016). Other mutants, with targeted mutation within the exon 4–9 sequence displayed sociability impairments (Wang et al., 2011) and altered male-female interaction (Bozdagi et al., 2010), while mice lacking Shank3 Pro-rich domain and exon 13 displayed altered social novelty recognition (Kouser et al., 2013; Jaramillo et al., 2017). Other behavioral traits, such as increased dominance has been reported in mice with point mutations of *Shank3* (Zhou et al., 2016). However, *Shank3* mutants lacking the exon 4–22 and exon 9, for example, displayed intact sociability (Wang et al., 2017; Bey et al., 2018). Moreover, considering the differential expression of *Shank3* across neuronal populations (Wang et al., 2014), specific behavioral tests are needed to assess the role of the protein in a discrete neuronal circuit. Previously, we showed that the developmental downregulation of *Shank3* in the VTA impaired social preference dynamics (Bariselli et al., 2016), pointing at a deficit in social motivation. Here, we found that insufficiency of SHANK3 in the VTA produces an aberrant habituation to non-familiar social stimuli, which is similar to our observation in another ASD-relevant animal model lacking Neuroligin 3 expression in VTA DA neurons (Bariselli et al., 2018). This indicates that different ASD-relevant mutations, within the same neuronal circuit, might lead to similar behavioral aberrancies.

Interestingly, we found that, although VTA-shShank3 mice discriminated between non-familiar conspecific-paired and non-social compartment at the post-TEST, they showed only a statistical trend towards an increase in their preference for the non-familiar conspecific-paired compartment before and after conditioning. These results might indicate subtle deficits in acquisition of non-familiar conspecific-induced contextual association. However, when VTA-shShank3 mice were repeatedly exposed to contextual cues in the absence of the social stimulus animal, their preference for the non-familiar conspecific-paired chamber became erratic and revealed an accelerated rate of extinction. This effect could be due to a reduced strength of the association as a consequence of *Shank3* downregulation in the VTA. According to the hypothesis that extinction is learning a new association, it is also plausible that in VTA-shShank3 mice the new association might easily overpower the weak primary association, thus resulting in an accelerated disappearance of the conditioned responses. To our knowledge, this is the first time that an extinction deficit is reported in

an ASD-related genetic dysfunction restricted to the VTA, but further investigation is warranted to understand the behavioral and neurobiological mechanisms underlying aberrant learning and extinction of those associations.

In conclusion, the CPP is a behavioral procedure classically used to assess the reinforcing properties of drugs of abuse and natural rewards. The observation of social-induced CPP in group-housed mice demonstrates that direct social interaction with a non-familiar conspecific can be reinforcing and can be studied without the confounding behavioral and neurobiological mal-adaptations induced by social isolation. Extinction and reinstatement of drug-induced CPP responses are behavioral procedures used to assess "drug-seeking" behavior in mice (Itzhak and Martin, 2002). For this reason, many studies have focused their attention on the cellular, synaptic and circuit adaptations that underlie "drug-seeking" behavior to facilitate extinction, to reduce reinstatement (Thanos et al., 2009; Voigt et al., 2011; Malvaez et al., 2013; Prast et al., 2014) and, ultimately, to aid the research for treating addiction. Similarly, the methods of extinction, and possibly reinstatement, of non-familiar conspecific-induced CPP responses are a way to observe and assess "social-seeking" behavior in mice. This paradigm could prove instrumental in identifying mechanisms underlying "social-seeking," and help to find pharmacological targets to promote social-induced learning in ASD patients.

AUTHOR CONTRIBUTIONS

SB, AC and ST performed the behavioral experiments. SB and AC prepared the figures. SM performed the qPCR analysis. SB and CB designed the study and wrote the manuscript.

FUNDING

CB is supported by the Swiss National Science Foundation, Pierre Mercier Foundation and NCCR Synapsy.

ACKNOWLEDGMENTS

We thank Jeremy Pantone, Giulia Casarotto and Lorena Jourdain for their technical contributions to the behavioral experiments and the histological validation.

REFERENCES

Adamantidis, A. R., Tsai, H.-C., Boutrel, B., Zhang, F., Stuber, G. D., Budygin, E. A., et al. (2011). Optogenetic interrogation of dopaminergic modulation of the multiple phases of reward-seeking behavior. *J. Neurosci.* 31, 10829–10835. doi: 10.1523/JNEUROSCI.2246-11.2011

Arakawa, H., Arakawa, K., Blanchard, D. C., and Blanchard, R. J. (2008). A new test paradigm for social recognition evidenced by urinary scent marking behavior in C57BL/6J mice. *Behav. Brain Res.* 190, 97–104. doi: 10.1016/j.bbr.2008.02.009

Bariselli, S., and Bellone, C. (2016). VTA DA neuron excitatory synapses in *Shank3* Δex^{4-9} mouse line. *Synapse* 71:e21955. doi: 10.1002/syn.21955

Bariselli, S., Hörnberg, H., Prévost-Solié, C., Musardo, S., Hatstatt-Burklé, L., Scheiffele, P., et al. (2018). Role of VTA dopamine neurons and neuroligin 3 in sociability traits related to nonfamiliar conspecific interaction. *Nat. Commun.* 9:3173. doi: 10.1038/s41467-018-05382-3

Bariselli, S., Tzanoulinou, S., Glangetas, C., Prévost-Solié, C., Pucci, L., Viguié, J., et al. (2016). SHANK3 controls maturation of social reward circuits in the VTA. *Nat. Neurosci.* 19, 926–934. doi: 10.1038/nn.4319

Bey, A. L., Wang, X., Yan, H., Kim, N., Passman, R. L., Yang, Y., et al. (2018). Brain region-specific disruption of *Shank3* in mice reveals a dissociation for cortical and striatal circuits in autism-related behaviors. *Transl. Psychiatry* 8:94. doi: 10.1038/s41398-018-0142-6

Bouton, M. E. (2004). Context and behavioral processes in extinction. *Learn. Mem.* 11, 485–494. doi: 10.1101/lm.78804

Bozdagi, O., Sakurai, T., Papapetrou, D., Wang, X., Dickstein, D. L., Takahashi, N., et al. (2010). Haploinsufficiency of the autism-associated Shank3 gene leads to deficits in synaptic function, social interaction and social communication. *Mol. Autism* 1:15. doi: 10.1186/2040-2392-1-15

Calcagnetti, D. J., and Schechter, M. D. (1992). Place conditioning reveals the rewarding aspect of social interaction in juvenile rats. *Physiol. Behav.* 51, 667–672. doi: 10.1016/0031-9384(92)90101-7

Calipari, E. S., Juarez, B., Morel, C., Walker, D. M., Cahill, M. E., Ribeiro, E., et al. (2017). Dopaminergic dynamics underlying sex-specific cocaine reward. *Nat. Commun.* 8:13877. doi: 10.1038/ncomms13877

Chevallier, C., Kohls, G., Troiani, V., Brodkin, E. S., and Schultz, R. T. (2012). The social motivation theory of autism. *Trends Cogn. Sci.* 16, 231–239. doi: 10.1016/j.tics.2012.02.007

Cohen, J. Y., Haesler, S., Vong, L., Lowell, B. B., and Uchida, N. (2012). Neuron-type-specific signals for reward and punishment in the ventral tegmental area. *Nature* 482, 85–88. doi: 10.1038/nature10754

Crawley, J. N., Belknap, J. K., Collins, A., Crabbe, J. C., Frankel, W., Henderson, N., et al. (1997). Behavioral phenotypes of inbred mouse strains: implications and recommendations for molecular studies. *Psychopharmacology* 132, 107–124. doi: 10.1007/s002130050327

Crowder, W. F., and Hutto, C. W. (1992). Operant place conditioning measures examined using two nondrug reinforcers. *Pharmacol. Biochem. Behav.* 41, 817–824. doi: 10.1016/0091-3057(92)90233-6

Cunningham, C. L., Howard, M. A., Gill, S. J., Rubinstein, M., Low, M. J., and Grandy, D. K. (2000). Ethanol-conditioned place preference is reduced in dopamine D2 receptor-deficient mice. *Pharmacol. Biochem. Behav.* 67, 693–699. doi: 10.1016/s0091-3057(00)00414-7

Dölen, G., Darvishzadeh, A., Huang, K. W., and Malenka, R. C. (2013). Social reward requires coordinated activity of nucleus accumbens oxytocin and serotonin. *Nature* 501, 179–184. doi: 10.1038/nature12518

Drapeau, E., Dorr, N. P., Elder, G. A., and Buxbaum, J. D. (2014). Absence of strong strain effects in behavioral analyses of Shank3-deficient mice. *Dis. Model. Mech.* 7, 667–681. doi: 10.1242/dmm.013821

Dunsmoor, J. E., Niv, Y., Daw, N., and Phelps, E. A. (2015). Rethinking extinction. *Neuron* 88, 47–63. doi: 10.1016/j.neuron.2015.09.028

El Rawas, R., Klement, S., Kummer, K. K., Fritz, M., Dechant, G., Saria, A., et al. (2012). Brain regions associated with the acquisition of conditioned place preference for cocaine vs. social interaction. *Front. Behav. Neurosci.* 6:63. doi: 10.3389/fnbeh.2012.00063

Engblom, D., Bilbao, A., Sanchis-Segura, C., Dahan, L., Perreau-Lenz, S., Balland, B., et al. (2008). Glutamate receptors on dopamine neurons control the persistence of cocaine seeking. *Neuron* 59, 497–508. doi: 10.1016/j.neuron.2008.07.010

Ferguson, J. N., Young, L. J., Hearn, E. F., Matzuk, M. M., Insel, T. R., and Winslow, J. T. (2000). Social amnesia in mice lacking the oxytocin gene. *Nat. Genet.* 25, 284–288. doi: 10.1038/77040

Ferhat, A.-T., Halbedl, S., Schmeisser, M. J., Kas, M. J., Bourgeron, T., and Ey, E. (2017). Behavioural phenotypes and neural circuit dysfunctions in mouse models of autism spectrum disorder. *Adv. Anat. Embryol. Cell Biol.* 224, 85–101. doi: 10.1007/978-3-319-52498-6_5

Fritz, M., El Rawas, R., Salti, A., Klement, S., Bardo, M. T., Kemmler, G., et al. (2011). Reversal of cocaine-conditioned place preference and mesocorticolimbic Zif268 expression by social interaction in rats. *Addict. Biol.* 16, 273–284. doi: 10.1111/j.1369-1600.2010.00285.x

Golden, S. A., Heshmati, M., Flanigan, M., Christoffel, D. J., Guise, K., Pfau, M. L., et al. (2016). Basal forebrain projections to the lateral habenula modulate aggression reward. *Nature* 534, 688–692. doi: 10.1038/nature18601

Hoffman, D. C., and Beninger, R. J. (1989). The effects of selective dopamine D1 or D2 receptor antagonists on the establishment of agonist-induced place conditioning in rats. *Pharmacol. Biochem. Behav.* 33, 273–279. doi: 10.1016/0091-3057(89)90499-1

Huang, W., Placzek, A. N., Di Prisco, G. V., Khatiwada, S., Sidrauski, C., Krnjević, K., et al. (2016). Translational control by eIF2α phosphorylation regulates vulnerability to the synaptic and behavioral effects of cocaine. *Elife* 5:e12052. doi: 10.7554/eLife.12052

Hung, L. W., Neuner, S., Polepalli, J. S., Beier, K. T., Wright, M., Walsh, J. J., et al. (2017). Gating of social reward by oxytocin in the ventral tegmental area. *Science* 357, 1406–1411. doi: 10.1126/science.aan4994

Itzhak, Y., and Martin, J. L. (2002). Cocaine-induced conditioned place preference in mice: induction, extinction and reinstatement by related psychostimulants. *Neuropsychopharmacology* 26, 130–134. doi: 10.1016/s0893-133x(01)00303-7

Jaramillo, T. C., Speed, H. E., Xuan, Z., Reimers, J. M., Escamilla, C. O., Weaver, T. P., et al. (2017). Novel Shank3 mutant exhibits behaviors with face validity for autism and altered striatal and hippocampal function. *Autism Res.* 10, 42–65. doi: 10.1002/aur.1664

Jiang, Y.-H., and Ehlers, M. D. (2013). Modeling autism by SHANK gene mutations in mice. *Neuron* 78, 8–27. doi: 10.1016/j.neuron.2013.03.016

Kouser, M., Speed, H. E., Dewey, C. M., Reimers, J. M., Widman, A. J., Gupta, N., et al. (2013). Loss of predominant Shank3 isoforms results in hippocampus-dependent impairments in behavior and synaptic transmission. *J. Neurosci.* 33, 18448–18468. doi: 10.1523/JNEUROSCI.3017-13.2013

Kummer, K., Klement, S., Eggart, V., Mayr, M. J., Saria, A., and Zernig, G. (2011). Conditioned place preference for social interaction in rats: contribution of sensory components. *Front. Behav. Neurosci.* 5:80. doi: 10.3389/fnbeh.2011.00080

Lahvis, G. P., Panksepp, J. B., Kennedy, B. C., Wilson, C. R., and Merriman, D. K. (2015). Social conditioned place preference in the captive ground squirrel *(Ictidomys tridecemlineatus)*: social reward as a natural phenotype. *J. Comp. Psychol.* 129, 291–303. doi: 10.1037/a0039435

Le Foll, B., Sokoloff, P., Stark, H., and Goldberg, S. R. (2005). Dopamine D3 receptor ligands block nicotine-induced conditioned place preferences through a mechanism that does not involve discriminative-stimulus or antidepressant-like effects. *Psychosom. Med.* 30, 720–730. doi: 10.1038/sj.npp.1300622

Livak, K. J., and Schmittgen, T. D. (2001). Analysis of relative gene expression data using real-time quantitative PCR and the $2^{-\Delta\Delta C_T}$ method. *Methods* 25, 402–408. doi: 10.1006/meth.2001.1262

Malvaez, M., McQuown, S. C., Rogge, G. A., Astarabadi, M., Jacques, V., Carreiro, S., et al. (2013). HDAC3-selective inhibitor enhances extinction of cocaine-seeking behavior in a persistent manner. *Proc. Natl. Acad. Sci. U S A* 110, 2647–2652. doi: 10.1073/pnas.1213364110

Mei, Y., Monteiro, P., Zhou, Y., Kim, J.-A., Gao, X., Fu, Z., et al. (2016). Adult restoration of Shank3 expression rescues selective autistic-like phenotypes. *Nature* 530, 481–484. doi: 10.1038/nature16971

Molas, S., Zhao-Shea, R., Liu, L., DeGroot, S. R., Gardner, P. D., and Tapper, A. R. (2017). A circuit-based mechanism underlying familiarity signaling and the preference for novelty. *Nat. Neurosci.* 20, 1260–1268. doi: 10.1038/nn.4607

Nadler, J. J., Moy, S. S., Dold, G., Trang, D., Simmons, N., Perez, A., et al. (2004). Automated apparatus for quantitation of social approach behaviors in mice. *Genes Brain Behav.* 3, 303–314. doi: 10.1111/j.1601-183x.2004.00071.x

Naisbitt, S., Kim, E., Tu, J. C., Xiao, B., Sala, C., Valtschanoff, J., et al. (1999). Shank, a novel family of postsynaptic density proteins that binds to the NMDA receptor/PSD-95/GKAP complex and cortactin. *Neuron* 23, 569–582. doi: 10.1016/s0896-6273(00)80809-0

Panksepp, J., and Beatty, W. W. (1980). Social deprivation and play in rats. *Behav. Neural Biol.* 30, 197–206. doi: 10.1016/s0163-1047(80)91077-8

Panksepp, J. B., and Lahvis, G. P. (2007). Social reward among juvenile mice. *Genes Brain Behav.* 6, 661–671. doi: 10.1111/j.1601-183x.2006.00295.x

Peça, J., Feliciano, C., Ting, J. T., Wang, W., Wells, M. F., Venkatraman, T. N., et al. (2011). *Shank3* mutant mice display autistic-like behaviours and striatal dysfunction. *Nature* 472, 437–442. doi: 10.1038/nature09965

Pickett, C. L., Gardner, W. L., and Knowles, M. (2004). Getting a cue: the need to belong and enhanced sensitivity to social cues. *Pers. Soc. Psychol. Bull.* 30, 1095–1107. doi: 10.1177/0146167203262085

Prast, J. M., Schardl, A., Schwarzer, C., Dechant, G., Saria, A., and Zernig, G. (2014). Reacquisition of cocaine conditioned place preference and its inhibition by previous social interaction preferentially affect D1-medium spiny neurons in the accumbens corridor. *Front. Behav. Neurosci.* 8:317. doi: 10.3389/fnbeh.2014.00317

Quirk, G. J., and Mueller, D. (2008). Neural mechanisms of extinction learning and retrieval. *Neuropsychopharmacology* 33, 56–72. doi: 10.1038/sj.npp.1301555

Rezayof, A., Zarrindast, M.-R., Sahraei, H., and Haeri-Rohani, A.-H.-R. (2002). Involvement of dopamine D2 receptors of the central amygdala on the acquisition and expression of morphine-induced place preference in rat. *Pharmacol. Biochem. Behav.* 74, 187–197. doi: 10.1016/s0091-3057(02)00989-9

Schultz, W., Dayan, P., and Montague, P. R. (1997). A neural substrate of prediction and reward. *Science* 275, 1593–1599. doi: 10.1126/science.275.5306.1593

Scott-Van Zeeland, A. A., Dapretto, M., Ghahremani, D. G., Poldrack, R. A., and Bookheimer, S. Y. (2010). Reward processing in autism. *Autism Res.* 3, 53–67. doi: 10.1002/aur.122

Stamatakis, A. M., Jennings, J. H., Ung, R. L., Blair, G. A., Weinberg, R. J., Neve, R. L., et al. (2013). A unique population of ventral tegmental area neurons inhibits the lateral habenula to promote reward. *Neuron* 80, 1039–1053. doi: 10.1016/j.neuron.2013.08.023

Stuber, G. D., Klanker, M., de Ridder, B., Bowers, M. S., Joosten, R. N., Feenstra, M. G., et al. (2008). Reward-predictive cues enhance excitatory synaptic strength onto midbrain dopamine neurons. *Science* 321, 1690–1692. doi: 10.1126/science.1160873

Thanos, P. K., Bermeo, C., Wang, G.-J., and Volkow, N. D. (2009). D-cycloserine accelerates the extinction of cocaine-induced conditioned place preference in C57bL/c mice. *Behav. Brain Res.* 199, 345–349. doi: 10.1016/j.bbr.2008.12.025

Thiel, K. J., Okun, A. C., and Neisewander, J. L. (2008). Social reward-conditioned place preference: a model revealing an interaction between cocaine and social context rewards in rats. *Drug Alcohol Depend.* 96, 202–212. doi: 10.1016/j.drugalcdep.2008.02.013

Trezza, V., Damsteegt, R., and Vanderschuren, L. J. M. J. (2009). Conditioned place preference induced by social play behavior: parametrics, extinction, reinstatement and disruption by methylphenidate. *Eur. Neuropsychopharmacol.* 19, 659–669. doi: 10.1016/j.euroneuro.2009.03.006

Tsai, H.-C., Zhang, F., Adamantidis, A., Stuber, G. D., Bonci, A., de Lecea, L., et al. (2009). Phasic firing in dopaminergic neurons is sufficient for behavioral conditioning. *Science* 324, 1080–1084. doi: 10.1126/science.1168878

Tzschentke, T. M. (2007). Measuring reward with the conditioned place preference (CPP) paradigm: update of the last decade. *Addict. Biol.* 12, 227–462. doi: 10.1111/j.1369-1600.2007.00070.x

Van den Berg, C. L., Pijlman, F. T., Koning, H. A., Diergaarde, L., Van Ree, J. M., and Spruijt, B. M. (1999). Isolation changes the incentive value of sucrose and social behaviour in juvenile and adult rats. *Behav. Brain Res.* 106, 133–142. doi: 10.1016/s0166-4328(99)00099-6

Vanderschuren, L. J., Stein, E. A., Wiegant, V. M., and Van Ree, J. M. (1995). Social isolation and social interaction alter regional brain opioid receptor binding in rats. *Eur. Neuropsychopharmacol.* 5, 119–127. doi: 10.1016/0924-977x(95)00010-m

Vidal-Infer, A., Roger-Sánchez, C., Daza-Losada, M., Aguilar, M. A., Miñarro, J., and Rodríguez-Arias, M. (2012). Role of the dopaminergic system in the acquisition, expression and reinstatement of MDMA-induced conditioned place preference in adolescent mice. *PLoS One* 7:e43107. doi: 10.1371/journal.pone.0043107

Voigt, R. M., Herrold, A. A., and Napier, T. C. (2011). Baclofen facilitates the extinction of methamphetamine-induced conditioned place preference in rats. *Behav. Neurosci.* 125, 261–267. doi: 10.1037/a0022893

Wang, X., Bey, A. L., Katz, B. M., Badea, A., Kim, N., David, L. K., et al. (2016). Altered mGluR5-Homer scaffolds and corticostriatal connectivity in a Shank3 complete knockout model of autism. *Nat. Commun.* 7:11459. doi: 10.1038/ncomms11459

Wang, W., Li, C., Chen, Q., van der Goes, M.-S., Hawrot, J., Yao, A. Y., et al. (2017). Striatopallidal dysfunction underlies repetitive behavior in *Shank3*-deficient model of autism. *J. Clin. Invest.* 127, 1978–1990. doi: 10.1172/JCI87997

Wang, X., McCoy, P. A., Rodriguiz, R. M., Pan, Y., Je, H. S., Roberts, A. C., et al. (2011). Synaptic dysfunction and abnormal behaviors in mice lacking major isoforms of *Shank3*. *Hum. Mol. Genet.* 20, 3093–3108. doi: 10.1093/hmg/ddr212

Wang, X., Xu, Q., Bey, A. L., Lee, Y., and Jiang, Y.-H. (2014). Transcriptional and functional complexity of *Shank3* provides a molecular framework to understand the phenotypic heterogeneity of *SHANK3* causing autism and *Shank3* mutant mice. *Mol. Autism* 5:30. doi: 10.1186/2040-2392-5-30

Whitaker, L. R., Degoulet, M., and Morikawa, H. (2013). Social deprivation enhances VTA synaptic plasticity and drug-induced contextual learning. *Neuron* 77, 335–345. doi: 10.1016/j.neuron.2012.11.022

Yang, M., Bozdagi, O., Scattoni, M. L., Wöhr, M., Roullet, F. I., Katz, A. M., et al. (2012). Reduced excitatory neurotransmission and mild autism-relevant phenotypes in adolescent *Shank3* null mutant mice. *J. Neurosci.* 32, 6525–6541. doi: 10.1523/JNEUROSCI.6107-11.2012

Zhou, Y., Kaiser, T., Monteiro, P., Zhang, X., Van der Goes, M. S., Wang, D., et al. (2016). Mice with *Shank3* mutations associated with ASD and schizophrenia display both shared and distinct defects. *Neuron* 89, 147–162. doi: 10.1016/j.neuron.2015.11.023

Conflict of Interest Statement: The authors declare that the research was conducted in the absence of any commercial or financial relationships that could be construed as a potential conflict of interest.

frontiers in Cellular Neuroscience

ORIGINAL RESEARCH
published: 22 October 2018
doi: 10.3389/fncel.2018.00374

Dietary Zinc Supplementation Prevents Autism Related Behaviors and Striatal Synaptic Dysfunction in *Shank3* Exon 13–16 Mutant Mice

Chantelle Fourie[1], *Yukti Vyas*[1], *Kevin Lee*[1], *Yewon Jung*[1], *Craig C. Garner*[2] *and Johanna M. Montgomery*[1]*

[1]Department of Physiology and Centre for Brain Research, University of Auckland, Auckland, New Zealand, [2]German Center for Neurodegenerative Disorders, Charité-Universitätsmedizin Berlin, Berlin, Germany

The SHANK family of synaptic proteins (SHANK1–3) are master regulators of the organizational structure of excitatory synapses in the brain. Mutations in *SHANK1–3* are prevalent in patients with autism spectrum disorders (ASD), and loss of one copy of *SHANK3* causes Phelan-McDermid Syndrome, a syndrome in which Autism occurs in >80% of cases. The synaptic stability of SHANK3 is highly regulated by zinc, driving the formation of postsynaptic protein complexes and increases in excitatory synaptic strength. As ASD-associated SHANK3 mutations retain responsiveness to zinc, here we investigated how increasing levels of dietary zinc could alter behavioral and synaptic deficits that occur with ASD. We performed behavioral testing together with cortico-striatal slice electrophysiology on a *Shank3*$^{-/-}$ mouse model of ASD (*Shank3*$^{ex13-1616-/-}$), which displays ASD-related behaviors and structural and functional deficits at striatal synapses. We observed that 6 weeks of dietary zinc supplementation in *Shank3*$^{ex13-16-/-}$ mice prevented ASD-related repetitive and anxiety behaviors and deficits in social novelty recognition. Dietary zinc supplementation also increased the recruitment of zinc sensitive SHANK2 to synapses, reduced synaptic transmission specifically through *N*-methyl-D-aspartate (NMDA)-type glutamate receptors, reversed the slowed decay tau of NMDA receptor (NMDAR)-mediated currents and occluded long term potentiation (LTP) at cortico-striatal synapses. These data suggest that alterations in NMDAR function underlie the lack of NMDAR-dependent cortico-striatal LTP and contribute to the reversal of ASD-related behaviors such as compulsive grooming. Our data reveal that dietary zinc alters neurological function from synapses to behavior, and identifies dietary zinc as a potential therapeutic agent in ASD.

Keywords: autism, SHANK3, zinc, synapse, NMDA receptor

OPEN ACCESS

Edited by:
Tobias Maria Boeckers, Universität Ulm, Germany

Reviewed by:
Michael J. Schmeisser, Medizinische Fakultät, Universitätsklinikum Magdeburg, Germany
Francesca Prestori, University of Pavia, Italy

***Correspondence:**
Johanna M. Montgomery
jm.montgomery@auckland.ac.nz

Received: *23 March 2018*
Accepted: *01 October 2018*
Published: *22 October 2018*

Citation:
Fourie C, Vyas Y, Lee K, Jung Y, Garner CC and Montgomery JM (2018) Dietary Zinc Supplementation Prevents Autism Related Behaviors and Striatal Synaptic Dysfunction in Shank3 Exon 13–16 Mutant Mice. Front. Cell. Neurosci. 12:374. doi: 10.3389/fncel.2018.00374

INTRODUCTION

The SHANK family of proteins (SHANK1–3) are localized at the core of the postsynaptic density (PSD) at glutamatergic synapses where they bind to structural proteins, glutamate receptors, and the actin cytoskeleton to modulate the structure, plasticity and maturation of excitatory synapses (Boeckers et al., 2002; Kreienkamp, 2008). SHANK proteins display a temporal

expression pattern at synapses, with SHANK2 being one of the first proteins concentrated at the developing PSD, followed by SHANK3 and SHANK1 (Bresler et al., 2004; Grabrucker et al., 2011a). SHANK3 strengthens glutamatergic α-amino-3-hydroxy-5-methyl-4-isoxazolepropionic acid receptor (AMPAR) and *N*-methyl-D-aspartate receptor (NMDAR) mediated synaptic transmission and increases glutamate release via the formation of trans-synaptic signaling complexes with neurexin and neuroligin (Arons et al., 2012). Multiple point mutations, deletions, and truncations occur in *SHANK1–3* in people with autism spectrum disorders (ASD), with *SHANK3* mutations mainly found in ASD individuals with moderate to severe intellectual disability (Leblond et al., 2014). In addition, loss of one copy of *SHANK3* causes Phelan-McDermid or 22q13 deletion syndrome, a syndrome in which Autism occurs in >80% of cases (Wilson et al., 2003; Phelan and McDermid, 2012; Soorya et al., 2013). ASD and 22q13 mutations in *SHANK3* disrupt AMPAR and NMDAR signaling and interfere with the ability of SHANK3 to alter presynaptic function via trans-synaptic signaling (Arons et al., 2012). Mouse models expressing ASD mutations in *Shank1–3* exhibit impaired glutamatergic synaptic function, decreased synaptic plasticity, increased anxiety and repetitive behaviors and impaired social interactions (Hung et al., 2008; Bozdagi et al., 2010; Peca et al., 2011; Schmeisser et al., 2012; Duffney et al., 2013; Lee et al., 2015; Speed et al., 2015; Mei et al., 2016). Moreover, restoring excitatory synaptic function (e.g., by altering NMDA or metabotropic-type glutamate receptor function, or restoring *Shank3* expression) improves ASD-related behaviors (Won et al., 2012; Chung et al., 2015; Lee et al., 2015; Mei et al., 2016). Therefore, glutamatergic synapses are a major focus for developing treatments for the behavioral deficits associated with ASD.

The C-terminal sterile alpha motif (SAM) domains in SHANK2 and SHANK3 are high affinity zinc binding sites (Boeckers et al., 2005), and zinc stabilizes synaptic SHANK localization and promotes the recruitment of pre- and postsynaptic protein complexes to excitatory synapses (Baron et al., 2006; Grabrucker et al., 2014; Arons et al., 2016). SHANK proteins containing ASD mutations retain their responsiveness to zinc: acute increases in zinc strengthen glutamatergic synaptic transmission and recruit postsynaptic protein complexes at excitatory synapses expressing ASD mutations in SHANK2 and SHANK3 (Lee et al., 2015; Arons et al., 2016), and trans-synaptic zinc mobilization reverses ASD-related behavioral deficits in *Shank2*$^{-/-}$ mice (Lee et al., 2015). Zinc is stored in glutamatergic synaptic vesicles where it is co-released with glutamate (Assaf and Chung, 1984; Howell et al., 1984; Westbrook and Mayer, 1987; Mayer and Vyklicky, 1989; Smart et al., 1994). Zinc enters the postsynapse via ion channels where it modulates synaptic transmission and plasticity (Mayer and Vyklicky, 1989; Izumi et al., 2006; Takeda et al., 2010; Pan et al., 2011). Zinc depletion induces disintegration of SHANK3 complexes and weakens glutamatergic synaptic strength (Arons et al., 2016). In human studies, chronic zinc deficiency is a risk factor for ASD, and low zinc levels have been reported in children with ASD (Faber et al., 2009; Yasuda et al., 2011). Together these data suggest that zinc mismanagement is a major factor in regulating both SHANK proteins at the cellular level and ASD at the behavioral level.

Here, we sought to determine whether dietary zinc supplementation is a viable strategy to rescue synaptic and behavioral deficits in *Shank3*$^{ex13-16-/-}$ mice that exhibit ASD-associated behavioral deficits and weakened synaptic function in the dorsolateral striatum (Peca et al., 2011). We performed behavioral and electrophysiological analysis on *Shank3*$^{ex13-16-/-}$ mice fed normal (30 ppm) or supplemented (150 ppm) zinc levels (Tallman and Taylor, 2003; Grabrucker et al., 2011b). Our data show that dietary zinc supplementation prevented ASD-associated behaviors by altering synaptic transmission through NMDARs as well as long term plasticity at cortico-striatal synapses.

MATERIALS AND METHODS

Animals

All animal experiments have been performed subject to regulations approved by the University of Auckland Animal Ethics Committee and adherence to the ARRIVE guidelines. *Shank3*$^{ex13-16-/-}$ mice (B6.129-*Shank3*^{tm2Gfng}/J; Peca et al., 2011) were imported from Jackson Laboratories, Bar Harbor, ME, USA and maintained at the University of Auckland, Auckland, New Zealand. Wild-type (WT), heterozygous and homozygous (Hom) mice were generated from heterozygous × heterozygous breeding pairs. All experimental animals were housed in a normal 12/12-h light dark cycle in groups of two to four per cage with mixed genotypes. Food and water were available *ad libitum*.

Experimental Design

Animals were randomly assigned to a normal zinc diet (30 ppm) or a zinc supplementation diet (150 ppm; Tallman and Taylor, 2003; Tran et al., 2009; Grabrucker et al., 2011b), purchased from Research Diets, Brunswick, NJ, USA (catalogs D19410B and D06041101, respectively) for 6 weeks from weaning (postnatal day 21). Aside from the zinc levels, the two diets were identical egg white based rodent diets. No adverse effects on animal health or development were evident on either diet. Behavioral, electrophysiological, and imaging experiments were performed at 9–10 weeks of age on males and females: in total 69 WT (38 male, 31 female) and 68 Hom (37 male and 31 female). Genotypes were determined by PCR as previously described (Peca et al., 2011). All experiments and analyses were performed with the experimenter blinded to genotype and zinc diet by independent animal coding with a unique identification number at weaning.

Behavioral Tests and Analysis

All behavioral experiments were recorded and analyzed with Ethovision (Noldus) software.

Grooming Behavior

Grooming behavior was recorded under low light conditions (40 lx), for 30 min and the time spent grooming during this period was timed. Grooming included face-wiping,

scratching/rubbing of head and ears, grooming of tail and full-body grooming (Chung et al., 2015; Pearson et al., 2011).

Dark-Light Emergence Test

Testing was conducted in a two-chambered apparatus where one chamber was in complete darkness and the other light (508 lx), with a door allowing mice to freely move between the two chambers. Mice were placed in the dark chamber for 5 min before the door was opened and the test mouse allowed to freely explore the apparatus for 10 min. The percentage of time spent in the light vs. dark chambers was used as an index of anxiety-like behaviors (Peca et al., 2011).

Three-Chamber Social Interaction Assay

The three-chamber social interaction assay was conducted under low light conditions (40 lx) and consisted of three phases, as previously described (Won et al., 2012; Lee et al., 2015). In the first phase, the test mouse was placed in the center chamber of the apparatus with two small containers in the left and right chamber, and was allowed to explore the environment freely for 10 min for habituation. The mouse was then guided to the center chamber, and the two side entrances were blocked while a stranger mouse (Stranger 1) was placed in one of the containers. Then, the two entrances were opened to allow the mouse to explore the new environment freely for 10 min. In the third phase, the test mouse was guided to the center chamber, and the entrances to the side chambers closed. A novel stranger mouse (Stranger 2) was then introduced into the empty container while the familiar (Stranger 1) mouse remained in the other container. The entrances were opened and the test mouse was allowed to explore Stranger 1 and 2 for 10 min. Social interaction was defined as the time the test mouse spent sniffing, orienting its nose towards, or interacting with the stranger mouse.

Cortico-Striatal Electrophysiology

Slice Preparation

Acute coronal cortico-striatal brain slices were prepared from 9 to 10 week-old mice, based on previous studies (Peca et al., 2011; Ting et al., 2014). Mice utilized for electrophysiological analysis were independent from mice used for behavioral analysis. Mice were culled with CO_2, decapitated and the brains removed into carbogenated (95% O_2, 5% CO_2) ice-cold protective cutting artificial cerebrospinal fluid (ACSF) with the composition (in mM): 93 NMDG, 2.5 KCl, 1.25 NaH_2PO_4, 30 $NaHCO_3$, 20 HEPES, 25 glucose, 2 thiourea, 5 L-ascorbic acid, 3 Na-pyruvate, 0.5 $CaCl_2$, 10 $MgSO_4.7H_2O$, (pH 7.4, osmolarity of 295–305 mOsm). The brains were rapidly sectioned at 300 μm using a vibratome and slices transferred for recovery in protective cutting ACSF at 34°C. Slices were maintained at room temperature (RT) in a holding chamber in carbogenated recording ACSF with the composition (in mM): 97 NaCl, 2.5 KCl, 1.25 NaH_2PO_4, 30 $NaHCO_3$, 25 glucose, 20 HEPES, 2 $CaCl_2$, 2 $MgSO_4.7H_2O$, 2 thiourea, 5 L-ascorbic acid, 3 Na-pyruvate (pH 7.4 with osmolarity of 295–305 mOsm). Fast inhibitory currents were not blocked. The dorsolateral striatum and individual medium spiny neurons (MSNs) were visualized with a Zeiss Axioskop microscope equipped with IR-DIC optics.

Presynaptic Stimulation and Postsynaptic Current Recording

A platinum iridium concentric bipolar stimulating electrode was placed on the inner border of the corpus callosum between the cortex and dorsolateral striatum for presynaptic stimulation of glutamatergic inputs to the dorsolateral striatum. Stimulation was performed with a Digitimer constant current stimulator with pulses delivered at 0.1 Hz. Whole-cell patch-clamp recordings were obtained from MSNs using glass recording electrodes (resistance 6–8 MΩ) filled with internal solution [in mM: 120 K gluconate (or 120 Cs gluconate for NMDAR EPSCs), 40 HEPES, 5 $MgCl_2$, 2 NaATP, 0.3 NaGTP and 5 QX314 (for NMDAR EPSCs), pH 7.2, 298mOsm]. Membrane currents and potentials were processed with a Multiclamp 700B commander (Axon Instruments, California, CA, USA) and digitized at 10 KHz (Digidata 1440, Axon Instruments, California, CA, USA) to convert analog to digital signals. Events were sampled at 10 KHz and low-pass filtered at 1 KHz. Series resistance (Rs) was measured and recordings with Rs variation greater than 20% were discarded. All data acquisition and analysis were performed using pClamp 10 acquisition software and Clampfit 10, respectively (Axon Instruments, California, CA, USA).

AMPA- and NMDA Receptor Current Recording and Analysis

The maximum AMPAR mediated excitatory postsynaptic current (EPSC) amplitude was determined and the stimulator set to deliver pulses that produced 50% of this amplitude. To record isolated NMDAR EPSCs, 10 μM 6-Cyano-7-nitroquinoxaline-2,3-dione (CNQX) was bath applied to block the AMPAR EPSCs and each neuron voltage clamped at +40 mV. NMDAR EPSCs were measured in response to presynaptic stimulation (50 μA pulses at 0.1 Hz stimulation). NMDAR decay kinetics were measured as previously described (Cathala et al., 2000): a double exponential function was fitted from the current peak to the baseline: $I(t) = I_f\exp((-t/\tau_f) + I_s\exp((-t/\tau_s)$, where I_f and I_s are the amplitudes of the fast and slow decay components, and τ_f and τ_s are their respective decay time constants. To compare decay times between different experiments we used a weighted mean decay time constant: $\tau_w = [I_f/(I_f + I_s)]/\tau_f + [I_s/(I_f + I_s)]/\tau_s$.

Synaptic Plasticity

For long term potentiation (LTP) experiments, a 5-min baseline of AMPAR EPSCs was recorded in response to 0.1 Hz presynaptic stimulation. LTP was then induced via four presynaptic stimulation trains of 100 Hz for 1 s, with a 10 s interval between trains while the postsynaptic cell was voltage clamped at 0 mV (Fino et al., 2005). The post-LTP induction EPSCs were subsequently recorded at 0.1 Hz. The omission of extracellular Mg^{2+}, nor the inclusion of $GABA_A$ receptor blockers was required for the induction of LTP. In previous studies, high frequency stimulation has also been shown to induce long-term depression (LTD) of AMPAR EPSCs in MSNs in the striatum (Calabresi et al., 1993; Walsh, 1993; Lovinger, 2010). However, it should be noted that the placement of the stimulating electrode together with

the level of postsynaptic depolarization play a major role in the LTP vs. LTD induction protocol (Spencer and Murphy, 2000).

Immunohistochemistry, Confocal Imaging and Image Analysis

We performed immunohistochemistry on 50 μm coronal sections from 4% paraformaldehyde immersion fixed WT and *Shank3*$^{ex13-16-/-}$ mice fed normal (30 ppm) and supplemented (150 ppm) zinc levels for 6 weeks. The sections were permeablized overnight with 0.25% Triton X-100 in 1 × PBS (PBST) at 4°C, non-specific binding was blocked by incubation in 10% normal goat serum in 1× PBST and then sections were immunostained for SHANK2 (1:500, Santa Cruz Biotechnology), VGluT1 (1:500, Neuromab) or VGluT2 (Synaptic Systems, 1:500) for 72 h at 4°C. The sections were washed in 1 × PBST, incubated for 4 h at RT with secondary antibodies, then washed and incubated with Hoechst (Sigma) for 20 min at RT and slide mounted. The dorsal striatum was imaged via high-resolution confocal microscopy (OLYMPUS FV1000) at 60× magnification (1.35 NA) with 3× digital zoom using FluoView 3.0 image acquisition software. Laser power, amplifier gain and offset were optimized for each antibody to accommodate the dynamic range of the signal, and then settings were kept consistent for all subsequent imaging. For each section, z-stacks were obtained (10 images taken 0.5 μm apart) from three regions within the dorsal striatum. Puncta-by-puncta analysis was performed with ImageJ software where images were thresholded to select puncta above image background, and then the maximum intensity of SHANK2 co-localized with VGluT1 or VGluT2 (synaptic SHANK2) and SHANK2 not co-localized with VGluT1 or VGluT2 (non-synaptic SHANK2) were measured within the same field of view. The 3D Objects Counter tool was utilized in ImageJ to analyze puncta and identify Shank2 and VGluT1/2 colocalization in a 3-dimensional space captured by the z-stack. Each plane of the z-stack was analyzed individually to ensure only SHANK2 and VGluT1/2 puncta truly co-localized in each z-plane were captured.

Statistical Analysis

All data represent mean ± SEM. Statistical analyses were performed using Graphpad Prism 6.0, with a p value < 0.05 considered significant. Tests for normality and homogeneity of variances were performed with the Shapiro-Wilk normality test and the Browne-Forsythe and Bartlett's tests for variance, to determine whether parametric vs. non-parametric testing was applied. Details of each statistical test for each data set (one-way ANOVA with *post hoc* comparison, Kruskal Wallis or two-tailed student's *t*-test) are provided in the figure legends.

RESULTS

ASD-Related Behavioral Deficits Can Be Reversed by Dietary Zinc Supplementation

To determine whether chronic changes in dietary zinc can alter the ASD-associated synaptic and behavioral deficits that occur in the striatum of the *Shank3*$^{ex13-16-/-}$ ASD mouse model (Peca et al., 2011), *Shank3*$^{ex13-16-/-}$ mice were fed normal (30 ppm) or high (150 ppm) dietary zinc levels for 6 weeks followed by analysis of ASD-related behaviors as well as glutamatergic excitatory synaptic transmission and plasticity in the cortico-striatal pathway. As expected, repetitive grooming behaviors in homozygous mice receiving normal dietary zinc ($Shank3^{ex13-16-/-}_{30\ ppm}$) were significantly increased compared to WT controls on the normal zinc diet ($WT_{30\ ppm}$) (**Figure 1A**; percentage time grooming $WT_{30\ ppm}$: 5.28 ± 1.23, $Shank3^{ex13-16-/-}_{30\ ppm}$ 12.70 ± 2.92, $p < 0.05$; Peca et al., 2011). Increasing dietary zinc in WT mice ($WT_{150\ ppm}$) resulted in no significant change in grooming behavior (percentage time grooming $WT_{150\ ppm}$ 8.24 ± 2.35; $p > 0.05$, **Figure 1A**). Strikingly, the repetitive grooming behavior observed in

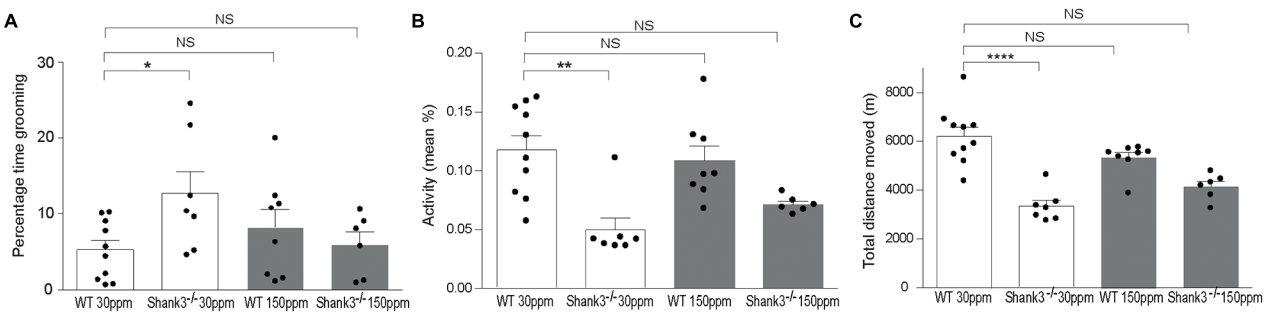

FIGURE 1 | *Shank3*$^{ex13-16-/-}$ autism spectrum disorder (ASD) mice repetitive grooming behaviors and reduced exploration behaviors are prevented with supplementation of dietary zinc. **(A)** Repetitive grooming in $Shank3^{ex13-16-/-}_{30\ ppm}$ mice was prevented in mice fed 150 ppm dietary zinc ($Shank3^{ex13-16-/-}_{150ppm}$). **(B)** Reduced exploratory behaviors in $Shank3^{ex13-16-/-}_{30\ ppm}$ mice, measured as a reduction in mean activity levels were no longer significantly different from Wild-type (WT) after dietary zinc supplementation. **(C)** Total distance moved by each mouse during the grooming test. Distance moved by *Shank3* $^{ex13-16-/-}$ mice was increased with 150 ppm dietary zinc ($Shank3^{ex13-16-/-}_{150\ ppm}$). All data represent mean ± SEM. Statistics: one-way ANOVA with Dunnett's *post hoc* test for **(A)** Kruskal-Wallis one-way ANOVA with Dunn's *post hoc* test was applied for **(B,C)** as not all groups were normally distributed and variances were not equal (see ""Materials and Methods" section). $WT_{30\ ppm}$ $n = 10$, $Shank3^{ex13-16-/-}_{30\ ppm}$ $n = 7$, $WT_{150\ ppm}$ $n = 8$, $Shank3^{ex13-16-/-}_{150\ ppm}$ $n = 6$ animals, $^{*}p < 0.05$, $^{**}p < 0.01$, $^{****}p < 0.0001$, NS, not significant.

Shank3$^{ex13-16-/-}$ mice was prevented when these mice were fed increased dietary zinc levels, such that the time spent grooming was no longer significantly different from WT mice (percentage time grooming *Shank3*$^{ex13-16-/-}_{150\ ppm}$ 6.00 ± 1.67, $p > 0.05$; **Figure 1A**). *Shank3*$^{ex13-16-/-}$ mice also displayed significantly decreased mean activity levels and total distance moved within the grooming arena compared with WT mice (**Figures 1B,C**; mean activity: $WT_{30\ ppm}$ 0.118 ± 0.012%, *Shank3*$^{ex13-16-/-}_{30\ ppm}$ 0.05 ± 0.01%, $p < 0.01$; total distance moved $WT_{30\ ppm}$ 6206.53 ± 366.88 cm, *Shank3*$^{ex13-16-/-}_{30\ ppm}$ 3339.97 ± 241.51 cm, $p < 0.01$). With increased dietary zinc, mean activity levels and total distance moved were no longer significantly decreased in *Shank3*$^{ex13-16-/-}_{150\ ppm}$ mice compared to WT controls (mean activity: *Shank3*$^{ex13-16-/-}_{150\ ppm}$ 0.072 ± 0.003%, $p > 0.05$; total distance moved *Shank3*$^{ex13-16-/-}_{150\ ppm}$ 4143.97 ± 219.47 cm, $p > 0.05$; **Figures 1B,C**). High dietary zinc did not significantly alter the activity and movement of WT mice (mean activity: $WT_{150\ ppm}$ 0.109 ± 0.012%; total distance moved $WT_{150\ ppm}$ 5326.71 ± 216.02 cm, $p > 0.05$ compared with $WT_{30\ ppm}$ mice in both cases).

Shank3$^{ex13-16-/-}_{30\ ppm}$ mice also displayed increased anxiety behavior, as assessed by the significant decrease in the percentage time spent in the light chamber in the dark-light emergence test compared with WT mice ($WT_{30\ ppm}$ 57.44 ± 3.54%, *Shank3*$^{ex13-16-/-}_{30\ ppm}$ 34.48 ± 5.41%; **Figures 2A,B**; $p < 0.01$; Peca et al., 2011). Increased dietary zinc did not significantly alter the percentage of time the WT mice spent in the light chamber ($WT_{150\ ppm}$ 53.25 ± 4.73%, $p > 0.05$; **Figures 2A,B**). *Shank3*$^{ex13-16-/-}$ mice fed high dietary zinc however spent a similar time in the light chamber as WT control mice, showing that the increase in anxiety in *Shank3*$^{ex13-16-/-}$ mice was also prevented by dietary zinc supplementation, rendering

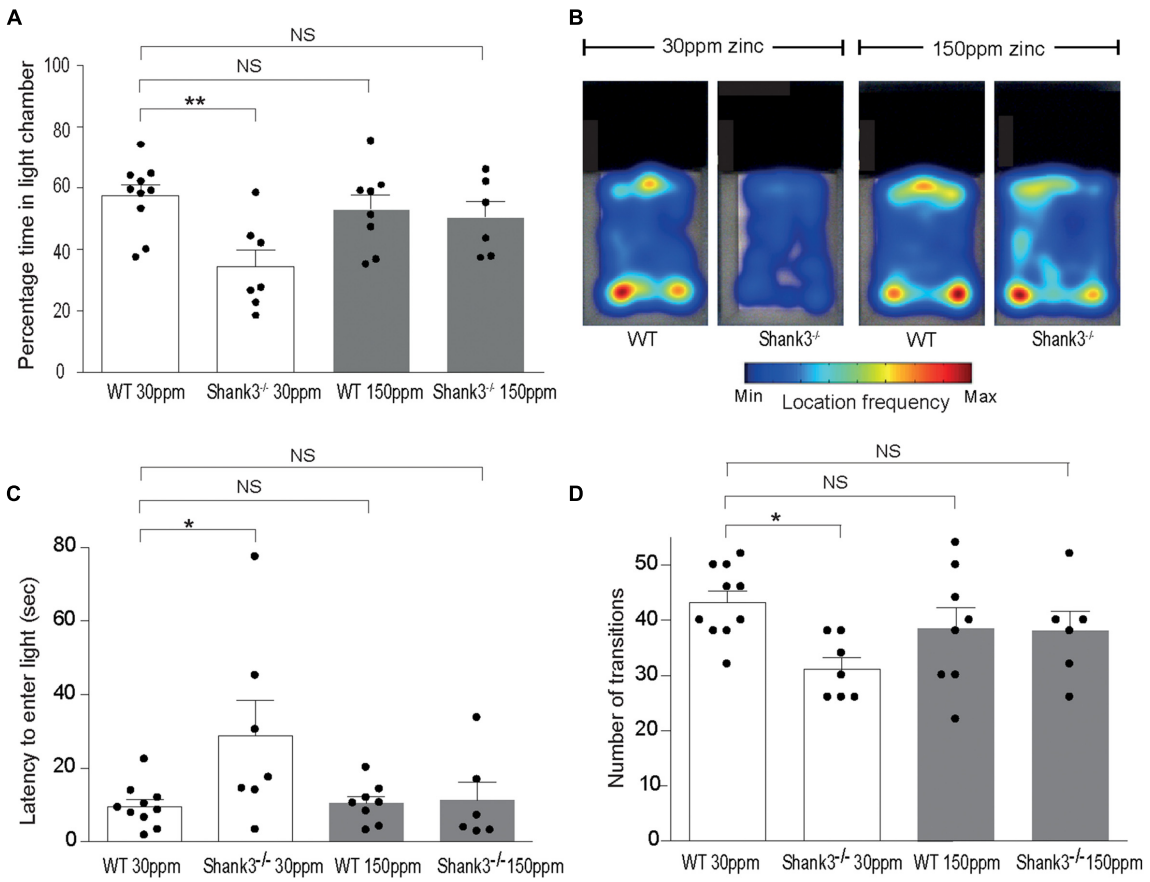

FIGURE 2 | ASD anxiety behaviors in *Shank3*$^{ex13-16-/-}$ mice are prevented with supplementation of dietary zinc. **(A)** Increased anxiety-type behaviors in *Shank3*$^{ex13-16-/-}_{30\ ppm}$ mice, reflected as a reduced percentage time spent in the light chamber, was prevented in mutant mice fed 150 ppm dietary zinc (*Shank3*$^{ex13-16-/-}_{150\ ppm}$). **(B)** Heat map example of WT and *Shank3*$^{ex13-16-/-}$ mice on 30 or 150 ppm dietary zinc. Note the significantly decreased time the *Shank3*$^{ex13-16-/-}_{30\ ppm}$ mice spend in the light, and how this increases in *Shank3*$^{ex13-16-/-}_{150\ ppm}$ mice. **(C)** *Shank3*$^{ex13-16-/-}_{30\ ppm}$ mice take significantly longer to first exit the dark chamber (latency), reflecting heightened anxiety, and this was prevented in mutant mice fed 150 ppm dietary zinc (*Shank3*$^{ex13-16-/-}_{150\ ppm}$). **(D)** The number of transitions between the light and dark chambers are significantly reduced in *Shank3*$^{ex13-16-/-}_{30\ ppm}$ mice, but no longer significantly different from WT controls in *Shank3*$^{ex13-16-/-}$ mice fed 150 ppm dietary zinc. All data represent mean ± SEM. Statistics: one-way ANOVA with Dunnett's *post hoc* test. $WT_{30\ ppm}$ $n = 10$, *Shank3*$^{ex13-16-/-}_{30\ ppm}$ $n = 7$, $WT_{150\ ppm}$ $n = 8$, *Shank3*$^{ex13-16-/-}_{150\ ppm}$ $n = 6$ animals, $^{*}p < 0.05$, $^{**}p < 0.01$, NS, not significant.

anxiety levels similar to control animals ($Shank3^{ex13\text{–}16-/-}_{150\ ppm}$ 50.50 ± 5.11%; **Figures 2A,B**). $Shank3^{ex13\text{–}16-/-}$ mice on the normal zinc diet showed an increased latency to enter the light chamber compared with WT mice on the same zinc diet (**Figure 2C**; latency $WT_{30\ ppm}$ 9.59 ± 1.83 s, $Shank3^{ex13\text{–}16-/-}_{30\ ppm}$ 28.91 ± 9.56 s, $p < 0.05$), and this latency returned to control levels after the $Shank3^{ex13\text{–}16-/-}$ mice were fed the high zinc diet (latency in $Shank3^{ex13\text{–}16-/-}_{150\ ppm}$ mice 11.29 ± 4.97 s; $p > 0.05$ compared to $WT_{30\ ppm}$; **Figure 2C**). WT mice fed the high zinc diet were not significantly different from WT mice on the control zinc diet (latency for $WT_{150\ ppm}$ mice 10.40 ± 1.93 s, $p > 0.05$ compared to $WT_{30\ ppm}$; **Figure 2C**). $Shank3^{ex13\text{–}16-/-}$ mice on the normal zinc diet also transitioned between the light and dark chambers significantly less than WT mice on the same diet (**Figure 2D**; number of transitions: $WT_{30\ ppm}$ 43.20 ± 2.07, $Shank3^{ex13\text{–}16-/-}_{30\ ppm}$ 31.14 ± 2.09; $p < 0.05$), however with increased dietary zinc $Shank3^{ex13\text{–}16-/-}_{150\ ppm}$ mice displayed a similar number of transitions to WT mice ($Shank3^{ex13\text{–}16-/-}_{150\ ppm}$ 38.00 ± 3.58; $p > 0.05$). No significant effect was observed for WT mice fed the high zinc diet ($WT_{150\ ppm}$ 38.50 ± 3.83, $p > 0.05$; **Figure 2D**).

We also examined social interaction in WT and $Shank3^{ex13\text{–}16-/-}$ mice fed with normal and supplemented zinc levels. WT and $Shank3^{ex13\text{–}16-/-}$ mice on either the normal or high zinc diet displayed normal social interaction during the phase II of the three-chamber social interaction test (**Figure 3A**; time sniffing stranger 1 vs. empty cage respectively, $p < 0.0001$ in all cases: $WT_{30\ ppm}$ 176.00 ± 18.39 s vs. 42.78 ± 4.18 s; $Shank3^{ex13\text{–}16-/-}_{30\ ppm}$ 190.00 ± 16.98 s vs. 58.00 ± 18.08 s; $WT_{150\ ppm}$ 182.13 ± 15.78 s vs. 41.00 ± 4.72 s; $Shank3^{ex13\text{–}16-/-}_{150\ ppm}$ 180.50 ± 21.52 s vs. 64.33 ± 11.55 s). In phase three of the social interaction test, $Shank3^{ex13\text{–}16-/-}_{30\ ppm}$ mice lacked social novelty recognition, showing no significant preference for the novel mouse in contrast to WT mice (time in close interaction with stranger 2 (novel) vs. stranger 1 (familiar): $WT_{30\ ppm}$ 101.56 ± 10.27 s vs. 61.44 ± 7.86 s, $p < 0.01$; $Shank3^{ex13\text{–}16-/-}_{30\ ppm}$ 101.83 ± 21.22 s vs. 100.17 ± 38.08 s, $p > 0.05$; **Figure 3B**). Similar to the other ASD behaviors, dietary zinc supplementation in $Shank3^{ex13\text{–}16-/-}$ mice also prevented the deficit in social novelty recognition as observed by the significant difference in time spent with the novel vs. familiar mouse in $Shank3^{ex13\text{–}16-/-}_{150\ ppm}$ mice (**Figures 3B,C**; $WT_{150\ ppm}$ 112.88 ± 11.01 s vs. 76.88 ± 8.87 s, $p < 0.05$; $Shank3^{ex13\text{–}16-/-}_{150\ ppm}$ 132.77 ± 19.86 s vs. 56.09 ± 11.23 s, $p < 0.05$).

Dietary Zinc Levels Also Affect Synaptic Function and Plasticity in $Shank3^{ex13\text{–}16-/-}$ Mice

Glutamatergic and GABAergic synapses are regulated by zinc, where it alters ion channel function (such as NMDA and GABA receptors), synaptic transmission, as well as the recruitment and stability of postsynaptic proteins including SHANKs (Mayer et al., 1989; Chen et al., 1997; Baron et al., 2006; Lee et al., 2015; Arons et al., 2016). As synaptic changes have been strongly linked to ASD-related behaviors (Won et al., 2012; Chung et al., 2015; Lee et al., 2015; Mei et al., 2016), we examined whether the observed dietary zinc-induced changes in ASD repetitive, anxiety, and social behaviors were accompanied by changes in function and plasticity at excitatory glutamatergic synapses in the dorsolateral striatum (**Figures 4A–D**). Cortico-striatal excitatory synaptic function was measured in acute slices prepared from WT and $Shank3^{ex13\text{–}16-/-}$ mice fed either normal (30 ppm) or supplemented (150 ppm) dietary zinc. Evoked AMPAR-mediated EPSC amplitudes were found to be significantly decreased in $Shank3^{ex13\text{–}16-/-}_{30\ ppm}$ mice compared to $WT_{30\ ppm}$ mice (average EPSC amplitudes were $WT_{30\ ppm}$ −576.02 ± 56.09 pA, $Shank3^{ex13\text{–}16-/-}_{30\ ppm}$ −442.24 ± 25.66 pA, $p < 0.05$), as also illustrated by a significant leftward shift towards smaller AMPAR EPSC amplitudes and a higher frequency of smaller amplitude events (**Figures 4B–D**). Average evoked AMPAR mediated EPSC amplitudes remained unchanged with increased dietary zinc levels, showing that increasing dietary zinc levels did not significantly alter the difference in AMPAR-mediated

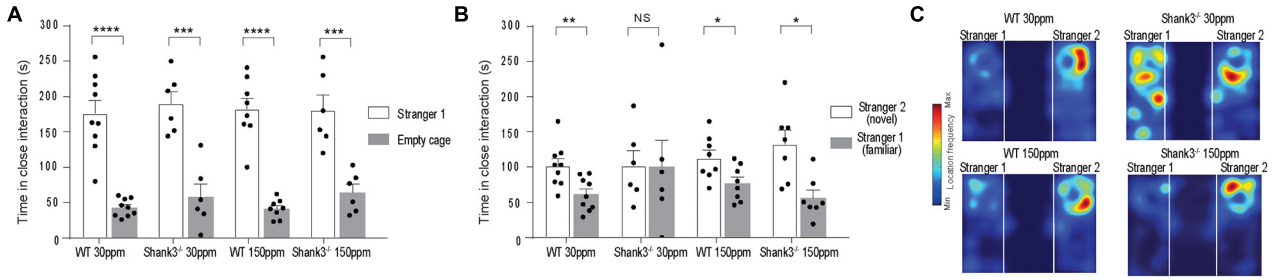

FIGURE 3 | ASD social interaction deficits in $Shank3^{ex13\text{–}16-/-}$ mice are prevented by increased dietary zinc. **(A)** All mice display normal social interaction during phase two of the three-chamber test. **(B)** $Shank3^{ex13\text{–}16-/-}_{30\ ppm}$ mice lack social novelty recognition during phase three, displaying no preference for the stranger or familiar mouse. Increased dietary zinc recovered the social novelty recognition behavior in $Shank3^{ex13\text{–}16-/-}$ mice. **(C)** Example heat maps of phase three of the social interaction test. WT mice on the normal and high zinc diet prefer the novel mouse as depicted by increased presence close to stranger 2. $Shank3^{ex13\text{–}16-/-}$ mice on the normal zinc diet show no preference for the novel mouse (stranger 2), but do show increased interaction with the novel mouse when fed the high zinc diet. All data represent mean ± SEM, two-tailed paired *t*-test. $WT_{30\ ppm}$ $n = 9$, $Shank3^{ex13\text{–}16-/-}_{30\ ppm}$ $n = 6$, $WT_{150\ ppm}$ $n = 8$, $Shank3^{ex13\text{–}16-/-}_{150\ ppm}$ $n = 7$ mice. $^{*}p < 0.05$, $^{**}p < 0.01$, $^{***}p < 0.001$, $^{****}p < 0.0001$, NS, not significant.

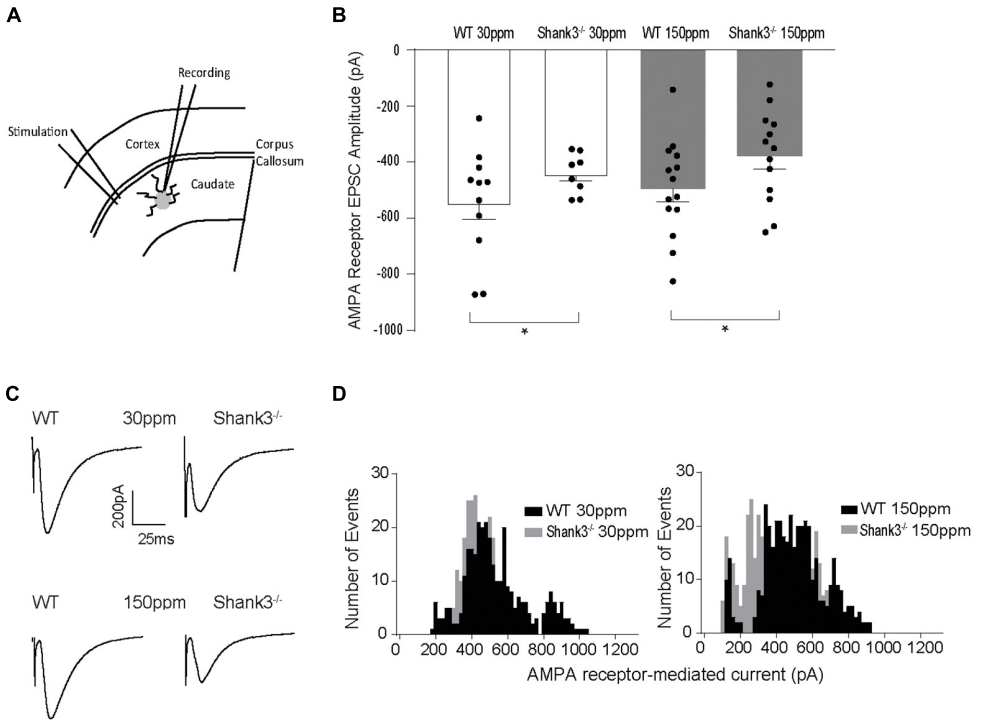

FIGURE 4 | Effect of dietary zinc on cortico-striatal AMPAR mediated EPSCs in WT and *Shank3*$^{ex13–16–/–}$ mice. **(A)** Schematic of electrode placement in dorsolateral striatum for all electrophysiology experiments. **(B)** *Shank3*$^{ex13–16–/–}$ induces a decrease in AMPAR EPSC amplitude, and this decrease is not altered when animals are fed a high zinc diet ($WT_{30\ ppm}$ $n = 11$ cells from nine animals, $Shank3^{ex13–16–/–}_{30\ ppm}$ $n = 8$ cells from seven animals, $WT_{150\ ppm}$ $n = 14$ cells from nine animals, $Shank3^{ex13–16–/–}_{150\ ppm}$ $n = 13$ cells from eight animals). **(C)** Example AMPAR mediated EPSCs from each animal genotype and zinc diet. **(D)** Frequency histograms of AMPAR EPSC amplitudes from WT and *Shank3*$^{ex13–16–/–}$ mice fed normal (left) or high zinc diet (right), illustrating the shift towards smaller AMPAR EPSC amplitudes in *Shank3*$^{ex13–16–/–}$ mice on either zinc diet. All data represent mean ± SEM. $^*p < 0.05$, student's *t*-test.

synaptic transmission at cortico-striatal synapses between WT and *Shank3*$^{ex13–16–/–}$ mice (average EPSC amplitudes were $WT_{150\ ppm}$ -536.37 ± 40.81 pA, $Shank3^{ex13–16–/–}_{150\ ppm}$ -378.56 ± 45.36 pA, $p < 0.05$; **Figures 4B–D**).

In contrast to AMPAR-mediated currents, NMDAR-mediated EPSC amplitudes were not significantly different between WT and *Shank3*$^{ex13–16–/–}$ mice fed normal dietary zinc (**Figure 5A**; average NMDAR EPSC amplitudes were: $WT_{30\ ppm}$

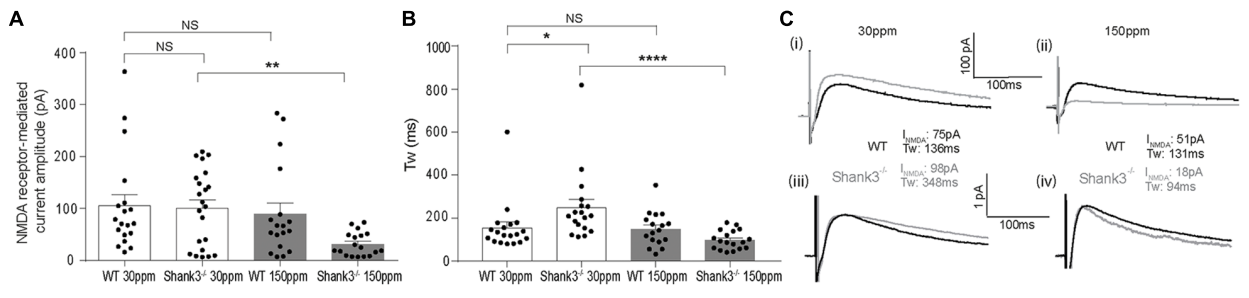

FIGURE 5 | Increased dietary zinc specifically decreases cortico-striatal *N*-methyl-D-aspartate receptor (NMDA) receptor (NMDAR) mediated EPSCs in $Shank3^{ex13–16–/–}_{150\ ppm}$ mice. **(A)** *Shank3*$^{ex13–16–/–}$ deletion ($Shank3^{ex13–16–/–}_{30\ ppm}$) had no effect on mean NMDAR mediated EPSC amplitude, but *Shank3*$^{ex13–16–/–}$ mice fed 150 ppm dietary zinc ($Shank3^{ex13–16–/–}_{150\ ppm}$) exhibited a decreased mean NMDAR EPSC amplitude (Kruskal-Wallis one-way ANOVA with Dunn's *post hoc* test; $WT_{30\ ppm}$ $n = 19$ cells from 10 animals, $Shank3^{ex13–16–/–}_{30\ ppm}$ $n = 22$ cells from nine animals, $WT_{150\ ppm}$ $n = 18$ cells from nine animals, $Shank3^{ex13–16–/–}_{150\ ppm}$ $n = 18$ cells from eight animals). **(B)** NMDAR decay kinetics, measured as the weighted time constant tau (τ_w), were significantly slowed in $Shank3^{ex13–16–/–}_{30\ ppm}$ mice. Increased dietary zinc in *Shank3*$^{ex13–16–/–}$ mice ($Shank3^{ex13–16–/–}_{150\ ppm}$) reversed the slowed kinetics (Kruskal-Wallis one-way ANOVA with Dunn's *post hoc* test). **(C)** Example NMDAR EPSCs from both genotypes and dietary zinc levels. (i) NMDAR EPSCs from WT (black) and *Shank3*$^{ex13–16–/–}$ (gray) mice on 30 ppm diet. (ii) NMDAR EPSCs from WT (black) and *Shank3*$^{ex13–16–/–}$ (gray) mice on 150 ppm diet. (iii) Scaled NMDAR EPSCs from WT (black) and *Shank3*$^{ex13–16–/–}$ (gray) mice on 30 ppm diet. (iv) Scaled NMDAR EPSCs from WT (black) and *Shank3*$^{ex13–16–/–}$ (gray) mice on 150 ppm diet. All data represent mean ± SEM. $^*p < 0.05$, $^{**}p < 0.01$, $^{****}p < 0.0001$, NS, not significant.

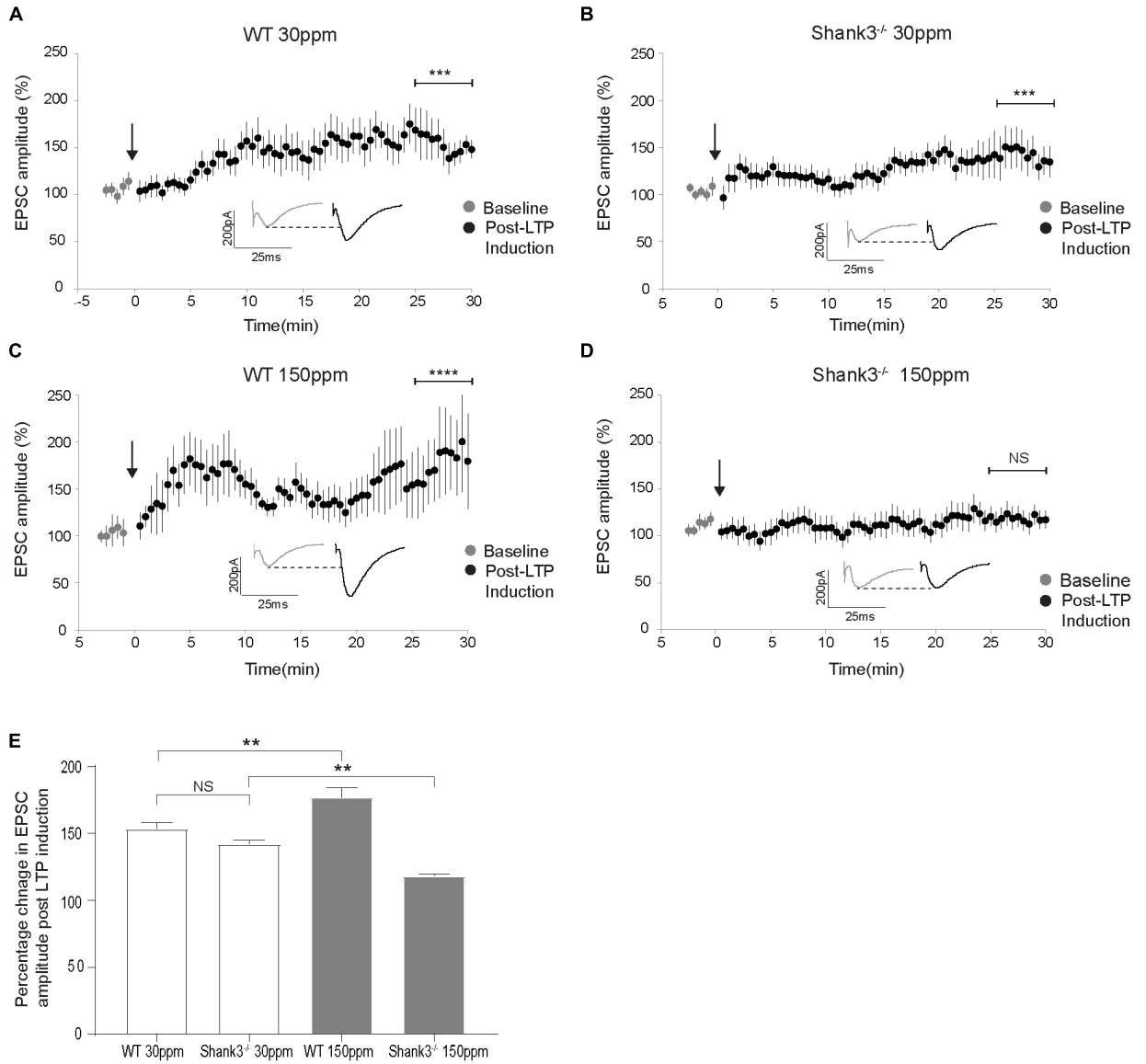

FIGURE 6 | Dietary zinc supplementation prevents long term potentiation (LTP) in the cortico-striatal pathway in *Shank3*$^{ex13-16-/-}$ mice. **(A–C)** $WT_{30\ ppm}$, $WT_{150\ ppm}$, and *Shank3*$^{ex13-16-/-}_{30\ ppm}$ mice all express LTP in response to tetanic stimulation (paired *t*-test, $WT_{30\ ppm}$ $n = 11$ cells from six animals, *Shank3*$^{ex13-16-/-}_{30\ ppm}$ $n = 16$ cells from six animals, $WT_{150\ ppm}$ $n = 7$ cells from four animals). **(D)** No significant change in AMPAR EPSC amplitude was observed 30 min after LTP induction in *Shank3*$^{ex13-16-/-}$ mice with dietary zinc supplementation (*Shank3*$^{ex13-16-/-}_{150\ ppm}$: paired *t*-test, n =11 cells from five animals). **(E)** Bar graph of average percent change in AMPAR EPSC amplitude measured at 30 min post LTP-induction. All data represent mean ± SEM. $^{**}p < 0.01$, $^{***}p < 0.001$, $^{****}p < 0.0001$, NS, not significant.

105.03 ± 23.14 pA, *Shank3*$^{ex13-16-/-}_{30\ ppm}$ 100.87 ± 16.93 pA, $p > 0.05$). Increasing dietary zinc in WT animals also had no effect on NMDAR-EPSC amplitudes (**Figure 5A**; $WT_{150\ ppm}$ 89.55 ± 25.31 pA). However, dietary zinc supplementation in *Shank3*$^{ex13-16-/-}$ mice induced a marked reduction in NMDAR-mediated EPSC amplitudes (**Figure 5A**), *Shank3*$^{ex13-16-/-}_{150\ ppm}$ 38.60 ± 13.78 pA, $p < 0.05$).

We also examined the decay kinetics of the evoked NMDAR mediated EPSCs in both WT and *Shank3*$^{ex13-16-/-}$ mice fed with normal and high zinc. The decay kinetics of NMDAR-mediated EPSCs were significantly slowed in *Shank3*$^{ex13-16-/-}_{30\ ppm}$ mice compared to $WT_{30\ ppm}$ mice (**Figure 5B**; weighted tau: $WT_{30\ ppm}$ 155.67 ± 26.55 ms, *Shank3*$^{ex13-16-/-}_{30\ ppm}$ 248.62 ± 38.67 ms, $p < 0.05$). Increasing dietary zinc has no effect on NMDAR EPSC decay tau in WT animals (**Figure 5B**; $WT_{150\ ppm}$ 150.04 ± 19.27 ms), however increased dietary zinc did reverse the decay tau in *Shank3*$^{ex13-16-/-}$ mice such that the NMDAR decay kinetics were no longer significantly increased compared to WT mice, but were significant decreased in comparison to *Shank3*$^{ex13-16-/-}$ mice fed normal zinc levels (**Figures 5B,C**; *Shank3*$^{ex13-16-/-}_{150\ ppm}$ 98.90 ± 10.25 ms, $p < 0.0001$).

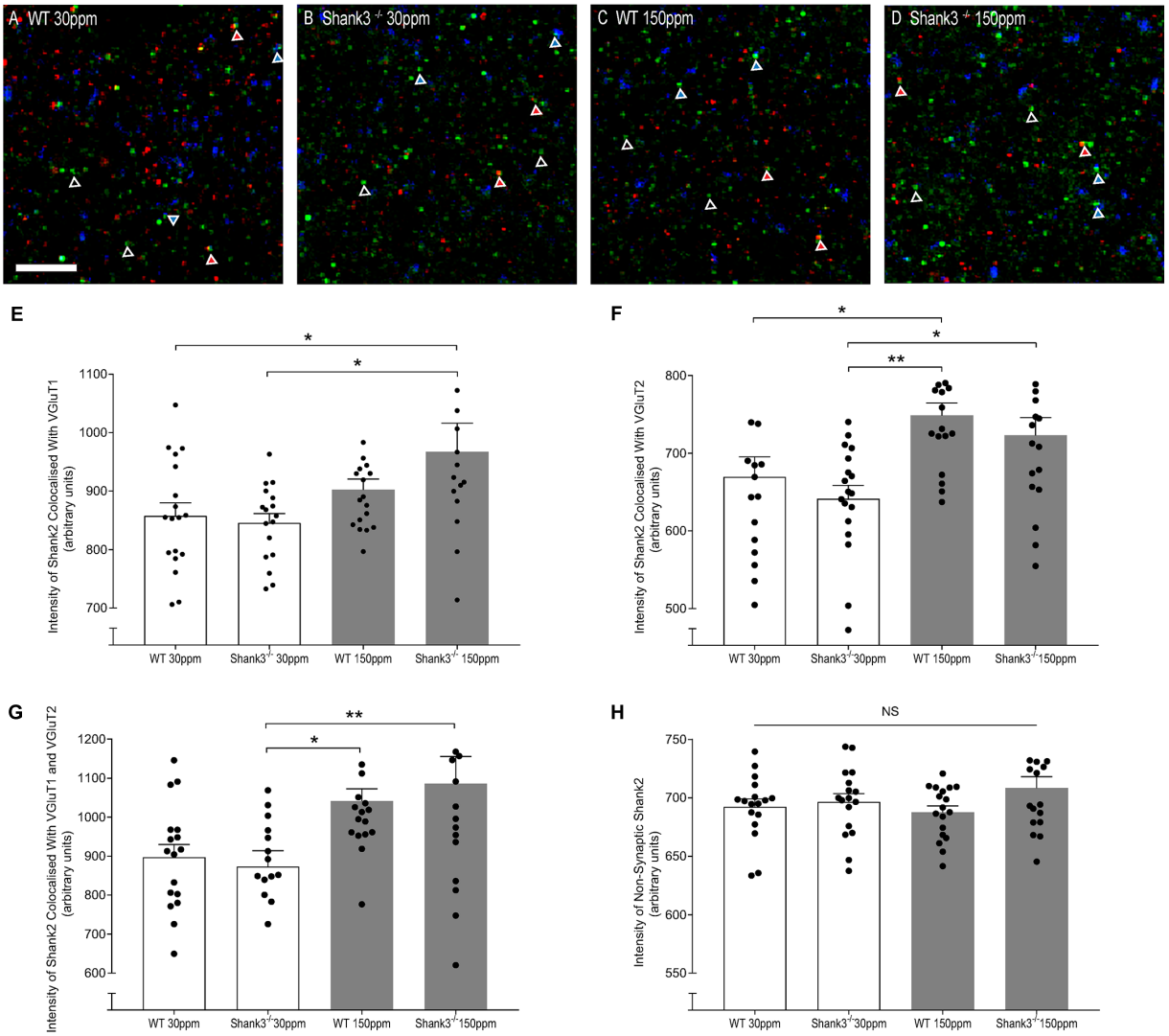

FIGURE 7 | Dietary zinc supplementation increases cortico-striatal and thalamo-striatal synaptic SHANK2 expression in *Shank3*$^{ex13-16-/-}$ mice. **(A–D)** Example overlaid images from WT and *Shank3*$^{ex13-16-/-}$ mice fed normal (30 ppm) or high dietary zinc (150 ppm), immunostained for SHANK2 (green), VGluT1 (red) or VGluT2 (blue). Red triangles denote example synaptic SHANK2 puncta colocalized with VGluT1, blue triangles denote example synaptic SHANK2 puncta colocalized with VGluT2, open triangles denote example non-synaptic SHANK2 puncta. Scale bar 5 μm. **(E)** SHANK2 puncta intensity at cortico-striatal synapses, i.e., puncta co-localized with VGluT1, was significantly increased in *Shank3*$^{ex13-16-/-}_{150\ ppm}$ mice. **(F)** SHANK2 puncta intensity at thalamocostriatal synapses, i.e., puncta co-localized with VGluT2, was significantly increased in WT and *Shank3*$^{ex13-16-/-}$ mice fed 150 ppm dietary zinc. **(G)** Total synaptic SHANK2, puncta co-localized with VGluT1 plus VGluT2, was significantly increased in both WT and *Shank3*$^{ex13-16-/-}$mice fed 150 ppm dietary zinc. **(H)** Non-synaptic SHANK2, i.e., puncta not co-localized with either VGluT1 or VGluT2, was not significantly different between WT and *Shank3*$^{ex13-16-/-}$ mice fed either diet. Data represent mean ± SEM from six *Shank3*$^{ex13-16-/-}$ mice and six WT mice. Statistical significance was determined by one-way ANOVA with Tukey's multiple comparisons test. $^{*}p < 0.05$, $^{**}p < 0.01$. NS, not significant.

The cortico-striatal pathway is linked to compulsive grooming behaviors and habit learning (Lewis and Kim, 2009). Because we observed that repetitive grooming behaviors could be prevented by increased dietary zinc in *Shank3*$^{ex13-16-/-}$ mice (**Figure 1**), and that dietary zinc significantly decreases NMDAR-mediated currents in *Shank3*$^{ex13-16-/-}$ mice (**Figure 5**), we next examined whether dietary zinc also alters NMDAR-dependent synaptic plasticity in this pathway in WT and *Shank3*$^{ex13-16-/-}$ mice fed with normal and supplemented zinc levels (**Figures 6A–E**). LTP was readily induced in the cortico-striatal pathway in WT mice fed 30 ppm zinc. Application of 4 × 100 Hz presynaptic stimulation trains for 1 s together with postsynaptic depolarization induced a significant increase in the AMPAR EPSC amplitude measured 30 min post stimulation in WT mice fed normal and increased zinc levels, and in *Shank3*$^{ex13-16-/-}$ mice fed normal zinc levels (% baseline AMPAR EPSC amplitude: $WT_{30\ ppm}$ 153.57 ± 4.31%, $p < 0.001$; $WT_{150\ ppm}$ 176.93 ± 7.41%, $p < 0.0001$; *Shank3*$^{ex13-16-/-}_{30\ ppm}$ 142.20 ± 2.68%,

$p < 0.001$; **Figures 6A–C,E**). In contrast, LTP was not able to be induced in the cortico-striatal pathway in *Shank3*$^{ex13-16-/-}$ mice fed increased zinc levels, with no significant difference in AMPAR mediated EPSC amplitudes measured after the LTP induction protocol was applied (**Figures 6D,E**; Average AMPAR EPSC amplitude was 118.30 ± 1.19% of baseline at 30 min post-LTP induction; $p > 0.05$).

Dietary Zinc Increases Synaptic Recruitment of Zinc-Responsive SHANK2

The rescue of ASD-related behaviors in *Shank3*$^{ex13-16-/-}$ mice suggests that other zinc-sensitive synaptic proteins may respond to increased dietary zinc. Like SHANK3, the SAM domain of SHANK2 also binds zinc (Boeckers et al., 2005). To explore the possibility that high dietary zinc increases the recruitment of zinc-sensitive SHANK2, we performed immunostaining to examine SHANK2 expression from WT and *Shank3*$^{ex13-16-/-}$ mice fed with normal and supplemented zinc levels. Our data show that synaptic SHANK2 intensity levels are significantly higher in mice fed 150 ppm zinc (**Figure 7**). Synaptic SHANK2, defined as SHANK2 puncta that co-localized with the synaptic markers VGluT1 or VGluT2 (to identify cortico-striatal and thalamo-striatal synapses respectively; Fremeau et al., 2001), was observed to increase in intensity in *Shank3*$^{ex13-16-/-}$ mice in response to dietary zinc supplementation (**Figures 7A–H**; At VGluT1 positive cortico-striatal synapses: $WT_{30\ ppm}$ 857.47 ± 22.41, $Shank3^{ex13-16-/-}_{30\ ppm}$ 845.57 ± 15.90; $Shank3^{ex13-16-/-}_{150\ ppm}$ 967.28 ± 48.76, $p < 0.05$, **Figure 7E**. At VGluT2 positive thalamo-striatal synapses: $WT_{30\ ppm}$ 669.53 ± 25.90, $Shank3^{ex13-16-/-}_{30\ ppm}$ 641.38 ± 17.08; $Shank3^{ex13-16-/-}_{150\ ppm}$ 722.99 ± 22.94, $p < 0.05$, **Figure 7F**). High dietary zinc also increased synaptic SHANK2 puncta intensity in WT mice, specifically at VGluT2 positive thalamo-striatal synapses ($WT_{150\ ppm}$ 748.87 ± 15.89, $p < 0.05$ compared with $WT_{30\ ppm}$) but not significantly at VGluT1 positive cortico-striatal synapses ($WT_{150\ ppm}$ 902.30 ± 18.17, $p > 0.05$ compared with $WT_{30\ ppm}$). SHANK2 increases were specific to synaptic sites, as no significant increases in SHANK2 were observed at non-synaptic sites (defined as SHANK2 puncta that did not colocalize with either VGluT1 or VGluT2; **Figure 7**); $WT_{30\ ppm}$ 692.31 ± 6.69, $Shank3^{ex13-16-/-}_{30\ ppm}$ 696.44 ± 7.17; $WT_{150\ ppm}$ 687.69 ± 5.31; $Shank3^{ex13-16-/-}_{150\ ppm}$ 708.33 ± 9.72; $p > 0.05$, **Figure 7H**).

DISCUSSION

Zinc is a known modulator of ion channels, synaptic transmission, and the recruitment of postsynaptic signaling protein complexes including SHANK2 and SHANK3 (Westbrook and Mayer, 1987; Chen et al., 1997; Yamada et al., 2002; Baron et al., 2006; Grabrucker et al., 2014; Arons et al., 2016). Interestingly, zinc responsiveness is maintained in SHANK3 containing ASD-associated mutations, and also in *Shank2*$^{-/-}$ ASD mice (Lee et al., 2015; Arons et al., 2016), implying that zinc restores loss of function at synapses by enhancing the activity of SHANK3 and/or SHANK2. Here we show that increasing dietary zinc reverses synaptic and behavioral changes in the *Shank3*$^{ex13-16-/-}$ model of ASD. Specifically, our data show that dietary zinc supplementation in *Shank3*$^{ex13-16-/-}$ mice prevents ASD-related repetitive and anxiety behaviors as well as social deficits, in parallel with increasing the synaptic recruitment of zinc-sensitive SHANK2, decreasing NMDAR-EPSC amplitudes, and altering NMDAR decay kinetics. In addition, increased dietary zinc altered LTP at cortico-striatal synapses in *Shank3*$^{ex13-16-/-}$ mice, a glutamatergic pathway implicated in repetitive behaviors (Lewis and Kim, 2009). Together these data suggest that increased dietary zinc affects synaptic and network function at synapses with reduced SHANK3 function by changing the functionality of synaptic zinc signaling systems. These appear to include alterations in NMDAR function that could contribute to the lack of cortico-striatal LTP (Calabresi et al., 1992) and thus ASD repetitive behaviors.

Differential Effects of Changes in Dietary Zinc

In our studies, we observed that increases in dietary zinc also prevented anxiety behaviors and social novelty recognition deficits in *Shank3*$^{ex13-16-/-}$ mice. Previous studies support the role of the amygdala in anxiety behaviors (Kalin et al., 2004; Etkin et al., 2009) as well as regulating social behaviors, especially those involving social novelty, with the most severe autistic-like social deficits occurring with combined damage to the amygdala and hippocampus (Sweeten et al., 2002). Dietary zinc supplementation therefore also likely alters glutamatergic synapses in the amygdala and/or hippocampus. Indeed, we have previously shown that zinc strengthens glutamatergic synaptic transmission in hippocampal neurons expressing SHANK3 ASD-associated mutations (Arons et al., 2016). Zinc mobilization has also been shown to restore glutamatergic synaptic transmission in the amygdala of *Tbr1*$^{-/-}$ ASD mice and in the hippocampus of *Shank2*$^{-/-}$ mice that was accompanied by a significant improvement in social interaction, but not anxiety behaviors, in both ASD mice models (Lee et al., 2015). The zinc responsiveness of the striatum, hippocampus, and amygdala together could underpin the normalization of ASD behaviors observed in these studies, although a complex balance likely exists between these key brain regions with respect to the zinc-induced changes at the synaptic, network and behavioral levels. The timing of zinc treatment also appears to influence the efficacy of the reversal of ASD-related anxiety behaviors, as certain ASD behaviors are irreversible in older mice (Mei et al., 2016). Therefore, a critical factor in the reversal of the observed social, anxiety, and repetitive ASD-related behaviors may be the increase in dietary zinc from weaning age.

NMDARs Are a Major Target for Dietary Zinc Changes

While the observed deficits in AMPAR currents may underpin ASD-related behaviors in *Shank3*$^{ex13-16-/-}$ mice, the dietary

zinc reversal of ASD behaviors occurs concurrently with alterations specifically in NMDAR currents, suggesting that rescue does not involve zinc-dependent changes in AMPAR-mediated synaptic transmission. A significant difference in the dietary zinc-induced effects we describe here on the cortico-striatal pathway is the direction of change in synaptic strength, with a marked zinc-induced decrease in NMDAR currents and LTP occurring in this region. This is in contrast to treatment-induced increases in NMDAR mediated currents observed concurrently with reversal of ASD-related behaviors in other ASD mouse models (e.g., Won et al., 2012; Lee et al., 2015). With regards to zinc-specific treatments, these data show that zinc differentially alters synaptic function in the dorsolateral striatum compared with the hippocampus and amygdala where increases in NMDAR and AMPAR currents were observed (Lee et al., 2015; Arons et al., 2016). Even within the hippocampus zinc differentially alters LTP, promoting presynaptic mossy fiber LTP but inhibiting postsynaptic LTP (Pan et al., 2011). How the dietary zinc-induced decrease in NMDAR currents and lack of LTP in the cortico-striatal pathway contributes to changes ASD-associated behaviors is unknown. As this form of LTP is present in WT animals without ASD-related behaviors, we predict that the zinc-induced decrease in synaptic weight alters striatal outputs to the basal ganglia and motor circuitry via the thalamus to normalize ASD behaviors. While we present here an NMDAR-linked pathway for the preventative effect of dietary zinc on grooming behavior at cortico-striatal synapses, a deeper understanding of the role of zinc at specific synapses in multiple brain regions will be important to decipher the differential effects of zinc on specific ASD-related behaviors.

Our data also show that the significantly decreased NMDAR current amplitude induced by dietary zinc in *Shank3*$^{ex13-16-/-}$ mice was accompanied by a lengthening of the decay time of NMDAR currents. This supports a mechanism whereby zinc induces a decrease in NMDAR synaptic expression and/or channel conductance, as well as a change in NMDAR subunit composition from GluN2B to GluN2A-containing receptors in *Shank3*$^{ex13-16-/-}$ mice (Monyer et al., 1994; Vicini et al., 1998; Cull-Candy et al., 2001). As the dietary zinc effect was observed to specifically occur in *Shank3*$^{ex13-16-/-}$ but not WT mice, the mechanisms underpinning changes induced by dietary zinc appear to require the absence of *Shank3* to exert their behavioral and synaptic effects. At WT synapses, SHANK3 has been shown to enhance the localization and stabilization of synaptic NMDAR expression by crosslinking NMDAR/PSD95 complexes with the underlying actin cytoskeleton (Naisbitt et al., 1999; Duffney et al., 2013). Synapses lacking SHANK3 will lack these cross-linkages, potentially leading to a decrease in the synaptic stability of NMDAR complexes. Additional zinc-sensitive signaling systems contributing to decreased NMDARs include a direct effect on the ion channels themselves, and/or zinc-dependent regulation of other zinc-dependent postsynaptic proteins such as SHANK2 or SAP102 (Firestein et al., 2000; Baron et al., 2006). With regards to the former, NMDARs contain zinc sensors in their N-terminal domains, enabling these receptors to detect zinc over a wide concentration range (Rachline et al., 2005). Zinc is a well-known inhibitor of NMDARs (Peters et al., 1987; Westbrook and Mayer, 1987; Mayer et al., 1989; Chen et al., 1997; Paoletti et al., 1997), particularly GluN2A-containing NMDARs which exhibit a higher zinc sensitivity (Chen et al., 1997; Rachline et al., 2005). This inhibition of NMDARs by zinc is decreased by PSD95 (Yamada et al., 2002). Therefore, the lack of SHANK3 crosslinked NMDAR/PSD95 complexes could also increase zinc inhibition of GluN2A-containing NMDARs, together resulting in decreased NMDAR-mediated currents and plasticity observed in *Shank3*$^{ex13-16-/-}$ mutant mice fed high dietary zinc.

An important observation from our studies is that normalization of ASD-related behaviors can occur in the absence of *Shank3*$^{ex13-16}$. However, this only became evident when dietary zinc levels were increased. These data suggest that there are still zinc sensitive molecules in *Shank3*$^{ex13-16-/-}$ mice that can compensate at least in part for the loss of the SHANK3α and SHANK3β isoforms. A reduced level of the SHANK3γ isoform persists at the PSD in *Shank3*$^{ex13-16-/-}$ mice (Peca et al., 2011), which may continue to respond to zinc-induced stabilization and recruitment of SHANK3 complexes (Baron et al., 2006; Arons et al., 2016). Moreover, an extensive array of SHANK3 isoforms has been described that are differentially regulated by activity, development, and epigenetics (Wang et al., 2014). Whether specific isoforms differentially contribute to zinc-responsiveness will also be of significant interest, especially splice isoforms within the zinc-binding SAM domains (Wang et al., 2014). SHANK2 may also compensate for the loss of *Shank3*$^{ex13-16-/-}$ with dietary zinc, as SHANK2 binds zinc and shows zinc-dependent synaptic recruitment (Grabrucker et al., 2014). Higher levels of SHANK2 have also been described in *Shank3*αβ$^{-/-}$ mice (Schmeisser et al., 2012), although this was not evident in our striatal immunohistochemical analysis in *Shank3*$^{ex13-16}$ mice, similar to that described in *Shank3*$^{InsG3680+/+}$ and *Shank3*$^{fx/fx}$ mutant mice (Mei et al., 2016; Zhou et al., 2016). Specifically, our data show that increased dietary zinc levels drive the recruitment of SHANK2 to cortico-striatal and thalamo-striatal synapses. SHANK2 plays a major role in the early steps of PSD assembly, before PSD95 and NMDAR complexes form (Bresler et al., 2004), followed by later recruitment of SHANK3 driving synaptic formation and maintenance, then lastly SHANK1 driving synaptic maturation (Roussignol et al., 2005; Grabrucker et al., 2011a). The observed increase in SHANK2 with dietary zinc may facilitate early postsynapse formation and contribute to normalization of ASD behaviors, but it does not appear to replace the role of SHANK3 in crosslinking and stabilizing PSD95-NMDAR complexes. Zinc may also engage SHANK2 in other brain regions such as the hippocampus and amygdala to restore normal behaviors. Animal models lacking both *Shank2* and *Shank3* will therefore be of interest to examine whether loss of both SHANK proteins further impairs the zinc sensitivity of these behaviors. It will also be of importance to determine whether increases in dietary zinc can prevent ASD behavioral deficits in mouse models expressing other ASD mutations in SHANKs (e.g., Wang et al., 2011; Schmeisser et al., 2012;

Won et al., 2012; Mei et al., 2016; Zhou et al., 2016) and also in other synaptic proteins (Ebert and Greenberg, 2013; Chen et al., 2014; Golden et al., 2018), to identify the breadth of dietary zinc as a potential therapeutic strategy, and the involvement of zinc-responsive SHANKs in restoring normal behaviors.

Importance of Dietary Zinc Levels

The observation that dietary zinc levels can significantly alter rodent behavior is important not only in the context of reversing ASD behaviors, but these data also have wider significance when comparing behavioral phenotypes in mouse models fed different "control" diets. Dietary zinc levels vary significantly between control diets sold commercially: an online search of control rodent diet chow composition reveals that different companies provide standard chow with zinc levels that range between 25 ppm and 120 ppm. This >4-fold difference in zinc levels could significantly alter rodent behavioral phenotypes, adding variability in the reproducibility of disorder-specific phenotypes and efficiency of treatment strategies across different laboratories. Indeed, discrepancies in ASD phenotypes have been observed in identical ASD mouse models, including the *Shank3*$^{ex13-16-/-}$ mutant mice employed in this study (Peca et al., 2001; Dhamne et al., 2017; Kabitzke et al., 2018). Recent studies have described these mice as having only "subtle" or "weak" social deficits (Dhamne et al., 2017; Kabitzke et al., 2018). We also observed limited social phenotypes in the *Shank3*$^{ex13-16-/-}$ mutant mice, as both WT and *Shank3*$^{ex13-16-/-}$ mutant mice spent significantly more time in close interaction with the stranger mouse compared to the empty chamber (**Figure 3**). However, we did observe a social novelty deficit in *Shank3*$^{ex13-16-/-}$ mutant mice consistent with Peca et al. (2011) but in contrast to Kabitzke et al. (2018), that was prevented by increased dietary zinc. These differences, and their responsiveness to dietary zinc, further highlight the importance of identifying dietary zinc levels in normal chow across studies, as these levels could underpin differences in ASD phenotypes such as sociability deficits.

Zinc deficiency has been observed in humans affected not only by ASD, but also in Phelan-McDermid syndrome in which heterozygous loss of *SHANK3* occurs (Faber et al., 2009; Yasuda et al., 2011; Grabrucker et al., 2014; Pfaender et al., 2017). Interestingly, SHANK3 is expressed in the gut epithelium in mice and in human induced enterocytes (Pfaender et al., 2017), suggesting its reduction in PMS patients and in ASD mice with *Shank3*αβ deletions may contribute to altered gut function in these disorders. A parallel reduction in zinc transporters in SHANK3 complexes (*ZIP2* and *ZIP4*; Pfaender et al., 2017) may therefore contribute to zinc deficiencies in ASD and PMS. The behavioral and synaptic responsiveness of *Shank3*$^{ex13-16-/-}$ mice to increased dietary zinc levels that were observed in the current study reflects an adequate level of gastrointestinal zinc absorption does occur in the gut of these mice. Therefore, despite a potential downregulation of specific zinc transporters, dietary zinc supplementation can overcome this deficit to influence ASD-related symptoms.

In summary, we have revealed that increased dietary zinc induces changes in synapse function and plasticity that occur in parallel with the reversal of ASD-related behaviors. Together these data identify the potential of chronically increasing dietary zinc as a viable strategy for altering cortico-striatal synaptic function and reversing specific behaviors related to ASD and Phelan-McDermid Syndrome.

AUTHOR CONTRIBUTIONS

CF performed experiments in **Figures 1–6** and analyzed data. JM designed the study and wrote the manuscript. YV and KL performed experiments in **Figure 7**. YJ assisted with electrophysiology experiments in **Figures 4–6**. CG assisted with the design of the study and the writing of the manuscript.

FUNDING

This work was funded by the Marsden Fund (award no. 13-UOA-053; Royal Society of New Zealand) and the Health Research Council of New Zealand award no. 17/052 to JM and the German Center for Neurodegenerative Diseases (DZNE) to CCG.

ACKNOWLEDGMENTS

We would like to thank members of the Montgomery lab for helpful discussion.

REFERENCES

Arons, M. H., Lee, K., Thynne, C. J., Kim, S. A., Schob, C., Kindler, S., et al. (2016). Shank3 is part of a zinc-sensitive signaling system that regulates excitatory synaptic strength. *J. Neurosci.* 36, 9124–9134. doi: 10.1523/jneurosci.0116-16.2016

Arons, M. H., Thynne, C. J., Grabrucker, A. M., Li, D., Schoen, M., Cheyne, J. E., et al. (2012). Autism associated mutations in ProSAP2/Shank3 impair synaptic transmission and neurexin-neuroligin mediated transsynaptic signaling. *J. Neurosci.* 32, 14966–14978. doi: 10.1523/JNEUROSCI.2215-12.2012

Assaf, S. Y., and Chung, S. H. (1984). Release of endogenous Zn^{2+} from brain tissue during activity. *Nature* 308, 734–736. doi: 10.1038/308734a0

Baron, M. K., Boeckers, T. M., Vaida, B., Faham, S., Gingery, M., Sawaya, M. R., et al. (2006). An architectural framework that may lie at the core of the postsynaptic density. *Science* 311, 531–535. doi: 10.1126/science.1118995

Boeckers, T. M., Bockmann, J., Kreutz, M. R., and Gundelfinger, E. D. (2002). ProSAP/Shank proteins-a family of higher order organizing molecules of the postsynaptic density with an emerging role in human neurological disease. *J. Neurochem.* 81, 903–910. doi: 10.1046/j.1471-4159.2002.00931.x

Boeckers, T. M., Liedtke, T., Spilker, C., Dresbach, T., Bockmann, J., Kreutz, M. R., et al. (2005). C-terminal synaptic targeting elements for postsynaptic density proteins ProSAP1/Shank2 and ProSAP2/Shank3. *J. Neurochem.* 92, 519–524. doi: 10.1111/j.1471-4159.2004.02910.x

Bozdagi, O., Sakurai, T., Papapetrou, D., Wang, X., Dickstein, D. L., Takahashi, N., et al. (2010). Haploinsufficiency of the autism-associated Shank3 gene leads to deficits in synaptic function, social interaction and social communication. *Mol. Autism* 1:15. doi: 10.3410/f.10696961.11583065

Bresler, T., Shapira, M., Boeckers, T., Dresbach, T., Futter, M., Garner, C. C., et al. (2004). Postsynaptic density assembly is fundamentally different from presynaptic active zone assembly. *J. Neurosci.* 24, 1507–1520. doi: 10.1523/jneurosci.3819-03.2004

Calabresi, P., Pisani, A., Mercuri, N. B., and Bernardi, G. (1992). Long-term potentiation in the striatum is unmasked by removing the voltage-dependent magnesium block of NMDA receptor channels. *Eur. J. Neurosci.* 4, 929–935. doi: 10.1111/j.1460-9568.1992.tb00119.x

Calabresi, P., Pisani, A., Mercuri, N. B., and Bernardi, G. (1993). Lithium treatment blocks long-term synaptic depression in the striatum. *Neuron* 10, 955–962. doi: 10.1016/0896-6273(93)90210-i

Cathala, L., Misra, C., and Cull-Candy, S. (2000). Developmental profile of the changing properties of NMDA receptors at cerebellar mossy fiber-granule cell synapses. *J. Neurosci.* 20, 5899–5905. doi: 10.1523/jneurosci.20-16-05899.2000

Chen, N., Moshaver, A., and Raymond, L. A. (1997). Differential sensitivity of recombinant N-methyl-D-aspartate receptor subtypes to zinc inhibition. *Mol. Pharmacol.* 51, 1015–1023. doi: 10.1124/mol.51.6.1015

Chen, J., Yu, S., Fu, Y., and Li, X. (2014). Synaptic proteins and receptors defects in autism spectrum disorders. *Front. Cell. Neurosci.* 8:276. doi: 10.3389/fncel.2014.00276

Chung, W., Choi, S. Y., Lee, E., Park, H., Kang, J., Park, H., et al. (2015). Social deficits in IRSp53 mutant mice improved by NMDAR and mGluR5 suppression. *Nat. Neurosci.* 18, 435–443. doi: 10.1038/nn.3927

Cull-Candy, S., Brickley, S., and Farrant, M. (2001). NMDA receptor subunits: diversity, development and disease. *Curr. Opin. Neurobiol.* 11, 327–335. doi: 10.1016/s0959-4388(00)00215-4

Dhamne, S. C., Silverman, J. L., Super, C. E., Lammers, S. H. T., Hameed, M. Q., Modi, M. E., et al. (2017). Replicable *in vivo* physiological and behavioral phenotypes of the *Shank3B* null mutant mouse model of autism. *Mol. Autism* 8:26. doi: 10.1186/s13229-017-0142-z

Duffney, L. J., Wei, J., Cheng, J., Liu, W., Smith, K. R., Kittler, J. T., et al. (2013). Shank3 deficiency induces NMDA receptor hypofunction via an actin-dependent mechanism. *J. Neurosci.* 33, 15767–15778. doi: 10.1523/jneurosci.1175-13.2013

Ebert, D. H., and Greenberg, M. E. (2013). Activity-dependent neuronal signalling and autism spectrum disorder. *Nature* 493, 327–337. doi: 10.1038/nature11860

Etkin, A., Prater, K. E., Schatzberg, A. F., Menon, V., and Greicius, M. D. (2009). Disrupted amygdalar subregion functional connectivity and evidence of a compensatory network in generalized anxiety disorder. *Arch. Gen. Psychiatry* 66, 1361–1372. doi: 10.1001/archgenpsychiatry.2009.104

Faber, S., Zinn, G. M., Kern, J. C., and Kingston, H. M. (2009). The plasma zinc/serum copper ratio as a biomarker in children with autism spectrum disorders. *Biomarkers* 14, 171–180. doi: 10.1080/13547500902783747

Fino, E., Glowinski, J., and Venance, L. (2005). Bidirectional activity-dependent plasticity at cortico-striatal synapses. *J. Neurosci.* 25, 11279–11287. doi: 10.1523/JNEUROSCI.4476-05.2005

Firestein, B. L., Craven, S. E., and Bredt, D. S. (2000). Postsynaptic targeting of MAGUKs mediated by distinct N-terminal domains. *Neuroreport* 11, 3479–3484. doi: 10.1097/00001756-200011090-00016

Fremeau, R. T. Jr. , Troyer, M. D., Pahner, I., Nygaard, G. O., Tran, C. H., Reimer, R. J., et al. (2001). The expression of vesicular glutamate transporters defines two classes of excitatory synapse. *Neuron* 31, 247–260. doi: 10.1016/s0896-6273(01)00344-0

Golden, C. E., Buxbaum, J. D., and De Rubeis, S. (2018). Disrupted circuits in mouse models of autism spectrum disorder and intellectual disability. *Curr. Opin. Neurobiol.* 48, 106–112. doi: 10.1016/j.conb.2017.11.006

Grabrucker, S., Jannetti, L., Eckert, M., Gaub, S., Chhabra, R., Pfaender, S., et al. (2014). Zinc deficiency dysregulates the synaptic ProSAP/Shank scaffold and might contribute to autism spectrum disorders. *Brain* 137, 137–152. doi: 10.1093/brain/awt303

Grabrucker, A. M., Knight, M. J., Proepper, C., Bockmann, J., Joubert, M., Rowan, M., et al. (2011a). Concerted action of zinc and ProSAP/Shank in synaptogenesis and synapse maturation. *EMBO J.* 30, 569–581. doi: 10.1038/emboj.2010.336

Grabrucker, A., Rowan, M., and Garner, C. (2011b). Brain-delivery of zinc-ions as potential treatment for neurological diseases: mini review. *Drug Deliv. Lett.* 1, 13–23. doi: 10.2174/2210303111101010013

Howell, G. A., Welch, M. G., and Frederickson, C. J. (1984). Stimulation-induced uptake and release of zinc in hippocampal slices. *Nature* 308, 736–738. doi: 10.1038/308736a0

Hung, A. Y., Futai, K., Sala, C., Valtschanoff, J. G., Ryu, J., Woodworth, M. A., et al. (2008). Smaller dendritic spines, weaker synaptic transmission, but enhanced spatial learning in mice lacking Shank1. *J. Neurosci.* 28, 1697–1708. doi: 10.1523/jneurosci.3032-07.2008

Izumi, Y., Auberson, Y. P., and Zorumski, C. F. (2006). Zinc modulates bidirectional hippocampal plasticity by effects on NMDA receptors. *J. Neurosci.* 26, 7181–7188. doi: 10.1523/jneurosci.1258-06.2006

Kabitzke, P. A., Brunner, D., He, D., Fazio, P. A., Cox, K., Sutphen, J., et al. (2018). Comprehensive analysis of two Shank3 and the Cacna1c mouse models of autism spectrum disorder. *Genes Brain Behav.* 17, 4–22. doi: 10.1111/gbb.12405

Kalin, N. H., Shelton, S. E., and Davidson, R. J. (2004). The role of the central nucleus of the amygdala in mediating fear and anxiety in the primate. *J. Neurosci.* 24, 5506–5515. doi: 10.1523/JNEUROSCI.0292-04.2004

Kreienkamp, H.-J. (2008). Scaffolding proteins at the postsynaptic density: shank as the architectural framework. *Handb. Exp. Pharmacol.* 186, 365–380. doi: 10.1007/978-3-540-72843-6_15

Leblond, C. S., Nava, C., Polge, A., Gauthier, J., Huguet, G., Lumbroso, S., et al. (2014). Meta-analysis of SHANK mutations in autism spectrum disorders: a gradient of severity in cognitive impairments. *PLoS Genet.* 10:e1004580. doi: 10.1371/journal.pgen.1004580

Lee, E.-J., Lee, H., Huang, T.-N., Chung, C., Shin, W., Kim, K., et al. (2015). Trans-synaptic zinc mobilization improves social interaction in two mouse models of autism through NMDAR activation. *Nat. Commun.* 6:7168. doi: 10.1038/ncomms8168

Lewis, M., and Kim, S.-J. (2009). The pathophysiology of restricted repetitive behavior. *J. Neurodev. Disord.* 1, 114–132. doi: 10.1007/s11689-009-9019-6

Lovinger, D. M. (2010). Neurotransmitter roles in synaptic modulation, plasticity and learning in the dorsal striatum. *Neuropharmacology* 58, 951–961. doi: 10.1016/j.neuropharm.2010.01.008

Mayer, M. L., Vyklicky, L. Jr., and Westbrook, G. L. (1989). Modulation of excitatory amino acid receptors by group IIB metal cations in cultured mouse hippocampal neurones. *J. Physiol.* 415, 329–350. doi: 10.1113/jphysiol.1989.sp017724

Mayer, M. L., and Vyklicky, L. Jr. (1989). The action of zinc on synaptic transmission and neuronal excitability in cultures of mouse hippocampus. *J. Physiol.* 415, 351–365. doi: 10.1113/jphysiol.1989.sp017725

Mei, Y., Monteiro, P., Zhou, Y., Kim, J.-A., Gao, X., Fu, Z., et al. (2016). Adult restoration of Shank3 expression rescues selective autistic-like phenotypes. *Nature* 530, 481–484. doi: 10.1038/nature16971

Monyer, H., Burnashev, N., Laurie, D. J., Sakmann, B., and Seeburg, P. H. (1994). Developmental and regional expression in the rat brain and functional properties of four NMDA receptors. *Neuron* 12, 529–540. doi: 10.1016/0896-6273(94)90210-0

Naisbitt, S., Kim, E., Tu, J. C., Xiao, B., Sala, C., Valtschanoff, J., et al. (1999). Shank, a novel family of postsynaptic density proteins that binds to the NMDA receptor/PSD-95/GKAP complex and cortactin. *Neuron* 23, 569–582. doi: 10.1016/s0896-6273(00)80809-0

Pan, E., Zhang, X. A., Huang, Z., Krezel, A., Zhao, M., Tinberg, C. E., et al. (2011). Vesicular zinc promotes presynaptic and inhibits postsynaptic long-term potentiation of mossy fiber-CA3 synapse. *Neuron* 71, 1116–1126. doi: 10.1016/j.neuron.2011.07.019

Paoletti, P., Ascher, P., and Neyton, J. (1997). High-affinity zinc inhibition of NMDA NR1-NR2A receptors. *J. Neurosci.* 17, 5711–5725. doi: 10.1523/jneurosci.17-20-j0001.1997

Pearson, B. L., Pobbe, R. L. H., Defensor, E. B., Oasay, L., Bolivar, V. J., Blanchard, D. C., et al. (2011). Motor and cognitive stereotypies in the BTBR T+tf/J mouse model of autism. *Genes Brain Behav.* 10, 228–235. doi: 10.1111/j.1601-183X.2010.00659.x

Peça, J., Feliciano, C., Ting, J. T., Wang, W., Wells, M. F., Venkatraman, T. N., et al. (2011). Shank3 mutant mice display autistic-like behaviours and striatal dysfunction. *Nature* 472, 437–442. doi: 10.1038/nature09965

Peters, S., Koh, J., and Choi, D. W. (1987). Zinc selectively blocks the action of N-methyl-D-aspartate on cortical neurons. *Science* 236, 589–593. doi: 10.1126/science.2883728

Pfaender, S., Sauer, A. K., Hagmeyer, S., Mangus, K., Linta, L., Liebau, S., et al. (2017). Zinc deficiency and low enterocyte zinc transporter expression in human patients with autism related mutations in SHANK3. *Sci. Rep.* 7:45190. doi: 10.1038/srep45190

Phelan, K., and McDermid, H. E. (2012). The 22q13.3 deletion syndrome (phelan-mcdermid syndrome). *Mol. Syndromol.* 2, 186–201. doi: 10.1159/000334260

Rachline, J., Perin-Dureau, F., Le Goff, A., Neyton, J., and Paoletti, P. (2005). The micromolar zinc-binding domain on the NMDA receptor subunit NR2B. *J. Neurosci.* 25, 308–317. doi: 10.1523/jneurosci.3967-04.2005

Roussignol, G., Ango, F., Romorini, S., Tu, J. C., Sala, C., Worley, P. F., et al. (2005). Shank expression is sufficient to induce functional dendritic spine synapses in aspiny neurons. *J. Neurosci.* 25, 3560–3570. doi: 10.1523/jneurosci.4354-04.2005

Schmeisser, M. J., Ey, E., Wegener, S., Bockmann, J., Stempel, A. V., Kuebler, A., et al. (2012). Autistic-like behaviours and hyperactivity in mice lacking ProSAP1/Shank2. *Nature* 486, 256–260. doi: 10.1038/nature11015

Smart, T. G., Xie, X., and Krishek, B. J. (1994). Modulation of inhibitory and excitatory amino acid receptor ion channels by zinc. *Prog. Neurobiol.* 42, 393–441. doi: 10.1016/0301-0082(94)90082-5

Soorya, L., Kolevzon, A., Zweifach, J., Lim, T., Dobry, Y., Schwartz, L., et al. (2013). Prospective investigation of autism and genotype-phenotype correlations in 22q13 deletion syndrome and SHANK3 deficiency. *Mol. Autism* 4:18. doi: 10.1186/2040-2392-4-18

Speed, H. E., Kouser, M., Xuan, Z., Reimers, J. M., Ochoa, C. F., Gupta, N., et al. (2015). Autism-associated insertion mutation (InsG) of Shank3 exon 21 causes impaired synaptic transmission and behavioral deficits. *J. Neurosci.* 35, 9648–9665. doi: 10.1523/jneurosci.3125-14.2015

Spencer, J. P., and Murphy, K. P. (2000). Bi-directional changes in synaptic plasticity induced at corticostriatal synapses *in vitro*. *Exp. Brain Res.* 135, 497–503.

Sweeten, T. L., Posey, D. J., Shekhar, A., and McDougle, C. J. (2002). The amygdala and related structures in the pathophysiology of autism. *Pharmacol. Biochem. Behav.* 71, 449–455. doi: 10.1016/s0091-3057(01)00697-9

Takeda, A., Iwaki, H., Ando, M., Itagaki, K., Suzuki, M., and Oku, N. (2010). Zinc differentially acts on components of long-term potentiation at hippocampal CA1 synapses. *Brain Res.* 1323, 59–64. doi: 10.1016/j.brainres.2010.01.085

Tallman, D. L., and Taylor, C. G. (2003). Effects of dietary fat and zinc on adiposity, serum leptin and adipose fatty acid composition in C57BL/6J mice. *J. Nutr. Biochem.* 14, 17–23. doi: 10.1016/s0955-2863(02)00228-0

Ting, J. T., Daigle, T. L., Chen, Q., and Feng, G. (2014). "Acute brain slice methods for adult and aging animals: application of targeted patch clamp analysis and optogenetics," in *Methods Mol. Biol.* 1183, 221–242. doi: 10.1007/978-1-4939-1096-0_14

Tran, C. D., Sundar, S., and Howarth, G. S. (2009). Dietary zinc supplementation and methotrexate-induced small intestinal mucositis in metallothionein-knockout and wild-type mice. *Cancer Biol. Ther.* 8, 1662–1667. doi: 10.4161/cbt.8.17.9293

Vicini, S., Wang, J. F., Li, J. H., Zhu, W. J., Wang, Y. H., Luo, J. H., et al. (1998). Functional and pharmacological differences between recombinant *N*-methyl-D-aspartate receptors. *J. Neurophysiol.* 79, 555–566. doi: 10.1152/jn.1998.79.2.555

Walsh, J. P. (1993). Depression of excitatory synaptic input in rat striatal neurons. *Brain Res.* 608, 123–128. doi: 10.1016/0006-8993(93)90782-i

Wang, X., McCoy, P. A., Rodriguiz, R. M., Pan, Y., Je, H. S., Roberts, A. C., et al. (2011). Synaptic dysfunction and abnormal behaviors in mice lacking major isoforms of Shank3. *Hum. Mol. Genet.* 20, 3093–3108. doi: 10.1093/hmg/ddr212

Wang, X., Xu, Q., Bey, A. L., Lee, Y., and Jiang, Y. H. (2014). Transcriptional and functional complexity of Shank3 provides a molecular framework to understand the phenotypic heterogeneity of SHANK3 causing autism and Shank3 mutant mice. *Mol. Autism.* 5:30. doi: 10.1186/2040-2392-5-30

Westbrook, G. L., and Mayer, M. L. (1987). Micromolar concentrations of Zn^{2+} antagonize NMDA and GABA responses of hippocampal neurons. *Nature* 328, 640–643. doi: 10.1038/328640a0

Wilson, H. L., Wong, A. C., Shaw, S. R., Tse, W. Y., Stapleton, G. A., Phelan, M. C., et al. (2003). Molecular characterization of the 22q13 deletion syndrome supports the role of haploinsufficiency of *SHANK3/PROSAP2* in the major neurological symptoms. *J. Med. Genet.* 40, 575–584. doi: 10.1136/jmg.40.8.575

Won, H., Lee, H. R., Gee, H. Y., Mah, W., Kim, J. I., Lee, J., et al. (2012). Autistic-like social behaviour in Shank2-mutant mice improved by restoring NMDA receptor function. *Nature* 486, 261–265. doi: 10.1038/nature11208

Yamada, Y., Iwamoto, T., Watanabe, Y., Sobue, K., and Inui, M. (2002). PSD-95 eliminates Src-induced potentiation of NR1/NR2A-subtype NMDA receptor channels and reduces high-affinity zinc inhibition. *J. Neurochem.* 81, 758–764. doi: 10.1046/j.1471-4159.2002.00886.x

Yasuda, H., Yoshida, K., Yasuda, Y., and Tsutsui, T. (2011). Infantile zinc deficiency: association with autism spectrum disorders. *Sci. Rep.* 1:129. doi: 10.1038/srep00129

Zhou, Y., Kaiser, T., Monteiro, P., Zhang, X., Van der Goes, M. S., Wang, D., et al. (2016). Mice with Shank3 mutations associated with ASD and schizophrenia display both shared and distinct defects. *Neuron* 89, 147–162. doi: 10.1016/j.neuron.2015.11.023

Conflict of Interest Statement: The authors declare that the research was conducted in the absence of any commercial or financial relationships that could be construed as a potential conflict of interest.

frontiers in Molecular Neuroscience

ORIGINAL RESEARCH
published: 09 November 2018
doi: 10.3389/fnmol.2018.00405

Shank and Zinc Mediate an AMPA Receptor Subunit Switch in Developing Neurons

Huong T. T. Ha[1,2†], Sergio Leal-Ortiz[3], Kriti Lalwani[1], Shigeki Kiyonaka[4], Itaru Hamachi[4], Shreesh P. Mysore[5], Johanna M. Montgomery[6], Craig C. Garner[7], John R. Huguenard[1]* and Sally A. Kim[1]**

[1]Department of Neurology & Neurological Sciences, School of Medicine, Stanford University, Stanford, CA, United States, [2]Neurosciences Graduate Program, School of Medicine, Stanford University, Stanford, CA, United States, [3]Department of Material Science & Engineering, School of Engineering, Stanford University, Stanford, CA, United States, [4]Department of Synthetic Chemistry & Biological Chemistry, Graduate School of Engineering, Kyoto University, Kyoto, Japan, [5]Department of Psychological & Brain Sciences, Johns Hopkins University, Baltimore, MD, United States, [6]Department of Physiology and Centre for Brain Research, University of Auckland, Auckland, New Zealand, [7]German Center for Neurodegenerative Diseases (DZNE), Charité—Universitätsmedizin Berlin, Berlin, Germany

OPEN ACCESS

Edited by:
Eunjoon Kim,
Institute for Basic Science (IBS),
South Korea

Reviewed by:
Silvia Bassani,
Istituto di Neuroscienze (IN), Italy
Yong-Seok Lee,
Seoul National University College of Medicine, South Korea

***Correspondence:**
Craig C. Garner
craig-curtis.garner@dzne.de
John R. Huguenard
huguenar@stanford.edu
Sally A. Kim
sallykim@stanford.edu

†Present address:
Huong T. T. Ha,
Department of Biomedical Engineering,
International University,
Vietnam National University—Ho Chi Minh City,
Ho Chi Minh City, Vietnam

Received: 25 July 2018
Accepted: 15 October 2018
Published: 09 November 2018

Citation:
Ha HTT, Leal-Ortiz S, Lalwani K, Kiyonaka S, Hamachi I, Mysore SP, Montgomery JM, Garner CC, Huguenard JR and Kim SA (2018) Shank and Zinc Mediate an AMPA Receptor Subunit Switch in Developing Neurons.
Front. Mol. Neurosci. 11:405.
doi: 10.3389/fnmol.2018.00405

During development, pyramidal neurons undergo dynamic regulation of AMPA receptor (AMPAR) subunit composition and density to help drive synaptic plasticity and maturation. These normal developmental changes in AMPARs are particularly vulnerable to risk factors for Autism Spectrum Disorders (ASDs), which include loss or mutations of synaptic proteins and environmental insults, such as dietary zinc deficiency. Here, we show how Shank2 and Shank3 mediate a zinc-dependent regulation of AMPAR function and subunit switch from GluA2-lacking to GluA2-containing AMPARs. Over development, we found a concomitant increase in Shank2 and Shank3 with GluA2 at synapses, implicating these molecules as potential players in AMPAR maturation. Since Shank activation and function require zinc, we next studied whether neuronal activity regulated postsynaptic zinc at glutamatergic synapses. Zinc was found to increase transiently and reversibly with neuronal depolarization at synapses, which could affect Shank and AMPAR localization and activity. Elevated zinc induced multiple functional changes in AMPAR, indicative of a subunit switch. Specifically, zinc lengthened the decay time of AMPAR-mediated synaptic currents and reduced their inward rectification in young hippocampal neurons. Mechanistically, both Shank2 and Shank3 were necessary for the zinc-sensitive enhancement of AMPAR-mediated synaptic transmission and act in concert to promote removal of GluA1 while enhancing recruitment of GluA2 at pre-existing Shank puncta. These findings highlight a cooperative local dynamic regulation of AMPAR subunit switch controlled by zinc signaling through Shank2 and Shank3 to shape the biophysical properties of developing glutamatergic synapses. Given the zinc sensitivity of young neurons and its dependence on Shank2 and Shank3, genetic mutations and/or environmental insults during early development could impair synaptic maturation and circuit formation that underlie ASD etiology.

Keywords: zinc signaling, AMPA receptor (AMPAR), GluA2 (GluR2), GluA1 (GluR1), Shank2, Shank3, synaptic development, subunit switch

INTRODUCTION

Autism Spectrum Disorders (ASDs) have symptom onset during the first three years of life, a period characterized by intense formation and refinement of synaptic connections. Therefore, it is not surprising that many ASD-associated genes encode synaptic proteins, such as neuroligins (NL3 and NL4; Jamain et al., 2003; Laumonnier et al., 2004), neurexins (Nrx1; Kim et al., 2008), and the Shank family of proteins (Durand et al., 2007; Berkel et al., 2010; Leblond et al., 2012; Sato et al., 2012). This suggests that changes in synaptic structure and function are causally associated with ASDs (Chen et al., 2014; Bourgeron, 2015). Synaptic deficits are also strongly linked with ASD-related environmental insults (such as prenatal inflammation and zinc deficiency) during the critical periods of brain development (Yasuda et al., 2011; Forrest et al., 2012; Grabrucker et al., 2014; Giovanoli et al., 2016), underscoring synapses as a potential focus for genetic and environmental interactions. Therefore, a better understanding of signaling pathways regulating synapse development is essential to discover effective pharmacotherapies for ASDs.

Mutations in the human *SHANK2* and *SHANK3* genes have been implicated in ASDs. Disruptions of these molecules serve as key models to study the underlying neuronal and synaptic dysfunction of ASDs (Harony et al., 2013; Jiang and Ehlers, 2013). The family of Shank proteins (Shank1, Shank2 and Shank3) are key multidomain molecules at excitatory synapses that interact with multiple glutamatergic receptors, cell adhesion molecules and cytoskeletal proteins (Boeckers et al., 1999; Naisbitt et al., 1999; Sheng and Kim, 2000; Arons et al., 2012). While they share high structural similarity and all localize to postsynaptic sites, Shank proteins are differentially expressed during development with Shank2 and Shank3 peaking before Shank1 (Boeckers et al., 1999; Grabrucker et al., 2011). Thus, Shank2 and Shank3 are thought to be critical for plastic aspects of synaptic activity during development and are the focus of this work. For example, Shank2 is thought to play a key role in growth cone function and nascent synapse formation (Du et al., 1998; Bresler et al., 2004) and Shank3 for dendritic spine morphogenesis (Roussignol et al., 2005). Both Shank2 and Shank3 knockout mice show impairments of synaptic plasticity and learning (Bozdagi et al., 2010; Peça et al., 2011; Won et al., 2012; Lee E. J. et al., 2015). Together, these data support the important roles of Shank2 and Shank3 in synapse formation and plasticity.

Shank2 and Shank3 have also been implicated in the maturation of synapses. For example, loss of Shank2 in mice resulted in reduced GluA1 levels, delayed synaptic maturation, and a reduction of AMPA receptor (AMPAR) function (Peter et al., 2016; Wegener et al., 2017). Similarly, Shank3 was shown to play a key role in the postnatal development of excitatory synapses, such that loss of Shank3 increased the AMPA/NMDA ratio and impaired the developmental AMPAR subunit switch (Peça et al., 2011; Bariselli et al., 2016). Such cellular and molecular deficits and autistic-like phenotypes in these mouse models were rescued by both genetic and pharmacological restoration of AMPAR functions (Bariselli et al., 2016; Mei et al., 2016). These findings suggest that Shank2 and Shank3 are critical for AMPAR recruitment and functionality in multiple brain circuits. Mechanistically, these Shank proteins could induce such changes by direct modulation of GluA1 trafficking via the Rich2 or mGluR dependent pathways, and/or indirectly through an interaction with GluA2 via GRIP (Sheng and Kim, 2000; Uchino et al., 2006; Verpelli et al., 2011; Raynaud et al., 2013). Understanding the interactions between Shank proteins and AMPAR will provide key insights into how they operate to regulate subunit switching of AMPARs during development.

Zinc has been shown to regulate the structure and function of Shank2 and Shank3 through its binding to the C-terminal sterile alpha motif (SAM) domain in these proteins. Both of these proteins require zinc binding for their synaptic localization, oligomerization, mobility and trans-synaptic signaling (Boeckers et al., 2005; Baron et al., 2006; Grabrucker et al., 2011; Arons et al., 2016). ASD-associated mutations in the SAM domain are associated with severe synaptic deficits in cell culture and mouse models (Baron et al., 2006; Durand et al., 2012; Speed et al., 2015). Interestingly, prenatal zinc deficiency also reduced expression level of Shank2 and Shank3 as well as Shank-binding partners, such as GluA1, suggesting that these Shank proteins act as mediators of zinc effects on synaptic function (Grabrucker et al., 2014). Furthermore, Shank3 was shown to be necessary for zinc-sensitive potentiation of AMPAR evoked EPSCs in young hippocampal neurons (Arons et al., 2016). In most neurons, basal free intracellular zinc is tightly regulated at very low picomolar concentrations (Maret, 2017). One endogenous source of free zinc for Shank modulation includes zinc release from synaptic vesicles which can enter postsynaptic sites via different ion channels, such as calcium-permeable AMPAR, NMDAR and voltage-gated calcium channels (Vogt et al., 2000; Frederickson et al., 2006; Vergnano et al., 2014). Synaptic activity could also trigger zinc release from postsynaptic zinc buffers, such as Metallothionein III or mitochondria (Masters et al., 1994; Cuajungco and Lees, 1998; Cole et al., 2000; Lee et al., 2003; Bossy-Wetzel et al., 2004). We thus hypothesize that zinc is well positioned to serve as a dynamic regulator to activate Shank-dependent pathways, such as regulating AMPAR subunit composition during synaptic development.

Here, we examine how Shank2, Shank3 and zinc mechanistically regulate AMPAR subunit composition and function in developing synapses. Our data reveal that during development, these Shank proteins exhibit increased synaptic localization in parallel with GluA2-containing AMPAR, supporting the hypothesis that they might play a role in the maturation of AMPARs. To test this, we studied whether neuronal activity regulated the level of postsynaptic zinc at glutamatergic synapses and in turn affected Shank and AMPAR localization and activity. We showed that K^+-induced neuronal depolarization elevated postsynaptic zinc transiently and reversibly. Zinc elevation was found to enhance synaptic efficacy by recruiting GluA2 and dispersing GluA1 at Shank-containing synapses in young neurons. Importantly, knockdown of either Shank2 or Shank3 function abolished the zinc-induced

enhancement of AMPAR-mediated transmission, indicating that Shank2 and Shank3 are critical mediators of a zinc-dependent AMPAR signaling pathway. Together, these data provide a potential mechanistic link between genetic mutations in Shank proteins and zinc deficiency in the etiology of ASD.

MATERIALS AND METHODS

Reagents

Drugs

Picrotoxin, 2,3-dihydroxy-6-nitro-7-sulfamoyl-benzo(f)quinoxa -line (NBQX), 6-cyano-7-nitroquinoxaline-2,3-dione (CNQX) and N-(2,6-dimethylphenylcarbamoylmethyl)triethylammonium bromide (QX314) were purchased from Tocris (R&D System Inc., Minneapolis, MN, USA). D-2-amino-5-phosphonopentanoic acid (D-AP5) and tetrodotoxin (TTX) were obtained from Abcam, Inc.

Antibodies

Primary antibodies used for immunocytochemistry and/or western blots included: Homer1 (1:750, Synaptic Systems; 160003), Shank2 (1:1,000, Synaptic Systems; 162204), Shank3 (1:500, Synaptic Systems; 162302 and 162304), GluA1 and GluA2 [1:8 for surface staining and 1:100 for whole cell staining, Millipore; PC246 and MAB397], VGluT1 (1:100, NeuroMab; N28/9), Shank2 (1:100, Neuromab; N23B/6), Shank3 (1:100, NeuroMab; N367/62), PSD-95 (1:100, NeuroMab; K28/43), MAP2 (1:5,000, Abcam; ab5392), green fluorescent protein (1:1,000, Abcam; ab13970), actin (1:1,000, Abcam; ab8227), and Shank2 (1:250, Cell Signaling; 12218). A custom-made VGluT1 antibody (1:500, polyclonal rabbit) was generously provided by Dr. Richard Reimer (Stanford University). All secondary antibodies (1:500, A11029, A11034, A11036, A11039, A11041, A11075, A21235 and A21449) were obtained from Life Technologies with the exception of the Dylight-350 antibody (1:250, Thermo Fisher; SA5-10069) and the HRP-conjugated antibodies (1:10,000, rabbit, mouse or guinea pig; Jackson ImmunoResearch; 706-035-148, 115-035-003 and 111-035-144).

Reagents and Chemicals

Cell culture reagents were purchased from Life Technologies [Trypsin-EDTA (0.05%), TrypLE, N-2-hydroxyethylpiperazine-N-2-ethane sulfonic acid (HEPES), Anti-Anti, B-27 supplement along with Neurobasal, Dulbecco's modified Eagle's media (DMEM) and Minimum Essential Media (MEM) medias], Sigma-Aldrich [Cytosine β-D-arabinofuranoside (Ara-C), poly-D-lysine (70–150 kDa), Hank's Balanced Salt Solution (HBSS), 1,4-Piperazinediethanesulfonic acid (PIPES), 3-(N-morpholino)propanesulfonic acid (MOPS), Ethylene glycol-bis(2-aminoethylether)-*N,N,N′,N′*-tetraacetic acid (EGTA), insulin, N-Acetyl Cysteine (NAC), hydrocortisone, sodium pyruvate and GlutaMAX], Worthington (Trypsin, Papain, Papain Dissociation Kit, and DNase), Atlanta Biologicals [Horse Serum (HS) and Fetal Bovine Serum (FBS)]. Zinc indicators (FluoZin-3 AM and Newport Green DCF) were obtained from Life Technologies. Vitamin MEM solution, amino acid MEM solution, $ZnCl_2$ (0.1 M stock solution), *N,N,N′,N′*-Tetrakis (2-pyridylmethyl)ethylenediamine (TPEN), 2-Mercaptopyridine *N*-oxide sodium salt (pyrithione) were all purchased from Sigma-Aldrich. For GluA2 surface labeling, Alexa 488-CAM2 and Alexa 647-CAM2 were designed and synthesized by the Hamachi research group (Kyoto University; Wakayama et al., 2017).

DNA Constructs

The mApple expression plasmid was generously provided by Dr. Neal Waxham (University of Texas Health Science Center at Houston).

Short-Hairpin RNA (shRNA) Design and Cloning

Sequences of *Rattus norvegicus* Shank2 and Shank3 from GenBank (NIH) were utilized to design short-hairpin RNA (shRNA) specifically targeting either Shank2 or Shank3. Online software (sidirect2.rnai.jp) was utilized to identify candidate sequences using criteria from three references (Amarzguioui and Prydz, 2004; Reynolds et al., 2004; Ui-Tei et al., 2004) with a maximal melting temperature (T_m) of 21°C. Literature searches for shRNA targeting Shank2 or Shank3 were also performed to provide a secondary selection of our custom designed shRNA. All candidate sequences were then further examined and modified using the iRNAi software (mekentosj.com). Forward and reverse oligo sequences were synthesized, annealed and cloned into the pZoff vector (see below; Leal-Ortiz et al., 2008). The different elements included: recognition sites of restriction enzymes used for cloning (underlined), structural elements of shRNA (5′ or 3′ Prefix—**Bold**, Loop –**Bold, underlined**) and specific shRNA sequences (red; **Supplementary Table S1**).

Forward: GATC**CCC** shRNA seq **TTCAAGAGA** complement shRNA seq **TTTTTGGAAA**

Reverse: AGCTT**TTCCAAAAA** shRNA seq **TCTCTTGAA** complement shRNA seq **GGG**

Constructs were transfected into rat hippocampal neurons, immunostained for both Shank2 and Shank3 and assessed for knockdown efficiency at synapses (**Supplementary Tables S1, S2**). Based on these data, we employed the following nucleotide siRNA sequences that target rat and mouse Shank2 (5′-3′: GGATAAACCGGAAGAGATA from *Rattus norvegicus* Shank2, GenBank accession no. NM133441.1; Berkel et al., 2012) or Shank3 (5′-3′: GTTTGGAGTCTGGACTAAG, GenBank accession no. NM021676.1; Bidinosti et al., 2016). As a control, a luciferase-targeting shRNA sequence was used (5′-3′: CTTACGCTGAGTACTTCGA; Bidinosti et al., 2016). For lentivirus production, the H1 promoter and shRNA elements were subcloned into a pFUGW H1 vector.

Cell Culture

Human Embryonic Kidney 293T Cells

HEK293T (ATCC CRL-3216) were maintained in DMEM (Invitrogen) supplemented with 10% FBS in a humidified

5% CO_2 incubator at 37°C and passaged every 2–3 days using TrypLE and mechanical trituration. Cells used for viral production were passaged fewer than 10 times after their initial acquisition from ATCC.

Primary Rat Hippocampal Neurons

Primary rat hippocampal neurons were prepared according to a Banker culture protocol from hippocampi of wildtype Sprague-Dawley rat embryos (embryonic day 18 or 19) with mixed gender (Kaech and Banker, 2006). Rats were handled in accordance with Stanford University Administrative Panel on Laboratory Animal (APLAC) guidelines (Protocol #14607). Hippocampi were dissected in ice cold HBSS supplemented with 10 mM HEPES pH 7.4, glucose and Anti-Anti and digested in trypsin in Neurobasal media at 37°C for 15 min. Cells were dissociated and plated at a density of 178 cells per mm^2 on poly-D-lysine-coated coverslips (Carolina Biological Supply Company) with paraffin feet in warmed neuronal plating media (0.6% glucose, 10% HS and 100 μM sodium pyruvate in MEM). After 1 h, coverslips were transferred in pairs to 60-mm dishes containing a glial feeder layer, where they were inverted and maintained in Neurobasal media containing B-27 and GlutaMAX in a humidified 5% CO_2 incubator at 37°C. Neurons were fed with a half media exchange twice per week. At 7 days *in vitro* (DIV 7), cells were treated with 800 nM Ara-C for approximately 24 h.

Primary Astrocyte Cultures

Primary astrocytes from the cortex of P0–2 rats with mixed gender were prepared according to the Papain Dissociation Kit. In brief, cortices from neonate rats were dissected, placed in dissection media, chopped into small pieces and then digested with papain and DNase. The astrocytes were cultured in glial media (10% FBS, 100 μM sodium pyruvate, 5 μg/ml N-acetyl-L-cysteine, 5 μg/ml insulin and 5 ng/ml hydrocortisone in DMEM). Microglia and other contaminating cells were shaken off of a confluent monolayer at one week, after which cells were allowed to recover. Upon reaching 80%–90% confluence, astrocytes were passaged, plated or harvested for cryopreservation. For use in Banker cultures, astrocytes were passed and plated one day prior to neuron preparation.

Gene Delivery

Neuronal Transfections

Neuronal transfections were performed using Lipofectamine 2000 as described by the manufacturer (Invitrogen) with the following modifications. Neurons were transfected at DIV 9–10 with a 1.8:1 ratio of Lipofectamine to DNA in transfection media (Neurobasal supplemented with Glutamax). After incubation at 37°C for 80 min, coverslips were placed back into their original 60 mm dishes with a half media exchange. Hippocampal neurons were incubated for 2–4 days prior to imaging experiments.

Lentivirus Production

To create lentivirus for expression of a given protein or shRNA, HEK293T cells were transfected in suspension with the lentiviral transfer plasmids FU-X-Wm, envelope plasmid pCMV-VSV-G, and packaging plasmid SPAX2 (2.8:1:1.5 ratio, respectively) using Lipofectamine 2000 to generate replication-incompetent lentivirus. The transfection media was replaced with complete Neurobasal media 6 h post-transfection, and cells were moved to a humidified 5% CO_2 incubator at 32°C. After 48–52 h, the lentivirus containing supernatant was collected, passed through a 0.45 μm filter to remove cellular debris and stored at -80°C until use. Biological Safety Level 2+ (BSL-2+) guidelines were applied for all lentiviral production and handling.

Lentiviral Infection

Hippocampal cultures were infected by the addition of 100–130 μL of lentivirus, to hippocampal neurons in 60 mm dishes at DIV 0–5 to infect 80%–100% of neurons depending on the day of infection.

Electrophysiological Recordings

General Experimental Conditions

Neurons were transferred to a recording chamber and perfused at a rate of 0.5 ml/min with HibernateE [in mM: 81.4 NaCl, 1.8 $CaCl_2$, 0.0025 $Fe(NO_3)_3{*}9H_2O$, 5.26 KCl, 0.812 $MgCl_2{*}6H_2O$, 0.880 $NaHCO_3$, 0.906 NaH_2PO_4, 34 D-glucose, 10 MOPS, 0.227 sodium pyruvate, Vitamin MEM (1:27) and Amino Acid MEM (1:26), pH 7.3, 235–240 mOs] at RT. Hibernate mimics the composition of Neurobasal media and improves both the stability and duration of recordings. Neurons were visualized using a 60× 0.9 NA LUMPlanFl/IR objective (Olympus Corporation) using differential contrast optics on an Axioskop 50 FS microscope (Zeiss) equipped with an X-Cite 120Q excitation light source. Pyramidal neurons were selected for electrophysiological recordings based on their pyramidal or pear-shaped somata with 3-4 primary dendrites.

Whole Cell Patch Clamp Recordings of AMPAR-Mediated Miniature EPSCs

Whole-cell recordings in voltage-clamp mode were obtained using borosilicate glass electrodes (Sutter Instrument) with a tip resistance of 3–7 MΩ. The internal solution contained (in mM): 114.5 gluconic acid, 114.5 CsOH, 2 NaCl, 8 CsCl, 10 MOPS, 4 EGTA, 4 MgATP and 0.3 Na_2GTP, pH 7.3, adjusted with CsOH.

Signals were amplified with a Multiclamp 700A amplifier, sampled at 20 kHz, filtered at 2.4 kHz, acquired using a Digidata 1440A digitizer and pClamp 10 (all from Molecular Devices). Cells were held at -60 mV, and AMPAR-mediated miniature EPSCS were isolated using bath application of TTX (1 μM), D-AP5 (50 μM) and picrotoxin (100 μM).

$ZnCl_2$ (10 μM) was bath applied in HibernateE to the cultured neurons. Series resistance (R_s) was monitored throughout the duration of all recordings, and data were excluded if R_s increased >20%.

Evoked AMPAR EPSC Recordings

AMPAR-mediated evoked EPSCs were pharmacologically isolated by bath application of a NMDAR blocker (50 μM

D-AP5) and GABAR blocker (100 μM picrotoxin). For these recordings, the internal pipette solution contained (in mM) 101 gluconic acid, 101 CsOH, 11 KCl, 10 MOPS, 2.9 QX 314, 1 $CaCl_2$, 5 EGTA, 2 MgATP, 0.3 Na_2GTP and 50 μM spermine, pH 7.3 adjusted with CsOH (250 mOsm). In addition to D-AP5 and picrotoxin, a very low concentration of NBQX (0.05 μM) was added to the bath to reduce spontaneous AMPAR-mediated synaptic activity that occurred under conditions of disinhibition (Kumar et al., 2002). To stimulate evoked AMPA EPSCs, a platinum parallel bipolar electrode (FHC) was placed in close proximity (∼1.5 mm) to the recorded neurons. Synaptic activity was evoked by delivering current pulses of 4–5 mA for 0.5 ms at intervals of 20 s. Post data collection, membrane potentials were corrected for a liquid junction potential of 18 mV.

Analysis

We detected and analyzed miniature EPSCs with wDetecta, a custom postsynaptic current detection program[1]. Numerical values are given as median ± SEM unless stated otherwise. Quantification of zinc conditions was performed using data after 10 min of zinc application to capture the plateau phase of the zinc effects. Wilcoxon matched-pairs signed rank tests were applied to compare between baseline and $ZnCl_2$ conditions for young or mature neurons. For shRNA experiments, the effect of genotypes on the zinc response were tested by two-way analysis of variance (ANOVA) and Sidak correction multiple *post hoc* comparison was applied to determine the difference between baseline and $ZnCl_2$ within the same genotype. Statistical significance was set at $p < 0.05$.

For cumulative probability distributions, each cohort population was composed of a random selection of equal number of events per condition from each cell (i.e., 600 events from 12 cells). Kolmogorov-Smirnov (K.S.) test was applied to determine statistical significance ($p < 0.005$) for experiments with two samples. Kruskal-Wallis one-way ANOVA with Dunn's correction *post hoc* multiple comparison was used for experiments with more than two samples.

For evoked AMPAR EPSC, current response at each holding voltage was measured by averaging the value within 3–6 ms of peak current using pClamp 10 (Molecular Devices). The I/V slope for negative and positive responses was calculated separately for each condition (baseline or $ZnCl_2$) of each cell using linear regression in Excel 2016 (Microsoft Office). For the population I/V curve, current responses were normalized to the value at the most negative potential. The rectification index was defined as the ratio of the I/V slope of negative responses over that of positive responses. The correlation between the rectification index and change in RI induced by $ZnCl_2$ application was calculated using a two-tailed Pearson correlation coefficient analysis, and statistical significance was set at $p < 0.05$.

All graphs and statistical analyses were done in Prism 6.0 (GraphPad Software).

[1]https://hlab.stanford.edu/wdetecta.php/

Immunoblot Analysis

Immunoblots of cellular lysates were prepared from lentiviral infected hippocampal neurons as described previously (Hsieh et al., 2016; Okerlund et al., 2017). In brief, neurons were infected with a lentiviral vector expressing shRNA and enhanced green fluorescent protein (eGFP) on DIV 1. Lysates from these neurons were harvested at DIV 14–15 in Laemmli loading buffer (Bio-Rad) with β-mercaptoethanol (Sigma). Lysates were loaded on either a 4%–15% or 4%–20% polyacrylamide gels (Bio-Rad) and transferred to a polyvinylidene fluoride (PVDF) membrane (Bio-Rad). After washing (0.1% Triton X-100 in phosphate buffered saline (PBS)) and blocking (5% non-fat powdered milk and 0.1% Triton X-100 in PBS) overnight at 4°C, membranes were probed with primary and secondary antibodies in blocking solution. Protein bands were visualized by West Dura ECL reagents (GE Healthcare). Membranes were either blotted simultanously with Shank and actin antibodies or blotted with Shank antibodies first, then stripped using Restore Western Blot Stripping Buffer (Thermo Fisher) and blotted again for actin to standardize protein levels. Representative blots of relevant protein bands are shown in the figures, and full blots are provided in the **Supplementary Material**.

Immunocytochemistry

Whole-Cell Staining

For whole-cell staining, wild-type (WT) or transfected rat hippocampal neurons were washed at room temperature (RT) with HibernateE solution. Cells were then placed in fixative solution [in mM: 60 PIPES, 25 HEPES, 120 sucrose, 2 $MgCl_2$, 10 EGTA and 4% paraformaldehyde (PFA), pH 7.4] for 10 min at RT. After fixation, cells were washed twice with PBS, permeabilized with 0.25% Triton X-100 (Thermo Scientific) in PBS for 2 min and washed twice with PBS at RT. Fixed and permeabilized cells were incubated in blocking solution (2% glycine, 2% bovine serum albumin, 0.2% gelatin, and 50 mM NH_4Cl in PBS, pH 7.4) for 30 min at RT, and then primary antibodies were applied in blocking solution overnight at 4°C. After the primary antibody incubation, cells were washed three times with blocking solution, followed by the addition of secondary antibodies for 1–2 h at RT. After secondary antibody application, cells were washed three times with PBS and rinsed quickly with water. Neurons were then mounted with Fluoromount-G (Southern Biotech) on pre-cleaned glass slides.

Surface Staining of AMPAR Subunits

The protocol for surface staining of AMPAR subunits was modified from published studies (Lu et al., 2001; Mangiavacchi and Wolf, 2004; Park et al., 2004). Coverslips were incubated in HibernateE solution with or without 10 μM $ZnCl_2$ for 20 min at RT. After treatment, coverslips were incubated with GluA1 or GluA2 antibodies in HibernateE with 2% BSA at 4°C on ice for 1 h. After primary antibody labeling, coverslips were washed twice with 2% BSA in HibernateE and placed in fixative solution. Neurons were then permeabilized and co-stained for

anti-Shank2 and anti-Shank3 antibodies using the whole-cell staining protocol (see previous section).

Chemical Labeling of Endogenous GluA2-Containing AMPAR Using CAM2

Labeling Conditions and Specificity Testing of CAM2 Reagent

For chemical labeling of endogenous GluA2-containing AMPAR in hippocampal neurons, labeling conditions were modified from the original published protocol (Wakayama et al., 2017) to allow for maximal labeling efficiency and minimal internalization of receptors. In brief, neurons were washed twice with Tyrode's solution [in mM: 96 NaCl, 5.4 KCl, 1 $MgCl_2$, 1.8 $CaCl_2$*$2H_2O$, 10 HEPES and 25 D-glucose, pH 7.3], then incubated in a humidified box for 3 h with 3 μM Alexa 647-CAM2 or Alexa 488-CAM2 in Tyrode's solution at 17°C to minimize internalization of AMPARs (Wakayama et al., 2017). To assess the specificity of the CAM2 reagent for tagging the GluA2 subunit, after labeling, neurons were washed three times with Tyrode's solution and then immunostained for GluA1 and GluA2 subunits using the whole-cell staining protocol described previously.

Sequential Dual-Labeling Experiment of Endogenous GluA2-Containing AMPAR

Neurons were first labeled with Alexa 647-CAM2 using the labeling protocol described above. Cells were then washed three times with Tyrode's solution, treated with 10 μM $ZnCl_2$ or $MgCl_2$ (control) in Tyrode's solution for 20 min at RT. After treatment, neurons were labeled again with Alexa 488-CAM2. After the second labeling, neurons were washed three times with Tyrode's solution and immunostained with MAP2 and either Shank2 or Shank3 antibodies using the whole-cell staining protocol described previously.

Zinc Imaging

Labeling

A high affinity zinc-sensitive fluorescent dye, FluoZin-3 AM (K_d for Zn^{2+} ~15 nM), was used for measuring total zinc and a low affinity zinc indicator, Newport Green DCF (NPG, K_d for Zn^{2+} ~1 μM), for free Zn^{2+}. For measuring intracellular zinc, neurons were loaded with FluoZin-3 (1–2 μM) or NPG (5 μM) for 30 min at RT, washed three times with Tyrode's solution and incubated for another 20–30 min at RT to allow for dye deesterification.

Experimental Set Up

To assess free zinc changes with extracellular manipulation of zinc, WT neurons were loaded with NPG as described above. Sister cultures were treated with different $ZnCl_2$ concentrations (with or without pyrithione, a zinc ionophore) and TPEN concentration (a zinc chelator) at RT. After 10 min of treatment, neurons were washed with Tyrode's solution, fixed, washed three times with PBS, and mounted onto slides. To monitor live zinc dynamics, WT neurons were utilized for whole-cell zinc assessment, and neurons pre-transfected with mApple were used for synaptic zinc imaging. After loading with FluoZin-3 as described above, neurons were utilized for time-lapse imaging experiments.

Image Acquisition

Imaging

Pyramidal neurons were selected for image acquisition based on their pyramidal or pear-shaped somata with 3–4 primary dendrites. Three-dimensional fluorescence images (16-bit, 512 × 512) were acquired using MetaMorph 7.0 (Universal Imaging) in conjunction with a Yokogawa CSU 10 spinning disk confocal (Perkin Elmer) fitted on a Zeiss Axiovert 200M inverted microscope. The excitation light of a Krypton/Argon ion laser (643-RYB-A02; Melles Griot) was selected by 488/10 nm, 568/10 nm or 647/10 nm filters (Sutter Lambda filter changer), reflected and then focused through a 63× 1.4 numerical aperture (NA) oil immersion Plan-Apochromat objective lens (Carl Zeiss MicroImaging, Inc.) or a 10× 0.45 NA Plan-Apochromat objective lens. Detection of the fluorescence emission, after passing a 525/50 nm bandpass filter for Alexa 488, a 607/45 nm bandpass filter for Alexa 568 or a 700/75 nm filter for Alexa 647, was obtained using a Cascade 512B camera (Roper). For between sample comparison, all images were acquired with the same settings without knowledge of the experimental condition during image acquisition. To acquire image stacks that could be deconvolved for further analysis, images were sampled using the Nyquist criterion.

Time-Lapse Imaging of Zinc Dynamics in Spines

For this experiment, three-dimensional fluorescence images (8-bit, 512 × 512) were acquired using a SP8 laser scanning confocal microscope (Leica Microsystems Inc.) with a white-light laser, hybrid (HyD) photodetectors and a tunable acousto-optical beam splitter. Custom band-passes (FluoZin-3, wavelength: 488 nm, bandwidth: 493–582 nm; mApple, wavelength: 568 nm, bandwidth: 583–602 nm) were set for FluoZin-3 and mApple based on their excitation and emission spectra (FluoZin-3 maxima, Excitation: 494 nm, Emission: 516 nm; mApple maxima, Excitation: 568 nm, Emission: 592 nm). Images were captured with a 63× 1.4 numerical aperture (NA) oil immersion HC PL Apo objective lens (Leica Microsystems Inc.) with a pinhole set at 1 Airy unit. For monitoring spine Zn^{2+} dynamics, images of both mApple and FluoZin-3 channels were captured every 40–60 s. After 5 min of baseline imaging, cells were perfused with high potassium Tyrode's solution (in mM: 11.5 NaCl, 90 KCl, 1 $MgCl_2$, 1.8 $CaCl_2$2H_2O, 10 HEPES and 25 glucose, pH 7.3) for 120–180 s and then washed out with regular Tyrode's solution for 5–10 min. Zinc increases were measured immediately post-HiK treatment to allow for full exchange of solution.

Image Analysis

Image Preprocessing

Image preprocessing was performed in ImageJ (NIH) unless otherwise specified.

3D Colocalization Analysis for Immunocytochemistry

Images were first preprocessed for analysis. Raw image stacks were background subtracted using a rolling ball radius of 50. They were then 3D deconvolved in Huygens Professional (Scientific Volume Imaging) software using the theoretically calculated point spread functions (PSF) and classic maximum likelihood estimation (CMLE) deconvolution algorithm. Next, primary dendrites were linearized and extracted from the full-frame image using the Straighten plugin for ImageJ.

The identification of protein puncta in straightened dendrites, and analysis of their colocalization in 3D was performed using a custom software package IMFLAN3D—a combination of ImageJ and MATLAB functions (Tai et al., 2007). In brief, straightened dendrites were sharpened, and regions of concentrated fluorophore intensity (puncta) within the images were segmented using a watershed algorithm (ImageJ). Once puncta separation was achieved in each channel, thresholding was done to remove low intensity noise while keeping higher intensities intact. Separate threshold values were determined for each channel, and this common set of threshold values was used to process all images from all conditions in a given experiment.

The resulting images with separated puncta were then processed using custom scripts in Matlab to calculate the properties of the individual 3D puncta. In brief, individual puncta were identified in the binary versions of the raw images using a standard image-processing technique for labeling groups of connected pixels (26-connectivity in 3D). Each separate puncta ended up with a unique label, and this identity information was then used to calculate distributions of individual puncta volume, intensity and other parameters in the raw images. For analyzing the percentage of colocalization between two proteins, the following equation was utilized:

$$\left.\begin{matrix}\%\text{ protein A overlap}\\ \text{with protein B}\end{matrix}\right\} = \frac{\text{Total \# overlapping protein A \& B puncta}}{\text{Total \# protein A puncta}}$$

2D Intensity Analysis of Shank Proteins in Dendritic Puncta vs. Spines

Raw image stacks were processed in Huygens Professional and ImageJ as described above. Deconvolved 3D images of linearized dendrites were then Z-projected (sum intensity). An intensity profile of puncta in the dendritic regions and in the spines were plotted in ImageJ, and the total intensity was quantified using area under the curve integration in Prism 6.0. The ratio of total Shank intensity in the dendritic shaft puncta vs. in the spines were quantified for each Shank protein in each dendrite as a metric for their relative contribution to the immature synapses vs. mature synapses (Niesmann et al., 2011; Valnegri et al., 2011).

2D Density and Fluorescence Intensity Analysis

For quantification of shRNA knockdown efficiency and GluA1/GluA2 expression over development, raw image stacks were background subtracted then Z-projected (average intensity) prior to use of SynPAnal analysis software (Danielson and Lee, 2014) to quantify 2D density and intensity values along primary dendrites. For identification of primary dendrites, the eGFP signal or the GluA1/2 signal was used, and puncta detection was accomplished by thresholding images and counting distinct cluster of four or more adjacent pixels above the intensity threshold. The same detection criteria were applied for different genotypes. Intensity and density values were extracted from the software.

2D Puncta Analysis of CAM2 Labeling of GluA2-Containing AMPAR

Raw image stacks were Z-projected (average intensity). Puncta-by-puncta analysis was performed using OpenView analysis software (Friedman et al., 2000; Arons et al., 2012). Shank2 or Shank3 immuno-positive fluorescent puncta were individually boxed using a Mexican hat filter and then selected based on the following criteria: selected puncta must be above background intensity values in immunostained and CAM2 channels, the puncta must be discrete and non-overlapping with good spatial separation, and the puncta must lie within four pixels of a MAP2-positive dendrite. Puncta fluorescence intensity values were determined, and subsequent data analysis revealed trends in the data.

Fluorescence Intensity Analysis of NPG DCF Signal

Raw image stacks were background subtracted and Z-projected (average intensity). Neuronal cells were identified based on morphology using bright field images of the same regions. NeuN staining was performed in an independent set of coverslips to further confirm the neuronal identity of these cells. Puncta intensity values of neuronal somas were then determined using the Time Series Analyzer plugin in ImageJ.

Fluorescence Intensity Analysis of FluoZin-3 Dynamics in Spines

Raw image stacks were background subtracted and Z-projected (sum intensity). Primary dendrites were then linearized and extracted from the full-frame image before being analyzed using custom scripts in Matlab (SpineZap; Mysore et al., 2007). To select spines, Z-projected images of FluoZin-3 signal at each time point and of mApple at the first time point were combined into a single stack and Z-projected (sum intensity; referred to as t-projection below). Individual boxes covering the spine and minimal extracellular space were then drawn around each spine so that the morphology of the spine was clearly visible but not in close proximity to axons, dendritic projections or tissue debris. The coordinates of each spine's box were then utilized to extract time-lapse images from the raw images in order to further verify visually whether or not the selected protrusions were spines. Mean fluorescence intensity values of spines were quantified using custom codes in MATLAB.

Statistical Analysis

All statistical tests of imaging data were performed in Prism 6.0. For cumulative probability distributions, each cohort population was composed of a random selection of an equal number of puncta values (50–100) from each cell per condition. The K.S. test

was applied to determine statistical significance ($p < 0.005$) for experiments with two samples. Kruskal-Wallis one-way ANOVA with Dunn's correction *post hoc* multiple comparisons was used in experiments with more than two samples. Two-way ANOVA was used to analyze the developmental difference in the ratio of Shank2 and Shank3 intensities in spines (mature) vs. in dendritic puncta (immature). The Mann-Whitney test was used for comparison of mean values between two non-paired conditions. Wilcoxon matched-pairs signed rank tests were applied to compare between baseline and high potassium conditions in time-lapse experiments and to compare the difference in the ratio of Shank2 and Shank3 intensity in dendritic puncta vs. spine at each time point.

RESULTS

Changes in Synaptic Expression of Zinc-Sensitive Shanks and VGluT1 During Development

To understand the roles of Shank2 and Shank3 on excitatory synaptic development, we compared the developmental changes of endogenous proteins in young (DIV 11) and mature (DIV 18) hippocampal neurons in culture (**Figure 1A** and **Supplementary Figure S1A**). Shank postsynaptic clusters (puncta) were analyzed using a three-dimensional blind analysis. Shank2 showed distinct clusters along the dendrites and was present in spines at DIV 11 (**Figure 1A**, left middle panel). Shank2 puncta remained stable with regard to intensity, density or volume between DIV 11 and DIV 18 (**Figure 1A**, middle panels and **Figures 1B–D**). In contrast, at DIV 11 Shank3 was present mainly in the dendritic shaft, especially in the proximal dendrites, and dendritic puncta with limited localization in spines (**Figure 1A**, left top panel). At DIV 18, the density of Shank3 puncta increased by 31.6% compared to DIV 11 ($p = 0.0092$; **Figure 1C**) without a change in puncta intensity or volume (**Figures 1B,D**). Additionally, Shank2 and Shank3 showed strong colocalization (**Figure 1E**) at DIV 11 (78.14 ± 2.43%) that remained stable through these developmental stages (DIV 18, 77.23 ± 2.58%), implying that both proteins might function in concert at the same synapses. Shank1 was weakly expressed in these cultures during this window (data not shown; Grabrucker et al., 2011) and was excluded from the rest of the study.

Motivated by the localization difference in Shank2 and Shank3 expression pattern at DIV 11 (**Figure 1A**), we further examined the contribution of each protein to mature vs. immature synapses at two additional time points (DIV 14 and 21). This contribution was measured by the ratio of Shank intensity in spines (mature) vs. in dendritic puncta (immature; **Figure 1H**; Valnegri et al., 2011). A ratio of zero means that Shank2 and Shank3 exclusively occupy immature synapses on the shaft whereas a ratio of one indicates they contribute equally to both immature synapses on the dendritic shaft and mature synapses on spines. In young neurons (DIV 11 and 14), Shank2 was more biased towards mature synapse localization in spines (0.69 and 0.67) compared to Shank3, which showed a stronger dendritic localization (0.51 and 0.58; $p = 0.0003$ and $p = 0.0024$; **Figure 1I**). Later in development (DIV 18 and 21), Shank3 localization mimicked Shank2 with an increased spine localization [0.70 at DIV 21 ($p = 0.0024$); **Figures 1H,I**]. Overall, these findings imply that Shank2 may serve as the primary scaffolding molecule occupying excitatory synapses early in development while Shank3 arrives later, which is consistent with previous studies (Boeckers et al., 1999; Bresler et al., 2004; Grabrucker et al., 2011).

Next, we wanted to understand the development of Shank-containing synapses by also looking at VGluT1 for visualization of presynaptic specializations to distinguish synaptic from non-synaptic puncta. Striking increases in VGluT1 during synapse maturation were seen in all measures (Intensity: 131.8% increase, $p < 0.0001$; Density: 34.078% increase, $p = 0.0004$; Volume: 96.91% increase, $p < 0.0001$), which is consistent with an earlier study (Wilson et al., 2005). Because of these large changes, we again looked at multiple time points (DIV 11, 14, 18 and 21). We found that VGluT1 showed developmental step-like changes in puncta intensity, density and volume between DIV 11 and 21, delineating a clear developmental profile of young neurons (DIV 11–14) and mature neurons (DIV 18–21; **Supplementary Figures S1B–E**). More than half of Shank2 (54.41%) and Shank3 (55.55%) clusters overlap with punctate VGluT1 staining at DIV 11 (**Figure 1E**). Concomitant with these developmental VGluT1 changes, significant increases with time were seen in all parameters (fraction, density and volume) of Shank-dependent synapses, as defined by Shank-VGluT1 overlapping puncta (**Figures 1E–G**).

Developmental Characterization of AMPAR Structure and Function

Since Shank2 and Shank3 serve as master scaffolding molecules that interact with glutamate receptors (Sheng and Kim, 2000; Uchino et al., 2006), we examined whether the developmental changes in AMPAR expression track with those of Shank. Here, we first compared the expression pattern of GluA1 and GluA2 at two different developmental stages (young—DIV 11 and mature—DIV 18) for GluA1 and GluA2 (**Figure 2A**). GluA1 puncta density and intensity remained the same between DIV 11 and DIV 18 (**Figures 2B,C**). However, GluA2 puncta density at DIV 18 more than doubled in comparison to that of DIV 11 [100.4 ± 15.31 puncta/μm at DIV 11 vs. 210.1 ± 17.03 puncta/μm at DIV 18 ($p = 0.004$; **Figure 2C**)]. These data identified the time frame for the AMPAR developmental subunit switch from GluA2-lacking to GluA2-containing receptors in our hippocampal cultures, similar to previous findings (Pickard et al., 2000; Kumar et al., 2002).

Considering the developmental increase of GluA2, we asked whether this contributes to different functional properties of these excitatory synapses. To address this question, AMPAR-mediated miniature EPSCs (mEPSCs) were recorded and compared between both groups of neurons (**Figure 2D**). AMPAR mEPSC decay time of mature neurons was longer than that of young neurons ($p \leq 0.005$; **Figures 2D,E**), a finding consistent with earlier work (Brill and Huguenard, 2008). No difference

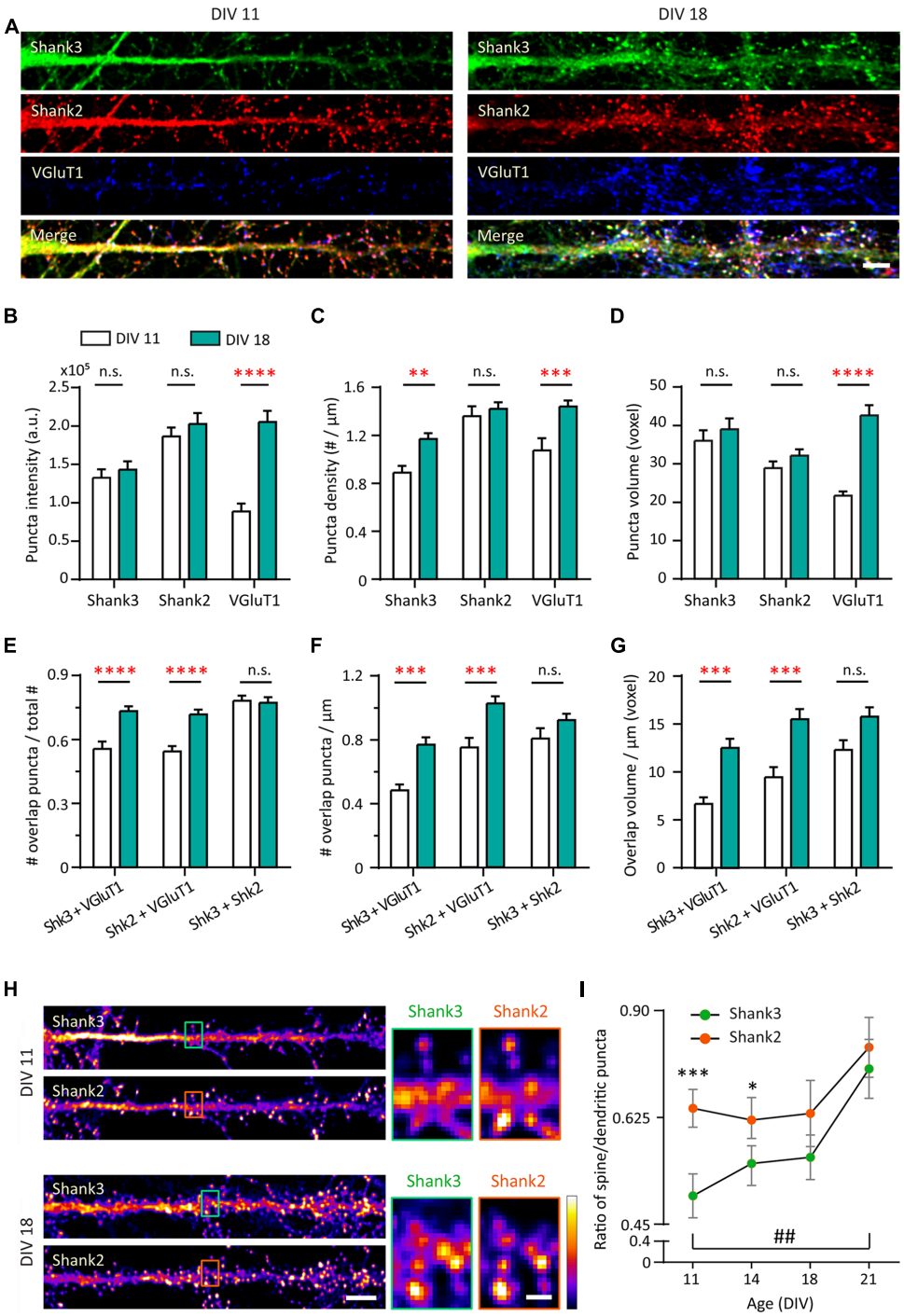

FIGURE 1 | Increase in synaptic expression of Shank2, Shank3 and VGluT1 during development. **(A)** Straightened dendrites of young (days *in vitro* 11, DIV 11) and mature (DIV 18) hippocampal neurons co-immunostained for Shank3 (A488, green), Shank2 (A568, red) and VGluT1 (A647, blue). White puncta in the merge images (bottom) indicate colocalization of all three proteins. Scale bar: 5 µm. **(B–D)** Three-dimensional analysis (IMFLAN3D) of Shank3 and Shank2 puncta at DIV 11 and 18 quantifying intensity **(B)**, density **(C)** or volume **(D)** (mean ± SEM). **(E–G)** Three-dimensional colocalization analysis of pairwise puncta overlap as measured by the ratio **(E)**, density **(F)** and volume **(G)** at DIV 11 and 18 [mean ± SEM; $N = 16$ dendrites from 10 to 12 neurons from two culture preparations (referred to as culture preps from now on; Mann-Whitney tests. n.s. $p \geq 0.05$, $^{**}p < 0.005$, $^{***}p < 0.0005$, $^{****}p < 0.0001$)]. **(H)** Straightened dendrites of young and mature hippocampal neurons immunostained for Shank3 and Shank2. Scale bar: Image, 5 µm; Corresponding inset, 1 µm. **(I)** Summary graphs showing quantification of Shank3 and Shank2 relative enrichment in spines vs. in dendritic puncta (DIV 21, $N = 18$; all others, $N = 16$ dendrites from 10 to 12 neurons from two cultures preps; Kruskal-Wallis one-way analysis of variance (ANOVA) followed by Dunn's correction *post hoc* multiple comparisons. Comparing between Shank2 and Shank3 at the same age: $^{*}p < 0.05$; $^{***}p < 0.0005$. Comparing Shank3 between different ages: $^{\#\#}p < 0.005$).

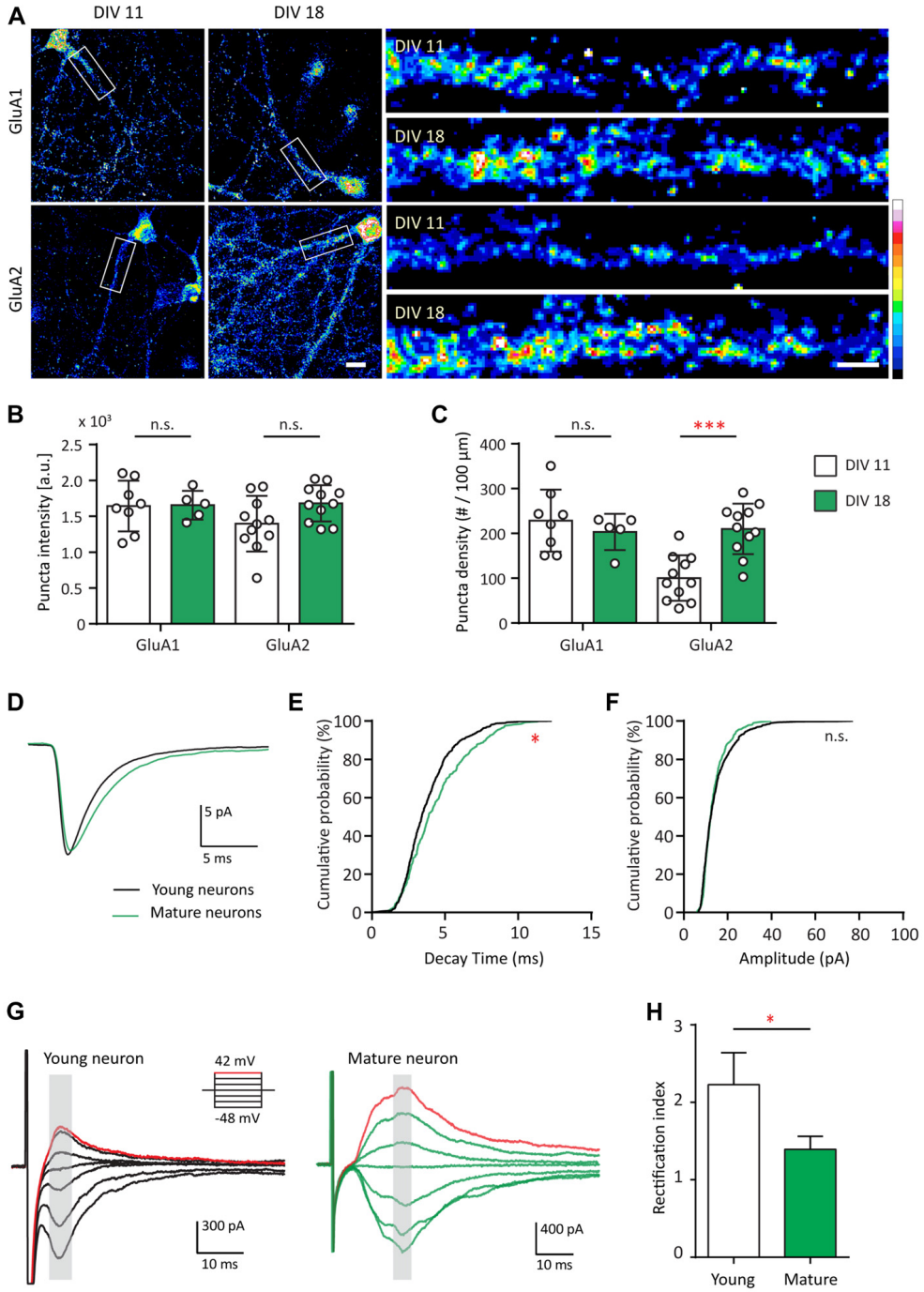

FIGURE 2 | AMPA receptor (AMPAR) subunit composition and functional change during development. **(A)** Hippocampal neurons were fixed and immunostained for GluA1 (top) or GluA2 (bottom) at DIV 11 and DIV 18. White boxes indicate the straightened dendrites (right). Scale bar: image, 15 µm; dendrite, 5 µm. **(B,C)** Summary graphs showing quantification of GluA1 and GluA2 puncta intensity (arbitrary fluorescent units—a.u.) **(B)** and density (puncta per 100 µm; **C**) [mean ± SEM; DIV 11, $N = 8$; DIV 18, $N = 5$ dendrites for GluA1; $N = 11$ for GluA2 from 5 to 10 neurons from two culture preps; Mann-Whitney test. n.s. $p \geq 0.05$, $^{***}p < 0.001$]. **(D)** Ensemble-averaged miniature EPSCs (mEPSCs) from all events recorded in young (black) or mature (green) neurons [$N = 11$ (young) and 10 (mature) neurons from 4 to 7 culture preps, which applies to all subsequent panels unless otherwise specified]. **(E,F)** Cumulative probability histograms of decay time **(E)** or amplitude **(F)** from all isolated events of young or mature neurons [Kolmogorov–Smirnov (K.S.) test, $N = 600$ events (young) and 400 events (for mature), n.s. $p \geq 0.005$, $^{*}p < 0.005$]. **(G)** AMPAR-mediated EPSCs (averaged from three trials) evoked at various holding potentials (see diagram, upper right) from a young (black, left) or mature (green, right) hippocampal neuron. Red traces correspond to the current response at the most positive holding potential. Gray shaded bars used for calculating peak current amplitude. **(H)** Summary graph showing the difference of AMPAR inward rectification property between young and mature neurons [mean ± SEM; $N = 29$ cells (young) and 13 cells (mature) from 3 to 5 culture preps. Mann-Whitney test, $^{*}p < 0.05$].

was found between young and mature neurons in terms of AMPAR mEPSC amplitude (**Figures 2D,F**) or frequency (data not shown). The developmental increase in decay time could be explained by the slower decay kinetics of GluA2-containing AMPAR (Geiger et al., 1995).

GluA2-lacking AMPARs are more sensitive to polyamine blockage at positive holding potentials and thus pass less outward current than inward current at equivalent distance from the reversal potential (Kumar et al., 2002). Therefore, we investigated whether inward rectification of electrically evoked AMPAR EPSCs changed during development. This was accomplished by measuring the AMPAR evoked response at different holding voltages (**Figure 2G**). In young neurons, AMPAR EPSCs were consistently smaller at positive holding potentials compared with those at corresponding negative potentials (**Figure 2G**, left). In mature neurons, AMPAR EPSCs were similar in magnitude at equipotential levels on either side of AMPAR reversal potential (∼3 mV in our experimental condition; **Figure 2G**, right), consistent with decreased rectification. For comparison, we employed a rectification index (RI) defined as the ratio of AMPA conductance measured at corresponding positive over negative holding potentials. The RI of young neurons was larger than that of the mature neurons (**Figure 2H**, 37.66%, $p = 0.04$). Thus, in young neurons, AMPAR-EPSCs were mostly characterized by inward rectification in contrast to mature neurons, similar to previous observations (Jonas et al., 1994; Geiger et al., 1995; Kumar et al., 2002; Brill and Huguenard, 2008; Bariselli et al., 2016). Together, these data indicate that AMPAR in young and mature neurons are fundamentally different in terms of their subunit compositions, leading to functional effects on their decay kinetics and inward rectification property.

Depolarization and Exogenous Zinc Cause an Increase in Intracellular Zinc

Due to the similar developmental expression profiles of GluA2 and synaptic Shank2 and Shank3 (**Figures 1**, **2**), we hypothesized that these Shank proteins could play a role in regulating AMPAR subunit composition during development. Previous work from our lab showed that Shank3 is required for zinc-induced AMPAR synaptic potentiation (Arons et al., 2016), Thus, zinc influx into the postsynaptic compartment could activate Shank-dependent regulation of AMPAR subunit composition. We next examined if neuronal stimulation affects the dynamics of postsynaptic zinc, which could enter from presynaptic-released zinc in the cleft or postsynaptic sources (Masters et al., 1994; Cole et al., 2000; Lee et al., 2003; Bossy-Wetzel et al., 2004; Frederickson et al., 2006).

Dissociated hippocampal neurons were transfected with mApple, as a structural marker, and then loaded with the membrane permeable fluorescent zinc indicator, FluoZin-3-AM (**Figure 3A**). FluoZin-3 fluorescence was present throughout the soma, dendrite and spines and co-localized with mApple (**Figures 3A,B**). Importantly, FluoZin-3 allows for the detection of small changes in intracellular zinc (K_d = 1.5 nM, detection range 10 nM-300 μM) and is unaffected by millimolar concentration of calcium (Zhao et al., 2008). In the absence of exogenous stimulation, the FluoZin-3 fluorescence signal remained stable over time (**Figure 3C**). To determine whether neural activity affects postsynaptic zinc levels, we briefly depolarized neurons by the application of 90 mM high potassium stimulation (HiK). Here, we observed a transient increase of FluoZin-3 intensity in spines (**Figures 3C–E**, 47.75% increase between baseline and during HiK, $p = 0.0001$). The elevation was fully reversible after washout (Baseline vs. Wash, $p > 0.05$; HiK vs. Wash, $p = 0.0001$). Together, these data show that zinc is elevated in postsynaptic spines during neuronal depolarization, which could bind to Shank2 and Shank3 and influence the activation of these proteins via conformational changes (Arons et al., 2016).

We then examined how extracellular manipulations of zinc change intracellular zinc levels (DIV 11–30). Here, Newport Green DCF (NPG) was used due to its lower affinity to zinc (K_d = 1.5 μM, detection range 1 μM-1 mM) for detection of free intracellular zinc (Thompson et al., 2002). With the application of 300 μM $ZnCl_2$, hot spots of NPG appeared along dendrites after a 10 min incubation, potentially indicating free zinc accumulation in synaptic puncta (**Supplementary Figure S2A**). Treatment with $ZnCl_2$ in the presence of a zinc ionophore, pyrithione (MNO), allowed the passive transport of zinc between the intra- and extracellular milieu and further induced the appearance of these putative zinc synaptic puncta (**Supplementary Figure S2A**). To assess the free zinc at baseline condition, we used a high affinity zinc chelator, TPEN (50 μM; K_d = 0.7 fM; Radford and Lippard, 2013). The zinc-chelating effect of TPEN was confirmed by its capacity to reduce somatic FluoZin-3 signal (data not shown). In contrast, we observed no quantifiable difference of NPG signal between baseline and zinc chelator (TPEN, 50 μM) treatment. This result showed that minimal, if any, free intracellular zinc is detectable by this method under baseline conditions (**Supplementary Figure S2C**), consistent with previous studies (Sensi et al., 1997; Canzoniero et al., 1999). At the population level, 10 μM extracellular $ZnCl_2$ application increased somatic NPG signal above baseline by 24.91% (**Supplementary Figures S2B,C**), and further increasing $ZnCl_2$ concentration to 300 μM raised the intracellular NPG signal even higher. Taken together, these results highlight the low levels of free intracellular zinc and that exogenous addition of $ZnCl_2$ can elevated this concentration above baseline. Based on these findings, we established our experimental conditions for further experiments using 10 μM $ZnCl_2$.

Zinc Treatment Enhances AMPAR-Mediated Synaptic Responses in Young Neurons

What are the functional consequences of the elevation of synaptic zinc? To test the functional effects of zinc on AMPAR, we recorded mEPSCs from young hippocampal neurons (DIV 11–14; **Figure 4A**). After a 10 min application, the addition of 10 μM $ZnCl_2$ was associated with a relative increase (39.69%, $p = 0.0186$) in a fraction of large amplitude events (event > 20 pA) and a consistent increase of peak amplitude

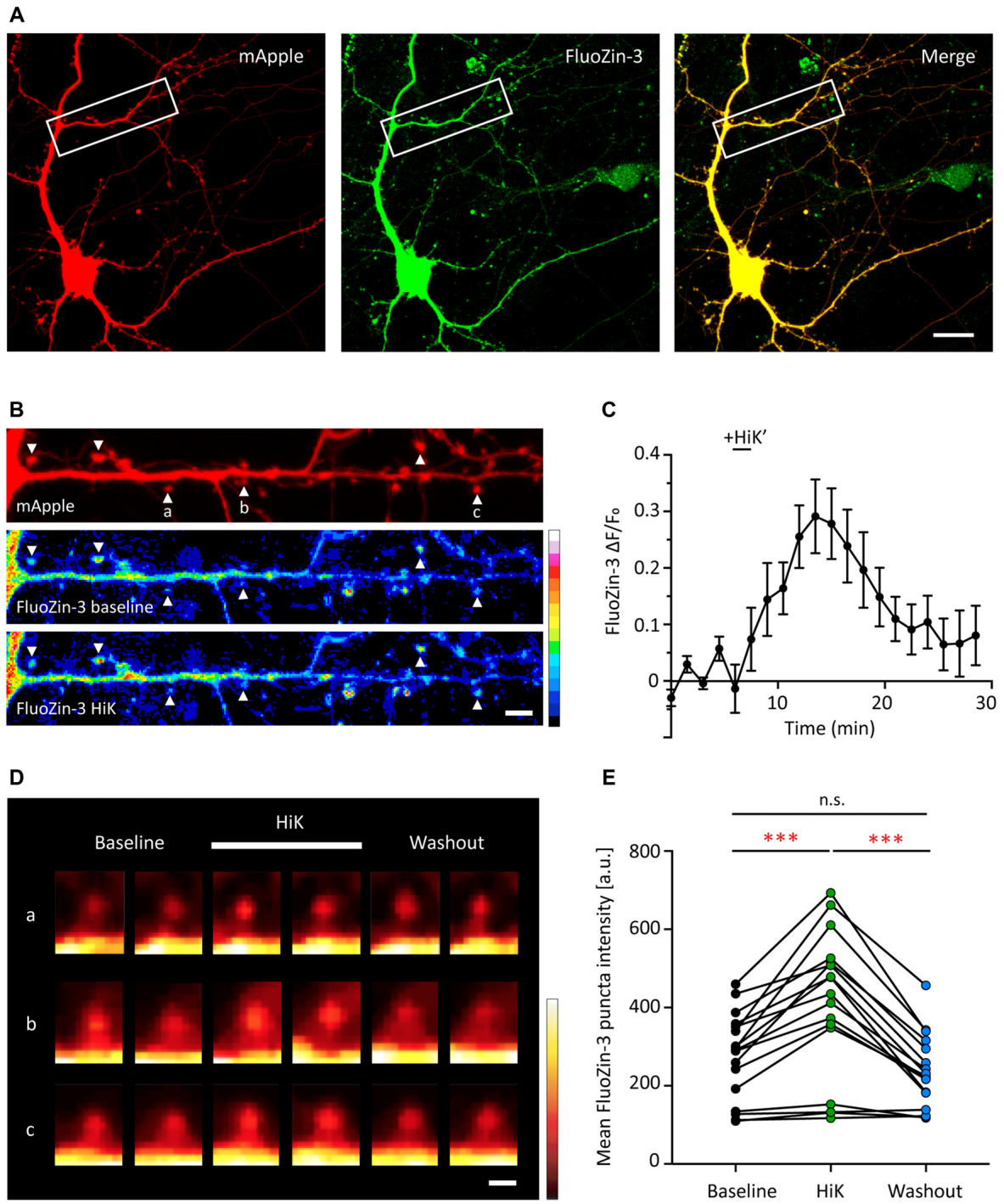

FIGURE 3 | Depolarization induces a transient and reversible increase of zinc in postsynaptic spines. **(A)** A young hippocampal neuron (DIV 14) transfected with mApple (left, red) and loaded with FluoZin-3 (middle, green). mApple was used as a morphological marker to indicate dendrites and postsynaptic spines. Yellow indicates clear colocalization in the merge image (far right). White boxes mark the dendrite shown in **(B)**. Scale bar: 10 μm. **(B)** Straightened dendrite with mApple (top) and FluoZin-3 at baseline (middle) and during depolarization conditions [bottom; 90 mM KCl (HiK), 120–180 s]. White arrowheads mark spines being quantified in **(C)** and shown in (**D**; indicated by a–c). Scale bar: 5 μm. **(C)** Time course of changes in FluoZin-3 ($\Delta F/F_o$) with depolarization for spines in **(B)**. Black line indicates when depolarization was applied (HiK'). Mean ± SEM for $N = 6$ spines in one dendrite, shown in **(B)**. **(D)** FluoZin-3 fluorescence changes in individual spines (a–c) under baseline, HiK (white line) and washout conditions indicated in **(B)**. Scale bar: 1 μm. **(E)** Effects of depolarization on FluoZin-3 in spines of individual hippocampal neurons averaged across baseline, during HiK and washout conditions (one-way ANOVA followed by Sidak's multiple comparisons, $N = 17$ dendrites from five neurons from four culture preps, n.s. $p > 0.05$, $^{***}p < 0.001$).

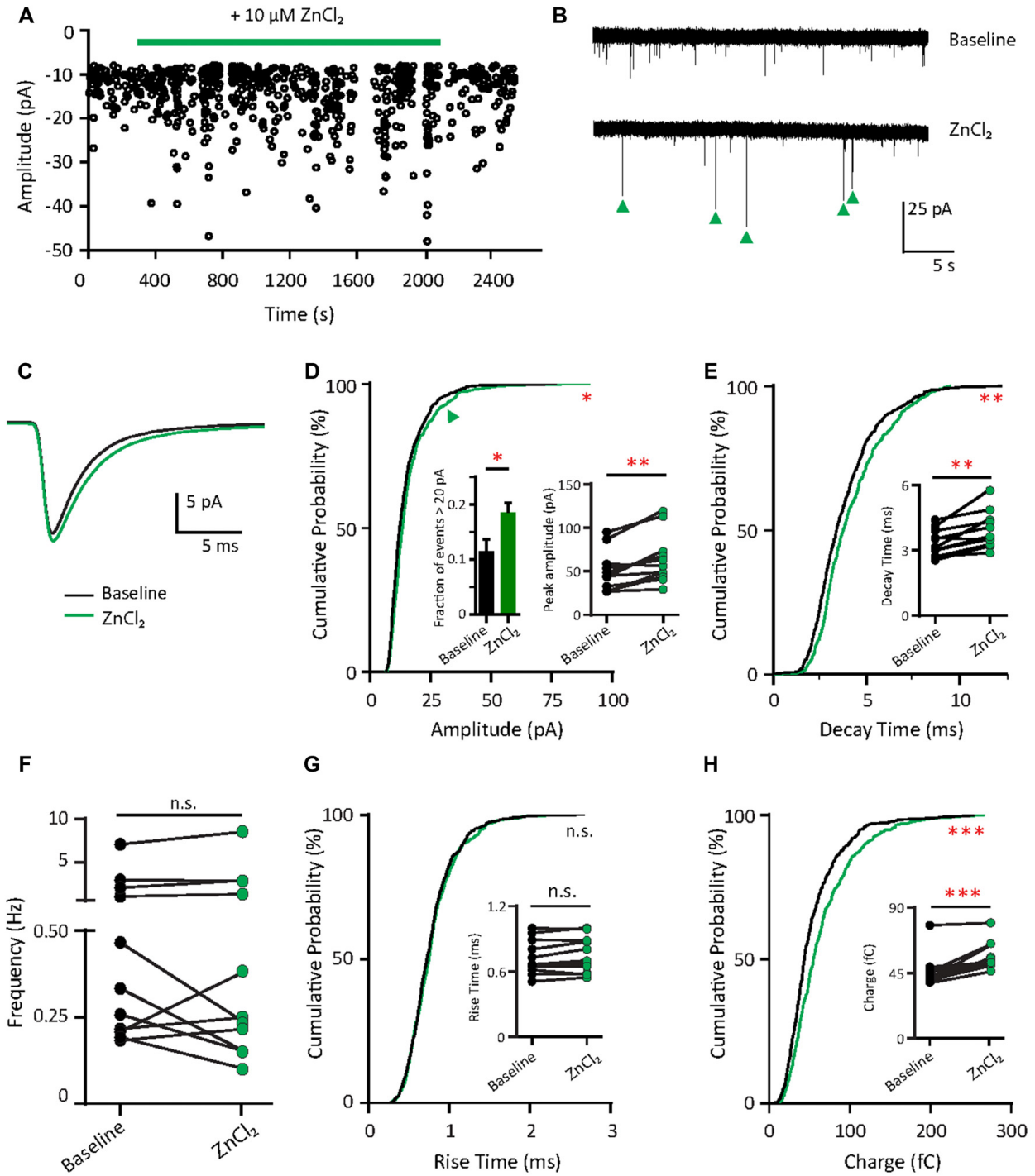

FIGURE 4 | Zinc treatment enhances synaptic efficacy of AMPAR mEPSCs in young neurons. **(A)** AMPAR mEPSCs were recorded from a young hippocampal neuron (DIV 11). Green bar: 10 μM $ZnCl_2$ application. **(B)** AMPAR mEPSC recording traces from the neuron shown in **(A)** at baseline (top) and during $ZnCl_2$ (bottom). Green arrowheads mark the events with larger amplitude during $ZnCl_2$ treatment. **(C)** Ensemble-averaged mEPSCs from the baseline and zinc conditions measured in the same neurons (baseline: black, $ZnCl_2$: green, $N = 11$ cells from seven culture preps, which applies to all subsequent panels unless otherwise specified). **(D,E,G,H)** Cumulative probability histograms of amplitude **(D)**, decay time **(E)**, rise time **(G)** and charge **(H)** of isolated events from baseline (black) and $ZnCl_2$ (green) conditions (K.S. test, $N = 600$ events. n.s. $p \geq 0.005$, $^{*}p < 0.005$, $^{**}p < 0.001$, $^{***}p < 0.0001$). First inset in **(D)**: summary graph showing the difference of fraction of events with amplitude >20 pA between baseline and $ZnCl_2$ conditions. All other insets show per-cell-basis pairwise comparison of amplitude **(D)**, decay time **(E)**, rise time **(G)** and charge **(H)** between baseline and $ZnCl_2$ conditions (Wilcoxon test, n.s. $p \geq 0.05$, $^{**}p < 0.01$, $^{***}p < 0.001$). **(F)** Pairwise comparison of AMPAR mEPSC frequency between baseline and $ZnCl_2$ conditions (Wilcoxon test, n.s. $p \geq 0.05$).

(29.93%, p = 0.002; **Figures 4B–D**). However, the frequency of AMPAR mEPSCs was unaffected by zinc application (**Figure 4F**), suggesting that the effect of zinc is likely postsynaptic. Consistent with a postsynaptic locus of action, zinc lengthened the decay times of AMPAR mEPSCs (19.76%, p = 0.002; **Figures 4C,E**) but did not affect rise time (**Figure 4G**). The increased amplitude and lengthened decay time resulted in increased synaptic efficacy as measured by the charge transfer (22.75%, p = 0.001; **Figure 4H**). These results reveal that zinc enhanced the strength of AMPAR-mediated synaptic transmission in young neurons, perhaps via activity at postsynaptic sites affecting AMPAR composition and hence response amplitude and kinetics.

Zinc Treatment Reduces Inward Rectification Property of AMPARs in Young Neurons

Since the decay time constant increases as a function of GluA2 content (**Figure 2**; Geiger et al., 1995), the zinc-induced slowing of decay might be due to the recruitment of GluA2. To assess how zinc alters the subunit composition of functional AMPARs in young neurons, we indirectly assessed GluA2 content by measuring the current to voltage relationship of evoked AMPA EPSCs (evoked EPSCs) at baseline and during zinc treatment. At baseline, synaptic currents were reliably smaller at positive holding potentials in comparison to those at corresponding negative levels, indicating these receptors were inwardly rectifying. The application of zinc led to a more linear current to voltage relationship (**Figures 5A,B**, right panels) and a reduction in the RI (32.8%, p = 0.0061; **Figure 5C**), observed after 10 min of treatment. Since more linear I/V curves are indicative of higher relative proportions of GluA2-containing AMPAR (Kumar et al., 2002; Brill and Huguenard, 2008), this result suggests that zinc specifically recruited receptors containing GluA2 subunits and/or reduced the synaptic level of GluA2-lacking AMPAR.

We also observed that AMPARs in young neurons have a wide range of RI (1.15–4.71) at baseline, implying variable basal synaptic GluA2 content. Motivated by this observation, we next examined the relationship between initial RI and magnitude of

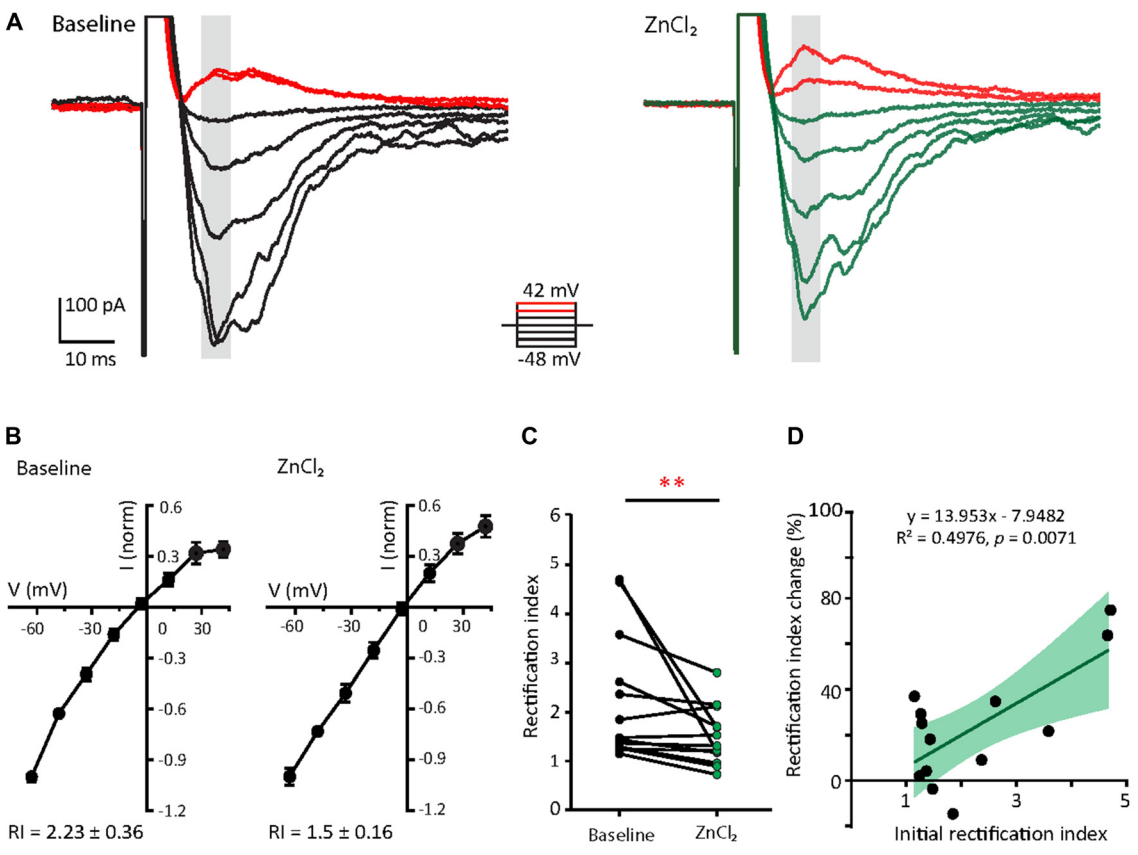

FIGURE 5 | Zinc treatment decreases AMPAR inward rectification in young neurons. **(A)** AMPAR-mediated EPSCs (averaged from three trials) evoked at various holding potentials [diagram (middle)] from a young hippocampal neuron during baseline (left) and after 10 min of 10 μM $ZnCl_2$ application (right). Red traces correspond to the current response at the two most positive holding potentials. Gray shaded bars used for calculating peak current amplitude in **(B)**. **(B)** Normalized current-voltage relationship of the pooled data recorded from the same neurons at baseline (left) and $ZnCl_2$ treatment (right; mean ± SEM for N = 13 cells from five culture preps, which applies to all subsequent panels unless otherwise specified). **(C)** Summary graph showing effect of $ZnCl_2$ application on the rectification indices (RI) of young neurons (Wilcoxon test, $^{**}p < 0.01$). **(D)** Relationship between initial RI (during baseline) and the magnitude of RI change with $ZnCl_2$ application (Pearson correlation, $^{**}p < 0.01$). Green shaded area indicates the 95% confidence interval region.

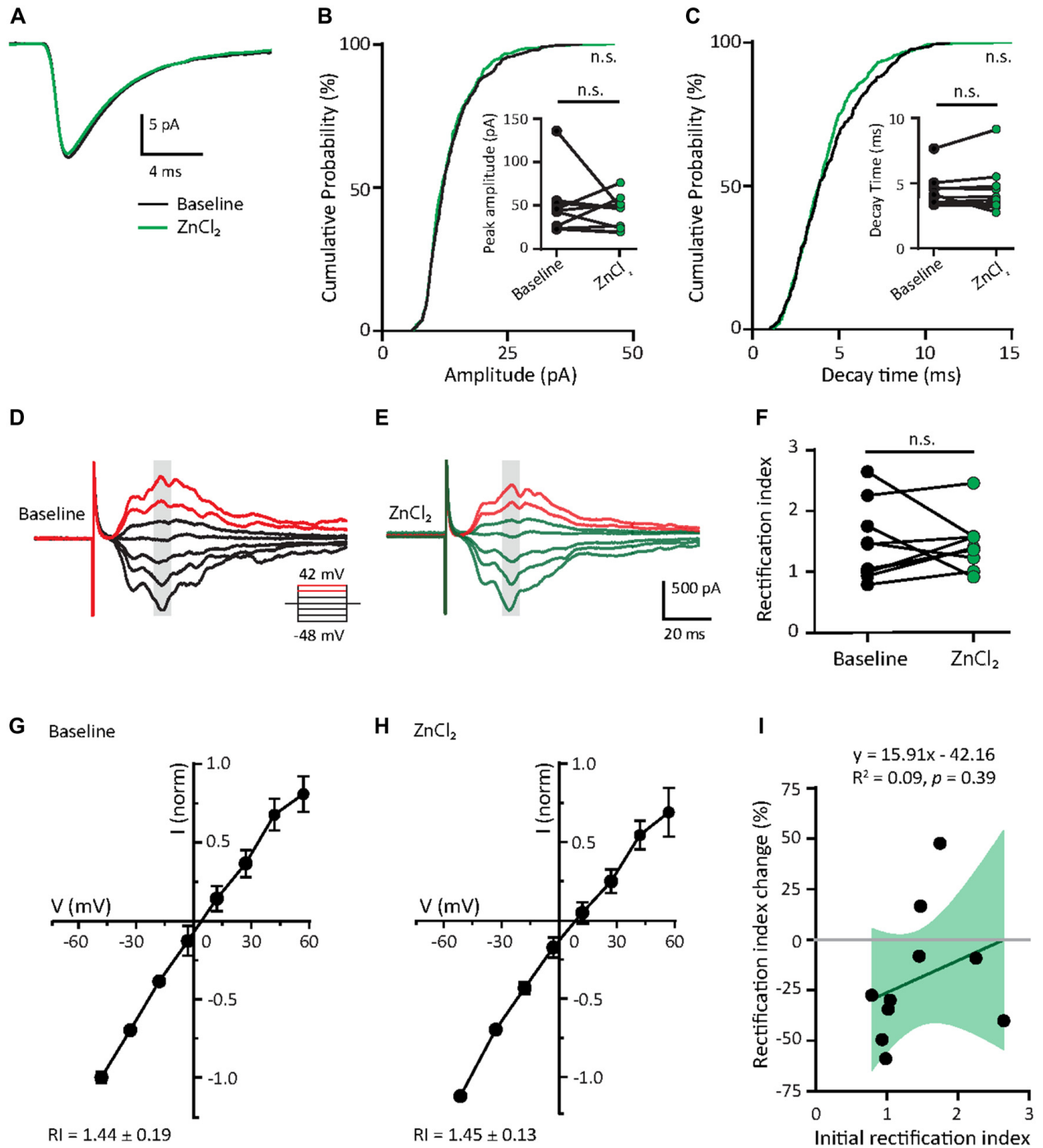

FIGURE 6 | Zinc treatment does not affect miniature or evoked AMPAR EPSCs in mature neurons. **(A)** Ensemble-averaged mEPSCs from the baseline and zinc conditions recorded in mature neurons (baseline: black, $ZnCl_2$: green, $N = 10$ cells). **(B,C)** Cumulative probability histograms of amplitude **(B)** or decay time **(C)** of isolated events from baseline and $ZnCl_2$ conditions (K.S. test, $N = 400$ events from 10 cells from four culture preps per condition, n.s. $p \geq 0.05$). Insets display per-cell-basis pairwise comparison of amplitude **(B)** and decay time (**C**; Wilcoxon test, $N = 10$ cells, n.s. $p \geq 0.05$). **(D,E)** AMPAR-mediated EPSCs (averaged from three trials) evoked at various holding potentials [diagram (middle)] from a mature hippocampal neuron (DIV 18) during baseline **(D)** and after 10 min of 10 μM $ZnCl_2$ application **(E)**. Red traces correspond to the current response at the two most positive holding potentials. Gray shaded bars mark the regions used for calculating peak current amplitude in **(G,H)**. **(F)** Summary graph showing effect of $ZnCl_2$ application on RI of mature neurons (Wilcoxon test, $N = 10$ cells from three culture preps, which applies to all subsequent panels unless otherwise specified; n.s. $p \geq 0.05$). **(G,H)** Normalized current-voltage relationship (mean ± SEM) of the pooled data recorded from the same neurons at baseline **(G)** and $ZnCl_2$ treatment **(H)**. **(I)** Relationship between the initial RI (during baseline) and the magnitude of RI change with $ZnCl_2$ application (Pearson correlation, n.s. $p \geq 0.05$). Green shaded area indicates the 95% confidence interval.

change induced by zinc. From this analysis, the magnitude of RI changes showed a strong positive correlation with the initial RI (**Figure 5D**; R^2 = 0.498, p = 0.0071). These data show that the initial GluA2 content affects the sensitivity of AMPAR to zinc application.

AMPARs of Mature Neurons Are Not Affected by Zinc Treatment

Given that the initial GluA2 content appears to predict the response to zinc treatment (**Figure 5D**) and mature neurons had higher GluA2 puncta density than young neurons (**Figures 2A–C**), we hypothesized that mature neurons would have limited sensitivity to zinc. We then recorded AMPAR mEPSCs in mature neurons (DIV 18–23) at baseline and examined the effect of zinc application. No detectable changes in any AMPAR mEPSC parameters (amplitude, kinetics or frequency) in mature neurons were observed with zinc application (**Figures 6A–C** and **Supplementary Figures S3A–E**), indicating that zinc has no significant influence on unitary synaptic strength, kinetics or active synapse numbers at this age of neuronal development. The insensitivity of AMPAR mEPSCs in mature neurons to zinc application is unlikely due to a ceiling effect since no difference in amplitude between young and mature neurons was observed (**Figure 2F**). Increasing zinc concentrations up to 30 μM also did not elicit any effect on AMPAR mEPSCs (data not shown). These results indicate that the insensitivity of AMPAR mEPSCs in mature neurons is independent of the availability of zinc.

Since zinc did not affect the decay kinetics of AMPAR mEPSCs, we predicted that it also would not alter the subunit composition of AMPARs. To indirectly test this, we assessed the rectification property, which would reflect the relative contribution of GluA2 to synaptic EPSCs (**Figures 6D,E,G,H**). In mature neurons, AMPAR-evoked EPSCs had a highly linear I/V relationship and low inward rectification (RI = 1.44 ± 0.19), similar to **Figures 2G,H**. This low IR remained unchanged with zinc application in these cells, suggesting that zinc exerted no effect on AMPAR subunit compositions (**Figures 6D–H**). As a result, no correlation was seen between initial RI and the magnitude of change induced by zinc treatment. Taken together, the addition of zinc had no significant effect on AMPAR function and subunit composition in mature neurons, likely due to the high basal level of GluA2-content in these cells (**Figure 2C**).

Zinc Recruits Surface GluA2-Containing AMPARs and Disperses GluA1 at Existing Shank-Positive Puncta

To understand the subunit composition changes induced by zinc, we examined the localization of GluA1 and GluA2 using an antibody directed against an extracellular epitope for each subunit (**Figure 7A**). Sister cultures were treated with either control or zinc conditions, immunolabeled and analyzed blind in three-dimensions for surface GluA1 or GluA2. This served as an immunocytochemical index of AMPAR subunit composition for comparison with mini and evoked recordings (Lu et al., 2001; Thiagarajan et al., 2005; Kalashnikova et al., 2010). Under control conditions, numerous, bright GluA1 clusters decorated the dendrite (**Figure 7A**, top left) in comparison to the low intensity levels of GluA2 puncta (**Figure 7A**, bottom left). Zinc treatment led to a marked increase of GluA2 puncta in terms of intensity (54.34%, p = 0.0001), volume (29.8%, p = 0.0077) and density (18%, p = 0.0016; **Figures 7B–D**). The modest change in density suggests that zinc has a stronger effect on GluA2 at preexisting synapses. This agrees with our findings in which zinc lengthened AMPAR mEPSC decay time and increased amplitude but did not affect frequency (**Figure 4**). Zinc also induced a reduction (19.6%, p = 0.0097) of GluA1 puncta density (**Figure 7C**), similar in magnitude to the increase in GluA2 density. This further emphasized that the major effect of zinc was to alter AMPAR subunit composition from GluA2-lacking to GluA2-containing at existing synapses.

Do the zinc-induced changes of AMPAR subunit composition involve Shank2 and Shank3? We looked at the pattern of surface GluA1 and GluA2 incorporation at (**Figure 8B**, **Supplementary Figure S4**) Shank-positive puncta with the same three-dimensional analysis described previously (**Figure 1**). The distribution of AMPARs and Shank puncta were analyzed (defined as overlap of GluA1 or GluA2 with Shank-positive or non-Shank puncta; **Figure 8**). A significant fraction of GluA2-positive puncta contained Shank2 (72.69%) and Shank3 (61.89%; **Figure 8B**, **Supplementary Figure S4**). A similar fraction of GluA1-positive puncta associated with Shank2 (73.55%) and Shank3 (78.38%) puncta (**Figure 8B**). This suggests that the majority of AMPAR (both GluA1 and GluA2 clusters) were found at Shank-positive puncta, consistent with previous findings on the interaction between both subunits with Shank2 and Shank3 (Sheng and Kim, 2000; Uchino et al., 2006). On the other hand, just over half of all Shank puncta were GluA2-positive (Shank2 56.76%; Shank3 54.82%; **Figure 8C**) with a higher fraction associated with GluA1 (Shank2 69.18%; Shank3 61.17%; **Figure 8C**).

Interestingly, with zinc treatment, there was a significant decrease in the fraction of GluA1 overlapping with Shank2 and Shank3 with a large concurrent increase of GluA1 at non-Shank sites (**Figure 8B** and **Table 1**). In contrast with regard to the total GluA2 population, there was no change in the fraction of overlap at any type of Shank or non-Shank puncta with zinc treatment. Instead, with regard to Shank puncta, zinc changed the distribution of GluA2, such that a higher fraction of Shank co-clustered with GluA2 than in control conditions (**Table 1**). A significant concomitant decrease in GluA2 was seen at both non-Shank2 and non-Shank3 sites (**Table 1**). Together, these data suggest that zinc preferentially recruits GluA2 to Shank puncta and disperses GluA1 to non-Shank sites.

Besides increasing the clustering density of GluA2 and Shank3, zinc treatment also led to an increase in fluorescence intensity (75.04%) and volume (40.19%) for GluA2 specifically at Shank3-positive puncta (**Figures 8D,E**), further supporting

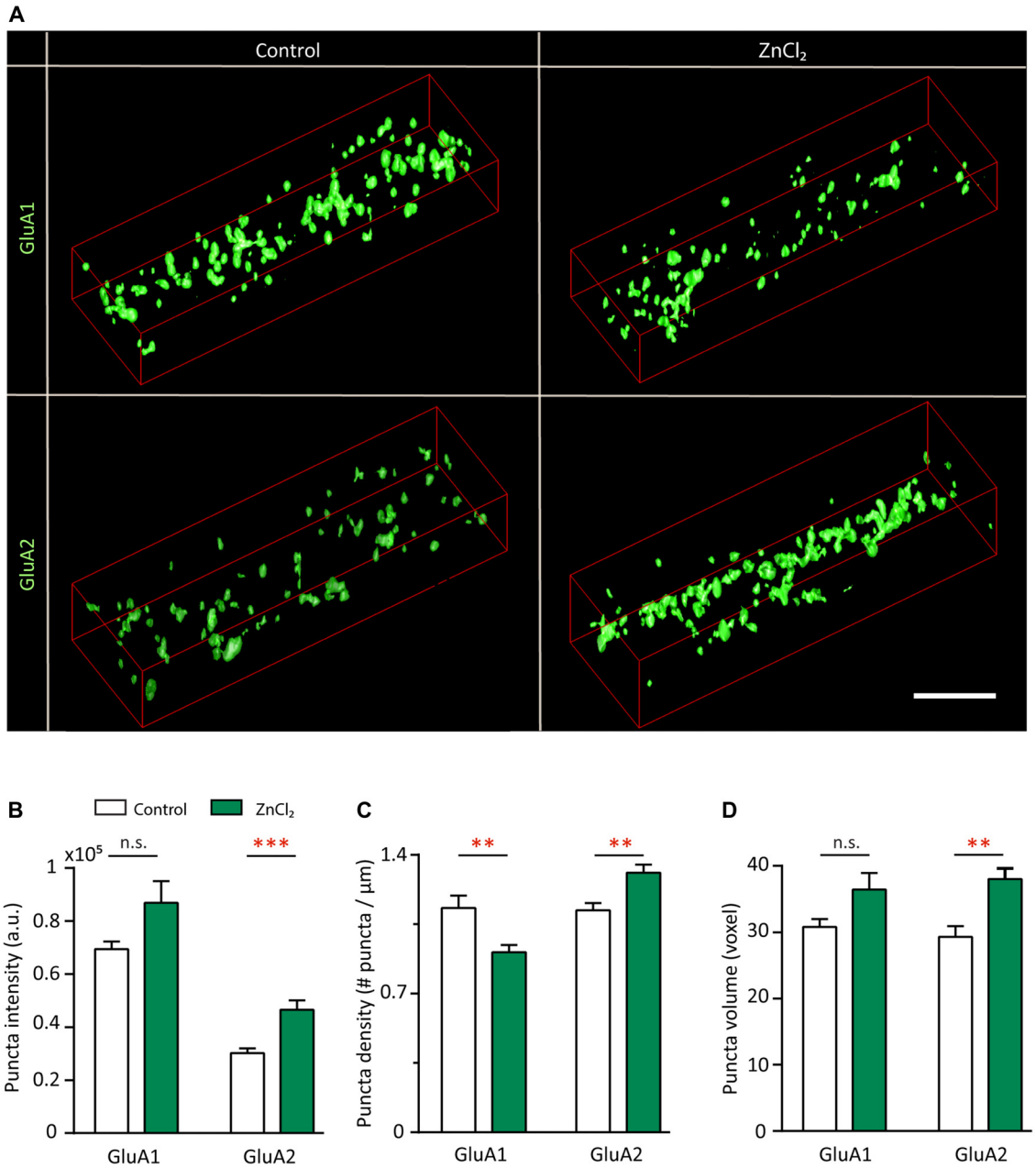

FIGURE 7 | Zinc treatment recruits surface GluA2 and disperses surface GluA1. **(A)** Straightened dendrites from young hippocampal neurons (DIV 14) treated with control (left) or 10 μM $ZnCl_2$ (right) conditions. Neurons were live surface labeled for GluA1 (top) or GluA2 (bottom). Scale bar: 4 μm. **(B–D)** Summary graphs showing quantification of GluA1 and GluA2 puncta intensity **(B)**, density **(C)** and volume **(D)** [mean ± SEM; Mann-Whitney test for GluA1, $N = 19$ (control), 22 ($ZnCl_2$) dendrites from 10 to 14 neurons from two culture preps; for GluA2, $N = 24$ dendrites from 10 to 14 neurons from two culture preps; n.s. $p \geq 0.05$, $^{**}p < 0.01$, $^{***}p < 0.001$].

the hypothesis that zinc selectively induces GluA2 incorporation to Shank3-positive puncta. A similar increase in intensity in response to zinc was seen in GluA2 at Shank2 puncta (64.05%) with no significant change in volume (**Figures 8D,E** and **Table 1**). In contrast, zinc decreased GluA1 overlap with Shank3 as measured by volume (**Figure 8E** and **Table 1**). A significant concomitant increase in intensity of GluA1 (132.65%; $p < 0.0004$) was seen at non-Shank2 sites (**Table 1**), perhaps corresponding with non-synaptic locations since Shank2 and Shank3 showed near 100% colocalization with other postsynaptic markers (Homer and PSD95) at this age (data not shown).

These findings implicate Shank2 and Shank3 as key players in the AMPAR subunit switch induced by zinc. Our treatment protocol did not elicit any changes of Shank2 or Shank3 puncta intensity, volume or density (data not shown), implying that zinc

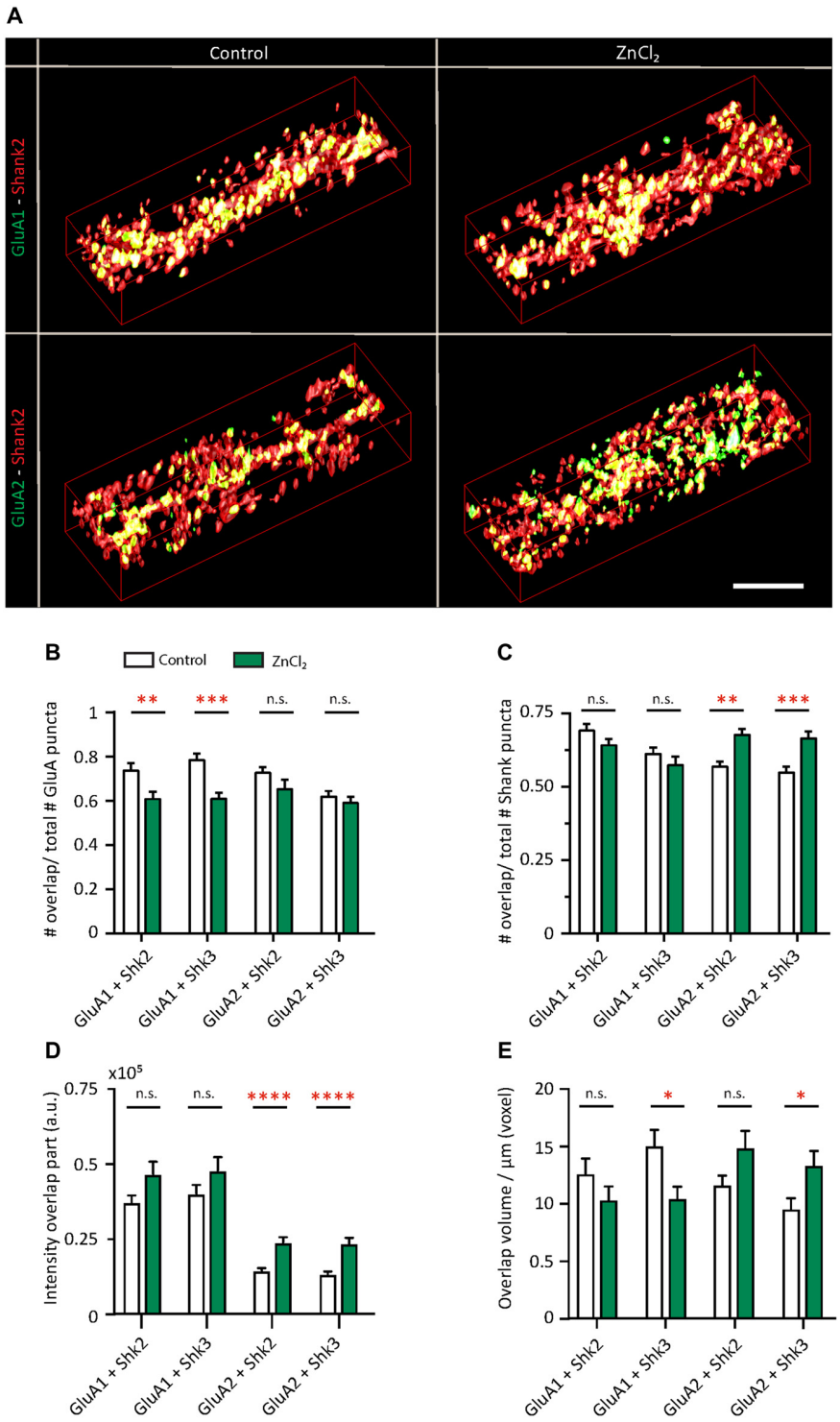

FIGURE 8 | Zinc treatment alters the colocalization between AMPAR subunits and Shank. **(A)** Straightened dendrites from young hippocampal neurons (DIV 14) treated with control (left) or 10 µM $ZnCl_2$ (right). Neurons were live surface labeled for GluA1 (green; top) or GluA2 (green; bottom) before being fixed and co-immunostained for both Shank2 (red) and Shank3 (not shown). Yellow indicates colocalization. Scale bar: 4 µm. **(B–E)** Three-dimensional colocalization analysis of pairwise puncta overlap using IMFLAN3D as measured by the fraction of overlap **(B,C)**, intensity **(D)** and volume **(E)** for baseline and $ZnCl_2$ conditions (mean ± SEM) [Mann-Whitney test, for GluA1 + Shank3 or Shank2, $N = 19$ (control) and 22 ($ZnCl_2$) dendrites from 10 to 14 neurons from two culture preps; for GluA2 + Shank3 or Shank2, $N = 24$ dendrites from 10 to 14 neurons from two culture preps; for Shank2 + Shank3, $N = 43$ (control) and 46 ($ZnCl_2$) dendrites from 20 to 25 neurons from four culture preps; n.s. $p \geq 0.05$, $^{*}p < 0.05$, $^{**}p < 0.01$, $^{***}p < 0.001$, $^{****}p < 0.0001$].

TABLE 1 | Effect of zinc on GluA—Shank colocalization.

		Intensity of overlap	Volume of overlap/μm	Fraction of overlap/total GluA	Fraction of overlap/total Shank
GluA1	**Shank2**	n.s.	n.s.	↓ 17.4% (0.0074)	n.s.
	Shank3	n.s.	↓ 30.51% (0.0209)	↓ 22.34% (0.0002)	n.s.
	Non-Shank2	↑ 132.65% (<0.0004)	n.s.	↑ 48.39% (0.0074)	n.s.
	Non-Shank3	n.s.	n.s.	↑ 80.99% (0.0002)	n.s.
GluA2	**Shank2**	↑ 64.05% (<0.0001)	n.s	n.s.	↑ 19.22% (0.0010)
	Shank3	↑ 75.04% (<0.0001)	↑ 40.19% (0.0153)	n.s.	↑ 21.32% (0.0008)
	Non-Shank2	n.s.	n.s.	n.s.	↓ 25.23% (0.0010)
	Non-Shank3	n.s.	n.s.	n.s.	↓ 25.87% (0.0008)

Values are expressed as % change of zinc condition in comparison to control, (p value). For p > 0.05, the values of changes are written as "n.s.". Red and green arrows indicate the direction of changes (Red arrow: Decrease, Green arrow: Increase)

mainly affects Shank activation (Arons et al., 2016) in association with a change in binding preference from GluA1 to GluA2.

Zinc-Sensitive Recruitment of GluA2 via Exocytosis and Lateral Diffusion Is Mediated by Shank3

To further understand which cellular processes underlie the zinc-dependent recruitment of GluA2, we performed a sequential dual-labeling experiment to monitor both lateral diffusion and exocytosis with zinc treatment. Here, we used a recently developed method to visualize native GluA2 using chemical AMPAR modification (CAM2) reagents that allow for covalent chemical labeling with a small fluorophore (Alexa fluors; Wakayama et al., 2017). Control experiments were performed to confirm the specificity and saturation binding of all surface GluA2 for this dual-labeling experiment in our neuronal culture system. Similar to the original study (Wakayama et al., 2017), we found that 80%–90% of CAM2 puncta colocalized with GluA2 staining, whereas there was limited colocalization between CAM2 and GluA1 (data not shown). We then next tested varying concentrations of CAM2 for labeling and chose an excess concentration (3 μM) for subsequent experiments to ensure saturated labeling of surface GluA2.

In order to examine AMPAR dynamics with zinc, surface GluA2 subunits were initially labeled with Alexa 647-CAM2 for saturated labeling. Neurons were then treated with control or $ZnCl_2$ conditions, which could recruit receptors from outside of the synapse and increase synaptic Alexa 647-CAM2 signal. If exocytosis was enhanced with zinc treatment, these new surface receptors would be labeled during the second labeling with Alexa 488-CAM2. Shank2 or Shank3 were also labeled as postsynaptic markers and used to understand their roles in zinc-sensitive AMPAR dynamics (**Figure 9A**).

To this end, we measured the fluorescence intensity in both CAM2 channels at Shank-positive puncta. Using puncta-by-puncta analysis (Friedman et al., 2000; Arons et al., 2012), we found that both lateral diffusion and exocytosis were involved with the zinc-dependent trafficking of GluA2 to synaptic sites as measured by the increase of both A647-CAM2 (16.61%, $p < 0.0001$) and A488-CAM2 puncta intensity (14.1%, $p < 0.0001$; **Figures 9B–D** and **Supplementary Figure S5A**). The total puncta density was not affected by zinc application (**Supplementary Figure S5B**), which agrees with the stable mEPSCs frequency during zinc treatment (**Figure 4F**). The relative rate between exocytosis and lateral diffusion was likely not affected by zinc since there was no difference in the slope of Alexa 647-CAM2 to Alexa 488-CAM2 (**Supplementary Figure S5C**).

Next, to assess whether there is a direct correlation between the amount of Shank2 or Shank3 and Alexa-labeled CAM2, we measured the fluorescence intensity of Shank at each individual puncta as well as the intensity of the CAM2 in both channels. Fluorescence intensities of individual Alexa-labeled CAM2 puncta were then plotted as a function of the corresponding colocalized Shank2 or Shank3 puncta intensities, and linear regression analysis applied for the individual synaptic intensities (**Figures 9E–H** and **Supplementary Figures S5D,E** O'Brien et al., 1998; Rumbaugh et al., 2003). Consistent with previous results (**Figures 8B,C**), we found a significant increase in the slope of A647-CAM2 intensity at Shank3-positive puncta with zinc treatment (**Figures 9E,G**), which means that for a given amount of Shank3 there is an increase in A647-CAM2. This can serve as a proxy for the increase in ratio of GluA2 to Shank3 through lateral diffusion (A647-CAM2; 139.8%, $p = 0.0001$; **Figure 9G**) or through exocytosis (A488-CAM2; 48.66%, $p = 0.0186$; **Figure 9H**). In contrast, the correlation between Shank2 and GluA2 for both processes was unchanged with zinc treatment (**Figures 5G,H** and **Supplementary Figures S5D,E**), implying that Shank2 did not directly influence the zinc-sensitive dynamics of GluA2. Taken together, these results imply that: (1) both lateral diffusion and exocytosis contributed to the GluA2 pool recruited by zinc; and (2) Shank3 was involved in both processes.

Characterization of Shank2 and Shank3 Knockdown in Young Neurons

To understand if Shank2 or Shank3 are required for the zinc-sensitive regulation of AMPAR structure and functions, we employed shRNA to decrease the endogenous expression of Shank2 or Shank3 in neurons (**Figure 10**). Multiple shRNA constructs for Shank2 and Shank3 were designed in a pZoff vector to target the various isoforms of each protein (**Supplementary Figures S6A,B** and **Supplementary Tables S1, S2**; Boeckers et al., 1999; Lim et al., 1999; Leal-Ortiz et al., 2008). To assess their efficacy in neurons, we used plasmid-based transfection and immunostained for

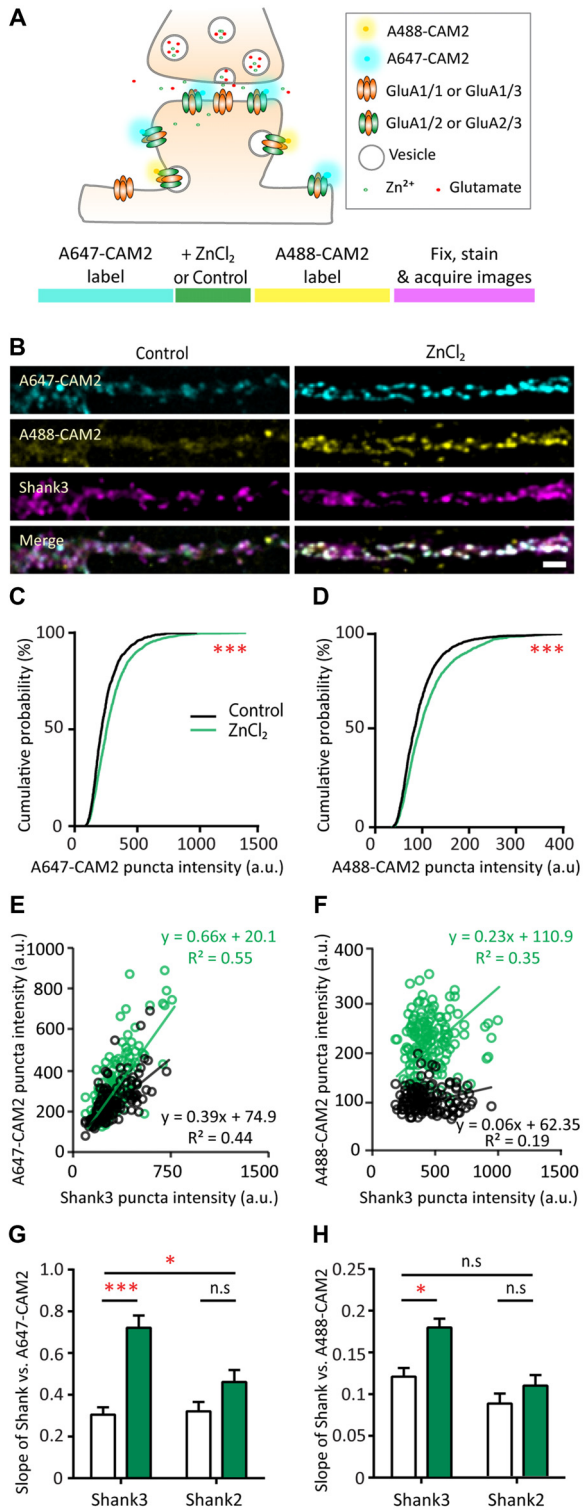

FIGURE 9 | Probing mechanisms of zinc-dependent AMPAR trafficking with CAM2. **(A)** Schematic of sequential dual chemical labeling of GluA2 subunit of AMPAR using A647-CAM2 and A488-CAM2 reagents (top). Sequence of the labeling experiment using CAM2 to probe zinc-dependent AMPAR trafficking (bottom). **(B)** Straightened dendrites of hippocampal neurons were pre-labeled (*Continued*)

FIGURE 9 | Continued
with A647-CAM2 (top), then treated with either control (10 μM $MgCl_2$, left) or 10 μM $ZnCl_2$ (right) conditions before being labeled with A488-CAM2 (second panel from the top), and finally fixed and stained for Shank3 (third panel from the top) and Shank2 (not shown). White puncta in the merge images (bottom) indicate colocalization of all three signals. Scale bar: 5 μm. **(C,D)** Cumulative probability histograms of puncta intensity from control and $ZnCl_2$ conditions for A647-CAM2 **(C)** and A488-CAM2 **(D)** signal (K.S., $N \sim 1500$ puncta from 25 (control) and 30 ($ZnCl_2$) cells from three culture preps; $^{***}p < 0.0001$). **(E,F)** Example of fluorescence intensities of individual colocalized CAM2 puncta (A647 or A488) plotted as a function of the corresponding colocalized Shank3 puncta intensities for two neurons. Comparisons were made between sister cultures. Linear regression is shown as a solid line for each condition (black = control; green = zinc). **(G)** Summary graph showing comparison of the slopes of linear regressions of puncta intensity between Shank3 or Shank2 and A647-CAM2 from control (white) and $ZnCl_2$ (green) conditions. **(H)** Similar to G but for Shank3 or Shank2 and A488-CAM2 [two-way ANOVA, Shank2 co-stained neurons, $N = 15$ (control) and 20 ($ZnCl_2$) cells from 3 to 4 coverslips from two culture preps; Shank3 co-stained, $N = 10$ cells from 3 to 4 coverslips from two culture preps; n.s. $p \geq 0.05$, $^{*}p < 0.05$. Sidak correction multiple *post hoc* comparisons; n.s. $p \geq 0.05$, $^{*}p < 0.05$, $^{***}p < 0.001$].

Shank2 and/or Shank3 (**Figures 10A,B** and **Supplementary Figure S6C**). shRNA-Shank2 (shShk2) targeting the proline-rich domain of Shank2 (* in **Supplementary Figure S6A**) was the most effective, reducing Shank2 puncta intensity by 87.5% ($p = 0.0335$; **Figure 10C**) and decreasing the puncta density by 90.56% ($p = 0.001$; **Figure 10D**). The most effective shRNA for Shank3 targeting the 3′UTR domain (shShk3; * in **Supplementary Figure S6B**) showed a significant decrease in Shank3 puncta density (35.56%, $p = 0.0372$; **Figure 10F**) and no change in intensity (**Figure 10E**), accompanied by a 122.08% increase of Shank2 puncta intensity ($p = 0.0233$; **Figure 10C**).

We next subcloned the two successful shRNAs described above into a lentivirus vector to create LV/eGFP/shRNA constructs (**Supplementary Figure S6D**) to ensure higher infection efficiency and avoid any potential overexpression artifacts associated with plasmid-based transfections. Lysates of hippocampal neurons infected with lentiviruses at 100% infectivity were harvested after 14 DIV and probed with antibodies for Shank2 and Shank3 (**Figures 10G,H** and **Supplementary Figures S6E,F**). With the shShk2, we observed a dramatic loss of most major Shank2 isoforms (**Figure 10I**) along with the reduction of the third longest isoform of Shank3 (c: 58.98% **Figure 10J**). The effect of shShk2 on Shank3 expression was similar to previous studies suggesting that Shank2 might be necessary for recruiting synaptic Shank3 over development (Grabrucker et al., 2011; Shi et al., 2017). On the other hand, the shShk3 produced ∼50%–80% loss of the three longest Shank3 isoforms (a: 70.05%, b: 80.01%, c: 53.6%; **Figure 10J**), which are the major zinc-binding isoforms. This shRNA also induced large increases of all Shank2 isoforms (**Figure 10I**), suggesting that there might be a compensation of Shank2 due to the loss of Shank3.

Next, we assessed the effects of Shank2 and Shank3 knockdown on AMPAR function. Here, we compared AMPAR-mediated mEPSCs from neurons infected with shLuci

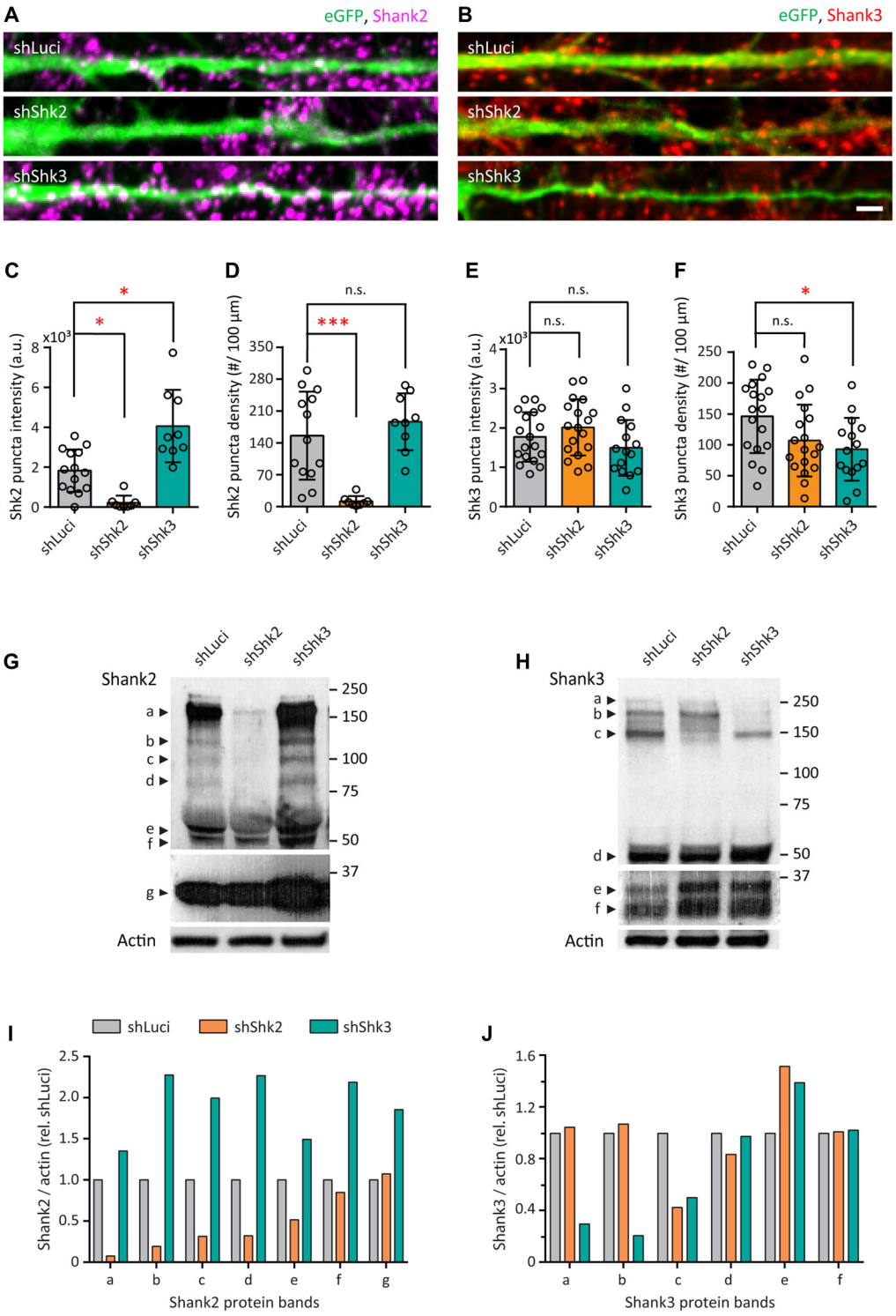

FIGURE 10 | Short-hairpin RNA (shRNA)-mediated knockdown of Shank2 and Shank3. **(A,B)** Straightened dendrites of transfected hippocampal neurons expressing a bicistronic construct with enhanced green fluorescent protein (eGFP; green) and shRNA hairpins for shLuciferase (shLuci, top), shShank2 (shShk2, middle) or shShank3 (shShk3, bottom) and immunostained for Shank2 (magenta; **A**) or Shank3 (red; **B**) after 14 DIV. Scale bar: 5 µm. **(C–F)** Summary graphs showing quantification of Shank2 **(C,D)** and Shank3 **(E,F)** puncta intensity and density (mean ± SEM) for different knockdown conditions (Kruskal-Wallis one-way ANOVA with Dunn's correction *post hoc* multiple comparisons, Shank2 staining: shLuci, $N = 14$; shShk2, $N = 8$; shShk3, $N = 9$ dendrites from 8 to 12 neurons from three culture preps. Shank3 staining: shLuci, $N = 18$; shShk2, $N = 18$; shShk3, $N = 15$ dendrites from 8 to 12 neurons from three culture preps; n.s. $p \geq 0.05$,

(*Continued*)

FIGURE 10 | Continued
$^{*}p < 0.05$, $^{***}p < 0.001$). **(G,H)** Western blots of cellular lysates from dissociated hippocampal neurons infected with lentivirus for shLuci, shShk2 or shShk3 immunoblotted for Shank2 **(G)** or Shank3 **(H)** antibodies. Protein molecular weights are indicated at the right in kDa. Different isoforms are labeled at the left. Top two panels in **(G,H)** show different exposures of the same films for optimal visualization of different isoforms. Actin was used as a loading control (bottom panels in **G,H**). **(I,J)** Quantification of Shank2 **(I)** or Shank3 **(J)** protein levels for different isoforms in hippocampal neurons for different knockdown conditions from two cultures per condition. "Shank/actin (rel. shLuci)" refers to the expression level of Shank2 or Shank3 normalized to actin and then to shLuci control.

(control), shShk2 or shShk3 (**Figure 11A**). Knockdown of Shank2 led to a modest reduction of mEPSCs amplitude as seen in the cumulative distribution (5.18%, $p = 0.0072$; **Supplementary Figure S7A**). In contrast, the AMPAR response in Shank3 knockdown neurons had a faster rise time (9.6%, $p = 0.0032$; **Supplementary Figure S7B**) and decay time (20.89%, $p < 0.0001$; **Figure 11B**). The faster kinetics led to a reduction in charge transferred by AMPAR in Shank3 knockdown neurons (16%, $p = 0.0004$, **Figure 11C**). Taken together, these results support that Shank3 is important for maintaining the kinetics, and hence, synaptic efficacy of AMPAR synaptic response in young neurons.

Zinc-Sensitive Regulation of AMPAR in Young Neurons Is Dependent on Shank2 and Shank3

Given that 10 μM zinc treatment led to increased incorporation of GluA2 to Shank puncta (**Figures 8**, **9**), we next asked whether Shank expression is necessary for the zinc-sensitive increase of AMPAR function. To address this question, we recorded and compared AMPAR mEPSCs from shLuci, shShk3 and shShk2 neurons at baseline and during zinc treatment (**Figure 11D**). Neurons infected with shLuci preserved their zinc-sensitivity with an increase in decay time (12.63%, $p = 0.0069$) and peak amplitude (30.44%, $p = 0.044$; **Figure 11E** and **Supplementary Figure S7C**). As a result, the charge transferred by AMPARs in shLuci neurons was increased by zinc treatment (16%, $p < 0.0001$; **Figure 11F**). The effects of zinc on shLuci neurons are comparable to those on untransfected neurons described in **Figure 4** ($p > 0.05$).

In contrast, we observed no zinc-sensitive increase in either decay time or charge with zinc addition in shShK3 neurons, confirming that synaptic expression of Shank3 is necessary for the zinc recruitment of GluA2-containing AMPARs (**Figures 11E,F**). Instead of being potentiated by zinc treatment, mEPSCs in Shank3 knockdown neurons displayed a decrease in peak amplitude (37.42%, $p = 0.012$) and frequency (34.78%, $p = 0.035$) upon zinc treatment (**Supplementary Figures S7C,E**). This observation revealed a separate zinc-dependent modulation of AMPAR activity, perhaps via the reduction of surface GluA1 as described in **Figure 7** from Shank synapses. Furthermore, knockdown of Shank2 also abolished the zinc sensitivity of AMPARs in all measures examined (decay time, charge, amplitude and rise time; **Figures 11E,F** and **Supplementary Figures S7C–E**). Together, these data revealed the necessity of both Shank2 and Shank3 expression to zinc-induced potentiation of AMPAR function.

DISCUSSION

The dynamic regulation of neurotransmitter receptor number and composition is a fundamental mechanism underlying synaptic plasticity, synaptic maturation and neural circuit development (Henley et al., 2011; Bassani et al., 2013; Henley and Wilkinson, 2016). This regulation is critical for the encoding of information, cognition and behavior and is vulnerable to genetic and environmental insults associated with ASD (Shepherd and Huganir, 2007; Lee et al., 2016; Kim et al., 2018). In this study, we explored the molecular mechanisms underlying zinc-dependent regulation of synaptic transmission via the postsynaptic scaffolding proteins Shank2 and Shank3. Our data reveal that young hippocampal neurons undergo a zinc-dependent subunit switch of AMPAR from GluA2-lacking to GluA2-containing receptors, which dictate their biophysical properties. In addition, we found that Shank proteins are key mediators of this regulation since they were necessary for this zinc-induced enhancement of AMPARs. Importantly, postsynaptic zinc, an activator of Shank2 and Shank3, was found to increase transiently and reversibly with neuronal depolarization, likely due to release of zinc from presynaptic vesicles or postsynaptic sources. Upon treatment with zinc, GluA2 was preferentially recruited into synapses by both lateral diffusion and exocytosis with a concomitant dispersion of GluA1. This occurred at pre-existing Shank2 and Shank3 puncta in young neurons, converting these synapses from GluA2-lacking to GluA2-containing. This zinc-stimulated subunit switch of surface GluA2 was accompanied by an increase in amplitude, longer decay time and reduced inward rectification of AMPAR-mediated currents and was dependent on Shank2 and Shank3. In summary, these results provide new insights into a cooperative dynamic regulation of AMPAR composition driven by the zinc signaling pathway via Shank2 and Shank3 at developing synapses, a critical period for local control of AMPAR composition.

Bimodal Action of Zinc on Shank2 and Shank3 for Dynamic Regulation of AMPA Receptors

During development and plasticity, GluA2 is a tightly regulated subunit of glutamate receptors (Isaac et al., 2007). GluA2-containing AMPARs at synapses are controlled through a variety of mechanisms and significantly increase with maturation (Pickard et al., 2000; Kumar et al., 2002; Brill and Huguenard, 2008; Mignogna et al., 2015). Here, we found GluA2 was recruited to an increasing number of synapses in dissociated hippocampal neurons, almost doubling during our developmental window of interest (**Figure 2**). Shank3 likewise increased in expression at individual synapses and number of synapses in this same period with a particular recruitment to

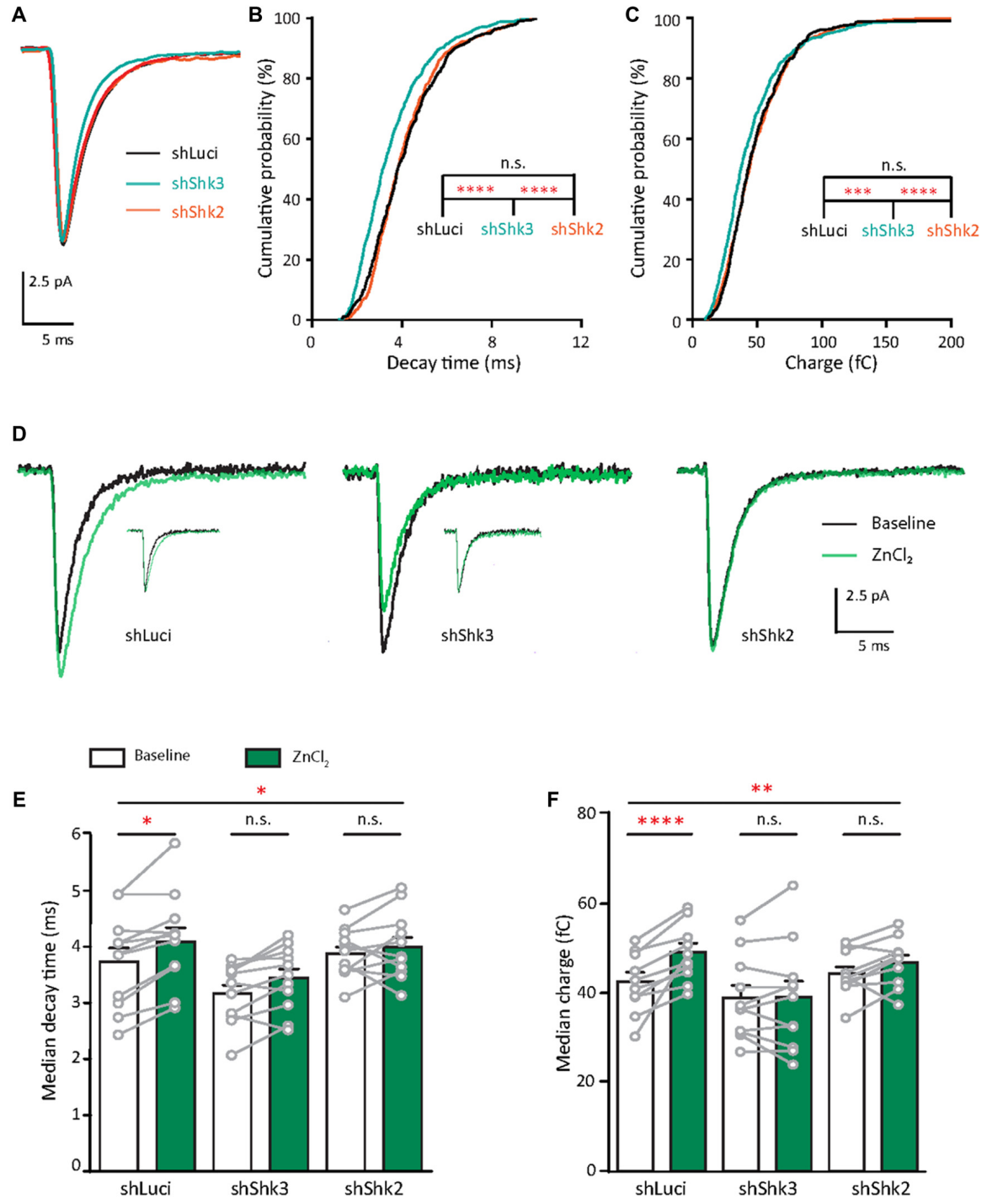

FIGURE 11 | Shank knockdown alters AMPAR function and suppresses their zinc-dependent changes. **(A)** Ensemble-averaged mEPSCs from recordings of hippocampal neurons infected with lentiviruses expressing shLuci (black), shShk3 (blue) or shShk2 (orange; $N = 11$ cells per condition from five to seven culture preps per condition). **(B,C)** Cumulative probability histograms of decay time **(B)** and charge **(C)** of isolated events of different conditions (Kruskal-Wallis one-way ANOVA followed by Dunn's correction *post hoc* multiple comparisons, $N = 400$–600 events from 11 neurons from five to seven culture preps per condition; n.s. $p \geq 0.05$, $^{***}p < 0.001$, $^{****}p < 0.0001$). **(D)** Average mEPSCs from recordings at baseline (black) and zinc (green) conditions of individual hippocampal neurons infected with lentiviruses expressing shLuci (left), shShk3 (middle) or shShk2 (right; $N = 11$ cells from five to seven culture preps per condition). mEPSCs normalized to baseline response are shown in corresponding insets to differentiate effect of zinc on decay kinetic. **(E,F)** Summary graphs with per-cell-basis pairwise comparisons of decay time **(E)** and charge **(F)** between baseline and $ZnCl_2$ conditions in different conditions (median ± SEM; two-way ANOVA; $^{*}p < 0.05$, $^{**}p < 0.01$. Sidak correction multiple *post hoc* comparisons, $N = 10$–11 cells from five to seven culture preps per condition; n.s. $p \geq 0.05$, $^{*}p < 0.05$, $^{****}p < 0.0001$).

mature synapses on dendritic spines (**Figure 1**). The SH3 domain of Shank proteins binds to GRIP suggesting that Shank3 might indirectly interact with and recruit GluA2 to synapses via the APB/GRIP complex (Sheng and Kim, 2000). Functionally, the knockdown of Shank3 has been shown to result in decreased GluA2 expression and GluA2-mediated AMPAR properties, such as reduced inward rectification (Bariselli et al., 2016; Mei et al., 2016). In our current study, Shank3 knockdown resulted in AMPAR mEPSCs with a faster decay time (**Figure 11**), which supports the concept that Shank3 can promote synaptic clusters of GluA2. Furthermore, Shank3 was shown to directly facilitate GluA2-containing AMPAR activity since zinc preferentially enhanced GluA2 at Shank3 puncta (**Figure 8** and **Table 1**). Both Shank2 and Shank3 appear to be necessary for the zinc-induced enhancement of synaptic AMPARs since knocking down either Shank3 or Shank2 eliminated the zinc effect. In both cases, this is likely due to a reduction of Shank3 at synapses (**Figure 10**), consistent with a recent study showing Shank2 is necessary for recruitment of Shank3 (Shi et al., 2017).

Clues to the mechanism for how Shank3 and zinc recruit GluA2-containing AMPAR to synapses can be found in the role of Shank3 in receptor trafficking (Okamoto et al., 2001; Lu et al., 2007; Verpelli et al., 2011; Raynaud et al., 2013), and zinc may be a key underlying driver. For example, zinc could facilitate the interaction between Shank3 and the Homer1b/dynamin-3 complex to tether the endocytic zone in close proximity to the PSD. This would allow for more rapid receptor recycling that could increase total surface GluA2 (Okamoto et al., 2001; Lu et al., 2007; Petrini et al., 2009). Using CAM2 labeling, we showed that the magnitude of the zinc-induced recruitment of GluA2 via lateral diffusion and exocytosis was correlated to the amount of synaptic Shank3 (**Figure 9**). Additionally, we found that elevating zinc induced a trafficking of GluA2 to Shank3-positive puncta from non-Shank3 sites (**Figure 8** and **Table 1**). These functions are plausible, especially considering the strong expression level of Shank3 in dendrites and its known interaction with the cytoskeleton via cortactin/actin binding (MacGillavry et al., 2016).

Since zinc-mediated recruitment of GluA2-containing AMPAR to Shank synapses did not strongly affect amplitude or frequency for AMPA mEPSCs, this implies that zinc might concomitantly induce the dispersion/removal of other types of synaptic AMPARs. Indeed, our data revealed that elevation of zinc also induced a synaptic removal of GluA1 from Shank2-positive synapses, indicating that GluA1 dispersion may be mediated by Shank2 (**Figures 8**, **11**). Consistent with this concept, previous studies showed that Shank2 directly associates and colocalizes with GluA1 and is critical for its synaptic expression, particularly at nascent synapses (Pickard et al., 2000; Uchino et al., 2006; Ha et al., 2016; Peter et al., 2016; Szíber et al., 2017). These findings indicate that Shank2 may regulate

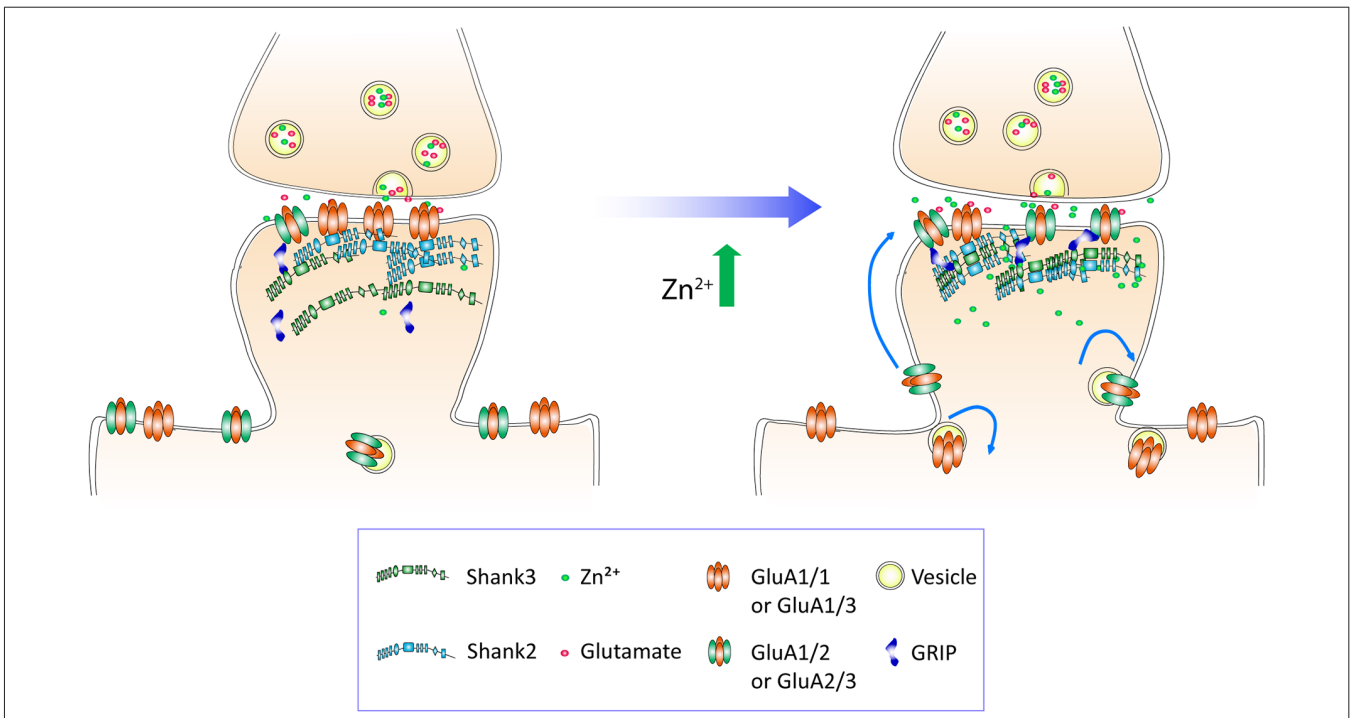

FIGURE 12 | A model for Shank mediation of zinc-dependent subunit switch of AMPAR in developing synapses. A glutamatergic synapse of a wild-type (WT) young neuron is shown with low levels of Shank3 (green) and GluA2 (teal) and high levels of Shank2 (blue) and GluA1 (orange). The synaptic complement changes with zinc-sensitive recruitment of synaptic GluA2 via exocytosis and lateral diffusion (blue arrows), leading to potentiation of AMPAR-mediated synaptic activity. The zinc-recruitment of GluA2 correlated with the level of synaptic Shank3. Zinc addition also led to reduction of synaptic GluA1, which is most likely driven by Shank2. Hence, loss of either Shank2 or Shank3 abolished the zinc-sensitive potentiation of AMPAR-mediated synaptic transmission.

the synaptic localization of GluA1. In support of this idea, our data confirmed that Shank2 initially co-clustered with surface GluA1 (**Figure 8** and **Table 1**) and knockdown of Shank2 led to reduction of AMPAR mEPSC amplitude (**Supplementary Figure S7**) in young neurons, potentially indicative of fewer GluA1 receptors. Furthermore, Shank2 overexpression, a condition induced by expressing shShk3, also resulted in synapses with faster kinetics (**Supplementary Figure S7B** and **Figures 11B,C**) perhaps via the increase recruitment of GluA1 to Shank2 sites. In contrast, elevating zinc reduced surface GluA1 puncta density. This could be due to increased endocytosis and/or diffusion of GluA1 away from Shank2-positive sites (**Figure 8** and **Table 1**). In line with a role of Shank2 and zinc in the synaptic removal of GluA1, our data showed that the zinc-induced reduction of AMPAR mEPSCs amplitude was prominent at synapses lacking Shank3 (**Supplementary Figure S7C**), a condition that creates synapses dominated by Shank2 (**Figure 10**). This effect of zinc, however, failed to occur in Shank2-lacking synapses (**Supplementary Figure S7C**).

Several mechanisms could explain the effects of zinc on downregulating GluA1 level at Shank2 sites. First, zinc binding to the SAM domain could favor a new conformation of Shank2 within the Shank scaffolding network or the complex with other molecules, all of which could have lower affinity or fewer docking sites for GluA1. This potential conformational change of Shank2 might affect its interaction with dynamin-2 (Okamoto et al., 2001) to facilitate GluA1 internalization (Carroll et al., 1999). Additionally, zinc could affect GluA1 synaptic dispersion by regulating the PKA, PKC or CaMKII-dependent phosphorylation of this AMPAR subunit either directly (Noh et al., 2001) or via crosstalk with calcium signaling (Hershfinkel et al., 2001; Takeda et al., 2008). Intriguingly, reduced phosphorylation of GluA1 at sites S831 and S845 has been reported in a Shank2 knockout mouse model (Won et al., 2012), raising yet another possible mechanism for zinc to regulate Shank2-dependent redistribution of GluA1.

In summary, the data presented in this study suggest a model for how zinc and zinc-sensitive Shank proteins regulate AMPAR function at developing synapses. Under basal conditions in young neurons, Shank2 appears to promote the synaptic localization and molecular anchoring of GluA1-containing receptors. Elevating zinc near synapses, as occurs during synaptic transmission, then exerts two effects: preferentially recruiting GluA2 to Shank3 synapses through both lateral diffusion and exocytosis, while simultanously promoting the removal of GluA1 receptors from Shank2 complexes (**Figure 12**). In this model, zinc interactions with Shank molecules may offer a general mechanism to shape the biophysical properties at developing glutamatergic synapses. While there are clear differences in the effects of shShk2 and shShk3 on Shank2 and Shank3 expression, both shRNAs induced changes in protein levels of these molecules. Future studies should attempt to parse the specific roles of Shank2 and Shank3 using strategies that result in cleaner knockdown or knockout of each protein.

Functional Implications of Zinc-Sensitive Control of AMPAR Subunit Composition

Our results suggest that a major function of the synaptic zinc-Shank pathway is to facilitate synaptic maturation. Shank3 was found to be necessary for AMPAR maturation in the ventral tegmental area (Bariselli et al., 2016). It is likely that during development of hippocampal neurons, Shank2 and Shank3 act as zinc-sensitive mediators to convert GluA2-lacking to GluA2-containing AMPAR synapses. More specifically, our data support the proposed model in which zinc could trigger Shank3 to accumulate more GluA2-containing AMPAR and act on Shank2 to remove GluA1-containing AMPAR over time. Perturbations of this pathway specifically during the prenatal period or early postnatal development have been linked to delayed AMPAR maturation, circuit dysfunction and behavioral deficits, further emphasizing the role of zinc-sensitive Shank proteins and zinc in synapse maturation and for the formation of associated brain circuits (Peça et al., 2011; Grabrucker et al., 2014; Bariselli et al., 2016; Mei et al., 2016). It is intriguing to speculate that other features of synaptic maturation, such as the subunit switch of NMDAR, might also be mediated by zinc and zinc-sensitive Shank proteins and that these processes might be shared mechanisms for synaptic development in pyramidal neurons of other brain areas. In order to directly understand whether zinc signaling mediates synaptic maturation, future studies could focus on revealing the effect of chronic chelation of zinc in the transition period from young to mature neurons during the development of synapses. However, a major challenge of such an approach is to select the appropriate zinc chelator that does not severely impair neuronal health, synapse stabilization or synaptic localization of Shank2 and Shank3 (Grabrucker et al., 2011; Arons et al., 2016). Moreover, since the source of zinc to activate Shank2 and Shank3 could be from either presynaptic vesicles or postsynaptic stores, both extracellular and intracellular zinc chelators should be considered to selectively chelate presynaptic- or postsynaptic-released zinc, respectively (Besser et al., 2009; Pan et al., 2011; Grabrucker et al., 2014).

The loss of AMPAR zinc-sensitivity in mature neurons (**Figure 6**) might be regulated by a variety of mechanisms. During early stages of development, the size of the synapse, and the number and composition of receptors with their complement of proteins are plastic (Craig et al., 1993; Rao et al., 1998; Boeckers et al., 1999; Kumar et al., 2002; Grabrucker et al., 2011; Valnegri et al., 2011). In the presence of zinc and zinc-sensitive Shank molecules, synapses are more dynamic and less stable (Grabrucker et al., 2011; Arons et al., 2012, 2016). Additionally, young synapses could have more available docking sites to accommodate zinc-induced recruitment of GluA2-containing receptors (Czöndör et al., 2012). Over development, the increase of Shank1 at synapses (Grabrucker et al., 2011) and the loss of zinc-sensitive recruitment of molecules may synergistically create a more stable/less plastic state. Also, a reduction in the diffusion rate of AMPAR could hinder zinc-sensitive recruitment of AMPAR via lateral diffusion in mature neurons (Groc et al.,

2006; Czöndör et al., 2012). Another possibility is that the high content of GluA2 in mature neurons (**Figure 2**) could result in the reduction of AMPAR zinc sensitivity (**Figure 5D**) by affecting zinc entry (Jia et al., 2002; Takeda et al., 2007). However, we found that intracellular zinc levels of neurons at different DIV (11–30) were similarly responsive to exogenous manipulations (**Supplementary Figure S2**), suggesting that the availability of zinc is not a limiting factor for mature neurons to respond to treatment. The mechanism shown here could allow for a means to downregulate AMPAR calcium signaling as seen in mature neurons. Considering that mature neurons can uptake zinc, it is possible a smaller subpopulation of synapses in mature neurons could undergo the AMPAR subunit switch dependent on their experience (Mattison et al., 2014). Furthermore, mature neurons may have other zinc-sensitive processes that play alternate roles in neuronal function, such as plasticity.

Does the zinc-sensitive dynamic control of AMPAR composition operate during plasticity? While zinc and zinc-sensitive Shank proteins may act together to regulate maturation of synapses, it is also reasonable to consider that they may additionally function to modulate AMPAR subunit composition during synaptic plasticity, e.g., during the induction and maintenance of long-term potentiation (LTP). More specifically, activity-dependent accumulation of postsynaptic zinc might activate Shank2 and Shank3 to replace GluA1-containing AMPARs with GluA2-containing receptors (Shi et al., 2001; Alberi et al., 2005). This AMPAR subunit switch mechanism might also enable synaptic long-term depression (LTD), especially at newly unsilenced synapses (Zhou et al., 2011; Selcher et al., 2012). Hence, the differential zinc sensitivity of synapses could allow them to be dynamically remodeled during Hebbian plasticity. Conversely, dysfunction of this pathway could contribute to the synaptic plasticity deficits seen in multiple Shank knockdown or zinc-deficient models (Lu et al., 2000; Jiang et al., 2011; Verpelli et al., 2011; Wang et al., 2011, 2016; Jaramillo et al., 2016). In another aspect of plasticity, a bidirectional model for synaptic scaling has emerged in which scaling up is dependent on increased synaptic accumulation of GluA2-containing receptors (Gainey et al., 2009; Anggono et al., 2011; Tatavarty et al., 2013; Ancona Esselmann et al., 2017). During synaptic scaling up due to chronic activity deprivation, one trafficking mechanism was shown in which GRIP was recruited to synaptic sites where it enhanced trafficking and/or stabilization of GluA2 (Gainey et al., 2015; Tan et al., 2015). Since Shank proteins have been reported to bind to GRIP and therefore could complex with GluA2 through the APB/GRIP (Sheng and Kim, 2000; Uemura et al., 2004), the zinc-sensitive dynamic regulation of AMPAR at developing synapses may converge in this same pathway. In general, this zinc-sensitive regulation of AMPAR could play roles to modulate receptor compositions and synaptic strength.

Zinc, Zinc-Sensitive Shank Proteins and Autism Spectrum Disorders

Our study revealed a novel zinc/Shank-dependent molecular pathway for regulating AMPAR subunit switching that could affect the formation, maturation and plasticity of excitatory synapses. Consistently, alterations of AMPAR subunit compositions and/or synaptic recruitment have been seen in multiple Shank2 and Shank3 mouse KO models of ASDs (Ramanathan et al., 2004; Mejias et al., 2011; Hayashi et al., 2013; Mignogna et al., 2015; Bariselli et al., 2016; Chanda et al., 2016; Wegener et al., 2017). Our findings also offer a novel mechanism for understanding how zinc deficiency or disrupted zinc dynamics might be linked to individuals with ASDs (Yasuda et al., 2011; Grabrucker et al., 2014; Curtin et al., 2018). Specifically, we anticipate that zinc deficiency during early brain development could disrupt Shank functions (Grabrucker et al., 2011; Grabrucker, 2014), the composition of synaptic AMPAR and ultimately synaptic plasticity, network formation and behavior. With shared molecular deficits to Shank knockout mice, zinc deficiency could result in similar circuit and behavioral deficits broadly in a number of relevant animal models (Halas and Sandstead, 1975; Sandstead et al., 1978; Lu et al., 2000; Grabrucker et al., 2014; Hagmeyer et al., 2015). Taken together, our study adds to the current understanding of how Shank2 and Shank3 regulate multiple aspects of synaptic functions during development and plasticity. These results also indicate that genetic mutations and environmental insults might predispose individuals to ASDs by impairing this process. This realization might help improve future diagnostics and development of effective pharmacotherapies for ASDs (Grabrucker et al., 2014; Lee J. et al., 2015; Bariselli et al., 2016; Hagmeyer et al., 2018).

AUTHOR CONTRIBUTIONS

CG, JM and SAK conceived and developed the initial concepts for the project. HH, CG, JH and SAK designed the research. HH and SAK performed all experiments and wrote the manuscript in consultation with CG and JH. SL-O helped design shRNA and provided technical input for cell culture and biochemistry experiments. IH and SK provided CAM2 reagents and technical consultation for CAM2 experiments. HH, KL and SAK analyzed the data. SPM wrote the IMFLAN3D and SpineZap analysis packages and gave technical support for image analysis. All authors revised the manuscript.

FUNDING

This work was supported by the Vietnam Education Foundation, the Stanford Graduate Fellowship, the Schlumberger Faculty for the Future Fellow Program and the Stanford Neurosciences Graduate Program to HH; Grant-in-Aid for Scientific Research on Innovative Areas Chemistry for Multimolecular Crowding Biosystems (JSPS KAKENHI Grant no. 17H06348) in Japan to IH; Marsden Fund (Royal Society of New Zealand, Project Grant 13-UOA-053) to JM; the Federal Government of Germany (DFG) SFB958 and German Center for Neurodegenerative Diseases (DZNE) to CG; the National Institutes of Health (Grant # R21MH100717 and R33MH100717) to JH; and the Phelan-McDermid Syndrome Foundation Fellowship (SAK).

ACKNOWLEDGMENTS

We would like to thank members of the Huguenard and Garner laboratories for helpful discussions. In particular, we would like to thank Dr. Austin Reese for scientific input on experimental design and data analysis and critical reading of the manuscript; Dr. Eric Danielson for assistance with synaptic analysis using his SynPAnal software; Drs. Richard Reimer and Neal Waxham for helpful comments on the manuscript; Drs. Dong Li, Dan Madison, Lu Chen and Thomas Launey for advice on cell culture and electrophysiology experiments; Dr. Jun Ding for use of the cell culture facility; Dr. Chung-han Hsieh and the Wang lab for technical assistance and resources for Western blot experiments; Remko Dijkstra for technical support with image deconvolution using Huygens software; Carl Pisaturo for his technical and engineering expertise; and Rachel Kim and Sophia Kim for general help and support.

SUPPLEMENTARY MATERIAL

The Supplementary Material for this article can be found online at: https://www.frontiersin.org/articles/10.3389/fnmol.2018.00405/full#supplementary-material

REFERENCES

Alberi, S., Boda, B., Steiner, P., Nikonenko, I., Hirling, H., and Muller, D. (2005). The endosomal protein NEEP21 regulates AMPA receptor-mediated synaptic transmission and plasticity in the hippocampus. *Mol. Cell. Neurosci.* 29, 313–319. doi: 10.1016/j.mcn.2005.03.011

Amarzguioui, M., and Prydz, H. (2004). An algorithm for selection of functional siRNA sequences. *Biochem. Biophys. Res. Commun.* 316, 1050–1058. doi: 10.1016/j.bbrc.2004.02.157

Ancona Esselmann, S. G., Díaz-Alonso, J., Levy, J. M., Bemben, M. A., and Nicoll, R. A. (2017). Synaptic homeostasis requires the membrane-proximal carboxy tail of GluA2. *Proc. Natl. Acad. Sci. U S A* 114, 13266–13271. doi: 10.1073/pnas.1716022114

Anggono, V., Clem, R. L., and Huganir, R. L. (2011). PICK1 loss of function occludes homeostatic synaptic scaling. *J. Neurosci.* 31, 2188–2196. doi: 10.1523/jneurosci.5633-10.2011

Arons, M. H., Lee, K., Thynne, C. J., Kim, S. A., Schob, C., Kindler, S., et al. (2016). Shank3 is part of a zinc-sensitive signaling system that regulates excitatory synaptic strength. *J. Neurosci.* 36, 9124–9134. doi: 10.1523/jneurosci.0116-16.2016

Arons, M. H., Thynne, C. J., Grabrucker, A. M., Li, D., Schoen, M., Cheyne, J. E., et al. (2012). Autism-associated mutations in ProSAP2/Shank3 impair synaptic transmission and neurexin-neuroligin-mediated transsynaptic signaling. *J. Neurosci.* 32, 14966–14978. doi: 10.1523/JNEUROSCI.2215-12.2012

Bariselli, S., Tzanoulinou, S., Glangetas, C., Prévost-Solié, C., Pucci, L., Viguié, J., et al. (2016). SHANK3 controls maturation of social reward circuits in the VTA. *Nat. Neurosci.* 19, 926–934. doi: 10.1038/nn.4319

Baron, M. K., Boeckers, T. M., Vaida, B., Faham, S., Gingery, M., Sawaya, M. R., et al. (2006). An architectural framework that may lie at the core of the postsynaptic density. *Science* 311, 531–535. doi: 10.1126/science.1118995

Bassani, S., Folci, A., Zapata, J., and Passafaro, M. (2013). AMPAR trafficking in synapse maturation and plasticity. *Cell. Mol. Life Sci.* 70, 4411–4430. doi: 10.1007/s00018-013-1309-1

Berkel, S., Marshall, C. R., Weiss, B., Howe, J., Roeth, R., Moog, U., et al. (2010). Mutations in the SHANK2 synaptic scaffolding gene in autism spectrum disorder and mental retardation. *Nat. Genet.* 42, 489–491. doi: 10.1038/ng.589

Berkel, S., Tang, W., Treviño, M., Vogt, M., Obenhaus, H. A., Gass, P., et al. (2012). Inherited and *de novo* SHANK2 variants associated with autism spectrum disorder impair neuronal morphogenesis and physiology. *Hum. Mol. Genet.* 21, 344–357. doi: 10.1093/hmg/ddr470

Besser, L., Chorin, E., Sekler, I., Silverman, W. F., Atkin, S., Russell, J. T., et al. (2009). Synaptically released zinc triggers metabotropic signaling via a zinc-sensing receptor in the hippocampus. *J. Neurosci.* 29, 2890–2901. doi: 10.1523/jneurosci.5093-08.2009

Bidinosti, M., Botta, P., Krüttner, S., Proenca, C. C., Stoehr, N., Bernhard, M., et al. (2016). CLK2 inhibition ameliorates autistic features associated with SHANK3 deficiency. *Science* 351, 1199–1203. doi: 10.1126/science.aad5487

Boeckers, T. M., Kreutz, M. R., Winter, C., Zuschratter, W., Smalla, K. H., Sanmarti-Vila, L., et al. (1999). Proline-rich synapse-associated protein-1/cortactin binding protein 1 (ProSAP1/CortBP1) is a PDZ-domain protein highly enriched in the postsynaptic density. *J. Neurosci.* 19, 6506–6518. doi: 10.1523/jneurosci.19-15-06506.1999

Boeckers, T. M., Liedtke, T., Spilker, C., Dresbach, T., Bockmann, J., Kreutz, M. R., et al. (2005). C-terminal synaptic targeting elements for postsynaptic density proteins ProSAP1/Shank2 and ProSAP2/Shank3. *J. Neurochem.* 92, 519–524. doi: 10.1111/j.1471-4159.2004.02910.x

Bossy-Wetzel, E., Talantova, M. V., Lee, W. D., Schölzke, M. N., Harrop, A., Mathews, E., et al. (2004). Crosstalk between nitric oxide and zinc pathways to neuronal cell death involving mitochondrial dysfunction and p38-activated K^+ channels. *Neuron* 41, 351–365. doi: 10.1016/s0896-6273(04)00015-7

Bourgeron, T. (2015). From the genetic architecture to synaptic plasticity in autism spectrum disorder. *Nat. Rev. Neurosci.* 16, 551–563. doi: 10.1038/nrn3992

Bozdagi, O., Sakurai, T., Papapetrou, D., Wang, X., Dickstein, D. L., Takahashi, N., et al. (2010). Haploinsufficiency of the autism-associated Shank3 gene leads to deficits in synaptic function, social interaction and social communication. *Mol. Autism* 1:15. doi: 10.1186/2040-2392-1-15

Bresler, T., Shapira, M., Boeckers, T., Dresbach, T., Futter, M., Garner, C. C., et al. (2004). Postsynaptic density assembly is fundamentally different from presynaptic active zone assembly. *J. Neurosci.* 24, 1507–1520. doi: 10.1523/jneurosci.3819-03.2004

Brill, J., and Huguenard, J. R. (2008). Sequential changes in AMPA receptor targeting in the developing neocortical excitatory circuit. *J. Neurosci.* 28, 13918–13928. doi: 10.1523/jneurosci.3229-08.2008

Canzoniero, L. M. T., Turetsky, D. M., and Choi, D. W. (1999). Measurement of intracellular free zinc concentrations accompanying zinc-induced neuronal death. *J. Neurosci.* 19:RC31. doi: 10.1523/jneurosci.19-19-j0005.1999

Carroll, R. C., Beattie, E. C., Xia, H., Lüscher, C., Altschuler, Y., Nicoll, R. A., et al. (1999). Dynamin-dependent endocytosis of ionotropic glutamate receptors. *Proc. Natl. Acad. Sci. U S A* 96, 14112–14117. doi: 10.1073/pnas.96.24.14112

Chanda, S., Aoto, J., Lee, S. J., Wernig, M., and Südhof, T. C. (2016). Pathogenic mechanism of an autism-associated neuroligin mutation involves altered AMPA-receptor trafficking. *Mol. Psychiatry* 21, 169–177. doi: 10.1038/mp.2015.20

Chen, J., Yu, S., Fu, Y., and Li, X. (2014). Synaptic proteins and receptors defects in autism spectrum disorders. *Front. Cell. Neurosci.* 8, 1–13. doi: 10.3389/fncel.2014.00276

Cole, T. B., Robbins, C. A., Wenzel, H. J., Schwartzkroin, P. A., and Palmiter, R. D. (2000). Seizures and neuronal damage in mice lacking vesicular zinc. *Epilepsy Res.* 39, 153–169. doi: 10.1016/s0920-1211(99)00121-7

Craig, A. M., Blackstone, C. D., Huganir, R. L., and Banker, G. (1993). The distribution of glutamate receptors in cultured rat hippocampal neurons: postsynaptic clustering of AMPA-selective subunits. *Neuron* 10, 1055–1068. doi: 10.1016/0896-6273(93)90054-u

Cuajungco, M. P., and Lees, G. J. (1998). Nitric oxide generators produce accumulation of chelatable zinc in hippocampal neuronal perikarya. *Brain Res.* 799, 118–129. doi: 10.1016/s0006-8993(98)00463-6

Curtin, P., Austin, C., Curtin, A., Gennings, C., Arora, M., Tammimies, K., et al. (2018). Dynamical features in fetal and postnatal zinc-copper metabolic cycles predict the emergence of autism spectrum disorder. *Sci. Adv.* 4:eaat1293. doi: 10.1126/sciadv.aat1293

Czöndör, K., Mondin, M., Garcia, M., Heine, M., Frischknecht, R., Choquet, D., et al. (2012). Unified quantitative model of AMPA receptor trafficking at synapses. *Proc. Natl. Acad. Sci. U S A* 109, 3522–3527. doi: 10.1073/pnas.1109818109

Danielson, E., and Lee, S. H. (2014). SynPAnal: Software for rapid quantification of the density and intensity of protein puncta from fluorescence microscopy images of neurons. *PLoS One* 9:e115298. doi: 10.1371/journal.pone.0115298

Du, Y., Weed, S. A., Xiong, W. C., Marshall, T. D., and Parsons, J. T. (1998). Identification of a novel cortactin SH3 domain-binding protein and its localization to growth cones of cultured neurons. *Mol. Cell. Biol.* 18, 5838–5851. doi: 10.1128/mcb.18.10.5838

Durand, C. M., Betancur, C., Boeckers, T. M., Bockmann, J., Chaste, P., Fauchereau, F., et al. (2007). Mutations in the gene encoding the synaptic scaffolding protein SHANK3 are associated with autism spectrum disorders. *Nat. Genet.* 39, 25–27. doi: 10.1038/ng1933

Durand, C. M., Perroy, J., Loll, F., Perrais, D., Fagni, L., Bourgeron, T., et al. (2012). SHANK3 mutations identified in autism lead to modification of dendritic spine morphology via an actin-dependent mechanism. *Mol. Psychiatry* 17, 71–84. doi: 10.1038/mp.2011.57

Forrest, C. M., Khalil, O. S., Pisar, M., Smith, R. A., Darlington, L., and Stone, T. W. (2012). Prenatal activation of Toll-like receptors-3 by administration of the viral mimetic poly(I:C) changes synaptic proteins, N-methyl-D-aspartate receptors and neurogenesis markers in offspring. *Mol. Brain* 5:22. doi: 10.1186/1756-6606-5-22

Frederickson, C. J., Giblin, L. J., Balaji, R. V., Masalha, R., Frederickson, C. J., Zeng, Y., et al. (2006). Synaptic release of zinc from brain slices: factors governing release, imaging, and accurate calculation of concentration. *J. Neurosci. Methods* 154, 19–29. doi: 10.1016/j.jneumeth.2005.11.014

Friedman, H. V., Bresler, T., Garner, C. C., and Ziv, N. E. (2000). Assembly of new individual excitatory synapses: time course and temporal order of synaptic molecule recruitment. *Neuron* 27, 57–69. doi: 10.1016/s0896-6273(00)00009-x

Gainey, M. A., Hurvitz-Wolff, J. R., Lambo, M. E., and Turrigiano, G. G. (2009). Synaptic scaling requires the GluR2 subunit of the AMPA receptor. *J. Neurosci.* 29, 6479–6489. doi: 10.1523/jneurosci.3753-08.2009

Gainey, M. A., Tatavarty, V., Nahmani, M., Lin, H., and Turrigiano, G. G. (2015). Activity-dependent synaptic GRIP1 accumulation drives synaptic scaling up in response to action potential blockade. *Proc. Natl. Acad. Sci. U S A* 112, E3590–E3599. doi: 10.1073/pnas.1510754112

Geiger, J. R. P., Melcher, T., Koh, D. S., Sakmann, B., Seeburg, P. H., Jonas, P., et al. (1995). Relative abundance of subunit mRNAs determines gating and Ca^{2+} permeability of AMPA receptors in principal neurons and interneurons in rat CNS. *Neuron* 15, 193–204. doi: 10.1016/0896-6273(95)90076-4

Giovanoli, S., Weber-Stadlbauer, U., Schedlowski, M., Meyer, U., and Engler, H. (2016). Prenatal immune activation causes hippocampal synaptic deficits in the absence of overt microglia anomalies. *Brain Behav. Immun.* 55, 25–38. doi: 10.1016/j.bbi.2015.09.015

Grabrucker, A. M. (2014). A role for synaptic zinc in ProSAP/Shank PSD scaffold malformation in autism spectrum disorders. *Dev. Neurobiol.* 74, 136–146. doi: 10.1002/dneu.22089

Grabrucker, S., Jannetti, L., Eckert, M., Gaub, S., Chhabra, R., Pfaender, S., et al. (2014). Zinc deficiency dysregulates the synaptic ProSAP/Shank scaffold and might contribute to autism spectrum disorders. *Brain* 137, 137–152. doi: 10.1093/brain/awt303

Grabrucker, A. M., Knight, M. J., Proepper, C., Bockmann, J., Joubert, M., Rowan, M., et al. (2011). Concerted action of zinc and ProSAP/Shank in synaptogenesis and synapse maturation. *EMBO J.* 30, 569–581. doi: 10.1038/emboj.2010.336

Groc, L., Gustafsson, B., and Hanse, E. (2006). AMPA signalling in nascent glutamatergic synapses: there and not there! *Trends Neurosci.* 29, 132–139. doi: 10.1016/j.tins.2006.01.005

Ha, S., Lee, D., Cho, Y. S., Chung, C., Yoo, Y. E., Kim, J., et al. (2016). Cerebellar Shank2 regulates excitatory synapse density, motor coordination and specific repetitive and anxiety-like behaviors. *J. Neurosci.* 36, 12129–12143. doi: 10.1523/JNEUROSCI.1849-16.2016

Hagmeyer, S., Haderspeck, J. C., and Grabrucker, A. M. (2015). Behavioral impairments in animal models for zinc deficiency. *Front. Behav. Neurosci.* 8:443. doi: 10.3389/fnbeh.2014.00443

Hagmeyer, S., Sauer, A. K., and Grabrucker, A. M. (2018). Prospects of zinc supplementation in autism spectrum disorders and Shankopathies such as Phelan McDermid Syndrome. *Front. Synaptic Neurosci.* 10:11. doi: 10.3389/fnsyn.2018.00011

Halas, E. S., and Sandstead, H. H. (1975). Some effects of prenatal zinc deficiency on behavior of the adult rat. *Pediatr. Res.* 9, 94–97. doi: 10.1203/00006450-197502000-00007

Harony, H., Günal, O. B., and Buxbaum, J. D. (2013). SHANK2 and SHANK3 mutations implicate glutamate signaling abnormalities in autism spectrum disorders. *Neurosci. Autism Spectr. Disord.* 3, 437–448. doi: 10.1016/b978-0-12-391924-3.00032-6

Hayashi, T., Yoshida, T., Ra, M., Taguchi, R., and Mishina, M. (2013). IL1RAPL1 associated with mental retardation and autism regulates the formation and stabilization of glutamatergic synapses of cortical neurons through RhoA signaling pathway. *PLoS One* 8:e66254. doi: 10.1371/journal.pone.0066254

Henley, J. M., Barker, E. A., and Glebov, O. O. (2011). Routes, destinations and delays: recent advances in AMPA receptor trafficking. *Trends Neurosci.* 34, 258–268. doi: 10.1016/j.tins.2011.02.004

Henley, J. M., and Wilkinson, K. A. (2016). Synaptic AMPA receptor composition in development, plasticity and disease. *Nat. Rev. Neurosci.* 17, 337–350. doi: 10.1038/nrn.2016.37

Hershfinkel, M., Moran, A., Grossman, N., and Sekler, I. (2001). A zinc-sensing receptor triggers the release of intracellular Ca^{2+} and regulates ion transport. *Proc. Natl. Acad. Sci. U S A* 98, 11749–11754. doi: 10.1073/pnas.201193398

Hsieh, C. H., Shaltouki, A., Gonzalez, A. E., Bettencourt da Cruz, A., Burbulla, L. F., St. Lawrence, E., et al. (2016). Functional impairment in Miro degradation and mitophagy is a shared feature in familial and sporadic Parkinson's disease. *Cell Stem Cell* 19, 709–724. doi: 10.1016/j.stem.2016.08.002

Isaac, J. T. R., Ashby, M. C., and McBain, C. J. (2007). The role of the GluR2 subunit in AMPA receptor function and synaptic plasticity. *Neuron* 54, 859–871. doi: 10.1016/j.neuron.2007.06.001

Jamain, S., Quach, H., Betancur, C., Råstam, M., Colineaux, C., Gillberg, I. C., et al. (2003). Mutations of the X-linked genes encoding neuroligins NLGN3 and NLGN4 are associated with autism. *Nat. Genet.* 34, 27–29. doi: 10.1038/ng1136

Jaramillo, T. C., Speed, H. E., Xuan, Z., Reimers, J. M., Liu, S., and Powell, C. M. (2016). Altered striatal synaptic function and abnormal behaviour in Shank3 exon 4-9 deletion mouse model of autism. *Autism Res.* 9, 350–375. doi: 10.1002/aur.1529

Jia, Y., Jeng, J. M., Sensi, S. L., and Weiss, J. H. (2002). Zn^{2+} currents are mediated by calcium-permeable AMPA/kainate channels in cultured murine hippocampal neurones. *J. Physiol.* 543, 35–48. doi: 10.1113/jphysiol.2002.020172

Jiang, Y. H., and Ehlers, M. D. (2013). Modeling autism by SHANK gene mutations in mice. *Neuron* 78, 8–27. doi: 10.1016/j.neuron.2013.03.016

Jiang, Y. G., Fang, H. Y., Pang, W., Liu, J., Lu, H., Ma, Q., et al. (2011). Depressed hippocampal MEK/ERK phosphorylation correlates with impaired cognitive and synaptic function in zinc-deficient rats. *Nutr. Neurosci.* 14, 45–50. doi: 10.1179/1476830510y.0000000002

Jonas, P., Racca, C., Sakmann, B., Seeburg, P. H., and Monyer, H. (1994). Differences in Ca^{2+} permeability of AMPA-type glutamate receptor channels in neocortical neurons caused by differential GluR-B subunit expression. *Neuron* 12, 1281–1289. doi: 10.1016/0896-6273(94)90444-8

Kaech, S., and Banker, G. (2006). Culturing hippocampal neurons. *Nat. Protoc.* 1, 2406–2415. doi: 10.1038/nprot.2006.356

Kalashnikova, E., Lorca, R. A., Kaur, I., Barisone, G. A., Li, B., Ishimaru, T., et al. (2010). SynDIG1: an activity-regulated, AMPA- receptor-interacting transmembrane protein that regulates excitatory synapse development. *Neuron* 65, 80–93. doi: 10.1016/j.neuron.2009.12.021

Kim, H. G., Kishikawa, S., Higgins, A. W., Seong, I. S., Donovan, D. J., Shen, Y., et al. (2008). Disruption of Neurexin1 associated with autism spectrum disorder. *Am. J. Hum. Genet.* 82, 199–207. doi: 10.1016/j.ajhg.2007.09.011

Kim, J. W., Park, K., Kang, R. J., Gonzales, E. L. T., Kim, D. G., Oh, H. A., et al. (2018). Pharmacological modulation of AMPA receptor rescues social impairments in animal models of autism. *Neuropsychopharmacology* doi: 10.1038/s41386-018-0098-5[Epub ahead of print].

Kumar, S. S., Bacci, A., Kharazia, V., and Huguenard, J. R. (2002). A developmental switch of AMPA receptor subunits in neocortical pyramidal neurons. *J. Neurosci.* 22, 3005–3015. doi: 10.1523/JNEUROSCI.22-08-03005.2002

Laumonnier, F., Bonnet-Brilhault, F., Gomot, M., Blanc, R., David, A., Moizard, M. P., et al. (2004). X-linked mental retardation and autism are

associated with a mutation in the NLGN4 gene, a member of the neuroligin family. *Am. J. Hum. Genet.* 74, 552–557. doi: 10.1086/382137

Leal-Ortiz, S., Waites, C. L., Terry-Lorenzo, R., Zamorano, P., Gundelfinger, E. D., and Garner, C. C. (2008). Piccolo modulation of Synapsin1a dynamics regulates synaptic vesicle exocytosis. *J. Cell Biol.* 181, 831–846. doi: 10.1083/jcb.200711167

Leblond, C. S., Heinrich, J., Delorme, R., Proepper, C., Betancur, C., Huguet, G., et al. (2012). Genetic and functional analyses of SHANK2 mutations suggest a multiple hit model of autism spectrum disorders. *PLoS Genet.* 8:e1002521. doi: 10.1371/journal.pgen.1002521

Lee, J., Chung, C., Ha, S., Lee, D., Kim, D.-Y., Kim, H., et al. (2015). Shank3-mutant mice lacking exon 9 show altered excitation/inhibition balance, enhanced rearing, and spatial memory deficit. *Front. Cell. Neurosci.* 9:94. doi: 10.3389/fncel.2015.00094

Lee, E. J., Lee, H., Huang, T. N., Chung, C., Shin, W., Kim, K., et al. (2015). Trans-synaptic zinc mobilization improves social interaction in two mouse models of autism through NMDAR activation. *Nat. Commun.* 6:7168. doi: 10.1038/ncomms8168

Lee, K., Goodman, L., Fourie, C., Schenk, S., Leitch, B., and Montgomery, J. M. (2016). AMPA receptors as therapeutic targets for neurological disorders. *Adv. Protein Chem. Struct. Biol.* 103, 203–261. doi: 10.1016/bs.apcsb.2015.10.004

Lee, J. Y., Kim, J. H., Palmiter, R. D., and Koh, J. Y. (2003). Zinc released from Metallothionein-III may contribute to hippocampal CA1 and thalamic neuronal death following acute brain injury. *Exp. Neurol.* 184, 337–347. doi: 10.1016/s0014-4886(03)00382-0

Lim, S., Naisbitt, S., Yoon, J., Hwang, J. I., Suh, P. G., Sheng, M., et al. (1999). Characterization of the Shank family of synaptic proteins: multiple genes, alternative splicing, and differential expression in brain and development. *J. Biol. Chem.* 274, 29510–29518. doi: 10.1074/jbc.274.41.29510

Lu, J., Helton, T. D., Blanpied, T. A., Rácz, B., Newpher, T. M., Weinberg, R. J., et al. (2007). Postsynaptic positioning of endocytic zones and AMPA receptor cycling by physical coupling of dynamin-3 to Homer. *Neuron* 55, 874–889. doi: 10.1016/j.neuron.2007.06.041

Lu, W. Y., Man, H. Y., Ju, W., Trimble, W. S., MacDonald, J. F., and Wang, Y. T. (2001). Activation of synaptic NMDA receptors induces membrane insertion of new AMPA receptors and LTP in cultured hippocampal neurons. *Neuron* 29, 243–254. doi: 10.1016/s0896-6273(01)00194-5

Lu, Y. M., Taverna, F. A., Tu, R., Ackerley, C. A., Wang, Y. T., and Roder, J. (2000). Endogenous Zn^{2+} is required for the induction of long-term potentiation at rat hippocampal mossy fiber-CA3 synapses. *Synapse* 38, 187–197. doi: 10.1002/1098-2396(200011)38:2<187::aid-syn10>3.0.co;2-r

MacGillavry, H. D., Kerr, J. M., Kassner, J., Frost, N. A., and Blanpied, T. A. (2016). Shank-cortactin interactions control actin dynamics to maintain flexibility of neuronal spines and synapses. *Eur. J. Neurosci.* 43, 179–193. doi: 10.1111/ejn.13129

Mangiavacchi, S., and Wolf, M. E. (2004). D1 dopamine receptor stimulation increases the rate of AMPA receptor insertion onto the surface of cultured nucleus accumbens neurons through a pathway dependent on protein kinase A. *J. Neurochem.* 88, 1261–1271. doi: 10.1046/j.1471-4159.2003.02248.x

Maret, W. (2017). Zinc in cellular regulation: the nature and significance of "zinc signals". *Int. J. Mol. Sci.* 18:E2285. doi: 10.3390/ijms18112285

Masters, B. A., Quaife, C. J., Erickson, J. C., Kelly, E. J., Froelick, G. J., Zambrowicz, B. P., et al. (1994). Metallothionein III is expressed in neurons that sequester zinc in synaptic vesicles. *J. Neurosci.* 14, 5844–5857. doi: 10.1523/JNEUROSCI.14-10-05844.1994

Mattison, H. A., Bagal, A. A., Mohammadi, M., Pulimood, N. S., Reich, C. G., Alger, B. E., et al. (2014). Evidence of calcium-permeable AMPA receptors in dendritic spines of CA1 pyramidal neurons. *J. Neurophysiol.* 112, 263–275. doi: 10.1152/jn.00578.2013

Mei, Y., Monteiro, P., Zhou, Y., Kim, J. A., Gao, X., Fu, Z., et al. (2016). Adult restoration of Shank3 expression rescues selective autistic-like phenotypes. *Nature* 530, 481–484. doi: 10.1038/nature16971

Mejias, R., Adamczyk, A., Anggono, V., Niranjan, T., Thomas, G. M., Sharma, K., et al. (2011). Gain-of-function glutamate receptor interacting protein 1 variants alter GluA2 recycling and surface distribution in patients with autism. *Proc. Natl. Acad. Sci. U S A* 108, 4920–4925. doi: 10.1073/pnas.1102233108

Mignogna, M. L., Giannandrea, M., Gurgone, A., Fanelli, F., Raimondi, F., Mapelli, L., et al. (2015). The intellectual disability protein RAB39B selectively regulates GluA2 trafficking to determine synaptic AMPAR composition. *Nat. Commun.* 6:6504. doi: 10.1038/ncomms7504

Mysore, S. P., Tai, C. Y., and Schuman, E. M. (2007). Effects of N-cadherin disruption on spine morphological dynamics. *Front. Cell. Neurosci.* 1:1. doi: 10.3389/neuro.03.001.2007

Naisbitt, S., Kim, E., Tu, J. C., Xiao, B., Sala, C., Valtschanoff, J., et al. (1999). Shank, a novel family of postsynaptic density proteins that binds to the NMDA receptor/PSD-95/GKAP complex and cortactin. *Neuron* 23, 569–582. doi: 10.1016/s0896-6273(00)80809-0

Niesmann, K., Breuer, D., Brockhaus, J., Born, G., Wolff, I., Reissner, C., et al. (2011). Dendritic spine formation and synaptic function require neurobeachin. *Nat. Commun.* 2:557. doi: 10.1038/ncomms1565

Noh, K. M., Kim, Y. H., and Koh, J. Y. (2001). Mediation by membrane protein kinase C of zinc-induced oxidative neuronal injury in mouse cortical cultures. *J. Neurochem.* 72, 1609–1616. doi: 10.1046/j.1471-4159.1999.721609.x

O'Brien, R. J., Kamboj, S., Ehlers, M. D., Rosen, K. R., Fischbach, G. D., and Huganir, R. L. (1998). Activity-dependent modulation of synaptic AMPA receptor accumulation. *Neuron* 21, 1067–1078. doi: 10.1016/s0896-6273(00)80624-8

Okamoto, P. M., Gamby, C., Wells, D., Fallon, J., and Vallee, R. B. (2001). Dynamin isoform-specific interaction with the Shank/ProSAP scaffolding proteins of the postsynaptic density and actin cytoskeleton. *J. Biol. Chem.* 276, 48458–48465. doi: 10.1074/jbc.m104927200

Okerlund, N. D., Schneider, K., Leal-Ortiz, S., Montenegro-Venegas, C., Kim, S. A., Garner, L. C., et al. (2017). Bassoon controls presynaptic autophagy through Atg5. *Neuron* 93, 897.e7–913.e7. doi: 10.1016/j.neuron.2017.01.026

Pan, E., Zhang, X. A., Huang, Z., Krezel, A., Zhao, M., Tinberg, C. E., et al. (2011). Vesicular zinc promotes presynaptic and inhibits postsynaptic long-term potentiation of mossy fiber-CA3 synapse. *Neuron* 71, 1116–1126. doi: 10.1016/j.neuron.2011.07.019

Park, M., Penick, E. C., Edwards, J. G., Kauer, J. A., and Ehlers, M. D. (2004). Recycling endosomes supply AMPA receptors for LTP. *Science* 305, 1972–1975. doi: 10.1126/science.1102026

Peça, J., Feliciano, C., Ting, J. T., Wang, W., Wells, M. F., Venkatraman, T. N., et al. (2011). Shank3 mutant mice display autistic-like behaviours and striatal dysfunction. *Nature* 472, 437–442. doi: 10.1038/nature09965

Peter, S., Ten Brinke, M. M., Stedehouder, J., Reinelt, C. M., Wu, B., Zhou, H., et al. (2016). Dysfunctional cerebellar Purkinje cells contribute to autism-like behaviour in Shank2-deficient mice. *Nat. Commun.* 7:12627. doi: 10.1038/ncomms12627

Petrini, E. M., Lu, J., Cognet, L., Lounis, B., Ehlers, M. D., and Choquet, D. (2009). Endocytic trafficking and recycling maintain a pool of mobile surface AMPA receptors required for synaptic potentiation. *Neuron* 63, 92–105. doi: 10.1016/j.neuron.2009.05.025

Pickard, L., Noël, J., Henley, J. M., Collingridge, G. L., and Molnar, E. (2000). Developmental changes in synaptic AMPA and NMDA receptor distribution and AMPA receptor subunit composition in living hippocampal neurons. *J. Neurosci.* 20, 7922–7931. doi: 10.1523/JNEUROSCI.20-21-07922.2000

Radford, R. J., and Lippard, S. J. (2013). Chelators for investigating zinc metalloneurochemistry. *Curr. Opin. Chem. Biol.* 17, 129–136. doi: 10.1016/j.cbpa.2013.01.009

Ramanathan, S., Woodroffe, A., Flodman, P. L., Mays, L. Z., Hanouni, M., Modahl, C. B., et al. (2004). A case of autism with an interstitial deletion on 4q leading to hemizygosity for genes encoding for glutamine and glycine neurotransmitter receptor sub-units (AMPA 2, GLRA3, GLRB) and neuropeptide receptors NPY1R, NPY5R. *BMC Med. Genet.* 5:10. doi: 10.1186/1471-2350-5-10

Rao, A., Kim, E., Sheng, M., and Craig, A. M. (1998). Heterogeneity in the molecular composition of excitatory postsynaptic sites during development of hippocampal neurons in culture. *J. Neurosci.* 18, 1217–1229.

Raynaud, F., Janossy, A., Dahl, J., Bertaso, F., Perroy, J., Varrault, A., et al. (2013). Shank3-Rich2 interaction regulates AMPA receptor recycling and synaptic long-term potentiation. *J. Neurosci.* 33, 9699–9715. doi: 10.1523/JNEUROSCI.2725-12.2013

Reynolds, A., Leake, D., Boese, Q., Scaringe, S., Marshall, W. S., and Khvorova, A. (2004). Rational siRNA design for RNA interference. *Nat. Biotechnol.* 22, 326–330. doi: 10.1038/nbt936

Roussignol, G., Ango, F., Romorini, S., Tu, J. C., Sala, C., Worley, P. F., et al. (2005). Shank expression is sufficient to induce functional dendritic spine synapses in aspiny neurons. *J. Neurosci.* 25, 3560–3570. doi: 10.1523/JNEUROSCI.4354-04.2005

Rumbaugh, G., Sia, G.-M., Garner, C. C., Huganir, R. L., and Malenka, R. C. (2003). Synapse-associated protein-97 isoform-specific regulation of surface AMPA receptors and synaptic function in cultured neurons. *J. Neurosci.* 23, 4567–4576. doi: 10.1523/JNEUROSCI.23-11-04567.2003

Sandstead, H. H., Strobel, D. A., Logan, G. M. Jr., Marks, E. O., and Jacob, R. A. (1978). Zinc deficiency in pregnant rhesus monkeys: effects on behavior of infants. *Am. J. Clin. Nutr.* 31, 844–849. doi: 10.1093/ajcn/31.5.844

Sato, D., Lionel, A. C., Leblond, C. S., Prasad, A., Pinto, D., Walker, S., et al. (2012). SHANK1 deletions in males with autism spectrum disorder. *Am. J. Hum. Genet.* 90, 879–887. doi: 10.1016/j.ajhg.2012.03.017

Selcher, J. C., Xu, W., Hanson, J. E., Malenka, R. C., and Madison, D. V. (2012). Glutamate receptor subunit GluA1 is necessary for long-term potentiation and synapse unsilencing, but not long-term depression in mouse hippocampus. *Brain Res.* 1435, 8–14. doi: 10.1016/j.brainres.2011.11.029

Sensi, S. L., Canzoniero, L. M., Yu, S. P., Ying, H. S., Koh, J. Y., Kerchner, G. A., et al. (1997). Measurement of intracellular free zinc in living cortical neurons: routes of entry. *J. Neurosci.* 17, 9554–9564. doi: 10.1523/JNEUROSCI.17-24-09554.1997

Sheng, M., and Kim, E. (2000). The Shank family of scaffold proteins. *J. Cell Sci.* 113, 1851–1856.

Shepherd, J. D., and Huganir, R. L. (2007). The cell biology of synaptic plasticity: AMPA receptor trafficking. *Annu. Rev. Cell Dev. Biol.* 23, 613–643. doi: 10.1146/annurev.cellbio.23.090506.123516

Shi, S.-H., Hayashi, Y., Esteban, J. A., and Malinow, R. (2001). Subunit-specific rules governing AMPA receptor trafficking to synapses in hippocampal pyramidal neurons. *Cell* 105, 331–343. doi: 10.1016/s0092-8674(01)00321-x

Shi, R., Redman, P., Ghose, D., Liu, Y., Ren, X., Ding, L. J., et al. (2017). Shank proteins differentially regulate synaptic transmission. *eNeuro* 4:ENEURO.0163–15.2017. doi: 10.1523/ENEURO.0163-15.2017

Speed, H. E., Kouser, M., Xuan, Z., Reimers, J. M., Ochoa, C. F., Gupta, N., et al. (2015). Autism-associated insertion mutation (InsG) of Shank3 exon 21 causes impaired synaptic transmission and behavioral deficits. *J. Neurosci.* 35, 9648–9665. doi: 10.1523/JNEUROSCI.3125-14.2015

Szíber, Z., Liliom, H., Morales, C. O. O., Ignácz, A., Rátkai, A. E., Ellwanger, K., et al. (2017). Ras and Rab interactor 1 controls neuronal plasticity by coordinating dendritic filopodial motility and AMPA receptor turnover. *Mol. Biol. Cell* 28, 285–285. doi: 10.1091/mbc.E16-07-0526

Tai, C.-Y., Mysore, S. P., Chiu, C., and Schuman, E. M. (2007). Activity-regulated N-Cadherin endocytosis. *Neuron* 54, 771–785. doi: 10.1016/j.neuron.2007.05.013

Takeda, A., Fuke, S., Minami, A., and Oku, N. (2007). Role of zinc influx via AMPA/kainate receptor activation in metabotropic glutamate receptor-mediated calcium release. *J. Neurosci. Res.* 85, 1310–1317. doi: 10.1002/jnr.21233

Takeda, A., Yamada, K., Tamano, H., Fuke, S., Kawamura, M., and Oku, N. (2008). Hippocampal calcium dyshomeostasis and long-term potentiation in 2-week zinc deficiency. *Neurochem. Int.* 52, 241–246. doi: 10.1016/j.neuint.2007.06.021

Tan, H. L., Queenan, B. N., and Huganir, R. L. (2015). GRIP1 is required for homeostatic regulation of AMPAR trafficking. *Proc. Natl. Acad. Sci. U S A* 112, 10026–10031. doi: 10.1073/pnas.1512786112

Tatavarty, V., Sun, Q., and Turrigiano, G. G. (2013). How to scale down postsynaptic strength. *J. Neurosci.* 33, 13179–13189. doi: 10.1523/JNEUROSCI.1676-13.2013

Thiagarajan, T. C., Lindskog, M., and Tsien, R. W. (2005). Adaptation to synaptic inactivity in hippocampal neurons. *Neuron* 47, 725–737. doi: 10.1016/j.neuron.2005.06.037

Thompson, R., Peterson, D., Mahoney, W., Cramer, M., Maliwal, B. P., Suh, S. W., et al. (2002). Fluorescent zinc indicators for neurobiology. *J. Neurosci. Methods* 118, 63–75. doi: 10.1016/s0165-0270(02)00144-9

Uchino, S., Wada, H., Honda, S., Nakamura, Y., Ondo, Y., Uchiyama, T., et al. (2006). Direct interaction of post-synaptic density-95/Dlg/ZO-1 domain-containing synaptic molecule Shank3 with GluR1 α-amino-3-hydroxy-5-methyl-4-isoxazole propionic acid receptor. *J. Neurochem.* 97, 1203–1214. doi: 10.1111/j.1471-4159.2006.03831.x

Uemura, T., Mori, H., and Mishina, M. (2004). Direct interaction of GluRδ2 with Shank scaffold proteins in cerebellar Purkinje cells. *Mol. Cell. Neurosci.* 26, 330–341. doi: 10.1016/j.mcn.2004.02.007

Ui-Tei, K., Naito, Y., Takahashi, F., Haraguchi, T., Ohki-Hamazaki, H., Juni, A., et al. (2004). Guidelines for the selection of highly effective siRNA sequences for mammalian and chick RNA interference. *Nucleic Acids Res.* 32, 936–948. doi: 10.1093/nar/gkh247

Valnegri, P., Montrasio, C., Brambilla, D., Ko, J., Passafaro, M., and Sala, C. (2011). The X-linked intellectual disability protein IL1RAPL1 regulates excitatory synapse formation by binding PTPδ and RhoGAP2. *Hum. Mol. Genet.* 20, 4797–4809. doi: 10.1093/hmg/ddr418

Vergnano, A. M., Rebola, N., Savtchenko, L. P., Pinheiro, P. S., Casado, M., Kieffer, B. L., et al. (2014). Zinc dynamics and action at excitatory synapses. *Neuron* 82, 1101–1114. doi: 10.1016/j.neuron.2014.04.034

Verpelli, C., Dvoretskova, E., Vicidomini, C., Rossi, F., Chiappalone, M., Schoen, M., et al. (2011). Importance of Shank3 protein in regulating metabotropic glutamate receptor 5 (mGluR5) expression and signaling at synapses. *J. Biol. Chem.* 286, 34839–34850. doi: 10.1074/jbc.M111.258384

Vogt, K., Mellor, J., Tong, G., and Nicoll, R. (2000). The actions of synaptically released zinc at hippocampal mossy fiber synapses. *Neuron* 26, 187–196. doi: 10.1016/s0896-6273(00)81149-6

Wakayama, S., Kiyonaka, S., Arai, I., Kakegawa, W., Matsuda, S., Ibata, K., et al. (2017). Chemical labelling for visualizing native AMPA receptors in live neurons. *Nat. Commun.* 8:14850. doi: 10.1038/ncomms14850

Wang, X., Bey, A. L., Katz, B. M., Badea, A., Kim, N., David, L. K., et al. (2016). Altered mGluR5-Homer scaffolds and corticostriatal connectivity in a Shank3 complete knockout model of autism. *Nat. Commun.* 7:11459. doi: 10.1038/ncomms11459

Wang, X., McCoy, P. A., Rodriguiz, R. M., Pan, Y., Je, H. S., Roberts, A. C., et al. (2011). Synaptic dysfunction and abnormal behaviors in mice lacking major isoforms of Shank3. *Hum. Mol. Genet.* 20, 3093–3108. doi: 10.1093/hmg/ddr212

Wegener, S., Buschler, A., Stempel, A. V., Shoichet, S. A., Manahan-Vaughan, D., and Schmitz, D. (2017). Defective synapse maturation and enhanced synaptic plasticity in Shank2$^{\Delta ex7-/-}$ mice. *bioRxiv*: 193078 [*Preprint*]. doi: 10.1101/193078

Wilson, N. R., Kang, J., Hueske, E. V., Leung, T., Varoqui, H., Murnick, J. G., et al. (2005). Presynaptic regulation of quantal size by the vesicular glutamate transporter VGLUT1. *J. Neurosci.* 25, 6221–6234. doi: 10.1523/JNEUROSCI.3003-04.2005

Won, H., Lee, H. R., Gee, H. Y., Mah, W., Kim, J. I., Lee, J., et al. (2012). Autistic-like social behaviour in Shank2-mutant mice improved by restoring NMDA receptor function. *Nature* 486, 261–265. doi: 10.1038/nature11208

Yasuda, H., Yoshida, K., Yasuda, Y., and Tsutsui, T. (2011). Infantile zinc deficiency: association with autism spectrum disorders. *Sci. Rep.* 1:129. doi: 10.1038/srep00129

Zhao, J., Bertoglio, B. A., Gee, K. R., and Kay, A. R. (2008). The zinc indicator FluoZin-3 is not perturbed significantly by physiological levels of calcium or magnesium. *Cell Calcium* 44, 422–426. doi: 10.1016/j.ceca.2008.01.006

Zhou, Z., Hu, J., Passafaro, M., Xie, W., and Jia, Z. (2011). GluA2 (GluR2) regulates metabotropic glutamate receptor-dependent long-term depression through N-Cadherin-dependent and Cofilin-mediated actin reorganization. *J. Neurosci.* 31, 819–833. doi: 10.1523/JNEUROSCI.3869-10.2011

Conflict of Interest Statement: The authors declare that the research was conducted in the absence of any commercial or financial relationships that could be construed as a potential conflict of interest.

frontiers in Molecular Neuroscience

ORIGINAL RESEARCH
published: 16 November 2018
doi: 10.3389/fnmol.2018.00419

Reduced Efficacy of d-Amphetamine and 3,4-Methylenedioxymethamphetamine in Inducing Hyperactivity in Mice Lacking the Postsynaptic Scaffolding Protein SHANK1

*A. Özge Sungur[1,2], Tobias M. Redecker[1], Elena Andres[3], Wiebke Dürichen[1], Rainer K. W. Schwarting[1,2], Adriana del Rey[3] and Markus Wöhr[1,2]**

[1] Behavioral Neuroscience, Experimental and Biological Psychology, Philipps University of Marburg, Marburg, Germany, [2] Center for Mind, Brain and Behavior, Philipps University of Marburg, Marburg, Germany, [3] Research Group Immunophysiology, Division of Neurophysiology, Institute of Physiology and Pathophysiology, Philipps University of Marburg, Marburg, Germany

OPEN ACCESS

Edited by:
Eunjoon Kim,
Institute for Basic Science (IBS),
South Korea

Reviewed by:
Christian P. Müller,
Friedrich-Alexander-Universität
Erlangen-Nürnberg, Germany
Damiana Leo,
University of Mons, Belgium

***Correspondence:**
Markus Wöhr
markus.woehr@staff.uni-marburg.de
orcid.org/0000-0001-6986-5684

Received: 01 August 2018
Accepted: 26 October 2018
Published: 16 November 2018

Citation:
Sungur AÖ, Redecker TM, Andres E, Dürichen W, Schwarting RKW, del Rey A and Wöhr M (2018) Reduced Efficacy of d-Amphetamine and 3,4-Methylenedioxymethamphetamine in Inducing Hyperactivity in Mice Lacking the Postsynaptic Scaffolding Protein SHANK1. Front. Mol. Neurosci. 11:419. doi: 10.3389/fnmol.2018.00419

Genetic defects in the three SH3 and multiple ankyrin repeat domains (SHANK) genes (*SHANK1*, *SHANK2*, and *SHANK3*) are associated with multiple major neuropsychiatric disorders, including autism spectrum disorder (ASD), schizophrenia (SCZ), and bipolar disorder (BPD). Psychostimulant-induced hyperactivity is a commonly applied paradigm to assess behavioral phenotypes related to BPD and considered to be the gold standard for modeling mania-like elevated drive in mouse models. Therefore, the goal of our present study was to test whether *Shank1* plays a role in the behavioral effects of psychostimulants and whether this is associated with genotype-dependent neurochemical alterations. To this aim, male and female null mutant *Shank1*$^{-/-}$ mice were treated with d-amphetamine (AMPH; 2.5 mg/kg) and 3,4-methylenedioxymethamphetamine (MDMA, commonly known as ecstasy; 20 mg/kg), and psychostimulant-induced hyperactivity was compared to heterozygous *Shank1*$^{+/-}$ and wildtype *Shank1*$^{+/+}$ littermate controls. Results show that *Shank1*$^{-/-}$ mice display reduced psychostimulant-induced hyperactivity, although psychostimulants robustly stimulated locomotor activity in littermate controls. *Shank1* deletion effects emerged throughout development, were particularly prominent in adulthood, and seen in response to both psychostimulants, i.e., AMPH and MDMA. Specifically, while AMPH-induced hyperactivity was reduced but still detectable in *Shank1*$^{-/-}$ mice, MDMA-induced hyperactivity was robustly blocked and completely absent in *Shank1*$^{-/-}$ mice. Reduced efficacy of psychostimulants to stimulate hyperactivity in *Shank1*$^{-/-}$ mice might be associated with alterations in the neurochemical architecture in prefrontal cortex, nucleus accumbens, and hypothalamus. Our observation that

psychostimulant-induced hyperactivity is reduced rather than enhanced in *Shank1*$^{-/-}$ mice clearly speaks against a behavioral phenotype with relevance to BPD. Lack of BPD-like phenotype is consistent with currently available human data linking mutations in *SHANK2* and *SHANK3* but not *SHANK1* to BPD.

Keywords: ecstasy, MDMA, dopamine, noradrenaline, norepinephrine, serotonin

INTRODUCTION

Genetic defects in the three SH3 and multiple ankyrin repeat domains (SHANK) genes (*SHANK1*, *SHANK2*, and *SHANK3*) are associated with multiple major neuropsychiatric disorders, including autism spectrum disorder (ASD), schizophrenia (SCZ), and bipolar disorder (BPD; Guilmatre et al., 2014; Bourgeron, 2015; de la Torre-Ubieta et al., 2016). Early genetic studies provided compelling evidence implicating *SHANK* mutations in the whole spectrum of ASD (Durand et al., 2007; Moessner et al., 2007; Gauthier et al., 2009; Berkel et al., 2010; Pinto et al., 2010; Sato et al., 2012). However, there is increasing evidence suggesting that *SHANK* mutations play a prominent role in other neuropsychiatric disorders as well. For instance, Fromer et al. (2014) reported a *de novo SHANK1* frameshift mutation in a SCZ patient, and Lennertz et al. (2012) found that a *SHANK1* promotor variant is associated with reduced auditory working memory capacity in SCZ patients. Mutations in *SHANK2* and *SHANK3* have likewise been described in individuals with SCZ (Gauthier et al., 2010; Peykov et al., 2015; Homann et al., 2016). Moreover, a duplication in *SHANK2* has been reported for a BPD patient (Noor et al., 2014) and BPD has been diagnosed also in individuals with the Phelan-McDermid 22q13 deletion syndrome lacking *SHANK3* (Sovner et al., 1996; Willemsen et al., 2011; Denayer et al., 2012; Verhoeven et al., 2012, 2013; Vucurovic et al., 2012). It thus appears that *SHANK* mutations are shared across multiple neuropsychiatric disorders similar to other genetic risk factors, pointing to extensive pleiotropy and challenging the biological validity of existing diagnostic approaches (Zhu et al., 2014; Geschwind and Flint, 2015; O'Donovan and Owen, 2016). However, the neurobiological mechanisms underlying the pleiotropic effects of *SHANK* mutations are not well understood.

The three *SHANK* genes code for several mRNA splice variants and generate multiple protein isoforms (Ting et al., 2012; Sala et al., 2015). Members of the SHANK protein family have five conserved protein domains through which they assemble into large molecular platforms in the postsynaptic density (PSD) at excitatory glutamatergic synapses. More than 30 synaptic proteins have been reported to form interactions with SHANK protein family members. As master scaffolding proteins, SHANKs anchor glutamate receptors and link them to the actin cytoskeleton and postsynaptic signaling pathways. They are thus strongly involved in several synaptic functions, including spine morphogenesis, synapse formation, glutamate receptor trafficking, and activity-dependent neuronal signaling.

Several *Shank* mouse models were generated during the last decade (Jiang and Ehlers, 2013; Yoo et al., 2013; Schmeisser and Verpelli, 2016). While *Shank2* and *Shank3* mutant mice have been extensively characterized (Peça et al., 2011; Wang et al., 2011; Schmeisser et al., 2012; Won et al., 2012), comparatively little is known about *Shank1* mutant mice (Sungur et al., 2018). Hung et al. (2008) generated *Shank1* mutant mice via deletion of exons 14 and 15 encoding almost the entire PDZ domain. This approach resulted in a complete knockout of all SHANK1 protein isoforms. Behavioral studies employing *Shank1*$^{-/-}$ mice almost exclusively focused on ASD-related behavioral phenotypes and cognitive deficits with relevance to intellectual disability (Silverman et al., 2010). Specifically, Hung et al. (2008) performed an extensive set of cognitive tasks and found that *Shank1*$^{-/-}$ mice display impaired contextual but intact cued fear memory, and enhanced acquisition but impaired retention of spatial memory, possibly resembling the aberrant cognitive phenotype present in some ASD cases. Extending these findings, we recently showed that *Shank1*$^{-/-}$ mice are severely impaired in novel object recognition memory and that this deficit is associated with increased expression of brain-derived neurotrophic factor BDNF in the hippocampus, possibly due to epigenetic modifications, as indicated by enrichment of histone H3 acetylation at the *Bdnf* promoter1 in *Shank1*$^{-/-}$ mice (Sungur et al., 2017). Consistent with ASD-related behavioral phenotypes, we further showed that *Shank1*$^{-/-}$ mice show prominent vocal and olfactory communication deficits (Wöhr et al., 2011; Wöhr, 2014; Sungur et al., 2016), together with a moderate increase in self-grooming behavior (Sungur et al., 2014) and mild alterations in social behavior (Silverman et al., 2011; Sungur et al., 2017).

However, because mutations in *SHANK* genes are associated with multiple major neuropsychiatric disorders, including SCZ and BPD besides ASD, we reasoned that a more comprehensive characterization of *Shank1*$^{-/-}$ mice might provide novel insights into the complex role *SHANK1* appears to play. A commonly applied paradigm to assess behavioral phenotypes related to SCZ and BPD in mouse models is psychostimulant-induced hyperactivity (Kato et al., 2007; Young et al., 2011). Psychostimulants, such as d-amphetamine (AMPH), can provoke mania-like symptoms in healthy subjects and exacerbate symptoms or induce a manic episode in BPD patients (Meyendorff et al., 1985; Peet and Peters, 1995; Hasler et al., 2006). AMPH-induced hyperactivity is thus considered to be the gold standard for modeling mania-like elevated drive in rodents (Berggren et al., 1978; Gould et al., 2001; Pereira et al., 2014). While AMPH affects primarily the catecholaminergic system and results in increased extracellular dopamine (DA) and noradrenaline (NA) concentrations through direct interaction with DA and NA transporters, other psychostimulants, such as 3,4-methylenedioxymethamphetamine (MDMA; commonly known as ecstasy), differ in their mode of action by having

particularly strong effects on serotonin (5-HT) in addition (Sulzer et al., 2005; Hutson et al., 2014). Importantly, *Shank3* overexpression was linked to increased locomotor activity in mice and Han et al. (2013) found that an acute injection of AMPH aggravated the hyperactivity of *Shank3* overexpressing mice to a greater extent than in controls. Moreover, Pappas et al. (2017) recently generated *Shank2* mutant mice lacking exon 24 (Δ24) and found that $Shank2^{\Delta 24-/-}$ mice display elevated levels of locomotor activity, which could be normalized by lithium and valproate treatment, but were further enhanced by AMPH administration. The augmentation with AMPH was more prominent in $Shank2^{\Delta 24-/-}$ mice than in wildtype $Shank2^{\Delta 24+/+}$ controls (Pappas et al., 2017).

Here, we therefore asked whether *Shank1* plays a role in the behavioral effects of psychostimulants and whether this is associated with genotype-dependent neurochemical alterations. Firstly, at the behavioral level, we assessed psychostimulant-induced hyperactivity in $Shank1^{-/-}$ null mutant mice in comparison to heterozygous $Shank1^{+/-}$ and wildtype $Shank1^{+/+}$ littermate controls across development. To this aim, juvenile and adult subject mice were treated with the psychostimulant AMPH primarily targeting DA and NA transporters, and their locomotor activity was assessed in an open field. To assess specificity and to evaluate generalizability, subject mice were further treated with the psychostimulant MDMA, which has particularly strong effects on the 5-HT transporter. Secondly, at the neurobiological level, we analyzed DA, NA, and 5-HT neurotransmitter concentrations together with their precursors and metabolites in relevant brain structures, namely prefrontal cortex, nucleus accumbens, and hypothalamus.

MATERIALS AND METHODS

Animals and Housing

Juvenile and adult $Shank1^{-/-}$ null mutant mice with a targeted replacement of exons 14 and 15 encoding almost the entire PDZ domain were compared to $Shank1^{+/-}$ heterozygous and $Shank1^{+/+}$ wildtype littermate control mice. Mice were obtained from mutant lines originally generated by Hung et al. (2008) on two independent background strains: C57BL/6J and 129SvJae. As high mortality rates were obtained in the C57BL/6J background strain and very low locomotion in the 129SvJae background strain (Hung et al., 2008; Silverman et al., 2011), the two lines were crossed for at least three generations to produce a mixed C57BL/6J/129SvJae background for the *Shank1* mutation. This mixed background was maintained since then and used in the present study, consistent with other studies focusing on this *Shank1* mutant (Hung et al., 2008; Wöhr et al., 2011; Silverman et al., 2011; Sungur et al., 2014, 2017, 2018; Wöhr, 2014). Using a heterozygous breeding protocol, $Shank1^{+/-}$ males and females were bred in a conventional vivarium at the Biomedical Research Center of the Philipps-University of Marburg, Germany. Approximately 2 weeks after pairing for breeding, females were individually housed and inspected daily for pregnancy and delivery. The day of birth was considered as postnatal day (PND) 0. After weaning on PND21, mice were socially housed in groups of 2–6 with same-sex partners in polycarbonate Makrolon type III IVC cages (L × W × H: 420 × 265 × 180 mm, 825 cm^2; Ehret, Emmendingen, Germany). Bedding and a wooden board were provided in each cage. Standard rodent chow and water were available ad libitum. The colony room was maintained on a 12:12 light/dark cycle (lights on: 06:00h) at approximately 22°C and 40–50% humidity. Pups were identified by paw tattoo, using non-toxic animal tattoo ink (Ketchum permanent Tattoo Inks green paste, Ketchum Manufacturing Inc., Brockville, ON, Canada). The ink was inserted subcutaneously through a 30 gauge hypodermic needle tip into the center of the paw. For genotyping, mouse tail snips were collected by dissecting ∼0.3 cm of tail between PND3-12. Genotyping was performed as described previously (Sungur et al., 2014). All procedures were approved by the ethical committee of the Regierungspräsidium Gießen, Germany [file reference: V54–19c 20 15 (1) MR20/35 Nr. 20/2010 and V54–19c 20 15 h 01 MR20/35 Nr. G 30/2018].

Experimental Design

For testing whether *Shank1* plays a role in the behavioral effects of psychostimulants, male and female null mutant $Shank1^{-/-}$ mice were treated with AMPH (2.5 mg/kg) and MDMA (20 mg/kg), and psychostimulant-induced hyperactivity was compared to heterozygous $Shank1^{+/-}$ and wildtype $Shank1^{+/+}$ littermate controls. AMPH-induced hyperactivity was assessed in juvenile ($Shank1^{+/+}$: $N = 15$; $Shank1^{+/-}$: $N = 20$; $Shank1^{-/-}$: $N = 16$) and adult ($Shank1^{+/+}$: $N = 24$; $Shank1^{+/-}$: $N = 28$; $Shank1^{-/-}$: $N = 28$) mice. MDMA-induced hyperactivity was determined in adulthood only ($Shank1^{+/+}$: $N = 14$; $Shank1^{+/-}$: $N = 19$; $Shank1^{-/-}$: $N = 14$). Drug doses are expressed as salt and were determined based on previous studies reporting psychostimulant-induced hyperactivity (Risbrough et al., 2006; Young et al., 2010).

Drug Treatment

d-amphetamine sulfate (AMPH; Sigma–Aldrich, MO, United States) and 3,4-Methylendioxy-*N*-methylamphetamin (MDMA; Lipomed, Switzerland) were dissolved in 0.9% saline and administered intraperitoneally (i.p.) at volume of 1 ml/kg. As vehicle control, 0.9% saline was used. Injections were performed immediately prior to open field exposure for locomotor activity assessment.

Open Field

Psychostimulant-induced hyperactivity was measured in an open field (50 cm × 50 cm × 35 cm; TSE Systems, Bad Homburg, Germany) under dim red light, according to a previously established protocol (Natusch and Schwarting, 2010). Individual mice were placed randomly in one of the corners of the open field and were allowed to explore the apparatus for 45 min on three consecutive days. On the first day (baseline), mice were habituated to the open field. On the second day (saline), mice were administered saline. On the third day (treatment), mice were administered AMPH or MDMA. Distance traveled, rearing behavior, and the time spent in the center (30 cm × 30 cm) were automatically collected using the TSE VideoMot2 analyzer

software (TSE Systems, Bad Homburg, Germany). Circling behavior, i.e., turning in a circular motion, was quantified by a trained observer.

Tissue Preparation

Drug-naïve juvenile mice of both sexes were individually caged and sacrificed by cervical dislocation. Immediately after the brain was removed, prefrontal cortex, nucleus accumbens, and hypothalamus were dissected using a special brain matrix, designed by Dr. J. Wildmann (Institute for Physiology and Pathophysiology, Philipps-University, Marburg). The different regions were divided into right and left parts, quickly frozen on dry ice, and stored at −80°C until used for neurotransmitter determination.

Neurotransmitter Determination

The concentration of catecholaminergic and indolaminergic neurotransmitters, metabolites, and precursors were measured using high performance liquid chromatography (HPLC), as previously described (Roggero et al., 2016). Briefly, frozen brain samples were homogenized in 0.4 M $HClO_4$ by sonication and 10 µl of the supernatant was injected for the analysis. The HPLC system used consists of a reversed-phase C-18 chromatography column (Supelco, Sigma–Aldrich, St. Louis, MO, United States) as stationary phase and an aqueous eluent containing 10% acetonitrile as mobile phase. Besides the neurotransmitters DA, NA, and 5-HT, the precursors tyrosine (Tyr) and tryptophan (Trp) as well as the metabolites dehydroxyphenylacetic acid (DOPAC), 4-hydroxy-3-methoxy-phenylglycol (MHPG), and 5-hydroxy-indol-acetic acid (5-HIAA) were quantified in each sample. Quantification was done by peak height evaluation or by area integration using Chromeleon software version 6.08 from Dionex (Sunnyvale, CA, United States).

Statistical Analysis

Distance traveled in the open field was analyzed using analyses of variance (ANOVAs) for repeated measurements with genotype and sex as between-subject factors and test day or test minute as within-subject factor. Comparison between test days for individual genotypes was performed by calculating paired samples *t*-tests. Neurotransmitter concentrations were analyzed using one-way ANOVAs with genotype as between-subject factor. For each neurotransmitter, values that were smaller than the lower quartile minus three times the interquartile range or larger than the upper quartile plus three times the interquartile range were considered as outliers and excluded from analysis. When appropriate, ANOVAs were followed by LSD *post hoc* analysis for comparing genotypes. A p-value of < 0.050 was considered statistically significant.

RESULTS

AMPH-Induced Hyperactivity

AMPH administration induced hyperactivity in juvenile mice ($F_{2,90} = 20.840$, $p < 0.001$), as evidenced by representative locomotor activity patterns in response to AMPH on test day 3 in comparison to saline on day 2 (**Figure 1A**). Importantly, there was also an overall effect of genotype ($F_{2,45} = 4.766$, $p = 0.013$; day × genotype: $F_{4,90} = 0.775$, $p = 0.545$), but no general sex effect and no sex interaction with AMPH treatment ($F_{1,45} = 0.139$, $p = 0.711$; sex × genotype: $F_{2,45} = 0.032$, $p = 0.968$; day × sex: $F_{2,90} = 0.198$, $p = 0.821$; day × sex × genotype: $F_{4,90} = 0.428$, $p = 0.788$). A comparison between test days revealed that the distanced traveled following AMPH treatment was clearly higher than the day before in response to saline ($p < 0.001$; **Figure 1B**). This difference held true for individual genotypes (*Shank1*$^{+/+}$: $t_{14} = 3.787$, $p = 0.001$, one-tailed; *Shank1*$^{+/-}$: $t_{19} = 2.953$, $p = 0.008$; *Shank1*$^{-/-}$: $t_{15} = 2.495$, $p = 0.025$; **Figure 1B′**). When comparing locomotor activity between individual genotypes separately for each test day, evidence for genotype-dependent differences in the distance traveled was obtained under baseline conditions ($F_{2,48} = 6.619$, $p = 0.003$; **Figure 2A**) and in response to saline ($F_{2,48} = 5.076$, $p = 0.010$; **Figure 2B**). Specifically, on day 1, *Shank1*$^{+/+}$ mice displayed slightly higher levels of locomotor activity than *Shank1*$^{-/-}$ mice ($p = 0.001$) but did not differ significantly from *Shank1*$^{+/-}$ mice ($p = 0.059$). Similarly, on day 2, *Shank1*$^{+/+}$ mice engaged more in locomotor activity than *Shank1*$^{-/-}$ ($p = 0.004$) and *Shank1*$^{+/-}$ mice ($p = 0.019$). Locomotor activity displayed by *Shank1*$^{+/-}$ and *Shank1*$^{-/-}$ mice did not differ from each other under baseline conditions ($p = 0.059$) and in response to saline ($p = 0.428$). Although there was only a trend for a genotype effect on AMPH-induced hyperactivity on the third test day and the overall level of locomotor activity was not significantly affected by *Shank1* deletion ($F_{2,48} = 2.602$, $p = 0.085$), the temporal response pattern differed between genotypes (genotype: $F_{2,45} = 2.186$, $p = 0.124$; time × genotype: $F_{88,1980} = 1.278$, $p = 0.045$; **Figure 2C**). After about 10 min with similar locomotor activity levels in all genotypes, *Shank1*$^{+/+}$ mice displayed a strong increase in locomotor activity and maintained high activity levels for about 30 min, whereas the AMPH-induced increase was less prominent in *Shank1*$^{+/-}$ and *Shank1*$^{-/-}$ mice (**Figures 2A′–C′**).

Of note, the time spent in the center of the open field was also affected and changed across test days ($F_{2,90} = 33.804$, $p < 0.001$). There were overall effects of genotype ($F_{2,45} = 9.573$, $p < 0.001$; day × genotype: $F_{4,90} = 2.774$, $p = 0.032$) and sex ($F_{1,45} = 7.393$, $p = 0.009$; sex × genotype: $F_{2,45} = 0.091$, $p = 0.914$), but no sex interaction with AMPH treatment (day × sex: $F_{2,90} = 0.352$, $p = 0.704$; day × sex × genotype: $F_{4,90} = 0.188$, $p = 0.944$). When comparing the time spent in the center between individual genotypes separately for each test day, prominent genotype differences were detected across all three test days. Specifically, under baseline conditions, genotypes differed from each other ($F_{2,48} = 9.360$, $p < 0.001$; **Supplementary Figure 1A**) and *Shank1*$^{+/+}$ mice spent more time in the center than *Shank1*$^{+/-}$ ($p = 0.018$) and *Shank1*$^{-/-}$ mice ($p < 0.001$), with the latter also differing from each other ($p = 0.037$). Similarly, center time differed between genotypes in response to saline on day 2 ($F_{2,48} = 4.388$, $p = 0.018$; **Supplementary Figure 1B**), with *Shank1*$^{+/+}$ mice again spending more time in the center than *Shank1*$^{+/-}$ ($p = 0.015$) and *Shank1*$^{-/-}$ mice ($p = 0.010$), but the latter not differing from each other ($p = 0.774$). A similar pattern was obtained also in response to AMPH on day 3 ($F_{2,48} = 5.367$,

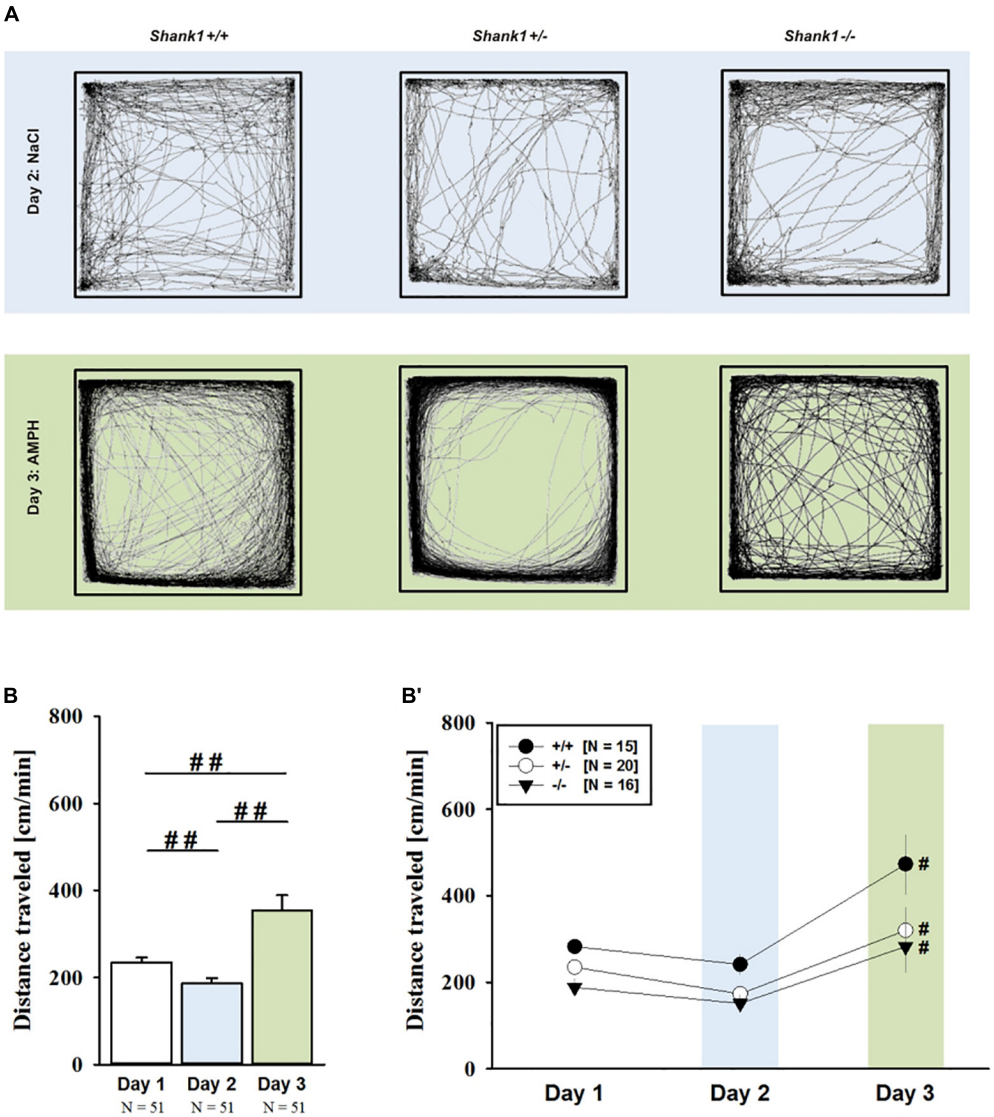

FIGURE 1 | AMPH-induced hyperactivity in juvenile *Shank1* mice. **(A)** Exemplary figure depicting the locomotor activity pattern of individual juvenile *Shank1*$^{+/+}$, *Shank1*$^{+/-}$, and *Shank1*$^{-/-}$ mice injected with saline (NaCl) on day 2 (upper panel) and with AMPH on day 3 (lower panel); measured over 45 min. **(B)** Bar graph depicting the distance traveled by all genotypes during baseline testing (white bar), following saline administration (blue bar), and after AMPH treatment (green bar). **(B')** Line graph depicting the distance traveled by *Shank1*$^{+/+}$ (black circle), *Shank1*$^{+/-}$ (white circle), and *Shank1*$^{-/-}$ (black triangle) over the three consecutive test days. Data are presented as means + SEM or means ± SEM. $^{\#\#}p < 0.001$ **(B)**, $^{\#}p < 0.05$ vs. day 2 **(B')**.

$p = 0.008$; **Supplementary Figure 1C**), with *Shank1*$^{+/+}$ mice spending more time in the center than *Shank1*$^{+/-}$ ($p = 0.011$) and *Shank1*$^{-/-}$ mice ($p = 0.004$), but the latter not differing from each other ($p = 0.546$).

Consistent with the data obtained in juveniles, AMPH administration induced hyperactivity in adult mice ($F_{2,148} = 107.888$, $p < 0.001$), and this is similarly evidenced by representative locomotor activity patterns on test day 3 in comparison to saline on day 2 (**Figure 3A**). Again, there was a general genotype effect ($F_{2,74} = 10.233$, $p < 0.001$), while sex had no prominent impact and did not modulate AMPH effects in a genotype-dependent manner ($F_{1,74} = 3.358$, $p = 0.064$; sex × genotype: $F_{2,74} = 0.349$, $p = 0.707$; day × sex: $F_{2,148} = 3.324$, $p = 0.039$; day × sex × genotype: $F_{4,148} = 0.957$, $p = 0.433$). This was further supported by a comparison between test days that revealed clearly higher levels of locomotor activity following AMPH treatment than the day before in response to saline ($p < 0.001$; **Figure 3B**) and this difference held true for individual genotypes (*Shank1*$^{+/+}$: $t_{23} = 5.800$, $p < 0.001$, one-tailed; *Shank1*$^{+/-}$: $t_{27} = 8.478$, $p < 0.001$; *Shank1*$^{-/-}$:

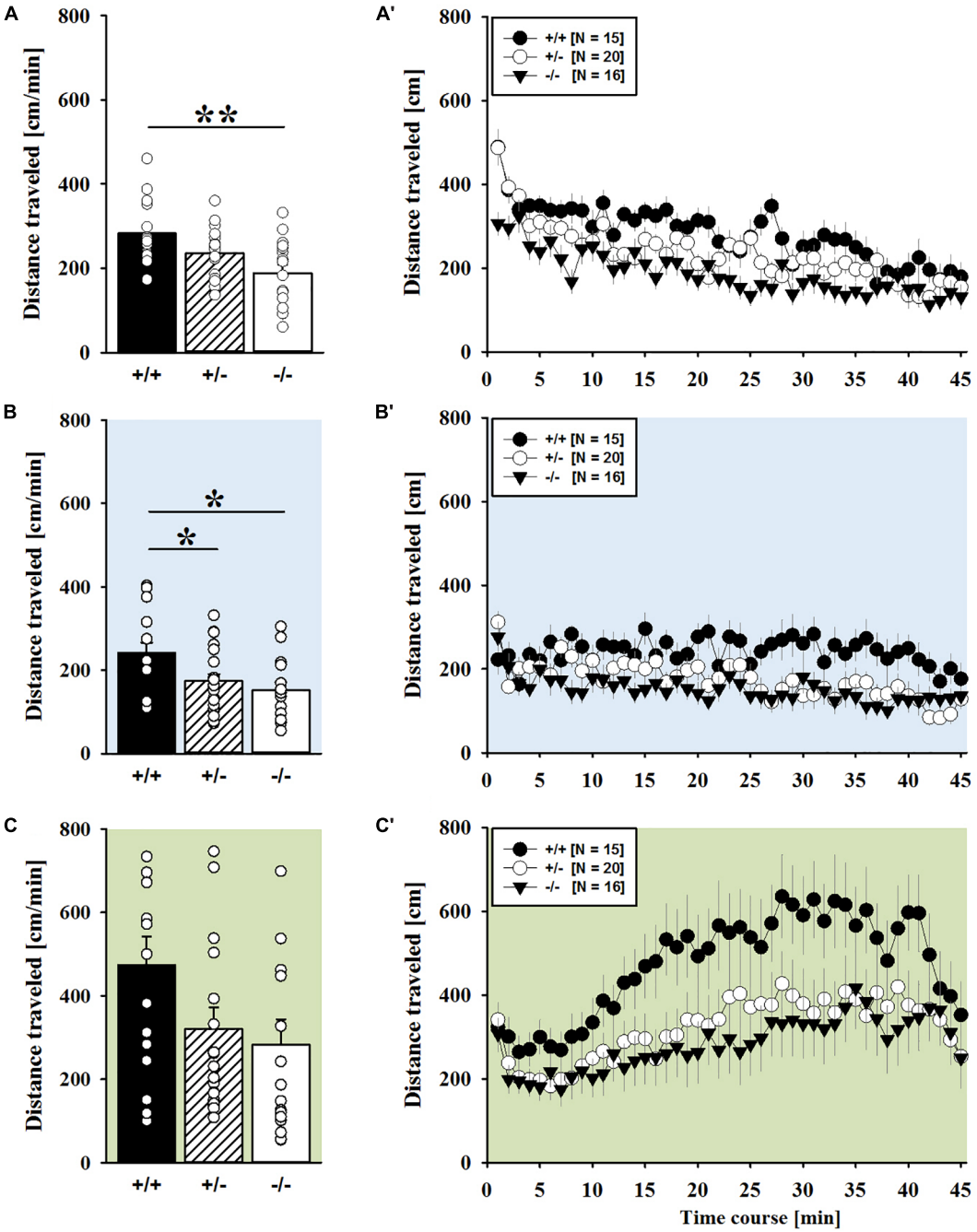

FIGURE 2 | AMPH-induced hyperactivity in juvenile *Shank1* mice. **(A–C)** Bar graphs and **(A′–C′)** line graphs depicting the distance traveled by *Shank1*$^{+/+}$ (black bar/black circle), *Shank1*$^{+/-}$ (striped bar/white circle), and *Shank1*$^{-/-}$ (white bar/black triangle). Locomotor activity was compared during baseline testing **(A,A′)**, following saline administration **(B,B′)**, and after AMPH treatment **(C,C′)**. Data are presented as means + SEM or means ± SEM. *$p < 0.05$, **$p < 0.001$.

$t_{27} = 5.123$, $p < 0.001$; **Figure 3B′**). Despite this general effect, however, AMPH responsivity in adult mice was strongly affected by *Shank1* deletion (day × genotype: $F_{4,148} = 10.030$, $p < 0.001$). While locomotor activity did not differ between genotypes under baseline conditions ($F_{2,77} = 0.980$, $p = 0.380$; **Figure 4A**) and no differences were evident in response to saline ($F_{2,77} = 0.801$, $p = 0.453$; **Figure 4B**), prominent genotype differences were evident following AMPH treatment. In contrast to juvenile mice, AMPH-induced hyperactivity was clearly dependent on genotype in adult mice ($F_{2,77} = 10.449$, $p < 0.001$). Specifically, in comparison to *Shank1*$^{-/-}$ mice, there was increased hyperactivity in *Shank1*$^{+/+}$ ($p < 0.001$) and *Shank1*$^{+/-}$ mice ($p < 0.001$) following AMPH treatment, whereas AMPH-induced hyperactivity did not differ between

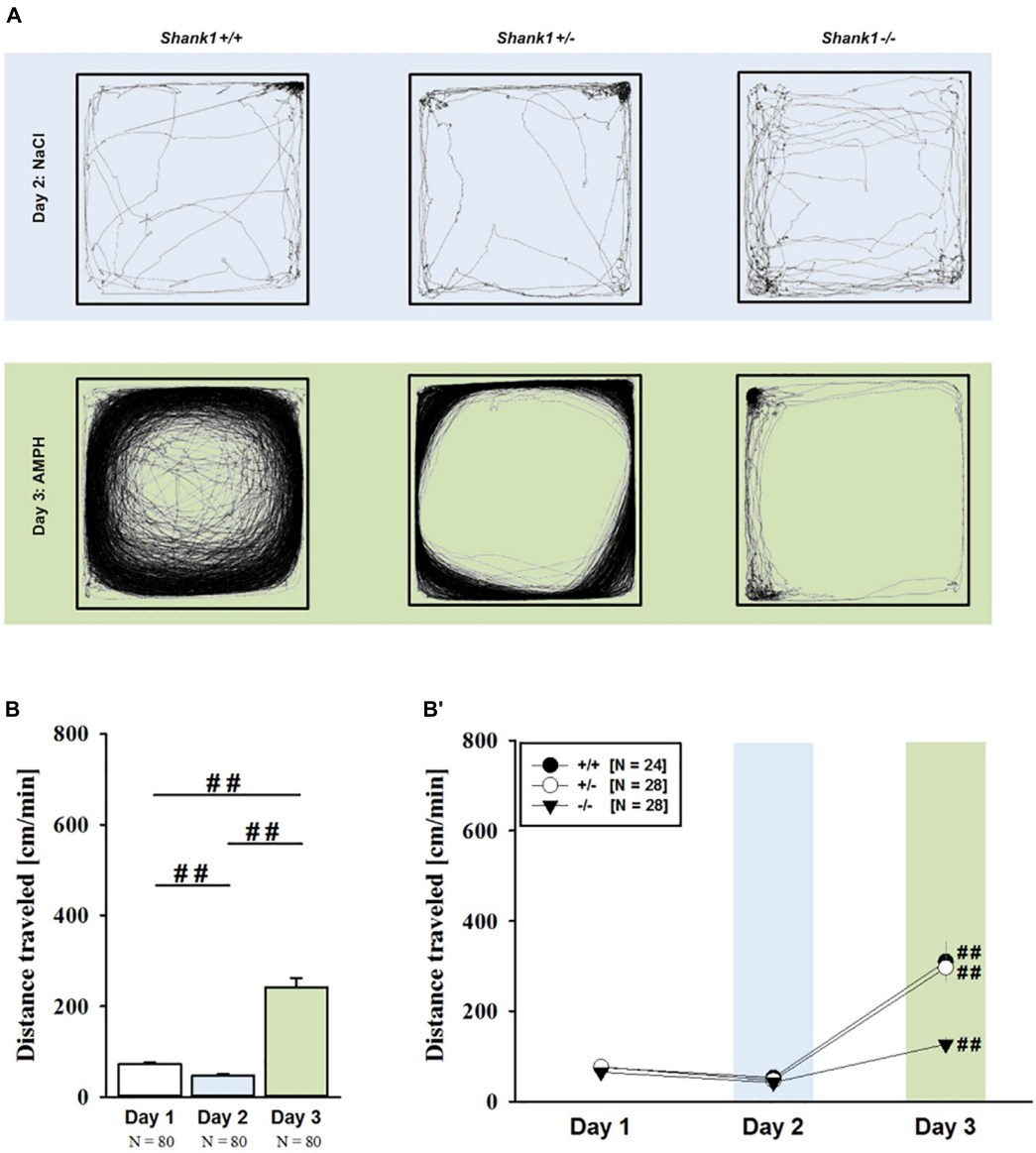

FIGURE 3 | (A) AMPH-induced hyperactivity in adult *Shank1* mice. Exemplary figure depicting the locomotor activity pattern of individual adult *Shank1*$^{+/+}$, *Shank1*$^{+/-}$, and *Shank1*$^{-/-}$ mice injected with saline (NaCl) on day 2 (upper panel) and with AMPH on day 3 (lower panel); measured over 45 min. **(B)** Bar graph depicting the distance traveled by all genotypes during baseline testing (white bar), following saline administration (blue bar), and after AMPH treatment (green bar). **(B′)** Line graph depicting the distance traveled by *Shank1*$^{+/+}$ (black circle), *Shank1*$^{+/-}$ (white circle), and *Shank1*$^{-/-}$ (black triangle) over the three consecutive test days. Data are presented as means + SEM or means ± SEM. $^{\#\#}p < 0.001$ **(B)**, $^{\#\#}p < 0.001$ vs. day 2 **(B′)**.

Shank1$^{+/+}$ and *Shank1*$^{+/-}$ mice ($p = 0.768$). This prominent genotype effect was also reflected in the temporal response pattern (genotype: $F_{2,77} = 10.449$, $p < 0.001$; time × genotype: $F_{88,3388} = 6.004$, $p < 0.001$; **Figure 4C**). After about 10 min with similar locomotor activity levels in all genotypes, *Shank1*$^{+/+}$ and *Shank1*$^{+/-}$ mice displayed a strong increase in locomotor activity and maintained high activity levels until the end of testing, whereas the AMPH-induced increase was very mild in *Shank1*$^{-/-}$ mice (**Figures 4A′–C′**).

Because *Shank1* deletion had prominent effects on the induction of locomotor activity following AMPH treatment in *Shank1*$^{-/-}$ mice but not *Shank1*$^{+/-}$ mice, we also tested whether rearing behavior was affected by genotype in a similar manner in adult mice. AMPH administration induced rearing behavior ($F_{2,148} = 3.885$, $p = 0.023$) and, alike locomotor activity, there was a general genotype effect on rearing behavior ($F_{2,74} = 7.794$, $p < 0.001$). Sex had no prominent impact and did not modulate AMPH effects ($F_{1,74} = 0.179$, $p = 0.674$; sex × genotype: $F_{2,74} = 0.578$, $p = 0.536$; day × sex: $F_{4,148} = 0.544$, $p = 0.582$; day × sex × genotype: $F_{4,148} = 1.815$, $p = 0.129$). Importantly, however, AMPH responsivity was again strongly affected by *Shank1* deletion (day × genotype: $F_{4,148} = 2.926$, $p = 0.023$).

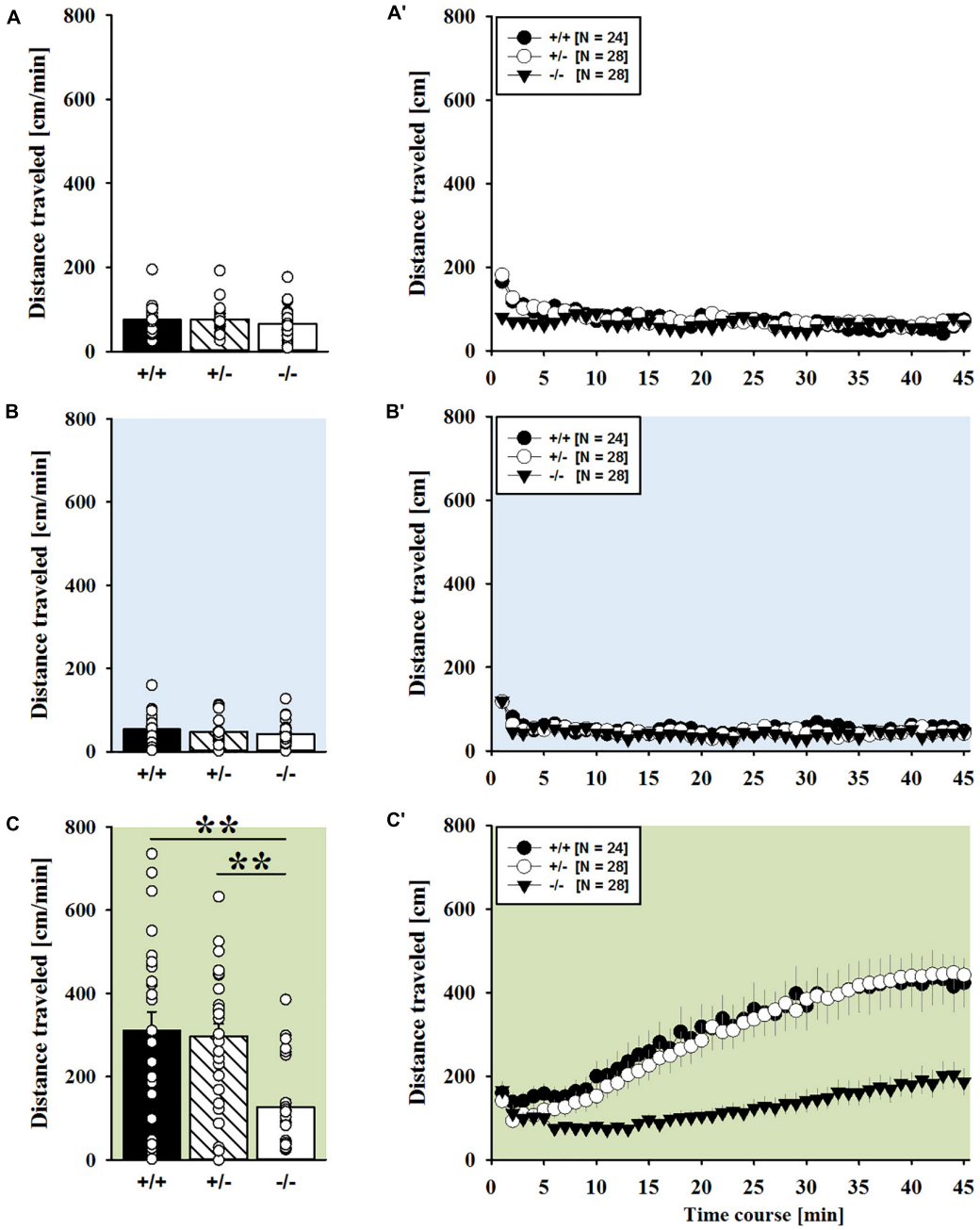

FIGURE 4 | AMPH-induced hyperactivity in adult *Shank1* mice. **(A–C)** Bar graphs and **(A′–C′)** line graphs depicting the distance traveled by *Shank1*$^{+/+}$ (black bar/black circle), *Shank1*$^{+/-}$ (striped bar/white circle), and *Shank1*$^{-/-}$ (white bar/black triangle). Locomotor activity was compared during baseline testing **(A,A′)**, following saline administration **(B,B′)**, and after AMPH treatment **(C,C′)**. Data are presented as means + SEM or means ± SEM. $^{**}p < 0.001$.

While rearing behavior did not differ between genotypes under baseline conditions ($F_{2,77} = 1.163$, $p = 0.318$; **Supplementary Figure 2A**) and no differences were evident in response to saline ($F_{2,77} = 1.406$, $p = 0.251$; **Supplementary Figure 2B**), prominent genotype differences were evident following AMPH treatment ($F_{2,77} = 8.629$, $p < 0.001$). Specifically, in comparison to *Shank1*$^{+/+}$ mice, there was reduced rearing behavior in *Shank1*$^{+/-}$ ($p < 0.001$) and *Shank1*$^{-/-}$ mice ($p < 0.001$) following AMPH treatment, whereas AMPH-induced rearing behavior did not differ between *Shank1*$^{+/-}$ and *Shank1*$^{-/-}$ mice ($p = 0.788$). This prominent genotype effect was also reflected in the temporal response pattern (genotype: $F_{2,77} = 8.629$, $p < 0.001$; time × genotype: $F_{88,3388} = 2.040$, $p < 0.001$; **Supplementary Figure 2C**). After about 10 min with similar levels of rearing behavior in all genotypes, only *Shank1*$^{+/+}$ mice displayed a strong increase in rearing behavior and maintained high rearing

levels until the end of testing, whereas the AMPH-induced increase was very mild in *Shank1*$^{+/-}$ and *Shank1*$^{-/-}$ mice (**Supplementary Figures 2A′–C′**).

Of note, the time spent in the center of the open field was also affected and changed across test days ($F_{2,148}$ = 30.879, $p < 0.001$), but no genotype-dependent differences were obtained ($F_{2,74}$ = 0.998, p = 0.373; day × genotype: $F_{4,148}$ = 1.579, p = 0.183), with sex having also no impact ($F_{1,74}$ = 0.270, p = 0.605; sex × genotype: $F_{2,74}$ = 0.138, p = 0.871; day × sex: $F_{2,148}$ = 1.543, p = 0.217; day × sex × genotype: $F_{4,148}$ = 0.660, p = 0.621). When comparing genotypes on individual test days, no differences were observed under baseline conditions ($F_{2,77}$ = 0.573, p = 0.566; **Supplementary Figure 3A**) and in response to saline on day 2 ($F_{2,77}$ = 2.590, p = 0.082; **Supplementary Figure 3B**), whereas genotypes differed from each other in response to AMPH on day 3 ($F_{2,77}$ = 4.318, p = 0.017; **Supplementary Figure 3C**). Specifically, *Shank1*$^{+/-}$ mice spent less time in the center than *Shank1*$^{+/+}$ mice (p = 0.005) but not than *Shank1*$^{-/-}$ mice (p = 0.055), with the latter also not differing from each other (p = 0.324).

MDMA-Induced Hyperactivity

MDMA administration induced hyperactivity in adult mice ($F_{2,82}$ = 9.290, $p < 0.001$), as again evidenced by representative locomotor activity patterns in response to MDMA on test day 3 in comparison to saline on day 2 (**Figure 5A**). Consistent with AMPH, there was a general genotype effect ($F_{2,41}$ = 13.153, $p < 0.001$), with sex having no prominent impact in modulating MDMA effects ($F_{1,41}$ = 0.689, p = 0.411; sex × genotype: $F_{2,41}$ = 4.155, p = 0.023; day × sex: $F_{2,82}$ = 2.487, p = 0.089; day × sex × genotype: $F_{4,82}$ = 0.534, p = 0.711). Again, this was further supported by a comparison between test days that revealed clearly higher levels of locomotor activity following MDMA treatment than the day before in response to saline (p = 0.003; **Figure 5B**). However, despite this difference held true for *Shank1*$^{+/+}$ (t_{13} = 2.000, p = 0.034, one-tailed) and *Shank1*$^{+/-}$ mice (t_{18} = 3.356, p = 0.004), no evidence for MDMA-induced hyperactivity was evident in *Shank1*$^{-/-}$ mice, with their level of locomotor activity being the same following MDMA as in response to saline (t_{13} = 1.188, p = 0.256; **Figure 5B′**). In fact, similar to AMPH, although more prominent, MDMA responsivity in adult mice was strongly affected by *Shank1* deletion (day × genotype: $F_{4,82}$ = 2.759, p = 0.033) and clear genotype differences in hyperactivity following MDMA administration were evident ($F_{2,44}$ = 6.606, p = 0.003). Importantly, the lack of MDMA-induced hyperactivity in *Shank1*$^{-/-}$ mice was not driven by baseline differences in locomotor activity. Although genotype differences were evident under baseline conditions ($F_{2,44}$ = 8.286, p = 0.001; **Figure 6A**) and *Shank1*$^{-/-}$ mice displayed lower locomotor activity compared to *Shank1*$^{+/+}$ ($p < 0.001$) and *Shank1*$^{+/-}$ mice (p = 0.040), with the latter also differing from each other (p = 0.029), locomotor activity did not differ between genotypes in response to saline ($F_{2,44}$ = 2.445, p = 0.098; **Figure 6B**). Specifically, as compared to *Shank1*$^{-/-}$ mice, increased MDMA-induced hyperactivity was detected in *Shank1*$^{+/+}$ (p = 0.002) and *Shank1*$^{+/-}$ mice (p = 0.004), whereas the latter two did not differ from each other (p = 0.652). This prominent genotype effect was also reflected in the temporal response pattern (genotype: $F_{2,44}$ = 6.606, p = 0.003; time × genotype: $F_{88,1936}$ = 0.999, p = 0.484; **Figure 6C**). While locomotor activity levels increased in *Shank1*$^{+/+}$ and *Shank1*$^{+/-}$ mice already from the very beginning of testing, MDMA treatment in *Shank1*$^{-/-}$ mice was associated with a decrease of locomotor activity, with very low activity levels being maintained in *Shank1*$^{-/-}$ mice throughout testing (**Figures 6A′–C′**).

Of note, the time spent in the center of the open field was also affected and changed across test days ($F_{2,82}$ = 43.972, $p < 0.001$), and genotype-dependent differences were obtained ($F_{2,41}$ = 5.374, p = 0.008; day × genotype: $F_{4,82}$ = 3.264, p = 0.016), with sex having no impact ($F_{1,41}$ = 0.001, p = 0.978; sex × genotype: $F_{2,41}$ = 0.823, p = 0.446 day × sex: $F_{2,82}$ = 0.061, p = 0.941; day × sex × genotype: $F_{4,82}$ = 0.148, p = 0.963). When comparing genotypes on individual test days, genotype differences were evident under baseline conditions ($F_{2,44}$ = 5.505, p = 0.007; **Supplementary Figure 4A**). Specifically, *Shank1*$^{+/+}$ mice spent more time in the center than *Shank1*$^{+/-}$ (p = 0.005) and *Shank1*$^{-/-}$ mice (p = 0.006), with the latter not differing from each other (p = 0.883). Genotypes did not differ from each other in terms of the time spent in the center on day 2 in response to saline ($F_{2,44}$ = 1.537, p = 0.226; **Supplementary Figure 4B**), and on day 3 in response to MDMA ($F_{2,44}$ = 1.170, p = 0.320; **Supplementary Figure 4C**).

Because MDMA-induced hyperactivity was completely absent in *Shank1*$^{-/-}$ mice, we also tested the hypothesis that MDMA treatment might have induced repetitive and stereotyped movement patterns, such as circling behavior (Powell et al., 2004; Risbrough et al., 2006). In fact, there was an overall increase in repetitive circling behavior following MDMA treatment ($F_{1,41}$ = 78.866, $p < 0.001$). Importantly, however, the increase in circling occurred irrespective of genotype and can thus not explain the lack of MDMA-induced hyperactivity in *Shank1*$^{-/-}$ mice. Specifically, there was no prominent effect of genotype ($F_{2,41}$ = 1.925, p = 0.159; day × genotype: $F_{2,41}$ = 1.678, p = 0.199) or sex ($F_{1,41}$ = 0.004, p = 0.953; sex × genotype: $F_{2,41}$ = 1.171, p = 0.320; day × sex: $F_{1,41}$ = 0.061, p = 0.806; day × sex × genotype: $F_{2,41}$ = 1.695, p = 0.196). A comparison between test days revealed that circling behavior following MDMA treatment was clearly higher than the day before in response to saline ($p < 0.001$; **Supplementary Figure 5A**), yet this increase occurred irrespective of genotype and held true for all individual genotypes (*Shank1*$^{+/+}$: t_{13} = 4.283, $p < 0.001$, one-tailed; *Shank1*$^{+/-}$: t_{18} = 7.681, $p < 0.001$; *Shank1*$^{-/-}$: t_{27} = 4.065, p = 0.001; **Supplementary Figure 5A′**).

Neurotransmitter Measurements

Prefrontal Cortex

Concentrations of the DA precursor Tyr in the prefrontal cortex did not differ between genotypes ($F_{2,39}$ = 0.364, p = 0.697; **Figure 7A**). *Shank1* deletion, however, affected the level of the 5-HT precursor Trp ($F_{2,40}$ = 3.933, p = 0.028; **Figure 7B**).

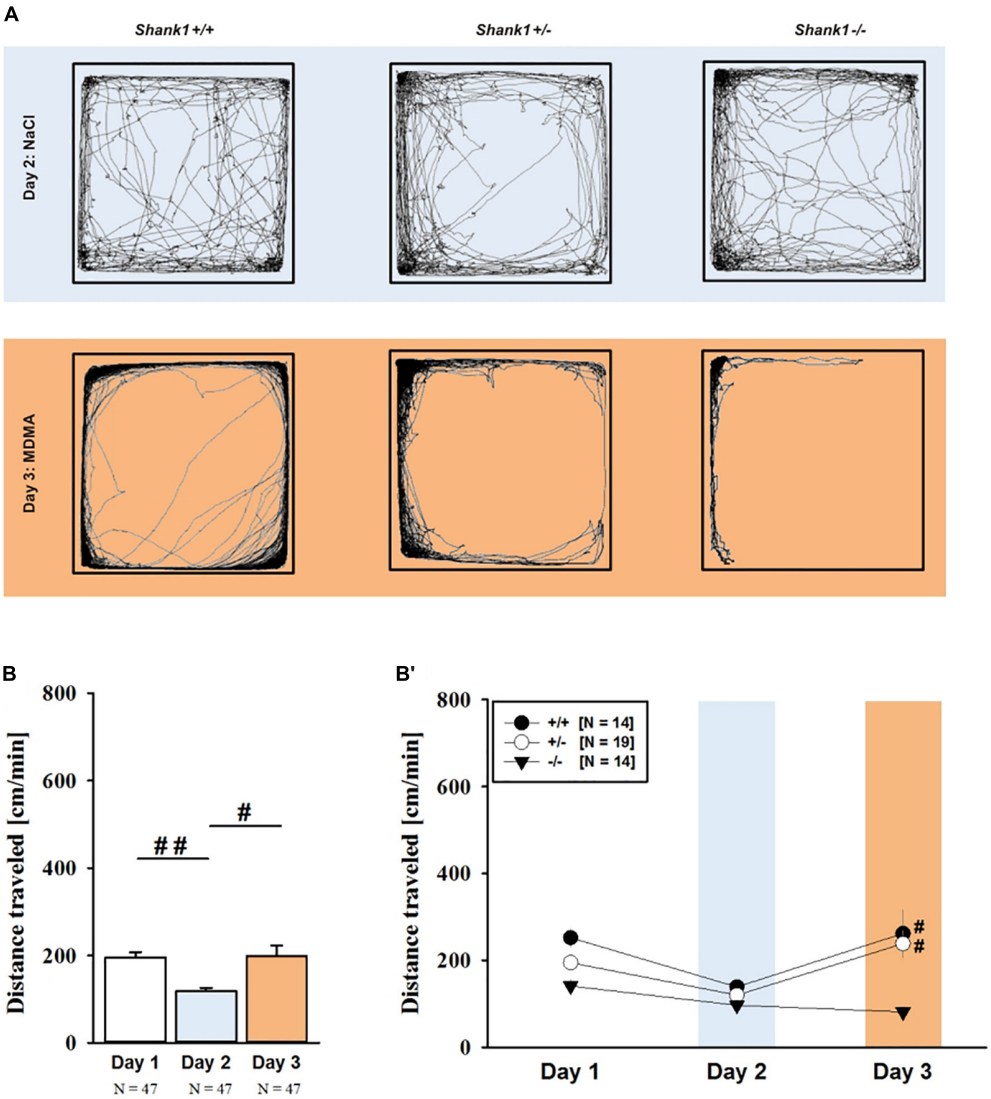

FIGURE 5 | MDMA-induced hyperactivity in adult *Shank1* mice. **(A)** Exemplary figure depicting the locomotor activity pattern of individual adult *Shank1*$^{+/+}$, *Shank1*$^{+/-}$, and *Shank1*$^{-/-}$ mice injected with saline (NaCl) on day 2 (upper panel) and with MDMA on day 3 (lower panel); measured over 45 min. **(B)** Bar graph depicting the distance traveled by all genotypes during baseline testing (white bar), following saline administration (blue bar), and after MDMA treatment (orange bar). **(B′)** Line graph depicting the distance traveled by *Shank1*$^{+/+}$ (black circle), *Shank1*$^{+/-}$ (white circle), and *Shank1*$^{-/-}$ (black triangle) over the three consecutive test days. Data are presented as means + SEM or means ± SEM. $^{\#}p < 0.05$, $^{\#\#}p < 0.001$ **(B)**, $^{\#}p < 0.05$ vs. day 2 **(B′)**.

Specifically, *Shank1*$^{-/-}$ mice had higher Trp concentrations in the prefrontal cortex than *Shank1*$^{+/+}$ ($p = 0.019$) and *Shank1*$^{+/-}$ mice ($p = 0.018$), with the latter two not differing from each other ($p = 0.910$).

Although basal DA levels clearly tended to be lower in *Shank1*$^{-/-}$ mice, apparent genotype differences in DA levels did not reach statistical significance ($F_{2,38} = 3.192$, $p = 0.052$; **Figure 7C**), while the concentration of the DA metabolite DOPAC differed between genotypes ($F_{2,40} = 3.879$, $p = 0.029$; **Figure 7D**). *Shank1*$^{+/+}$ mice had higher DOPAC concentrations than *Shank1*$^{-/-}$ ($p = 0.008$) but not *Shank1*$^{+/-}$ mice ($p = 0.290$), with *Shank1*$^{-/-}$ and *Shank1*$^{+/-}$ mice also not differing from each other ($p = 0.102$). The DOPAC/DA ratio, however, was not affected by *Shank1* deletion ($F_{2,38} = 0.261$, $p = 0.772$; **Figure 7E**).

While DA levels were not significantly affected by genotype, *Shank1* deletion affected basal NA concentrations ($F_{2,35} = 6.597$, $p = 0.004$; **Figure 7F**). *Shank1*$^{-/-}$ mice had higher concentrations of NA as compared to *Shank1*$^{+/+}$ ($p = 0.003$) and *Shank1*$^{+/-}$ mice ($p = 0.003$), while *Shank1*$^{+/+}$ and *Shank1*$^{+/-}$ mice did not differ in that aspect ($p = 0.797$). There were no differences between genotypes in the concentrations of the NA metabolite MHPG ($F_{2,39} = 1.604$, $p = 0.214$; **Figure 7G**), yet the MHPG/NA ratio differed between genotypes ($F_{2,34} = 4.066$, $p = 0.026$; **Figure 7H**). The MHPG/NA ratio was lower in *Shank1*$^{-/-}$ mice as compared to *Shank1*$^{+/-}$

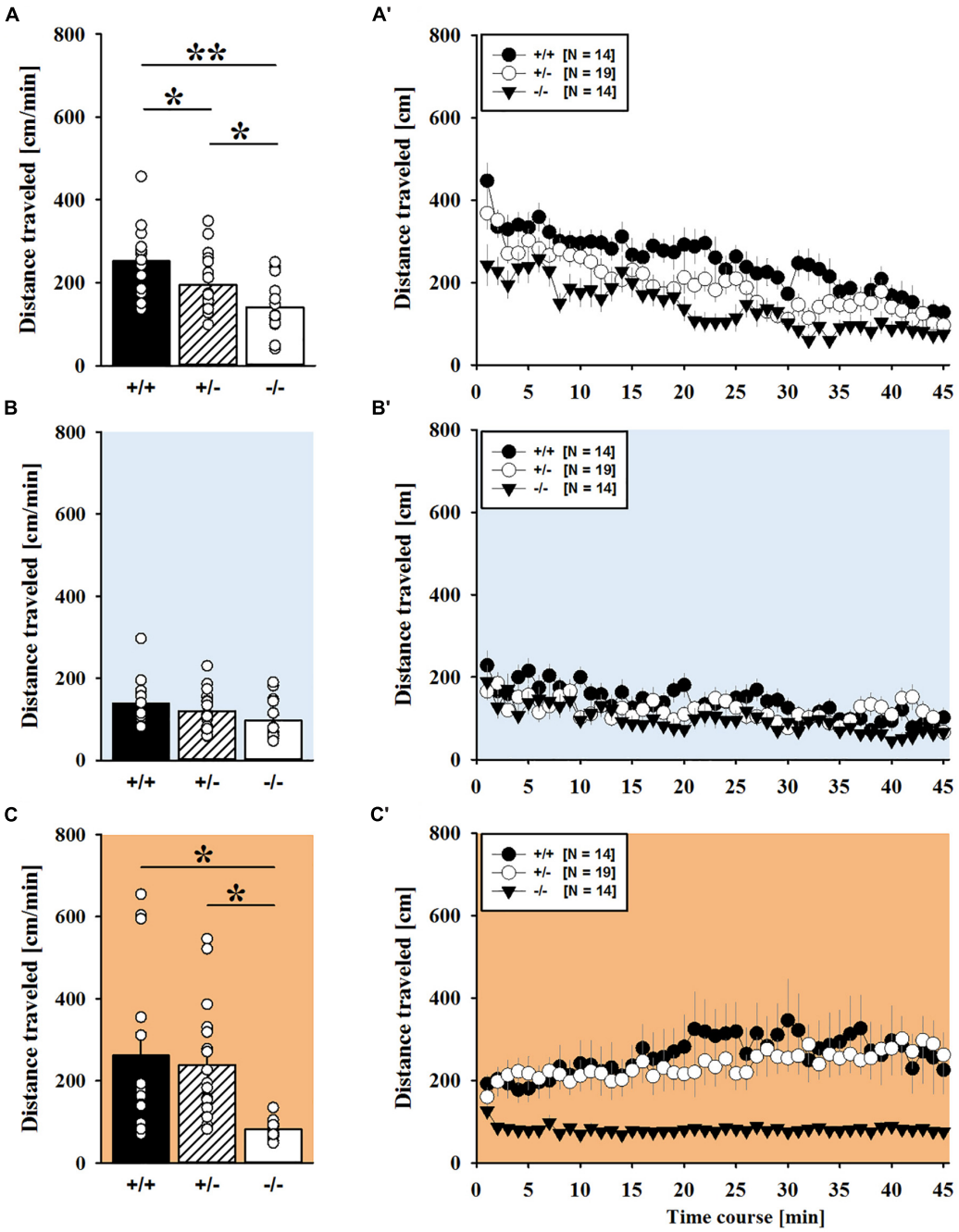

FIGURE 6 | MDMA-induced hyperactivity in adult *Shank1* mice. **(A–C)** Bar graphs and **(A′–C′)** line graphs depicting the distance traveled by *Shank1*$^{+/+}$ (black bar/black circle), *Shank1*$^{+/-}$ (striped bar/white circle), and *Shank1*$^{-/-}$ (white bar/black triangle). Locomotor activity was compared during baseline testing **(A,A′)**, following saline administration **(B,B′)**, and after MDMA treatment **(C,C′)**. Data are presented as means + SEM or means ± SEM. *$p < 0.05$, **$p < 0.001$.

mice ($p = 0.007$) but not as compared to *Shank1*$^{+/+}$ mice ($p = 0.140$). No significant differences in MHPG/NA ratio between *Shank1*$^{+/+}$ and *Shank1*$^{+/-}$ mice were detected ($p = 0.114$).

The 5-HT system was not affected by *Shank1* deletion. Specifically, basal 5-HT concentrations, the levels of the main 5-HT metabolite 5-HIAA, and the 5-HIAA/5-HT ratio did not differ between genotypes (all p-values > 0.100; **Figures 7I–K**).

Nucleus Accumbens

In the nucleus accumbens, *Shank1* deletion affected the concentration of the DA precursor Tyr ($F_{2,40} = 3.421$, $p = 0.043$; **Figure 8A**) and the 5-HT precursor Trp ($F_{2,40} = 3.709$,

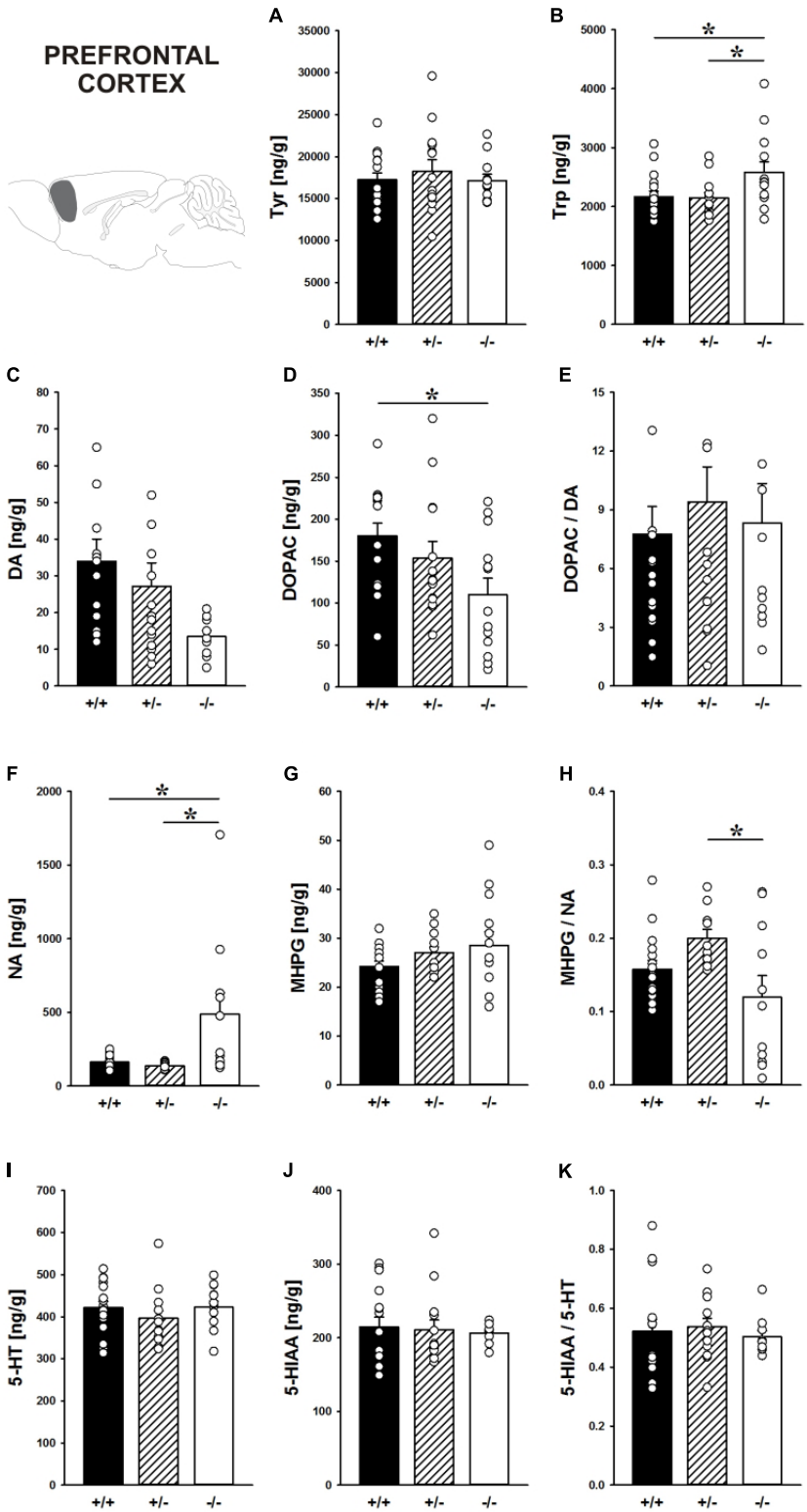

FIGURE 7 | Catecholamine/indolamine, precursor, and metabolite concentrations in the prefrontal cortex of *Shank1* mice. Basal levels of **(A)** Tyrosine (Tyr), **(B)** Tryptophan (Trp), **(C)** Dopamine (DA), **(D)** DA-metabolite dehydroxyphenylacetic acid (DOPAC), **(E)** DOPAC/DA ratio, **(F)** Noradrenaline (NA), **(G)** NA-metabolite 4-hydroxy-3-methoxy-phenylglycol (MHPG), **(H)** MHPG/NA ratio, **(I)** 5-hydroxytryptamine (5-HT; serotonin), **(J)** 5-HT-metabolite 5-hydroxy-indol-acetic acid (5-HIAA), and **(K)** 5-HIAA/5-HT ratio in *Shank1*$^{+/+}$ (black bar), *Shank1*$^{+/-}$ (striped bar), and *Shank1*$^{-/-}$ mice (white bar). *N* = 10–16 per genotype. Data are presented as means + SEM. *$p < 0.05$. Schematic representation of the prefrontal cortex was adapted from Paxinos and Franklin (2001).

$p = 0.033$; **Figure 8B**). Specifically, *Shank1*$^{-/-}$ mice had higher Tyr concentrations than *Shank1*$^{+/+}$ mice ($p = 0.013$) but not *Shank1*$^{+/-}$ mice ($p = 0.281$), with the latter also not differing from each other ($p = 0.143$). Trp levels in *Shank1*$^{-/-}$ mice were higher than in *Shank1*$^{+/+}$ ($p = 0.018$) and *Shank1*$^{+/-}$ mice ($p = 0.028$), whereas the latter did not differ from each other ($p = 0.901$).

However, despite genotype differences in the levels of the precursors, there were no differences between genotypes in DA, DOPAC, DOPAC/DA ratio, NA, MHPG, MHPG/NA ratio, 5-HT, 5-HIAA, and 5-HIAA/5-HT ratio (all p-values > 0.100; **Figures 8C–K**).

Hypothalamus

Concentrations of the precursors Tyr tended to be affected by *Shank1* deletion in the hypothalamus ($F_{2,38} = 2.902$, $p = 0.067$; **Figure 9A**). Trp in the hypothalamus did not differ between genotypes ($F_{2,39} = 0.864$, $p = 0.429$; **Figure 9B**).

Moreover, the DA system was not affected by *Shank1* deletion. DA, DOPAC, and DOPAC/DA ratio did not differ between genotypes (all p-values > 0.100; **Figures 9C–E**).

While NA concentrations were not affected by *Shank1* deletion ($F_{2,37} = 0.598$, $p = 0.555$; **Figure 9F**), MHPG levels differed between genotypes ($F_{2,37} = 3.596$, $p = 0.037$; **Figure 9G**). Specifically, MHPG concentrations in the hypothalamus of *Shank1*$^{-/-}$ mice were higher than *Shank1*$^{+/+}$ mice ($p = 0.012$) but not *Shank1*$^{+/-}$ mice ($p = 0.263$), with no difference between *Shank1*$^{+/+}$ and *Shank1*$^{+/-}$ mice ($p = 0.121$). Genotype-dependent differences in the MHPG/NA ratio were not evident ($F_{2,36} = 1.041$, $p = 0.363$; **Figure 9H**).

Finally, there were genotype-dependent differences in 5-HT concentrations in the hypothalamus ($F_{2,38} = 5.437$, $p = 0.008$; **Figure 9I**). While *Shank1*$^{-/-}$ mice had higher 5-HT concentrations than *Shank1*$^{+/+}$ mice ($p = 0.002$), this difference was not present between *Shank1*$^{-/-}$ and *Shank1*$^{+/-}$ mice ($p = 0.113$) or between *Shank1*$^{+/+}$ and *Shank1*$^{+/-}$ mice ($p = 0.095$). In conjunction, there was a trend for differences in 5-HIAA concentrations ($F_{2,38} = 2.581$, $p = 0.089$; **Figure 9J**). No genotype-dependent differences in the 5-HIAA/5-HT ratio were observed ($F_{2,38} = 0.480$, $p = 0.622$; **Figure 9K**).

DISCUSSION

The goal of our present study was to test whether *Shank1* plays a role in the behavioral effects of psychostimulants and whether this is associated with genotype-dependent neurochemical alterations. To this aim, null mutant *Shank1*$^{-/-}$ mice were treated with AMPH (2.5 mg/kg) and MDMA (20 mg/kg), and psychostimulant-induced hyperactivity was compared to heterozygous *Shank1*$^{+/-}$ and wildtype *Shank1*$^{+/+}$ littermate controls. Results show that *Shank1*$^{-/-}$ mice display reduced psychostimulant-induced hyperactivity, although psychostimulants robustly stimulated locomotor activity in littermate controls. *Shank1* deletion effects emerged throughout development, were particularly prominent in adulthood, and seen in response to both psychostimulants, i.e., AMPH and MDMA.

Mutations in *SHANK* genes are associated with multiple major neuropsychiatric disorders, including SCZ and BPD besides ASD (Guilmatre et al., 2014; Bourgeron, 2015; de la Torre-Ubieta et al., 2016). Because psychostimulants, such as AMPH, can provoke mania-like symptoms in healthy subjects and exacerbate symptoms or induce a manic episode in BPD patients (Meyendorff et al., 1985; Peet and Peters, 1995; Hasler et al., 2006), we expected that *Shank1* deletion leads to increased AMPH-induced hyperactivity. In fact, AMPH-induced hyperactivity is a commonly applied paradigm to assess behavioral phenotypes related to BPD and considered to be the gold standard for modeling mania-like elevated drive in mouse models (Berggren et al., 1978; Gould et al., 2001; Kato et al., 2007; Young et al., 2011). Unexpectedly, however, *Shank1*$^{-/-}$ mice displayed reduced psychostimulant-induced hyperactivity. This was reflected in a weaker increase in locomotor activity and a complete lack of induction of rearing behavior following AMPH. Supporting a gene dosage effect, *Shank*$^{+/-}$ mice displayed an intermediate phenotype. While locomotor activity was increased following AMPH to levels similar to littermate controls, induction of rearing behavior following AMPH was absent, with rearing levels being similar to *Shank1*$^{-/-}$ mice. Our observation that AMPH-induced hyperactivity is reduced rather than enhanced following *Shank1* deletion thus clearly speaks against a behavioral phenotype with relevance to BPD. The lack of a BPD-like phenotype is consistent with currently available human data linking mutations in *SHANK2* and *SHANK3* but not *SHANK1* to BPD. Specifically, a duplication in *SHANK2* has been reported for a BPD patient (Noor et al., 2014) and four point mutations in *SHANK2* (c.3979G > A; c.2900A > G; c.4461C > T; c.4926G > A) have been identified very recently in BPD patients (Yang et al., 2018). Moreover, in a substantial number of individuals lacking *SHANK3* and diagnosed with the Phelan-McDermid 22q13 deletion syndrome BPD was evident (Sovner et al., 1996; Willemsen et al., 2011; Denayer et al., 2012; Verhoeven et al., 2012, 2013; Vucurovic et al., 2012). Notably, *SHANK3* duplications were also associated with BPD in humans (Han et al., 2013). In contrast, mutations in *SHANK1* have been associated with SCZ but not BPD. Fromer et al. (2014) reported a *de novo SHANK1* frameshift mutation in a SCZ patient. Lennertz et al. (2012) found that the T allele of the *SHANK1* promotor variant rs3810280 leads to impaired auditory working memory capacity as assessed with digit span in SCZ patients and subjects clinically at risk for developing a psychosis but not in healthy controls.

The clinical pattern is reflected in relevant *Shank* mouse models. For instance, Pappas et al. (2017) recently reported BPD-like phenotypes in *Shank2*$^{\Delta 24-/-}$ mice. Specifically, they observed increased locomotor activity indicative of elevated drive and perturbed circadian rhythms, which could be normalized by lithium and valproate treatment. Importantly, the increase in locomotor activity caused by *Shank2* deletion could be augmented by AMPH administration and the augmentation was more prominent in *Shank2*$^{\Delta 24-/-}$ mice than in *Shank2*$^{\Delta 24+/+}$ controls (Pappas et al., 2017). *Shank2* deficiency limited to

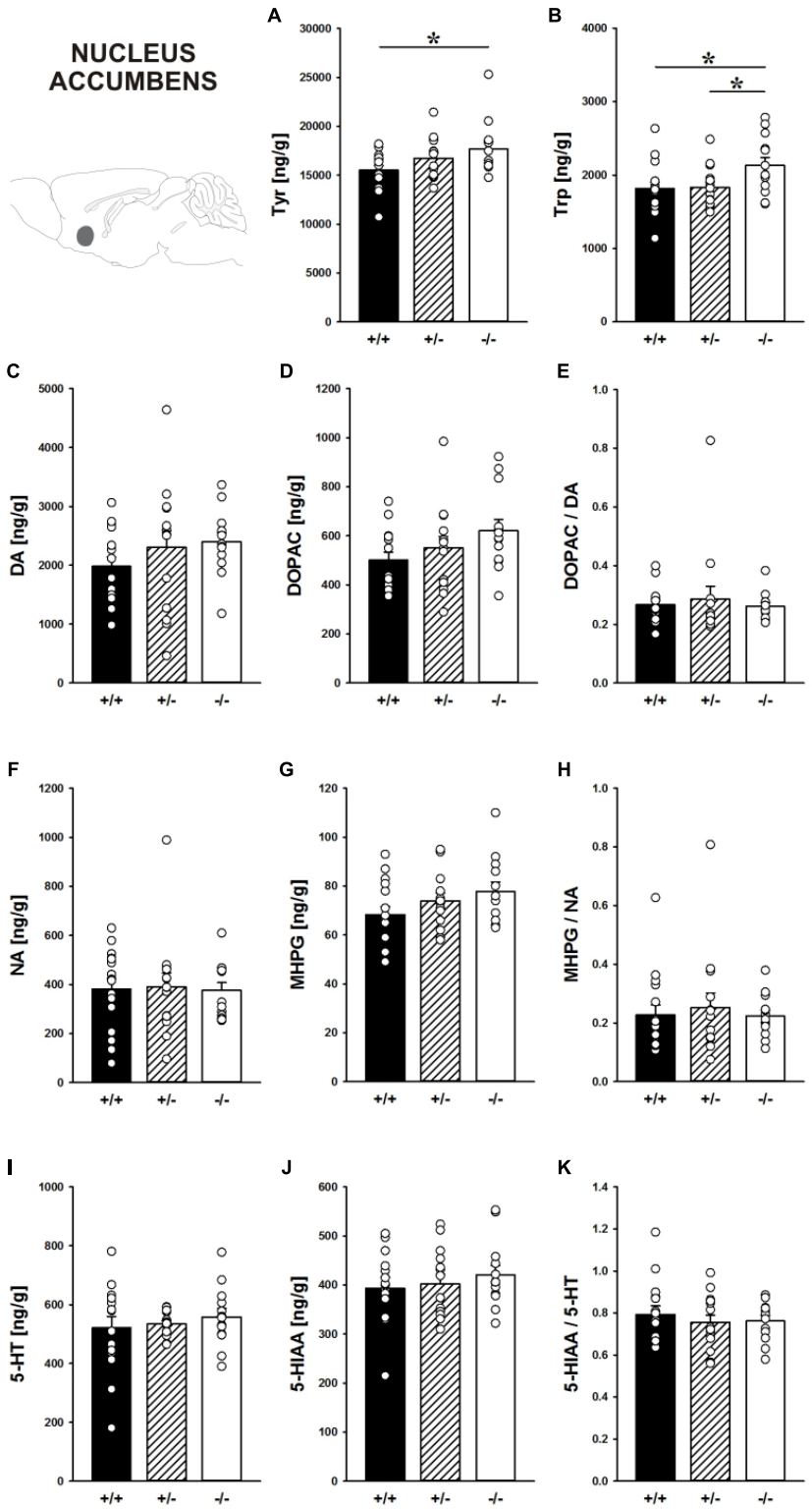

FIGURE 8 | Catecholamine/indolamine, precursor, and metabolite concentrations in the nucleus accumbens of *Shank1* mice. Basal levels of **(A)** Tyrosine (Tyr), **(B)** Tryptophan (Trp), **(C)** Dopamine (DA), **(D)** DA-metabolite dehydroxyphenylacetic acid (DOPAC), **(E)** DOPAC/DA ratio, **(F)** Noradrenaline (NA), **(G)** NA-metabolite 4-hydroxy-3-methoxy-phenylglycol (MHPG), **(H)** MHPG/NA ratio, **(I)** 5-hydroxytryptamine (5-HT; serotonin), **(J)** 5-HT-metabolite 5-hydroxy-indol-acetic acid (5-HIAA), and **(K)** 5-HIAA/5-HT ratio in *Shank1*$^{+/+}$ (black bar), *Shank1*$^{+/-}$ (striped bar), and *Shank1*$^{-/-}$ mice (white bar). N = 13–16 per genotype. Data are presented as means + SEM. *$p < 0.05$. Schematic representation of the nucleus accumbens was adapted from Paxinos and Franklin (2001).

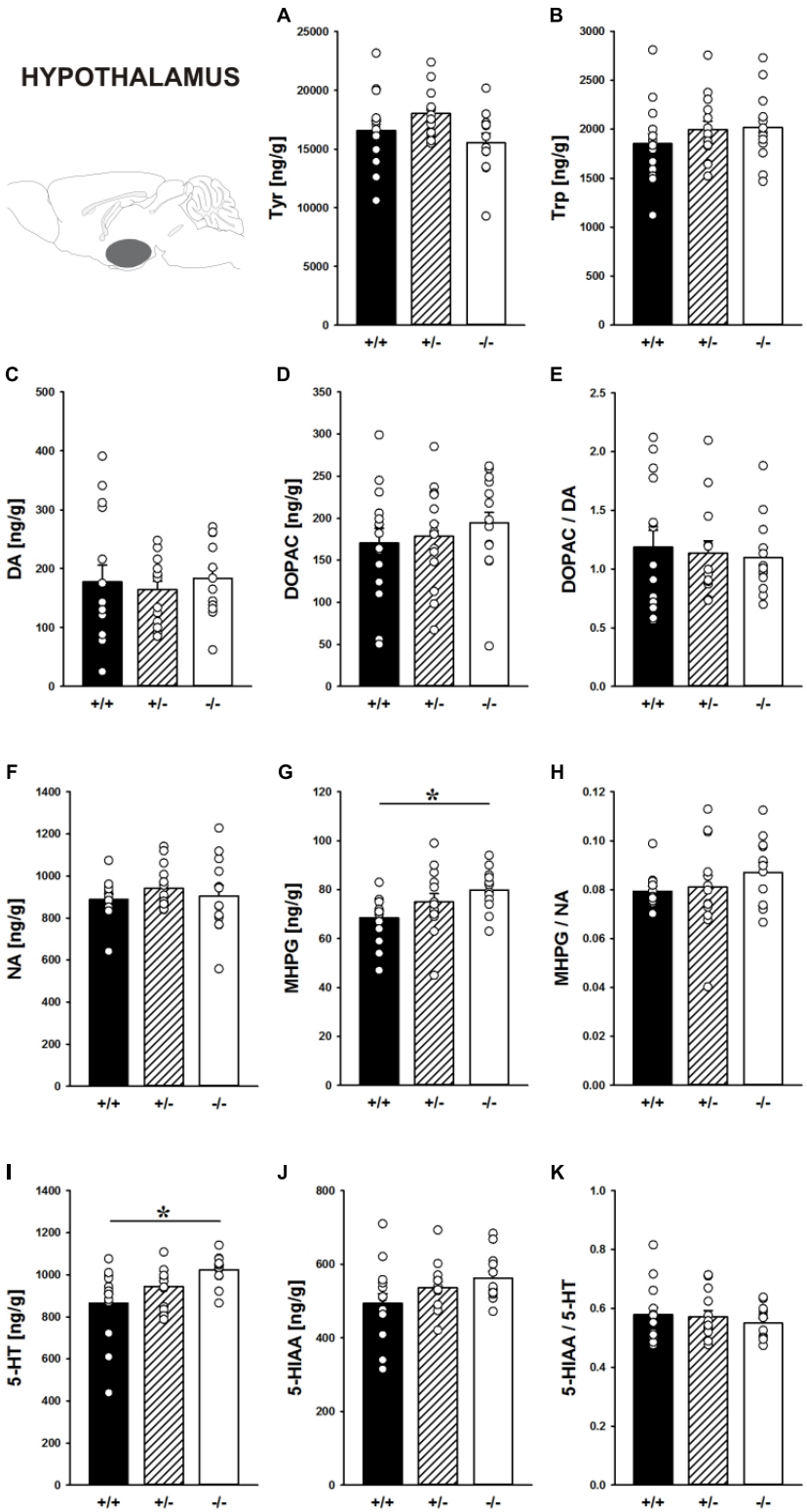

FIGURE 9 | Catecholamine/indolamine, precursor, and metabolite concentrations in the hypothalamus of *Shank1* mice. Basal levels of **(A)** Tyrosine (Tyr), **(B)** Tryptophan (Trp), **(C)** Dopamine (DA), **(D)** DA-metabolite dehydroxyphenylacetic acid (DOPAC), **(E)** DOPAC/DA ratio, **(F)** Noradrenaline (NA), **(G)** NA-metabolite 4-hydroxy-3-methoxy-phenylglycol (MHPG), **(H)** MHPG/NA ratio, **(I)** 5-hydroxytryptamine (5-HT; serotonin), **(J)** 5-HT-metabolite 5-hydroxy-indol-acetic acid (5-HIAA), and **(K)** 5-HIAA/5-HT ratio in *Shank1*$^{+/+}$ (black bar), *Shank1*$^{+/-}$ (striped bar), and *Shank1*$^{-/-}$ mice (white bar). *N* = 12–15 per genotype. Data are presented as means + SEM. *$p < 0.05$. Schematic representation of the hypothalamus was adapted from Paxinos and Franklin (2001).

the forebrain recapitulated the BPD-like phenotype, which was associated with alterations in the composition and function of NMDA and AMPA receptors (Pappas et al., 2017). Moreover, *Shank2*$^{\Delta 7-/-}$ mice likewise display enhanced levels of locomotor activity but augmentation by methylphenidate was weaker in *Shank2*$^{\Delta 7-/-}$ mice than in *Shank2*$^{\Delta 7+/+}$ controls (Ey et al., 2018). Finally, *Shank3* overexpression in mice was linked to a BPD-like phenotype characterized by increased locomotor activity and abnormal circadian rhythms (Han et al., 2013). Importantly, hyperactivity of *Shank3* overexpressing mice following an acute injection of AMPH aggravated to a greater extent than in controls. The BPD-like phenotype was rescued by valproate but not lithium treatment. To our knowledge, no studies on *Shank3* deletion effects on AMPH-induced hyperactivity are available. Together, this might suggest that *Shank1* deletion leads to specific alterations in brain structure or function reducing rather than enhancing the efficacy of AMPH to stimulate hyperactivity not present in other relevant *Shank* mouse models.

Sold as speed, AMPH is among the most commonly used illicit drugs, but is also available by prescription and is widely used for treating weight control, narcolepsy, and attention deficit disorder (Sulzer et al., 2005). AMPH acts primarily as a DA and NA releaser by induction of reverse transport of catecholamines through plasma membrane uptake carries, i.e., the DA and NA transporters, and redistribution of catecholamines from synaptic vesicles to the cytosol, with little affinity for receptors (Sulzer et al., 2005; Hutson et al., 2014), although prominent effects on the 5-HT system were also reported (Pum et al., 2007). In mice, the stimulatory effects of AMPH are widely believed to be driven by increased synaptic DA levels and subsequent activation of postsynaptic receptors. In fact, while mice deficient for the NA transporter are supersensitive (Xu F. et al., 2000), AMPH-induced hyperactivity is enhanced in DA transporter overexpressing mice (Salahpour et al., 2008) but completely abolished in mice lacking the DA transporter (Giros et al., 1996), an effect mediated by the 5-HT system (Gainetdinov et al., 1999). Yet, it is not affected by deletion of the gene for the 5-HT transporter (Bengel et al., 1998), although, to a lesser extent, AMPH affects 5-HT transporters as well (Steele et al., 1987; Crespi et al., 1997). Postsynaptically, AMPH action was reported to depend on D2 but less on D3 and not on D4 receptors, with mixed results for the D1 receptor (Xu M. et al., 2000; McNamara et al., 2006; Fan and Hess, 2007; Fan et al., 2010). Various 5-HT receptors play a modulating role as well and it was shown that AMPH-induced hyperactivity is increased in 5-HT1A (van den Buuse et al., 2011), 5-HT1B (Bronsert et al., 2001), and 5-HT2A (Salomon et al., 2007) receptor knockout mice. Partially conflicting evidence was obtained in pharmacological studies, with 8-OH-DPAT (Przegalinski et al., 2000) and SB216641 (Przegalinski et al., 2001), 5-HT1A agonist and 5-HT1B antagonist, respectively, reducing AMPH-induced hyperactivity, while CP94,253, a 5-HT1B agonist, further enhances AMPH-induced hyperactivity (Przegalinski et al., 2001). Mixed results were obtained for the 5-HT2A (Carlsson et al., 1999; Sorensen et al., 1993) and the 5-HT2C (O'Neill et al., 1999; Marquis et al., 2007) receptor. For a more comprehensive overview including other species besides mice, the reader is referred to two excellent reviews (Hutson et al., 2014; Müller and Homberg, 2015).

While AMPH-induced hyperactivity was reduced but still detectable in *Shank1*$^{-/-}$ mice, MDMA-induced hyperactivity was robustly blocked and completely absent in *Shank1*$^{-/-}$ mice. Because a genetic manipulation affecting psychostimulant-induced hyperactivity may easily look like an attenuation when the dose-response curve is in fact shifted to the left, but now producing motor stereotypies instead of ambulation, we measured repetitive circling behavior (Powell et al., 2004; Risbrough et al., 2006). We focused on mice treated with MDMA, mostly for two reasons. Firstly, the *Shank1* deletion effect was most prominent in response to MDMA. Secondly, the MDMA dose applied here can be considered relatively high, making it particularly likely that motor stereotypies, such as repetitive circling behavior occur. However, while there was an overall increase in repetitive circling behavior following MDMA treatment, the increase in circling occurred irrespective of genotype and can thus not explain the lack of MDMA-induced hyperactivity in *Shank1*$^{-/-}$ mice. Although this speaks against a dose-response curve that is shifted to the left following *Shank1* deletion, a future dose-response study including several MDMA doses appears warranted.

Sold as ecstasy, MDMA is also among the most widely used illicit drugs, yet with little therapeutic use (Sulzer et al., 2005). MDMA acts primarily as a 5-HT and DA releaser by blocking reuptake transporters. However, relative to AMPH, MDMA is more potent at releasing 5-HT than DA (Steele et al., 1987; Crespi et al., 1997). In mice, it was repeatedly shown that MDMA leads to hyperactivity, and hyperactivity induced by low doses of MDMA of up to 10 mg/kg has previously been found to be blocked by deletion of the genes for either the 5-HT1B receptor (Scearce-Levie et al., 1999; Jean et al., 2012), the 5-HT2B receptor (Doly et al., 2008; Doly et al., 2009), or the 5-HT transporter (Bengel et al., 1998), while it is potentiated in 5-HT2A receptor knockout mice (Orejarena et al., 2011). Consistently, MDMA-induced hyperactivity was reported to be reduced by the 5-HT1B antagonist GR127935 (Scearce-Levie et al., 1999), the 5-HT2B antagonist RS127445 (Doly et al., 2008; Doly et al., 2009), the 5-HT2C antagonist RS102221 (Conductier et al., 2005), the 5-HT4 antagonist RS39604 (Jean et al., 2012), and the 5-HT uptake inhibitor fluoxetine (Fantegrossi et al., 2003). Higher MDMA doses, however, induced late-phase increases in hyperactivity in 5-HT1B (Scearce-Levie et al., 1999) and 5-HT2B (Doly et al., 2009) receptor knockout mice, possibly due to a delayed increase in DA release (White et al., 1994, 1996; Yamamoto and Spanos, 1988). Risbrough et al. (2006) found that late-phase increases in hyperactivity evoked by MDMA are enhanced in D1 knockout mice but reduced in D2 and D3 knockout mice. In DA transporter knockout mice, the typical hyperactivity displayed by these mice is reduced in response to MDMA (Powell et al., 2004). Benturquia et al. (2008) reported that MDMA-induced hyperactivity is antagonized by SCH23390, a D1 antagonist. Alike for AMPH, the reader is referred to two excellent reviews for a more comprehensive overview including other species besides mice (Sulzer et al., 2005; Müller and Homberg, 2015).

Very little is known about interactions between SHANK1 and the major neurotransmitters affected by AMPH and MDMA, i.e., DA, NA, and 5-HT. Azdad et al. (2009) obtained evidence indicating that in striatal neurons D2 receptors regulate NMDA-mediated neuronal excitation resulting in a depolarized plateau potential and spike firing through a mechanism requiring scaffolding proteins of the SHANK family including SHANK1. Buonaguro et al. (2017) showed that 3 weeks of treatment with the D2 antagonist haloperidol led to a reduction of SHANK1 mRNA expression in the anterior cingulate cortex and the insula as well as the nucleus accumbens. Li et al. (2015) reported that vortioxetine but not fluoxetine treatment leads to enhanced levels of SHANK1 mRNA in the hippocampus. Vortioxetine acts through increasing 5-HT concentrations in the synaptic cleft by inhibiting reuptake and through modulating 5-HT receptors. Finally, Pal and Das (2013) reported upregulation of SHANK1 mRNA and protein levels in cortex and midbrain following chronic morphine treatment.

In an initial effort to better understand the effects of *Shank1* deletion on the neurochemical architecture, we analyzed DA, NA, and 5-HT neurotransmitter concentrations together with their precursors and metabolites in relevant brain structures, namely prefrontal cortex, nucleus accumbens, and hypothalamus. In the prefrontal cortex, which plays a key role in maintaining inhibitory control over striatal mechanisms involved in the effects of drugs of abuse (Everitt and Robbins, 2016), basal DA levels tended to be affected by *Shank1* deletion, with lower DA concentrations in *Shank1*$^{-/-}$ mice. Moreover, the concentration of the DA metabolite DOPAC differed between genotypes and DOPAC levels were reduced in *Shank1*$^{-/-}$ mice. The DOPAC/DA ratio, however, was not affected. Concentrations of the DA precursor Tyr also did not differ between genotypes. Besides DA, basal NA concentrations in the prefrontal cortex were affected by *Shank1* deletion, with higher NA concentrations in *Shank1*$^{-/-}$ mice. There were no differences between genotypes in the concentrations of the NA metabolite MHPG, yet the MHPG/NA ratio differed between genotypes and was lower in *Shank1*$^{-/-}$ mice. Importantly, the decreased MHPG/NA ratio in *Shank1*$^{-/-}$ mice, which was paralleled by increases in NA concentrations in absence of changes in MHPG, might indicate decreased NA metabolism in *Shank1*$^{-/-}$ mice. Finally, *Shank1* deletion affected the level of the 5-HT precursor Trp in the prefrontal cortex, with *Shank1*$^{-/-}$ mice having higher Trp concentrations. However, basal 5-HT concentrations, the levels of the main 5-HT metabolite 5-HIAA, and the 5-HIAA/5-HT ratio did not differ between genotypes.

In the nucleus accumbens, a key brain structure strongly implicated in the rewarding actions of drugs of abuse (Everitt and Robbins, 2016), *Shank1* deletion affected the concentration of the DA precursor Tyr and the 5-HT precursor Trp, with the levels of both precursors being higher in *Shank1*$^{-/-}$ mice. Despite these genotype differences in the levels of the precursors, DA, NA, and 5-HT concentrations as well as their metabolites were not affected in this brain region.

In the hypothalamus, a brain region less heavily involved in the actions of drugs of abuse (Everitt and Robbins, 2016), no prominent genotype effects on the levels of the precursors Tyr and Trp were evident and DA, DOPAC as well as the DOPAC/DA ratio also did not differ between genotypes. However, while NA concentrations were not affected by *Shank1* deletion, MHPG levels were higher in the hypothalamus of *Shank1*$^{-/-}$ mice. Genotype-dependent differences in the MHPG/NA ratio were not evident. Finally, there were genotype-dependent differences in 5-HT concentrations in the hypothalamus, with *Shank1*$^{-/-}$ mice having higher concentrations. In conjunction, there was a trend for a similar genotype pattern in 5-HIAA concentrations. No genotype-dependent differences in the 5-HIAA/5-HT ratio were observed.

Together, this shows that *Shank1* deletion leads to alterations in the neurochemical architecture of the brain regions evaluated, with most prominent effects being evident in the prefrontal cortex. This is remarkable because SHANK1 expression is particularly high in cortex, but low in striatum and hypothalamus (Peça et al., 2011), suggesting local effects of *Shank1* deletion. It is tempting to speculate that the opposite alterations in DA and NA concentrations together with the decreased NA metabolism in the prefrontal cortex of *Shank1*$^{-/-}$ mice affect the fronto-striatal circuitry in mediating inhibitory control. Reduced prefrontal inhibitory control was strongly implicated in dominance of subcortically mediated responding to drugs of abuse (Everitt and Robbins, 2016). Of note, the increase of Trp in prefrontal cortex and nucleus accumbens is interesting because the essential amino acid Trp is not only the precursor of 5-HT, but also gives rise to melatonin and kynurenines, which have all been implicated, in one or the other way, in ASD, SCZ, and BPD (Morera-Fumero and Abreu-Gonzalez, 2013; Rossignol and Frye, 2014; Geoffroy et al., 2015; Lim et al., 2016; Erhardt et al., 2017).

To our knowledge, it is currently not known whether *Shank1* deletion affects the expression and/or function of the AMPH and MDMA targets, i.e., plasma membrane uptake carries for DA, NA, and 5-HT. Because reduced efficacy to stimulate hyperactivity in *Shank1*$^{-/-}$ mice is seen in response to both AMPH and MDMA, alterations in the NA transporter are not prime candidates driving the effects. Another candidate for the reduced efficacy of psychostimulants to stimulate hyperactivity in *Shank1*$^{-/-}$ mice is the DA transporter. Although reduced expression and/or function of the DA transporter could explain reduced efficacy of psychostimulants, this also appears unlikely to be the case. This is because DA transporter knockout mice display increased locomotor activity under drug free conditions (Giros et al., 1996; Gainetdinov et al., 1999; Powell et al., 2004), whereas *Shank1* deletion leads to mild hypoactivity (Hung et al., 2008; Silverman et al., 2011; Wöhr et al., 2011). Finally, the 5-HT transporter appears of relevance because MDMA-induced hyperactivity is abolished in mice lacking the 5-HT transporter (Bengel et al., 1998), yet this as well does not explain the full result pattern because AMPH-induced hyperactivity is not affected by deletion of the gene for the 5-HT transporter (Bengel et al., 1998). Of note, the time spent in the center was not affected by AMPH or MDMA treatment in a genotype-dependent manner and the reduction in center time seen following *Shank1* deletion might reflect a mild increase in anxiety levels and is consistent with the literature (Hung et al., 2008; Silverman et al., 2011). Together, this might thus indicate that postsynaptic receptors implicated

in psychostimulant-induced hyperactivity, such as D1 and D2 (Xu M. et al., 2000; Fan and Hess, 2007; Fan et al., 2010) as well as 5-HT1B (Scearce-Levie et al., 1999; Jean et al., 2012) and 5-HT2B (Doly et al., 2008; Doly et al., 2009) receptors, drive the effects of *Shank1* deletion. However, to our knowledge, there is no study on the expression of relevant receptors in mice lacking SHANK1 available. Future studies on the effects of *Shank1* deletion on DA, NA, and 5-HT transporters and receptors appear therefore warranted.

As master scaffolding proteins enriched in the PSD at excitatory glutamatergic synapses, SHANKs anchor glutamate receptors and link them to the actin cytoskeleton and postsynaptic signaling pathways (Ting et al., 2012; Sala et al., 2015). In the first study on the effects of *Shank1* deletion, Hung et al. (2008) focused on the forebrain and hippocampus and demonstrated that *Shank1* is important for regulating dendritic spine morphology and synaptic strength. Standard measures of synaptic plasticity, however, were unchanged, with intact hippocampal long-term potentiation. NMDA, AMPA, and metabotropic glutamate receptors were also not affected (Hung et al., 2008). AMPA and NMDA receptors appear to play a role in acquisition and reinstatement of conditioned place preference, as, for instance, induced by MDMA (García-Pardo et al., 2015; García-Pardo et al., 2018).

More recently, Sungur et al. (2017) studied the effects of *Shank1* deletion on protein expression levels of the brain-derived neurotrophic factor BDNF together with its epigenetic regulation. Partial genetic depletion of BDNF was repeatedly associated with stronger AMPH-induced hyperactivity and associated with increased striatal DA concentrations (Dluzen et al., 2001; Saylor and McGinty, 2008; Manning et al., 2016). Similar findings were obtained for MDMA (Mouri et al., 2017). Sungur et al. (2017) found that *Shank1* deletion has no effect on basal BDNF expression levels, yet in response to learning a memory task hippocampal BDNF expression was particularly enhanced in *Shank1*$^{-/-}$ mice. A subsequent investigation of the epigenetic regulation revealed enrichment of histone H3 acetylation at the *Bdnf* promoter1 in *Shank1*$^{-/-}$ mice. Because BDNF is an important regulator of gene expression stimulating D3 receptor expression (Guillin et al., 2001) and D3 receptor activation was reported to inhibit psychostimulant-induced hyperactivity (McNamara et al., 2006), altered BDNF expression and its epigenetic regulation might thus be associated with the reduced efficacy of psychostimulants to stimulate hyperactivity in *Shank1*$^{-/-}$ mice.

Finally, another relevant factor that possibly contributes to the reduced efficacy of psychostimulants in *Shank1*$^{-/-}$ mice might be parvalbumin (PV) expression. PV is a calcium-binding protein important for the maintenance of the excitation/inhibition balance in the brain (Hu et al., 2014), repeatedly associated with major neuropsychiatric disorders, including ASD, SCZ, and BPD (Marín, 2012). Acute AMPH treatment stimulates robust firing of striatal PV-positive GABAergic interneurons (Wiltschko et al., 2010). Moreover, AMPH was reported to induce expression of the activity-inducible transcription factor Fos in PV-positive GABAergic interneurons in the nucleus accumbens, together with phosphorylation of the methyl-DNA-binding protein MeCP2 at Ser421 (Deng et al., 2010), the latter being associated with SHANK1 protein expression (Du et al., 2016). Very recently, it was further shown that AMPH treatment in mice with silenced PV-positive GABAergic interneurons evoked stronger activation in both D1 and D2 receptor-expressing medium spiny neurons in the nucleus accumbens (Wang et al., 2018). Importantly, silencing PV-positive GABAergic interneurons in the nucleus accumbens selectively inhibited the expression of locomotor sensitization following repeated injections of AMPH and blocked AMPH-induced conditioned place preference without affecting AMPH-induced DA release and hyperactivity (Wang et al., 2018). This is relevant because SHANK1 protein is highly co-localized with PV-expressing fast-spiking inhibitory interneurons (Mao et al., 2015) and *Shank1* deletion was shown to result in reduced PV expression (Filice et al., 2016). It would thus be interesting to test whether psychostimulant-induced hyperactivity is altered in PV-deficient mice, which display behavioral phenotypes with relevance to ASD (Wöhr et al., 2015). Specifically, Filice et al. (2016) found that the reduction of PV-immunoreactive neurons caused by *Shank1* deletion was due to a reduction in *Pvalb* mRNA and PV protein, without any indication for PV-expressing GABAergic interneuron loss. Importantly, PV protein expression levels were selectively decreased in those brain regions normally expressing high levels of SHANK1, such as the somatosensory cortex. However, no evidence for effects of *Shank1* deletion was obtained in the striatum, a region with low SHANK1 expression levels in *Shank1*$^{+/+}$ mice, similar to the local effects on neurochemical architecture in the present study.

CONCLUSION

Shank1$^{-/-}$ mice display reduced psychostimulant-induced hyperactivity, although psychostimulants robustly stimulated locomotor activity in littermate controls. *Shank1* deletion effects emerged throughout development, were particularly prominent in adulthood, and seen in response to both psychostimulants, i.e., AMPH and MDMA. Specifically, while AMPH-induced hyperactivity was reduced but still detectable in *Shank1*$^{-/-}$ mice, MDMA-induced hyperactivity was robustly blocked and completely absent in *Shank1*$^{-/-}$ mice. Reduced efficacy of psychostimulants to stimulate hyperactivity in *Shank1*$^{-/-}$ mice might be associated with alterations in the neurochemical architecture in prefrontal cortex, nucleus accumbens, and hypothalamus. Our observation that psychostimulant-induced hyperactivity is reduced rather than enhanced in *Shank1*$^{-/-}$ mice clearly speaks against a behavioral phenotype with relevance to BPD. Lack of BPD-like phenotype is consistent with currently available human data linking mutations in *SHANK2* and *SHANK3* but not *SHANK1* to BPD.

AUTHOR CONTRIBUTIONS

AS, TR, EA, and WD performed the experiments and/or data analysis. AS, RS, AdR, and MW wrote the manuscript. AS, AdR, and MW designed the study and supervised the project.

MW acquired funding. All authors were involved in data interpretation.

FUNDING

This work was supported by a grant from the Deutsche Forschungsgemeinschaft to MW (DFG; WO 1732/1-1).

ACKNOWLEDGMENTS

The authors wish to thank Jacqueline Crawley, University of California Davis School of Medicine, and the Howard Hughes Medical Institute investigators Albert Hung and Morgan Sheng for providing the *Shank1* mouse line. The authors also wish to thank Dr. J. Wildmann, Philipps-University of Marburg, for his help in this project.

SUPPLEMENTARY MATERIAL

The Supplementary Material for this article can be found online at: https://www.frontiersin.org/articles/10.3389/fnmol.2018.00419/full#supplementary-material

FIGURE S1 | Time spent in the center in juvenile *Shank1* mice treated with AMPH. **(A–C)** Bar graphs depicting the time spent in the center by *Shank1*$^{+/+}$ (black bar), *Shank1*$^{+/-}$ (striped bar), and *Shank1*$^{-/-}$ (white bar). Center time was compared during baseline testing **(A)**, following saline administration **(B)**, and after AMPH treatment **(C)**. Data are presented as means + SEM. *$p < 0.05$, **$p < 0.001$.

FIGURE S2 | AMPH-induced rearing behavior in adult *Shank1* mice. **(A–C)** Bar graphs and **(A′–C′)** line graphs depicting the rearing behavior by *Shank1*$^{+/+}$ (black bar/black circle), *Shank1*$^{+/-}$ (striped bar/white circle), and *Shank1*$^{-/-}$ (white bar/black triangle). Rearing behavior was compared during baseline testing **(A,A′)**, following saline administration **(B,B′)**, and after AMPH treatment **(C,C′)**. Data are presented as means + SEM or means ± SEM. **$p < 0.001$.

FIGURE S3 | Time spent in the center in adult *Shank1* mice treated with AMPH. **(A–C)** Bar graphs depicting the time spent in the center by *Shank1*$^{+/+}$ (black bar), *Shank1*$^{+/-}$ (striped bar), and *Shank1*$^{-/-}$ (white bar). Center time was compared during baseline testing **(A)**, following saline administration **(B)**, and after AMPH treatment **(C)**. Data are presented as means + SEM. *$p < 0.05$.

FIGURE S4 | Time spent in the center in adult *Shank1* mice treated with MDMA. **(A–C)** Bar graphs depicting the time spent in the center by *Shank1*$^{+/+}$ (black bar), *Shank1*$^{+/-}$ (striped bar), and *Shank1*$^{-/-}$ (white bar). Center time was compared during baseline testing **(A)**, following saline administration **(B)**, and after MDMA treatment **(C)**. Data are presented as means + SEM. *$p < 0.05$.

FIGURE S5 | MDMA-induced repetitive and stereotyped circling behavior in adult *Shank1* mice treated with MDMA. **(A)** Bar graph depicting the circling behavior displayed by all genotypes following saline administration (blue bar) and after MDMA treatment (orange bar). **(A′)** Line graph depicting the circling behavior displayed by *Shank1*$^{+/+}$ (black circle), *Shank1*$^{+/-}$ (white circle), and *Shank1*$^{-/-}$ (black triangle) over two consecutive test days, i.e., following saline administration (blue are) and after MDMA treatment (orange area). Data are presented as means + SEM or means ± SEM. $^{\#\#}p < 0.001$ **(A)**, $^{\#}p < 0.05$ and $^{\#\#}p < 0.001$ vs. day 2 **(A′)**.

REFERENCES

Azdad, K., Gall, D., Woods, A. S., Ledent, C., Ferré, S., and Schiffmann, S. N. (2009). Dopamine D2 and adenosine A2A receptors regulate NMDA-mediated excitation in accumbens neurons through A2A-D2 receptor heteromerization. *Neuropsychopharmacology* 34, 972–986. doi: 10.1038/npp.2008.144

Bengel, D., Murphy, D. L., Andrews, A. M., Wichems, C. H., Feltner, D., Heils, A., et al. (1998). Altered brain serotonin homeostasis and locomotor insensitivity to 3, 4-methylenedioxymethamphetamine ("Ecstasy") in serotonin transporter-deficient mice. *Mol. Pharmacol.* 53, 649–655. doi: 10.1124/mol.53.4.649

Benturquia, N., Courtin, C., Noble, F., and Marie-Claire, C. (2008). Involvement of D1 dopamine receptor in MDMA-induced locomotor activity and striatal gene expression in mice. *Brain Res.* 1211, 1–5. doi: 10.1016/j.brainres.2008.03.016

Berggren, U., Tallstedt, L., Ahlenius, S., and Engel, J. (1978). The effect of lithium on amphetamine-induced locomotor stimulation. *Psychopharmacology* 59, 41–45. doi: 10.1007/BF00428028

Berkel, S., Marshall, C. R., Weiss, B., Howe, J., Roeth, R., Moog, U., et al. (2010). Mutations in the SHANK2 synaptic scaffolding gene in autism spectrum disorder and mental retardation. *Nat. Genet.* 42, 489–491. doi: 10.1038/ng.589

Bourgeron, T. (2015). From the genetic architecture to synaptic plasticity in autism spectrum disorder. *Nat. Rev. Neurosci.* 16, 551–563. doi: 10.1038/nrn3992

Bronsert, M. R., Mead, A. N., Hen, R., and Rocha, B. A. (2001). Amphetamine-induced locomotor activation in 5-HT(1B) knockout mice: effects of injection route on acute and sensitized responses. *Behav. Pharmacol.* 12, 549–555. doi: 10.1097/00008877-200111000-00017

Buonaguro, E. F., Iasevoli, F., Marmo, F., Eramo, A., Latte, G., Avagliano, C., et al. (2017). Re-arrangements of gene transcripts at glutamatergic synapses after prolonged treatments with antipsychotics: a putative link with synaptic remodeling. *Prog. Neuropsychopharmacol. Biol. Psychiatry* 76, 29–41. doi: 10.1016/j.pnpbp.2017.02.012

Carlsson, M. L., Martin, P., Nilsson, M., Sorensen, S. M., Carlsson, A., Waters, S., et al. (1999). The 5-HT2A receptor antagonist M100907 is more effective in counteracting NMDA antagonist- than dopamine agonist-induced hyperactivity in mice. *J. Neural Transm.* 106, 123–129. doi: 10.1007/s007020050144

Conductier, G., Crosson, C., Hen, R., Bockaert, J., and Compan, V. (2005). 3,4-N-methlenedioxymethamphetamine-induced hypophagia is maintained in 5-HT1B receptor knockout mice, but suppressed by the 5-HT2C receptor antagonist RS102221. *Neuropsychopharmacology* 30, 1056–1063. doi: 10.1038/sj.npp.1300662

Crespi, D., Mennini, T., and Gobbi, M. (1997). Carrier-dependent and Ca^{2+}-dependent 5-HT and dopamine release induced by (+)-amphetamine, 3,4-methylendioxymethamphetamine, p-chloroamphetamine and (+)-fenfluramine. *Br. J. Pharmacol.* 121, 1735–1743. doi: 10.1038/sj.bjp.0701325

de la Torre-Ubieta, L., Won, H., Stein, J. L., and Geschwind, D. H. (2016). Advancing the understanding of autism disease mechanisms through genetics. *Nat. Med.* 22, 345–361. doi: 10.1038/nm.4071

Denayer, A., van Esch, H., de Ravel, T., Frijns, J. P., van Buggenhout, G., Vogels, A., et al. (2012). Neuropsychopathology in 7 patients with the 22q13 deletion syndrome: presence of bipolar disorder and progressive loss of skills. *Mol. Syndromol.* 3, 14–20. doi: 10.1159/000339119

Deng, J. V., Rodriguiz, R. M., Hutchinson, A. N., Kim, I. H., Wetsel, W. C., and West, A. E. (2010). MeCP2 in the nucleus accumbens contributes to neural and behavioral responses to psychostimulants. *Nat. Neurosci.* 13, 1128–1136. doi: 10.1038/nn.2614

Dluzen, D. E., Gao, X., Story, G. M., Anderson, L. I., Kucera, J., and Walro, J. M. (2001). Evaluation of nigrostriatal dopaminergic function in adult +/+ and +/- BDNF mutant mice. *Exp. Neurol.* 170, 121–128. doi: 10.1006/exnr.2001.7698

Doly, S., Bertran-Gonzalez, J., Callebert, J., Bruneau, A., Banas, S. M., Belmer, A., et al. (2009). Role of serotonin via 5-HT2B receptors in the reinforcing effects of MDMA in mice. *PLoS One* 4:e7952. doi: 10.1371/journal.pone.0007952

Doly, S., Valjent, E., Setola, V., Callebert, J., Hervé, D., Launay, J. M., et al. (2008). Serotonin 5-HT2B receptors are required for 3,4-methylenedioxymethamphetamine-induced hyperlocomotion and

5-HT release in vivo and in vitro. *J. Neurosci.* 28, 2933–2940. doi: 10.1523/JNEUROSCI.5723-07.2008

Du, F., Nguyen, M. V., Karten, A., Felice, C. A., Mandel, G., and Ballas, N. (2016). Acute and crucial requirement for MeCP2 function upon transition from early to late adult stages of brain maturation. *Hum. Mol. Genet.* 25, 1690–1702. doi: 10.1093/hmg/ddw038

Durand, C. M., Betancur, C., Boeckers, T. M., Bockmann, J., Chaste, P., Fauchereau, F., et al. (2007). Mutations in the gene encoding the synaptic scaffolding protein SHANK3 are associated with autism spectrum disorders. *Nat. Genet.* 39, 25–27. doi: 10.1038/ng1933

Erhardt, S., Schwieler, L., Imbeault, S., and Engberg, G. (2017). The kynurenine pathway in schizophrenia and bipolar disorder. *Neuropharmacology* 112, 297–306. doi: 10.1016/j.neuropharm.2016.05.020

Everitt, B. J., and Robbins, T. W. (2016). Drug addiction: updating actions to habits to compulsions ten years on. *Annu. Rev. Psychol.* 67, 23–50. doi: 10.1146/annurev-psych-122414-033457

Ey, E., Torquet, T., de Chaumont, F., Lévi-Strauss, J., Ferhat, A. T., Le Sourd, A. M., et al. (2018). SHANK2 mutant mice display hyperactivity insensitive to methylphenidate and reduced flexibility in social motivation, but normal social recognition. *Front. Mol. Neurosci.* 11:365. doi: 10.3389/fnmol.2018.00365

Fan, X., and Hess, E. J. (2007). D2-like dopamine receptors mediate the response to amphetamine in a mouse model of ADHD. *Neurobiol. Dis.* 26, 201–211. doi: 10.1016/j.nbd.2006.12.011

Fan, X., Xu, M., and Hess, E. J. (2010). D2 dopamine receptor subtype-mediated hyperactivity and amphetamine responses in a model of ADHD. *Neurobiol. Dis.* 37, 228–236. doi: 10.1016/j.nbd.2009.10.009

Fantegrossi, W. E., Godlewski, T., Karabenick, R. L., Stephens, J. M., Ullrich, T., Rice, K. C., et al. (2003). Pharmacological characterization of the effects of 3,4-methylenedioxymethamphetamine ("ecstasy") and its enantiomers on lethality, core temperature, and locomotor activity in singly housed and crowded mice. *Psychopharmacology* 166, 202–211. doi: 10.1007/s00213-002-1261-5

Filice, F., Vörckel, K. J., Sungur, A. Ö., Wöhr, M., and Schwaller, B. (2016). Reduction in parvalbumin expression not loss of the parvalbumin-expressing GABA interneuron subpopulation in genetic parvalbumin and shank mouse models of autism. *Mol. Brain* 9:e10. doi: 10.1186/s13041-016-0192-8

Fromer, M., Pocklington, A. J., Kavanagh, D. H., Williams, H. J., Dwyer, S., Gormley, P., et al. (2014). De novo mutations in schizophrenia implicate synaptic networks. *Nature* 506, 179–184. doi: 10.1038/nature12929

Gainetdinov, R. R., Wetsel, W. C., Jones, S. R., Levin, E. D., Jaber, M., and Caron, M. G. (1999). Role of serotonin in the paradoxical calming effect of psychostimulants on hyperactivity. *Science* 283, 397–401. doi: 10.1126/science.283.5400.397

García-Pardo, M. P., Escobar-Valero, C., Rodríguez-Arias, M., Miñarro, J., and Aguilar, M. A. (2015). Involvement of NMDA glutamate receptors in the acquisition and reinstatement of the conditioned place preference induced by MDMA. *Behav. Pharmacol.* 26, 411–417. doi: 10.1097/FBP.0000000000000138

García-Pardo, M. P., Miñarro, J., and Aguilar, M. A. (2018). Role of AMPA glutamate receptors in the conditioned rewarding effects of MDMA in mice. *Behav. Brain Res.* 347, 57–60. doi: 10.1016/j.bbr.2018.03.010

Gauthier, J., Champagne, N., Lafrenière, R. G., Xiong, L., Spiegelman, D., Brustein, E., et al. (2010). De novo mutations in the gene encoding the synaptic scaffolding protein SHANK3 in patients ascertained for schizophrenia. *Proc. Natl. Acad. Sci. U.S.A.* 107, 7863–7868. doi: 10.1073/pnas.0906232107

Gauthier, J., Spiegelman, D., Piton, A., Lafrenière, R. G., Laurent, S., St-Onge, J., et al. (2009). Novel de novo SHANK3 mutation in autistic patients. *Am. J. Med. Genet. Part B Neuropsychiatr. Genet.* 150B, 421–424. doi: 10.1002/ajmg.b.30822

Geoffroy, P. A., Etain, B., Franchi, J. A., Bellivier, F., and Ritter, P. (2015). Melatonin and melatonin agonists as adjunctive treatments in bipolar disorders. *Curr. Pharm. Des.* 21, 3352–3358. doi: 10.2174/1381612821666150619093448

Geschwind, D. H., and Flint, J. (2015). Genetics and genomics of psychiatric disease. *Science* 349, 1489–1494. doi: 10.1126/science.aaa8954

Giros, B., Jaber, M., Jones, S. R., Wightman, R. M., and Caron, M. G. (1996). Hyperlocomotion and indifference to cocaine and amphetamine in mice lacking the dopamine transporter. *Nature* 379, 606–612. doi: 10.1038/379606a0

Gould, T. J., Keith, R. A., and Bhat, R. V. (2001). Differential sensitivity to lithium's reversal of amphetamine-induced open-field activity in two inbred strains of mice. *Behav. Brain Res.* 118, 95–105. doi: 10.1016/S0166-4328(00)00318-1

Guillin, O., Diaz, J., Carroll, P., Griffon, N., Schwartz, J. C., and Sokoloff, P. (2001). BDNF controls dopamine D3 receptor expression and triggers behavioural sensitization. *Nature* 411, 86–89. doi: 10.1038/35075076

Guilmatre, A., Huguet, G., Delorme, R., and Bourgeron, T. (2014). The emerging role of SHANK genes in neuropsychiatric disorders. *Dev. Neurobiol.* 74, 113–122. doi: 10.1002/dneu.22128

Han, K., Holder, J. L. Jr., Schaaf, C. P., Lu, H., Chen, H., Kang, H., et al. (2013). SHANK3 overexpression causes manic-like behaviour with unique pharmacogenetic properties. *Nature* 503, 72–77. doi: 10.1038/nature12630

Hasler, G., Drevets, W. C., Gould, T. D., Gottesman, I. I., and Manji, H. K. (2006). Toward constructing an endophenotype strategy for bipolar disorders. *Biol. Psychiatry* 60, 93–105. doi: 10.1016/j.biopsych.2005.11.006

Homann, O. R., Misura, K., Lamas, E., Sandrock, R. W., Nelson, P., McDonough, S. I., et al. (2016). Whole-genome sequencing in multiplex families with psychoses reveals mutations in the SHANK2 and SMARCA1 genes segregating with illness. *Mol. Psychiatry* 21, 1690–1695. doi: 10.1038/mp.2016.24

Hu, H., Gan, J., and Jonas, P. (2014). Interneurons. Fast-spiking, parvalbumin^{+} GABAergic interneurons: from cellular design to microcircuit function. *Science* 345:1255263. doi: 10.1126/science.1255263

Hung, A. Y., Futai, K., Sala, C., Valtschanoff, J. G., Ryu, J., Woodworth, M. A., et al. (2008). Smaller dendritic spines, weaker synaptic transmission, but enhanced spatial learning in mice lacking SHANK1. *J. Neurosci.* 28, 1697–1708. doi: 10.1523/JNEUROSCI.3032-07.2008

Hutson, P. H., Tarazi, F. I., Madhoo, M., Slawecki, C., and Patkar, A. A. (2014). Preclinical pharmacology of amphetamine: implications for the treatment of neuropsychiatric disorders. *Pharmacol. Ther.* 143, 253–264. doi: 10.1016/j.pharmthera.2014.03.005

Jean, A., Laurent, L., Bockaert, J., Charnay, Y., Dusticier, N., Nieoullon, A., et al. (2012). The nucleus accumbens 5-HT$_4$-CART pathway ties anorexia to hyperactivity. *Transl. Psychiatry* 2:e203. doi: 10.1038/tp.2012.131

Jiang, Y., and Ehlers, M. D. (2013). Modeling autism by SHANK gene mutations in mice. *Neuron* 78, 8–27. doi: 10.1016/j.neuron.2013.03.016

Kato, T., Kubota, M., and Kasahara, T. (2007). Animal models of bipolar disorder. *Neurosci. Biobehav. Rev.* 31, 832–842. doi: 10.1016/j.neubiorev.2007.03.003

Lennertz, L., Wagner, M., Wölwer, W., Schuhmacher, A., Frommann, I., Berning, J., et al. (2012). A promoter variant of SHANK1 affects auditory working memory in schizophrenia patients and in subjects clinically at risk for psychosis. *Eur. Arch. Psychiatry Clin. Neurosci.* 262, 117–124. doi: 10.1007/s00406-011-0233-3

Li, Y., Abdourahman, A., Tamm, J. A., Pehrson, A. L., Sánchez, C., and Gulinello, M. (2015). Reversal of age-associated cognitive deficits is accompanied by increased plasticity-related gene expression after chronic antidepressant administration in middle-aged mice. *Pharmacol. Biochem. Behav.* 135, 70–82. doi: 10.1016/j.pbb.2015.05.013

Lim, C. K., Essa, M. M., de Paula Martins, R., Lovejoy, D. B., Bilgin, A. A., Waly, M. I., et al. (2016). Altered kynurenine pathway metabolism in autism: implication for immune-induced glutamatergic activity. *Autism Res.* 9, 621–631. doi: 10.1002/aur.1565

Manning, E. E., Halberstadt, A. L., and van den Buuse, M. (2016). BDNF-deficient mice show reduced psychosis-related behaviors following chronic methamphetamine. *Int. J. Neuropsychopharmacol.* 19:yv116. doi: 10.1093/ijnp/pyv116

Mao, W., Watanabe, T., Cho, S., Frost, J. L., Truong, T., Zhao, X., et al. (2015). SHANK1 regulates excitatory synaptic transmission in mouse hippocampal parvalbumin-expressing inhibitory interneurons. *Eur. J. Neurosci.* 41, 1025–1035. doi: 10.1111/ejn.12877

Marín, O. (2012). Interneuron dysfunction in psychiatric disorders. *Nat. Rev. Neurosci.* 13, 107–120. doi: 10.1038/nrn3155

Marquis, K. L., Sabb, A. L., Logue, S. F., Brennan, J. A., Piesla, M. J., Comery, T. A., et al. (2007). WAY-163909 [(7bR,10aR)-1,2,3,4,8,9,10,10a-octahydro-7bH-cyclopenta-[b][1,4]diazepino [6,7,1hi]indole]: a novel 5-hydroxytryptamine 2C receptor-selective agonist with preclinical antipsychotic-like activity. *J. Pharmacol. Exp. Ther.* 320, 486–496. doi: 10.1124/jpet.106.106989

McNamara, R. K., Logue, A., Stanford, K., Xu, M., Zhang, J., and Richtand, N. M. (2006). Dose-response analysis of locomotor activity and stereotypy in dopamine D3 receptor mutant mice following acute amphetamine. *Synapse* 60, 399–405. doi: 10.1002/syn.20315

Meyendorff, E., Lerer, B., Moore, N. C., Bow, J., and Gershon, S. (1985). Methylphenidate infusion in euthymic bipolars: effect of carbamazepine pretreatment. *Psychiatry Res.* 16, 303–308. doi: 10.1016/0165-1781(85)90121-0

Moessner, R., Marshall, C. R., Sutcliffe, J. S., Skaug, J., Pinto, D., Vincent, J., et al. (2007). Contribution of SHANK3 mutations to autism spectrum disorder. *Am. J. Hum. Genet.* 81, 1289–1297. doi: 10.1086/522590

Morera-Fumero, A. L., and Abreu-Gonzalez, P. (2013). Role of melatonin in schizophrenia. *Int. J. Mol. Sci.* 14, 9037–9050. doi: 10.3390/ijms14059037

Mouri, A., Noda, Y., Niwa, M., Matsumoto, Y., Mamiya, T., Nitta, A., et al. (2017). The involvement of brain-derived neurotrophic factor in 3,4-methylenedioxymethamphetamine-induced place preference and behavioral sensitization. *Behav. Brain Res.* 329, 157–165. doi: 10.1016/j.bbr.2017.04.052

Müller, C. P., and Homberg, J. R. (2015). The role of serotonin in drug use and addiction. *Behav. Brain Res.* 277, 146–192. doi: 10.1016/j.bbr.2014.04.007

Natusch, C., and Schwarting, R. K. W. (2010). Using bedding in a test environment critically affects 50-kHz ultrasonic vocalizations in laboratory rats. *Pharmacol. Biochem. Behav.* 96, 251–259. doi: 10.1016/j.pbb.2010.05.013

Noor, A., Lionel, A. C., Cohen-Woods, S., Moghimi, N., Rucker, J., Fennell, A., et al. (2014). Copy number variant study of bipolar disorder in Canadian and UK populations implicates synaptic genes. *Am. J. Med. Genet. B Neuropsychiatr. Genet.* 165B, 303–313. doi: 10.1002/ajmg.b.32232

O'Donovan, M. C., and Owen, M. J. (2016). The implications of the shared genetics of psychiatric disorders. *Nat. Med.* 22, 1214–1219. doi: 10.1038/nm.4196

O'Neill, M. F., Heron-Maxwell, C. L., and Shaw, G. (1999). 5-HT2 receptor antagonism reduces hyperactivity induced by amphetamine, cocaine, and MK-801 but not D1 agonist C-APB. *Pharmacol. Biochem. Behav.* 63, 237–243. doi: 10.1016/S0091-3057(98)00240-8

Orejarena, M. J., Lanfumey, L., Maldonado, R., and Robledo, P. (2011). Involvement of 5-HT2A receptors in MDMA reinforcement and cue-induced reinstatement of MDMA-seeking behaviour. *Int. J. Neuropsychopharmacol.* 14, 927–940. doi: 10.1017/S1461145710001215

Pal, A., and Das, S. (2013). Chronic morphine exposure and its abstinence alters dendritic spine morphology and upregulates SHANK1. *Neurochem. Int.* 62, 956–964. doi: 10.1016/j.neuint.2013.03.011

Pappas, A. L., Bey, A. L., Wang, X., Rossi, M., Kim, Y. H., Yan, H., et al. (2017). Deficiency of SHANK2 causes mania-like behavior that responds to mood stabilizers. *JCI Insight* doi: 10.1172/jci.insight.92052 [Epub ahead of print].

Paxinos, G., and Franklin, K. B. J. (2001). *The Mouse Brain in Stereotaxic Coordinates*, 2nd Edn. San Diego, CA: Academic Press.

Peça, J., Feliciano, C., Ting, J. T., Wang, W., Wells, M. F., Venkatraman, T. N., et al. (2011). SHANK3 mutant mice display autistic-like behaviours and striatal dysfunction. *Nature* 472, 437–442. doi: 10.1038/nature09965

Peet, M., and Peters, S. (1995). Drug-induced mania. *Drug Saf.* 12, 146–153. doi: 10.2165/00002018-199512020-00007

Pereira, M., Andreatini, R., Schwarting, R. K. W., and Brenes, J. C. (2014). Amphetamine-induced appetitive 50-kHz calls in rats: a marker of affect in mania? *Psychopharmacology* 231, 2567–2577. doi: 10.1007/s00213-013-3413-1

Peykov, S., Berkel, S., Schoen, M., Weiss, K., Degenhardt, F., Strohmaier, J., et al. (2015). Identification and functional characterization of rare SHANK2 variants in schizophrenia. *Mol. Psychiatry* 20, 1489–1498. doi: 10.1038/mp.2014.172

Pinto, D., Pagnamenta, A. T., Klei, L., Anney, R., Merico, D., Regan, R., et al. (2010). Functional impact of global rare copy number variation in autism spectrum disorders. *Nature* 466, 368–372. doi: 10.1038/nature09146

Powell, S. B., Lehmann-Masten, V. D., Paulus, M. P., Gainetdinov, R. R., Caron, M. G., and Geyer, M. A. (2004). MDMA "ecstasy" alters hyperactive and perseverative behaviors in dopamine transporter knockout mice. *Psychopharmacology* 173, 310–317. doi: 10.1007/s00213-003-1765-7

Przegalinski, E., Siwanowicz, J., Baran, L., and Filip, M. (2000). Activation of serotonin (5-HT)1A receptors inhibits amphetamine sensitization in mice. *Life Sci.* 66, 1011–1019. doi: 10.1016/S0024-3205(99)00666-9

Przegalinski, E., Siwanowicz, J., Nowak, E., Papla, I., and Filip, M. (2001). Role of 5-HT(1B) receptors in the sensitization to amphetamine in mice. *Eur. J. Pharmacol.* 422, 91–99. doi: 10.1016/S0014-2999(01)01079-2

Pum, M., Carey, R. J., Huston, J. P., and Müller, C. P. (2007). Dissociating effects of cocaine and d-amphetamine on dopamine and serotonin in the perirhinal, entorhinal, and prefrontal cortex of freely moving rats. *Psychopharmacology* 193, 375–390. doi: 10.1007/s00213-007-0791-2

Risbrough, V. B., Masten, V. L., Caldwell, S., Paulus, M. P., Low, M. J., and Geyer, M. A. (2006). Differential contributions of dopamine D1, D2, and D3 receptors to MDMA-induced effects on locomotor behavior patterns in mice. *Neuropsychopharmacology* 31, 2349–2358. doi: 10.1038/sj.npp.1301161

Roggero, E., Pérez, A. R., Pollachini, N., Villar, S. R., Wildmann, J., Besedovsky, H., et al. (2016). The sympathetic nervous system affects the susceptibility and course of *Trypanosoma cruzi* infection. *Brain Behav. Immun.* 58, 228–236. doi: 10.1016/j.bbi.2016.07.163

Rossignol, D. A., and Frye, R. E. (2014). Melatonin in autism spectrum disorders. *Curr. Clin. Pharmacol.* 9, 326–334. doi: 10.2174/1574884711308660072

Sala, C., Vicidomini, C., Bigi, I., Mossa, A., and Verpelli, C. (2015). Shank synaptic scaffold proteins: keys to understanding the pathogenesis of autism and other synaptic disorders. *J. Neurochem.* 135, 849–858. doi: 10.1111/jnc.13232

Salahpour, A., Ramsey, A. J., Medvedev, I. O., Kile, B., Sotnikova, T. D., Holmstrand, E., et al. (2008). Increased amphetamine-induced hyperactivity and reward in mice overexpressing the dopamine transporter. *Proc. Natl. Acad. Sci. U.S.A.* 105, 4405–4410. doi: 10.1073/pnas.0707646105

Salomon, L., Lanteri, C., Godeheu, G., Blanc, G., Gingrich, J., and Tassin, J. P. (2007). Paradoxical constitutive behavioral sensitization to amphetamine in mice lacking 5-HT2A receptors. *Psychopharmacology* 194, 11–20. doi: 10.1007/s00213-007-0810-3

Sato, D., Lionel, A. C., Leblond, C. S., Prasad, A., Pinto, D., Walker, S., et al. (2012). SHANK1 deletions in males with autism spectrum disorder. *Am. J. Hum. Genet.* 90, 879–887. doi: 10.1016/j.ajhg.2012.03.017

Saylor, A. J., and McGinty, J. F. (2008). Amphetamine-induced locomotion and gene expression are altered in BDNF heterozygous mice. *Genes Brain Behav.* 7, 906–914. doi: 10.1111/j.1601-183X.2008.00430.x

Scearce-Levie, K., Viswanathan, S. S., and Hen, R. (1999). Locomotor response to MDMA is attenuated in knockout mice lacking the 5-HT1B receptor. *Psychopharmacology* 141, 154–161. doi: 10.1007/s002130050819

Schmeisser, M. J., Ey, E., Wegener, S., Bockmann, J., Stempel, A. V., Kuebler, A., et al. (2012). Autistic-like behaviours and hyperactivity in mice lacking ProSAP1/SHANK2. *Nature* 486, 256–260. doi: 10.1038/nature11015

Schmeisser, M. J., and Verpelli, C. (2016). "SHANK mutations in intellectual disability and autism spectrum disorder," in *Neuronal and Synaptic Dysfunction in Autism Spectrum Disorder and Intellectual Disability*, eds C. Sala and C. Verpelli (Cambridge, MA: Academic Press), 151–160. doi: 10.1016/B978-0-12-800109-7.00010-8

Silverman, J. L., Turner, S. M., Barkan, C. L., Tolu, S. S., Saxena, R., Hung, A. Y., et al. (2011). Sociability and motor functions in SHANK1 mutant mice. *Brain Res.* 1380, 120–137. doi: 10.1016/j.brainres.2010.09.026

Silverman, J. L., Yang, M., Lord, C., and Crawley, J. N. (2010). Behavioural phenotyping assays for mouse models of autism. *Nat. Rev. Neurosci.* 11, 490–502. doi: 10.1016/j.brainres.2010.09.026

Sorensen, S. M., Kehne, J. H., Fadayel, G. M., Humphreys, T. M., Ketteler, H. J., Sullivan, C. K., et al. (1993). Characterization of the 5-HT2 receptor antagonist MDL 100907 as a putative atypical antipsychotic: behavioral, electrophysiological and neurochemical studies. *J. Pharmacol. Exp. Ther.* 266, 684–691.

Sovner, R., Stone, A., and Fox, C. (1996). Ring chromosome 22 and mood disorders. *J. Intellect. Disabil. Res.* 40, 82–86. doi: 10.1111/j.1365-2788.1996.tb00607.x

Steele, T. D., Nichols, D. E., and Yim, G. K. (1987). Stereochemical effects of 3,4-methylenedioxymethamphetamine (MDMA) and related amphetamine derivatives on inhibition of uptake of [3H]monoamines into synaptosomes from different regions of rat brain. *Biochem. Pharmacol.* 36, 2297–2303. doi: 10.1016/0006-2952(87)90594-6

Sulzer, D., Sonders, M. S., Poulsen, N. W., and Galli, A. (2005). Mechanisms of neurotransmitter release by amphetamines: a review. *Prog. Neurobiol.* 75, 406–433. doi: 10.1016/j.pneurobio.2005.04.003

Sungur, A. Ö., Jochner, M. C. E., Harb, H., Kılıç, A., Garn, H., Schwarting, R. K. W., et al. (2017). Aberrant cognitive phenotypes and altered hippocampal BDNF expression related to epigenetic modifications in mice lacking the post-synaptic scaffolding protein SHANK1: implications for autism spectrum disorder. *Hippocampus* 27, 906–919. doi: 10.1002/hipo.22741

Sungur, A. Ö., Schwarting, R. K. W., and Wöhr, M. (2016). Early communication deficits in the SHANK1 knockout mouse model for autism spectrum disorder: developmental aspects and effects of social context. *Autism Res.* 9, 696–709. doi: 10.1002/aur.1564

Sungur, A. Ö., Schwarting, R. K. W., and Wöhr, M. (2018). Behavioral phenotypes and neurobiological mechanisms in the SHANK1 mouse model for autism spectrum disorder: a translational perspective. *Behav. Brain Res.* 352, 46–61. doi: 10.1016/j.bbr.2017.09.038

Sungur, A. Ö., Vörckel, K. J., Schwarting, R. K. W., and Wöhr, M. (2014). Repetitive behaviors in the SHANK1 knockout mouse model for autism spectrum disorder: developmental aspects and effects of social context. *J. Neurosci. Methods* 234, 92–100. doi: 10.1016/j.jneumeth.2014.05.003

Ting, J. T., Peça, J., and Feng, G. (2012). Functional consequences of mutations in postsynaptic scaffolding proteins and relevance to psychiatric disorders. *Annu. Rev. Neurosci.* 35, 49–71. doi: 10.1146/annurev-neuro-062111-150442

van den Buuse, M., Ruimschotel, E., Martin, S., Risbrough, V. B., and Halberstadt, A. L. (2011). Enhanced effects of amphetamine but reduced effects of the hallucinogen, 5-MeO-DMT, on locomotor activity in 5-HT(1A) receptor knockout mice: implications for schizophrenia. *Neuropharmacology* 61, 209–216. doi: 10.1016/j.neuropharm.2011.04.001

Verhoeven, W. M., Egger, J. I., Willemsen, M. H., de Leijer, G. J., and Kleefstra, T. (2012). Phelan-McDermid syndrome in two adult brothers: atypical bipolar disorder as its psychopathological phenotype? *Neuropsychiatr. Dis. Treat.* 8, 175–179. doi: 10.2147/NDT.S30506

Verhoeven, W. M. A., Egger, J. I. M., Cohen-Snuijf, R., Kant, S. G., and de Leeuw, N. (2013). Phelan-McDermid syndrome: clinical report of a 70-year-old woman. *Am. J. Med. Genet. A* 161, 158–161. doi: 10.1002/ajmg.a.35597

Vucurovic, K., Landais, E., Delahaigue, C., Eutrope, J., Schneider, A., Leroy, C., et al. (2012). Bipolar affective disorder and early dementia onset in a male patient with SHANK3 deletion. *Eur. J. Med. Genet.* 55, 625–629. doi: 10.1016/j.ejmg.2012.07.009

Wang, X., Gallegos, D. A., Pogorelov, V. M., O'Hare, J. K., Calakos, N., Wetsel, W. C., et al. (2018). Parvalbumin interneurons of the mouse nucleus accumbens are required for amphetamine-induced locomotor sensitization and conditioned place preference. *Neuropsychopharmacology* 43, 953–963. doi: 10.1038/npp.2017.178

Wang, X., McCoy, P. A., Rodriguiz, R. M., Pan, Y., Je, H. S., Roberts, A. C., et al. (2011). Synaptic dysfunction and abnormal behaviors in mice lacking major isoforms of SHANK3. *Hum. Mol. Genet.* 20, 3093–3108. doi: 10.1093/hmg/ddr212

White, S. R., Duffy, P., and Kalivas, P. W. (1994). Methylenedioxymethamphetamine depresses glutamate-evoked neuronal firing and increases extracellular levels of dopamine and serotonin in the nucleus accumbens in vivo. *Neuroscience* 62, 41–50. doi: 10.1016/0306-4522(94)90313-1

White, S. R., Obradovic, T., Imel, K. M., and Wheaton, M. J. (1996). The effects of methylenedioxymethamphetamine (MDMA, "Ecstasy") on monoaminergic neurotransmission in the central nervous system. *Prog. Neurobiol.* 49, 455–479. doi: 10.1016/0301-0082(96)00027-5

Willemsen, M. H., Rensen, J. H. M., van Schrojenstein-Lantman de Valk, H. M. J., Hamel, B. C. J., and Kleefstra, T. (2011). Adult phenotypes in angelman- and rett-like syndromes. *Mol. Syndromol.* 2, 217–234. doi: 10.1159/000335661

Wiltschko, A. B., Pettibone, J. R., and Berke, J. D. (2010). Opposite effects of stimulant and antipsychotic drugs on striatal fast-spiking interneurons. *Neuropsychopharmacology* 35, 1261–1270. doi: 10.1038/npp.2009.226

Wöhr, M. (2014). Ultrasonic vocalizations in Shank mouse models for autism spectrum disorders: detailed spectrographic analyses and developmental profiles. *Neurosci. Biobehav. Rev.* 43, 199–212. doi: 10.1016/j.neubiorev.2014.03.021

Wöhr, M., Orduz, D., Gregory, P., Moreno, H., Khan, U., Vörckel, K. J., et al. (2015). Lack of parvalbumin in mice leads to behavioral deficits relevant to all human autism core symptoms and related neural morphofunctional abnormalities. *Transl. Psychiatry* 5:e525. doi: 10.1038/tp.2015.19

Wöhr, M., Roullet, F. I., Hung, A. Y., Sheng, M., and Crawley, J. N. (2011). Communication impairments in mice lacking SHANK1: reduced levels of ultrasonic vocalizations and scent marking behavior. *PLoS One* 6:e20631. doi: 10.1371/journal.pone.0020631

Won, H., Lee, H. R., Gee, H. Y., Mah, W., Kim, J. I., Lee, J., et al. (2012). Autistic-like social behaviour in SHANK2-mutant mice improved by restoring NMDA receptor function. *Nature* 486, 261–265. doi: 10.1038/nature11208

Xu, F., Gainetdinov, R. R., Wetsel, W. C., Jones, S. R., Bohn, L. M., Miller, G. W., et al. (2000). Mice lacking the norepinephrine transporter are supersensitive to psychostimulants. *Nat. Neurosci.* 3, 465–471. doi: 10.1038/74839

Xu, M., Guo, Y., Vorhees, C. V., and Zhang, J. (2000). Behavioral responses to cocaine and amphetamine administration in mice lacking the dopamine D1 receptor. *Brain Res.* 852, 198–207. doi: 10.1016/S0006-8993(99)02258-1

Yamamoto, B. K., and Spanos, L. J. (1988). The acute effects of methylenedioxymethamphetamine on dopamine release in the awake-behaving rat. *Eur. J. Pharmacol.* 148, 195–203. doi: 10.1016/0014-2999(88)90564-X

Yang, Y., Wang, X., and Jiang, Y. H. (2018). SHANK2 harbors potentially pathogenic mutations associated with bipolar disorder. *Bipolar Disord.* 20, 63–141. doi: 10.1111/bdi.12619

Yoo, J., Bakes, J., Bradley, C., Collingridge, G. L., and Kaang, B. K. (2013). Shank mutant mice as an animal model of autism. *Philos. Trans. R. Soc. Lond. B Biol. Sci.* 369:20130143. doi: 10.1098/rstb.2013.0143

Young, J. W., Goey, A. K. L., Minassian, A., Perry, W., Paulus, M. P., and Geyer, M. A. (2010). GBR 12909 administration as a mouse model of bipolar disorder mania: mimicking quantitative assessment of manic behavior. *Psychopharmacology* 208, 443–454. doi: 10.1007/s00213-009-1744-8

Young, J. W., Henry, B. L., and Geyer, M. A. (2011). Predictive animal models of mania: hits, misses and future directions. *Br. J. Pharmacol.* 164, 1263–1284. doi: 10.1111/j.1476-5381.2011.01318.x

Zhu, X., Need, A. C., Petrovski, S., and Goldstein, D. B. (2014). One gene, many neuropsychiatric disorders: lessons from Mendelian diseases. *Nat. Neurosci.* 17, 773–781. doi: 10.1038/nn.3713

Conflict of Interest Statement: The authors declare that the research was conducted in the absence of any commercial or financial relationships that could be construed as a potential conflict of interest.

frontiers in Neural Circuits

ORIGINAL RESEARCH
published: 22 February 2019
doi: 10.3389/fncir.2019.00006

Shank3 Transgenic and Prenatal Zinc-Deficient Autism Mouse Models Show Convergent and Individual Alterations of Brain Structures in MRI

*Michael Schoen[1†], Harun Asoglu[1†], Helen F. Bauer[1], Hans-Peter Müller[2], Alireza Abaei[3], Ann Katrin Sauer[4], Rong Zhang[5,6,7], Tian-jia Song[5,6,7], Juergen Bockmann[1], Jan Kassubek[2], Volker Rasche[3], Andreas M. Grabrucker[4,8,9] and Tobias M. Boeckers[1]**

[1]Institute for Anatomy and Cell Biology, Ulm University, Ulm, Germany, [2]Neurology Department, Ulm University, Ulm, Germany, [3]Core Facility Small Animal MRI, Ulm University, Ulm, Germany, [4]Department of Biological Sciences, University of Limerick, Limerick, Ireland, [5]Neuroscience Research Institute, Peking University, Beijing, China, [6]Department of Neurobiology, School of Basic Medical Sciences, Peking University, Beijing, China, [7]Key Laboratory for Neuroscience, Ministry of Education/National Health and Family Planning Commission, Peking University, Beijing, China, [8]Bernal Institute, University of Limerick, Limerick, Ireland, [9]Health Research Institute (HRI), University of Limerick, Limerick, Ireland

OPEN ACCESS

Edited by:
Tommaso Pizzorusso,
Italian National Research Council (CNR), Italy

Reviewed by:
Eunjoon Kim,
Institute for Basic Science (IBS), South Korea
Maija Liisa Castrén,
University of Helsinki, Finland
Alessandro Gozzi,
Fondazione Istituto Italiano di Tecnologia, Italy

***Correspondence:**
Tobias M. Boeckers
tobias.boeckers@uni-ulm.de

[†]These authors have contributed equally to this work

Received: 05 April 2018
Accepted: 16 January 2019
Published: 22 February 2019

Citation:
Schoen M, Asoglu H, Bauer HF, Müller H-P, Abaei A, Sauer AK, Zhang R, Song T, Bockmann J, Kassubek J, Rasche V, Grabrucker AM and Boeckers TM (2019) Shank3 Transgenic and Prenatal Zinc-Deficient Autism Mouse Models Show Convergent and Individual Alterations of Brain Structures in MRI. Front. Neural Circuits 13:6. doi: 10.3389/fncir.2019.00006

Research efforts over the past decades have unraveled both genetic and environmental factors, which contribute to the development of autism spectrum disorders (ASD). It is, to date, largely unknown how different underlying causes result in a common phenotype. However, the individual course of development and the different comorbidities might reflect the heterogeneous genetic and non-genetic contributions. Therefore, it is reasonable to identify commonalities and differences in models of these disorders at the different hierarchical levels of brain function, including genetics/environment, cellular/synaptic functions, brain regions, connectivity, and behavior. To that end, we investigated *Shank3* transgenic mouse lines and compared them with a prenatal zinc-deficient (PZD) mouse model of ASD at the level of brain structural alterations in an 11,7 T small animal magnetic resonance imaging (MRI). Animals were measured at 4 and 9 weeks of age. We identified a decreased total brain volume (TBV) and hippocampal size of *Shank3*$^{-/-}$ mice but a convergent increase of basal ganglia (striatum and globus pallidus) in most mouse lines. Moreover, *Shank3* transgenic mice had smaller thalami, whereas PZD mice had this region enlarged. Intriguingly, *Shank3* heterozygous knockout mice mostly showed minor abnormalities to full knockouts, which might reflect the importance of proper *Shank3* dosage in neuronal cells. Most reported volume changes seemed to be more pronounced at younger age. Our results indicate both convergent and divergent brain region abnormalities in genetic and non-genetic models of ASD. These alterations of brain structures might be mirrored in the reported behavior of both models, which have not been assessed in this study.

Keywords: ASD, autism mouse models, zinc deficiency, SHANK3, brain structures, animal MRI

Abbreviations: ASD, autism spectrum disorder(s); MRI, magnetic resonance imaging; ppm, parts per million; PZD, prenatal zinc-deficient; SHANK, SH3 and multiple ankyrin repeat domains; TBV, total brain volume; TCS, Tissue Classification Software.

INTRODUCTION

Autism spectrum disorders (ASD) belong to the most common neurodevelopmental disorders with a prevalence of approximately 1% in the population. Affected individuals demonstrate as consensus criteria abnormal social behavior and communication as well as repetitive behavior. However, a majority also presents a wide variety of comorbidities such as intellectual disability, language impairment, anxiety, hyperactivity, and sensory deficits (Levy et al., 2009).

The underlying pathomechanisms are not yet fully understood, while the causative factors have been unraveled within the last decades. Genetic alterations account for approximately two thirds of all cases (Huguet et al., 2016), and studies on identical twins show high concordance rates with strong penetrance of mutations. We know some of the genetic factors, however, the number of possible mutations is daunting with hundreds of genes potentially contributing to the phenotype (Ellegood, 2012). Nevertheless, there is a large cluster of genes coding for synaptic proteins. In fact, ASD are currently also perceived as synaptopathies (Brose et al., 2010). Mutations in the gene coding for the postsynaptic scaffolding protein SH3 and multiple ankyrin repeat domains 3 (SHANK3) are one of the rather common monogenetic causes of syndromic ASD. The most prominent example of a SHANK3 deficiency is the 22q13.3 deletion syndrome, also known as Phelan-McDermid syndrome, however, intragenic mutations have also been found in autistic cohorts (Grabrucker et al., 2011b). Apart from the strong genetic component in autism, environmental factors and gene-environment interactions are contributing factors. For unknown reasons, every second autistic individual demonstrates zinc deficiency very early in life (Grabrucker, 2012; Grabrucker et al., 2014). Intriguingly, zinc is strongly concentrated in brain tissue and there it effects, among others, the homomerization of SHANK molecules, including SHANK3 (Grabrucker et al., 2011a; Grabrucker, 2014). Maternal zinc deficiency in mice results in ASD-like behavior in the offspring (Grabrucker et al., 2016, 2014).

Neuroanatomical alterations are a frequent finding in many neurological and psychiatric disorders. Kanner (1943) already reported an increased head circumference in 5 of 11 case reports in the initial description of autism. However, head size correlates with brain size only in early childhood but Kanner's case reports were mostly beyond that period (Kanner, 1943). Approximately 20% of all autistic patients show macrocephaly, at least in a certain period throughout development. Beginning in the 1980ies with computer tomography and further followed with magnetic resonance imaging (MRI), researchers and physicians found a common pattern seen in a large number of affected individuals: the brain size at birth is usually normal, while an accelerated growth can be observed in early childhood (up to 4 years), which affects up to 90%. Then, a deceleration follows with a plateau phase until normal volume values are reached again by entry into adolescence or early adulthood (Chen et al., 2011; Stigler et al., 2011; Zielinski et al., 2014). The detailed volumetric deviation of specific parts of the brain is highly heterogeneous, which is attributable to age, intelligence quotient, but predominantly to the underlying genetic alterations. To reduce this factor, it has been reasoned to analyze neuroanatomy of syndromal ASD in humans and to model the different disease entities in mouse models, which allow for a specific genotype-phenotype correlation (Ellegood, 2012).

Nieman et al. (2007) analyzed mouse models mimicking a variety of different neurological diseases and, thereby, observed detectable changes in 90% of them. A proper model for a neuropsychiatric disease such as autism harbors the same mutations as in humans, demonstrates comparable phenotypes, and, finally, also the same underlying molecular, cellular, or neuroanatomical changes, which are ideally reproducible (Ellegood and Crawley, 2015). To date, several autism mouse models have been analyzed on the level of neuroanatomical changes with MRI. These studies included mutations in synaptic genes (Ellegood et al., 2010, 2011, 2012, 2015a; Peça et al., 2011; Kumar et al., 2014; Steadman et al., 2014), CNVs (copy number variations; Horev et al., 2011; Ellegood et al., 2015a,b), and inbred mouse strains including the BTBR mouse with autistic-like behavior (Ellegood et al., 2013, 2015a). An important conclusion is that the commonness of neuroanatomical alterations is even higher as compared to humans and that the heterogeneity is as high as observed in autistic individuals. However, the reproducibility of findings in the same model seems to be remarkably high (Ellegood and Crawley, 2015).

Along this line, we aimed at adding a longitudinal study with measurement points in: (1) the juvenile age; and (2) early adulthood by comparing a genetic model with an environmental model of autism, which have already been extensively characterized by our workgroups. The transgenic *Shank3* isoform-specific knockout mice have not been assessed on behavioral level by us (Schmeisser et al., 2012), but similar models show social abnormalities, reduced vocalization, and repetitive behavior (Bozdagi et al., 2010; Peça et al., 2011; Wang et al., 2011; Bozdagi et al., 2013). Non-genetic autism models have hardly been described but Grabrucker et al. (2014) introduced a model of prenatal zinc deficiency (PZD). Female mice undergo a temporary nutritional deprivation from zinc before and during pregnancy. The PZD offspring demonstrates autistic-like behavior. Intriguingly, one feature of these mice is a synaptic downregulation of SHANK3 levels that recovers only after birth with adequate zinc supply, and a loss of excitatory synapses in several brain regions (Grabrucker et al., 2014). Therefore, PZD and transgenic *Shank3* mice have a shared feature on a molecular level with a functional relationship at synapses. Our hypothesis is that it is possible to gain further insights in the neurobiology underlying the ASD phenotypes by further analyzing the neuroanatomy with MRI of two different models of ASD, one produced by a genetic and one by a non-genetic factor. It is plausible to assume: (1) convergent neuroanatomical changes associated with common autistic phenotypes; and (2) divergent findings may relate to specific comorbidities present in only one model.

MATERIALS AND METHODS

Animal Ethics Statement

All animal experiments were performed in compliance with the guidelines for the welfare of experimental animals issued by the Federal Government of Germany, the National Institutes of Health and the Max Planck Society. The experiments in this study were approved by the review board of the Land Baden-Württemberg (Regierungspräsidium Tübingen) and the local ethics committee at Ulm University, permit number 1239.

Animal Breeding

All animals were bred and mated in the animal facility of Ulm University.

Shank3 Transgenic Mice

Prosap2/*Shank3* mutants were generated by Genoway (Lyon, France) on a C57BL/6 strain background. The targeting strategy of the isoform-specific knockout has been described from our laboratory by Schmeisser et al. (2012). In synopsis, exon 11 in the SH3 domain was deleted, thereby, resulting in a translational stop sequence. The western blot phenotype with missing α- and β-isoforms was referred to the genotype *Prosap2/Shank3*$\alpha\beta^{-/-}$ (Schmeisser et al., 2012). The strains are, further on, named as *Shank3*$^{+/-}$ for heterozygous and *Shank3*$^{-/-}$ for homozygous animals.

Prenatal Zinc-Deficient Mice

PZD mice were generated as described previously (Grabrucker et al., 2014, 2016) using C57BL/6 mice purchased from Janvier Labs. In brief, 8-week-old mice were purchased from Janvier Labs and housed in plastic cages under standard laboratory conditions [22°C, 12 h rhythm (lights on at 7 am)], and provided with food and water available *ad libitum*. After 1 week of acclimation, mice were divided into two groups; one group was fed a zinc-deficient diet [4 parts per million (ppm; zinc, SSNIFF diets, Germany)] with demineralized drinking water, whereas the control group was fed with standard laboratory food (35 ppm zinc). After 5 weeks, females of the control and zinc-deficient group were mated and maintained on their respective diet during pregnancy. To prevent zinc contamination, feeding jars, water bottles, and plastic cages were rinsed with HCl and deionized water. After birth, offspring from both control and PZD mice received milk from mice on standard laboratory diet and were fed standard laboratory food after weaning.

Small Animal MRI

The MRI measurements were performed in the small animal MRI of Ulm University.

Animal Narcosis

High-resolution MRI experiments on age-matched control, PZD, and *Shank3* transgenic mice were carried out under isoflurane anesthesia (5% for induction, 1.5% for maintenance, mixed with air).

Structural MRI Scans

All data were acquired on a dedicated small bore animal scanner (Biospec 117/16, Bruker, Ettlingen, Germany) equipped with a cryogenically cooled two-element surface (MRI CryoProbeTM, Bruker BioSpec, Ettlingen, Germany) transmit/receive coil. Anatomical brain images were acquired in axial, sagittal, and coronal slice orientation applying a gradient-echo (FLASH) sequence with acquisition parameters as: TE/TR 2.2/193 ms (TE, echo time; TR, repetition time), matrix 260 × 260, $\Delta r = 65 \times 65 \times 500\ \mu m^3$.

In order to not overburden the mice, all measurements together were at an upper limit of narcosis time, thus, the resolution of the scans had to be restricted, e.g., to 500 μm slice thickness for the FLASH sequence [similar resolution as already was used in (Braunstein et al., 2010; Wiesner et al., 2015)]. Thus, we focussed especially on those brain regions, which: (1) are clearly distinguishable; (2) have a certain extension mediolaterally (for sagittal plane analyses) or rostrocaudally (for coronal plane analyses); and (3) have a supposedly high relevance in autism development.

Data Analysis

Volumetric tissue analysis followed previously established semi-automatic procedures in (Wiesner et al., 2015; Braunstein et al., 2010): data processing was performed by the in-house developed software package Tissue Classification Software (TCS). For optimized visualization, the acquisition matrix of 260 × 260 voxels was transformed into a 768 × 768 grid by nearest neighbor interpolation. Slicewise filtering was applied to equalize intensity gradients caused by recording. TCS includes mouse-based drawing tools for tissue/voxel selection. In order to define clearly visible regions, drawing was supported by a two-level thresholded conventional region-grow algorithm. Following the operator-defined intensity threshold, all connected voxels with respect to their intensity within the predefined intensity range were selected (process described in **Supplementary Figure S1**). The analysis was blinded and evaluated by the same experienced investigator. All regions were checked again by several investigators.

Brain regions and bregma coordinates were identified manually according to Allen Brain Atlas (Allen Institute for Brain Science, 2011) and Franklin and Paxinos (2007). In the following, brain region delineation is described in more detail. Total brain volume (TBV) and cerebellum were analyzed in sagittal planes. In order to separate left and right hemispheres, the midsagittal section volume was assigned half to both volumes each. Brain-spinal cord transition was determined as a tangential line at the posterior end of the cerebellum. All other brain areas were analyzed in coronal planes. In the following, we refer to the analyzed areas as they are named in the Allen Brain Atlas. Hippocampus was analyzed as denominated hippocampal region and subiculum under the hippocampal formation structures. Striatum was analyzed as denominated caudoputamen. Globus pallidus was analyzed as denominated globus pallidus, external and internal segment in the atlas. Thalamus was analyzed as denominated thalamus.

TBV and striatum in PZD mice were already analyzed by Grabrucker et al. (2018) however, with a different anaylsis tool, which resulted in slightly different anatomical boundaries.

Cortical thickness was measured at the bregma coordinates −0.82 mm, −1.28 mm, and −2.75 mm (adult mouse brain atlas of the Allen Brain Atlas) for both hemispheres. Thereby, a perpendicular line was drawn at the most dorsal extension of the corpus callosum. Brains at 4 and 9 weeks were not obviously different at the mentioned bregma coordinates, which is reflected in the almost identical TBV.

Statistical analysis was performed with GraphPad Prism 5 for **Supplementary Figures** and 7 for main figures (GraphPad Software, La Jolla, USA).

Significances were calculated with a two-way analysis of variance (ANOVA) with a Bonferroni *post hoc* test. Significance levels are as follows according to the p-value threshold: $^{*}p < 0.05$, $^{**}p < 0.01$, $^{***}p < 0.001$.

RESULTS

Study Concept

The study was conceptualized longitudinally with horizontal measurements at two different ages: postnatal day (PD) 28–30 (4 weeks) and PD 63–65 (9 weeks; **Figure 1A**). This interval spans the time corresponding to human adolescence and early adulthood, respectively. Per group, two different cohorts were measured and the measurement regimen for both ages was kept unchanged during the entire study. Three different autism mouse models were analyzed, namely a heterozygous and a full knockout of *Shank3* isoforms (*Shank3*$^{+/-}$ and *Shank3*$^{-/-}$), and a model of PZD (**Figure 1B**). All shown data points including mean values, standard error of the mean, standard deviation, and p-values of the main figures are provided in **Supplementary Table S1**.

Analysis of Total Brain Volume and Cortical Brain Regions

The analysis encompassed the TBV, the cerebellar volume, and the following cortical areas: cortical thickness at three corresponding points at the bregma coordinates −0.82 mm, −1.28 mm, and −2.75 mm (no volume measured), and hippocampus. All measurements were conducted on right and left parts of the brain (**Figure 2**).

Initially, the TBV was investigated (**Figure 2A**). The comparison also included right vs. left hemispheres of the brain. The only significant finding was in *Shank3*$^{-/-}$ mice at 4 weeks of age, a trend is seen in both hemispheres at this age, however, not significant. A trend can still be observed for this strain at 9 weeks.

The cerebellar volume was not majorly different between the cohorts (**Figure 2B**). However, there was an increase of the left hemisphere in *Shank3*$^{+/-}$. This alteration seemed to vanish over time.

Next, the cortical thickness was determined at three different bregma coordinates (**Figure 2C**). No significant alterations were detected. In some of the autism mouse models at 9 weeks, a slight tendency of increased thickness could be observed.

Finally, we were interested in the volume of the archicortex, namely the hippocampus (**Figure 2D**). Here, the *Shank3*$^{-/-}$ mice showed a marked decrease in volume at the early age, which seemed to largely disappear later. These results are attributable to changes in both hemispheres, however, not significant. A non-significant trend can also be seen in the heterozygous *Shank3*$^{+/-}$ animals.

Analysis of Subcortical Brain Regions

In **Figure 3**, the analysis for size differences for the subcortical regions striatum, globus pallidus, and thalamus are displayed. The striatum was tendentially bigger in all autism mouse models at both ages, however, only significant in the PZD mice at 9 weeks (**Figure 3A**).

The globus pallidus volumetry revealed significant differences in the *Shank3* mouse models (**Figure 3B**). The added hemisphere volumes of this structure were increased in volume at both ages, however, significant only for *Shank3*$^{+/-}$ at 4 weeks.

Lastly, the thalamus measurements revealed a reduction of volume in both *Shank3* models, which was only significant for the late measurement (**Figure 3C**). Interestingly, the PZD mice showed, in turn, an increase of the thalamic volume on both sides and throughout development. These differences seemed to be attributable to both hemispheres.

Region Volumetry Relative to TBV and Sex Differences

Finally, we aimed at investigating, in how the brain region volumes depend on the respective TBV. Results were not majorly different, however, some signficicancies hold, others disapper (see **Supplementary Figure S2**).

Although most significant results disappear because of low individual male and female numbers, we found it interesting to split the groups according to sex (**Supplementary Figure S3**).

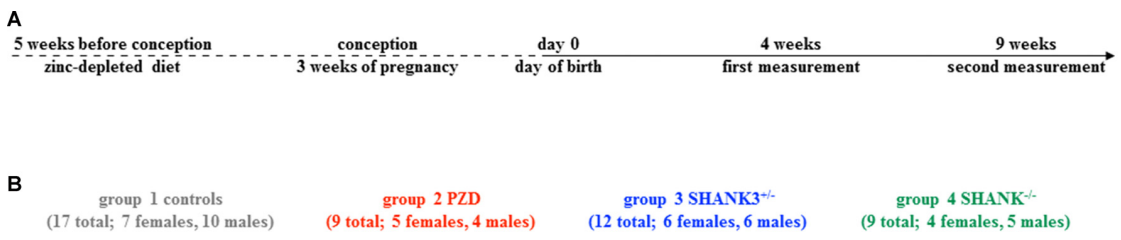

FIGURE 1 | Study design with autism mouse models measured at adolescent and adult ages. **(A)** The timeline of this longitudinal study shows the two measurement points at 4 weeks and 9 weeks. **(B)** In total, 17 controls (7 females, 10 males), nine PZD (5 females, 4 males), 12 *Shank3*$^{+/-}$ (6 females, 6 males), and nine *Shank3*$^{-/-}$ (4 females, 5 males) mice were measured.

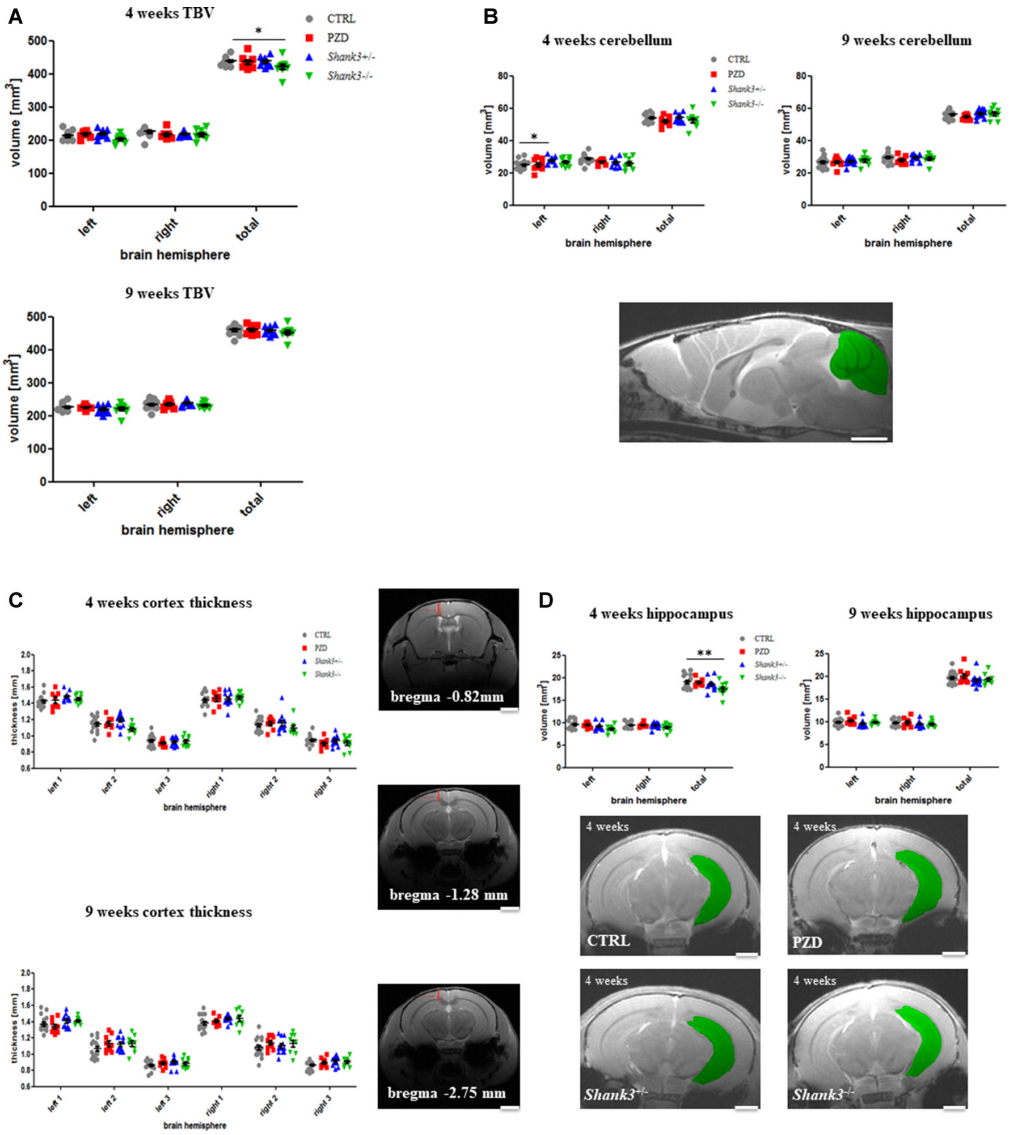

FIGURE 2 | Brain region volumetry of the total brain and cortical structures. Volumetric and thickness analyses are provided for the total brain **(A)**, the cerebellum **(B)**, cortical thickness **(C)**, and hippocampus **(D)**. Exemplary images are displayed of a 4-weeks-old control line mouse as a mid-sagittal section with the cerebellum in green **(B)**, at the three bregma coordinates of a control mouse in coronal sections **(C)**, and as 2D images in coronal sections at 4 weeks for the hippocampus measurements **(D)**. The hippocampus is highlighted in green. CTRL, controls; L, left; PZD, prenatal zinc-deficient mice; R, right; *Shank3*, SH3 and multiple ankyrin repeat domains 3; TBV, total brain volume. The mean values in the diagrams are presented with standard errors of the mean. Significance levels are as follows according to the *p*-value threshold: < 0.05 = *, < 0.01 = **. Scale bars represent 2 mm.

Interestingly, when significances remained, they usually could be attributed to the male mice.

DISCUSSION

Main Findings

In a longitudinal study, we compared brain anatomical alterations with small animal MRI in two different mouse models of ASD, a non-genetic, and a *Shank3* transgenic model with two different gene dosages. We have, to our knowledge, performed the first study analyzing a non-genetic autism mouse model in comparison to a genetic model in order to investigate the shared neurobiological substrate of their common ASD behavioral phenotype. The study revealed the following main findings:

1. All ASD models in this study show largely unaltered cerebellar volumes, cortical thickness, however, TBV and hippocampus are diminished in *Shank3* full knockout mice.
2. A convergent finding is an increased size of basal ganglia structures; striatum is significantly enlarged in PZD mice as was *Shank3* mice globus pallidus in all models.
3. *Shank3* models additionally show a decrease in the thalamus volume, on the contrary, PZD mice had this area enlarged.

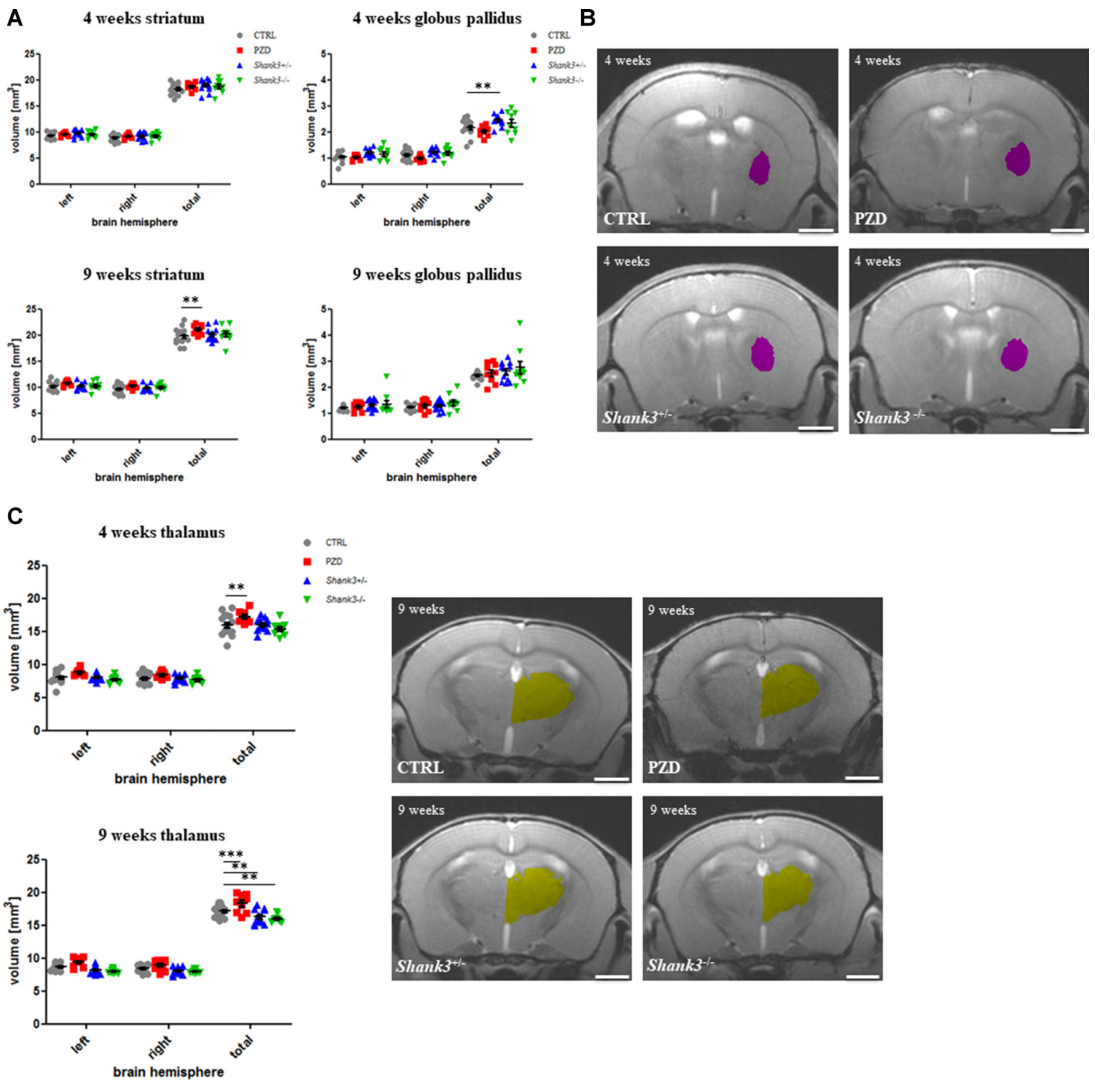

FIGURE 3 | Brain region volumetry of subcortical areas. The volumetric results of the subcortical nuclei are shown for the striatum **(A)**, globus pallidus **(B)**, and thalamus **(C)**. Exemplary images of coronal sections of 4-weeks-old mice are depicted for globus pallidus (violet, **B**) and of 9-week-old mice for thalamus (yellow, **C**). CTRL, controls; L, left; PZD, prenatal zinc-deficient mice; R, right; *Shank3*, SH3 and multiple ankyrin repeat domains 3. The mean values in the diagrams are presented with standard errors of the mean. Significance levels are as follows according to the *p*-value threshold: < 0.01 = **, < 0.001 = ***. Scale bars represent 2 mm.

4. Both heterozygous and full *Shank3* isoform-specific knockout mice display gene-dosage dependent alterations with more pronounced changes in full knockout animals.
5. Male mice show more significant alterations.
6. Some of the alterations are transient, with early brain development being more divergent from control mice.

Shank3 and PZD Mice Demonstrate Convergent Basal Ganglia but Divergent Total Brain Volume, Thalamic and Hippocampal Alterations

In the following, the results of this study will be discussed with regard to previous investigations for neuroanatomical alterations in mouse models and comparable observations in humans. The focus will, further on, be set on both similarities and discrepant results.

Brain Structures in Mouse Models for ASD

To date, most analyzed autism mouse models have not been studied longitudinally as in our study. In the majority of cases, MRI scans represented endpoints of the studies with *post mortem* MRI. Only in one previous work the developmental stages are comparable to our early measurements at about 4 weeks of age, resembling the human juvenile age, (Ellegood et al., 2010), whereas most measurements were conducted at an age around our second time-point, which corresponds to early adulthood (Ellegood et al., 2012, 2013, 2015a,b). Only Kumar et al. (2014)

conducted a longitudinal study with three consecutive measurements starting at PD 30 followed by two more runs with two 20 days intervals. They report that the neuroanatomical changes are developmentally stable (Kumar et al., 2014). Along these lines, our results with regard to dynamic over time are important information, as not all anatomical alterations were maintained during development. For example, the changes in the TBV, the subtle changes in hemispheric cerebellar, hippocampal, and globus pallidus volumes of *Shank3* models were more pronounced at younger age. The alterations of brain structures in the non-genetic PZD model seemed to be more stable over time, e.g., in the thalamus. We want to emphasize that demarcation of the respective brain regions might be subtly different in the conducted studies. We strictly followed anatomical descriptions of the Allen Brain Atlas (Allen Institute for Brain Science, 2011).

Changes in the volume of basal ganglia (especially striatum) of autism mouse models have repeatedly been reported. But most models show a decrease, such as models with a *Nlgn3* knock-in (Ellegood et al., 2011; Kumar et al., 2014), 15q11–13 duplication (Ellegood et al., 2015a), an *Fmr1* knockout (Ellegood et al., 2010), an *Itgβ3* model (Ellegood et al., 2012), and the BTBR inbred strain (Ellegood et al., 2013). Ellegood and colleagues showed in a cross-sectional study with 26 autism mouse models in 8-week-old mice that only six had an increased striatal size, including a *Shank3* isoform-specific knockout at approx. the same age as our later measurement point (Ellegood et al., 2015a). Interestingly, we could only detect a non-significant enlargement of the striatum and globus pallidus in both *Shank3* models at this age. The slight differences to our study might be due to the different knockout strategy used for the generation of the *Shank3* model; their model had exons 4–9 deleted. Peça et al. (2011) reported an enlarged striatum earlier in the same model. An increased striatal volume in the PZD model was already reported by us earlier with a different analysis method (Grabrucker et al., 2018). It can be concluded that basal ganglia enlargement is a common phenomenon in PZD mice and SHANK3 deficiency, however, it might be dosage-dependent of the remaining isoforms.

Our *Shank3* heterozygous and full knockout mice additionally demonstrated a smaller thalamus as is also observed in a *Nlgn3* knock-in model (Ellegood et al., 2011) and a 15q11–13 duplication model. A comparable situation reported for the striatum is also seen for the thalamus in another study from Ellegood et al. (2015a), showing no alterations in the heterozygous *Shank3* animals but a slight decrease, as seen in our model, in the full knockout. A thalamic enlargement, as seen in the PZD model, is rather rare (Ellegood et al., 2015a). Finally, a change in hippocampus volume is not uncommon in autism mouse models. In line with our study, this archicortical structure is mostly decreased in size including *Shank3* KOs with a different targeting strategy (Ellegood et al., 2011, 2012, 2015a). Also in agreement with Ellegood et al. (2015a), the TBV was reduced in our *Shank3* full KO animals (Ellegood et al., 2015a). In conclusion, although other groups analyzed *Shank3* models with different isoform-specific knockdown strategies, most alterations are in line with previous studies.

Interestingly, when relating the volumes of each brain region to the TBV of the same animals, results were majorly in accordance with the total volume comparison. However, some regions became significantly different or became trends only, e.g., the striatum and the thalamus in *Shank3* transgenic mice, respectively. We recommend to show both total and relative volumes in future studies to unravel or relativize the data.

Moreover, after splitting the data according to sex, we observed more alterations in the male cohorts, which is in line with the male dominance in ASD (Levy et al., 2009). To our knowledge, this is the first study to explicetly report on male-female differences in autism mouse models.

Brain Structures in Human Individuals With ASD

Human MRI has a long tradition for diagnosing and monitoring anatomical changes and brain functions in neurological disorders (Anderson and Frank, 2007). Intriguingly, the partly recovery of neuroanatomical changes from adolescence to early adulthood in our study is much in line with what has been observed as a common phenomenon in ASD: an accelerated growth of brain structures during postnatal development with a normalization of most parts until adulthood (Chen et al., 2011; Stigler et al., 2011; Zielinski et al., 2014). Common findings in structural MRI in autistic individuals are an increased TBV, white matter anomalies (including corpus callosum thinning as most frequent neuroanatomical alteration), but also common are alterations of the cerebellum, the hippocampus, the striatum, and the thalamus (Stigler et al., 2011). This is very much in line with our results.

Some models such as a Rett syndrome mouse model have shown quite comparable neuroanatomical alterations as are observed in human patients (Ellegood, 2012). Phelan-McDermid syndrome, which oftentimes goes along with a syndromal variant of ASD, is a SHANK3 deficiency disorder and patients frequently have low zinc levels, which can be a modifying factor of their phenotype (Pfaender et al., 2017). We reasoned that some of the neuroanatomical peculiarities in this syndrome might be replicable in our models. Although several studies have analyzed the brains of affected individuals, the number of included patients was quite low; also the measurements were not always standardized and did not always include thorough volumetric analyses of various brain structures. However, neuroanatomical alterations are abundant in the syndrome including corpus callosum thinning, ventriculomegaly, cortical atrophy, cerebellar malformations, and arachnoid cysts (Aldinger et al., 2013; Soorya et al., 2013; Figura et al., 2014; Philippe et al., 2015). In line with these data, we detected subtle cerebellar changes in one of the *Shank3* mouse models. Future studies ought to focus on precise volumetry of cortical and subcortical structures and would ideally include more cases with isolated *SHANK3* gene disruptions or intragenic mutations to exclude the possibility that other genes than *SHANK3* cause the anatomical alterations. In addition, with reference to the PZD model, it would now be interesting to study a correlation of specific volumetric changes in the subgroup of ASD and Phelan-McDermid syndrome patients with a zinc deficiency as we have seen them in our model organism.

Abnormal Brain Structure Associated With Neurobiological and Behavioral Changes in ASD

The following paragraph deals with the question how our observed alterations fit to previous studies on these models. Our *Shank3* model has previously been compared to a *Shank2* full knockout from our lab (Schmeisser et al., 2012). Although behavior was not assessed, similar *Shank3* knockout models display autism-related behavior (Bozdagi et al., 2010; Peça et al., 2011; Wang et al., 2011). Repetitive behavior is the predominant phenotype of these models, which is related to striatal changes (Stigler et al., 2011). This structure is the best analyzed structure in these models and shows most significant alterations with disrupted synaptic assembly and diminished glutamatergic signaling (Peça et al., 2011; Schmeisser et al., 2012). Fitting to our results of volumetric changes in the basal ganglia (striatum and globus pallidus) and thalamus, SHANK3 expression was shown to be predominantly high in these brain regions in comparison to SHANK1 and 2 (Peça et al., 2011).

Also in line with alterations in the striatum, zinc is specifically highly concentrated in this brain region. The PZD model has been shown to display a reduction of excitatory synapses in this area (Grabrucker et al., 2014), where zinc was also shown to interact with SHANK3 at the postsynaptic density. Further, an altered brain lateralization, which among others, affects the dopaminergic transmission in the striatum of these mice was reported (Grabrucker et al., 2018). On behavioral level, this correlates with stereotyped repetitive behaviors such as abnormal circling and altered marble burying that has been reported in PZD mice (Grabrucker et al., 2016), but also other ASD mouse models.

In line with the hippocampus affection that was specific for *Shank3* full KO mice, previous studies report learning and memory deficits (Wang et al., 2011; Yang et al., 2012).

Conclusions and Outlook

In this study on autism mouse models, SHANK3-deficient mice were compared to PZD mice in terms of neuroanatomical peculiarities measured by structural MRI. While both models display enlarged basal ganglia strucutres, thalami in *Shank3* models were smaller, while they were enlarged in the PZD mice. Especially the latter observation remained significant until early adulthood. Only *Shank3* full knockout mice showed decreased total brain and hippocampal volumes.

Our study harbors several limitations. Because of inter-individual differences, several observed alterations did not turn out be significant or were significant in the early measurement but not in the later analysis. Also, when splitting the group according to sex, we lost some of the significant results. This is most likely attributable to a combination of a low number of individuals and a concomitant low effect size. Future studies might include either more animals or might employ higher resolution. Furthermore, we can only speculate on functional consequences of the observed alterations by reviewing literature on these or comparable models, or the situation in humans. Further, in this study, we cannot answer the question what is happening on the cellular or even molecular levels of the affected areas.

Nevertheless, the results reported here might pave the way for future investigations in order to further scrutinize these observations. This way might lead upstream to unravel the molecular and neurocellular alterations, which could have led to the alterations observed. Moreover, this might give rise to a better understanding of underlying pathomechanisms and to identify therapeutic targets that are shared between the plethora of different causes of ASD. However, based on these data, it is also important to seek downstream to more specifically analyze the models for specific behavioral alterations, which might refer to the brain region alterations in the analyzed models and might be related to specific comorbidities observed in addition to the core features of ASD.

So far, two studies had a glimpse on what is happening on the level of neuronal function and morphology. In an *Fmr1* KO model of autism, two cerebellar nuclei were found to be decreased in size; immunohistochemistry unraveled a loss of neurons accounting for the shrinkage (Ellegood et al., 2010). Peça et al. (2011) nicely showed in *Shank3* transgenic mice, how medium spiny neurons of the striatum are significantly more branched, which goes along with diminished cortico-striatal transmission. In line with our results, the striatum is larger in this model, and the authors suggest these striatal changes to underlie the strong repetitive behavior in this model (Peça et al., 2011). This represents an exemplary study to scrutinize a behavioral alteration on the level of cellular morphology up to the resulting function. Thus, they found a neuroanatomical phenotype on the mesoscopic scale resulting in a distinguishable phenotype. Future investigations might verify these hypotheses of a brain-region—phenotype association by specifical knockdowns of autism-related genes in certain brain regions or key pathways. It could prove the suggested associations between brain regions and a certain phenotype: striatum/globus pallidus—repetitive behavior, hippocampus and thalamus—learning, processing of highly associated sensory input. In line with this, the striatal size in human individuals is negatively correlated with stereotypies but positively with difficulties in problem solving (Stigler et al., 2011). Our data also shows that despite different etiologies of ASDs such as genetic or non-genetic ones, the search of commonalities between different models may identify the neurobiological correlate of the shared behavioral impairments.

Another interesting lesson we learn from our results and by reviewing different mouse models is that it is rather the affection of a certain brain area than the dynamic of increase or decrease in volume, which correlates with a phenotype. This holds true both for human individuals as well as for autism mouse models. An intriguing path would be to correlate the volumetric changes to altered connectivity between brain regions, which has been used to study ASD in both humans as well as mouse models by applying diffusion tensor imaging (DTI).

For our models, it is most intriguing that SHANK3 and zinc have repeatedly been shown to preferentially localize in the same

brain areas, to even interact molecularly, and a reduction of both players seems to result in an overlapping phenotype (Bozdagi et al., 2010; Peça et al., 2011; Schmeisser et al., 2012; Grabrucker et al., 2014). However, on the level of neuroanatomical alterations they show similarities but also differ in some respect. This might indicate that the zinc-SHANK3 interaction may be a major driver for the ASD-associated behavioral impairments seen in PZD mice, but also hints toward other SHANK3-independent functions of zinc signaling in the brain. The shared but also unique functions of zinc and possibly a variety of genetic and non-genetic factors may account for the phenotypic heterogeneity of ASD despite the occurrence of common core features. However, it is possible that the molecular and cellular changes might be very similar despite differences in volume changes of certain brain regions. For instance, both *Shank3* and PZD models demonstrate decreased glutamatergic transmission in both the striatum and hippocampus (Bozdagi et al., 2010; Peça et al., 2011; Schmeisser et al., 2012; Grabrucker et al., 2014), but effects on hippocampal volume were only seen in *Shank3* mice.

Intriguingly, our analyzed heterozygous *Shank3* KO was generally less affected than the full KO. This should be further scrutinized on other levels, cellular and behavioral ones, since heterozygous *Shank3* KO more closely resembles the human pathology on the genetic level. Furthermore, it would be worth to study the affection of the thalamus in *Shank3* models in more detail. A common observation in patients with SHANK3 deficiency (Soorya et al., 2013) and mouse models is an altered perception of inconvenient sensations such as heat or pain. If this is only attributable to peripheral neurons as suggested by Han et al. (2016) or also includes higher brain function with sensory processing in the thalamus remains elusive. Moreover, future studies on human individuals with either SHANK3 loss or early life exposure to zinc deficiency might now seek for similar alterations as we have seen them in the corresponding animal models.

Taken together, efforts in describing the brain anatomy in ASD and respective models might be important to: (1) find diagnostic criteria based on MRI-detectable changes (Stevenson and Kellett, 2010); and to (2) pinpoint clusters of ASD variants with same anatomical alterations, maybe associated with similar symptoms constellations, which might then be grouped and subjected to a more specific symptom-based therapy. Intriguingly, such a therapeutic intervention and the putative positive effect might even be measurable as was shown for a Rett model, in which alterations in brain structures was used as marker. After exposure to an enriched environment, some of the neuroanatomical alterations could be rescued (Nag et al., 2009).

AUTHOR CONTRIBUTIONS

TB, MS, JS, AA, AG, RZ, TS, and VR designed and outlined this study. HA, AA, MS, and AS carried out all experiments. JB took care of animal breeding. HA, HB, H-PM, JK, and MS jointly analyzed the data. HA, HB, and MS composed the figures. MS, TB, AG, H-PM, and JK jointly wrote the manuscript.

FUNDING

AG was supported by the Juniorprofessuren-Program of the State of Baden-Württemberg. TB is supported by the BIU2 program at Ulm University and by the DFG (SFB1149, A02). The Helmholtz Gesellschaft ("RNA Dysmetabolism in ALS and FTD") and the Innovative Medicines Initiative (IMI) Joint Undertaking under grant agreement no 115300 and 777394, resources of which are composed of financial contribution from the European Union and EFPIA companies in kind contribution.

ACKNOWLEDGMENTS

We would like to thank Natalie Damm, Ursula Pika-Hartlaub, and Anne Subgang for excellent technical support and acknowledge networking support by the COST Action TD1304 (Zinc-Net).

SUPPLEMENTARY MATERIAL

The Supplementary Material for this article can be found online at: https://www.frontiersin.org/articles/10.3389/fncir.2019.00006/full#supplementary-material

FIGURE S1 | Volumetric analysis cascade. Original data were optionally gradient filtered and an intensity thresholding supported the user-defined selection of the respective brain region. Volumetric marked regions were then analyzed for the respective slices.

FIGURE S2 | Volumes relative to TBV. Each measured brain region (not the cortical thickness) was calculated as the percentage of the total brain volume of the same animal. CTRL, controls; L, left; PZD, prenatal zinc-deficient mice; R, right; *Shank3*, SH3 and multiple ankyrin repeat domains 3; TBV, total brain volume. The mean values in the diagrams are presented with standard errors of the mean. Significance levels are as follows according to the *p*-value threshold: $< 0.05 = *$, $< 0.01 = **$, $< 0.001 = ***$.

FIGURE S3 | Sex differences. Animals were split according to sex. CTRL, controls; f, female; L, left; m, male; PZD, prenatal zinc-deficient mice; R, right; *Shank3*, SH3 and multiple ankyrin repeat domains 3; TBV, total brain volume. The mean values in the diagrams are presented with standard errors of the mean. Significance levels are as follows according to the *p*-value threshold: $< 0.05 = *$, $< 0.01 = **$, $< 0.001 = ***$.

TABLE S1 | Raw volume data and statistics for **Figures 1**,**2**.

REFERENCES

Aldinger, K. A., Kogan, J., Kimonis, V., Fernandez, B., Horn, D., Klopocki, E., et al. (2013). Cerebellar and posterior fossa malformations in patients with autism-associated chromosome 22q13 terminal deletion. *Am. J. Med. Genet. A* 161A, 131–136. doi: 10.1002/ajmg.a.35700

Allen Institute for Brain Science. (2011). *Allen Brain Atlas API*. Available online at: http://atlas.brain-map.org/

Anderson, S. A., and Frank, J. A. (2007). MRI of mouse models of neurological disorders. *NMR Biomed.* 20, 200–215. doi: 10.1002/nbm.1167

Bozdagi, O., Sakurai, T., Papapetrou, D., Wang, X., Dickstein, D. L., Takahashi, N., et al. (2010). Haploinsufficiency of the autism-associated Shank3 gene leads to deficits in synaptic function, social interaction, and social communication. *Mol. Autism* 1:15. doi: 10.1186/2040-2392-1-15

Bozdagi, O., Tavassoli, T., and Buxbaum, J. D. (2013). Insulin-like growth factor-1 rescues synaptic and motor deficits in a mouse model of autism and developmental delay. *Mol. Autism* 4:9. doi: 10.1186/2040-2392-4-9

Braunstein, K. E., Eschbach, J., Ròna-Vörös, K., Soylu, R., Mikrouli, E., Larmet, Y., et al. (2010). A point mutation in the dynein heavy chain gene leads to striatal atrophy and compromises neurite outgrowth of striatal neurons. *Hum. Mol. Genet.* 19, 4385–4398. doi: 10.1093/hmg/ddq361

Brose, N., O'Connor, V., and Skehel, P. (2010). Synaptopathy: dysfunction of synaptic function? *Biochem. Soc. Trans.* 38, 443–444. doi: 10.1042/bst0380443

Chen, R., Jiao, Y., and Herskovits, E. H. (2011). Structural MRI in autism spectrum disorder. *Pediatr. Res.* 69, 63R–68R. doi: 10.1203/pdr.0b013e318212c2b3

Ellegood, J. (2012). Magnetic resonance imaging as a tool for the study of mouse models of autism. *Autism* 01:008. doi: 10.4172/2165-7890.s1-008

Ellegood, J., Anagnostou, E., Babineau, B. A., Crawley, J. N., Lin, L., Genestine, M., et al. (2015a). Clustering autism: using neuroanatomical differences in 26 mouse models to gain insight into the heterogeneity. *Mol. Psychiatry* 20, 118–125. doi: 10.1038/mp.2014.98

Ellegood, J., Nakai, N., Nakatani, J., Henkelman, M., Takumi, T., and Lerch, J. (2015b). Neuroanatomical phenotypes are consistent with autism-like behavioral phenotypes in the 15q11–13 duplication mouse model. *Autism Res.* 8, 545–555. doi: 10.1002/aur.1469

Ellegood, J., Babineau, B. A., Henkelman, R. M., Lerch, J. P., and Crawley, J. N. (2013). Neuroanatomical analysis of the BTBR mouse model of autism using magnetic resonance imaging and diffusion tensor imaging. *Neuroimage* 70, 288–300. doi: 10.1016/j.neuroimage.2012.12.029

Ellegood, J., and Crawley, J. N. (2015). Behavioral and neuroanatomical phenotypes in mouse models of autism. *Neurotherapeutics* 12, 521–533. doi: 10.1007/s13311-015-0360-z 4

Ellegood, J., Henkelman, R. M., and Lerch, J. P. (2012). Neuroanatomical assessment of the integrin β3 mouse model related to autism and the serotonin system using high resolution MRI. *Front. Psychiatry* 3:37. doi: 10.3389/fpsyt.2012.00037

Ellegood, J., Lerch, J. P., and Henkelman, R. M. (2011). Brain abnormalities in a neuroligin3 R451C knockin mouse model associated with autism. *Autism Res.* 4, 368–376. doi: 10.1002/aur.215

Ellegood, J., Pacey, L. K., Hampson, D. R., Lerch, J. P., and Henkelman, R. M. (2010). Anatomical phenotyping in a mouse model of fragile X syndrome with magnetic resonance imaging. *Neuroimage* 53, 1023–1029. doi: 10.1016/j.neuroimage.2010.03.038

Figura, M. G., Coppola, A., Bottitta, M., Calabrese, G., Grillo, L., Luciano, D., et al. (2014). Seizures and EEG pattern in the 22q13.3 deletion syndrome: clinical report of six italian cases. *Seizure* 23, 774–779. doi: 10.1016/j.seizure.2014.06.008

Franklin, K. B. J., and Paxinos, G. (2007). *The Mouse Brain in Stereotaxic Coordinates*. 3rd Edn. San Diego, CA: Academic Press.

Grabrucker, A. M., Knight, M. J., Proepper, C., Bockmann, J., Joubert, M., Rowan, M., et al. (2011a). Concerted action of zinc and ProSAP/Shank in synaptogenesis and synapse maturation. *EMBO J.* 30, 569–581. doi: 10.1038/emboj.2010.336

Grabrucker, A. M., Schmeisser, M. J., Schoen, M., and Boeckers, T. M. (2011b). Postsynaptic ProSAP/Shank scaffolds in the cross-hair of synaptopathies. *Trends Cell Biol.* 21, 594–603. doi: 10.1016/j.tcb.2011.07.003

Grabrucker, A. M. (2012). Environmental factors in autism. *Front. Psychiatry* 3:118. doi: 10.3389/fpsyt.2012.00118

Grabrucker, A. M. (2014). A role for synaptic zinc in ProSAP/Shank PSD scaffold malformation in autism spectrum disorders. *Dev. Neurobiol.* 74, 136–146. doi: 10.1002/dneu.22089

Grabrucker, S., Boeckers, T. M., and Grabrucker, A. M. (2016). Gender dependent evaluation of autism like behavior in mice exposed to prenatal zinc deficiency. *Front. Behav. Neurosci.* 10:37. doi: 10.3389/fnbeh.2016.00037

Grabrucker, S., Haderspeck, J. C., Sauer, A. K., Kittelberger, N., Asoglu, H., Abaei, A., et al. (2018). Brain lateralization in mice is associated with zinc signaling and altered in prenatal zinc deficient mice that display features of autism spectrum disorder. *Front. Mol. Neurosci.* 10:450. doi: 10.3389/fnmol.2017.00450

Grabrucker, S., Jannetti, L., Eckert, M., Gaub, S., Chhabra, R., Pfaender, S., et al. (2014). Zinc deficiency dysregulates the synaptic ProSAP/Shank scaffold and might contribute to autism spectrum disorders. *Brain* 137, 137–152. doi: 10.1093/brain/awt303

Han, Q., Kim, Y. H., Wang, X., Liu, D., Zhang, Z. J., Bey, A. L., et al. (2016). SHANK3 deficiency impairs heat hyperalgesia and TRPV1 signaling in primary sensory neurons. *Neuron* 92, 1279–1293. doi: 10.1016/j.neuron.2016.11.007

Horev, G., Ellegood, J., Lerch, J. P., Son, Y.-E., Muthuswamy, L., Vogel, H., et al. (2011). Dosage-dependent phenotypes in models of 16p11.2 lesions found in autism. *Proc. Natl. Acad. Sci. U S A* 108, 17076–17081. doi: 10.1073/pnas.1114042108

Huguet, G., Benabou, M., and Bourgeron, T. (2016). *The Genetics of Autism Spectrum Disorders. Edited by Paolo Sassone-Corsi and Yves Christen. A Time for Metabolism and Hormones. Research and Perspectives in Endocrine Interactions.* Cham: Springer International Publishing.

Kanner, L. (1943). Autistic disturbance of affective contact. *Nervous Child* 2, 217–250.

Kumar, M., Duda, J. T., Hwang, W.-T., Kenworthy, C., Ittyerah, R., Pickup, S., et al. (2014). High resolution magnetic resonance imaging for characterization of the neuroligin-3 knock-in mouse model associated with autism spectrum disorder. *PLoS One* 9:e109872. doi: 10.1371/journal.pone.0109872

Levy, S. E., Mandell, D. S., and Schultz, R. T. (2009). Autism. *Lancet* 374, 1627–1638. doi: 10.1016/S0140-6736(09)61376-3

Nag, N., Moriuchi, J. M., Peitzman, C. G., Ward, B. C., Kolodny, N. H., and Berger-Sweeney, J. E. (2009). Environmental enrichment alters locomotor behaviour and ventricular volume in Mecp2 1lox mice. *Behav. Brain Res.* 196, 44–48. doi: 10.1016/j.bbr.2008.07.008

Nieman, B. J., Lerch, J. P., Bock, N. A., Chen, X. J., Sled, J. G., and Henkelman, R. M. (2007). Mouse behavioral mutants have neuroimaging abnormalities. *Hum. Brain Mapp.* 28, 567–575. doi: 10.1002/hbm.20408

Peça, J., Feliciano, C., Ting, J. T., Wang, W., Wells, M. F., Venkatraman, T. N., et al. (2011). *Shank3* mutant mice display autistic-like behaviours and striatal dysfunction. *Nature* 472, 437–442. doi: 10.1038/nature09965

Pfaender, S., Sauer, A. K., Hagmeyer, S., Mangus, K., Linta, L., Liebau, S., et al. (2017). Zinc deficiency and low enterocyte zinc transporter expression in human patients with autism related mutations in SHANK3. *Sci. Rep.* 7:45190. doi: 10.1038/srep45190

Philippe, A., Craus, Y., Rio, M., Bahi-Buisson, N., Boddaert, N., Malan, V., et al. (2015). Case report: an unexpected link between partial deletion of the *SHANK3* gene and heller's *dementia infantilis*, a rare subtype of autism spectrum disorder. *BMC Psychiatry* 15:256. doi: 10.1186/s12888-015-0631-6

Schmeisser, M. J., Ey, E., Wegener, S., Bockmann, J., Stempel, A. V., Kuebler, A., et al. (2012). Autistic-like behaviours and hyperactivity in mice lacking ProSAP1/Shank2. *Nature* 486, 256–260. doi: 10.1038/nature11015

Soorya, L., Kolevzon, A., Zweifach, J., Lim, T., Dobry, Y., Schwartz, L., et al. (2013). Prospective investigation of autism and genotype-phenotype correlations in 22q13 deletion syndrome and *SHANK3* deficiency. *Mol. Autism* 4:18. doi: 10.1186/2040-2392-4-18

Steadman, P. E., Ellegood, J., Szulc, K. U., Turnbull, D. H., Joyner, A. L., Henkelman, R. M., et al. (2014). Genetic effects on cerebellar structure across mouse models of autism using a magnetic resonance imaging atlas. *Autism Res.* 7, 124–137. doi: 10.1002/aur.1344

Stevenson, J. L., and Kellett, K. A. (2010). Can magnetic resonance imaging aid diagnosis of the autism spectrum? *J. Neurosci.* 30, 16763–16765. doi: 10.1523/JNEUROSCI.4946-10.2010

Stigler, K. A., McDonald, B. C., Anand, A., Saykin, A. J., and McDougle, C. J. (2011). Structural and functional magnetic resonance imaging of autism spectrum disorders. *Brain Res.* 1380, 146–161. doi: 10.1016/j.brainres.2010.11.076

Wang, X., McCoy, P. A., Rodriguiz, R. M., Pan, Y., Je Shawn, H., Roberts, A. C., et al. (2011). Synaptic dysfunction and abnormal behaviors in mice lacking

major isoforms of Shank3. *Hum. Mol. Genet.* 20, 3093–3108. doi: 10.1093/hmg/ddr212

Wiesner, D., Sinniger, J., Henriques, A., Dieterlé, S., Müller, H.-P., Rasche, V., et al. (2015). Low dietary protein content alleviates motor symptoms in mice with mutant dynactin/dynein-Mediated neurodegeneration. *Hum. Mol. Genet.* 24, 2228–2240. doi: 10.1093/hmg/ddu741

Yang, M., Bozdagi, O., Scattoni, M. L., Wöhr, M., Roullet, F. I., Katz, A. M., et al. (2012). Reduced excitatory neurotransmission and mild autism-relevant phenotypes in adolescent Shank3 null mutant mice. *J. Neurosci.* 32, 6525–6541. doi: 10.1523/JNEUROSCI.6107-11.2012

Zielinski, B. A., Prigge, M. B. D., Nielsen, J. A., Froehlich, A. L., Abildskov, T. J., Anderson, J. S., et al. (2014). Longitudinal changes in cortical thickness in autism and typical development. *Brain* 137, 1799–1812. doi: 10.1093/brain/awu083

Conflict of Interest Statement: The authors declare that the research was conducted in the absence of any commercial or financial relationships that could be construed as a potential conflict of interest.

The Reviewer EK is currently editing a Research Topic with one of the authors TB, and confirms the absence of any other collaboration.

frontiers in Molecular Neuroscience

ORIGINAL RESEARCH
published: 18 June 2019
doi: 10.3389/fnmol.2019.00155

Shank3 Mice Carrying the Human Q321R Mutation Display Enhanced Self-Grooming, Abnormal Electroencephalogram Patterns, and Suppressed Neuronal Excitability and Seizure Susceptibility

*Ye-Eun Yoo[1], Taesun Yoo[1], Seungjoon Lee[1], Jiseok Lee[2], Doyoun Kim[2], Hye-Min Han[3], Yong-Chul Bae[3] and Eunjoon Kim[1,2]**

[1] Department of Biological Sciences, Korea Advanced Institute of Science and Technology, Daejeon, South Korea, [2] Center for Synaptic Brain Dysfunctions, Institute for Basic Science, Daejeon, South Korea, [3] Department of Anatomy and Neurobiology, School of Dentistry, Kyungpook National University, Daegu, South Korea

Shank3, a postsynaptic scaffolding protein involved in regulating excitatory synapse assembly and function, has been implicated in several brain disorders, including autism spectrum disorders (ASD), Phelan-McDermid syndrome, schizophrenia, intellectual disability, and mania. Here we generated and characterized a *Shank3* knock-in mouse line carrying the Q321R mutation (*Shank3*^{Q321R} mice) identified in a human individual with ASD that affects the ankyrin repeat region (ARR) domain of the Shank3 protein. Homozygous *Shank3*$^{Q321R/Q321R}$ mice show a selective decrease in the level of Shank3a, an ARR-containing protein variant, but not other variants. CA1 pyramidal neurons in the *Shank3*$^{Q321R/Q321R}$ hippocampus show decreased neuronal excitability but normal excitatory and inhibitory synaptic transmission. Behaviorally, *Shank3*$^{Q321R/Q321R}$ mice show moderately enhanced self-grooming and anxiolytic-like behavior, but normal locomotion, social interaction, and object recognition and contextual fear memory. In addition, these mice show abnormal electroencephalogram (EEG) patterns and decreased susceptibility to induced seizures. These results indicate that the Q321R mutation alters Shank3 protein stability, neuronal excitability, repetitive and anxiety-like behavior, EEG patterns, and seizure susceptibility in mice.

Keywords: Shank3, autism spectrum disorder, patient mutations, self-grooming, anxiety-like behavior, excitability, EEG, seizure susceptibility

OPEN ACCESS

Edited by:
Michael J. Schmeisser, Johannes Gutenberg University Mainz, Germany

Reviewed by:
Gaia Novarino, Institute of Science and Technology Austria (IST Austria), Austria
Peter Jedlicka, Goethe-Universität Frankfurt am Main, Germany

***Correspondence:**
Eunjoon Kim
kime@kaist.ac.kr

Received: *01 August 2018*
Accepted: *03 June 2019*
Published: *18 June 2019*

Citation:
Yoo Y-E, Yoo T, Lee S, Lee J, Kim D, Han H-M, Bae Y-C and Kim E (2019) Shank3 Mice Carrying the Human Q321R Mutation Display Enhanced Self-Grooming, Abnormal Electroencephalogram Patterns, and Suppressed Neuronal Excitability and Seizure Susceptibility. Front. Mol. Neurosci. 12:155. doi: 10.3389/fnmol.2019.00155

INTRODUCTION

Shank proteins, a family of postsynaptic scaffolding proteins with three known members, have been implicated in the regulation of excitatory synapse assembly and function (Sheng and Kim, 2000, 2011; Sheng and Sala, 2001; Boeckers et al., 2002; Sheng and Hoogenraad, 2007; Grabrucker et al., 2011; Jiang and Ehlers, 2013; Sala et al., 2015; Monteiro and Feng, 2017; Mossa et al., 2017). The third member of the family, Shank3, also known as ProSAP2, contains multiple domains

for protein-protein interactions, including an SPN (Shank/ProSAP N-terminal) domain, ankyrin repeats, an SH3 domain, a PDZ domain, a proline-rich region, and a SAM (sterile alpha motif) domain (Du et al., 1998; Boeckers et al., 1999; Lim et al., 1999; Naisbitt et al., 1999; Sheng and Kim, 2000). These domains mediate interactions with diverse synaptic proteins, including GKAP (also known as SAPAP1 and DLGAP1) and Homer.

Clinically, *SHANK3* has been implicated in multiple neurodevelopmental and psychiatric disorders, including autism spectrum disorders (ASD), Phelan-McDermid syndrome (PMS), schizophrenia, intellectual disability, and mania (Bonaglia et al., 2001; Wilson et al., 2003; Durand et al., 2007; Moessner et al., 2007; Gauthier et al., 2010; Bonaglia et al., 2011; Hamdan et al., 2011; Leblond et al., 2012; Boccuto et al., 2013; Han et al., 2013; Guilmatre et al., 2014; Leblond et al., 2014; Cochoy et al., 2015; Nemirovsky et al., 2015; de Sena Cortabitarte et al., 2017; De Rubeis et al., 2018). Importantly, *SHANK3* mutations have been shown to account for ∼1% of all ASD cases (Leblond et al., 2014). Multiple lines of *Shank3*-mutant mice and, more recently, rats that carry global, conditional and point mutations in *Shank3*, have been generated and characterized, providing information about normal and disease-related functions of Shank3 (Bozdagi et al., 2010; Peca et al., 2011; Wang et al., 2011; Schmeisser et al., 2012; Yang et al., 2012; Han et al., 2013; Kouser et al., 2013; Lee et al., 2015; Speed et al., 2015; Jaramillo et al., 2016, 2017; Mei et al., 2016; Wang et al., 2016; Zhou et al., 2016; Harony-Nicolas et al., 2017; Vicidomini et al., 2017; Amal et al., 2018; Berg et al., 2018; Bey et al., 2018; Drapeau et al., 2018; Engineer et al., 2018; Fourie et al., 2018; Heise et al., 2018; Jin et al., 2018; Ma et al., 2018; Qin et al., 2018; Yoo et al., 2018; Zhu et al., 2018; Balaan et al., 2019; Rendall et al., 2019). These animals display diverse synaptic, neuronal, circuit and behavioral abnormalities, providing substantial insight into how *Shank3* mutations lead to various phenotypic abnormalities in mice (Jiang and Ehlers, 2013; Harony-Nicolas et al., 2015; Sala et al., 2015; Ferhat et al., 2017; Monteiro and Feng, 2017; Mossa et al., 2017; Tan and Zoghbi, 2018). However, with the exception of recent studies on two mouse lines carrying an ASD-linked InsG3680 mutation and a schizophrenia-linked R1117X mutation (Zhou et al., 2016) and a mouse line carrying the S685I mutation (Wang et al., 2019), mouse lines expressing point mutations of *Shank3* identified in human individuals with ASD, PMS, or other disorders have not been reported.

The Shank3 Q321R mutation was identified as a de novo mutation in an individual with ASD who displayed symptoms including social and language deficits, repetitive behaviors (verbal repetitive behaviors, hair pulling, but no motor stereotypies), restricted interests, inattention and irritability (Moessner et al., 2007). This mutation has been shown to decrease excitatory synaptic targeting of Shank3 and Shank3-dependent dendritic spine development, decrease F-actin levels in spines, and suppress excitatory synaptic transmission in cultured hippocampal neurons (Durand et al., 2012). In a more recent study, this mutation was shown to enhance the interaction of Shank3 with Sharpin, but not with α-fodrin (Mameza et al., 2013), two known ligands of the ARR (ankyrin repeat region) domain of Shank3 (Bockers et al., 2001; Lim et al., 2001). In addition, the Q321R mutation has stronger influences on excitatory synapses, as compared with other Shank3 mutations such as R12C and R300C (Durand et al., 2012). These results indicate that the Q321R mutation exerts a significant influence on ASD-related behaviors and excitatory synapse development and function. However, *in vivo* functions of the Q321R mutation have not been explored.

In the present study, we generated and characterized a new *Shank3*-mutant mouse line carrying the Q321R mutation (*Shank3*^{Q321R} mice) and studied its *in vivo* effects. We found that this mutation leads to destabilization of Shank3 protein, decreased excitability in hippocampal CA1 pyramidal neurons, enhanced self-grooming and anxiolytic-like behavior, altered electroencephalogram (EEG) patterns, and decreased seizure susceptibility.

MATERIALS AND METHODS

Structural Modeling of the Shank3 Protein Containing a Q321R Mutation

The structure of the SPN and ARR domains of the mouse Shank3 protein containing the p.Q321R missense mutation was modeled using the mutagenesis function in PyMOL software (version 1.3) (DeLano, 2009) based on the crystal structure of the SPN and ARR domains of the rat Shank3 protein (PDB ID: 5G4X). Energy minimization and loop flexible modeling were performed using Modeller software (Fiser et al., 2000). Electrostatic charge distribution surfaces were calculated and represented using PyMOL software (version 1.3) (DeLano, 2009). All structural figures were prepared using PyMOL software (version 1.3) (DeLano, 2009).

Stability Prediction of Mutant Shank3 Proteins

The stability of the SPN and ARR domains of Shank3 containing the ASD-risk missense mutations, p.R12C, p.L68P, p.A198G, p.R300C, or p.Q321R, were predicted using the *in silico* algorithm in I-Mutant 2.0 (version 2.0)[1] under conditions of pH 7.0 and 25°C (Capriotti et al., 2005). I-Mutant 2.0 is a support vector machine (SVM)-based web server for automatic prediction of stability changes upon a single point mutation. We used the crystal structure of the SPN and ARR domains of Shank3 protein (PDB ID: 5G4X) as a template structure to calculate changes in the stability of the protein containing ASD-risk missense mutations. The $\Delta\Delta G$ value was calculated by subtracting the unfolding Gibbs free energy of wild-type (WT) protein from that of the mutated protein (kcal/mol). A negative $\Delta\Delta G$ value indicates a decrease in the stability of the mutated protein.

Animals

A mouse embryonic stem (ES) cell line harboring the Shank3 Q321R mutation was generated by Cyagen. ES cells were injected into C57BL/6N blastocysts to produce chimeric mice, which were crossed with WT C57BL/6J to produce heterozygous knock-in

[1] http://folding.biofold.org/i-mutant/i-mutant2.0.html

(KI) F1 mice. F1 mice were then crossed with *protamine-Cre* mice to remove the Neo cassette, followed by backcrossing into a C57BL/6J background for more than five generations. All mice used for experiments in the present study were obtained by mating heterozygotes (HT x HT). The average WT:HT:KI ratio was 0.94:1.94:1.12, consistent with the expected 1:2:1 Mendelian ratio. Breeding was successful in >95% of cases, and homozygous *Shank3*^{Q321R} mice showed survival rates and body weights comparable to those of WT mice. The mice were fed *ad libitum* under 12-h light-dark cycles, and 2–6 mice were grouped in each cage. Mice were bred and maintained according to the Animal Research Requirements of KAIST, and all procedures were approved by the Committee of Animal Research at KAIST (2016-30). For PCR genotyping, the following oligonucleotide primers were used to detect a band of 478 base pairs for WT allele and a band of 622 base pairs for the Q321R mutant allele: forward, 5′-CAT GAG GCA CCC TTT TCT GT-3′, reverse, 5′-TGT CCC TAA CCC CAA TGT GT-3′.

Western Blot

Brains from *Shank3*^{Q321R} mice (*Shank3*$^{Q321R/Q321R}$ and *Shank3*$^{+/Q321R}$) and their WT littermates (3 months) were extracted in ice-cold homogenization buffer (0.32 M sucrose, 10 mM HEPES, 2 mM EDTA, 2 mM EGTA, protease inhibitors and phosphatase inhibitors) and homogenized by motorized tissue grinder. Brain whole lysates were prepared by boiling with β-mercaptoethanol. After immunoblotting with antibodies to Shank3 (Santa Cruz SC-30193; H-160) and α-tubulin (Sigma T5168), fluorescent secondary antibody signals were detected using Odyssey Fc Dual Mode Imaging System.

Immunohistochemistry

Adult mice (2 months, female) were anesthetized and perfused transcardially with 4% paraformaldehyde. Brains were removed and post-fixed overnight at 4°C followed by Vibratome sectioning (50 μm; Leica VT 1200S). After washing in phosphate-buffered saline (PBS), brain sections were blocked in 5% bovine serum albumin (BSA) in PBS for 3–5 h. Brain sections were incubated with primary antibodies (NeuN, 1:1000, Millipore) in 5% BSA overnight at 4°C and washed three times for 20 min in 0.2% TritonX-100 in PBS (PBST). After incubation with Alexa 594 secondary antibody (1:500, Jackson ImmunoResearch) at room temperature for 1 h, sections were washed three times for 10 min in PBST. Brain sections were mounted with DAPI mounting medium. Brain sections were imaged with a confocal microscope (10x objective; LSM780, Carl Zeiss).

Behavioral Assays

Behavioral analyses were performed during light-off periods on male 2–4-month-old male or female mice in their home cages. WT and mutant littermates (partly pairs) from several mother mice were used to form a cohort. All mice were handled for 10 min per day for 3 days by experienced researchers prior to behavioral experiments. Mouse behavioral assays were performed in the following order: Laboras monitoring of 96-h movements, open-field test, novel-object–recognition test, repetitive behaviors, three-chamber social-interaction test, elevated plus-maze (EPM) test, light-dark test, courtship adult ultrasonic vocalization (USV), and contextual fear conditioning.

Laboras

Long-term locomotion and behaviors of mice were recorded and analyzed using the Laboratory Animal Behavior Observation Registration and Analysis System (LABORAS^{TM}) by Metris. Mice without habitation to the behavioral booth or Laboras cages were put into Laboras cages where recordings were conducted for 96 consecutive hours. Laboras results were not validated by manual analyses because similar Laboras validations have been reported (Van de Weerd et al., 2001; Quinn et al., 2003; Quinn et al., 2006; Dere et al., 2015).

Open-Field Test

The open-field test was performed as described previously (Gould et al., 2009). A subject mouse was gently introduced into the center zone of the white acryl chamber (40 × 40 × 40 cm) and recorded of movements for 1 h. Locomotor activities and time spent in the center region (20 × 20 cm) of the open field arena were analyzed using EthoVision XT 10 (Noldus).

Novel Object Recognition Test

Novel object recognition memory (Antunes and Biala, 2012) was measured as follows. Briefly, after 1-h habituation in the white acryl chamber 1 day before the experimental day, the subject mouse was allowed to explore two objects of the same shape and material placed symmetrically in the center of the chamber for 10 min. Twenty-four hour later, one object was replaced by a novel object, and the subject mouse was allowed to explore the two objects (one novel and the other familiar) for 10 min. Exploration was defined as events in which the mouse sniffs the object within 1 cm distance or climbs up the object. Time spent in sniffing each object was analyzed by EthoVision XT 10 (Noldus) using the movies from the first 5 min to minimize saturation effects. Genotype comparisons were made using the discrimination index [time spent exploring novel object – time spent exploring familiar object)/(time spent exploring novel + familiar objects) * 100], as previously described (Stefanko et al., 2009; Vogel-Ciernia and Wood, 2014).

Repetitive Behaviors

Autism-relevant repetitive behaviors (Silverman et al., 2010) was measured as follows. The subject mice were allowed to freely move in a clean new home cage with bedding (∼60 lux). Time spent in digging and self-grooming during the 10-min session from a single recording was measured manually in a blind manner. Digging was defined as a mouse uses its head or forelimbs to dig out beddings. Self-grooming was defined as a mouse stroking or scratching its face or body area, or licking its body.

Three-Chamber Social Interaction Test

The three-chamber test, known to measure social approach and social novelty-recognition behavior (Moy et al., 2004; Nadler et al., 2004; Silverman et al., 2010), was performed as previously described (Lee et al., 2015). Briefly, the subject mice were isolated for 4 days before this assay. Three-chambered apparatus

(60 × 40 × 20 cm) consisted of the left, center, and right chamber with two entrances to the center chamber. Two empty containers were located in the corner of left and right chamber but not the center chamber. This assay consisted of three sessions. First, the subjects were allowed to freely explore all three chambers for 10 min. Second, the subject mouse was allowed to explore the containers with a stranger 1 (S1) or a novel object (O) for 10 min. Finally, the novel object was replaced with a stranger 2 (S2), and the subject mouse was allowed to explore S1 and S2 for 10 min. During the interval between each session, the subject was gently guided to the center chamber and the two entrances were blocked. Analysis of time spent in sniffing stranger/object was performed using EthoVision XT 10 (Noldus)

Elevated Plus-Maze Test

The EPM test (Pellow et al., 1985) was performed as follows. Briefly, the EPM apparatus, located 75 cm above the floor, consisted of two open arms (30 × 5 × 0.5 cm), two closed arms (30 × 5 × 30 cm), and a center zone with access to both arms. Light conditions were 180 lux for open arms and 20 lux for closed arms. A subject mouse was gently introduced into the center zone and allowed to move freely the open and closed arms for 8 min. Time spent in open/closed arms was measured using EthoVision XT 10 (Noldus).

Light-Dark Test

The light-dark test (Bourin and Hascoet, 2003) was performed as previously described (Ikeda et al., 1995) with minor modifications. Animals were placed in the light chamber with their heads toward the opposite wall from the dark chamber, and allowed to explore the light-dark apparatus (20 × 30 × 20 cm, 670 lux for light chamber, 20 × 13 × 20 cm, 5 lux for dark chamber), which has a 5-cm wide entrance between the two chambers. Time spent in the light chamber was analyzed using EthoVision XT 10 (Noldus).

Direct Social Interaction Test

Direct social interaction test was performed as described previously (Chung et al., 2015). Mice, which were isolated in their home cage for 4 days, were used in this assay. On the day of habituation, mice were individually habituated in gray acryl box (33 × 33 × 22 cm) for 10 min. On the day for experiments, two mice in the same genotype that never met each other previously were put into the habituated box and allowed to freely interact each other for 10 min while all behaviors were recorded. Time spent in interaction such as nose-to-nose sniffing, following, nose-to-tail sniffing, and other interactions such as body contacts and huddling were measured manually in a blind manner.

Courtship Adult Ultrasonic Vocalization

Courtship ultrasonic vocalizations (Portfors, 2007) was measured as follows. Male adult subject mice were socially isolated in their home cages for 4 days to allow them to recognize the cage as their own territory. Female adult stranger mice were group-caged prior to these experiments on the assumption that group housing might synchronize female cycles. A subject male mouse was habituated to a novel test cage for 5 min while recording its basal vocalizations in the absence of a female stranger. Next, a female stranger mouse was introduced into the subject's cage, and the two mice were allowed to interact freely with each other while recording courtship USVs of the subject mouse for 5 min. Because courtship USVs in the context of male-female encounters are mainly produced by males (Maggio and Whitney, 1985; Egnor and Seagraves, 2016), USVs were not categorized as arising from male or female mice. Avisoft SASLab Pro was used to analyze USVs.

Contextual Fear Conditioning and Extinction Test

Contextual fear conditioning and extinction (Phillips and LeDoux, 1992; Milad and Quirk, 2002) were measured as described previously (Lee et al., 2012). The fear conditioning test consisted of two sessions performed on consecutive days. On day 1, subject mice were introduced to the conditioning box and allowed to freely explore the environment for 120 s, and then received a series of 0.8 mA electric foot shocks (1 s; without associated auditory cue) for five times at intervals of 120 s. After the last shock the mice were left in the box for an additional 120 s, making the total experimental time 12 min. On day 2, the mice were placed in the same conditioning box and allowed to freely explore for 10 min without any stimuli, and the freezing levels of the mice on the test day (day 2) were quantified for the first 3 min. These mice, which were tested for 24-h fear memory, were exposed to the same context for 5 min to measure fear extinction every day during the following 7 days (days 3–9). All freezing behaviors were recorded and analyzed using FreezeFrame software (Coulbourn Instruments).

Hot Plate Test

Hot plate test was performed as previously described (Ankier, 1974) with minor modifications. The subject mice were placed in the clear acryl chamber (10 × 10 × 15 cm), which was located on an aluminum heat controller (Sun Electronics Co.) maintained at 50–51°C. Times taken for the animals to lick their fore-/hindpaws or to jump were measured.

Von Frey Test

The von Frey test was performed according to the standard operating procedures of the Jackson Laboratory Mouse Neurobehavioral Phenotyping Facility (JAX-MNBF). The von Frey test apparatus consisted of a wire floor grid and a clear observation arena with aerated lids (Stoelting Co.). A subject mouse was gently introduced in the observation arena and habituated for 1 h until the activity levels become low. Beginning with the left hind paw, stimuli of von Frey filaments (Stoelting Co.) were presented perpendicularly to the plantar surface of the hind paws of the subject mice for two trials. The initial stimulus started with a von Frey filament with 0.4 g bending force. When there is a withdrawal response, the strength of the stimulus was gradually decreased to lower bending forces (0.16 to 0.02 g), while the stimulus was increased to a higher bending force (0.6 g) when there was no response. The minimum threshold required to induce a withdrawal response for left and right paws was recorded. A withdrawal response is defined as the mouse lifting up their hind paws when a filament is pushed with increasing

pressure until it bends. All experimental procedures and analysis were performed in a double-blinded manner.

Electrophysiology

Male or female mice were used for electrophysiological measurements (details are described in figure legends). After anesthetization with isoflurane, mouse brains were removed, and sagittal sections (300 μm) including hippocampus or striatum were prepared using a Vibratome (Leica VT 1200S) in ice-cold section buffer (in mM: 212 sucrose, 25 $NaHCO_3$, 5 KCl, 1.25 NaH_2PO_4, 10 D-glucose, 1.2 L-ascorbic acid, 2 Na-pyruvate, 3.5 $MgSO_4$, 0.5 $CaCl_2$). Slices were maintained in artificial cerebrospinal fluid (ACSF) (in mM: 124 NaCl, 25 $NaHCO_3$, 10 glucose, 2.5 KCl, 1 NaH_2PO_4, 2.5 $CaCl_2$, 1.25 $MgCl_2$) bubbled with 95% O_2 and 5% CO_2 for 30 min at 32°C followed by incubation for 30 min at room temperature. For mEPSC measurements, ACSF contained tetrodotoxin (0.5 μM) and picrotoxin (60 μM). Whole-cell recordings of pyramidal neurons in the hippocampal CA1 region were performed using a recording pipette filled with internal solution (in mM: 100 $CsMeSO_4$, 10 TEA-Cl, 8 NaCl, 10 HEPES, 5 QX-314-Cl, 2 Mg-ATP, 0.3 Na-GTP and 10 EGTA with pH 7.25, 295 mOsm). For mIPSC measurement, ACSF contained tetrodotoxin (0.5 μM), NBQX (10 μM), and AP5 (50 μM). Whole-cell recordings of pyramidal neurons in the hippocampal CA1 region were performed with a recording pipette filled with internal solution (in mM: 115 CsCl, 10 TEA-Cl, 8 NaCl, 10 HEPES, 5 Qx-314-Cl, 4 Mg-ATP, 0.3 Na-GTP, 10 EGTA with pH 7.35, 295 mOsm). For neuronal excitability measurement, ACSF contained picrotoxin (60 μM), NBQX (10 μM), and AP5 (50 μM). Whole-cell recordings in pyramidal neurons in the hippocampus CA1 region were performed with a recording pipette filled with internal solution (in mM: 137 K-gluconate, 5 KCl, 10 HEPES, 0.2 EGTA, 10 Na_2-phosphocreatine, 4 Mg-ATP, 0.5 Na-GTP with pH 7.2, 280 mOsm). First minimal currents were introduced to hold the membrane potential around −70 to −75 mV in a current clamp mode. To evoke depolarizing voltage sag responses, increasing amounts of depolarizing step currents (by 10 pA, −150 to 20 pA) were injected. Then, to elicit action potentials, increasing amounts of depolarizing currents (0 to 330 pA) were injected in a stepwise manner. Input resistance was calculated as the linear slope of current-voltage plots generated from a series of increasing current injection steps. The sag ratio was determined as the ratio of a steady state value to repolarized peak at the entire length of injected current at each step. The synaptic responses were amplified (Multiclamp 700B, Molecular Devices) and digitized (Digidata 1550, Molecular Devices) for analyses. mE/IPSCs were analyzed using Clamfit 10.4 software and horizontally spread-out currents where the high noise levels that are visible in horizontally compressed currents do not inhibit accurate analyses of the currents.

Electroencephalography

Electroencephalography (EEG) recording was performed as previously described with minor modifications (Lee et al., 2018). An EEG driver was composed of a small header pin connector socket (Hirose Electric, H2021-ND) connected with six stainless steel screws (1 mm × 3 mm) through soldered coated stainless steel wire. All screws were implanted on the skull (two for bilateral frontal, +1.8 mm AP, ±1.0 mm ML; two for bilateral parietal, −2.0 mm AP and ±1.8 mm ML; two for animal ground and reference, −1.0 mm AP and ±1.0 mm ML from lambda). After recovery 1 week after the surgery, EEG recordings were performed using a Cheetah Data Acquisition System (Neuralynx). The subject mice were allowed to freely move around in a white acryl box (25 × 25 × 35 cm) with synchronized video recording. After 20-min habituation in the box, EEGs were recorded for 40 min. EEG data were analyzed using a customized MATLAB code. Baseline EEGs were analyzed using 5-min serial samplings, and the total power spectral density (PSD) was averaged per mouse by applying Fast Fourier Transform (FFT). EEG frequency ranges were defined as follows; Delta, 0–4 Hz; theta, 4–12 Hz; alpha, 12–30 Hz; low gamma, 30–80 Hz; high gamma, 80–130 Hz.

PTZ-Induced Seizure Susceptibility

To determine the susceptibility of mice to PTZ-induced seizures, we performed the experiments using mice that did not receive EEG driver surgery for cleaner results. After intraperitoneal injection of PTZ (Sigma; 50 mg/kg), subject mice were placed in a clean new home cage. Video recordings for 20 min were used to analyze seizure stages defined as follows; stage 1, behavioral arrest; stage 2, myoclonic (jerk) seizures; stage 3: general tonic-clonic seizures, as previously described (Naydenov et al., 2014). The seizure susceptibility score was defined as follows; 0.2 × (latency to stage 1) + 0.3 × (latency to stage 2) + 0.5 × (latency to stage 3).

Statistical Analysis

All behavioral, biochemical, and electrophysiological experiments were performed by researchers blinded to the experimental conditions. Statistical analyses were performed using GraphPad Prism 7 and MATLAB. Data sets, after removal of outliers, were analyzed for significance using unpaired two-tailed Student's *t*-test, Mann–Whitney *U*-test, one-sample *t*-test, log-rank test, and two-way analysis of variance (ANOVA) with *post hoc* multiple comparisons test when appropriate. The n values and statistical significance values are indicated in figure legends. Statistical significance values are indicated as follows in the figures: $^{*}P < 0.05$; $^{**}P < 0.01$; $^{***}P < 0.001$; ns, not significant. Additional statistical details and results, as well as information on sex, age and numbers of mice used, are presented in **Supplementary Table S1**.

RESULTS

Molecular Modeling of the Shank3 Q321R Mutation

The Q321R mutation in the *SHANK3* gene (Moessner et al., 2007), which strongly influences the synaptic targeting of Shank3 and the development and function of dendritic spines and excitatory synapses (Durand et al., 2012), is located in the

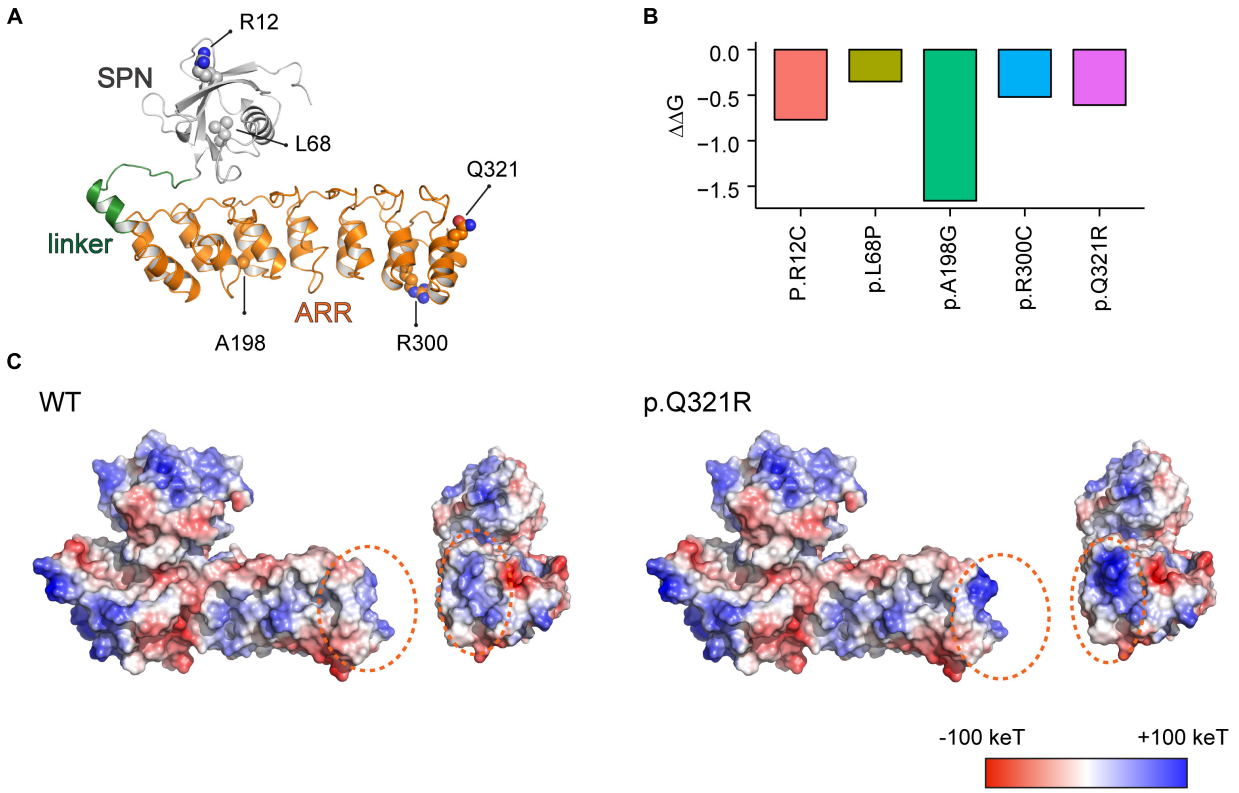

FIGURE 1 | Molecular modeling-based predictions of protein stability and surface charge distribution in SPN-ARR domains of the Shank3 protein harboring Q321R and other ASD-risk mutations. **(A)** Structure of the SPN and ARR domains of the Shank3 protein (PDB ID: 5G4X), with the locations of amino acid residues mutated in autistic individuals (R12C, L68P, A198G, R300C, and Q321R) indicated. The SPN domain, the linker connecting the SPN and ARR domains, and the ARR domain of Shank3 are indicated in gray, green, and orange colors, respectively, as a ribbon diagram. The ASD-risk residues are indicated by ball-and-stick models. **(B)** Stability predictions of SPN and ARR domains of the Shank3 protein containing the indicated ASD-risk mutations, obtained using I-Mutant 2.0 software. A negative predicted free energy change (ΔΔG, in kcal/mol) indicates a decrease in the stability of the mutant protein. **(C)** Electrostatic surface charge distribution patterns in WT and mutant (Q321R) SPN and ARR domains of the Shank3 protein. Negative and positive surface charges are indicated in red and blue, respectively. Hydrophobic surfaces are indicated in white. Surface areas with the Shank3 Q321R mutation are indicated by dotted orange circles.

ARR domain of the protein. The ARR domain of Shank3 has been shown to interact with the N-terminal SPN domain of Shank3 in an intramolecular manner, leading to suppression of the binding of the ARR domain to Sharpin and α-fodrin (Mameza et al., 2013). These results suggest the possibility that these intra- and intermolecular interactions of the SPN and ARR domains of Shank3 might underlie the effects of the Q321R mutation.

Using the recently reported X-ray crystal structure of the N-terminal SPN and ARR domains of Shank3 (Lilja et al., 2017), we attempted molecular modeling of the SPN and ARR domains harboring the Q321R mutation to determine whether the mutation could interfere with the interaction between these two domains (**Figure 1A**). We also included the following additional ASD-risk Shank3 mutations in SPN and ARR domains in our modeling (Durand et al., 2007; Moessner et al., 2007; Gauthier et al., 2010): L68P, which disrupts the interaction between the SPN and ARR domains and enhances the interactions of the ARR with Sharpin (Mameza et al., 2013); R12C, which affects excitatory synapse structure and function (Durand et al., 2012) and disrupts SPN binding to GTP-bound Ras and Rap small GTPases to suppress integrin signaling (Lilja et al., 2017); and R300C, which affects excitatory synapse structure and function (Durand et al., 2012).

We found that the Q321R mutation, unlike the L68P mutation, is located in the C-terminal region of the ARR domain, away from the interface of the SPN and ARR domains, and thus is unlikely to affect the SPN-ARR interaction (**Figure 1A**). We next tested whether these mutations affect the stability of SPN and ARR domains by calculating changes in free energy. All five mutations, including the Shank3 Q321R mutation, induced significant decreases in the stability of the protein, with the A198G mutation exerting the strongest effect (**Figure 1B**), although the impact of the A198G mutation has not been explored in previous *in vitro* studies (Durand et al., 2012; Mameza et al., 2013). In addition, an analysis of surface charge distribution indicated that the Q321R mutation induces a substantial increase in the local positive charge density (**Figure 1C**). These results suggest that the Q321R mutation is less likely to affect the intramolecular SPN-ARR interaction, but more likely to affect the protein stability or intermolecular interactions of Shank3.

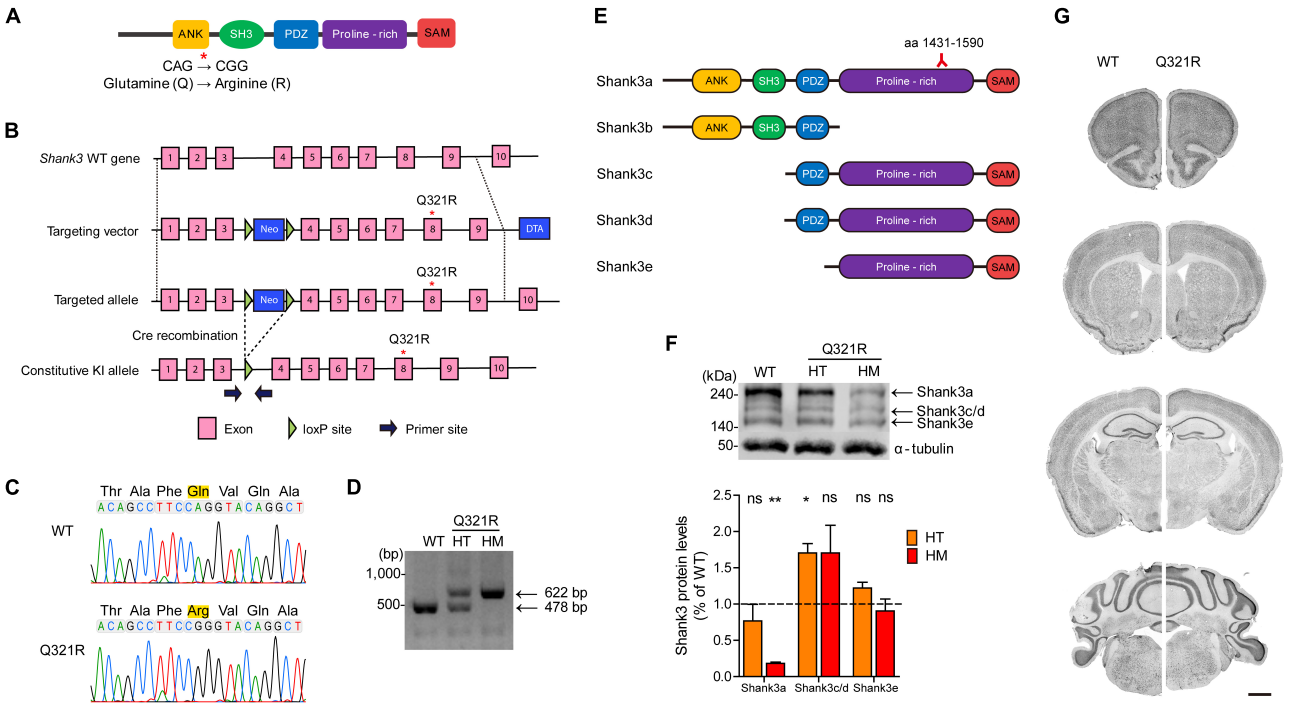

FIGURE 2 | Generation and characterization of *Shank3*^{Q321R} mice. **(A)** A schematic diagram showing the location of the Shank3 Q321R mutation in the Shank3 protein. Ank, ankyrin repeat region; SH3, Src homology 3 domain; PDZ, PSD-95/Dlg/ZO-1 domain; Proline-rich, proline-rich region; SAM, sterile alpha motif domain. **(B)** A schematic diagram showing the gene-targeting strategy used to generate *Shank3*^{Q321R} mice. Note that the mutated codon corresponding to the Q321R mutation is located in exon 8 of the *Shank3* gene. Primers (forward and reverse) for PCR genotyping are indicated. Neo, neomycin resistance; DTA, diphtheria toxin. **(C)** Confirmation of the *Shank3*^{Q321R} mutation by genomic DNA sequencing of *Shank3*$^{Q321R/Q321R}$ mice. Results from a wild-type (WT) mouse are shown for comparison. **(D)** PCR genotyping of *Shank3*$^{Q321R/Q321R}$ (HM/homozygous) and *Shank3*$^{+/Q321R}$ (HT/heterozygous) mice. **(E)** Known Shank3 protein variants. The target region (aa 1431–1590) of the Shank3 antibody used in the immunoblot analysis **(F)** is indicated. **(F)** The levels of Shank3a, but not Shank3c/d or Shank3e, protein variants, are substantially decreased in whole-brain lysates from WT and *Shank3*$^{Q321R/Q321R}$ and *Shank3*$^{+/Q321R}$ mice (2 months; female), as determined by immunoblot analysis using Shank3-specific antibodies targeting amino acids 1431–1590 in the proline-rich region of the protein that can detect all three protein splice variants. $n = 3$ mice (WT, HT, and HM), $^{*}P < 0.05$, $^{**}P < 0.01$, ns, not significant, One sample *t*-test. **(G)** Normal gross morphology of the brains of WT and homozygous *Shank3*$^{Q321R/Q321R}$ mice (2 months; female), as shown by immunostaining of coronal sections for the neuronal marker, NeuN. Scale bar, 1 mm.

Generation and Characterization of *Shank3*^{Q321R} Mice

To determine *in vivo* impacts of the Shank3 Q321R mutation, we generated a new knock-in (KI) mouse line carrying this mutation (*Shank3*^{Q321R} mice) (**Figures 2A,B**). DNA sequencing confirmed the *Shank3*^{Q321R} mutation (**Figure 2C**), and wild-type (WT) and *Shank3*^{Q321R} mice (heterozygous *Shank3*$^{+/Q321R}$ and homozygous *Shank3*$^{Q321R/Q321R}$) were detected by polymerase chain reaction (PCR) genotyping (**Figure 2D**).

The mutated codon corresponding to the Shank3 Q321R mutation is located in exon 8 of the *Shank3* gene, which encodes the C-terminal region of the ARR domain of the Shank3 protein. Therefore, among the multiple variants of the Shank3 protein, Shank3a and Shank3b, containing the ARR domain (**Figure 2E**), would be most strongly affected compared with ARR-lacking Shank3c/d/e variants (Lim et al., 1999; Maunakea et al., 2010; Wang et al., 2011, 2014; Waga et al., 2014; Zhu et al., 2014). Indeed, the levels of Shank3a, the longest (∼240 kDa) variant, which is readily detected by an antibody targeting the proline-rich region (aa 1431–1590), were significantly decreased (by ∼18%) in homozygous *Shank3*$^{Q321R/Q321R}$ brains (**Figure 2F**), in line with the predicted destabilization of the Shank3 protein noted above. Detection of Shank3b protein, which lacks a large portion of the proline-rich region, was not possible because the antibody used targets the proline-rich region. In heterozygous *Shank3*$^{+/Q321R}$ brains, Shank3a levels were comparable to those in WT mice, indicative of less severe protein degradation of the mutant Shank3 protein in the heterozygous *Shank3*-mutant brain.

Shank3$^{Q321R/Q321R}$ and *Shank3*$^{+/Q321R}$ mice were born in the expected Mendelian ratios. In addition, *Shank3*$^{Q321R/Q321R}$ mice displayed no detectable abnormalities in the size or gross morphology of the brain, as shown by staining for the neuronal marker, NeuN (**Figure 2G**).

Suppressed Neuronal Excitability in Homozygous *Shank3*$^{Q321R/Q321R}$ Hippocampal CA1 Pyramidal Neurons

To determine the effect of the Shank3 Q321R mutation on synaptic transmission and neuronal excitability, we first measured spontaneous synaptic transmission in the hippocampus, a brain region implicated in ASD (Amaral et al., 2008). The frequency and amplitude of miniature excitatory

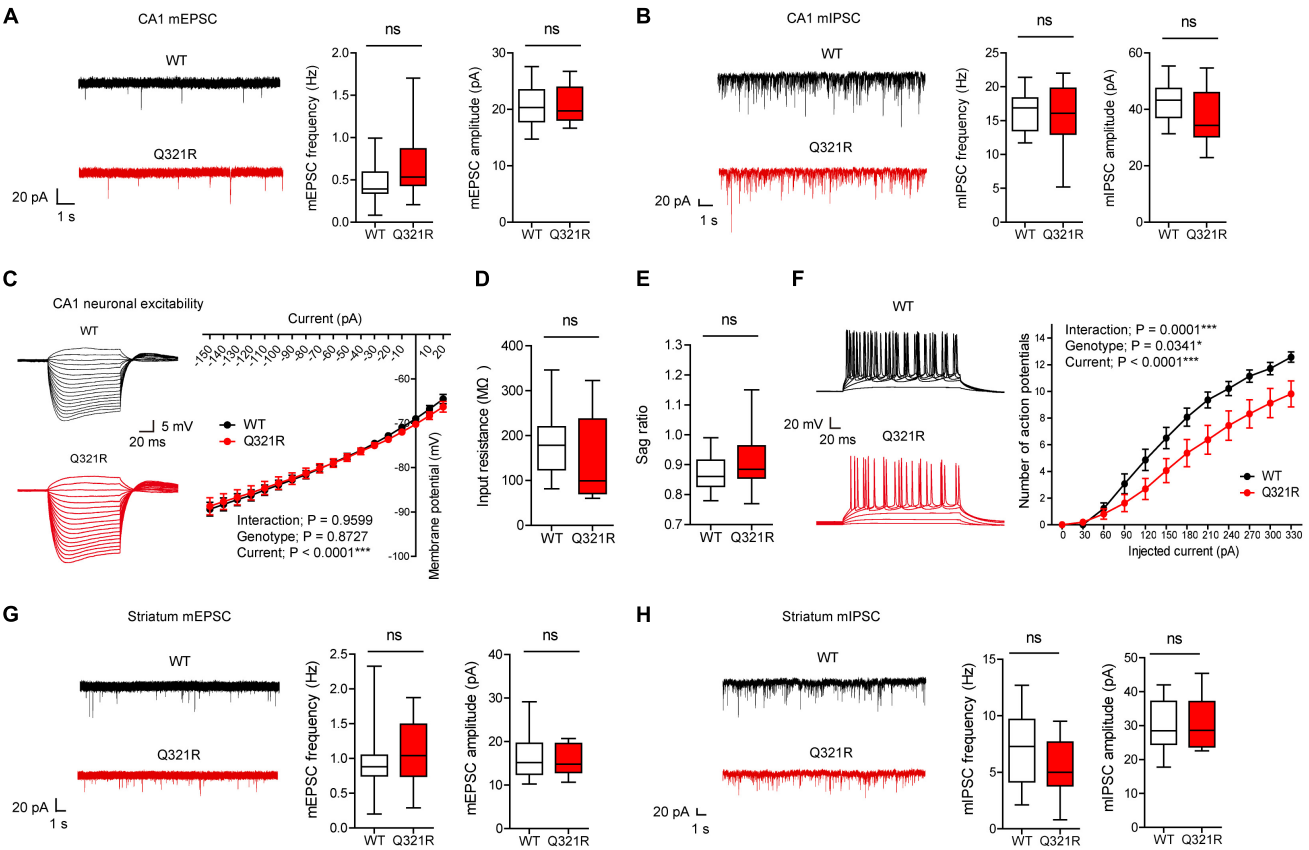

FIGURE 3 | Suppressed neuronal excitability but normal mEPSCs and mIPSCs in hippocampal CA1 pyramidal neurons from male *Shank3*$^{Q321R/Q321R}$ mice. **(A)** Normal mEPSC frequency and amplitude in CA1 pyramidal neurons in the hippocampus of male *Shank3*$^{Q321R/Q321R}$ mice (P21–25). The indicated values represent means ± SEM. *n* = 14 neurons from 3 mice (WT) and 15 neurons from 3 mice (Q321R), ns, not significant, Mann–Whitney *U*-test (for frequency) and Student's *t*-test (for amplitude). **(B)** Normal mIPSC frequency and amplitude in CA1 pyramidal neurons in the hippocampus of male *Shank3*$^{Q321R/Q321R}$ mice (P21–25). *n* = 12 neurons from 5 mice (WT) and 13 neurons from 3 mice (Q321R), ns, not significant, Student's *t*-test (for frequency) and Student's *t*-test (for amplitude). **(C–F)** Suppressed neuronal excitability in hippocampal CA1 pyramidal neurons from male *Shank3*$^{Q321R/Q321R}$ mice (P22–26), as shown by the number of action potential fired plotted against injected currents **(F)**. Note that the current-voltage relationship **(C)**, input resistance **(D)**, and Sag ratio **(E)** were not changed. *n* = 14 neurons from 5 mice (WT) and 16 neurons from 4 mice (Q321R), $^{*}P < 0.05$, $^{***}P < 0.001$, ns, not significant, repeated measures two-way ANOVA (for current-membrane potential and current-firing curves) and Mann–Whitney *U*-test (for input resistance and sag ratio). **(G)** Normal mEPSC frequency and amplitude in dorsolateral striatal neurons from male *Shank3*$^{Q321R/Q321R}$ mice (P28–43). *n* = 16 neurons from 4 mice (WT) and 16 neurons from 5 mice (Q321R), ns, not significant, Mann–Whitney *U*-test (for frequency) and Student's *t*-test (for amplitude). **(H)** Normal mIPSC frequency and amplitude in dorsolateral striatal neurons from male *Shank3*$^{Q321R/Q321R}$ mice (P28–43). *n* = 16 neurons from 6 mice (WT) and 17 neurons from 7 mice (Q321R), ns, not significant, Student's *t*-test (for frequency) and Mann–Whitney *U*-test (for amplitude).

postsynaptic currents (mEPSCs) in CA1 pyramidal neurons from the hippocampus of homozygous *Shank3*$^{Q321R/Q321R}$ mice (P21–25; male) were comparable to those from WT neurons (**Figure 3A**). Similarly, the frequency and amplitude of miniature inhibitory postsynaptic currents (mIPSCs) were normal in hippocampal CA1 pyramidal neurons from male *Shank3*$^{Q321R/Q321R}$ mice (P21–25; male) (**Figure 3B**).

When female mice were tested for mEPSCs and mIPSCs, the frequency, but not amplitude, of mIPSCs was increased in CA1 pyramidal neurons (P22–26), whereas mEPSC frequency and amplitude in these neurons (P21–27) were normal (**Supplementary Figures S1A,B**). Given that Shank proteins are mainly present at excitatory, but not inhibitory, synapses (Boeckers et al., 1999; Naisbitt et al., 1999; Tu et al., 1999; Yao et al., 1999; Bockmann et al., 2002; Heise et al., 2016), these results likely represent a secondary change rather than the direct consequence of *Shank3* deletion in pyramidal neurons.

We next measured the neuronal excitability of CA1 pyramidal neurons from *Shank3*$^{Q321R/Q321R}$ mice (P22–26; male). Neuronal excitability was decreased, as evidenced by the relationship between the amount of injected current and the number of action potentials fired, but the current-voltage relationship, input resistance, and Sag ratio were normal (**Figures 3C–F**). These results collectively suggest that the Shank3 Q321R mutation suppresses neuronal excitability in male CA1 pyramidal neurons, which would suppress the output function of these neurons.

In addition to the hippocampus, we measured mEPSCs and mIPSCs in the striatum, a brain region strongly implicated in the pathophysiology of Shank3-related autistic-like phenotypes in mice (Peca et al., 2011; Peixoto et al., 2016; Lee et al., 2017).

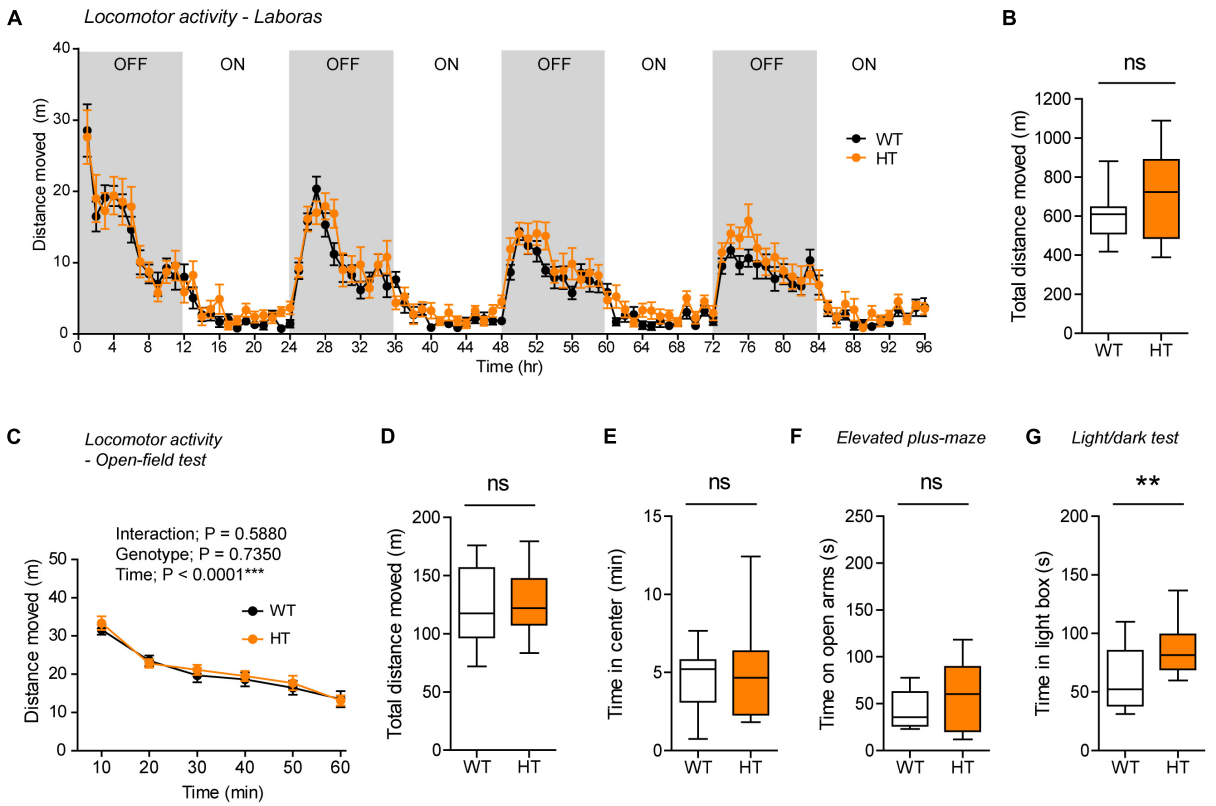

FIGURE 4 | Normal locomotor activity and moderate anxiolytic-like behavior in heterozygous *Shank3*$^{+/Q321R}$ mice. **(A,B)** Normal locomotor activity in *Shank3*$^{+/Q321R}$ mice (2–3 months; male) in Laboras cages, where locomotor activity was measured together with other movements for four consecutive days in the absence of habituation. OFF/ON, light-off/on. n = 13 mice (WT) and 13 mice (HT), ns, not significant, two-way ANOVA (genotype main effect p-value = 0.1813 in **A**), and Student's t-test **(B)**. **(C,D)** Normal locomotor activity in *Shank3*$^{+/Q321R}$ mice (2–3 months; male) in the open-field test, as shown by the distance moved. n = 13 mice (WT) and 13 mice (HT), ns, not significant, repeated measures two-way ANOVA **(C)** and Student's t-test **(D)**. **(E)** Normal anxiety-like behavior in *Shank3*$^{+/Q321R}$ mice (2–3 months; male) in the open-field test, as shown by the time spent in the center region of the open-field arena. n = 13 mice (WT) and 13 mice (HT), ns, not significant, Mann–Whitney U-test. **(F)** Normal anxiety-like behavior in *Shank3*$^{+/Q321R}$ mice (2–3 months; male) in the elevated plus-maze test, as shown by the time spent in the open arms of the maze. n = 13 mice (WT) and 13 mice (HT), ns, not significant, Welch's t-test. **(G)** Anxiolytic-like behavior in *Shank3*$^{+/Q321R}$ mice (2–3 months; male) in the light-dark test, as shown by the time spent in the light chamber of the light-dark apparatus. n = 13 mice (WT) and 12 mice (HT), $^{**}P < 0.01$, Student's t-test.

We found that the frequency and amplitude of mEPSCs in dorsolateral striatal neurons in *Shank3*$^{Q321R/Q321R}$ mice (P28–43; male) were normal (**Figure 3G**). In addition, mIPSC frequency and amplitude were normal in these neurons (P28–43; male) (**Figure 3H**). These results suggest that the *Shank3* Q321R homozygous mutation does not affect spontaneous excitatory or inhibitory synaptic transmission in the dorsolateral striatum in male mice.

Normal Locomotion and Moderate Anxiolytic-Like Behavior in Heterozygous *Shank3*$^{+/Q321R}$ Mice

To determine the behavioral impacts of the Shank3 Q321R mutation, we next subjected *Shank3*$^{+/Q321R}$ and *Shank3*$^{Q321R/Q321R}$ mice to a battery of behavioral tests. Previous studies on *Shank3*-mutant mice have shown that *Shank3* heterozygosity can lead to ASD-related behavioral abnormalities (Bozdagi et al., 2010; Yang et al., 2012; Duffney et al., 2015; Jaramillo et al., 2016, 2017). We thus first analyzed behavioral abnormalities in heterozygous *Shank3*$^{+/Q321R}$ mice.

Continuous monitoring of mouse movements for four consecutive days in Laboras cages, representing a familiar environment, revealed that *Shank3*$^{+/Q321R}$ mice have normal locomotor activity compared with WT mice (**Figures 4A,B**). Similarly, *Shank3*$^{+/Q321R}$ mice displayed normal locomotor activity in the open-field test, a novel environment (**Figures 4C,D**). These results suggest that locomotor activities in both familiar and novel environments are not affected by the heterozygous Shank3 Q321R mutation.

Shank3$^{+/Q321R}$ and WT mice spent comparable amounts of time in the center region of the open-field arena (**Figure 4E**). In addition, *Shank3*$^{+/Q321R}$ mice spent normal amounts of time in the open arms of the EPM (**Figure 4F**). In contrast, these mice spent more time in the light chamber of the light-dark apparatus (**Figure 4G**). Together, these results suggest that the heterozygous Shank3 Q321R mutation leads to moderate anxiolytic-like behavior but does not affect locomotor activity.

Normal Social Interaction, Moderately Enhanced Social Communication and Self-Grooming, and Suppressed Digging in Heterozygous *Shank3*$^{+/Q321R}$ Mice

Shank3$^{+/Q321R}$ and WT mice showed comparable levels of social approach in the three-chamber test, as shown by time spent sniffing social and object targets (**Figure 5A**). Social novelty recognition could not be assessed because WT mice failed to recognize a novel stranger mouse. In tests for USVs in adult male mice encountering a novel female mouse (courtship USVs), *Shank3*$^{+/Q321R}$ mice emitted normal numbers of USVs, but the mean duration of each call was increased (**Figure 5B**), indicative of a moderate and abnormal increase in social communication.

In tests for repetitive behaviors, *Shank3*$^{+/Q321R}$ mice displayed enhanced self-grooming and suppressed digging in novel home cages with bedding (10 min; ∼60 lux) (**Figures 5C,D**), suggesting that the suppressed digging might result from the enhanced self-grooming. However, long-term (96-h) monitoring of behavior in Laboras cages showed that *Shank3*$^{+/Q321R}$ mice exhibit normal self-grooming during the first 10 min, the first 1 or 12 h, the entire session (96 h), and during light-off and light-on periods (48 h each) (**Figures 5E–I**). These results collectively suggest that the heterozygous Shank3 Q321R mutation does not affect social approach, moderately enhances social communication and self-grooming, and suppresses digging in mice.

Homozygous *Shank3*$^{Q321R/Q321R}$ Mice Show Behaviors That Are Largely Similar to Those Observed in Heterozygous *Shank3*$^{+/Q321R}$ Mice

To test whether there are any dose-dependent effects of the Shank3 Q321R mutation on mouse behaviors, we subjected homozygous *Shank3*$^{Q321R/Q321R}$ mice to a battery of behavioral tests that were used for heterozygous *Shank3*$^{+/Q321R}$ mice. *Shank3*$^{Q321R/Q321R}$ mice showed normal levels of locomotor activity in Laboras cages and in the open-field test (**Figures 6A–D**). In addition, these mice showed moderately increased anxiolytic-like behaviors, as shown by normal levels of center time in the open-field test but increased open-arm time in the EPM and increased light-box time in the light-dark test (**Figures 6E–G**), similar to heterozygous *Shank3*$^{+/Q321R}$ mice.

Social behavior was normal in homozygous *Shank3*$^{Q321R/Q321R}$ mice, as shown by the three-chamber test (**Figure 7A**), similar to heterozygous *Shank3*$^{+/Q321R}$ mice. Again, social novelty recognition could not be assessed because WT mice failed to recognize a novel stranger mouse. *Shank3*$^{Q321R/Q321R}$ and WT mice showed comparable levels of social interaction in the direct social interaction test, as shown by the total time spent interacting with an age- and sex-matched male stranger mouse (**Figure 7B**).

Homozygous *Shank3*$^{Q321R/Q321R}$ mice displayed normal courtship USVs, as shown by the number of USV calls as well as the duration of each USV calls (**Figure 7C**), partly similar to heterozygous *Shank3*$^{+/Q321R}$ mice that displayed a normal number of courtship USV calls but increased duration of each USV calls. Lastly, homozygous *Shank3*$^{Q321R/Q321R}$ mice displayed increased self-grooming and decreased digging in novel home cages with bedding (10 min) (**Figures 7D,E**), but normal Laboras-cage self-grooming (**Figures 7F–J**), largely similar to heterozygous *Shank3*$^{+/Q321R}$ mice.

Because the differences between novel home-cage and Laboras-cage environments, where both *Shank3*$^{+/Q321R}$ and *Shank3*$^{Q321R/Q321R}$ mice showed positive and negative repetitive self-grooming, respectively, include the novelty of the space (less novel in new home cages and more novel in Laboras cages) and the light intensity (bright light in home cages and complete darkness in Laboras cages). To differentiate these factors, we first tested a new condition, novel home-cage environment without light, and, intriguingly, could not observe enhanced self-grooming in *Shank3*$^{Q321R/Q321R}$ mice (**Supplementary Figure 2A**), suggesting that the presence of light is important. However, the presence of light in Laboras cages did not enhance self-grooming in *Shank3*$^{Q321R/Q321R}$ mice during the first 10 min (**Supplementary Figure 2B**), similar to the results from Laboras cages without light. Furthermore, the presence of light in a novel open-field arena did not enhance self-grooming in *Shank3*$^{Q321R/Q321R}$ mice (**Supplementary Figure 2C**). These results indicate that self-grooming in *Shank3*$^{Q321R/Q321R}$ mice is enhanced selectively in novel home cages in the presence of light. In addition, these results suggest that novelty of space/environment *per se* is not important, but, rather, an increase in stress associated with the light in novel home cages (but not in other environments) strongly enhances self-grooming in *Shank3*$^{Q321R/Q321R}$ mice.

Together, these results suggest that homozygous *Shank3*$^{Q321R/Q321R}$ mice show behavioral abnormalities that are largely similar to those observed in heterozygous *Shank3*$^{+/Q321R}$ mice such as moderately enhanced anxiolytic-like behavior and self-grooming, although there were minor differences in a sub-parameter of USVs (duration of each USV calls). In addition, the largely similar behaviors of *Shank3*$^{+/Q321R}$ and *Shank3*$^{Q321R/Q321R}$ mice suggest that there is no strong dose-dependent effect of the Shank3 Q321R mutation on mouse behaviors.

Normal Novel Object-Recognition and Contextual Fear Memory in Homozygous *Shank3*$^{Q321R/Q321R}$ Mice

In the novel object–recognition test, in which a mouse is exposed to two identical objects on day 1 and then to one original object and a new object on day 2, *Shank3*$^{Q321R/Q321R}$ and WT mice showed similar discrimination index scores for the novel object (**Figure 8A**), indicative of normal object-recognition memory in the mutant mice.

In the contextual fear-conditioning test, *Shank3*$^{Q321R/Q321R}$ mice showed normal acquisition of fear memory on the training day (day 1) (**Figure 8B**). Twenty-four hours later (day 2), *Shank3*$^{Q321R/Q321R}$ and WT mice showed comparable levels of freezing in the same context, suggestive of normal retrieval of contextual fear memory. When these mice were subsequently exposed to the same context every day for seven consecutive

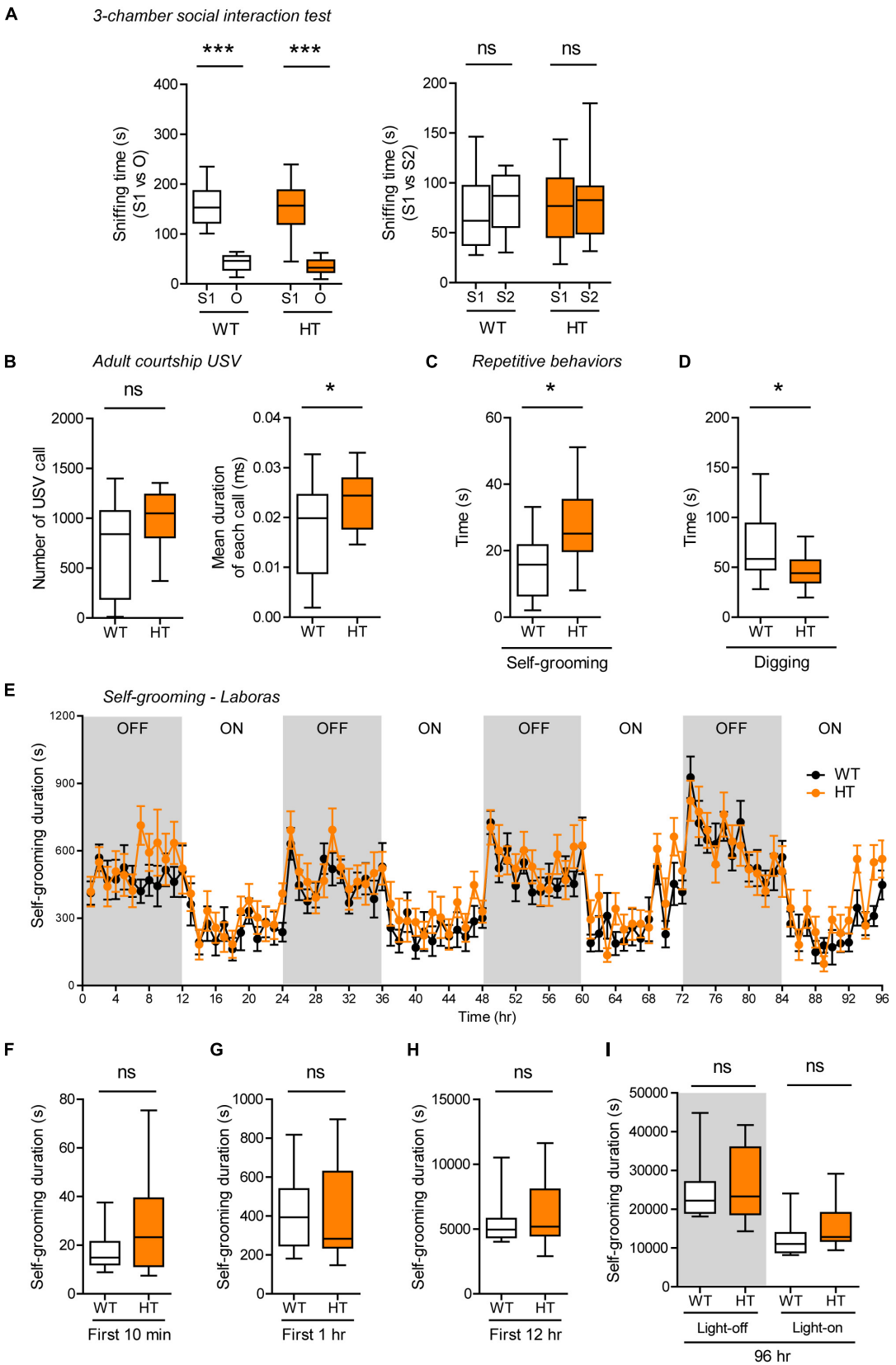

FIGURE 5 | Continued

FIGURE 5 | Normal social interaction, moderately enhanced social communication and self-grooming, and suppressed digging in heterozygous *Shank3*$^{+/Q321R}$ mice. **(A)** Normal social approach in *Shank3*$^{+/Q321R}$ mice (2–3 months; male) in the three-chamber test, as shown by time spent sniffing. S1, a stranger; O, object; S2, new stranger. Social novelty recognition, measured by the preference for new stranger (S2) over old stranger (S1), could not be determined due the lack of normal social novelty recognition in WT mice. n = 10 mice (WT), 13 mice (HT), ***$P < 0.001$, ns, not significant, Welch's t-test, Mann–Whitney U-test, and Student's t-test. **(B)** Moderately increased courtship USVs emitted by *Shank3*$^{+/Q321R}$ mice (2–3 months; male) upon encounter with a novel female stranger, as shown by the normal number of USVs but increased mean duration of each USV calls. n = 12 mice (WT), 12 mice (HT), *$P < 0.05$, ns, not significant, Student's t-test. **(C)** Enhanced self-grooming in *Shank3*$^{+/Q321R}$ mice (2–3 months; male) in home cages with bedding (10 min), as shown by total self-grooming time. n = 12 mice (WT), 13 mice (HT), *$P < 0.05$, Student's t-test. **(D)** Suppressed digging in *Shank3*$^{+/Q321R}$ mice (2–3 months; male) in home cages with bedding (10 min), as shown by total digging time. n = 12 mice (WT), 13 mice (HT), *$P < 0.05$, Welch's t-test. **(E–I)** Normal self-grooming in *Shank3*$^{+/Q321R}$ mice (2–3 months; male) in Laboras cages, as shown by total self-grooming duration. n = 13 mice (WT), 13 mice (HT), ns, not significant, two-way ANOVA (genotype main effect p-value = 0.4087 in **E**), Mann-Whitney test **(F,H,I)**, Student's t-test **(G)**.

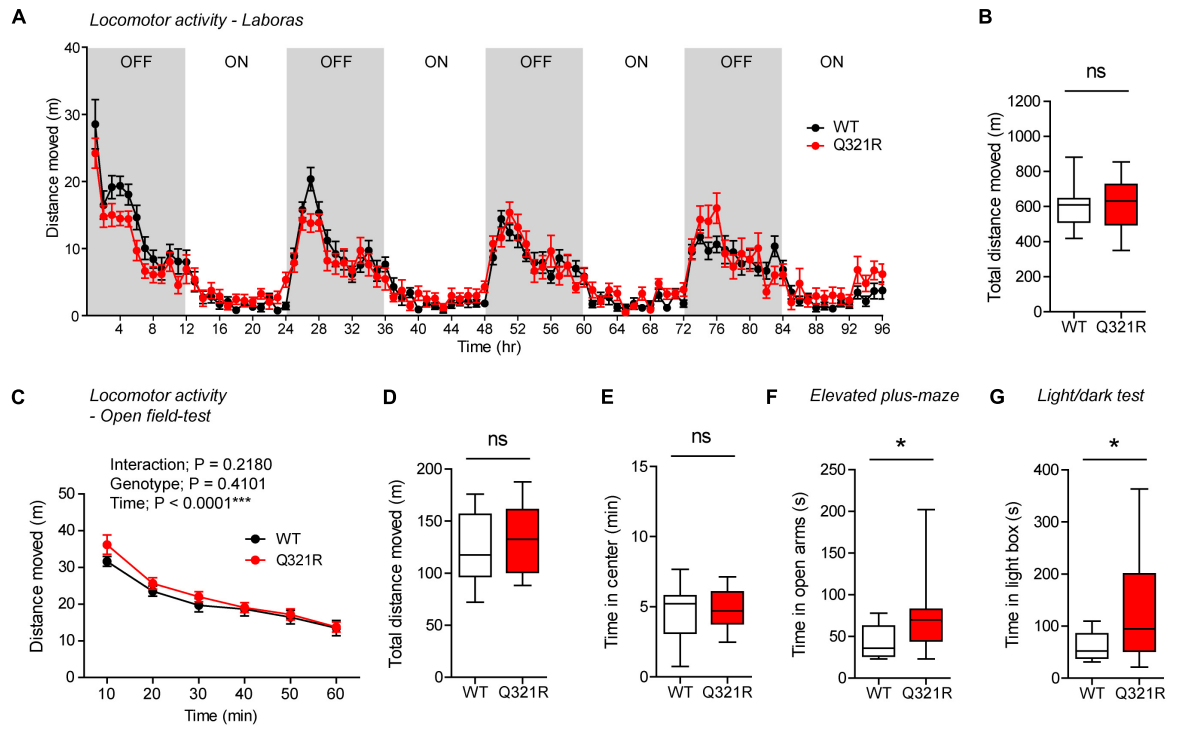

FIGURE 6 | Normal locomotor activity and moderate anxiolytic-like behavior in homozygous *Shank3*$^{Q321R/Q321R}$ mice. **(A,B)** Normal locomotor activity in *Shank3*$^{Q321R/Q321R}$ mice (2–4 months; male), in Laboras cages, where locomotor activity was measured together with other movements for four consecutive days in the absence of habituation. Note that the WT data in this panel and other panels in this figure are identical to those shown in **Figure 4** because WT, heterozygous, and homozygous mice were tested together in the same behavioral tests. OFF/ON, light-off/on. n = 13 mice (WT) and 14 mice (Q321R), ns, not significant, two-way ANOVA (**A**, genotype main effect p-value = 0.9356) and Student's t-test **(B)**. **(C,D)** Normal locomotor activity in *Shank3*$^{Q321R/Q321R}$ mice (2 months; male) in the open-field test, as shown by the distance moved. Note that *Shank3*^{Q321R} mice spent a normal amount of time in the center region of the open-field arena, suggestive of normal anxiety-like behavior. n = 13 mice (WT) and 14 mice (Q321R), ***$P < 0.001$, ns, not significant, repeated measures two-way ANOVA **(C)** and Student's t-test **(D)**. **(E)** Normal anxiety-like behavior in *Shank3*$^{Q321R/Q321R}$ mice (2 months; male) in the open-field test, as shown by the time spent in the center region of the open-field arena. n = 13 mice (WT) and 14 mice (Q321R), ns, not significant, Student's t-test. **(F)** Anxiolytic-like behavior in *Shank3*$^{Q321R/Q321R}$ mice (2 months; male) in the elevated plus-maze test, as shown by the increased time spent in the open arms of the maze. n = 13 mice (WT) and 14 mice (Q321R), *$P < 0.05$, Mann–Whitney U-test. **(G)** Anxiolytic-like behavior in *Shank3*$^{Q321R/Q321R}$ mice (2 months; male) in the light-dark test, as shown by the increased time spent in the light chamber of the light-dark apparatus. n = 13 mice (WT) and 14 mice (Q321R), *$P < 0.05$, Welch's t-test.

days (day 3–9) for fear extinction, they displayed comparable decreases in freezing levels, suggestive of normal fear extinction in *Shank3*$^{Q321R/Q321R}$ mice.

In addition, *Shank3*$^{Q321R/Q321R}$ mice showed normal levels of somatosensory functions, as determined by the hot plate and von Frey tests (**Figures 8C,D**). These results collectively suggest that the homozygous Shank3 Q321R mutation does not affect object-recognition memory, acquisition, or extinction of contextual fear memory, or somatosensory functions.

Female Homozygous *Shank3*$^{Q321R/Q321R}$ Mice Show Normal Anxiety-Like Behavior and Reduced Self-Grooming

To test whether there is a male-female difference in the impacts of the Shank3 Q321R mutation on behaviors, we subjected female *Shank3*$^{Q321R/Q321R}$ mice to the behavioral tests in which male *Shank3*$^{Q321R/Q321R}$ mice showed abnormal behaviors. To our surprise, female *Shank3*$^{Q321R/Q321R}$ mice

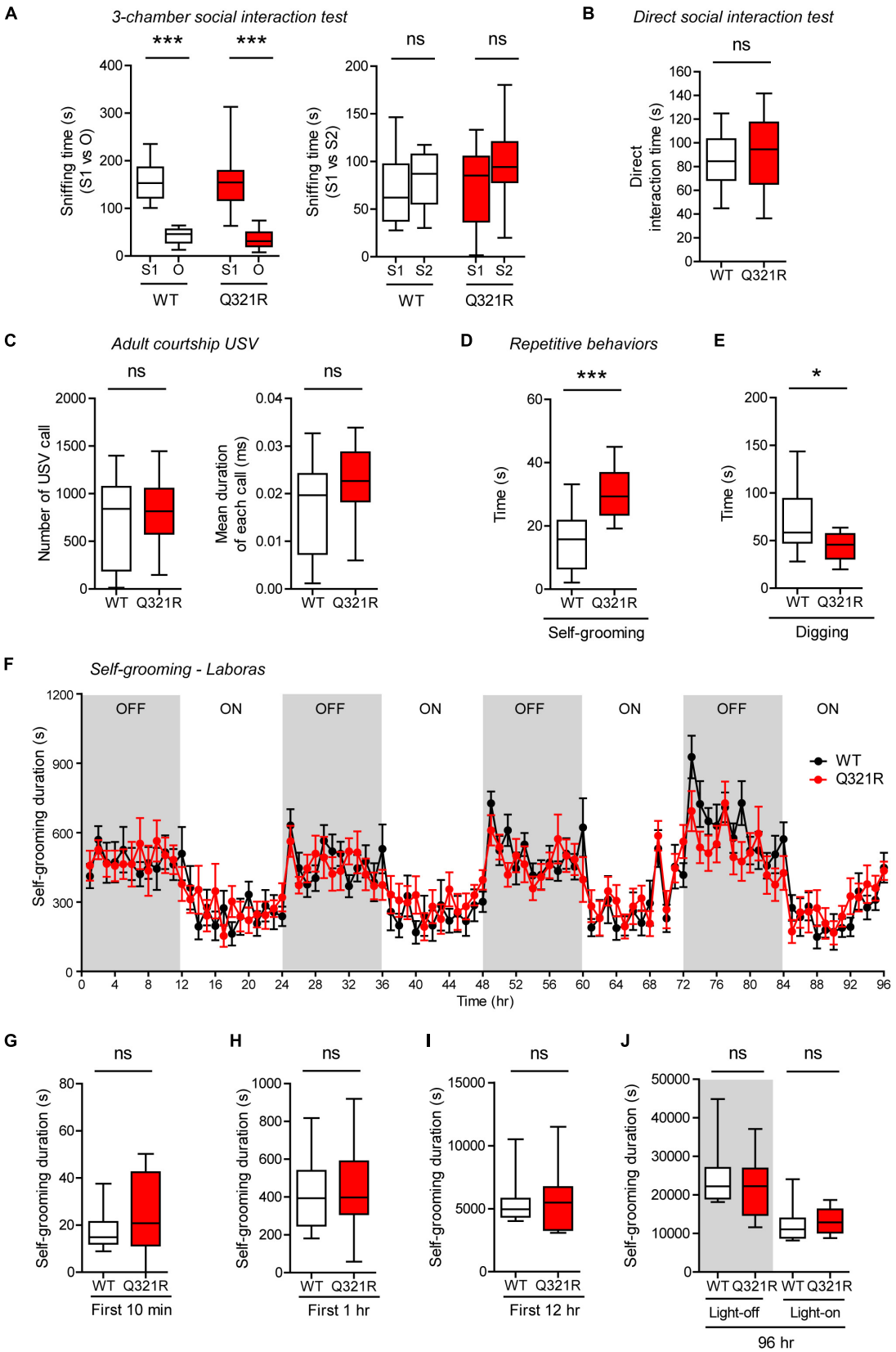

FIGURE 7 | Continued

FIGURE 7 | Normal social interaction and communication, moderately enhanced stress-induced self-grooming, and suppressed digging in homozygous *Shank3*$^{Q321R/Q321R}$ mice. **(A)** Normal social approach in *Shank3*$^{Q321R/Q321R}$ mice (3 months; male) in the three-chamber test, as shown by time spent sniffing social (S1) or object (O) target. Social novelty recognition, measured by the preference for new stranger (S2) over old stranger (S1), could not be determined due the lack of normal social novelty recognition in WT mice. Note that the WT data in this panel and other panels in this figure are identical to those shown in **Figure 5** because WT, heterozygous, and homozygous mice were tested together in the same behavioral tests. n = 10 mice (WT), 14 mice (Q321R), $^{***}P < 0.001$, ns, not significant, Welch's t-test (for S1 vs. O) and Student's t-test (for S1 vs. S2). **(B)** Normal social interaction in *Shank3*$^{Q321R/Q321R}$ mice (3 months; male) in bidirectional direct social-interaction tests, as shown by total time spent in social interaction. n = 10 pairs (WT), 13 pairs (Q321R), ns, not significant, Student's t-test. **(C)** Normal USVs emitted by *Shank3*$^{Q321R/Q321R}$ mice (4 months; male) upon encounter with a novel female stranger (courtship USVs), as shown by the total number of USVs and the mean duration of each USV calls. n = 12 mice (WT), 14 mice (Q321R), ns, not significant, Student's t-test. **(D)** Enhanced self-grooming in *Shank3*$^{Q321R/Q321R}$ mice (2 months; male) in home cages with bedding (10 min), as shown by total self-grooming time. n = 12 mice (WT), 13 mice (Q321R), $^{***}P < 0.001$, Student's t-test. **(E)** Suppressed digging in *Shank3*$^{Q321R/Q321R}$ mice (2 months; male) in home cages with bedding (10 min), as shown by total digging time. n = 12 mice (WT), 13 mice (Q321R), $^{*}P < 0.05$, Welch's t-test. **(F–J)** Normal self-grooming in *Shank3*$^{Q321R/Q321R}$ mice (2 months; male) in Laboras cages, where self-grooming was measured together with other movements for four consecutive days in the absence of habituation. OFF/ON, light-off/on. Note that there are no genotype differences during the first 10 min, 1 or 12 h, the entire session (96 h), or during light-off and light-on periods (48 h each). n = 13 mice (WT) and 14 mice (Q321R), ns, not significant, two-way ANOVA (genotype main effect p-value = 0.9754 in **F**), Student's t-test **(H)** and Mann–Whitney U-test **(G,I,J)**.

showed normal levels of anxiety-like behaviors in both EPM and light-dark tests (**Supplementary Figures 1C,D**), dissimilar to male *Shank3*$^{Q321R/Q321R}$ mice that showed anxiolytic-like behavior in both tests (**Figures 6F,G**).

Furthermore, female *Shank3*$^{Q321R/Q321R}$ mice showed normal levels of self-grooming and digging in novel home cages with bedding (10 min) (**Supplementary Figures 1E,F**), again dissimilar to male *Shank3*$^{Q321R/Q321R}$ mice that showed enhanced self-grooming and reduced digging in novel home cages (**Figures 7D,E**). These results collectively suggest that female *Shank3*$^{Q321R/Q321R}$ mice do not show anxiolytic-like behavior or enhanced self-grooming, dissimilar to male *Shank3*$^{Q321R/Q321R}$ mice.

Abnormal EEG Patterns and Decreased Susceptibility to Induced Seizures in Homozygous Male *Shank3*$^{Q321R/Q321R}$ Mice

Abnormal electroencephalogram (EEG) patterns have been observed in ASD (Wang et al., 2013), ASD and PMS associated with *SHANK3* mutations (Moessner et al., 2007; Soorya et al., 2013; Figura et al., 2014; Holder and Quach, 2016), as well as in *Shank3*-mutant mouse models (Han et al., 2013; Dhamne et al., 2017). In particular, the individual with ASD carrying the Q321R mutation was reported to display abnormal EEG, bilateral epileptiform discharges without seizures, and severe sleep disorders (Moessner et al., 2007). We thus attempted bilateral EEG recordings in the frontal and parietal lobes of the male *Shank3*$^{Q321R/Q321R}$ brain using EEG drivers implanted on the skull. The power of EEG in the delta range, but not other frequency ranges (0–4 Hz), was decreased in the frontal lobes, whereas EEG power in the alpha frequency range (12–30 Hz) was increased in the parietal lobes (**Figures 9A,B**).

Abnormalities in the left-right hemispheric asymmetry of EEGs have also been observed in ASD (Wang et al., 2013). We thus analyzed the changes in EEGs in left and right hemispheres of the *Shank3*$^{Q321R/Q321R}$ brain separately. In the frontal lobe, left and right hemispheres showed similar decreases in normalized EEG power in the delta range, but not other ranges (**Supplementary Figure 3A**). Intriguingly, in the parietal lobe, the right but not left hemisphere showed decreased EEG power in the delta range and increased EEG power in theta and alpha ranges (**Supplementary Figure 3B**). These results suggest that the decreased delta-band EEG power in the frontal lobe likely involves both hemispheres, whereas the increase alpha-band EEG power in the parietal lobe likely involves the right parietal lobe.

These abnormal EEG patterns in the *Shank3*$^{Q321R/Q321R}$ brain and reduced neuronal excitability in *Shank3*$^{Q321R/Q321R}$ hippocampal CA1 neurons (**Figure 3**) suggest the possibility that the *Shank3*$^{Q321R/Q321R}$ mutation disrupts the balance between neuronal excitation and inhibition in the brain, a mechanism suggested to underlie ASD (Rubenstein and Merzenich, 2003). To test this, we assessed the susceptibility of *Shank3*$^{Q321R/Q321R}$ mice to seizures induced by the $GABA_A$ receptor antagonist pentylenetetrazole (PTZ).

We found that male *Shank3*$^{Q321R/Q321R}$ mice are less susceptible to PTZ-induced seizures compared with WT mice, as shown by the latency to seizure stage 1 (although not stage 2), latency-based seizure susceptibility index, and final seizure stages reached (**Figure 10**). Spontaneous behavioral seizures were not observed in the absence of PTZ injection. These results collectively suggest that the homozygous Shank3 Q321R mutation induces abnormal EEG patterns and decreased PTZ-induced seizure susceptibility in male mice.

DISCUSSION

Our results indicate that the Shank3 Q321R mutation, located in exon 8 of the *Shank3* gene encoding the C-terminal part of the ARR domain of the protein, leads to substantial destabilization of the ARR-containing Shank3a protein variant and synaptic, behavioral, and EEG/seizure abnormalities in mice.

Our *in vivo* data from *Shank3*$^{Q321R/Q321R}$ mice indicate that the Q321R mutation induces a substantial decrease (∼18% of WT levels) in the total level of the ARR-containing Shank3a protein variant in the *Shank3*$^{Q321R/Q321R}$ brain (**Figure 2F**). In addition, our molecular modeling analyses suggest that the Q321R mutation is less likely to affect the intramolecular SPN-ARR interaction but more likely to affect the protein stability or intermolecular interactions of Shank3. The ARR domain of Shank3 is known to interact with Sharpin and α-fodrin (Bockers et al., 2001; Lim et al., 2001), and the Q321R mutation has

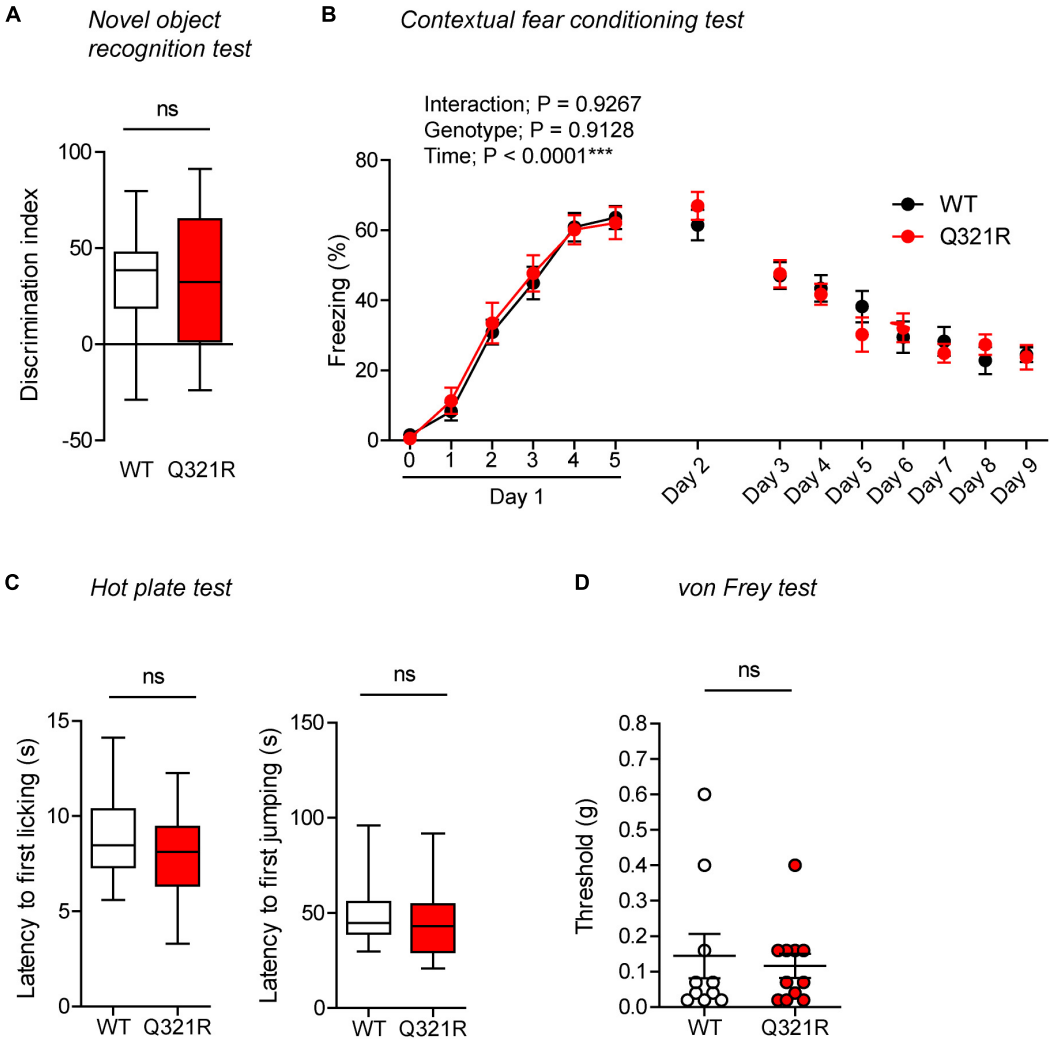

FIGURE 8 | Normal object-recognition and fear memory in homozygous male *Shank3*$^{Q321R/Q321R}$ mice. **(A)** Normal levels of object recognition memory in *Shank3*$^{Q321R/Q321R}$ mice (2–4 months; male) in the novel object recognition test, as shown by the discrimination index over a familiar object and a novel object (see Materials and Methods for details) presented 24 h after exploring two identical objects on the first day. *n* = 11 mice (WT), 13 mice (Q321R), ns, not significant, Student's *t*-test. **(B)** Normal acquisition, retrieval, and extinction of contextual fear memory *Shank3*$^{Q321R/Q321R}$ mice (3–6 months; male), as shown by freezing levels. Mice were given 5 foot shocks (2-min intervals) during the 12-min fear memory acquisition phase (day 1), and were consecutively exposed to the same context 24 h after the training (day 2) and also during days 3–9 for fear extinction. *n* = 13 mice (WT), 17 mice (Q321R), repeated measures two-way ANOVA. **(C)** Normal somatosensory function in *Shank3*$^{Q321R/Q321R}$ mice (6 months; male) in the hot plate test, as shown by latency to first licking/jumping. *n* = 17 mice (WT) and 20 mice (Q321R), ns, not significant, Student's *t*-test (for latency to first licking), and Mann–Whitney *U*-test (for latency to first jumping). **(D)** Normal somatosensory function in *Shank3*$^{Q321R/Q321R}$ mice (2 months; male) in the von Frey test, as shown by threshold for response to stimulation. *n* = 10 mice (WT) and 11 mice (Q321R), ns, not significant, Mann–Whitney *U*-test.

been shown to enhance Shank3 binding to Sharpin but not α-fodrin (Mameza et al., 2013). Given that Shank proteins can be ubiquitinated and deubiquitinated in an activity-dependent manner to regulate excitatory synapse structure and function (Ehlers, 2003; Kerrisk Campbell and Sheng, 2018) and that Sharpin is a component of the E3 ligase complex termed LUBAC (linear ubiquitin chain assembly complex) (Ikeda et al., 2011; Tokunaga et al., 2011; Iwai et al., 2014; Hrdinka and Gyrd-Hansen, 2017), it is tempting to speculate that the strong decrease in the levels of the mutant Shank3 protein (Q321R) might involve enhanced protein ubiquitination. Dissimilar to the results from *Shank3*$^{Q321R/Q321R}$ mice, however, *Shank3*$^{+/Q321R}$ mice show normal levels of Shank3 proteins, as compared with WT mice (**Figure 2F**). Therefore, distinct pathophysiological mechanisms of the Shank3 Q321R mutation at the protein level (i.e., decreased protein levels vs. abnormal protein function) might lead to similar behavioral abnormalities in *Shank3*$^{Q321R/Q321R}$ and *Shank3*$^{+/Q321R}$ mice, likely by acting on similar sets of neurons in the brain.

Electrophysiologically, there were no changes in the frequency or amplitude of mEPSCs in male *Shank3*$^{Q321R/Q321R}$ CA1 pyramidal or dorsolateral striatal neurons (**Figure 3**; summarized

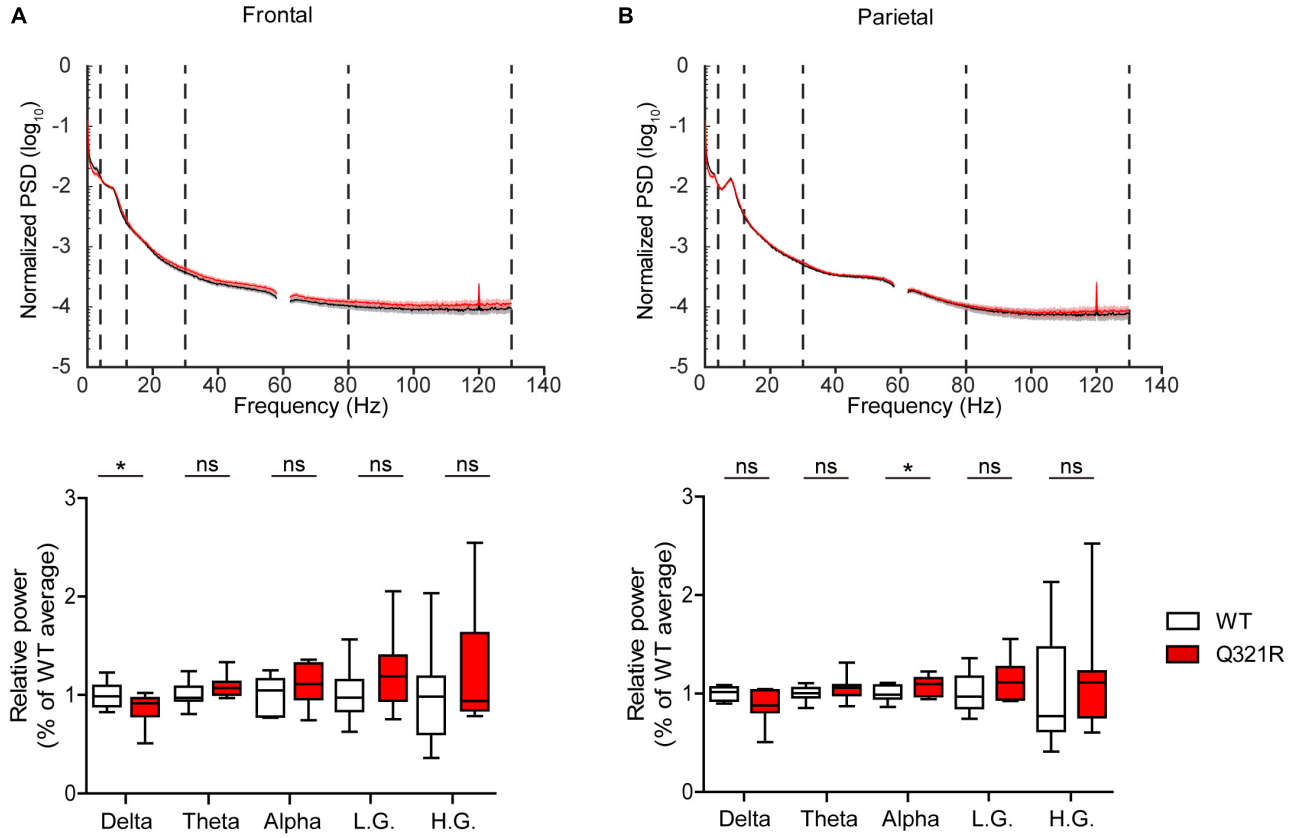

FIGURE 9 | Abnormal EEG patterns in *Shank3*$^{Q321R/Q321R}$ mice. **(A,B)** Abnormal EEG patterns in frontal and parietal lobes of the *Shank3*$^{Q321R/Q321R}$ brain (3 months; male). EEG power was calculated by combining data from both left and right hemispheres in the frontal or parietal lobe. Note that the EEG power in the delta frequency range is decreased, whereas that in the alpha frequency range is increased. The vertical dotted lines in the power spectral density (PSD) diagrams indicate the boundaries between different frequency ranges (delta, 0–4 Hz; theta, 4–12 Hz; alpha, 12–30 Hz; low gamma, 30–80 Hz; high gamma, 80–130 Hz). n = 10 mice (WT) and 10 mice (Q321R) for frontal lobe and 9 mice (WT) and 10 mice (Q321R) for parietal lobe, $^*P < 0.05$, ns, not significant, Student's t-test, Mann–Whitney U-test, Welch's t-test.

in **Table 1**). These results suggest that homozygous deletion of ARR-containing Shank3 protein variants does not affect mEPSCs in hippocampal or striatal neurons. Potential reasons for these results could be that ARR-containing Shank3 protein variants only minimally affect excitatory synapse development and function in hippocampal and striatal neurons or that some compensatory changes have occurred. Similar to our results, mEPSC frequency and amplitude are unchanged in *Shank3* mouse lines carrying similar ARR deletions, including *Shank3*$^{\Delta 9}$ mice (lacking exon 9) (Lee et al., 2015) and *Shank3*$^{\Delta 4-9}$ mice (lacking exons 4–9) (Wang et al., 2011; Jaramillo et al., 2016). Notably, however, heterozygous deletion of *Shank3* exons 4–9 in mice induces an increase in mEPSC frequency and a decrease in mEPSC amplitude (Bozdagi et al., 2010), suggesting different effects of homozygous and heterozygous deletions.

Whereas mEPSCs and mIPSCs were unchanged in male *Shank3*$^{Q321R/Q321R}$ CA1 pyramidal neurons, and mEPSCs were unchanged in female *Shank3*$^{Q321R/Q321R}$ CA1 pyramidal neurons, the frequency but not amplitude of mIPSCs was increased in female CA1 neurons (**Figure 3** and **Supplementary Figures 1A,B**). These changes may involve some presynaptic changes given that Shank3 proteins are mainly localized at excitatory postsynaptic sites. Alternatively, the Shank3 protein with Q321R mutation might be localized at subcellular sites other than excitatory postsynaptic sites or even at inhibitory postsynaptic sites in CA1 pyramidal neurons, although our Shank3 antibodies were not good enough for immunohistochemical analyses at the electron microscopic level. Intriguingly, a similar increase in mIPSC frequency has been reported in *Shank3*$^{\Delta 9}$ CA1 pyramidal neurons (Lee et al., 2015), although mIPSCs were not affected in Shank3$^{\Delta 4-9}$ CA1 pyramidal neurons (Wang et al., 2011).

Our data indicate a decrease in neuronal excitability in male *Shank3*$^{Q321R/Q321R}$ CA1 pyramidal neurons, a conclusion supported by the current-firing curve (**Figure 3**). However, there were no changes in the current-voltage relationship, input resistance, or Sag ratio. These results suggest potential changes in the threshold or properties of action potentials involving sodium or potassium channels, rather than changes in resting conductance involving HCN (hyperpolarization-activated cyclic nucleotide–gated) channels. Notably, a previous study has reported that cultured hippocampal neurons obtained from

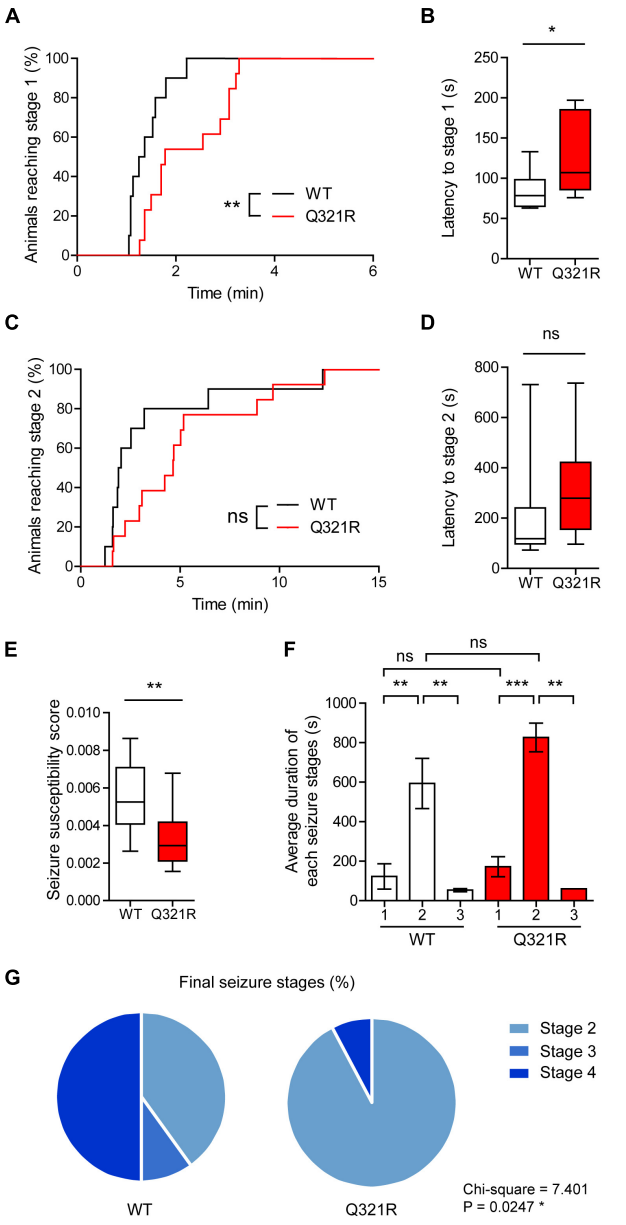

FIGURE 10 | Decreased susceptibility to PTZ-induced seizures in *Shank3*$^{Q321R/Q321R}$ mice. **(A)** Percentage of animals that can reach stage 1 (behavioral arrest) seizures. Seizures were induced in WT and *Shank3*$^{Q321R/Q321R}$ mice (3–4 months; male) by intraperitoneal injection of PTZ (50 mg/kg). n = 10 mice (WT), 13 mice (Q321R), $^{**}P < 0.01$, log-rank (Mantel-Cox) test ($p = 0.0047$). **(B)** Latency to reach stage 1 (behavioral arrest) seizures. $^{*}P < 0.05$, Mann–Whitney U-test. **(C)** Percentage of animals that can reach stage 2 (myoclonic) seizures. ns, not significant, log-rank (Mantel-Cox) test ($p = 0.1881$). **(D)** Latency to reach stage 2 (myoclonic) seizures. ns, not significant, Mann–Whitney U-test. **(E)** Seizure susceptibility based on the latencies to reach stage 1, 2, or 3 seizure (see Materials and Methods for details on the definition of seizure susceptibility). $^{**}P < 0.01$, Student's t-test. **(F)** Duration of seizure stages 1, 2, and 3. $^{**}P < 0.01$, $^{***}P < 0.001$, ns, not significant, one-way ANOVA with Kruskal–Wallis/Holm–Sidak test (within-genotype stage 1/2/3 comparison) and Mann–Whitney U-test (between-genotype stage 1/2/3 comparison). **(G)** Final seizure stages that animals reached, expressed as a percentage of animals. $^{*}P < 0.05$, Chi-square test.

Shank3 mice carrying heterozygous and homozygous deletion of exons 13–16 encoding the PDZ domain of Shank3 (Peca et al., 2011) display markedly increased neuronal excitability in association with increased input resistance and decreased hyperpolarization-activated currents (I_h). Moreover, human neurons with a *SHANK3* exon 13 deletion display similar changes (Yi et al., 2016). This difference may be attributable to differences in the specific exons of the Shank3 gene affected: exon 8 in our study of the Q321R mutation and exons 13–16 in these previous studies. The former encompasses mainly ARR-containing Shank3 protein variants, whereas the latter encompasses almost all Shank3 protein variants. Although further details remain to be elucidated, our electrophysiology results suggest that, at minimum, the decreased neuronal excitability and increased mIPSC frequency in *Shank3*$^{Q321R/Q321R}$ CA1 pyramidal neurons would substantially suppress the output functions of these neurons.

Behaviorally, heterozygous *Shank3*$^{+/Q321R}$ mice show moderately enhanced social communication and self-grooming and moderate anxiolytic-like behaviors in the light-dark tests (although open-field center activity and EPM performance were normal), while showing normal levels of locomotor activity and three-chamber social interaction (**Figures 4**, **5**). Homozygous *Shank3*$^{Q321R/Q321R}$ mice show behaviors that are largely similar to those in heterozygous *Shank3*$^{+/Q321R}$ mice, displaying moderately enhanced self-grooming, moderate anxiolytic-like behaviors in EPM and light-dark tests (although open-field center activity was normal), while showing normal levels of locomotor activity, social interaction (three-chamber and direct social interaction), social communication (courtship USV), and object–recognition and contextual fear memory (**Figures 6–8**; summarized in **Table 1**).

Notably, *Shank3*$^{\Delta 9}$ mice, which carry a similar alteration in the ARR domain, show behaviors that are largely similar to those of *Shank3*$^{Q321R/Q321R}$ mice, displaying normal levels of locomotor activity, anxiety-like behavior (open-field center time), social interaction and communication (three-chamber and pup USV), and object–recognition memory, although self-grooming was also normal in these mice (Lee et al., 2015). Behavioral impacts in other ARR-deletion–carrying mouse lines are more severe compared with those reported here, a difference that is likely attributable to larger deletions in the ARR domain of the Shank3 protein. Specifically, self-grooming is enhanced in *Shank3*$^{\Delta 4-9}$ mice, similar to our mice, but these former mice additionally show altered social interaction and communication and impaired novel object–recognition memory (Bozdagi et al., 2010; Wang et al., 2011; Yang et al., 2012; Jaramillo et al., 2016; Dhamne et al., 2017). In addition, *Shank3*$^{\Delta 4-7}$ mice show abnormal social novelty recognition, but normal self-grooming (Peca et al., 2011), again different from our mice.

Identifying synaptic mechanisms and neural circuits associated with the behavioral phenotypes in *Shank3*^{Q321R} mice will require additional investigation. Notably, however, while male *Shank3*$^{Q321R/Q321R}$ mice show normal mEPSCs and mIPSCs in the hippocampus and anxiolytic-like behavior, enhanced self-grooming, and suppressed digging, female *Shank3*$^{Q321R/Q321R}$ mice show increased mIPSC frequency in the

TABLE 1 | Summary of electrophysiological, behavioral, and brain function phenotypes in *Shank3*$^{Q321R/Q321R}$ mice.

	Subcategory	Measurement	Results
Electrophysiology	Hippocampal CA1 pyramidal neurons	mEPSC	Frequency -, amplitude -
		mIPSC	Frequency -, amplitude -
		Neuronal excitability	↓
	Dorsolateral striatal neurons	mEPSC	Frequency -, amplitude -
		mIPSC	Frequency -, amplitude -
Behavior			
	Social interaction	Three-chamber (social approach)	–
		Direct interaction	–
	Social communication	Adult courtship USV	–
	Repetitive behavior	Self-grooming (Laboras cage)	–
		Self-grooming (novel home cage)	↑
		Digging (novel home cage)	↓
	Locomotor activity	Laboras	–
		Open-field	–
	Anxiety-like behavior	Open field center time	–
		Elevated plus-maze (open-arm time)	↓
		Light/dark box (light-chamber time)	↓
	Learning and memory	Novel object recognition	–
		Contextual fear conditioning, retrieval, and extinction	Acquisition (day 1) - 24-h retrieval (day 2) - Extinction (days 3–9) -
Brain function	EEG	Baseline EEG	Frontal-delta ↓ Parietal-alpha ↑ Left-right asymmetry
	Seizure	Susceptibility to PTZ-induced seizure	↓

Up and down arrows, increases and decreases, respectively; –, no significant change. Male mice were used to obtain the results listed in the table. Additional measurements for select electrophysiological and behavioral parameters were also made in females and described in Results but not summarized in this table.

hippocampus and normal anxiety-like behavior, self-grooming, and digging (**Figures 3**, **6**, **7** and **Supplementary Figures 1C–F**). Therefore, the increased mIPSC frequency in female mice might represent a part of the compensatory changes that might have normalized the anxiety-like behaviors and repetitive behaviors in female *Shank3*$^{Q321R/Q321R}$ mice.

In addition, the most strongly affected Shank3 protein variant in our mice was Shank3a, which is abundantly expressed in the striatum among many brain regions (Wang et al., 2014). In addition, the striatopallidal pathway has been shown to regulate self-grooming in *Shank3*$^{\Delta 13-16}$ mice (Wang et al., 2017). In addition, the striatum has emerged as one of the key brain regions involved in the regulation of anxiety-like behaviors, in addition to the amygdala, bed nucleus of the stria terminalis, hippocampus, and ventromedial prefrontal cortex (Lago et al., 2017). Therefore, it is tempting to speculate that striatal dysfunctions might contribute to the self-grooming and anxiolytic-like behavior in *Shank3*^{Q321R} mice. Although male *Shank3*$^{Q321R/Q321R}$ mice displayed normal levels of excitatory and inhibitory spontaneous synaptic transmission (mEPSCs and mIPSCs) in the dorsolateral striatum (**Figures 3G,H**), additional investigations might reveal some other striatal dysfunctions in synaptic transmission and plasticity. For instance, previous studies have reported decreased NMDA/AMPA ratio but normal mEPSCs and mIPSCs in the dorsal striatum of homozygous and heterozygous *Shank3*$^{\Delta 4-9}$ mice (Jaramillo et al., 2016).

Shank3$^{Q321R/Q321R}$ mice (males) display abnormal baseline EEG patterns, with a decreased delta band in the frontal lobe and increased alpha band in the parietal lobe (**Figure 9**). In addition, we found left-right asymmetry in the parietal, but not frontal, lobe of the *Shank3*^{Q321R} brain. Understanding the biological significances of these results would have to involve, for instance, additional analyses of sleep behaviors and rhythms in *Shank3*$^{Q321R/Q321R}$ mice and acquisition of EEG- and sleep-related details from the individual carrying the Q321R mutation (Moessner et al., 2007). Nonetheless, our data are in line with the previous studies in ASD that have reported abnormalities in the power, coherence, and asymmetry of EEGs in the delta and alpha ranges in addition to other frequency ranges (Wang et al., 2013). Moreover, the individual carrying the *SHANK3* Q321R mutation was shown to display abnormal EEG patterns (Moessner et al., 2007), although it is unclear whether the abnormal EEGs were observed in similar frequency ranges. Notably, a previous study on *Shank3*$^{\Delta 13-16}$ mice reported abnormally enhanced EEGs in the low gamma range (30–80 Hz), known to be associated with parvalbumin-positive GABAergic neurons (Sohal et al., 2009), but normal EEGs in other frequency ranges (Dhamne et al., 2017). This difference could again reflect

differences in the exons deleted in the two mutant mouse lines, with *Shank3*$^{\Delta 13-16}$ mice lacking a larger number of Shank3 splice variants.

Our *Shank3*$^{Q321R/Q321R}$ mice (males) are more resistant to PTZ-induced seizures and do not display spontaneous behavioral seizures (**Figure 10**). These results are in line with the suppressed excitability of CA1 pyramidal neurons in these animals. Similar to our results, a previous study on *Shank3*$^{\Delta 13-16}$ mice revealed a decrease in susceptibility to PTZ-induced seizures (Dhamne et al., 2017) and lack of spontaneous behavioral seizures (Peca et al., 2011). In addition, *Shank3*$^{\Delta 4-22}$ mice show tonic hyperactivity in the cortico-striatal-thalamic axis, revealed by multi-site *in vivo* recordings, but do not show spontaneous behavioral seizures (Wang et al., 2016). In contrast, a transgenic mouse line carrying duplicated *Shank3* shows enhanced epileptiform spikes in the dentate gyrus and electrographic seizures (Han et al., 2013). These results collectively suggest that Shank3 is an important regulator of excitatory drive in the brain. Perhaps more importantly, the individual with the Q321R mutation was shown to display bilateral epileptiform discharges without seizures, in addition to abnormal EEG patterns (Moessner et al., 2007). Therefore, the EEG and seizure phenotypes of our *Shank3*^{Q321R} mice may serve as potential biomarkers for future studies.

CONCLUSION

Our data suggest that the Shank3 Q321R mutation in mice has significant influences on Shank3 protein stability, hippocampal neuronal excitability, anxiety-like and repetitive behaviors, EEG, and seizure susceptibility.

ETHICS STATEMENT

The mice were bred and maintained according to the Animal Research Requirements of KAIST, and all procedures were approved by the Committee of Animal Research at KAIST (2016-30).

AUTHOR CONTRIBUTIONS

JL generated the mice. Y-EY and TY performed the electrophysiological and behavioral experiments. Y-EY performed the immunoblot experiments. SL performed the immunohistochemistry and behavioral experiments. Y-EY, SL, and TY performed the EEG experiments. DK performed the structural modeling. H-MH, Y-CB, and EK wrote the manuscript.

FUNDING

This study was supported by the National Research Foundation of Korea (NRF-2017R1A5A2015391 to Y-CB) and the Institute for Basic Science (IBS-R002-D1 to EK).

SUPPLEMENTARY MATERIAL

The Supplementary Material for this article can be found online at: https://www.frontiersin.org/articles/10.3389/fnmol.2019.00155/full#supplementary-material

FIGURE S1 | Female *Shank3*$^{Q321R/Q321R}$ mice show increased mIPSC frequency in CA1 pyramidal neurons but normal anxiety-like and repetitive behaviors. **(A)** Normal mEPSCs in CA1 pyramidal neurons in the hippocampus of female *Shank3*$^{Q321R/Q321R}$ mice (P21–27). The indicated values represent means ± SEM. n = 14 neurons from 4 mice (WT; female) and 15 neurons from 4 mice (Q321R), ns, not significant, Mann–Whitney U-test (for frequency) and Student's t-test (for amplitude). **(B)** Increased frequency, but normal amplitude, of mIPSCs in CA1 pyramidal neurons in the hippocampus of female *Shank3*$^{Q321R/Q321R}$ mice (P22–26). n = 12 neurons from 4 mice (WT) and 13 neurons from 4 mice (Q321R), $^{*}P < 0.05$, ns, not significant, Student's t-test. **(C)** Normal anxiety-like behavior in female *Shank3*$^{Q321R/Q321R}$ mice (3–5 months) in the elevated plus-maze test, as shown by time spent in open arms of the maze. n = 9 mice (WT) and 12 mice (Q321R), ns, not significant, Mann–Whitney U-test. **(D)** Normal anxiety-like behavior in female *Shank3*$^{Q321R/Q321R}$ mice (3–5 months) in the light-dark test, as shown by time spent in light chamber of the light-dark apparatus. n = 9 mice (WT) and 12 mice (Q321R), ns, not significant, Mann–Whitney U-test. **(E)** Normal self-grooming in female *Shank3*$^{Q321R/Q321R}$ mice (3–5 months) in home cages with bedding (10 min), as shown by total self-grooming time. n = 9 mice (WT) and 11 mice (Q321R), ns, not significant, Welch's t-test. **(F)** Normal digging in female *Shank3*$^{Q321R/Q321R}$ mice (3–5 months) in home cages with bedding (10 min), as shown by total digging time. n = 9 mice (WT) and 11 mice (Q321R), ns, not significant, Student's t-test.

FIGURE S2 | *Shank3*$^{Q321R/Q321R}$ mice show normal self-grooming in novel home cages without light, Laboras cages with light, and open-field arena with light. **(A)** Normal self-grooming in *Shank3*$^{Q321R/Q321R}$ mice (4–5 months; male) in novel home cages without light (0 lux; 10 min). n = 16 mice (WT), 20 mice (Q321R), ns, not significant, Mann–Whitney U-test. **(B)** Normal self-grooming in *Shank3*$^{Q321R/Q321R}$ mice (4–5 months; male) in Laboras cages (a novel environment) with light (∼50 lux; 10 min). n = 9 mice (WT), 8 mice (Q321R), ns, not significant, Mann–Whitney U-test. **(C)** Normal self-grooming in *Shank3*$^{Q321R/Q321R}$ mice (2–3 months; male) in an open-field arena (a novel environment) with light (∼100 lux; 10 min). n = 13 mice (WT), 14 mice (Q321R), ns, not significant, Student's t-test.

FIGURE S3 | Abnormal EEG patterns in the left and right hemispheres in *Shank3*$^{Q321R/Q321R}$ mice. **(A,B)** Altered left and right hemispheric EEG powers in the frontal and parietal lobes of the *Shank3*$^{Q321R/Q321R}$ brain (3 months; male). Note that the frontal lobe displays decreased delta power in both left and right hemispheres, whereas the parietal lobe displays decreased delta power and increased theta and alpha powers only in the right hemisphere. n = 10 mice (WT) and 10 mice (Q321R) for frontal lobe and 9 mice (WT) and 10 mice (Q321R) for parietal lobe, $^{*}P < 0.05$, $^{**}P < 0.01$, ns, not significant, Student's t-test, Mann–Whitney U-test, Welch's t-test.

TABLE S1 | Statistical details.

REFERENCES

Amal, H., Barak, B., Bhat, V., Gong, G., Joughin, B. A., Wishnok, J. S., et al. (2018). Shank3 mutation in a mouse model of autism leads to changes in the S-nitroso-proteome and affects key proteins involved in vesicle release and synaptic function. *Mol. Psychiatry* [Epub ahead of print].

Amaral, D. G., Schumann, C. M., and Nordahl, C. W. (2008). Neuroanatomy of autism. *Trends Neurosci.* 31, 137–145.

Ankier, S. I. (1974). New hot plate tests to quantify antinociceptive and narcotic antagonist activities. *Eur. J. Pharmacol.* 27, 1–4. doi: 10.1016/0014-2999(74)90195-2

Antunes, M., and Biala, G. (2012). The novel object recognition memory: neurobiology, test procedure, and its modifications. *Cognit. Process* 13, 93–110. doi: 10.1007/s10339-011-0430-z

Balaan, C., Corley, M. J., Eulalio, T., Leite-Ahyo, K., Pang, A. P. S., Fang, R., et al. (2019). Juvenile Shank3b deficient mice present with behavioral phenotype relevant to autism spectrum disorder. *Behav. Brain Res.* 356, 137–147. doi: 10.1016/j.bbr.2018.08.005

Berg, E. L., Copping, N. A., Rivera, J. K., Pride, M. C., Careaga, M., Bauman, M. D., et al. (2018). Developmental social communication deficits in the Shank3 rat model of phelan-mcdermid syndrome and autism spectrum disorder. *Autism Res.* 11, 587–601. doi: 10.1002/aur.1925

Bey, A. L., Wang, X., Yan, H., Kim, N., Passman, R. L., Yang, Y., et al. (2018). Brain region-specific disruption of Shank3 in mice reveals a dissociation for cortical and striatal circuits in autism-related behaviors. *Transl. Psychiatry* 8:94.

Boccuto, L., Lauri, M., Sarasua, S. M., Skinner, C. D., Buccella, D., Dwivedi, A., et al. (2013). Prevalence of SHANK3 variants in patients with different subtypes of autism spectrum disorders. *Eur. J. Hum. Genet.* 21, 310–316. doi: 10.1038/ejhg.2012.175

Bockers, T. M., Mameza, M. G., Kreutz, M. R., Bockmann, J., Weise, C., Buck, F., et al. (2001). Synaptic scaffolding proteins in rat brain. Ankyrin repeats of the multidomain Shank protein family interact with the cytoskeletal protein alpha-fodrin. *J. Biol. Chem.* 276, 40104–40112. doi: 10.1074/jbc.m102454200

Bockmann, J., Kreutz, M. R., Gundelfinger, E. D., and Bockers, T. M. (2002). ProSAP/Shank postsynaptic density proteins interact with insulin receptor tyrosine kinase substrate IRSp53. *J. Neurochem.* 83, 1013–1017. doi: 10.1046/j.1471-4159.2002.01204.x

Boeckers, T. M., Bockmann, J., Kreutz, M. R., and Gundelfinger, E. D. (2002). ProSAP/Shank proteins – a family of higher order organizing molecules of the postsynaptic density with an emerging role in human neurological disease. *J. Neurochem.* 81, 903–910. doi: 10.1046/j.1471-4159.2002.00931.x

Boeckers, T. M., Kreutz, M. R., Winter, C., Zuschratter, W., Smalla, K. H., Sanmarti-Vila, L., et al. (1999). Proline-rich synapse-associated protein-1/cortactin binding protein 1 (ProSAP1/CortBP1) is a PDZ-domain protein highly enriched in the postsynaptic density. *J. Neurosci.* 19, 6506–6518. doi: 10.1523/jneurosci.19-15-06506.1999

Bonaglia, M. C., Giorda, R., Beri, S., De Agostini, C., Novara, F., Fichera, M., et al. (2011). Molecular mechanisms generating and stabilizing terminal 22q13 deletions in 44 subjects with Phelan/McDermid syndrome. *PLoS Genet.* 7:e1002173. doi: 10.1371/journal.pgen.1002173

Bonaglia, M. C., Giorda, R., Borgatti, R., Felisari, G., Gagliardi, C., Selicorni, A., et al. (2001). Disruption of the ProSAP2 gene in a t(12;22)(q24.1;q13.3) is associated with the 22q13.3 deletion syndrome. *Am. J. Hum. Genet.* 69, 261–268. doi: 10.1086/321293

Bourin, M., and Hascoet, M. (2003). The mouse light/dark box test. *Eur. J. Pharmacol.* 463, 55–65. doi: 10.1016/s0014-2999(03)01274-3

Bozdagi, O., Sakurai, T., Papapetrou, D., Wang, X., Dickstein, D. L., Takahashi, N., et al. (2010). Haploinsufficiency of the autism-associated Shank3 gene leads to deficits in synaptic function, social interaction, and social communication. *Mol. Autism* 1:15. doi: 10.1186/2040-2392-1-15

Capriotti, E., Fariselli, P., and Casadio, R. (2005). I-Mutant2.0: predicting stability changes upon mutation from the protein sequence or structure. *Nucleic Acids Res.* 33, W306–W310.

Chung, W., Choi, S. Y., Lee, E., Park, H., Kang, J., Park, H., et al. (2015). Social deficits in IRSp53 mutant mice improved by NMDAR and mGluR5 suppression. *Nat. Neurosci.* 18, 435–443. doi: 10.1038/nn.3927

Cochoy, D. M., Kolevzon, A., Kajiwara, Y., Schoen, M., Pascual-Lucas, M., Lurie, S., et al. (2015). Phenotypic and functional analysis of SHANK3 stop mutations identified in individuals with ASD and/or ID. *Mol. Autism* 6:23.

De Rubeis, S., Siper, P. M., Durkin, A., Weissman, J., Muratet, F., Halpern, D., et al. (2018). Delineation of the genetic and clinical spectrum of Phelan-McDermid syndrome caused by SHANK3 point mutations. *Mol. Autism* 9:31.

de Sena Cortabitarte, A., Degenhardt, F., Strohmaier, J., Lang, M., Weiss, B., Roeth, R., et al. (2017). Investigation of SHANK3 in schizophrenia. *Am. J. Med. Genet. B Neuropsychiatr. Genet.* 174, 390–398. doi: 10.1002/ajmg.b.32528

DeLano, W. L. (2009). *PyMOL Molecular Viewer: Updates and Refinements*. Washington, DC: American Chemical Society, 238.

Dere, E., Winkler, D., Ritter, C., Ronnenberg, A., Poggi, G., Patzig, J., et al. (2015). Gpm6b deficiency impairs sensorimotor gating and modulates the behavioral response to a 5-HT2A/C receptor agonist. *Behav. Brain Res.* 277, 254–263. doi: 10.1016/j.bbr.2014.04.021

Dhamne, S. C., Silverman, J. L., Super, C. E., Lammers, S. H. T., Hameed, M. Q., Modi, M. E., et al. (2017). Replicable in vivo physiological and behavioral phenotypes of the Shank3B null mutant mouse model of autism. *Mol. Autism* 8:26.

Drapeau, E., Riad, M., Kajiwara, Y., and Buxbaum, J. D. (2018). Behavioral phenotyping of an improved mouse model of phelan-mcdermid syndrome with a complete deletion of the Shank3 gene. *eNeuro* 5:ENEURO.46–ENEURO.18.

Du, Y., Weed, S. A., Xiong, W. C., Marshall, T. D., and Parsons, J. T. (1998). Identification of a novel cortactin SH3 domain-binding protein and its localization to growth cones of cultured neurons. *Mol. Cell Biol.* 18, 5838–5851. doi: 10.1128/mcb.18.10.5838

Duffney, L. J., Zhong, P., Wei, J., Matas, E., Cheng, J., Qin, L., et al. (2015). Autism-like deficits in Shank3-deficient mice are rescued by targeting actin regulators. *Cell Rep.* 11, 1400–1413. doi: 10.1016/j.celrep.2015.04.064

Durand, C. M., Betancur, C., Boeckers, T. M., Bockmann, J., Chaste, P., Fauchereau, F., et al. (2007). Mutations in the gene encoding the synaptic scaffolding protein SHANK3 are associated with autism spectrum disorders. *Nat. Genet.* 39, 25–27. doi: 10.1038/ng1933

Durand, C. M., Perroy, J., Loll, F., Perrais, D., Fagni, L., Bourgeron, T., et al. (2012). SHANK3 mutations identified in autism lead to modification of dendritic spine morphology via an actin-dependent mechanism. *Mol. Psychiatry* 17, 71–84. doi: 10.1038/mp.2011.57

Egnor, S. R., and Seagraves, K. M. (2016). The contribution of ultrasonic vocalizations to mouse courtship. *Curr. Opin. Neurobiol.* 38, 1–5. doi: 10.1016/j.conb.2015.12.009

Ehlers, M. D. (2003). Activity level controls postsynaptic composition and signaling via the ubiquitin-proteasome system. *Nat. Neurosci.* 6, 231–242. doi: 10.1038/nn1013

Engineer, C. T., Rahebi, K. C., Borland, M. S., Buell, E. P., Im, K. W., Wilson, L. G., et al. (2018). Shank3-deficient rats exhibit degraded cortical responses to sound. *Autism Res.* 11, 59–68. doi: 10.1002/aur.1883

Ferhat, A. T., Halbedl, S., Schmeisser, M. J., Kas, M. J., Bourgeron, T., and Ey, E. (2017). Behavioural phenotypes and neural circuit dysfunctions in mouse models of autism spectrum disorder. *Adv. Anat. Embryol. Cell Biol.* 224, 85–101. doi: 10.1007/978-3-319-52498-6_5

Figura, M. G., Coppola, A., Bottitta, M., Calabrese, G., Grillo, L., Luciano, D., et al. (2014). Seizures and EEG pattern in the 22q13.3 deletion syndrome: clinical report of six Italian cases. *Seizure* 23, 774–779. doi: 10.1016/j.seizure.2014.06.008

Fiser, A., Do, R. K., and Sali, A. (2000). Modeling of loops in protein structures. *Protein Sci.* 9, 1753–1773. doi: 10.1110/ps.9.9.1753

Fourie, C., Vyas, Y., Lee, K., Jung, Y., Garner, C. C., and Montgomery, J. M. (2018). Dietary zinc supplementation prevents autism related behaviors and striatal synaptic dysfunction in Shank3 exon 13-16 mutant mice. *Front. Cell Neurosci.* 12:374. doi: 10.3389/fncel.2018.00374

Gauthier, J., Champagne, N., Lafreniere, R. G., Xiong, L., Spiegelman, D., Brustein, E., et al. (2010). De novo mutations in the gene encoding the synaptic scaffolding protein SHANK3 in patients ascertained for schizophrenia. *Proc. Natl. Acad. Sci. U.S.A.* 107, 7863–7868. doi: 10.1073/pnas.0906232107

Gould, T. D., Dao, D. T., and Kovacsics, C. E. (2009). "The open field test," in *Mood and Anxiety Related Phenotypes in Mice*, ed. T. D. Gould (Totowa, NJ: Humana Press).

Grabrucker, A. M., Schmeisser, M. J., Schoen, M., and Boeckers, T. M. (2011). Postsynaptic ProSAP/Shank scaffolds in the cross-hair of synaptopathies. *Trends Cell Biol.* 21, 594–603. doi: 10.1016/j.tcb.2011.07.003

Guilmatre, A., Huguet, G., Delorme, R., and Bourgeron, T. (2014). The emerging role of SHANK genes in neuropsychiatric disorders. *Dev. Neurobiol.* 74, 113–122. doi: 10.1002/dneu.22128

Hamdan, F. F., Gauthier, J., Araki, Y., Lin, D. T., Yoshizawa, Y., Higashi, K., et al. (2011). Excess of de novo deleterious mutations in genes associated with glutamatergic systems in nonsyndromic intellectual disability. *Am. J. Hum. Genet.* 88, 306–316. doi: 10.1016/j.ajhg.2011.02.001

Han, K., Holder, J. L. Jr., Schaaf, C. P., Lu, H., Chen, H., et al. (2013). SHANK3 overexpression causes manic-like behaviour with unique pharmacogenetic properties. *Nature* 503, 72–77. doi: 10.1038/nature12630

Harony-Nicolas, H., De Rubeis, S., Kolevzon, A., and Buxbaum, J. D. (2015). Phelan McDermid syndrome: from genetic discoveries to animal models and treatment. *J. Child Neurol.* 30, 1861–1870. doi: 10.1177/0883073815600872

Harony-Nicolas, H., Kay, M., Hoffmann, J. D., Klein, M. E., Bozdagi-Gunal, O., Riad, M., et al. (2017). Oxytocin improves behavioral and electrophysiological deficits in a novel Shank3-deficient rat. *Elife* 6:e18904.

Heise, C., Preuss, J. M., Schroeder, J. C., Battaglia, C. R., Kolibius, J., Schmid, R., et al. (2018). Heterogeneity of cell surface glutamate and GABA receptor expression in shank and CNTN4 autism mouse models. *Front. Mol. Neurosci.* 11:212. doi: 10.3389/fnmol.2018.00212

Heise, C., Schroeder, J. C., Schoen, M., Halbedl, S., Reim, D., Woelfle, S., et al. (2016). Selective localization of shanks to VGLUT1-positive excitatory synapses in the mouse hippocampus. *Front. Cell. Neurosci.* 10:106. doi: 10.3389/fncel.2016.00106

Holder, J. L. Jr., and Quach, M. M. (2016). The spectrum of epilepsy and electroencephalographic abnormalities due to SHANK3 loss-of-function mutations. *Epilepsia* 57, 1651–1659. doi: 10.1111/epi.13506

Hrdinka, M., and Gyrd-Hansen, M. (2017). The met1-linked ubiquitin machinery: emerging themes of (De)regulation. *Mol. Cell* 68, 265–280. doi: 10.1016/j.molcel.2017.09.001

Ikeda, F., Deribe, Y. L., Skanland, S. S., Stieglitz, B., Grabbe, C., Franz-Wachtel, M., et al. (2011). SHARPIN forms a linear ubiquitin ligase complex regulating NF-kappaB activity and apoptosis. *Nature* 471, 637–641. doi: 10.1038/nature09814

Ikeda, K., Araki, K., Takayama, C., Inoue, Y., Yagi, T., Aizawa, S., et al. (1995). Reduced spontaneous activity of mice defective in the epsilon 4 subunit of the NMDA receptor channel. *Brain Res. Mol. Brain Res.* 33, 61–71. doi: 10.1016/0169-328x(95)00107-4

Iwai, K., Fujita, H., and Sasaki, Y. (2014). Linear ubiquitin chains: NF-kappaB signalling, cell death and beyond. *Nat. Rev. Mol. Cell Biol.* 15, 503–508. doi: 10.1038/nrm3836

Jaramillo, T. C., Speed, H. E., Xuan, Z., Reimers, J. M., Escamilla, C. O., Weaver, T. P., et al. (2017). Novel Shank3 mutant exhibits behaviors with face validity for autism and altered striatal and hippocampal function. *Autism Res.* 10, 42–65. doi: 10.1002/aur.1664

Jaramillo, T. C., Speed, H. E., Xuan, Z., Reimers, J. M., Liu, S., and Powell, C. M. (2016). Altered striatal synaptic function and abnormal behaviour in Shank3 Exon4-9 deletion mouse model of autism. *Autism Res.* 9, 350–375. doi: 10.1002/aur.1529

Jiang, Y. H., and Ehlers, M. D. (2013). Modeling autism by SHANK gene mutations in mice. *Neuron* 78, 8–27. doi: 10.1016/j.neuron.2013.03.016

Jin, C., Kang, H., Ryu, J. R., Kim, S., Zhang, Y., Lee, Y., et al. (2018). Integrative brain transcriptome analysis reveals region-specific and broad molecular changes in Shank3-overexpressing mice. *Front. Mol. Neurosci.* 11:250. doi: 10.3389/fnmol.2018.00250

Kerrisk Campbell, M., and Sheng, M. (2018). USP8 deubiquitinates SHANK3 to control synapse density and SHANK3 activity-dependent protein levels. *J. Neurosci.* 38, 5289–5301. doi: 10.1523/jneurosci.3305-17.2018

Kouser, M., Speed, H. E., Dewey, C. M., Reimers, J. M., Widman, A. J., Gupta, N., et al. (2013). Loss of predominant Shank3 isoforms results in hippocampus-dependent impairments in behavior and synaptic transmission. *J. Neurosci.* 33, 18448–18468. doi: 10.1523/jneurosci.3017-13.2013

Lago, T., Davis, A., Grillon, C., and Ernst, M. (2017). Striatum on the anxiety map: small detours into adolescence. *Brain Res.* 1654, 177–184. doi: 10.1016/j.brainres.2016.06.006

Leblond, C. S., Heinrich, J., Delorme, R., Proepper, C., Betancur, C., Huguet, G., et al. (2012). Genetic and functional analyses of SHANK2 mutations suggest a multiple hit model of autism spectrum disorders. *PLoS Genet.* 8:e1002521. doi: 10.1371/journal.pgen.1002521

Leblond, C. S., Nava, C., Polge, A., Gauthier, J., Huguet, G., Lumbroso, S., et al. (2014). Meta-analysis of SHANK mutations in autism spectrum disorders: a gradient of severity in cognitive impairments. *PLoS Genet.* 10:e1004580. doi: 10.1371/journal.pgen.1004580

Lee, J., Chung, C., Ha, S., Lee, D., Kim, D. Y., Kim, H., et al. (2015). Shank3-mutant mice lacking exon 9 show altered excitation/inhibition balance, enhanced rearing, and spatial memory deficit. *Front. Cell Neurosci.* 9:94. doi: 10.3389/fncel.2015.00094

Lee, S., Ahmed, T., Lee, S., Kim, H., Choi, S., Kim, D. S., et al. (2012). Bidirectional modulation of fear extinction by mediodorsal thalamic firing in mice. *Nat. Neurosci.* 15, 308–314. doi: 10.1038/nn.2999

Lee, S., Lee, E., Kim, R., Kim, J., Lee, S., Park, H., et al. (2018). Shank2 deletion in parvalbumin neurons leads to moderate hyperactivity, enhanced self-grooming and suppressed seizure susceptibility in mice. *Front. Mol. Neurosci.* 11:209. doi: 10.3389/fnmol.2018.00209

Lee, Y., Kim, S. G., Lee, B., Zhang, Y., Kim, Y., Kim, S., et al. (2017). Striatal transcriptome and interactome analysis of Shank3-overexpressing mice reveals the connectivity between Shank3 and mTORC1 signaling. *Front. Mol. Neurosci.* 10:201. doi: 10.3389/fnmol.2017.00201

Lilja, J., Zacharchenko, T., Georgiadou, M., Jacquemet, G., De Franceschi, N., Peuhu, E., et al. (2017). SHANK proteins limit integrin activation by directly interacting with Rap1 and R-Ras. *Nat. Cell Biol.* 19, 292–305. doi: 10.1038/ncb3487

Lim, S., Naisbitt, S., Yoon, J., Hwang, J. I., Suh, P. G., Sheng, M., et al. (1999). Characterization of the shank family of synaptic proteins. Multiple genes, alternative splicing, and differential expression in brain and development. *J. Biol. Chem.* 274, 29510–29518. doi: 10.1074/jbc.274.41.29510

Lim, S., Sala, C., Yoon, J., Park, S., Kuroda, S., Sheng, M., et al. (2001). Sharpin, a novel postsynaptic density protein that directly interacts with the shank family of proteins. *Mol. Cell. Neurosci.* 17, 385–397. doi: 10.1006/mcne.2000.0940

Ma, K., Qin, L., Matas, E., Duffney, L. J., Liu, A., and Yan, Z. (2018). Histone deacetylase inhibitor MS-275 restores social and synaptic function in a Shank3-deficient mouse model of autism. *Neuropsychopharmacology* 43, 1779–1788. doi: 10.1038/s41386-018-0073-1

Maggio, J. C., and Whitney, G. (1985). Ultrasonic vocalizing by adult female mice (Mus musculus). *J. Comp. Psychol.* 99, 420–436. doi: 10.1037//0735-7036.99.4.420

Mameza, M. G., Dvoretskova, E., Bamann, M., Honck, H. H., Guler, T., Boeckers, T. M., et al. (2013). SHANK3 gene mutations associated with autism facilitate ligand binding to the Shank3 ankyrin repeat region. *J. Biol. Chem.* 288, 26697–26708. doi: 10.1074/jbc.m112.424747

Maunakea, A. K., Nagarajan, R. P., Bilenky, M., Ballinger, T. J., D'souza, C., Fouse, S. D., et al. (2010). Conserved role of intragenic DNA methylation in regulating alternative promoters. *Nature* 466, 253–257. doi: 10.1038/nature09165

Mei, Y., Monteiro, P., Zhou, Y., Kim, J. A., Gao, X., Fu, Z., et al. (2016). Adult restoration of Shank3 expression rescues selective autistic-like phenotypes. *Nature* 530, 481–484. doi: 10.1038/nature16971

Milad, M. R., and Quirk, G. J. (2002). Neurons in medial prefrontal cortex signal memory for fear extinction. *Nature* 420, 70–74. doi: 10.1038/nature01138

Moessner, R., Marshall, C. R., Sutcliffe, J. S., Skaug, J., Pinto, D., Vincent, J., et al. (2007). Contribution of SHANK3 mutations to autism spectrum disorder. *Am. J. Hum. Genet.* 81, 1289–1297. doi: 10.1086/522590

Monteiro, P., and Feng, G. (2017). SHANK proteins: roles at the synapse and in autism spectrum disorder. *Nat. Rev. Neurosci.* 18, 147–157. doi: 10.1038/nrn.2016.183

Mossa, A., Giona, F., Pagano, J., Sala, C., and Verpelli, C. (2017). SHANK genes in autism: defining therapeutic targets. *Prog. Neuropsychopharmacol. Biol. Psychiatry* 84, 416–423. doi: 10.1016/j.pnpbp.2017.11.019

Moy, S. S., Nadler, J. J., Perez, A., Barbaro, R. P., Johns, J. M., Magnuson, T. R., et al. (2004). Sociability and preference for social novelty in five inbred strains: an approach to assess autistic-like behavior in mice. *Genes Brain Behav.* 3, 287–302. doi: 10.1111/j.1601-1848.2004.00076.x

Nadler, J. J., Moy, S. S., Dold, G., Trang, D., Simmons, N., Perez, A., et al. (2004). Automated apparatus for quantitation of social approach behaviors in mice. *Genes Brain Behav.* 3, 303–314. doi: 10.1111/j.1601-183x.2004.00071.x

Naisbitt, S., Kim, E., Tu, J. C., Xiao, B., Sala, C., Valtschanoff, J., et al. (1999). Shank, a novel family of postsynaptic density proteins that binds to the NMDA

receptor/PSD-95/GKAP complex and cortactin. *Neuron* 23, 569–582. doi: 10.1016/s0896-6273(00)80809-0

Naydenov, A. V., Horne, E. A., Cheah, C. S., Swinney, K., Hsu, K. L., Cao, J. K., et al. (2014). ABHD6 blockade exerts antiepileptic activity in PTZ-induced seizures and in spontaneous seizures in R6/2 mice. *Neuron* 83, 361–371. doi: 10.1016/j.neuron.2014.06.030

Nemirovsky, S. I., Cordoba, M., Zaiat, J. J., Completa, S. P., Vega, P. A., Gonzalez-Moron, D., et al. (2015). Whole genome sequencing reveals a de novo SHANK3 mutation in familial autism spectrum disorder. *PLoS One* 10:e0116358. doi: 10.1371/journal.pone.0116358

Peca, J., Feliciano, C., Ting, J. T., Wang, W., Wells, M. F., Venkatraman, T. N., et al. (2011). Shank3 mutant mice display autistic-like behaviours and striatal dysfunction. *Nature* 472, 437–442. doi: 10.1038/nature09965

Peixoto, R. T., Wang, W., Croney, D. M., Kozorovitskiy, Y., and Sabatini, B. L. (2016). Early hyperactivity and precocious maturation of corticostriatal circuits in Shank3B(-/-) mice. *Nat. Neurosci.* 19, 716–724. doi: 10.1038/nn.4260

Pellow, S., Chopin, P., File, S. E., and Briley, M. (1985). Validation of open:closed arm entries in an elevated plus-maze as a measure of anxiety in the rat. *J. Neurosci. Methods* 14, 149–167. doi: 10.1016/0165-0270(85)90031-7

Phillips, R. G., and LeDoux, J. E. (1992). Differential contribution of amygdala and hippocampus to cued and contextual fear conditioning. *Behav. Neurosci.* 106, 274–285. doi: 10.1037//0735-7044.106.2.274

Portfors, C. V. (2007). Types and functions of ultrasonic vocalizations in laboratory rats and mice. *J. Am. Assoc. Lab. Anim. Sci.* 46, 28–34.

Qin, L., Ma, K., Wang, Z. J., Hu, Z., Matas, E., Wei, J., et al. (2018). Social deficits in Shank3-deficient mouse models of autism are rescued by histone deacetylase (HDAC) inhibition. *Nat. Neurosci.* 21, 564–575. doi: 10.1038/s41593-018-0110-8

Quinn, L. P., Stean, T. O., Chapman, H., Brown, M., Vidgeon-Hart, M., Upton, N., et al. (2006). Further validation of LABORAS using various dopaminergic manipulations in mice including MPTP-induced nigro-striatal degeneration. *J. Neurosci. Methods* 156, 218–227. doi: 10.1016/j.jneumeth.2006.03.013

Quinn, L. P., Stean, T. O., Trail, B., Duxon, M. S., Stratton, S. C., Billinton, A., et al. (2003). LABORAS: initial pharmacological validation of a system allowing continuous monitoring of laboratory rodent behaviour. *J. Neurosci. Methods* 130, 83–92. doi: 10.1016/s0165-0270(03)00227-9

Rendall, A. R., Perrino, P. A., Buscarello, A. N., and Fitch, R. H. (2019). Shank3B mutant mice display pitch discrimination enhancements and learning deficits. *Int. J. Dev. Neurosci.* 72, 13–21. doi: 10.1016/j.ijdevneu.2018.10.003

Rubenstein, J. L., and Merzenich, M. M. (2003). Model of autism: increased ratio of excitation/inhibition in key neural systems. *Genes Brain Behav.* 2, 255–267. doi: 10.1034/j.1601-183x.2003.00037.x

Sala, C., Vicidomini, C., Bigi, I., Mossa, A., and Verpelli, C. (2015). Shank synaptic scaffold proteins: keys to understanding the pathogenesis of autism and other synaptic disorders. *J. Neurochem.* 135, 849–858. doi: 10.1111/jnc.13232

Schmeisser, M. J., Ey, E., Wegener, S., Bockmann, J., Stempel, A. V., Kuebler, A., et al. (2012). Autistic-like behaviours and hyperactivity in mice lacking ProSAP1/Shank2. *Nature* 486, 256–260. doi: 10.1038/nature11015

Sheng, M., and Hoogenraad, C. C. (2007). The postsynaptic architecture of excitatory synapses: a more quantitative view. *Annu. Rev. Biochem.* 76, 823–847. doi: 10.1146/annurev.biochem.76.060805.160029

Sheng, M., and Kim, E. (2000). The Shank family of scaffold proteins. *J. Cell Sci.* 113(Pt 11), 1851–1856.

Sheng, M., and Kim, E. (2011). The postsynaptic organization of synapses. *Cold Spring Harb. Perspect. Biol.* 3:a005678. doi: 10.1101/cshperspect.a005678

Sheng, M., and Sala, C. (2001). PDZ domains and the organization of supramolecular complexes. *Annu. Rev. Neurosci.* 24, 1–29. doi: 10.1146/annurev.neuro.24.1.1

Silverman, J. L., Yang, M., Lord, C., and Crawley, J. N. (2010). Behavioural phenotyping assays for mouse models of autism. *Nat. Rev. Neurosci.* 11, 490–502. doi: 10.1038/nrn2851

Sohal, V. S., Zhang, F., Yizhar, O., and Deisseroth, K. (2009). Parvalbumin neurons and gamma rhythms enhance cortical circuit performance. *Nature* 459, 698–702. doi: 10.1038/nature07991

Soorya, L., Kolevzon, A., Zweifach, J., Lim, T., Dobry, Y., Schwartz, L., et al. (2013). Prospective investigation of autism and genotype-phenotype correlations in 22q13 deletion syndrome and SHANK3 deficiency. *Mol. Autism* 4, 18. doi: 10.1186/2040-2392-4-18

Speed, H. E., Kouser, M., Xuan, Z., Reimers, J. M., Ochoa, C. F., Gupta, N., et al. (2015). Autism-associated insertion mutation (InsG) of Shank3 Exon 21 causes impaired synaptic transmission and behavioral deficits. *J. Neurosci.* 35, 9648–9665. doi: 10.1523/jneurosci.3125-14.2015

Stefanko, D. P., Barrett, R. M., Ly, A. R., Reolon, G. K., and Wood, M. A. (2009). Modulation of long-term memory for object recognition via HDAC inhibition. *Proc. Natl. Acad. Sci. U.S.A.* 106, 9447–9452. doi: 10.1073/pnas.0903964106

Tan, Q., and Zoghbi, H. Y. (2018). Mouse models as a tool for discovering new neurological diseases. *Neurobiol. Learn Mem.* [Epub ahead of print].

Tokunaga, F., Nakagawa, T., Nakahara, M., Saeki, Y., Taniguchi, M., Sakata, S., et al. (2011). SHARPIN is a component of the NF-kappaB-activating linear ubiquitin chain assembly complex. *Nature* 471, 633–636. doi: 10.1038/nature09815

Tu, J. C., Xiao, B., Naisbitt, S., Yuan, J. P., Petralia, R. S., Brakeman, P., et al. (1999). Coupling of mGluR/Homer and PSD-95 complexes by the Shank family of postsynaptic density proteins. *Neuron* 23, 583–592. doi: 10.1016/s0896-6273(00)80810-7

Van de Weerd, H. A., Bulthuis, R. J., Bergman, A. F., Schlingmann, F., Tolboom, J., Van Loo, P. L., et al. (2001). Validation of a new system for the automatic registration of behaviour in mice and rats. *Behav. Processes* 53, 11–20. doi: 10.1016/s0376-6357(00)00135-2

Vicidomini, C., Ponzoni, L., Lim, D., Schmeisser, M. J., Reim, D., Morello, N., et al. (2017). Pharmacological enhancement of mGlu5 receptors rescues behavioral deficits in SHANK3 knock-out mice. *Mol. Psychiatry* 22, 689–702. doi: 10.1038/mp.2016.30

Vogel-Ciernia, A., and Wood, M. A. (2014). Examining object location and object recognition memory in mice. *Curr. Protoc. Neurosci.* 69 8, 31–17.

Waga, C., Asano, H., Sanagi, T., Suzuki, E., Nakamura, Y., Tsuchiya, A., et al. (2014). Identification of two novel Shank3 transcripts in the developing mouse neocortex. *J. Neurochem.* 128, 280–293. doi: 10.1111/jnc.12505

Wang, J., Barstein, J., Ethridge, L. E., Mosconi, M. W., Takarae, Y., and Sweeney, J. A. (2013). Resting state EEG abnormalities in autism spectrum disorders. *J. Neurodev. Disord.* 5:24.

Wang, L., Pang, K., Han, K., Adamski, C. J., Wang, W., He, L., et al. (2019). An autism-linked missense mutation in SHANK3 reveals the modularity of Shank3 function. *Mol. Psychiatry* [Epub ahead of print].

Wang, W., Li, C., Chen, Q., Van Der Goes, M. S., Hawrot, J., Yao, A. Y., et al. (2017). Striatopallidal dysfunction underlies repetitive behavior in Shank3-deficient model of autism. *J. Clin. Investig.* 127, 1978–1990. doi: 10.1172/jci87997

Wang, X., Bey, A. L., Katz, B. M., Badea, A., Kim, N., David, L. K., et al. (2016). Altered mGluR5-Homer scaffolds and corticostriatal connectivity in a Shank3 complete knockout model of autism. *Nat. Commun.* 7:11459.

Wang, X., Mccoy, P. A., Rodriguiz, R. M., Pan, Y., Je, H. S., Roberts, A. C., et al. (2011). Synaptic dysfunction and abnormal behaviors in mice lacking major isoforms of Shank3. *Hum. Mol. Genet.* 20, 3093–3108. doi: 10.1093/hmg/ddr212

Wang, X., Xu, Q., Bey, A. L., Lee, Y., and Jiang, Y. H. (2014). Transcriptional and functional complexity of Shank3 provides a molecular framework to understand the phenotypic heterogeneity of SHANK3 causing autism and Shank3 mutant mice. *Mol. Autism* 5:30. doi: 10.1186/2040-2392-5-30

Wilson, H. L., Wong, A. C., Shaw, S. R., Tse, W. Y., Stapleton, G. A., Phelan, M. C., et al. (2003). Molecular characterisation of the 22q13 deletion syndrome supports the role of haploinsufficiency of SHANK3/PROSAP2 in the major neurological symptoms. *J. Med. Genet.* 40, 575–584. doi: 10.1136/jmg.40.8.575

Yang, M., Bozdagi, O., Scattoni, M. L., Wohr, M., Roullet, F. I., Katz, A. M., et al. (2012). Reduced excitatory neurotransmission and mild autism-relevant phenotypes in adolescent Shank3 null mutant mice. *J. Neurosci.* 32, 6525–6541. doi: 10.1523/jneurosci.6107-11.2012

Yao, I., Hata, Y., Hirao, K., Deguchi, M., Ide, N., Takeuchi, M., et al. (1999). Synamon, a novel neuronal protein interacting with synapse-associated protein 90/Postsynaptic density-95-associated protein. *J. Biol. Chem.* 274, 27463–27466. doi: 10.1074/jbc.274.39.27463

Yi, F., Danko, T., Botelho, S. C., Patzke, C., Pak, C., Wernig, M., et al. (2016). Autism-associated SHANK3 haploinsufficiency causes Ih channelopathy in human neurons. *Science* 352:aaf2669. doi: 10.1126/science.aaf2669

Yoo, T., Cho, H., Lee, J., Park, H., Yoo, Y. E., Yang, E., et al. (2018). GABA neuronal deletion of Shank3 exons 14-16 in mice suppresses striatal excitatory synaptic input and induces social and locomotor abnormalities. *Front. Cell Neurosci.* 12:341. doi: 10.3389/fncel.2018.00341

Zhou, Y., Kaiser, T., Monteiro, P., Zhang, X., Van Der Goes, M. S., Wang, D., et al. (2016). Mice with Shank3 mutations associated with ASD and schizophrenia display both shared and distinct defects. *Neuron* 89, 147–162. doi: 10.1016/j.neuron.2015.11.023

Zhu, L., Wang, X., Li, X. L., Towers, A., Cao, X., Wang, P., et al. (2014). Epigenetic dysregulation of SHANK3 in brain tissues from individuals with autism spectrum disorders. *Hum. Mol. Genet.* 23, 1563–1578. doi: 10.1093/hmg/ddt547

Zhu, M., Idikuda, V. K., Wang, J., Wei, F., Kumar, V., Shah, N., et al. (2018). Shank3-deficient thalamocortical neurons show HCN channelopathy and alterations in intrinsic electrical properties. *J. Physiol.* 596, 1259–1276. doi: 10.1113/jp275147

Conflict of Interest Statement: The authors declare that the research was conducted in the absence of any commercial or financial relationships that could be construed as a potential conflict of interest.

Advantages of publishing in Frontiers

OPEN ACCESS
Articles are free to read for greatest visibility and readership

FAST PUBLICATION
Around 90 days from submission to decision

HIGH QUALITY PEER-REVIEW
Rigorous, collaborative, and constructive peer-review

TRANSPARENT PEER-REVIEW
Editors and reviewers acknowledged by name on published articles

Frontiers
Avenue du Tribunal-Fédéral 34
1005 Lausanne | Switzerland

Visit us: www.frontiersin.org
Contact us: info@frontiersin.org | +41 21 510 17 00

REPRODUCIBILITY OF RESEARCH
Support open data and methods to enhance research reproducibility

DIGITAL PUBLISHING
Articles designed for optimal readership across devices

FOLLOW US
@frontiersin

IMPACT METRICS
Advanced article metrics track visibility across digital media

EXTENSIVE PROMOTION
Marketing and promotion of impactful research

LOOP RESEARCH NETWORK
Our network increases your article's readership